ORNL-2217
C-84 – Reactors–Special Features
of Aircraft Reactors

This document consists of 252 pages.

Copy 194 of 211 copies. Series A.

Contract No. W-7405-eng-26

METALLURGY DIVISION

SEMIANNUAL PROGRESS REPORT

for Period Ending October 10, 1956

J. H. Frye, Jr., Director
W. D. Manly, Associate Director
J. E. Cunningham, Assistant Director

DATE ISSUED

DEC 19 1956

OAK RIDGE NATIONAL LABORATORY
Operated by
UNION CARBIDE NUCLEAR COMPANY
A Division of Union Carbide and Carbon Corporation
Post Office Box X
Oak Ridge, Tennessee

DISCLAIMER

Reports previously issued in this series are as follows:

ORNL-28	Period Ending March 1, 1948
ORNL-69	Period Ending May 31, 1948
ORNL-407	Period Ending July 31, 1949
ORNL-511	Period Ending October 31, 1949
ORNL-583	Period Ending January 31, 1950
ORNL-754	Period Ending April 30, 1950
ORNL-827	Period Ending July 31, 1950
ORNL-910	Period Ending October 31, 1950
ORNL-987	Period Ending January 31, 1951
ORNL-1033	Period Ending April 30, 1951
ORNL-1108	Period Ending July 31, 1951
ORNL-1161	Period Ending October 31, 1951
ORNL-1267	Period Ending January 31, 1952
ORNL-1302	Period Ending April 30, 1952
ORNL-1366	Period Ending July 31, 1952
ORNL-1437	Period Ending October 31, 1952
ORNL-1503	Period Ending January 31, 1953
ORNL-1551	Period Ending April 10, 1953
ORNL-1625	Period Ending October 10, 1953
ORNL-1727	Period Ending April 10, 1954
ORNL-1875	Period Ending October 10, 1954
ORNL-1911	Period Ending April 10, 1955
ORNL-1988	Period Ending October 10, 1955
ORNL-2080	Period Ending April 10, 1956

INTERNAL DISTRIBUTION

1. C. E. Center
2. Biology Library
3. Health Physics Library
4. Metallurgy Library
5-7. Central Research Library
8. Reactor Experimental Engineering Library
9-13. Laboratory Records Department
14. Laboratory Records, ORNL RC
15. A. M. Weinberg
16. L. B. Emlet (K-25)
17. J. P. Murray (Y-12)
18. J. A. Swartout
19. E. H. Taylor
20. E. J. Murphy
21. E. D. Shipley
22. J. H. Frye, Jr.
23. M. L. Nelson
24. W. H. Jordan
25. R. A. Charpie
26. S. C. Lind
27. F. L. Culler
28. A. H. Snell
29. A. Hollaender
30. M. T. Kelley
31. K. Z. Morgan
32. T. A. Lincoln
33. A. S. Householder
34. C. S. Harrill
35. C. E. Winters
36. D. S. Billington
37. D. W. Cardwell
38. E. M. King
39. A. J. Miller
40. D. D. Cowen
41. P. M. Reyling
42. W. H. Bridges
43. G. C. Williams
44. S. Cromer
45. L. K. Jetter
46. R. R. Dickison
47. W. D. Manly
48. C. D. Susano
49. W. W. Parkinson
50. R. J. Gray
51. H. L. Yakel
52. P. Patriarca
53. C. P. Keim
54. G. P. Smith
55. J. E. Cunningham
56. R. S. Crouse
57. R. E. Adams
58. J. H. Erwin
59. J. O. Betterton, Jr.
60. W. O. Harms (consultant)
61. G. M. Adamson
62. E. S. Bomar
63. R. J. Beaver
64. T. W. Fulton
65. C. J. McHargue
66. R. B. Oliver
67. J. T. Howe
68. T. H. Blewitt
69. C. R. Boston
70. J. H. Crawford, Jr.
71. J. C. Wilson
72. H. W. Savage
73. E. E. Hoffman
74. W. J. Leonard
75. J. A. Milko
76. L. M. Doney
77. R. W. Johnson
78. J. A. Lane
79. G. E. Boyd
80. R. S. Livingston
81. A. L. Boch
82. J. H. DeVan
83. J. H. Coobs
84. D. A. Douglas
85. J. P. Hammond
86. T. T. Hikido
87. M. R. Hill
88. M. L. Picklesimer
89. A. Taboada
90. H. G. MacPherson
91. E. C. Cruetz (consultant)
92. E. P. Wigner (consultant)
93. N. J. Grant (consultant)
94. T. S. Shevlin (consultant)
95. H. Leidheiser, Jr. (consultant)

96. E. E. Stansbury (consultant)
97. C. S. Smith (consultant)
98. ORNL – Y-12 Technical Library, Document Reference Section

EXTERNAL DISTRIBUTION

99. AF Plant Representative, Baltimore
100. AF Plant Representative, Burbank
101. AF Plant Representative, Marietta
102-104. AF Plant Representative, Santa Monica
105-106. AF Plant Representative, Seattle
107. AF Plant Representative, Wood-Ridge
108. Air Materiel Area
109. Air Research and Development Command (RDGN)
110. Air Technical Intelligence Center
111. Allison Division
112-114. ANP Project Office, Fort Worth
115. Albuquerque Operations Office
116. Argonne National Laboratory
117. Armed Forces Special Weapons Project, Sandia
118. Armed Forces Special Weapons Project, Washington
119. Assistant Secretary of the Air Force, R&D
120-125. Atomic Energy Commission, Washington
126. Battelle Memorial Institute
127-128. Bettis Plant (WAPD)
129. Bureau of Aeronautics
130. Bureau of Aeronautics (Code 24)
131. Bureau of Aeronautics General Representative
132. Chicago Operations Office
133. Chicago Patent Group
134. Chief of Naval Research
135. Convair-General Dynamics Corporation
136. Engineer Research and Development Laboratories
137-140. General Electric Company (ANPD)
141. Hartford Area Office
142. Headquarters, Air Force Special Weapons Center
143. Idaho Operations Office
144. Knolls Atomic Power Laboratory
145. Lockheed Aircraft Corporation (R. G. Rowe)
146. Lockland Area Office
147. Los Alamos Scientific Laboratory
148. National Advisory Committee for Aeronautics, Cleveland
149. National Advisory Committee for Aeronautics, Washington
150. Naval Air Development and Material Center
151. Naval Research Laboratory
152. New York Operations Office
153. North American Aviation, Inc. (Aerophysics Division)
154. North American Aviation, Inc. (Canoga Park)
155. Nuclear Development Corporation of America
156. Office of the Chief of Naval Operations (OP-361)

157. Patent Branch, Washington
158-161. Pratt and Whitney Aircraft Division (Fox Project)
162. Sandia Corporation
163. School of Aviation Medicine
164. Sylvania Electric Products, Inc.
165. USAF Project RAND
166. University of California Radiation Laboratory, Livermore
167-184. Wright Air Development Center (WCOSI-3)
185-209. Technical Information Service Extension, Oak Ridge
210. Technical Research Group, New York
211. Division of Research and Development, AEC, ORO

CONTENTS

HRP METALLURGY

APPLIED METALLURGY

FUNDAMENTAL METALLURGY

PUBLICATIONS

G. P. Smith, M. E. Steidlitz, and E. E. Hoffman, *Experimental Procedures Used for the Measurement of Corrosion and Metal Transport in Fused Sodium Hydroxides*, ORNL-2125 (Sept. 25, 1956).

J. R. Johnson and G. D. White, "Note on a High Temperature Attachment for an X-Ray Spectrometer," *J. Am. Chem. Soc.* 6, 227–228 (1956).

G. M. Slaughter, P. Patriarca, W. D. Manly, and R. L. Heestand, *Fabrication of Heat Exchangers and Radiators for High Temperature Reactor Applications*, ORNL-1955 (June 14, 1956).

S. G. Holder, Jr., E. E. Stansbury, and J. H. Frye, Jr., "Internal Friction Studies on Silver and Certain Silver-Base Solid Solutions," *J. Metals* 8(II), 993 (1956). Paper presented *Am. Inst., Mech. Engr.*, New York, Feb. 1956.

J. H. Frye, Jr., and J. L. Gregg, "Economic Atomic Power Depends on Materials of Construction," *Metal Progr.* 70(3), 92–96B (1956).

G. P. Smith, *Problems Pertaining to the Dehydration of Sodium Hydroxide by Volatization of Water*, ORNL-2130 (Aug. 28, 1956).

J. A. Milko, *Impact Behavior of Thorium*, ORNL-2122 (Sept. 5, 1956).

J. V. Cathcart, L. L. Hall, and G. P. Smith, *The Oxidation Characteristics of the Alkali Metals I. The Oxidation Rate of Sodium Between 79 and 48°C*, ORNL-2054 (June 14, 1956).

D. A. Douglas and W. D. Manly, *A Laboratory for the High-Temperature Creep Testing of Metals and Alloys in Controlled Environment*, ORNL-2053 (Sept. 18, 1956).

W. D. Manly, *Fundamentals of Liquid Metal Corrosion*, ORNL-2055 (July 12, 1956); *Corrosion* 12, 46–52 (1956). Paper presented at NACA Meeting, Chicago, March 10, 1955, and Houston, Oct. 1955.

C. R. Johnson and J. M. Warde, *Bulk ThO_2, A Reactor Material*, ORNL-2041 (May 22, 1956).

G. E. Elder, E. C. Miller, L. F. Bledsoe, and F. V. Daly, "Fabrication of a Large Zirconium Tank," *J. Metals* 8(I), 648 (1956). Paper presented at the Engineers Joint Council, *Am. Inst. Mech. Engr.* Meeting in Cleveland, Ohio, Dec. 12–16, 1955.

E. C. Miller, W. R. Gall, L. F. Bledsoe, and F. V. Daly, "Fabrication of the Homogeneous Reactor Test Vessel Assembly," *Welding J.* (N.Y.) 35, 997–1006 (1956). Presented at 1956 AWS National Spring Meeting in Buffalo, N. Y., May 7–11.

METALLURGY DIVISION
SEMIANNUAL PROGRESS REPORT

SUMMARY

ANP METALLURGY

General Corrosion. – The results of two beryllium-Inconel-sodium compatibility tests are given. Direct contact between Inconel and beryllium specimens while immersed in sodium at 1300°F for 1000 hr results in 25 mils of brittle alloy formation (principally $Be_{21}Ni_5$). Chromium plating of the Inconel has been effective in reducing the thickness of alloy formed, Be_2Cr being the compound formed in this case.

Two Inconel-sodium thermal-convection-loop tests have been conducted to determine the effect of a diffusion cold trap on the amount of mass transfer observed in the cold leg of the loop. Corrosion and mass transfer were found to be less in the loop with the diffusion cold trap than in a standard loop with no trap.

The results of 17 lithium thermal-convection-loop tests on various grades of the stainless steels and Inconel are given. None of the stainless steels had satisfactory resistance to mass transfer at hot-zone temperatures of 1500°F, and Inconel was not satisfactory at a temperature of 1300°F.

Corrosion tests in seesaw apparatus have been conducted on a series of Coast Metals No. 52 (89% Ni–5% Si–4% B–2% Fe) buttons to obtain some information on the depleted region found at the edge of this alloy after exposure to liquid metal or fuel salts. It was found that the depth of the depleted region is time-dependent and that boron is leached out of this area when tested in the fuel bath. Similar tests were conducted on Coast Metals No. 53 (81% Ni–8% Cr–4% Si–4% B–3% Fe) with the expectation that the high chromium content would tie up the boron and prevent it from being leached into the fuel bath.

Recrystallized tube-to-header joints welded and supplied by The Glenn L. Martin Co. show good resistance to the NaF-ZrF_4-UF_4 (50-46-4 mole %) and NaK (56-44 wt %) baths during corrosion tests at 1500°F for 100 hr. The welds are made by forging a preflared tube into a drilled header plate; the edge of the header hole is heated to a plastic state which allows the tube to be forged into position.

Inconel thermal-convection loops with the 70% Ni–13% Ge–11% Cr–6% Si brazing alloy located in the hot-leg section have been tested at 1500°F for 500 hr with NaK (56-44 wt %) and NaF-ZrF_4-UF_4 (53.5-40.0-6.5 mole %) as circulating fluids. The alloy showed a 1- to 1.5-mil attack in the NaK loop. Depth of attack on the alloy in the fuel loop averaged approximately 5 mils. A third thermal-convection loop with the 82% Au–18% Ni brazing alloy in the hot leg was operated with NaF-ZrF_4-UF_4 (50-46-4 mole %) as circulating fluid for 500 hr at 1500°F. Attack on this brazing alloy averaged 8 mils.

Pure niobium has been static tested in sodium for 1000 hr at 1500°F in Inconel and type 304 stainless steel capsules. A small amount of surface roughening and weight loss was found on the specimens after the test.

Some Thermenol (82% Fe–15% Al–3% Mo) samples have been statically tested in sodium for 100 hr at 1500°F using 1035 steel and type 430 stainless steel capsules. A small weight and thickness loss was found on the tested specimens.

Haynes alloy No. 40, nominal composition 13.5% Cr–4.5% Fe–3.9% Si–3.2% B–1.0% Co–0.42% C–0.25% Mn–bal Ni, shows good corrosion resistance to NaK but only fair resistance to an NaF-ZrF_4-UF_4 (50-46-4 mole %) mixture during a dynamic corrosion test at 1500°F for 100 hr.

Screening corrosion tests on nickel and Inconel by using an $NaCl$-$MgCl_2$-UCl_3 (50.0-33.3-16.7 mole %) bath show that nickel mass-transfers quite readily in this bath at 1800°F during a 100-hr test. Inconel showed trace amounts of mass transfer under the same conditions and a 2-mil subsurface type attack in a 500-hr test at 1350°F in the same bath.

Tests with seesaw apparatus which was operated for 100 hr at 1500°F revealed little attack of Inconel and type 316 stainless steel by NaK and lithium. Thermal-convection-loop tests which were

conducted for 1000 hr at 1500°F with a 5% lithium addition revealed no change in attack on the Inconel, but the stainless steel was attacked to a depth of 6 mils in the cold leg.

Long-duration tests of $NaF-UF_4-ZrF_4$ (56-4-40 mole %) in Inconel, in which a temperature gradient was used to make the more volatile ZrF_4 "snow" crystallize above the fused-salt bath, revealed that no attack occurred in the "snow" region and that the attack in the bath region was less than that normally observed in fused salt–Inconel tests.

No mass transfer or attack occurred in tests by seesaw apparatus of zirconium in lithium and in sodium. Niobium capsules, tested in sodium and in lithium under similar test conditions, were subjected to some attack and to a very small amount of dissimilar-metal mass transfer to the walls of the Hastelloy B and Inconel protective containers.

Several Inconel castings tested statically for 1000 hr at 1500°F in an $NaF-ZrF_4-UF_4$ (50-46-4 mole %) wrought Inconel system were more severely attacked than is normally experienced in wrought Inconel.

Rubidium standpipe and corrosion tests by seesaw apparatus in Hastelloy B and in molybdenum capsules which were performed for 500 hr at various temperatures produced no mass transfer and little attack of the two materials.

Of the four materials subjected to carburization by sodium with varying graphite additions, the heaviest amount of carburization and deepest carbon penetration occurred, in descending order, in type 430 stainless steel, type 316 stainless steel, Hastelloy B, and type 310 stainless steel.

In 100-hr screening tests at 1500°F, the corrosion resistance of intermetallics of NiAl, NiAl + 5% Ni, NiAl + 4% Zr, and MoAl was good in static sodium and poor in static $NaF-ZrF_4-UF_4$ (53.5-40.0-6.5 mole %).

A ceramic of rare-earth oxides with an apparent porosity to water of 53.5% had an apparent porosity to sodium of 52% when exposed to static sodium for 100 hr at 1300°F. A ceramic body of the same rare-earth oxides with an apparent porosity to water of 46.4% had an apparent porosity to sodium of 51.0% when exposed to static sodium for 473 hr at 1350°F plus 81 hr of 3-hr cycles between 1350 and 1100°F.

Solid-phase-bonding screening tests have been made for molybdenum in contact at 20,000 psi (calculated) with K150A (80% TiC–10% $NbTaTiC_3$–10% Ni) and K152B (64% TiC–6% $NbTaTiC_3$–30% Ni) for 100 hr in $NaF-ZrF_4-UF_4$ (50-46-4 mole %) at 1500°F. Bonding occurred between K152B and molybdenum.

No bonding was found between specimens of Stellite 6 in contact at 50,000 psi (calculated) for 200 hr in sodium at 1200°F.

Dynamic Corrosion. – Two Inconel pump loops were operated to study the effects of increasing cold-leg surface area on corrosion in fused fluoride No. 30. One of the loops contained a standard cooling coil, while in the other a special coil was employed to double the effective cooler surface. No difference in attack between the loops was observed over a 1000-hr period.

A standard forced-circulation loop, which was designed to study effects of bulk fluoride temperatures on corrosion, operated with No. 30 fused salt at a 1700°F maximum wall temperature, 1500°F maximum fluid temperature, and 200°F temperature drop. The attack in this loop was 9 mils and compares closely with the attack in a loop operated at a similar wall temperature and temperature drop but at a 1650°F fluid temperature. The agreement in corrosion results is attributed to the importance of wall temperature in fluoride corrosion.

Two Inconel pump loops were examined following 1000-hr operation with fuel No. 70, a fluoride mixture composed of $NaF-ZrF_4-UF_4$ (56.0-39.0-5.0 mole %). The purpose of these tests was to compare the corrosion properties of this fuel mixture with those of fuel No. 30. The loops were operated at 1500 and 1650°F maximum fluid temperatures with temperature gradients of 200°F. Maximum attack in both loops reached 7 mils, values which show good agreement with similarly operated loops circulating fuel No. 30. However, very thin metallic deposits were noted in the cooling coils of both loops in contrast with fuel No. 30 loops, which normally have shown no deposits.

A Hastelloy B forced-circulation loop has been operated 1000 hr with the fluoride mixture $NaF-KF-LiF-UF_4$ (11.2-41-45.3-2.5 mole %). The fluoride was circulated at a maximum fluid temperature of 1500°F and a temperature drop of 200°F. Metallographic examination of the hot leg revealed only very slight attack in the form of surface roughening and pitting. The cold leg metallographically showed no deposits or attack, although some evidence of very minute metal particles was found on visual inspection.

The operation of an Inconel pump loop, conducted as an endurance test with fuel No. 30, was terminated after 8300 hr by a pump drive failure. The loop was gas-fired and operated with a maximum fluoride temperature of 1450°F. Hot-leg attack occurred as subsurface void formation to a depth of 25 mils. The cold-leg surface was roughened but showed no evidence of mass-transferred deposits. A second loop of relatively long duration operated for 3000 hr with fuel No. 30 at a maximum temperature of 1600°F. Hot-leg attack in this loop was 25 mils in depth, and again no deposits were noted in the cold leg.

An Inconel pump loop, using sodium specially treated to remove oxide contamination, has operated 1000 hr at 1500°F. The sodium was cold-trapped at 300°F before entry into the test loop, where it was again cold-trapped. An examination of mass transfer in this loop showed the weight of deposit to be equivalent to loops operating with normal sodium either with or without bypass cold traps.

Several Inconel pump loops have completed operation with sodium at temperatures from 1250 to 1500°F. A loop operated at a temperature of 1350°F with a 300°F temperature drop revealed only scattered metal deposits in the cooler after 1000 hr. A relatively heavy deposit resulted in a loop operated at 1500°F with a temperature gradient of 400°F. Two loops, one at 1250°F and the other at 1300°F, were operated in conjunction with beryllium inserts. At the higher temperature, the insert revealed scattered void formation to 7 mils. Alloying between the beryllium and the Inconel in contact with it produced a brittle layer $3\frac{1}{2}$ mils thick. At the lower temperature, void formation in the beryllium progressed to 5 mils with no evidence of alloy formation with Inconel. To determine whether increasing the surface area of beryllium will affect its compatibility in an Inconel-sodium system, two tests were conducted at 1250°F in which equivalent surface areas of Inconel and beryllium were in contact in molten sodium. Visually, no increase in mass transfer was seen in either of these tests, compared with tests of smaller inserts.

Severe fluoride corrosion of cast Inconel was observed in standard Inconel thermal-convection loops containing the castings as hot-leg inserts. These loops operated 500 hr with NaF-ZrF_4-UF_4 (50-46-4 mole %) at 1500°F. The castings contained approximately 1.2% Mn, 2% Nb, and 1 to 2% Si. The inserts with the lowest and the highest silicon contents were evaluated in tests with fuel No. 30, while the insert with the intermediate silicon content was operated with sodium. The fluoride attack, which reached in the most severe case to a depth of 70 mils, appeared as subsurface voids with very deep intergranular penetration. Metal deposits were also observed in the loops.

The casting with the intermediate silicon content, which was tested in sodium, showed very little corrosion, although metallic deposits were observed in the cold-leg area of the loop.

Thermal-convection loops constructed of Monel and operated with NaF-LiF-KF-UF_4 (11.2-41.0-45.3-2.5 mole %) at 1500°F showed very little hot-leg attack, 1 mil, in various tests conducted from 500 to 1339 hr.

Hastelloy X exhibited poor fluoride corrosion resistance in thermal-convection-loop tests conducted 1000 hr with NaF-ZrF_4-UF_4 (50-46-4 mole %) at 1500°F. The hot-leg attack, 27 to 35 mils in depth, appeared as deep intergranular subsurface void formations. Cold-leg deposits were observed in these tests.

No deposits or attack was observed in thermal-convection loops constructed of Hastelloy X and operated 1000 hr with sodium at 1500°F.

Several Hastelloy W thermal-convection loops were operated 1000 hr with sodium, NaF-ZrF_4-UF_4 (50-46-4 mole %), and NaF-LiF-KF-UF_4 (11.2-41.0-45.3-2.5 mole %) all at 1500°F. No hot-leg attack was observed in the sodium tests, but metallic deposits were observed in the cold legs of the loops. Also, no hot-leg attack or cold-leg deposits were observed in the NaF-ZrF_4-UF_4 (50-46-4 mole %) tests. A maximum attack of 2 mils was observed in the loops operating 1000 hr with NaF-LiF-KF-UF_4 (11.2-41.0-45.3-2.5 mole %) at 1500°F. Alloying of nickel and beryllium was observed in Hastelloy B thermal-convection loops containing beryllium inserts in the hot legs and operating 1000 hr with sodium at 1200 and 1300°F. However, this alloying occurred only at the areas of contact, and alloying was not observed where a spacing of 0.020 ± 0.005 in. was provided. A maximum attack of 3 mils occurred on the outside diameter of the beryllium insert where the sodium flow was somewhat restricted.

Inconel-beryllium-sodium studies at sodium operating temperatures of 1200, 1250, 1300, 1400, and 1500°F were conducted with standard Inconel

thermal-convection loops containing beryllium inserts in the hot legs. All tests were operated for 1000 hr. Nickel-beryllium alloy formation was observed in tests conducted at temperatures of 1300°F and above. Maximum attack of the beryllium was 13 mils and occurred on the outside diameter of the insert in the loop which operated at 1500°F.

A reduction in maximum hot-leg attack was observed in standard Inconel thermal-convection loops operating 500 hr with specially prepared fuels ($NaF-ZrF_4-UF_4$, 50-46-4 mole %).

Two types of fuel were used; one contained specially prepared ZrF_4, and the other had been used and reclaimed.

Screening tests of special fuel mixtures are under way. Tests were conducted to study the effect on corrosion of different alkali-metal fluorides as components of the basic fluoride-fuel mixture $MF-ZrF_4-UF_4$ (50-46-4 mole %), where M stands for potassium, rubidium, or lithium. The attack with the lithium-bearing mixture was severe, but the attack with potassium and rubidium mixtures was similar to that normally found with $NaF-ZrF_4-UF_4$.

Also, tests were completed in which the alkali metal and ZrF_4 content of the $MF-ZrF_4-UF_4$ fuel system were varied. Lowering the ZrF_4 content from 46 to 40 mole %, but keeping the UF_4 content at 4 mole %, had no effect on attack by the NaF-containing mixtures, but the attack by the KF- and RbF-containing mixtures increased from 1 to 2 mils. The attack by the LiF-containing mixture decreased significantly with the decrease in ZrF_4 content, although this result is in doubt. Traces of metallic crystals were found in the cold legs of loops containing 56 mole % of the alkali-metal fluoride, except the loop containing KF.

An increase in UF_4 content from 5 to 26 mole % in the $NaF-ZrF_4-UF_4$ system shows an increase in fluoride attack with an increase in UF_4 content. Cold-leg deposits, possibly uranium, were observed in all loops.

The special fuels in which the $NaF-BeF_2$ ratio was varied do not exhibit a definite corrosion pattern. However, in the instances where the NaF was replaced with LiF in these beryllium systems, the attack was increased almost twofold. Also, increasing the LiF in these mixtures appears to increase the maximum hot-leg attack.

Mechanical Properties. – Relaxation tests of Inconel at 1300 and 1500°F have been completed. Results indicate that relaxation rates tend to vary with the load rate up to the proportional limit. At stresses above the proportional limit the relaxation rate is independent of the load rate.

Creep tests of Inconel specimens with varying section thicknesses were conducted in liquid No. 30. It can be noted that, for sections of 0.020 in. and less, the stress-rupture properties are very drastically affected, as compared with the tests for sections from 0.060 to 0.125 in., which show good correlation.

Extensive mechanical tests of beryllium at elevated temperatures in argon have been conducted by The Brush Beryllium Co. In this laboratory a few creep tests have been performed on beryllium specimens in sodium. A comparison of the results with those obtained by The Brush Beryllium laboratory indicates that no detrimental effects will be attributable to this environment.

Lead alloyed with 0.06% copper for better elevated temperature strength is in test at 230°F. It is desirable that this material deform less than 0.5% in a year at a stress of 100 psi. Results to date indicate that the alloy does not possess this strength.

Results of tests of Hastelloy B and Hastelloy W in several environments including liquid No. 107 show that, except for very high stresses, no differences in creep properties are noted. Hastelloy X shows good corrosion resistance in liquid No. 30 at 1500°F but is heavily attacked with a corresponding loss in creep properties at higher temperatures.

The creep properties of an 80% Mg–20% Li alloy, proposed as neutron shielding material for crew compartments, are being investigated. The oxidation resistance of the material, even at room temperature, is so poor that a method was devised for producing a protective film at the surface. The results of tests at 200°F show that the alloy is so weak that a stress of 500 psi will produce rupture in 1000 hr.

Nondestructive Testing. – Most of the available manpower and equipment time has been devoted to the routine inspection of approximately 17,000 ft of pipe and tubing for the reactor construction program. Both encircling-coil-eddy-current and immersed-ultrasound methods of inspection were used. Part of the remaining effort was employed in the metallographic examination of regions which showed defect indications so that the defect types

and sizes could be correlated with the data presented by the inspection instruments. This has been valuable experience.

The balance of the efforts of this group has been devoted to the development of an inspection method to detect small lamination-like defects in sheet material. After consideration and rejection of such techniques as ultrasonic resonance, conventional pulse-echo ultrasound, and transmission-attenuation of ultrasound by using transducers on opposite sides of the sheet, a new ultrasonic method was conceived and is presently being investigated. This method requires a pulse of ultrasound of 5- to 20-μsec duration tuned to such a frequency that the sheet thickness is an exact multiple of the half-wave length. Under these conditions a reverberation or ringing of the ultrasound between the two sheet surfaces is obtained and presence of laminations is detected by a decrease in this ringing. The reflectoscope is being modified for application to this sheet inspection technique.

Inspection. – Inspection of 4959 critical weldments in the Y-12 area resulted in an 11% rejection rate for porosity, cracks, misalignment, lack of fusion, and lack of penetration.

Over 20,000 ft of tubing and various amounts of pipe, plate, sheet, rod, and other Inconel material were inspected. The rejection rate for pipe and tubing averaged approximately 10%, except for two lots which were completely rejected, one because of oxidation of the inside-diameter surface and the other because of numerous defects. Rejection rates for other shapes were not greater than 5% in any case and averaged much less.

Sixty feet of Inconel W and 208 ft of Hastelloy B tubing were also inspected. The former was found to be acceptable, while the latter was over 65% rejectable. However, because of the need for this material, it was reworked, and all but the most gross defects were accepted.

Inspection of items fabricated by outside vendors included thermal-convection loops, pressed dished Inconel heads, small heat exchangers, and ½-Mw high-conductivity fin radiators.

Fluorescent penetrant inspection equipment has been installed and tests are under way to compare this type of inspection with the dye penetrant process it will replace. It appears that higher quality tubing can be ensured by the greater sensitivity of the new method.

A report of the number of qualified welders currently employed in the ANP program is presented.

Welding and Brazing. – Weld shrinkage studies have been conducted to permit the accumulation of empirical data pertaining to the fabrication of Inconel reactor components. A special welding procedure has been developed for fabricating Inconel pump volutes to the desired tolerances. Metallographic examinations on radiators after service have indicated that the incorporation of various suggested design modifications has been beneficial. The results of a heat exchanger failure analysis are also reported.

A continuous furnace for the production of sintered brazing alloy rings has been developed, and a production rate has been established. Approximately 50,000 rings could be produced in an 8-hr day, with a probable cost per ring of a fraction of a cent.

The development of a suitable technique for joining various cermet valve components is also reported. A metallurgical bond can be formed directly between nickel and the nickel–titanium carbide cermets at temperatures of approximately 1350°C. Preliminary work on an evaluation of the weldabilities of several nickel-molybdenum alloys has been initiated.

Fabrication. – Conditions for the extrusion of nickel-molybdenum-base alloys, including Hastelloys B and W, have been developed to the point where tube blanks of these materials can be successfully fabricated on a laboratory scale. Slow extrusion rates and improved lubrication were found to be the most desirable conditions. This laboratory-established information has been successfully applied for the extrusion of Hastelloys B, W, and X on a commercial scale for the first time.

Twenty-five feet of high-quality seamless Hastelloy W tubing, 0.187 in. in outside diameter by 0.025 in. in wall thickness, was redrawn from the first successful laboratory extrusion of this alloy. This demonstrates the feasibility of producing seamless tubing of this type of alloy for heat-exchanger applications.

A high-strength, corrosion-resistant nickel-molybdenum-base alloy is being developed that will not be embrittled as a result of aging, as is the case for Hastelloys B and W. Various experimental nickel-molybdenum-base alloys received from the

International Nickel Company, Inc., and Battelle Memorial Institute were extruded into tube blanks and further processed into seamless tubing by the Superior Tube Co. The alloys which contained moderately high carbon contents of 0.12 to 0.25% tended to crack badly during tube processing. Metallographic examination revealed stringers of carbides in the microstructure; it was along these stringers that the cracks tended to propagate. Those alloys which yielded acceptable tubing are being evaluated for their corrosion resistance.

Ternary alloys, based on the 17% Mo–Ni alloy with additions of Ti, Al, W, Nb, Cr, Fe, and V, have been fabricated into tubing for corrosion testing in order to determine the upper limit of the third element added to increase the strength of the alloy.

In order to gain production experience with special nickel-molybdenum-base alloys, the International Nickel Company has prepared 4800-lb heats of six alloys. One composition, 1.5% Ti–2% Al–17% Mo–Ni, was not forged successfully during the initial ingot breakdown and was virtually 100% scrap. Seamless tubing, plate, sheet, wire, and rod products are being prepared from the other five compositions.

The effect of consumable-electrode arc melting on the strength and fabricability of nickel and several nickel-molybdenum-base alloys is being investigated. It is hoped that the high arc temperatures will vaporize "tramp" elements and that the resulting melts will have improved mechanical properties. Electrodes of each composition of interest were arc-melted at Battelle Memorial Institute and have been returned to ORNL for evaluation.

The oxidation of Hastelloy B in static air has been investigated at 1200, 1400, 1600, and 1800°F. The curves of weight gain vs time were parabolic at all test temperatures; and, thus, the oxide scale ($NiMoO_4$) that forms on the surface appears to be protective. Evidence has been found that the formation of $NiMoO_4$ depends on the molybdenum content of the alloy, as well as on the test temperature.

The fabrication of experimental compositions of tungsten carbide with nickel-alloy binders, for use in the ART pump-impeller shield plug, was continued. It was established that a composition of 25 to 30% Hastelloy C with tungsten carbide had optimum properties. Hot-pressed models of the gamma shield were successfully brazed to Inconel plate.

Specimens of ZrO_2 were fabricated and tested for use in the thermal shield of the shield plug and were found to be satisfactory.

A sample of the type 430 stainless-steel-clad Cu-B_4C shield material, which was fabricated by the Alleghany Ludlum Steel Corp., was evaluated. The sample plate was satisfactory except for thickness deviations and surface roughness.

Sample tiles of B_4C submitted by The Carborundum Company and the Norton Company were evaluated. Tiles submitted by The Carborundum Company were unsatisfactory because of voids and low boron density, whereas the Norton Company tiles met or exceeded all specifications.

Dispersions of CaB_6 and BN in iron and nickel were investigated as possible substitutes for the B_4C-Cu layer. Dispersions of BN in nickel were easily fabricated and were found to be stable at 2000°F.

Samples of steel and stainless steel containing up to 1.0% boron were prepared for strength and irradiation tests.

The preparation of copper coatings on B_4C tiles was investigated by The Vitro Mfg. Co. Uniform, adherent coatings were produced by a two-step process consisting of deposition of Cu_2O, followed by reduction with a mixture of argon and hydrogen.

A promising phosphate-base coating for the 20% Li–80% Mg alloy was developed and was tested in tensile and creep tests for comparison with previous samples. Coated specimens had strength equivalent to previous uncoated samples and had much greater ductility.

A powder-base substitute for the lithium-magnesium alloy was developed; it consisted of Li_2O dispersed in aluminum. Dispersions containing 50 vol % Li_2O were readily fabricated into plates clad with aluminum. Such clad plates have a lithium density greater than that with lithium-magnesium alloy.

Encouraging results were obtained on the fabrication of tubular control rods by coextrusion. The proposed rods would utilize a core of 70% Ni–30% Lindsay oxide. The thermal conductivity of the core material was also determined.

Simulated fuel-element tubing redrawn from three-ply tube blanks was received and evaluated. The redrawn tubing, containing fine oxide with an average particle size of 15 μ, showed tensile fractures in the core, whereas the redrawn tubing containing coarse oxide of 44- to 105-μ particle

size showed excessive stringering of oxide particles in the core.

The study of flow patterns in three-ply extrusions was continued. The effects of sectional cores and cores with tapered ends were investigated.

The evaluation of arc-melted niobium is being carried out by comparing its properties with those of powder-base wrought material. An alloy of 80% Nb–20% U is also being fabricated into strip for mechanical testing and cladding experiments.

A research program has been initiated to investigate the hydrides of zirconium and of zirconium-yttrium alloys for high-temperature-moderator applications. The Ceramics Group is building the furnace and the gas purification system for the program.

High-Temperature Reactions of Metals and Ceramics. – A spectrophotometer has been constructed for the measurement of absorption spectra of fused salts at temperatures up to 800°C. Measurements have been made of fused silver halide–alkali metal halide solutions over the spectral range of 450 to 800 mμ. These measurements are being extended down to 200 mμ.

Other apparatus are being constructed for the measurement of nuclear magnetic resonances in fused salts and for the measurement of the self-decomposition of fused hydroxides.

Continuing studies of the kinetics of the oxidation of alkali metals have shown that potassium forms a highly protective oxide film at –50°C during 10^5 min of reaction, whereas at –20°C the oxide film was found to transform from protective to non-protective after about 200 min.

Studies were made of the reaction between fused sodium hydroxide and a number of alloys in which rate processes in the solid alloy were found to play a prominent role in the reaction mechanism. In most instances the reaction proceeded by a complex mechanism which for certain alloys was found to involve a stress-corrosion process in which the reaction itself induced the stress.

HRP METALLURGY

To confirm the phase boundary temperatures reported previously for short-time specimens, specimens of Zircaloy-2 have been held for two weeks at temperature. Preferred orientation measurements have been made in order to determine the change in the amount of preferred orientation caused by the "randomizing" heat treatment. A multipass weld in Zircaloy-2 plate has been examined metallographically and a hardness traverse made. The data are reported with micrographs.

Crystal-bar zirconium and Zircaloy-2 specimens have been hydrided and either step-cooled to show near-equilibrium structures or mercury-quenched to retain as much hydrogen as possible. Microstructures are shown.

A series of crystal-bar and sponge-base zirconium alloys with Nb, Mo, Fe, Ta, Pd, and Pt as binary and ternary alloy additions have been cast, rolled, and given a variety of heat treatments. No ternary addition tried will completely suppress the formation of alpha plates on quenching the Nb alloys even at 20% Nb. The addition of 5% Pd or Pt to zirconium will permit the retention of a completely beta structure on quenching from 800°C or above. The eutectoid composition and temperature are near 5% and 700°C for both systems. At 10% Pd or Pt, a second phase appears at and above 800°C that is not alpha zirconium. Decomposition of retained beta in the Pd and Pt alloys is very rapid at 600 and 700°C.

APPLIED METALLURGY

Process Metallurgy. – Fifty-two APPR fuel and absorber components were manufactured and delivered to the critical facility of ALCO Products, Inc. During production of these fuel elements it was discovered that the type 304L stainless steel cladding material was carburized by diffusion of carbon from the fuel core matrix type 302B stainless steel, rendering the material susceptible to intergranular attack in the reducing acid cleaning solution. Investigation of substitute material combinations revealed that plates containing type 347 stainless steel, either as the core matrix or clad material, or both, passed the Strauss test.

Results of the corrosion testing program have revealed that APPR fuel plates, clad with sensitized type 304 stainless steel, appeared to be corrosion-resistant in 1200 psi, 295°C pressurized water after extensive testing. Further information has also been obtained on the corrosion resistance of various UO_2-cermet fuel core material and of brazed stainless steel joints.

Efforts have been successful in developing and manufacturing control rod plates for the APPR, which consisted of a 3.2 wt % boron dispersion in iron, by utilizing powder metallurgy processing and cladding with wrought stainless steel. Irradiation testing is being conducted to determine the damage to this material.

Progress has been made in evaluating the factors contributing to segregation in the uranium-aluminum alloy containing 48 wt % uranium. Efforts to extrude the alloy into rods have been successful, and plans have been laid to extrude the material into plates.

Manufacturing of a test fuel element containing the 48 wt % uranium–aluminum alloy has been hampered by two problems; (1) the serious "dog-boning" of the end of the fuel core and resultant localized thinning of the cladding, and (2) the blistering of the fuel elements during brazing. Investigations are being directed toward improving the bonding in the composite fuel plate, which is believed to be the source of the blisters.

Development of high-strength aluminum fuel elements has revealed the possibility of substitution of age-hardenable type 6061 aluminum for the type 1100 aluminum as the cladding and side plate material. Experimental Special Power Excursion Reactor Test (SPERT) B fuel elements have been brazed, air quenched, and aged, with the type 6061 material approaching a strength of 32,000 psi after this heat treatment.

Fuel plates containing a 10 wt % Pu–Al alloy, clad with aluminum, have been fabricated into composite plates for irradiation in the MTR.

Development of the aluminum-uranium-boron and aluminum-boron alloys has been concluded and will be reported in a detailed topical report to be published in the near future.

Metallurgical Materials and Processing. – Fifteen pounds of thorium from the Metallex process has been arc-melted in a nonconsumable-electrode furnace. Only traces of mercury were found to have deposited on cold portions of the furnace following melting. The results of several experiments indicate that a better formed thorium product may result from a retorting cycle which includes a holding period at about 140°C. No transfer of iron, nickel, or chromium from the steel retort to the thorium charge was detected during the retorting cycle. Cursory tests of several materials indicate that tungsten or tantalum would serve best as liner materials in preventing contact between the thorium charge and the steel retort.

The high silicon content of type 302B stainless steel has been found to reduce the effectiveness of treatments to promote intergranular corrosion as an aid in recovering uranium from carburized stainless steel fuel elements. Experiments show that uranium has a limited solubility in aluminum-tin-uranium baths; uranium has been recovered from such baths by filtration to remove the compound USn_3. Zirconium was found to resist dissolution by both tin and bismuth; therefore it is not likely that uranium can be recovered from zirconium alloys by dissolution and filtration.

Metallography. – A high-velocity heat exchanger, SHE No. 1, was operated for a total period of 1648 hr with fluoride salt (fuel) and NaK. For the study of mass-transfer effects, a wide temperature differential was maintained during the last 456 hr of operation.

Upon postoperational examination of the heat exchanger it was found that failure was imminent, as the sum of the depths of the intergranular attack on the inner NaK surface (0.003 in.) and the depth of the subsurface voids on the fuel side (0.007 in.) amounted to more than half of the wall thickness of the Inconel tubing. The most severe deterioration of the tubing was in the hot end of the heat exchanger.

The operating temperatures (1505°F for fuel and 1495°F for NaK) in the hot end caused the probable elemental diffusion of Cr, Ti, Al, and C into the NaK and fuel and a resultant decrease in the amount of precipitate in the microstructure.

The larger grain size in the tubing at the hot end of the heat exchanger resulted from the absence of precipitate, the presence of biaxial stresses due to thermal expansion and to a thermal differential, and the increased temperature. Also, the strain anneal effect due to thermal cycling would accelerate grain growth.

Metallographic examination of Hastelloy B, heat-treated isothermally at temperatures ranging from 1300 to 1800°F up to a period of 1600 hr, revealed an age-hardening alloy between 1300 and 1500°F. Age-hardening results from a Widmanstätten type of precipitate, which becomes finer the lower the temperature of the heat treatment. Hardness increases with the fineness of the precipitate. Above

1500°F the amount of precipitate decreases, and that which forms tends to spheroidize.

Ceramics Research. – The production of large UO_3 crystals has been improved; differences in the conditions required for production of depleted and of normal UO_3 crystals have been found.

The production of Si-SiC fuel plates has been continued, with emphasis on a thinner plate with higher fuel contents.

Fabrication of ceramic compacts of CaF_2, Al_2O_3, rare-earth oxides, nickel plus rare-earth oxides, cadmium silicate, and other materials has been continued in support of the critical experiment work of Pratt & Whitney.

Construction of a system for the production of ZrH and YH is nearing completion. The production of a BeO protection tube is under investigation. The synthesis of ZrC is the subject of a series of experiments.

Enthalpy data for various ceramic and metallic materials are being collected. The discontinuity in several of the curves is being thoroughly investigated.

X-ray diffraction traces of Hastelloy B to 700°C were obtained in order to look for a possible inversion at 600°C; no inversion was found.

The petrography of fluoride fuels continues as in the past. A bulletin containing optical and x-ray data of a large number of fluoride compounds will be issued in the near future.

The effect of the lead ion on the UO_2 lattice parameter has been found to be negligible.

The feasibility of fixation of radioisotopes in clay-flux mixes is being further studied.

The properties of beryllia hot-pressed by the Saclay Laboratories in France have been determined.

FUNDAMENTAL METALLURGY

Fundamental Physico-Metallurgical Research. – In the phase-diagram study of zirconium alloys, the results of a preliminary study of the cadmium-zirconium system show that at least two intermediate phases, Zr_2Cd and $ZrCd_2$, occur in this system with no indication, at the present time, of extensive solid solubility of cadmium in zirconium. The investigation of the lead-zirconium system has been renewed, and the effect of lead on the hardness of zirconium is described. Additional experiments on the Ag-Zr, In-Zr, and Sb-Zr systems are reported and confirm the phase diagrams presented earlier. A determination of the α/β transition temperature for zone-refined zirconium shows that this temperature is 870 ± 3°C.

A thorium bar was extruded at 850°C such that the recrystallization which occurred during deformation had a duplex texture, $\{001\}<\bar{1}00>$ and near $\{034\}<\bar{4}\bar{1}1>$. After being reduced 75% in thickness by cold rolling, the sheet had textures described as $\{148\}<\bar{4}\bar{1}1>$, $\{011\}<\bar{3}\bar{2}2>$, and $\{034\}<\bar{1}00>$. A 95% reduction in thickness by cold rolling resulted in textures described as near $\{113\}<\bar{2}\bar{1}1>$, $\{011\}<\bar{1}00>$, and near $\{011\}<\bar{2}\bar{1}1>$. Annealing textures were $\{017\}<\bar{1}00>$ for a prior reduction of 75% and $\{001\}<100>$ for one of 95%. A relationship between mechanical properties and preferred orientation was established.

ANP METALLURGY

W. D. Manly

GENERAL CORROSION

E. E. Hoffman W. H. Cook D. H. Jansen
Metallurgy Division
R. Carlander
Pratt & Whitney Aircraft

BERYLLIUM-INCONEL-SODIUM COMPATIBILITY IN A STATIC SYSTEM (TEST NO. 1)

E. E. Hoffman

It has been indicated that type 430 stainless-steel-clad copper plus B_4C cermet in the ART will be canned in Inconel which will be in direct contact with the beryllium hemispheres. The tests to be discussed were conducted in order to determine what thickness of Inconel might be consumed by the alloying reaction between Inconel and beryllium when these materials are in direct contact under pressure while immersed in sodium at 1300°F. The surfaces of two of the Inconel specimens in test No. 1 (Figs. 1 and 2) were chromium-plated to study the effect of chromium in reducing the extent of the alloy formation between the nickel (from the Inconel) and the beryllium. The test specimens measured $\frac{1}{4} \times \frac{1}{2} \times 1$ in., with the $\frac{1}{2} \times 1$ in. surfaces in contact. Sufficient load was applied to the specimens through a compression rod and bellows to yield a 500-psi stress on the test specimens. The test assembly was loaded with sodium and held at 1300°F for 1000 hr. The load was applied to the specimens when the test temperature was reached.

Following the test the sodium was drained from the test pot, the pot was filled with oil, and the specimens were removed. Residual oil and sodium were removed from the specimens by placing the specimens in ethyl alcohol. The Inconel specimens which were chromium-plated could be separated from the adjacent beryllium specimen; however, it was impossible to separate the Inconel specimens from the beryllium specimens where no chromium plate had been applied to the Inconel.

The results of metallographic examination of the four specimen interfaces are listed in Table 1. Examination of these results indicates that thin chromium platings on Inconel do not eliminate alloying reactions with beryllium when the two materials are placed in contact while immersed in high-temperature sodium. However, these platings did substantially reduce the extent of alloy formation. Approximately 4 mils of Inconel was consumed in the formation of the 24-mil nickel-beryllium alloy layer which was found where the Inconel and beryllium were in direct contact. The major portion of the reaction layer which forms between Inconel and beryllium is $Be_{21}Ni_5$, with a small percentage of BeNi adjacent to the Inconel.

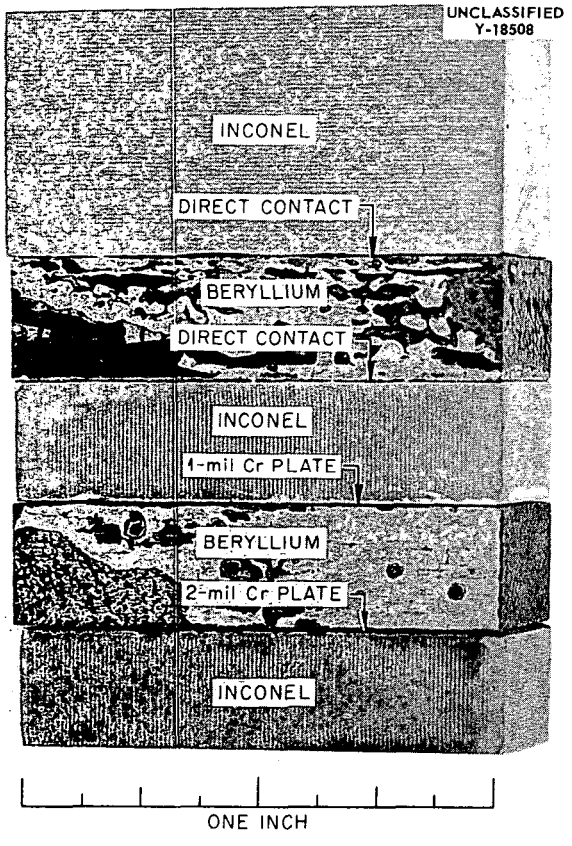

Fig. 1. Compatibility Test Specimens (See Fig. 2) Following 1000-hr Exposure to Sodium at 1300°F. Inconel specimens chromium-plated as indicated. (Secret with caption)

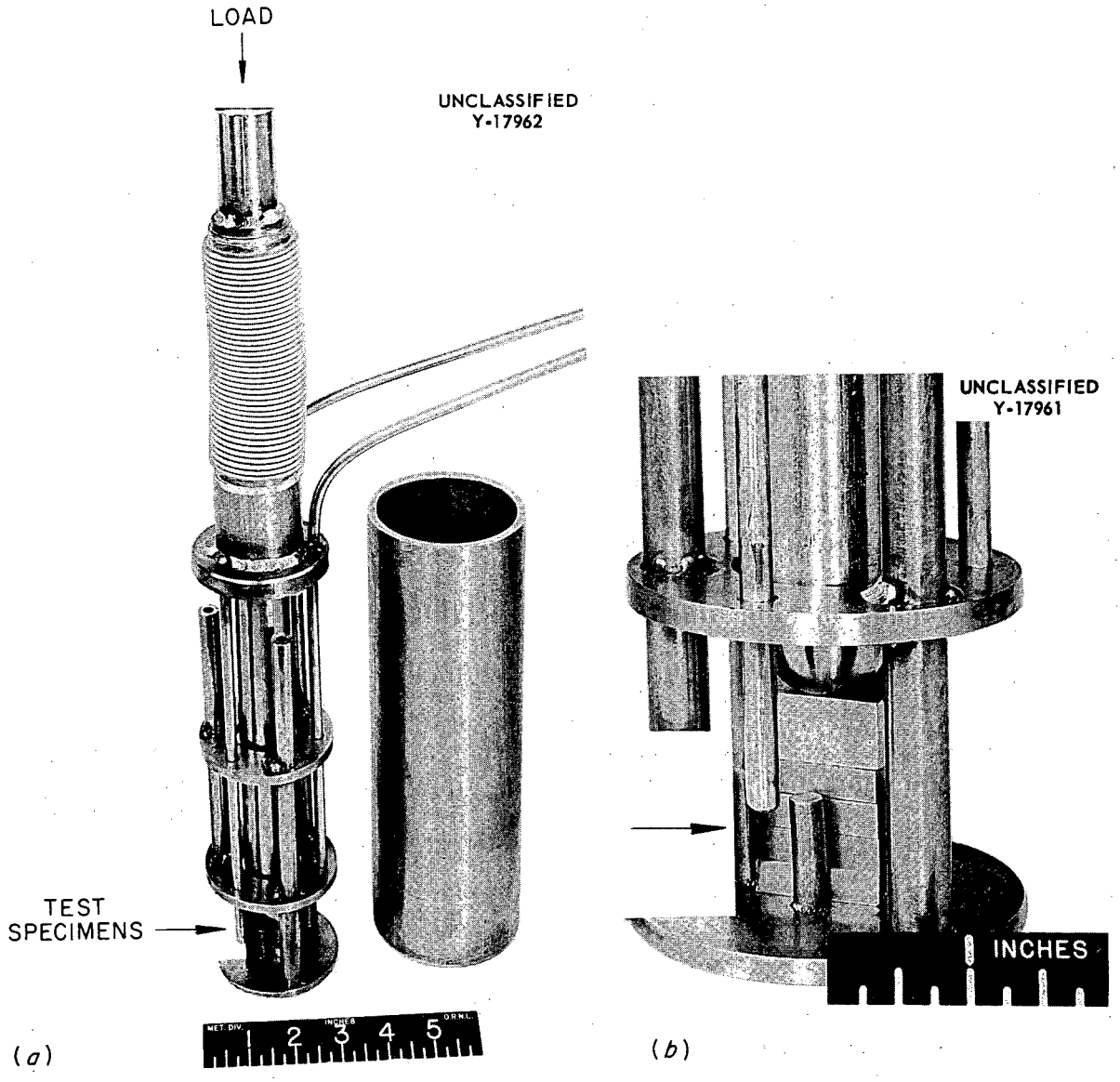

Fig. 2. Compatibility Test Rig. (*a*) Apparatus used to study extent of alloying between beryllium and various metals under stress while immersed in molten sodium. (*b*) Enlarged view of test specimens. (Secret with caption)

TABLE 1. RESULTS OF METALLOGRAPHIC EXAMINATION OF SPECIMEN INTERFACES (SEE FIG. 1)

Test Conditions: sodium; 1000 hr; 1300°F; 500 psi stress

Interface	Results
A-B (Inconel vs beryllium – direct contact)	10 to 24 mils of alloy formation ($Be_{21}Ni_5$ plus BeNi) along interface; 4 mils of Inconel consumed in the production of this thickness of reaction layer
B-C (beryllium vs Inconel – direct contact)	22 to 24 mils of uniform alloy formation along interface
C-D (Inconel plus 1 mil of chromium vs beryllium)	3.5 to 7 mils of alloy formation; 7-mil layer occurred where chromium plating was thinnest
D-E (beryllium vs 2 mils of chromium on Inconel)	2 mils of interaction between specimens along 90% of interface; 6 mils of alloy detected at one area where plating appears to have been defective

BERYLLIUM-INCONEL-SODIUM COMPATIBILITY IN A STATIC SYSTEM (TEST NO. 2)

E. E. Hoffman

The results of Beryllium-Inconel-Sodium compatibility test No. 1 indicated that a chromium plate on the Inconel surface in contact with the beryllium would reduce the extent of the alloying reaction which occurs when Inconel and beryllium are in direct contact in sodium. The thin chromium platings (1 and 2 mils) used in the first test were entirely consumed by alloying during the 1000-hr test period at 1300°F. Therefore a second test was conducted in which heavier platings were used. A beryllium oxide specimen was also included in this test to determine whether a reaction would occur between beryllium oxide and beryllium or beryllium oxide and Inconel.

The results of this test are given in Table 2. The reference test with Inconel and beryllium in direct contact resulted in approximately 25 mils of alloy formation (Fig. 3). The presence of a chromium-plate "diffusion barrier" on the Inconel specimen resulted in the formation of an alloy layer (principally Be_2Cr) which was approximately one-third the thickness of the alloy layer which forms when Inconel is placed in direct contact with beryllium under the conditions of this test.

Analysis of the test results indicates that a minimum of 5 mils of chromium plate will be necessary to ensure that all the chromium is not consumed by the alloying reaction with beryllium. The Be_2Cr phase was identified by x-ray analysis. This phase has a Vickers hardness of 2440 as compared with hardnesses of 1495 for $Be_{21}Ni_5$, the phase which forms when Inconel and beryllium are in direct contact, and 180 for Inconel (Figs. 4 and 5). No reactions were anticipated between beryllium oxide and beryllium or beryllium oxide and Inconel, and none were found to have occurred during this test.

TABLE 2. RESULTS OF METALLOGRAPHIC EXAMINATION OF INTERFACES OF SPECIMENS FROM SODIUM-BERYLLIUM-INCONEL COMPATIBILITY TEST NO. 2

Test duration: 1000 hr
Test temperature: 1300°F
Contact pressure between specimens: 500 psi

Interface	Results of Metallographic Examination
Inconel vs beryllium, direct contact (standard)	Alloy formation ($Be_{21}Ni_5$ and BeNi) 25 mils deep along interface; in earlier test 24 mils of alloy formed; 4 to 5 mils of Inconel consumed by alloying reaction
Inconel plus 4-mil chromium plate vs beryllium	Alloys formed between chromium plate and beryllium to a depth of 8 mils which consisted of 7 mils of Be_2Cr and 1 mil of Be_5Cr(?); 0 to 2 mils of chromium plate remained after the test; 2 to 3 mils of Inconel consumed, probably by alloying with the chromium plate
Inconel plus 6-mil chromium plate vs beryllium	Alloys formed between chromium plate and beryllium to a depth of 9 mils which consisted of 8 mils of Be_2Cr and 1 mil of Be_5Cr(?); 3 mils of chromium plate remained after the test; approximately 2 mils of Inconel consumed by alloying with the chromium plate
Beryllium vs beryllium oxide	Surface of beryllium oxide discolored slightly; specimens were easily separated and no bonding was evident
Beryllium oxide vs Inconel	Neither the beryllium oxide nor the Inconel surfaces affected by test

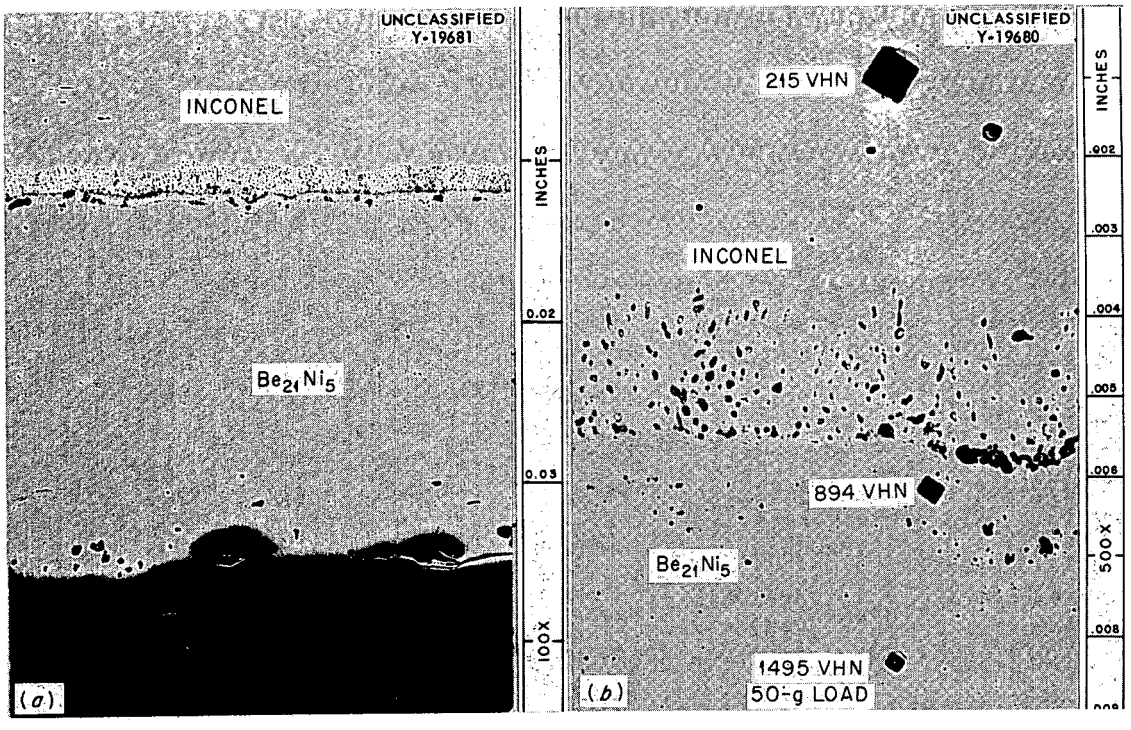

Fig. 3. Alloying (~25 mils) Between Inconel and Beryllium While Held in Direct Contact (500 psi) in Sodium for 1000 hr at 1300°F at (*a*) 100X; (*b*) 500X, Enlarged View of the $Be_{21}Ni_5$-Inconel Interface. Note hardness of $Be_{21}Ni_5$. Unetched. Reduced 17%. (Secret with caption)

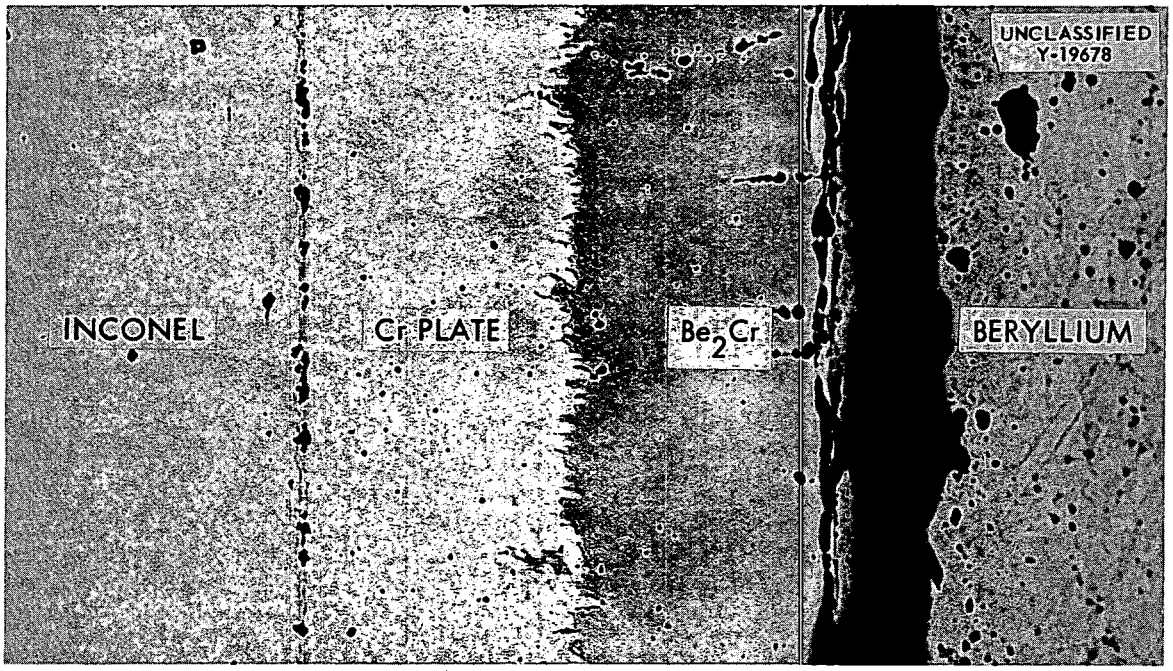

Fig. 4. Alloying Reactions Between Chromium-plated Inconel and Beryllium During 1000-hr–1300°F Compatibility Test. Dark area between Be_2Cr and beryllium is due to separation of specimens following test. Unetched. 300X. (Secret with caption)

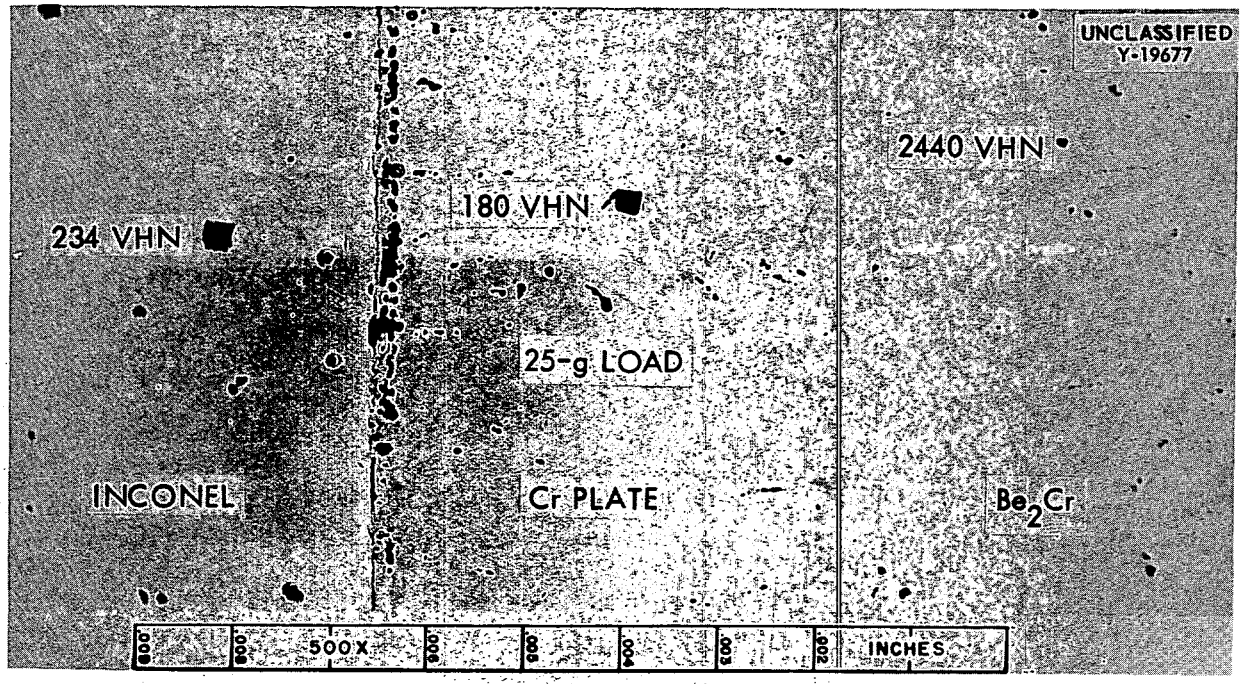

Fig. 5. Enlarged View of Area Shown in Fig. 4. Note extreme hardness of Be_2Cr phase as compared with hardness of Inconel and chromium plate. Unetched. (Secret with caption)

EFFECT OF DIFFUSION COLD TRAPS ON MASS TRANSFER IN INCONEL-SODIUM THERMAL-CONVECTION LOOPS

E. E. Hoffman

The purpose of operation of the two Inconel-sodium thermal-convection loops discussed here was to determine whether the presence of a diffusion cold trap would affect the extent of mass transfer observed in the cold legs. The loops were loaded with sodium which had been pretreated by cold trapping for several months to lower the oxygen content. One loop was provided with a diffusion cold trap near the bottom of the cold leg in order to reduce the sodium oxide content during operation, while the other loop was of standard design, with no cold trap.

Although many thermal-convection-loop tests conducted on Inconel-sodium systems in the past have failed to show any mass transfer, it has been demonstrated that mass transfer will occur in such systems if the hot-zone temperature is in excess of 1500°F and if a steep temperature gradient is induced in the cold leg by directing an air blast on a small area near the bottom of the cold leg. These loops (Nos. 28 and 29) were therefore operated for 1000 hr at hot- and cold-zone temperatures of 1600 and 990°F, respectively. The loops were carefully stripped of sodium after the tests. The mass-transfer deposits found in the cold zones of these loops are shown in Fig. 6. Although only small amounts of mass-transfer crystals were found in these loops, it is apparent that slightly more deposition occurred in the loop which had no diffusion cold trap than in the loop which included a cold trap. The results of spectrographic analysis of the metallic crystals recovered from these loops are presented in Table 3, along with the analysis of the Inconel pipe prior to test. More tests will be required to establish whether the differences in chromium and iron contents of the crystals from the two loops are significant. The mass-transfer crystals found in a thermal-convection loop operated previously at a hot-zone temperature of 1500°F had a much lower iron concentration.[1] The results of metallographic examination of specimens from similar locations in the loops are given in Table 4. Examinations of these results indicate that the loop with no cold trap (loop No. 29) had slightly heavier attack in the hot leg (Fig. 7) than the loop with a cold trap (loop No. 28). The deposits found on the cold-leg surfaces of these loops may be seen in Fig. 8.

[1] E. E. Hoffman, *ANP Quar. Prog. Rep. Sept. 10, 1955*, ORNL-1947, p 113.

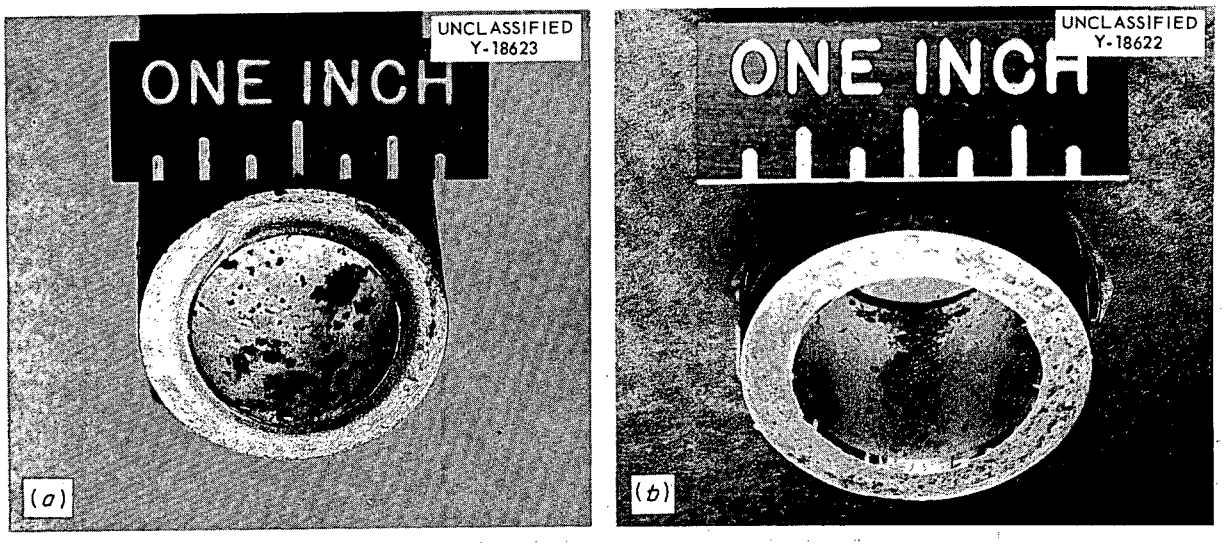

Fig. 6. Mass Transfer in Inconel-Sodium Thermal-Convection Loop Tests. (*a*) Cold-zone section of loop which had no diffusion cold trap (loop 29). (*b*) Cold-zone section of loop which had a diffusion cold trap (loop 28).

TABLE 3. ANALYSES OF MASS-TRANSFER CRYSTALS FROM INCONEL-SODIUM THERMAL-CONVECTION LOOPS

Operating period: 1000 hr
Hot-zone temperature: 1600°F
Cold-zone temperature: 990°F

Material Analyzed	Chemical Analysis (wt %)				
	Ni	Cr	Fe	Cu	Mn
Crystals from loop No. 28 which included a diffusion cold trap	84.4	10.6	4.6	0.33	0.07
Crystals from loop No. 29 which had no cold trap	77.4	13.3	9.1	0.06	0.08
Inconel (as-received)	73.15	14.81	6.62		0.40

TABLE 4. RESULTS OF METALLOGRAPHIC EXAMINATION OF VARIOUS SECTIONS FROM INCONEL-SODIUM THERMAL-CONVECTION-LOOP TESTS

Location	Operating Temperature (°F)	Loop No. 28 (Diffusion cold trap)	Loop No. 29 (No diffusion cold trap)
Top of hot leg	1600	Grain boundary voids to a depth of less than 1 mil	1 to 2 mils of grain boundary attack
Top of cold leg	1350	Slightly irregular surface	Slightly irregular surface
Bottom of cold leg	990	Two-phase surface layer, 0.5 mil thick	Two-phase surface layer on wall of pipe, 0.5 mil thick

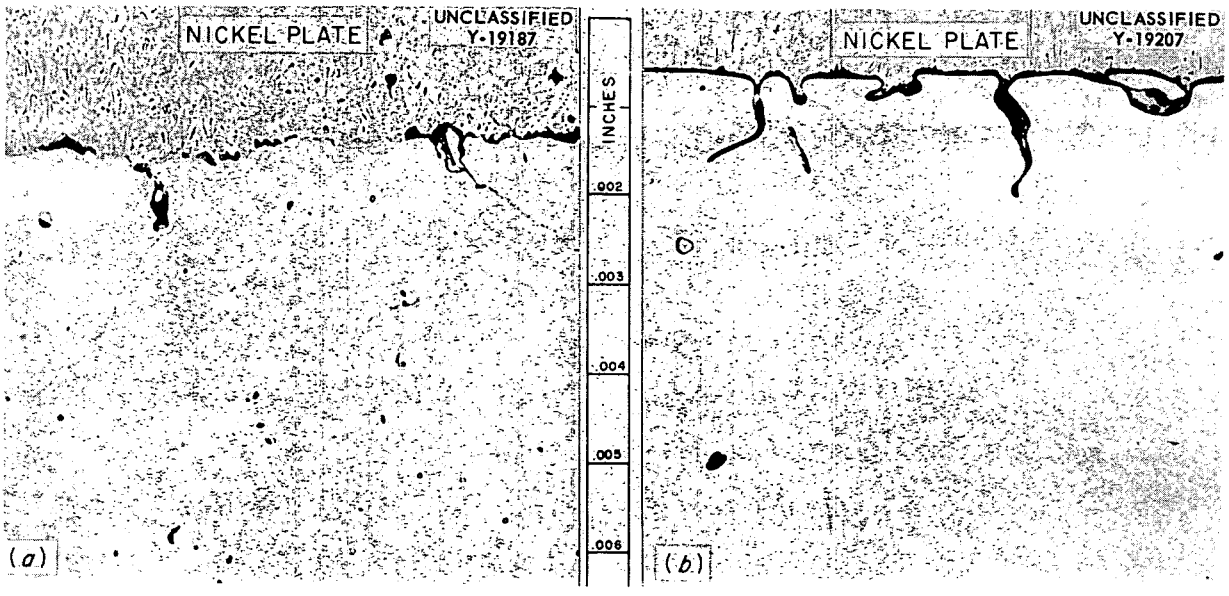

Fig. 7. Hot-Leg Surfaces of Inconel-Sodium Thermal-Convection Loops. (*a*) Loop 28, with diffusion cold trap. (*b*) Loop 29, with no diffusion cold trap. Etched with aqua regia. 500X. Reduced 5%.

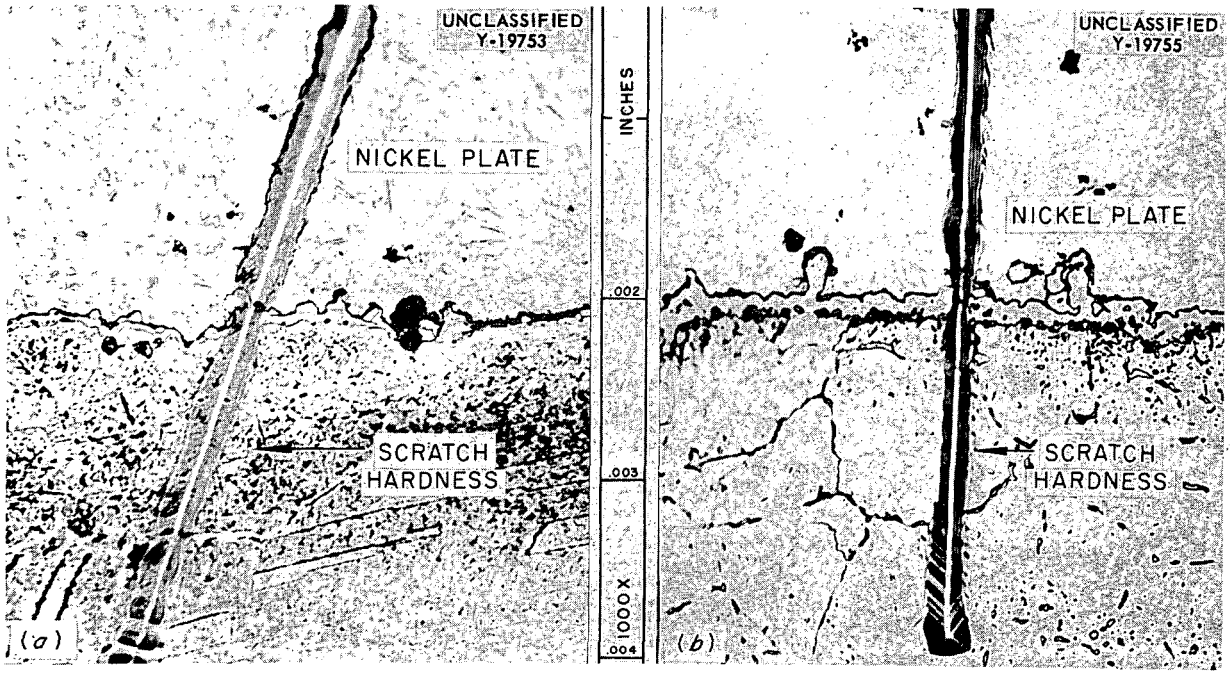

Fig. 8. Cold-Leg Surfaces of Inconel-Sodium Thermal-Convection Loops Showing Mass-Transfer Deposits. (*a*) Loop 28, with diffusion cold trap. (*b*) Loop 29, with no diffusion cold trap. The decreased width of the scratch at the edge of the specimens indicates that this deposit is quite hard (possibly a carbide) as compared with Inconel or nickel plate. Etched with aqua regia. 1000X. Reduced 5%.

LITHIUM THERMAL-CONVECTION-LOOP TESTS

E. E. Hoffman

There has been considerable interest in the possible application of lithium as a reactor coolant and, in particular, as a coolant for a solid-fuel-element aircraft reactor. The corrosion problems encountered in attempting to contain lithium high-temperature systems are much more difficult than those found in liquid sodium. Analyses of a large number of static tests have indicated that nickel and nickel-base alloys are very heavily attacked even by static, isothermal lithium, and thus many of the commercially available high-temperature alloys are eliminated from consideration. Pure iron has shown good resistance to lithium, and therefore considerable effort has been directed toward tests on iron-base alloys, in particular, the stainless steels. The results of lithium thermal-convection loop tests of various materials are summarized in Table 5. The important information contained in this table is whether or not the loop plugged, the weight of metal crystals recovered from the cold leg of the loop, and the depth of attack in the hot leg. All the loops were constructed of ½-in., sched-40 pipe (0.84-in. OD, 0.622-in. ID).

The low-sodium-content lithium used in these tests was received from the vendor packed in gas-tight helium-filled containers. The loops were loaded with lithium and were inert-gas arc-welded inside an inert atmosphere chamber.

Inconel (nominal composition, in wt %: Ni, 77; Cr, 15; Fe, 7) showed extensive mass transfer and hot-leg attack, even at hot-leg temperatures as low as 1300°F (cold leg, 1200°F). This result is typical of the nickel-base alloys exposed to lithium under these conditions.

The six loops of type 316 stainless steel (nominal composition in wt %: Fe, 68; Cr, 17; Ni, 12; Mo, 2) which were tested showed less mass transfer and less of a tendency to plug in the three tests conducted with hot-leg temperatures of approximately 1500°F than in other tests conducted at hot-zone temperatures of approximately 1400 and 1300°F (Figs. 9 and 10). The loop (No. 25) operated with a hot-zone temperature

TABLE 5. RESULTS OF THERMAL-CONVECTION-LOOP TESTS OF VARIOUS ALLOYS EXPOSED TO CIRCULATING LITHIUM

Material	System Temperatures (°F)			Test Duration (hr)	Metallographic Results	
	Hot Leg	Cold Leg	Differential		Hot-Leg Attack (mils)	Cold Leg
Inconel	1300	1200	100	1000	16	15.1 g of crystals
Stainless steel	1500	1292	208	500	13	0.5 g of crystals
Type 316	1490	1220	270	1000	1.5	0.1 g of crystals
	1472	1335	117	1000	3	0.1 g of crystals
	1400	1130	270	2150*	23	4.7 g of crystals
	1310	1058	252	290*	2	0.8 g of crystals
	1292	1094	198	1000	15	0.25 g of crystals
Type 321	1500	1220	280	204*	0.5	1.0 g of crystals
	1310	980	330	1230*	3.0	0.7 g of crystals
Type 347	1500	1112	388	280*	2	1.5 g of crystals
	1310	1060	250	1000	3.0	1.3 g of crystals
	1000	618	382	1000	1	Crystals 0.2 mil thick
	1000	618	382	3000	1.5	Crystals 0.3 mil thick
Type 430	1500	1220	280	1500	4.0	1.0 g of crystals
Type 446	1500	1166	334	864*	1.0	9 g of crystals (84 mils of attack)
	1500	1200	300	700*	16	6.8 g of crystals (84 mils of attack)
	1292	1058	234	1500	25	0.23 g of crystals (65 mils of attack)

*Loop plugged with crystals.

of 1400°F had more mass-transfer crystals in the cold leg than did the loop (No. 16) operated with a hot-zone temperature of 1310°F; however, loop No. 25 operated over seven times longer before it plugged than did loop No. 16. The hot- and cold-leg surfaces of loop No. 25 after the test are shown in Fig. 11, and the hot- and cold-leg surfaces of loop No. 16, which plugged in 290 hr, are shown in Fig. 12. The formation of carbide crystals on the surfaces of lithium loops has been noted in almost all tests conducted with stainless steels, and it usually occurs in that section of the loop which is at a temperature of approximately 1300°F. The carbide deposits have been found in the hot legs of some loops and in the cold legs of others.

Loops of type 321 stainless steel (nominal composition, in wt %: Fe, 70; Cr, 18; Ni, 10; Ti, 0.5), when tested at a hot-leg temperature of 1500°F, completely plugged with crystals in 204 hr. Loops of type 347 stainless steel (nominal composition, in wt %: Fe, 70; Cr, 18; Ni, 10; Nb, 1) showed results similar to those of type 321 stainless steel, with plugging occurring in 280 hr with a 1500°F hot-leg temperature. A 3000-hr test of a type 347 stainless steel loop with a hot-leg temperature of 1000°F indicated that this material would be satisfactory for operation in this temperature range for very long periods of time if a small amount of attack and mass transfer could be tolerated.

A loop of type 430 stainless steel (nominal composition, in wt %: Fe, 83; Cr, 16; C, 0.10) operated at a hot-leg temperature of 1500°F (cold-leg temperature, 1220°F) for 1500 hr without plugging, but it showed considerable mass transfer

(Fig. 13). Two loops of type 446 stainless steel (nominal composition, in wt %: Fe, 74; Cr, 25; C, 0.35) which were tested at a hot-leg temperature of 1500°F (cold-leg temperature, 1200°F) completely plugged in less than 900 hr and had 6.8 and 9 g of metal crystals in the cold legs (Fig. 14). The wall-crystal interface on the cold-leg surface

UNCLASSIFIED
Y-18640

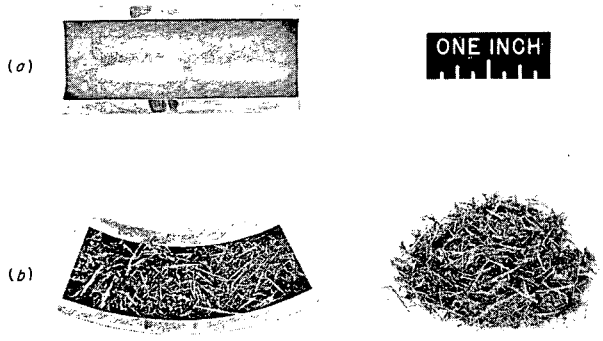

Fig. 9. Portions of Hot and Cold Legs of a Type 316 Stainless Steel Thermal-Convection Loop in Which Lithium Was Circulated for 2150 hr. (*a*) Hot zone, 1400°F. (*b*) Cold zone, 1130°F.

UNCLASSIFIED
Y-18373

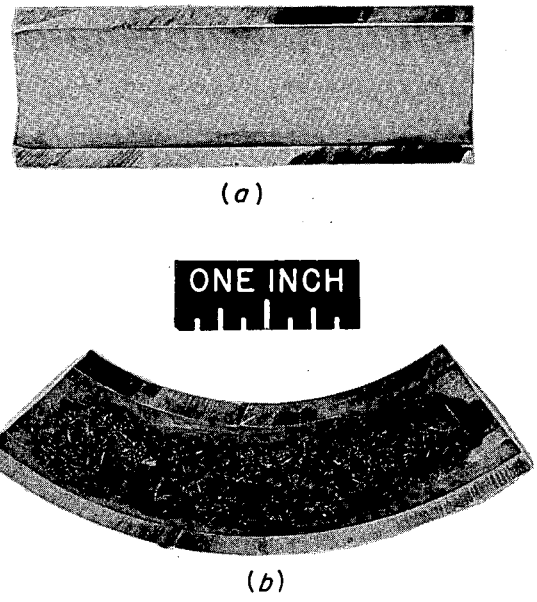

Fig. 10. Portions of Hot and Cold Legs of a Type 316 Stainless Steel Thermal-Convection Loop in Which Lithium Was Circulated for 290 hr. (*a*) Hot zone, 1310°F. (*b*) Cold zone, 1060°F.

UNCLASSIFIED
Y-19162

UNCLASSIFIED
Y-14932

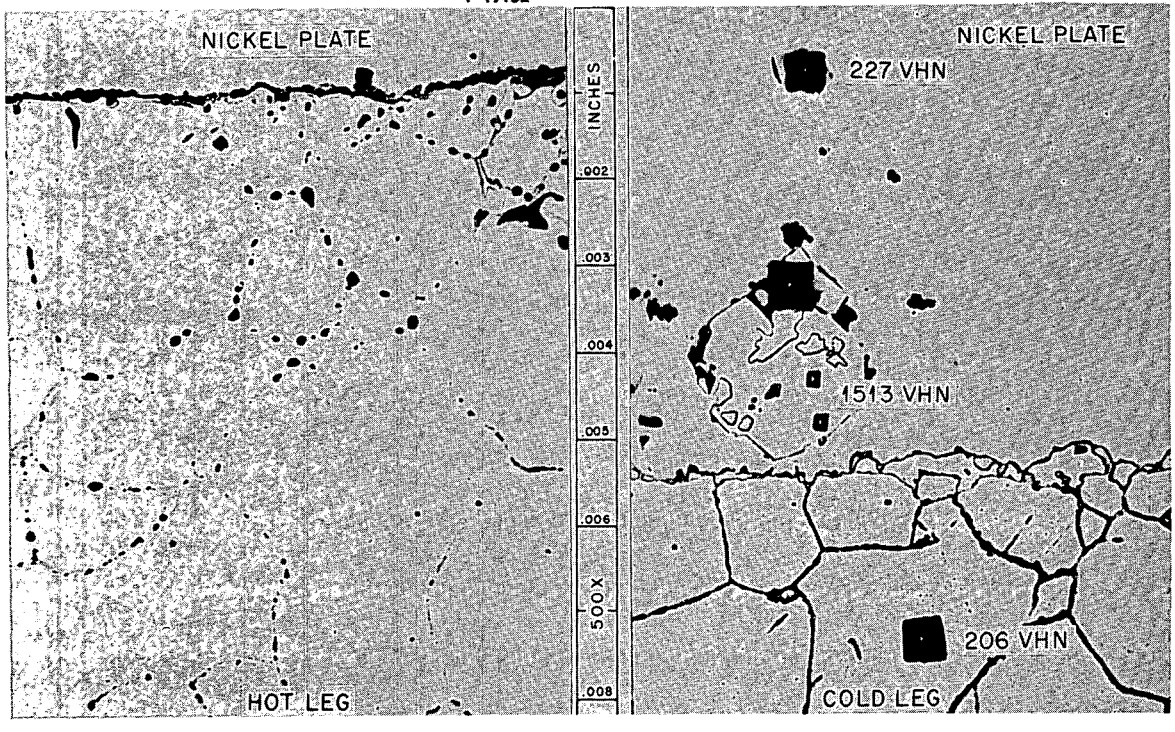

Fig. 11. Hot- and Cold-Leg Surfaces of Loop 25 – Type 316 Stainless Steel (See Fig. 9). Hot-leg surface attacked along grain-boundary carbides. Two-phase mass-transfer crystal of chromium carbide (VHN 1513) plus attached crystal containing iron, nickel, and chromium are shown on cold-leg surface. Specimen nickel-plated following test. Etchant: glyceria regia. 500X. Reduced 8.5%.

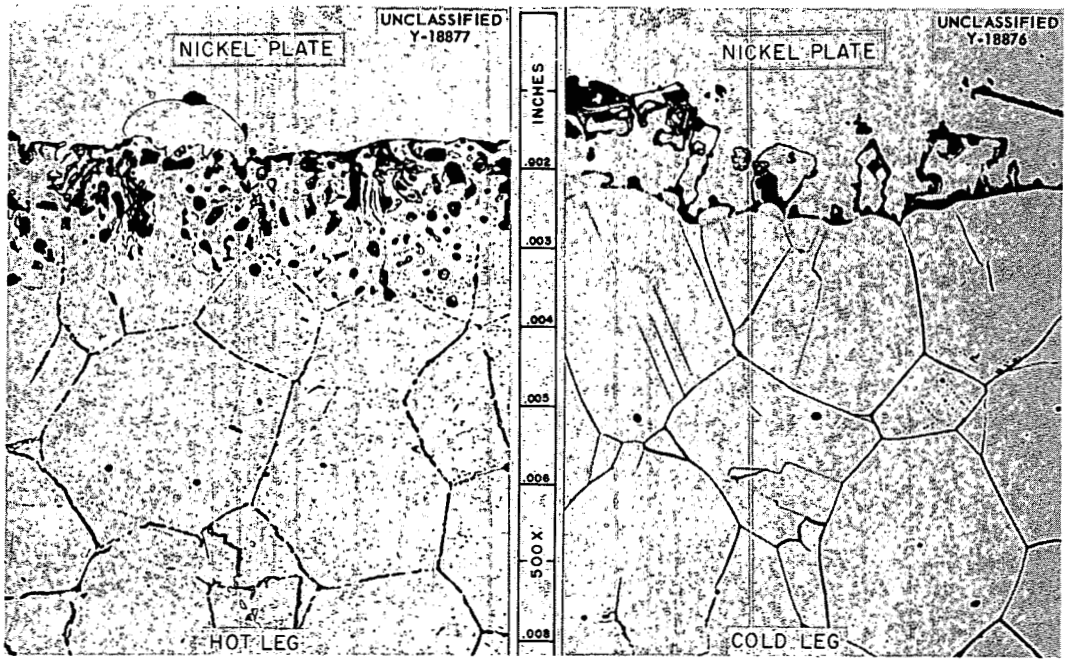

Fig. 12. Hot- and Cold-Leg Surfaces of Loop 16 – Type 316 Stainless Steel (See Fig. 10). Crystal on hot-leg surface is chromium carbide. Note mass-transfer crystals on cold-leg surface. Specimen nickel-plated following test. Etchant: glyceria regia. 500X. Reduced 5%.

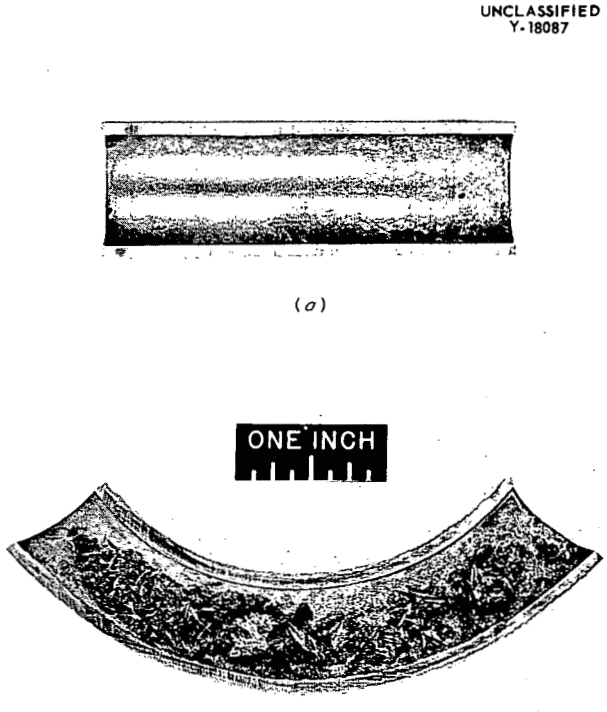

Fig. 13. Portions of Hot and Cold Legs of a Type 430 Stainless Steel Thermal-Convection Loop in Which Lithium Was Circulated for 1500 hr. (*a*) Hot zone, 1500°F. (*b*) Cold zone, 1220°F.

is shown in Fig. 15. The bulk of the crystals are ferrite (composition, in wt %: Fe, 90; Cr, 6), while those attached to the surface of the type 446 stainless steel wall have been identified by x-ray analysis as $Cr_{23}C_6$. The relative hardnesses of these two phases may be noted in the photomicrograph.

The results of chemical analysis of the mass-transfer crystals from the nickel-iron-chromium and iron-chromium alloy loops show that all three metals are transferred in appreciable quantities. If the alloy contains nickel, the mass-transfer crystals are richer in nickel than the container alloy. In iron-chromium alloy loops, the crystals deposited are richer in iron than the container alloy. Of the three metals – nickel, iron, and chromium – chromium has the least tendency to mass transfer but is still found to be present to the extent of 5 to 10% in the mass-transfer crystals found in stainless steel–lithium tests.

The data obtained in these thermal-convection-loop tests indicate clearly that further work needs to be done to resolve the apparent discrepancies which exist between the results for type 316 stainless steel and other austenitic stainless steels which contain little or no molybdenum. Also, types 317 and 318 stainless steels, which contain more molybdenum than type 316 stainless

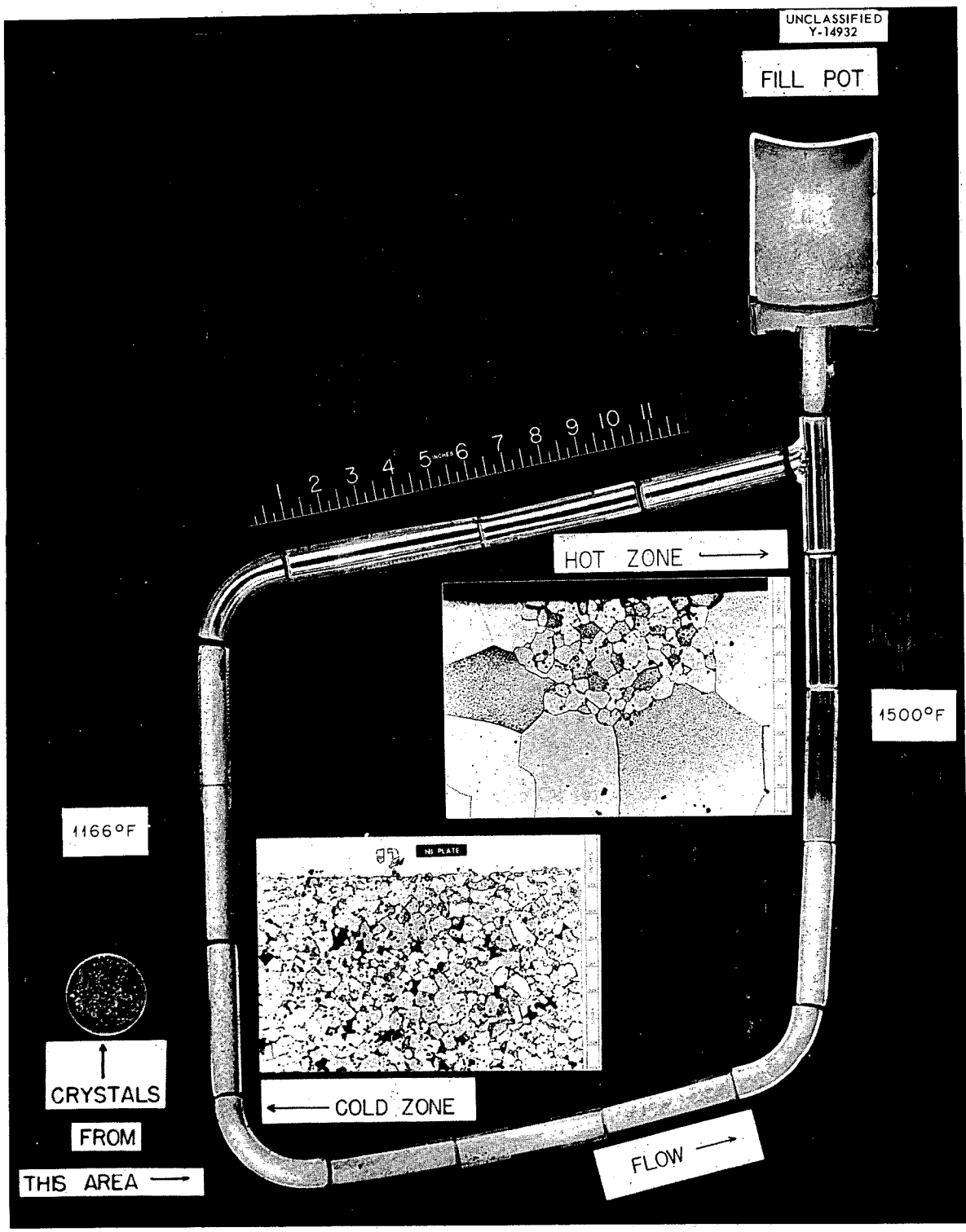

Fig. 14. Type 446 Stainless Steel Thermal-Convection Loop in Which Lithium Was Circulated for 864 hr.

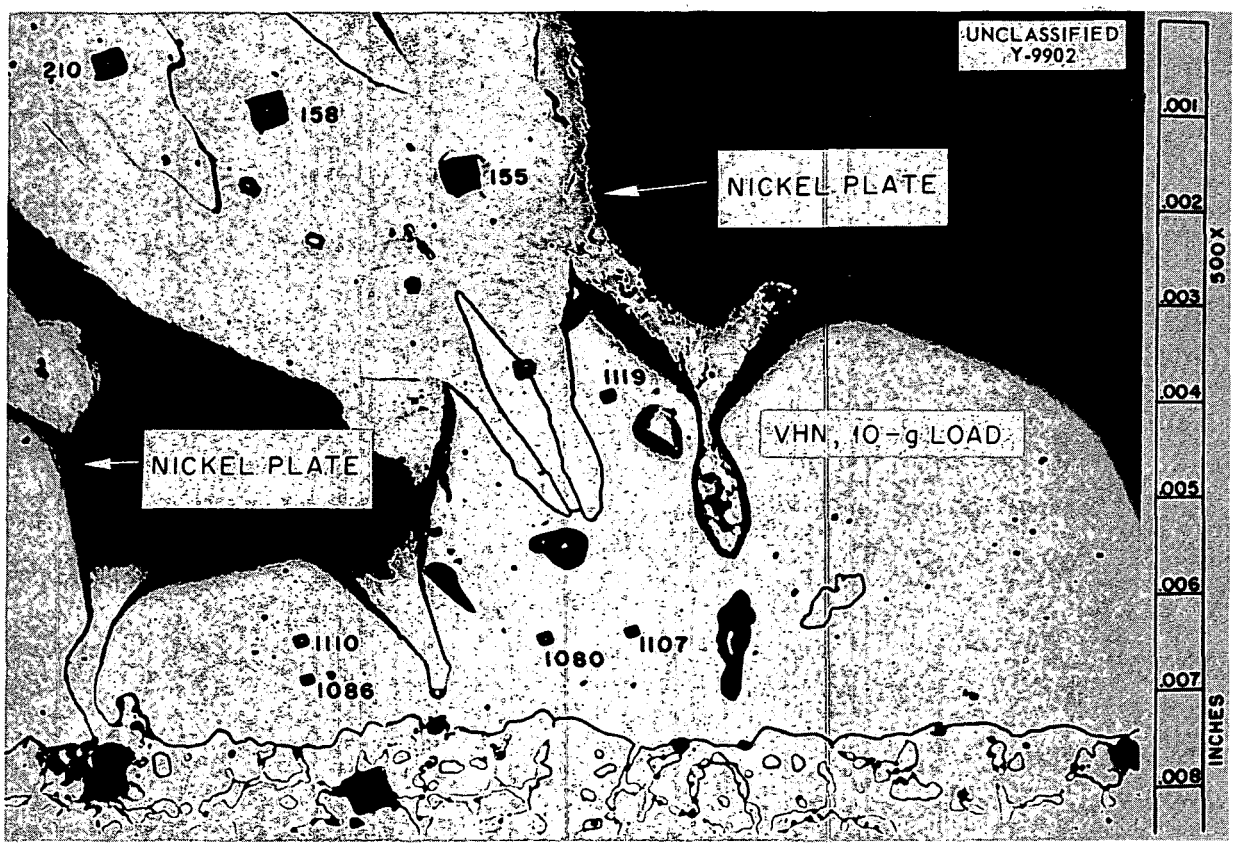

Fig. 15. Cold-Leg Wall of Type 446 Stainless Steel Loop Following Exposure to Lithium (See Fig. 13). Very hard phase (VHN ~1100) is $Cr_{23}C_6$, while soft crystal attached to it is a ferrite crystal of $Fe_{90}Cr_6$. Specimen was nickel-plated (VHN 210) following test. Etchant: glyceria regia.

steel, will be tested to determine the effect of molybdenum on the mass-transfer tendency of stainless steels in contact with molten lithium. The ferritic stainless steel test results are not encouraging, especially those for type 446 stainless steel, which suffers very deep intergranular attack because of preferential attack of the grain-boundary carbides. Further tests are planned for type 430 stainless steel. The superior corrosion resistance of type 430 stainless steel, in comparison with type 446 stainless steel, can be attributed to the lower carbon content of type 430 stainless steel (0.10% C maximum). Type 446 stainless steel has a maximum of 0.35% C.

The data obtained in static and thermal-convection-loop tests are summarized in Fig. 16, which shows that the alloys tested thus far are unsatisfactory as containers for lithium at hot-leg temperatures of approximately 1500°F in flowing systems. Tests are presently being conducted on niobium, molybdenum, and zirconium in dynamic systems. It is believed that these refractory metals, especially molybdenum, will withstand the corrosive action of lithium under these conditions, but, as yet, this has not been demonstrated. The effect of various amounts of nitride contamination on the amount of mass transfer will be studied further. Experiments will be conducted in order to determine the maximum temperature (in the range from 1000 to 1300°F) at which a stainless steel–dynamic lithium system may be operated, since these alloys at present seem to be satisfactory at 1000°F and, in general, unsatisfactory at 1300°F. The temperature limits indicated in Fig. 16 are merely estimates derived by evaluating the data obtained thus far, and they may be in error by as much as 100°F.

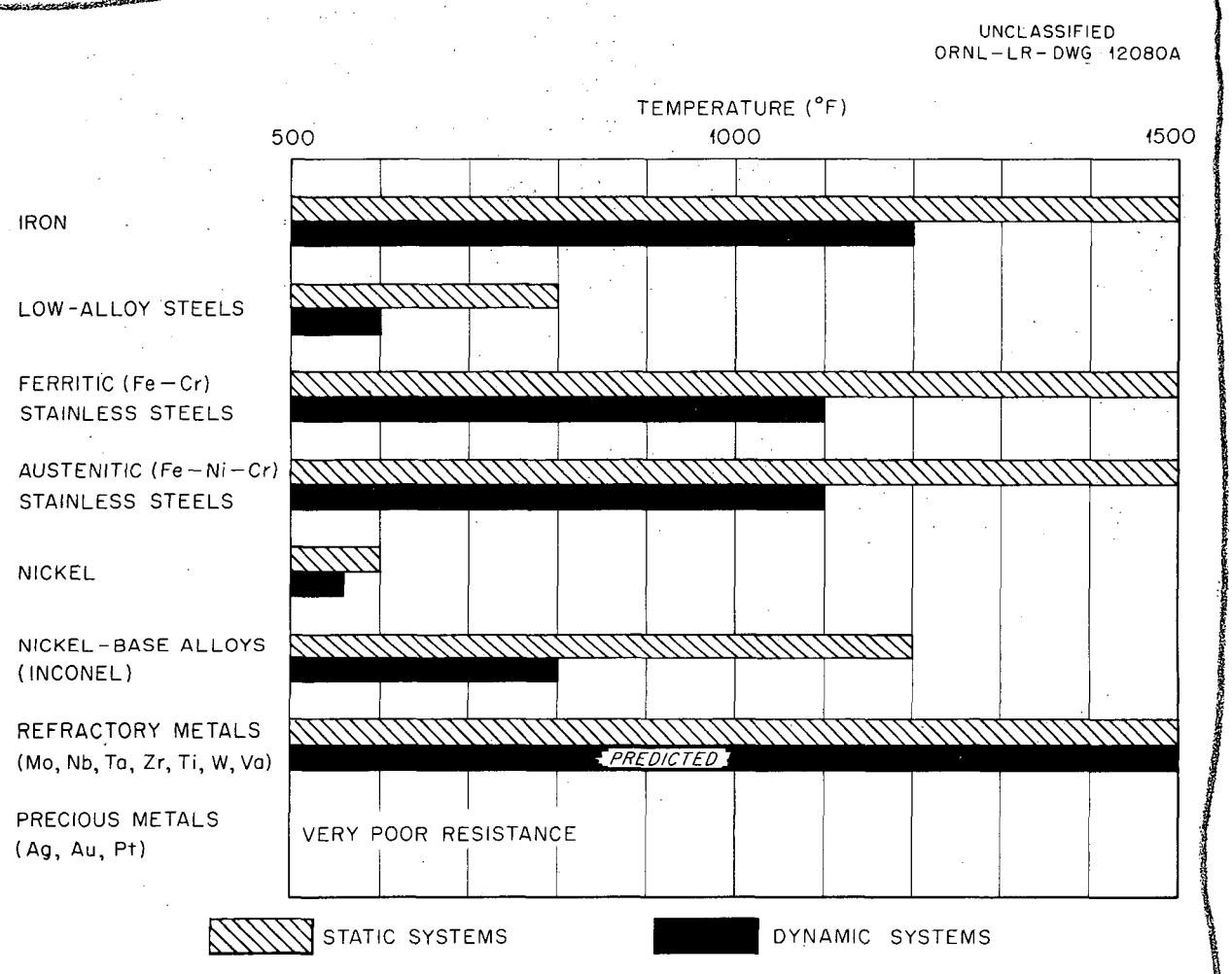

Fig. 16. Corrosion Resistance of Various Metals and Alloys in Lithium. Bars indicate approximate temperatures below which a system might be operated for 1000 hr with less than 0.005 in. of attack or container surface removal. (Confidential with caption)

SEESAW CORROSION TESTS ON COAST METALS BRAZING ALLOYS

D. H. Jansen

Previous corrosion tests of the Coast Metals No. 52 brazing alloy (89% Ni–5% Si–4% B–2% Fe) in fused salts and NaK baths have indicated that a constituent is removed at the surface of the alloy. More recent corrosion tests of this alloy have been conducted to determine whether the depth of this depleted region is time-dependent and to obtain some information concerning the composition of the edge after exposure to the above baths.

All the recent tests were conducted in nickel capsules with a hot-zone temperature of 1500°F. Individual results of these tests are listed in Table 6.

The depth of the depleted region is time-dependent. The No. 52 alloy is shown in Fig. 17 after exposure to the fused salt bath for 100 and 500 hr. A microspark traverse on the sample from test D showed that the boron concentration (nominal composition 4% by weight) dropped to one-third its normal value from the edge to a depth of 8 mils into the alloy sample. Microdrillings from this edge were analyzed for boron.

TABLE 6. RESULTS OF SEESAW CORROSION TESTS ON COAST METALS NO. 52 (89% Ni–5% Si–4% B–2% Fe) BRAZING ALLOY IN NaK AND $NaF\text{-}ZrF_4\text{-}UF_4$ (53.5-40.0-6.5 MOLE %)

Test	Bath	Time	Temperature		Weight Loss (%)	Depth of Depleted Edge (mils)
			Hot Zone	Cold Zone		
A	NaK	100	1500	1100	−0.07	0.5
B	NaK	350	1500	1100	−0.23	4
C	Salt	100	1500	1200	−0.06	3
D	Salt	500	1500	1200	−0.34	6

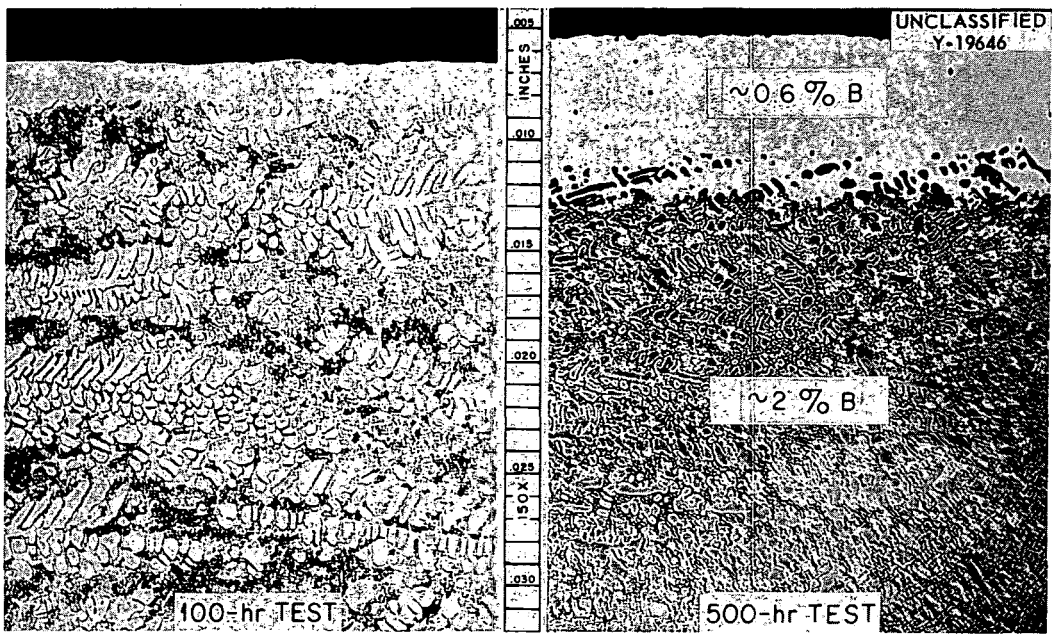

Fig. 17. Coast Metals No. 52 Alloy After Seesaw Testing in $NaF\text{-}ZrF_4\text{-}UF_4$ (53.5-40.0-6.5 mole %) for 100 and 500 hr. The leached-out region was 2.3 mils deep on the 100-hr test and was 6 mils deep on the 500-hr test. (Secret with caption)

The upper limit of boron concentration in the layer was approximately 0.6% by weight. Hardness measurements on the interior of the alloy sample exposed to NaK for 350 hr showed a 716 DPH, while measurements at the edge showed 145 DPH (Fig. 18). Hardness traverses on the alloy samples tested in the fused salt baths exhibited similar hardness results.

Since Coast Metals No. 52 alloy has been used to fabricate NaK-to-fuel heat exchangers, and since the boron leaching may become a pressing problem, a series of tests has been initiated with this alloy to determine the rate at which boron is depleted from the alloy during exposure to the fuel mixtures. This series will include corrosion tests in NaK and fuel baths at 1400, 1500, and 1600°F for 100 hr and at 1500°F for 500 and 1000 hr.

A substitute alloy which might not be as susceptible to boron leaching but still maintain a good corrosion resistance to the fused salts has been corrosion-tested. Coast Metals No. 53

(81% Ni–8% Cr–4% B–4% Si–3% Fe) was corrosion-tested in $NaF\text{-}ZrF_4\text{-}UF_4$ (53.5-40.0-6.5 mole %) and NaK (56-44 wt %) in the hope that the chromium would tie up the boron and retard its removal from the surface of the alloy.

The same type of depleted area was found on the surface of the No. 53 alloy (Figs. 19 and 20) as was detected on the No. 52 alloy. A spectrographic traverse on the alloy button tested in NaK at 1500°F for 100 hr showed that, between

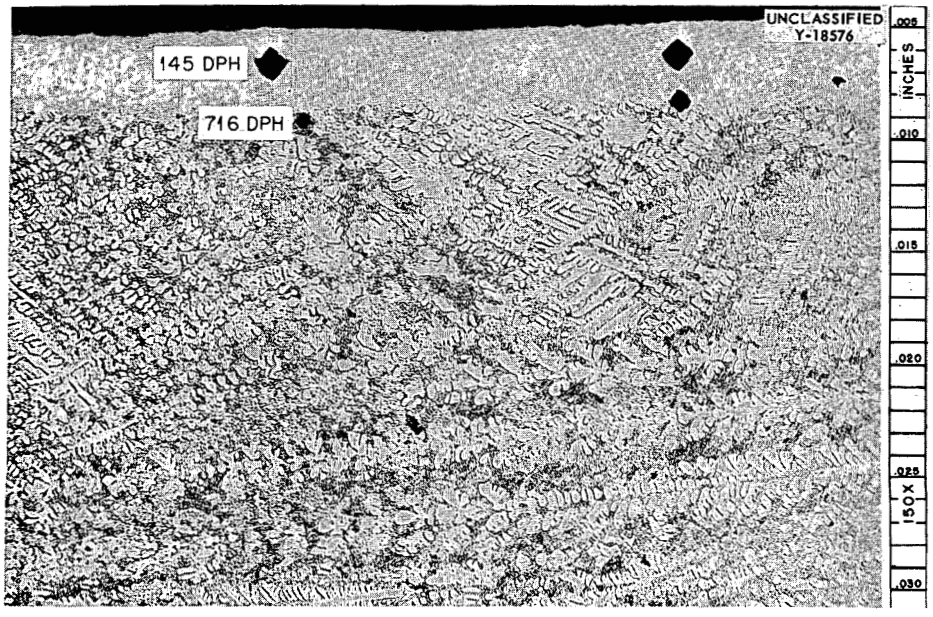

Fig. 18. Coast Metals No. 52 Alloy Button Tested in NaK for 350 hr. Note the difference in hardness. Etchant: 10% oxalic acid. Reduced 21.5%.

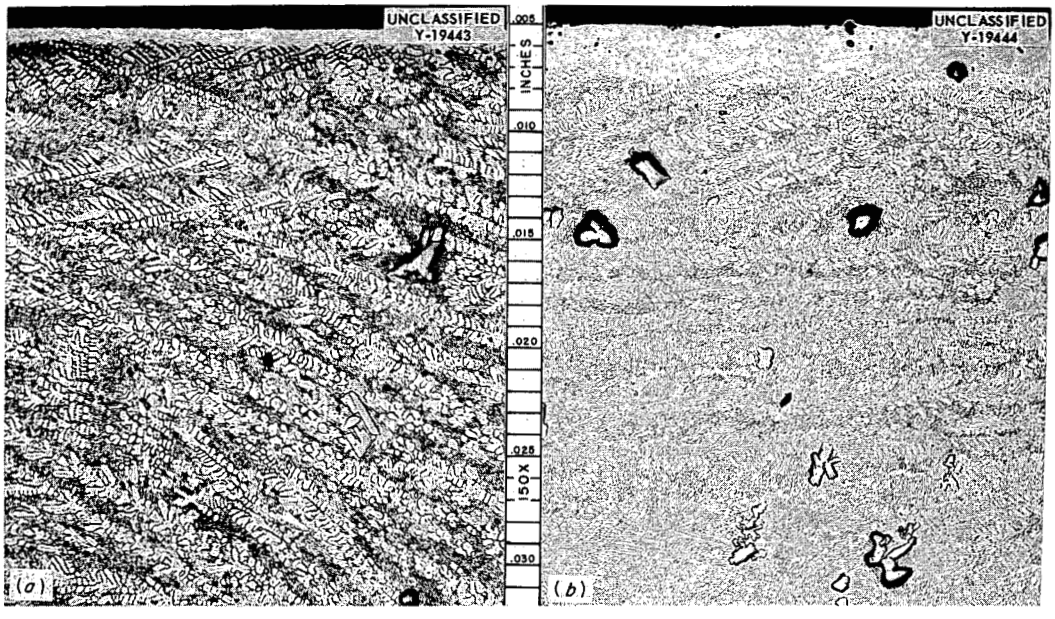

Fig. 19. Coast Metals No. 53 Alloy Seesaw Corrosion-Tested in NaK (56-44 wt %) for 100 hr at (*a*) 1400°F and (*b*) 1500°F. The constituent removal is greater at the higher temperature. Etchant: 10% oxalic acid. 50X. Reduced 24%.

the surface and a depth of 6 to 7 mils, the concentration of boron was less than one-third its value in the interior.

All the test systems had surface-to-volume ratios of 0.83-in.$^{-1}$. This ratio was calculated by using only the surface area of the alloy buttons; the area of the capsule wall that was covered with the test bath was not included. Tests will be conducted later in which the surface-to-volume ratio will be altered to determine whether it has any effect on the rate of depletion. Results of these tests are given in Table 7.

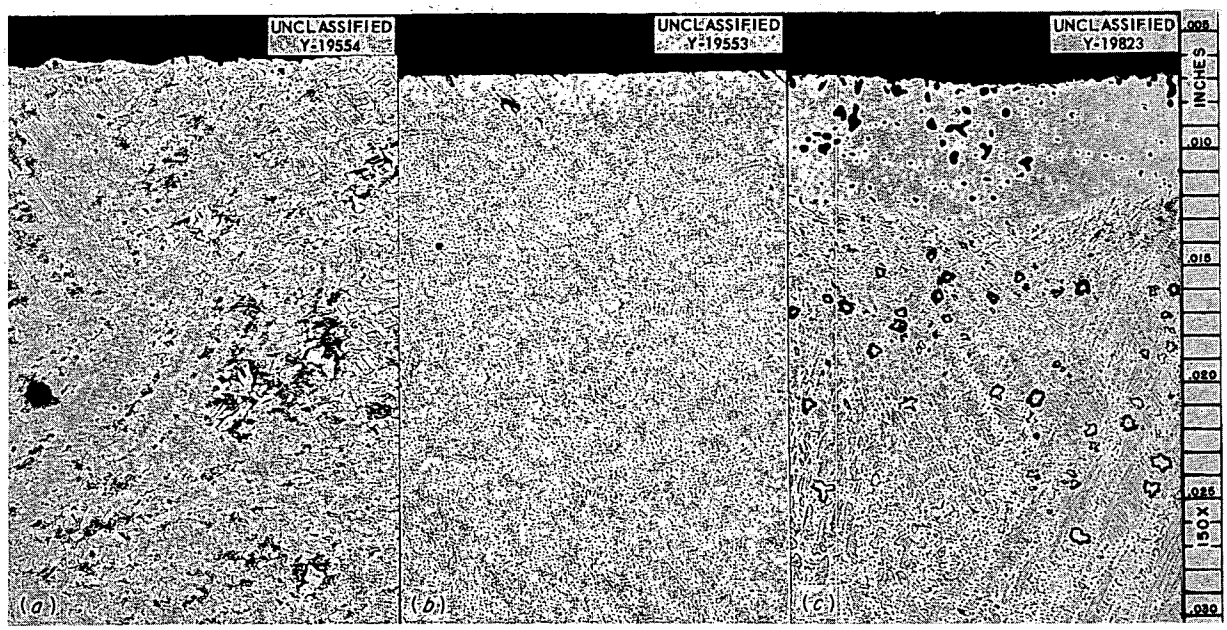

Fig. 20. Coast Metals No. 53 (81 Ni–8 Cr–4 Si–4 B–3 Fe) Alloy Seesaw Corrosion-Tested in NaF-ZrF_4-UF_4 (53.5-40.0-6.5 mole %) at (*a*) 1400°F for 100 hr, (*b*) 1500°F for 100 hr, and (*c*) 1500°F for 500 hr. Etchant: 10% oxalic acid. 50X. Reduced 17%. (Secret with caption)

TABLE 7. RESULTS OF SEESAW CORROSION TESTS ON COAST METALS NO. 53 BRAZING ALLOYS IN NaK (56-44 wt %) AND NaF-ZrF_4-UF_4 (53.5-40.0-6.5 MOLE %) AT VARIOUS TEMPERATURES AND TIMES

Bath	Time	Temperature (°F)	Depth of Depleted Area (mils)	Metallographic Notes
NaK	100	1400	0.8	No apparent attack
NaK	100	1500	2.5	Small subsurface voids in depleted area
Fluoride No. 44	100	1400	0.0	Small subsurface intermittent voids along edge to maximum of 0.5 mil
Fluoride No. 44	100	1500	1.5	Small intermittent stringers along edge to a maximum depth of 1.5 mils
Fluoride No. 44	500	1500	6	Subsurface voids in depleted region to maximum depth of 5 mils

TESTS ON INCONEL TUBE-TO-HEADER JOINTS WITH RECRYSTALLIZATION WELDS IN NaK AND IN FLUORIDE FUEL

D. H. Jansen

Welded Inconel tube-to-header joints fabricated by The Glenn L. Martin Co. were corrosion-tested in NaK (56-44 wt %) and in the fuel mixture (No. 30) $NaF-ZrF_4-UF_4$ (50-46-4 mole %) in seesaw apparatus at 1500°F for 100 hr. The test specimens were resistance-welded by using the "flange-during-welding method."[2] These welds are made by forging a preflared tube into a drilled header plate; the edge of the header hole is heated to a plastic state, which allows the tube to be forged into position, as shown in Figs. 21 and 22. The bond is achieved by recrystallization of the tube-to-header interface. The purpose of the tests was to determine the corrosion resistance of this recrystallized area. It was found that the NaK attacked the specimen to a maximum depth of 0.5 mil in the recrystallized area and the header plate (Fig. 23). The fused salt attacked the header plate to a maximum of 1.5 mils in the form of small, subsurface voids, but this attack dropped to a maximum of about 0.5 mil in the worked tube and recrystallized area (Figs. 24 and 25).

[2] J. J. Mueller, C. Shaeffer, and C. L. Lawrence, *Special Welding Techniques, Summary Report*, The Glenn L. Martin Co. (Jan. 1956).

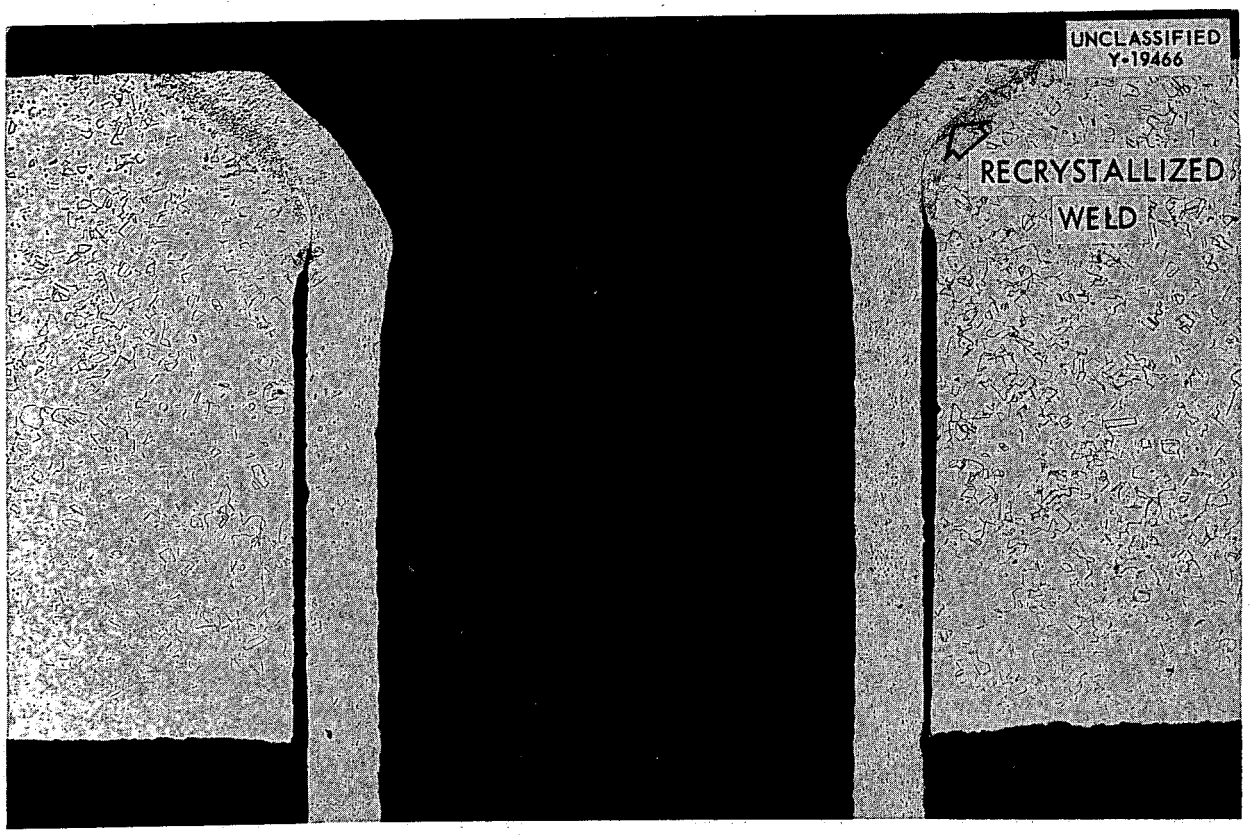

Fig. 21. As-received Tube-to-Header Joint Welded by the "Flange-During-Welding Method." The recrystallization weld and worked portion of the tube can be seen at the top of the header plate. Etchant: glyceria regia. 15X.

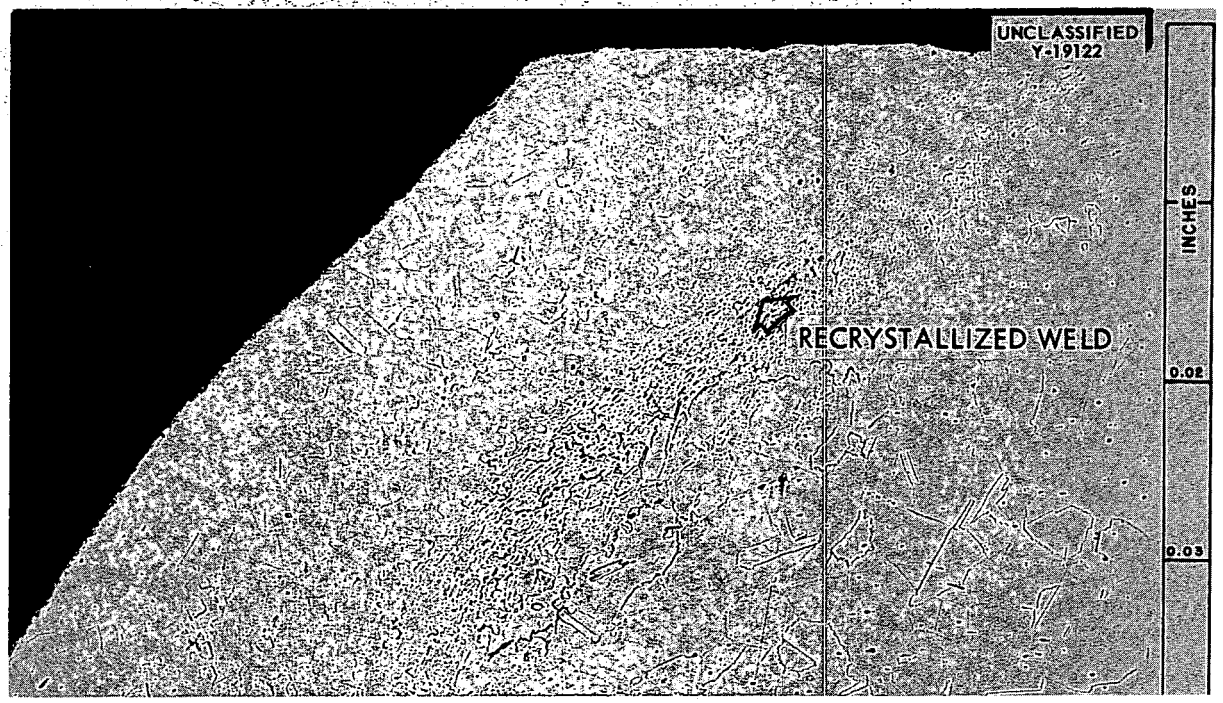

Fig. 22. Enlarged View of Recrystallization Weld Shown in Fig. 21. Etchant: glyceria regia. 100X. Reduced 4%.

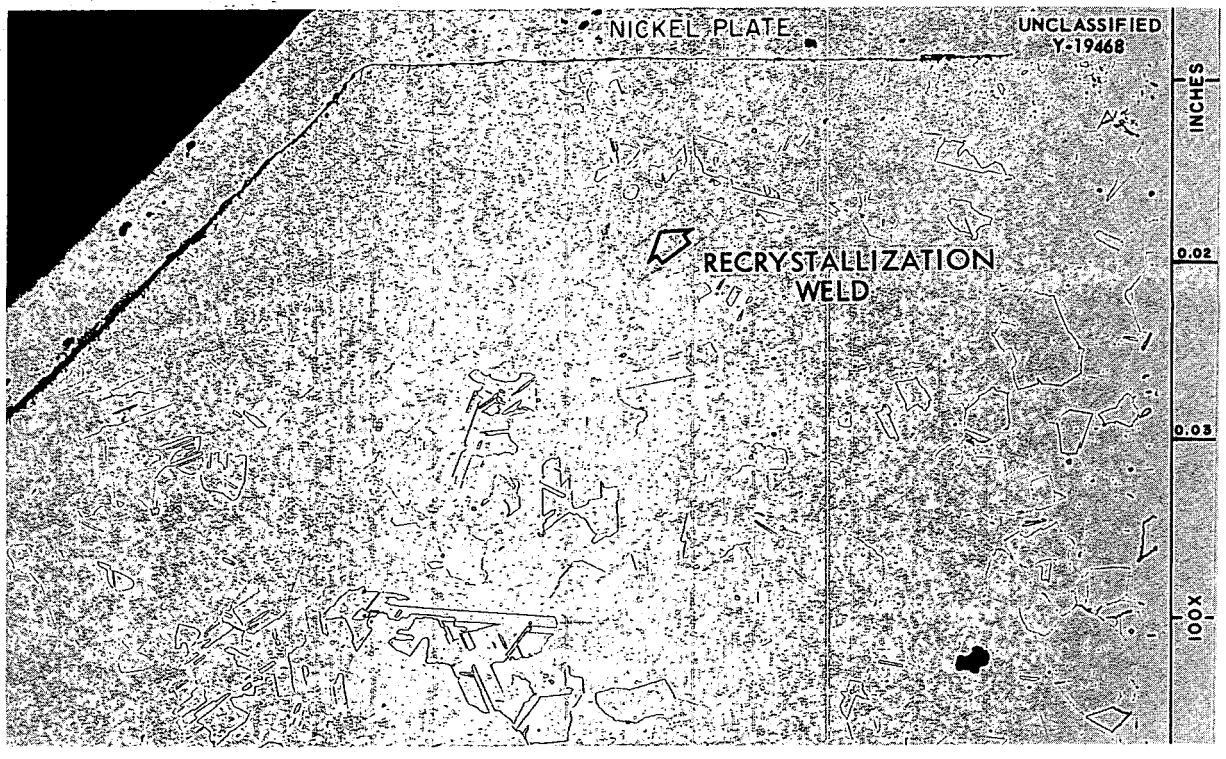

Fig. 23. Recrystallization Weld of Tube-to-Header Joint Seesaw Corrosion-Tested in NaK (56-44 wt%) for 100 hr at 1500°F. Etchant: glyceria regia. 100X. Reduced 3%.

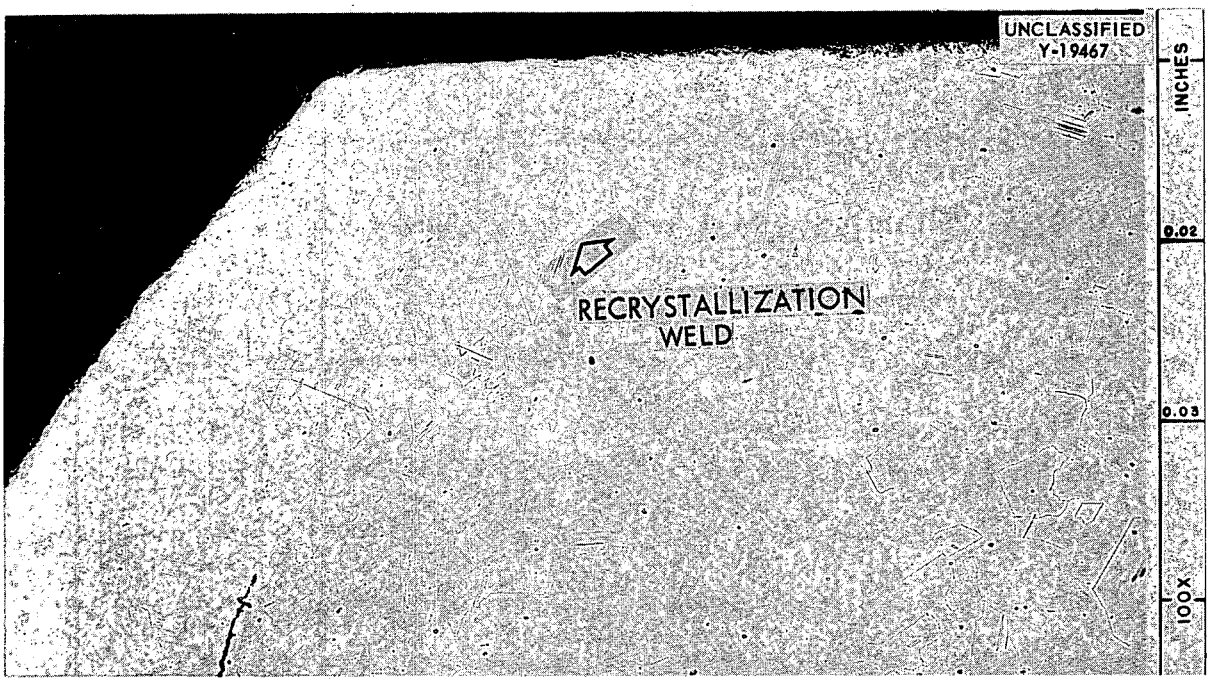

Fig. 24. Recrystallization Weld of Inconel Tube-to-Header Joint Seesaw Corrosion-Tested in NaF-ZrF_4-UF_4 (50-0-46.0-4.0 mole %) for 100 hr at 1500°F. Etchant: glyceria regia. 100X. Reduced 4%. (Secret with caption)

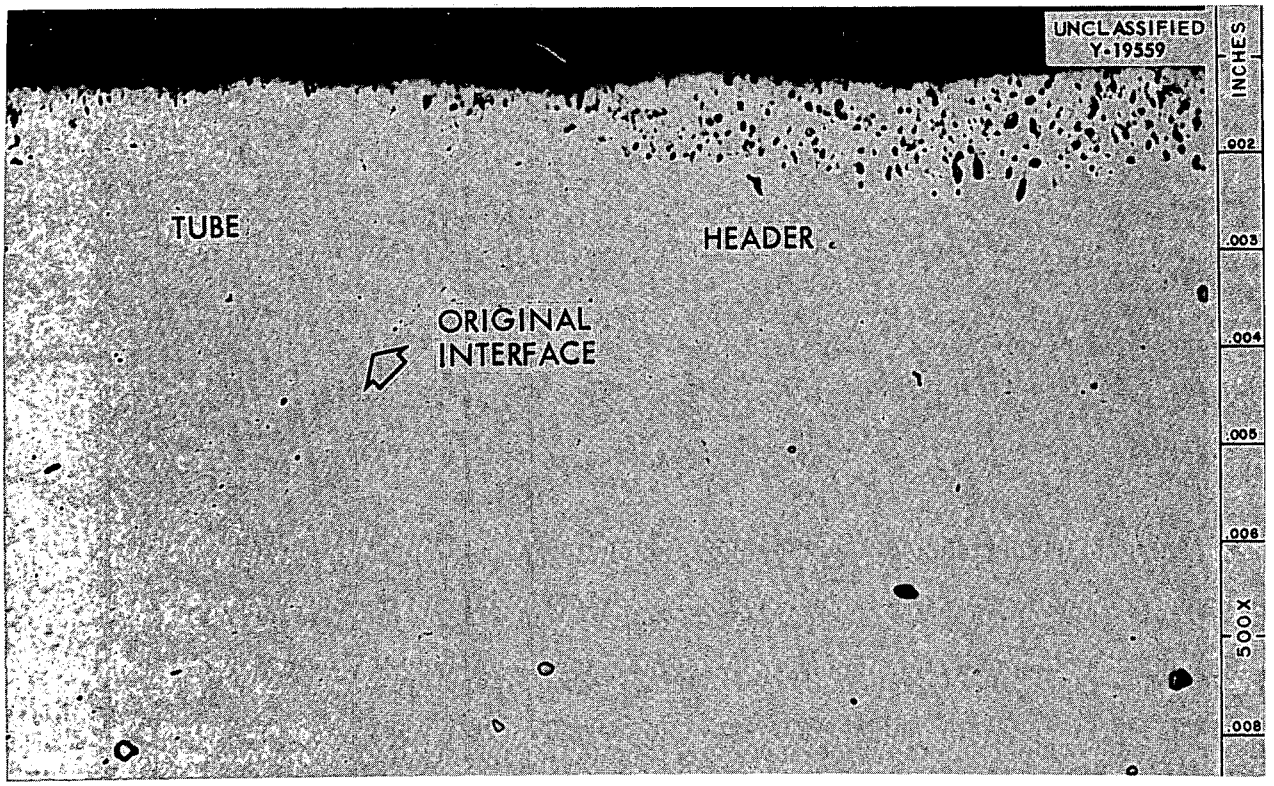

Fig. 25. Enlarged View of Recrystallization Weld Shown in Fig. 24. Note how attack by the NaF-ZrF_4-UF_4 (50.0-46.0-4.0 mole %) bath decreases in the worked tube area. Etchant: glyceria regia. (Secret with caption)

BRAZING-ALLOY–THERMAL-CONVECTION-LOOP TESTS

D. H. Jansen

Two Inconel thermal-convection loops containing the 70% Ni–13% Ge–11% Cr–6% Si brazing alloy in the hot-leg section have been operated for 500 hr. One loop was operated with NaK (56-44 wt %) as the circulating media, the other with NaF-ZrF_4-UF_4 (53.5-40.0-6.5 mole %). The Ni-Ge-Cr-Si alloy was placed in these loops by brazing together seven Inconel segments having slip-type joints and then replacing the hot-leg section with this assembly. This type of thermal-convection loop has been described earlier.[3] Hot-leg temperatures were maintained at 1500°F on both loops for the duration of the tests. Cold-leg temperatures were held at 1165 and 1150°F on the NaK and fused salt loops, respectively.

The inner walls of the Inconel segments and two samples from each brazed joint were examined, after the tests, for any evidence of attack. The results of the examinations are summarized in Table 8.

The brazing alloy showed good corrosion resistance to NaK (Fig. 26), but some large cracks which extended halfway through the tube wall were found in some of the brazed joints (Fig. 27). It is not known whether these cracks are caused by thermal stress or shrinkage, since no as-received joints were available for examination. NaK samples from this loop showed 1160-ppm oxygen content after test. This is admittedly high, but no efforts were made to purify the NaK since it is received in container lots.

Attack by the fused salt bath averaged approximately 5 mils on the brazed joints in this loop. Figure 28*a* shows the type of attack found. The Inconel tubing adjacent to the brazed joints showed attack ranging from 4.5 mils in the coldest region of the hot leg to 9 mils at the hottest portion of the hot leg (Fig. 28*b*). A slight trace of metallic crystals was found in the coldest portion of the fused salt loop. Spectrographic analyses of these crystals showed strong traces of chromium and nickel, while weak lines for iron were present.

A third Inconel thermal-convection loop containing the 82% Au–18% Ni brazing alloy was tested with NaF-ZrF_4-UF_4 (50-46-4 mole %) for 500 hr. Hot- and cold-leg temperatures were maintained at 1500 and 1175°F, respectively. Microscopic examination of samples from each brazed joint show attack on the alloy which averages about 8 mils.

[3] D. H. Jansen, *ANP Quar. Prog. Rep. Dec. 10, 1955*, ORNL-2012, p 112–13.

TABLE 8. RESULTS OF METALLOGRAPHIC EXAMINATION OF INCONEL JOINTS BRAZED WITH THE 70% Ni–13% Ge–11% Cr–6% Si BRAZING ALLOY LOCATED IN THE HOT-LEG SECTION OF INCONEL THERMAL CONVECTION LOOPS WITH NaK (56-44 wt %) AND NaF-ZrF_4-UF_4 (53.5-40.0-6.5 MOLE %) AS CIRCULATING MEDIA

Test Conditions: time, 500 hr; hot leg temperature, 1500°F

Brazed Joint	Metallographic Notes			
	Attack on NaK Loop (mils)		Attack on Fused Salt Loop (mils)	
	Braze	Inconel Tube	Braze	Inconel Tube
1	None	None	4.5	9.5
2	0.5	None	4.5	7
3	None	None	6	7.5
4	0.5	None	3	4.5
5	None	None	5	4.5
6	1.5	None	5	4.5

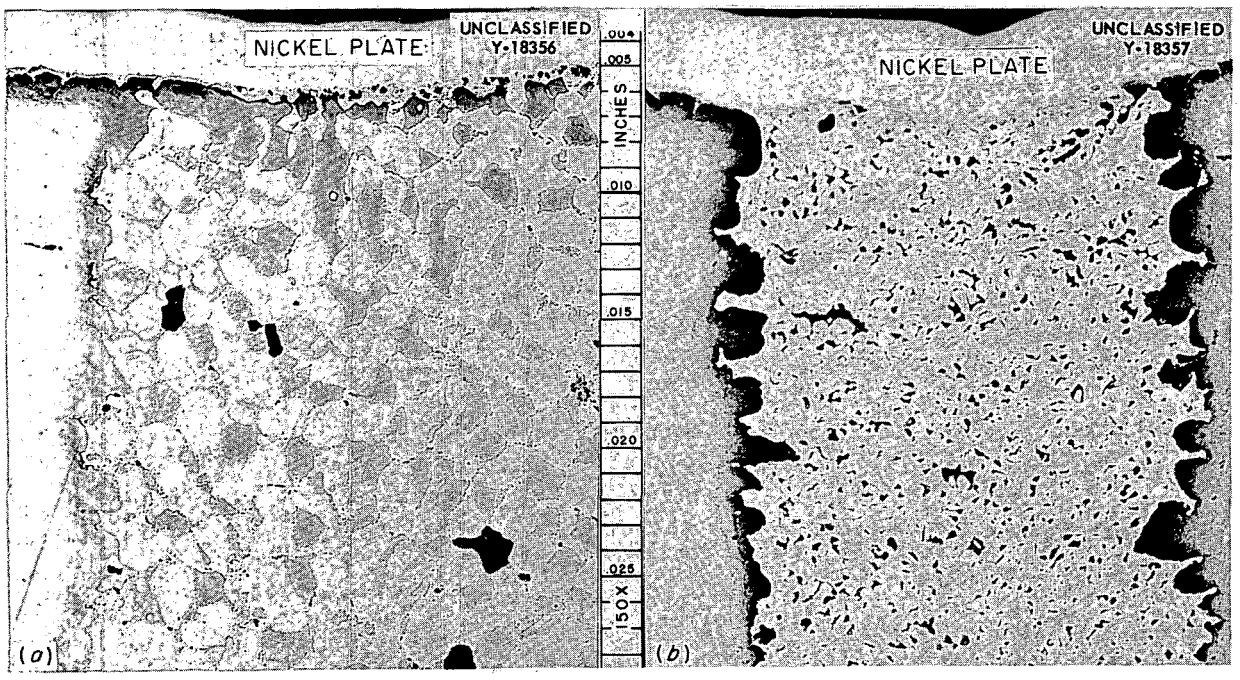

Fig. 26. Brazed Joints 2 (*a*) and 6 (*b*) of Inconel-NaK Thermal-Convection Loop Showing a Slight Attack on Brazing Alloy. These two samples were the only ones examined in which a large crack in the brazing alloy was not found. Specimens were nickel-plated to preserve edge during polishing. Etchant: 10% oxalic acid. 50X. Reduced 11%.

Fig. 27. Large-Type Crack Found in Brazed Joints in the Inconel-NaK Loop. Etchant: 10% oxalic acid. 100X. Reduced 34%.

NIOBIUM IN STATIC SODIUM

D. H. Jansen

At the request of the Mechanical Testing Group, specimens of niobium were tested in static sodium at 1500°F for 1000 hr to determine the suitability of this bath as a protective environment for niobium. The purpose of these tests was to determine if the niobium would be corroded by the sodium at this temperature and if the hardness of the niobium would be appreciably altered due to oxygen pickup.

The niobium specimens were contained in type 304 stainless steel and Inconel capsules, and the variables such as the volume of bath, the container size, and the area of the specimens were adjusted to obtain a surface-area-to-volume ratio that would conform as closely as possible to that found in creep-test equipment. Cold traps were utilized on the bottom of each capsule to reduce the amount of oxide in the sodium bath.

The niobium specimen tested in the type 304 stainless steel capsule showed more evidence of surface roughening than did the specimen tested in the Inconel capsule (Fig. 29), and the thickness loss was also more than that of the specimen

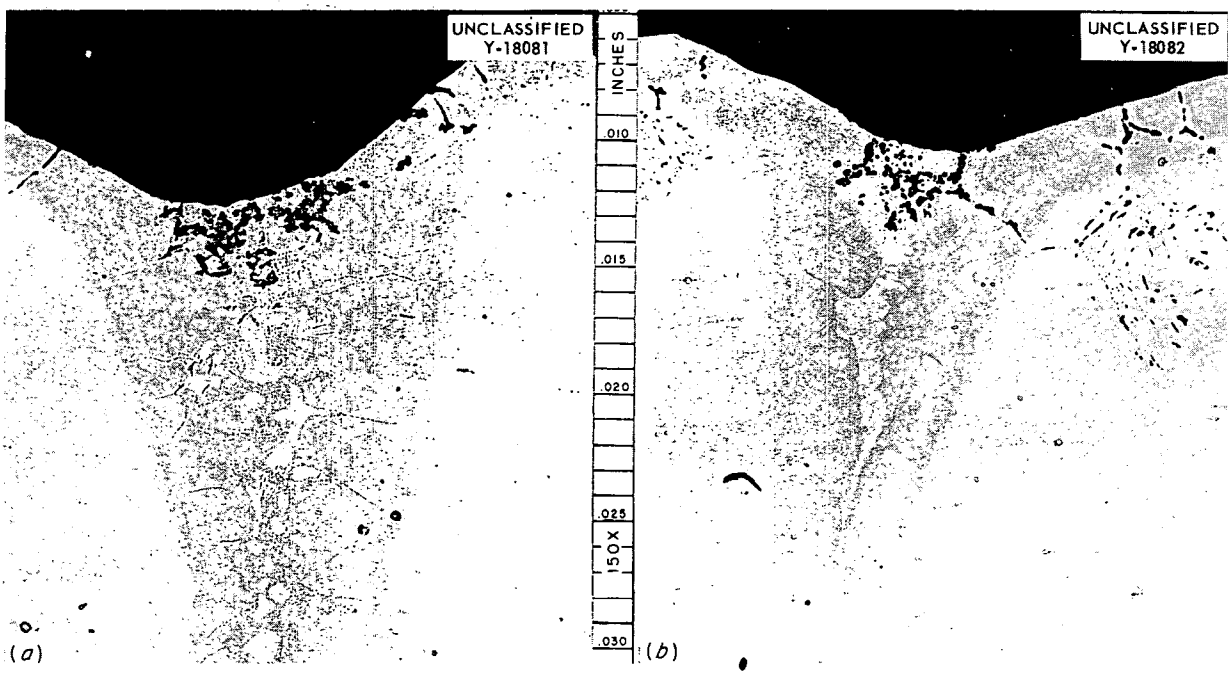

Fig. 28. Brazed Joints Located in (*a*) Cool Section, 1450°F, and (*b*) Hottest Section, 1500°F, of Hot Leg in Inconel–NaF-ZrF_4-UF_4 (50-46-4 mole %) Thermal-Convection Loop. Etchant: 10% oxalic acid. 50X. Reduced 11%. (Secret with caption)

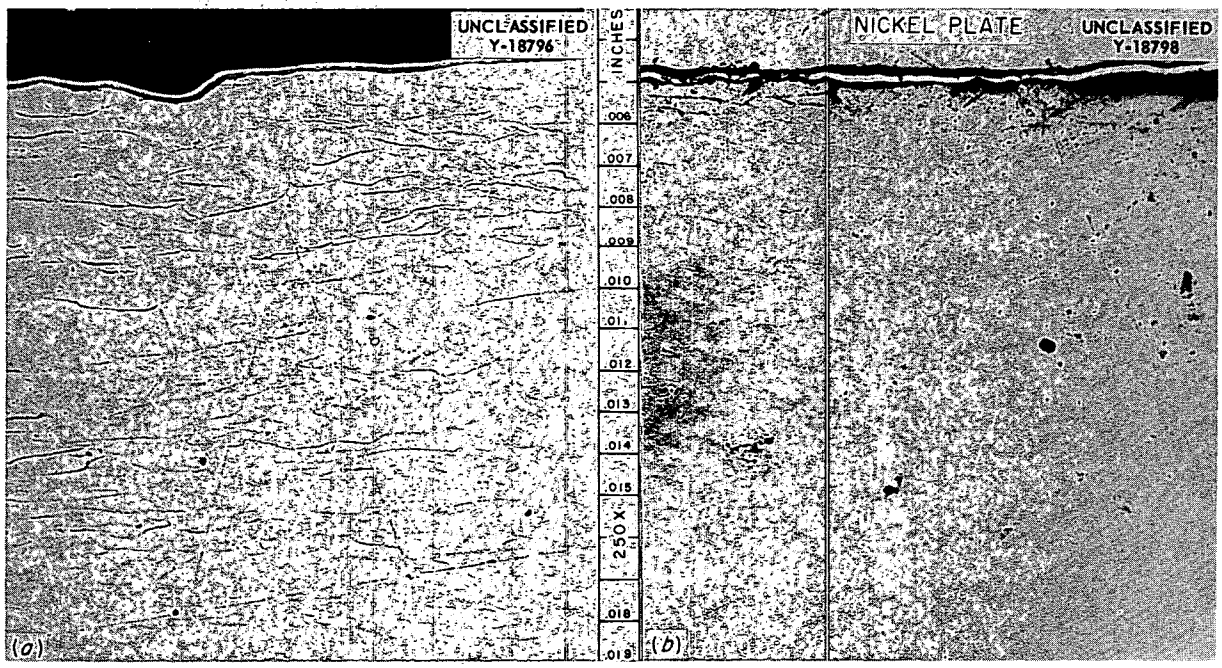

Fig. 29. Niobium Specimens Tested in Liquid Sodium for 1000 hr in (*a*) Inconel and (*b*) Type 304 Stainless Steel Containers. Specimen nickel-plated to preserve edge during polishing. Etchant: 25% HF, 25% H_2SO_4, 50% H_2O. 250X. Reduced 12%.

tested in the Inconel capsule (Table 9). Both tested specimens showed a thin, brittle layer approximately 0.3 mil thick that had formed on the surface during the test (Fig. 30). Since specimens are nickel-plated to protect their edges during metallographic polishing operations, it was not possible to have this film analyzed by x-ray techniques. Therefore, a short-term (200 hr) niobium-sodium static test at 1700°F was performed to duplicate this layer. This layer was identified by x-ray analysis to be Nb_4C_3.

Vickers hardness traverses taken on the specimens subjected to the 1000-hr tests show that the hardness of the niobium tested in the type 304 stainless steel capsule increased (130 to 135 VHN) during the test, whereas the hardness of the

TABLE 9. RESULTS OF TESTS OF NIOBIUM IN STATIC SODIUM

Test Conditions: time, 1000 hr; temperature, 1500°F

Sample	Hardness (VHN)	Thickness Loss (mils)	Chemical Analysis (ppm)			
			H_2	O_2	N_2	C
As-received material	130		2.4	40	125	300
Tested in type 304	135	3.0	3.8	84	250	370
Tested in Inconel	116	1.8	3.4	90	92	1180

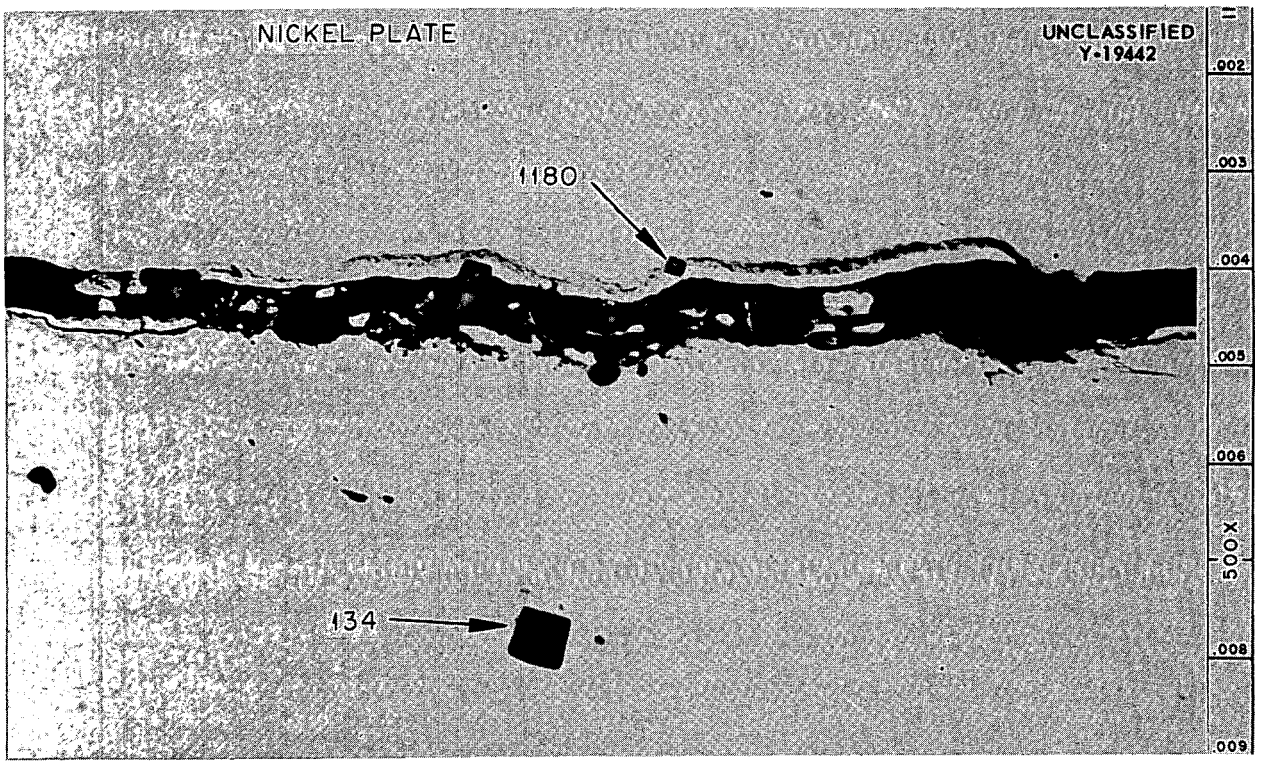

Fig. 30. Niobium Specimen Tested in Static Sodium in Type 304 Stainless Steel Container at 1500°F for 1000 hr Showing Comparative Hardness of Layer Formed on Surface and on the Niobium Specimen. The value 1180 VHN is approximate. Etchant: 25% HF, 25% H_2SO_4, 50% H_2O.

specimen tested in the Inconel capsule decreased (130 to 116 VHN).

From the chemical analysis, nitrogen seems to be the major hardening agent, as noted by the hardness of the tested specimens and by the corresponding nitrogen contents.

THERMENOL-SODIUM SCREENING TESTS

D. H. Jansen

Samples of Thermenol (82% Fe–15% Al–3% Mo) from a piece of hot-rolled strip have been screen-tested in static sodium for 100 hr at 1500°F. The tests were conducted in AISI 1035 steel and type 304 stainless steel capsules.

Weight and thickness changes of the tested specimens are listed in Table 10.

TABLE 10. RESULTS OF STATIC CORROSION TESTS ON THERMENOL (82% Fe–15% Al–3% Mo) IN SODIUM

Test Conditions: 1500°F; 100 hr

Capsule Material	Weight Change (%)	Thickness Change (%)
AISI 1035 steel	−0.22	+0.1
Type 430 stainless steel	−0.07	+0.3

A slight roughening on the surfaces of both samples was found after test (Fig. 31). Neither capsule showed any evidence of attack.

Analysis of the solvent used to dissolve the sodium baths after test showed the presence of aluminum.

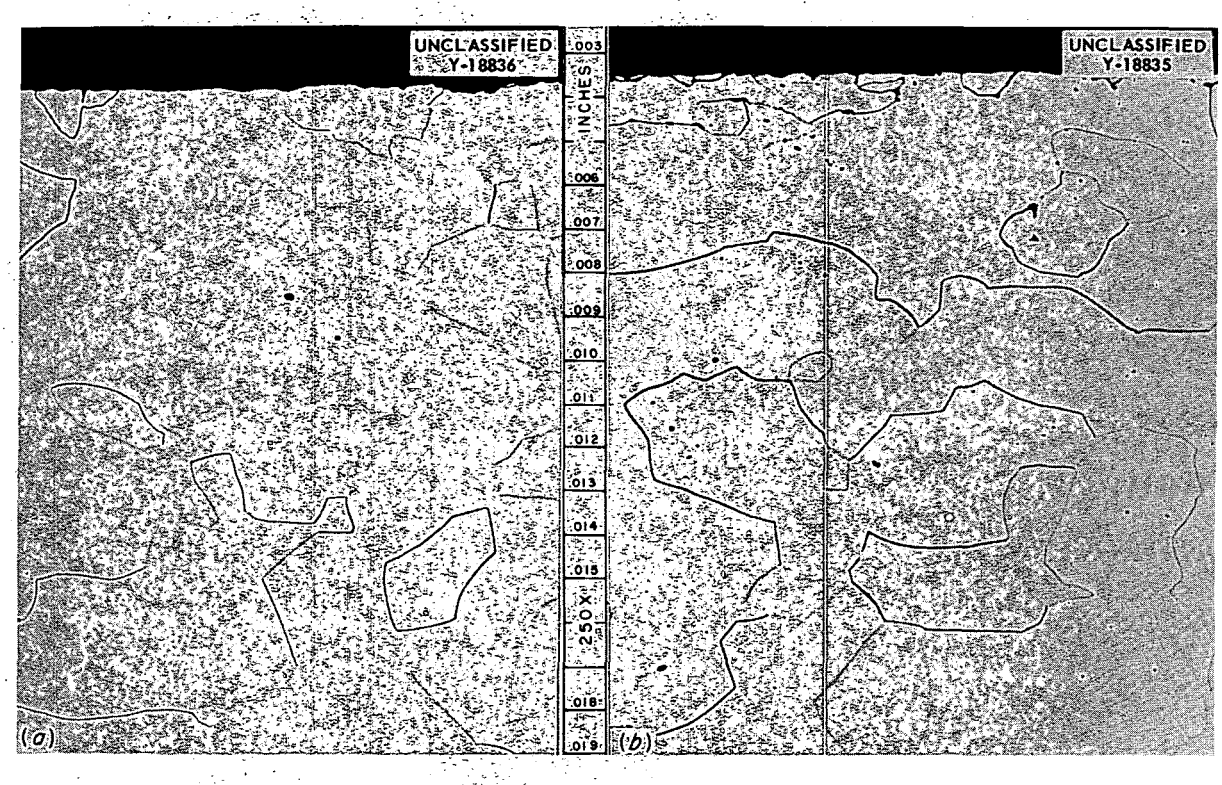

Fig. 31. As-tested Thermenol (82 Fe–15 Al–3 Mo) Specimens After Exposure to Static Sodium at 1500°F for 100 hr in (*a*) Type 430 Stainless Steel and (*b*) AISI 1035 Steel Capsules. Etchant: aqua regia. 250X. Reduced 7%.

TESTS OF HAYNES BRAZING ALLOY NO. 40 IN NaK AND IN FLUORIDE FUELS

D. H. Jansen

Inconel tube-to-header joints brazed with Haynes brazing alloy No. 40 (nominal composition, in wt %: Cr, 13.5; Fe, 4.5; Si, 3.9; B, 3.2; Co, 1.0; C, 0.42; Mn, 0.25; Ni, balance) were corrosion-tested in the fuel mixture (No. 30) $NaF-ZrF_4-UF_4$ (50-46-4 mole %) and NaK (56-44 wt %) in seesaw apparatus. The test periods were 100 hr, and the hot zone was maintained at 1500°F. The specimens were retained in the hot zones of the capsules during the tests.

The alloy showed good corrosion resistance to NaK but only fair resistance (2.5- to 3-mil attack) to the fuel mixture. There was attack to a depth of 2.5 to 3 mils on the specimen exposed to the fuel mixture, as shown in Fig. 32. A considerable amount of porosity was found in the braze fillets.

CHLORIDE CORROSION TESTS

D. H. Jansen

Screening tests on nickel and Inconel by using an $NaCl-Mg_2Cl-UCl_3$ (50.0-33.3-16.7 mole %) bath have been performed at the request of a Reactor School study group. Two sets of Inconel and nickel capsules loaded with the chloride bath were tested in seesaw apparatus. The test periods were 100 hr, and the hot zone was maintained at 1800°F for the first set of capsules. The second set of capsules was tested for 500 hr at a hot-zone temperature of 1350°F.

Both the Inconel and nickel capsules tested at 1800°F showed evidence of mass-transfer crystals, the nickel capsule having the greater amount, as shown in Fig. 33.

The hot-zone portion of the Inconel capsule from this test showed a maximum attack of 4 mils in the form of subsurface voids (Fig. 34). This

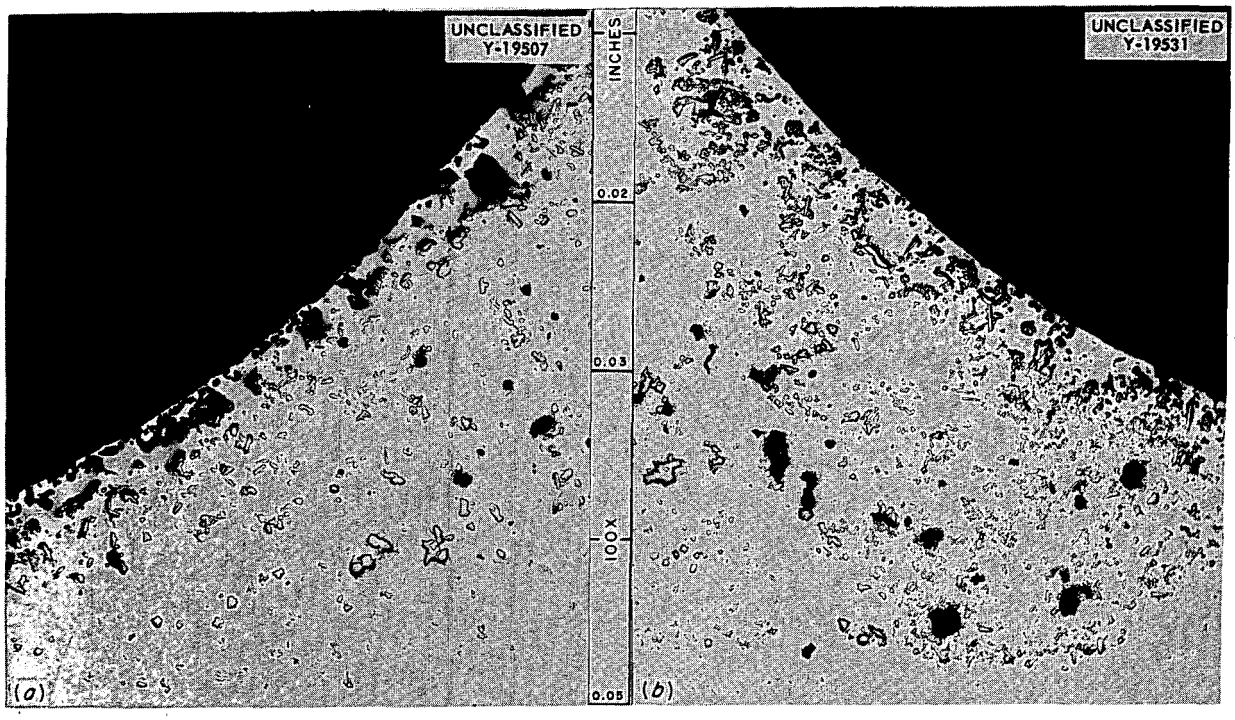

Fig. 32. Haynes No. 40 Alloy After 100-hr Seesaw Test in (*a*) $NaF-ZrF_4-UF_4$ (50.0-46.0-4.0 mole %) and (*b*) NaK (56-44 wt %) at 1500°F. As polished. 100X. Reduced 11%. (Secret with caption)

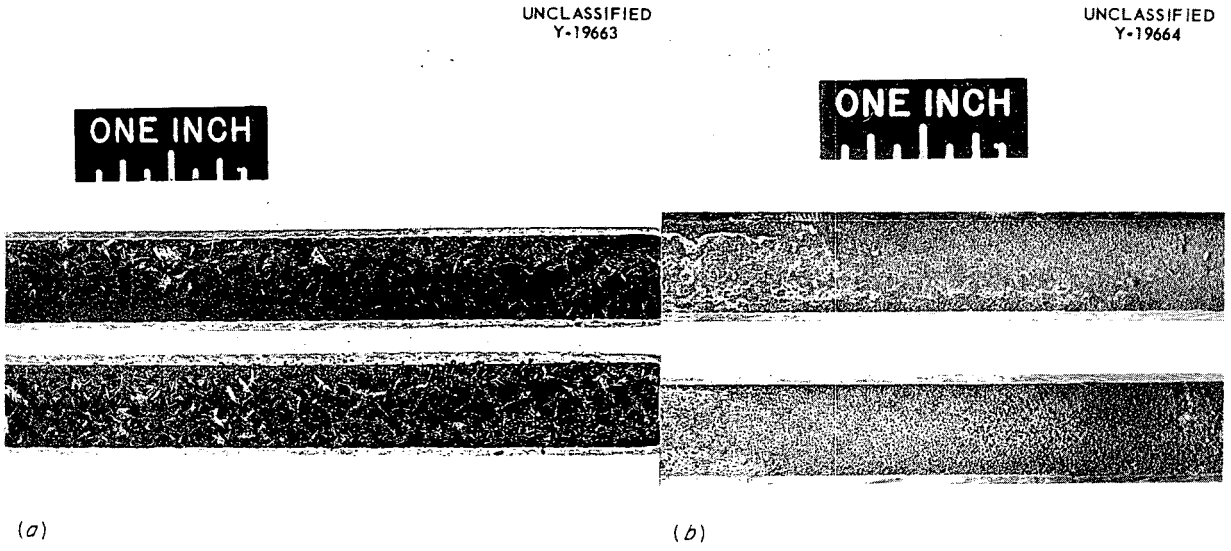

Fig. 33. Cold Zones of (*a*) Nickel and (*b*) Inconel Capsules Seesawed for 100 hr at 1800°F in NaCl-$MgCl_2$-UCl_3 (50.0-33.3-16.7 mole %). Note greater amount of mass-transfer crystals in the nickel capsule. 1.2X. Reduced 12%. (Secret with caption)

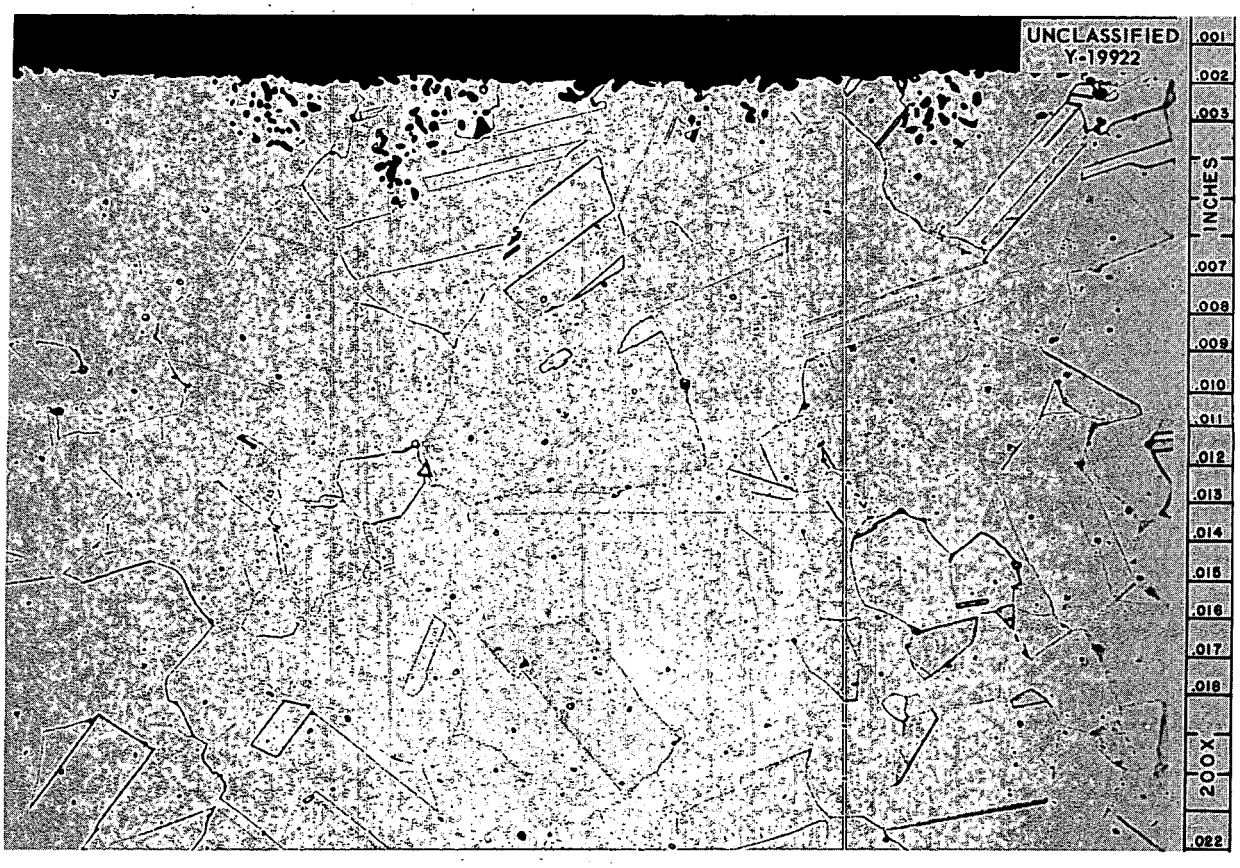

Fig. 34. Hot Zone from Inconel Capsule Subjected to NaCl-$MgCl_2$-UCl_3 (50.0-33.3-16.7 mole %) Bath for 500 hr at 1350°F. A spotty subsurface void attack to a maximum depth of 4 mils can be seen. Etchant: copper regia. (Secret with caption)

is the same type of attack found on Inconel when exposed to the fluoride baths.

The 500-hr tests (1350°F hot zone) showed no mass transfer in the nickel capsule, but a slight amount of metallic crystals was observed in the cold zone of the Inconel capsule. Chemical analyses on these crystals are incomplete.

Tube thickness measurements from the hot and cold zones of all the tests indicated a uniform removal of container material from the hot zones.

CORROSION TESTS OF INCONEL AND TYPE 316 STAINLESS STEEL IN NaK AND LITHIUM

R. Carlander

The corrosion resistance of type 316 stainless steel and Inconel to NaK (56-44 wt %) with lithium additions was determined under dynamic conditions (seesaw and thermal-convection-loop tests).

The tests in seesaw apparatus were made from 12-in.-long capsules which were filled to 40% of their volume with NaK plus 5 or 10 wt % lithium. The tests were conducted for 100 hr in a tilting-type furnace (1 cpm) with the hot zone at 1500°F and the cold zone at 1100°F. No mass transfer occurred in any of the systems. The Inconel with a 10 wt % addition of lithium was attacked to a depth of 1 mil in the hot zone, while the other systems were unattacked.

The thermal-convection-loop tests were conducted for 1000 hr at a hot-leg temperature of 1500°F (cold-leg temperature 1220°F) with a 5 wt % lithium addition. A slight amount of mass transfer in the form of small adherent crystals containing 71.5% Ni–4.6% Cr–0.7% Fe occurred in the Inconel loop, while no mass transfer was found in the stainless steel loop. Figures 35 and 36 show portions of the hot and cold legs of the Inconel and stainless steel loops. The Inconel was attacked to a depth of 1½ mils in the hot and cold legs. The stainless steel was unattacked in the hot leg but was attacked to a depth of 6 mils in the cold leg. Photomicrographs of the cold legs of the Inconel and the stainless steel loops are shown in Fig. 37. The addition of 5 wt % lithium to NaK did not decrease the corrosion resistance of Inconel, but did decrease that of type 316 stainless steel. The difference in attack between the hot and cold legs of the stainless steel loop may be attributed to the larger amount

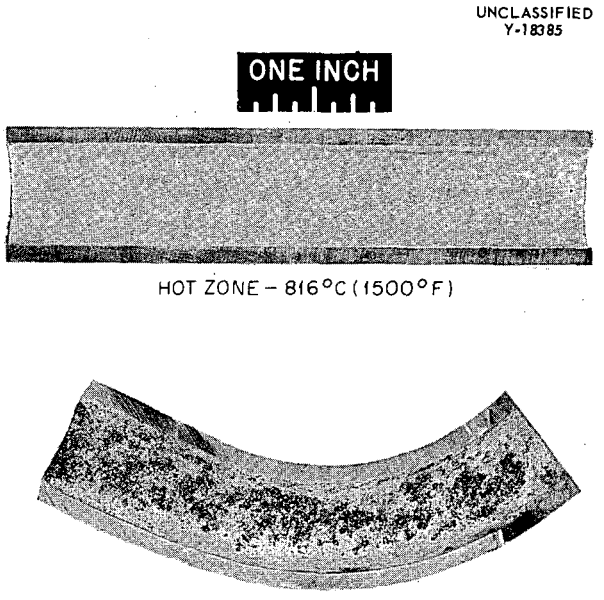

Fig. 35. Inconel Thermal-Convection Loop Operated for 1000 hr with 95 wt % NaK (56-44 wt %) + 5 wt % Li as Circulating Medium. (Secret with caption)

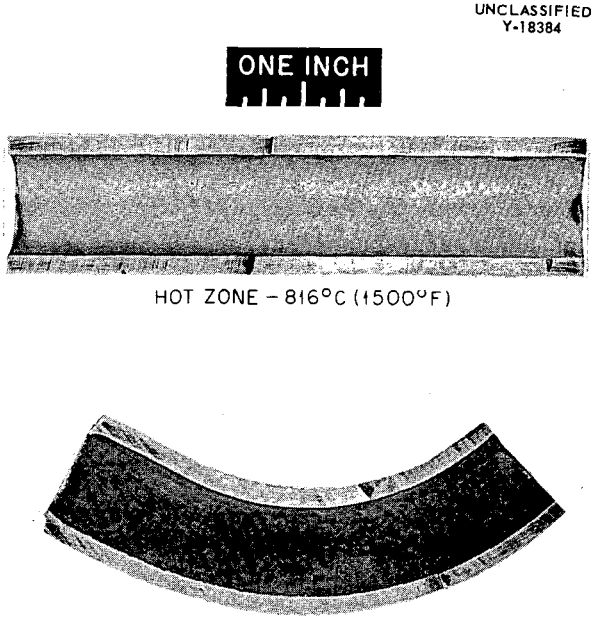

Fig. 36. Type 316 Stainless Steel Thermal-Convection Loop Operated for 1000 hr with 95 wt % NaK (56-44 wt %) + 5% Li as Circulating Medium. (Secret with caption)

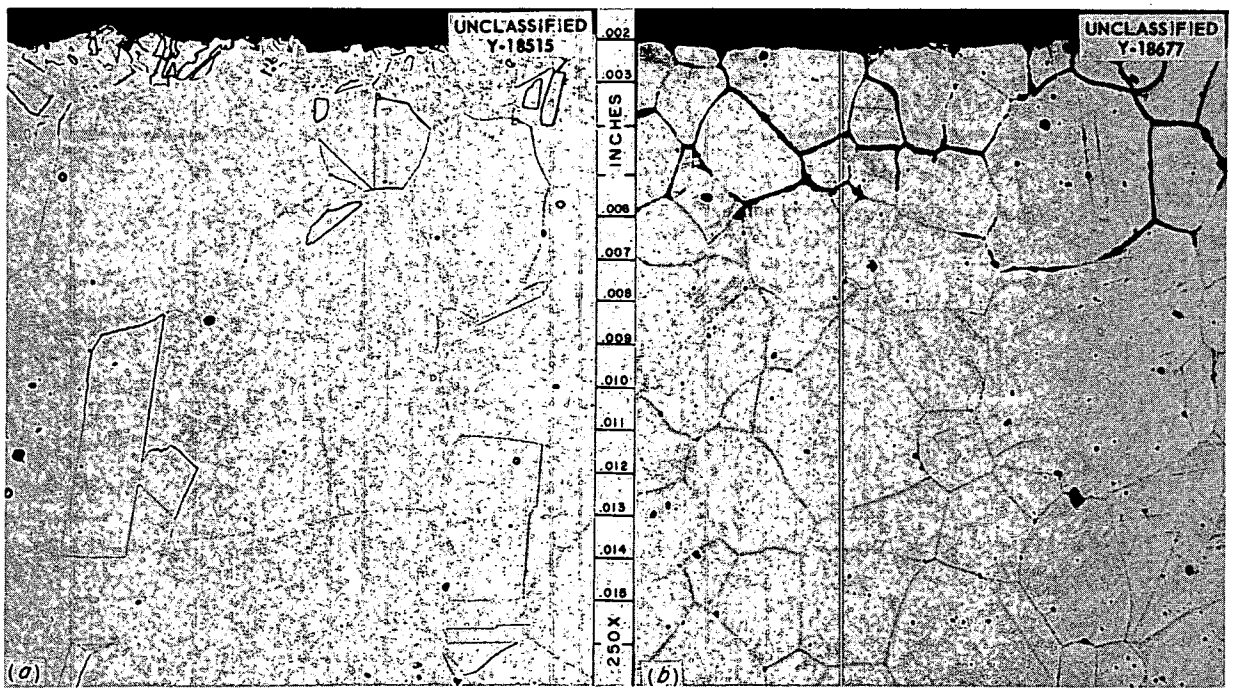

Fig. 37. Cold Legs of (*a*) Inconel and of (*b*) Type 316 Stainless Steel Thermal-Convection Loops Operated for 1000 hr at 1500°F with NaK + 5 wt % Li as Circulating Medium. Etchant: aqua regia. 250X. Reduced 10%. (Secret with caption)

of carbides present at the lower temperature of the cold leg than at the higher temperature of the hot leg.

VAPOR-ZONE ATTACK IN INCONEL-FLUORIDE FUEL SYSTEMS

R. Carlander

In several creep experiments on Inconel in the fuel mixture (No. 44) NaF-ZrF_4-UF_4 (53.5-40-6.5 mole %), extremely heavy attack on portions of the system in the regions above the bath level has been detected. This type of attack was also noted in experimental tests of a ZrF_4 "snow trap" (a system in which the more volatile ZrF_4 was made to deposit from the fused salt bath by means of a temperature gradient) fabricated from type 316 stainless steel. The following test was conducted in a manner to approximate roughly the conditions in the creep experiments where this heavy attack on Inconel was originally noted.

Evacuated Inconel capsules were exposed to static NaF-ZrF_4-UF_4 (53.5-40-6.5 mole %) at 1600°F for 500 and 1000 hr. Two 12-in.-long capsules were used in which ½-in.-dia Inconel thermocouple probes extended to within 1 in. of the bottom. The level of the fluoride bath and the height of the heated zone was 4 in. A temperature gradient was maintained over the rest of the system. Examinations of the capsules after the tests revealed that the ZrF_4 "snow" deposited around the walls of the capsule approximately 1 in. above the original bath level, where the temperature was approximately 1100°F. A hard layer that reached a maximum thickness of ¼ in. and that consisted of the fluorides (NaF, ZrF_4, and UF_4) and small particles of NiO, Fe, and Cr was found in a region ½ in. above and below the original bath level. A picture of the capsule tested for 1000 hr is shown in Fig. 38. Chemical analysis of the bath and of the thermocouple probe revealed that chromium, as could be expected, was the main element leached out of the Inconel in both tests. A sample of the fluoride mixture taken from the bottom of the bath was richer in chromium than a sample taken from the top. The results of the chemical analyses are given in Table 11.

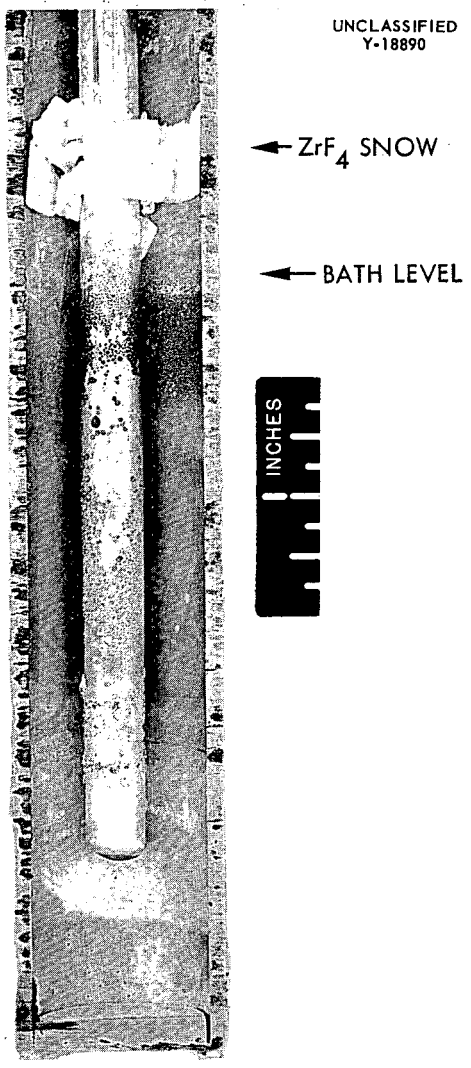

Fig. 38. Inconel Capsule and Probe Following Exposure to NaF-ZrF_4-UF_4 (53.5-40-6.5 mole %) for 1000 hr at 1600°F. (Secret with caption)

Metallographic examination revealed that the portion of the capsule wall around which the "snow" deposited was unattacked in both capsules. The heaviest attack occurred in the bath zone of both capsules. The attack reached a maximum depth of 4 mils in the 500-hr test and 5 mils in the 1000-hr test (Fig. 39). The depletion of ZrF_4 from the fused salt bath actually decreased the attack from that normally observed, and this attack, by itself, could not have caused the failures in the creep tests.

TABLE 11. CHEMICAL ANALYSES OF THE NaF-ZrF_4-UF_4 (53.5-40-6.5 MOLE %) BATH AND THE INCONEL CAPSULE FOLLOWING A TEST FOR 1000 hr AT 1600°F

Location of Sample	Amount (wt %)		
	Ni	Fe	Cr
Inconel probe (vapor zone)	75.00	7.39	16.08
Inconel probe (bath zone)	75.80	7.42	14.37
Top of fused salt bath	< 0.01	0.068	0.002
Bottom of fused salt bath	0.32	0.61	3.95

NIOBIUM AND ZIRCONIUM DYNAMIC CORROSION TESTS IN SODIUM AND IN LITHIUM

R. Carlander

Seesaw apparatus was used for corrosion tests of niobium and zirconium in sodium and in lithium in order to determine the corrosion resistance of these two materials in the dynamic system. Two niobium capsules and two zirconium capsules, 15 in. long, were filled to 40% of their volume – one capsule of each material with sodium and one capsule of each material with lithium – and sealed under an inert atmosphere. The capsules filled with lithium were enclosed in Hastelloy B containers. The niobium capsule filled with sodium was enclosed in an Inconel container, while the zirconium capsule which contained sodium was protected by a type 430 stainless steel jacket. The spaces between the capsules and the jackets were then filled to 40% of their volumes with sodium in order to obtain good heat transfer between the capsules and the containers (Fig. 40). The capsules were tested in a tilting furnace at 1 cpm for 100 hr with the hot zone at 1535°F and the cold zone at 995°F. No mass transfer was detectable in the zirconium tests, while some dissimilar-metal mass transfer was observed on the surface of the Hastelloy B and Inconel in the niobium tests (Fig. 41). The attack in all the tests was small. Photomicrographs of the zirconium capsule that contained lithium and of the niobium capsule that contained lithium are shown in Fig. 42. The results of metallographic examination of the test specimens are given in Table 12.

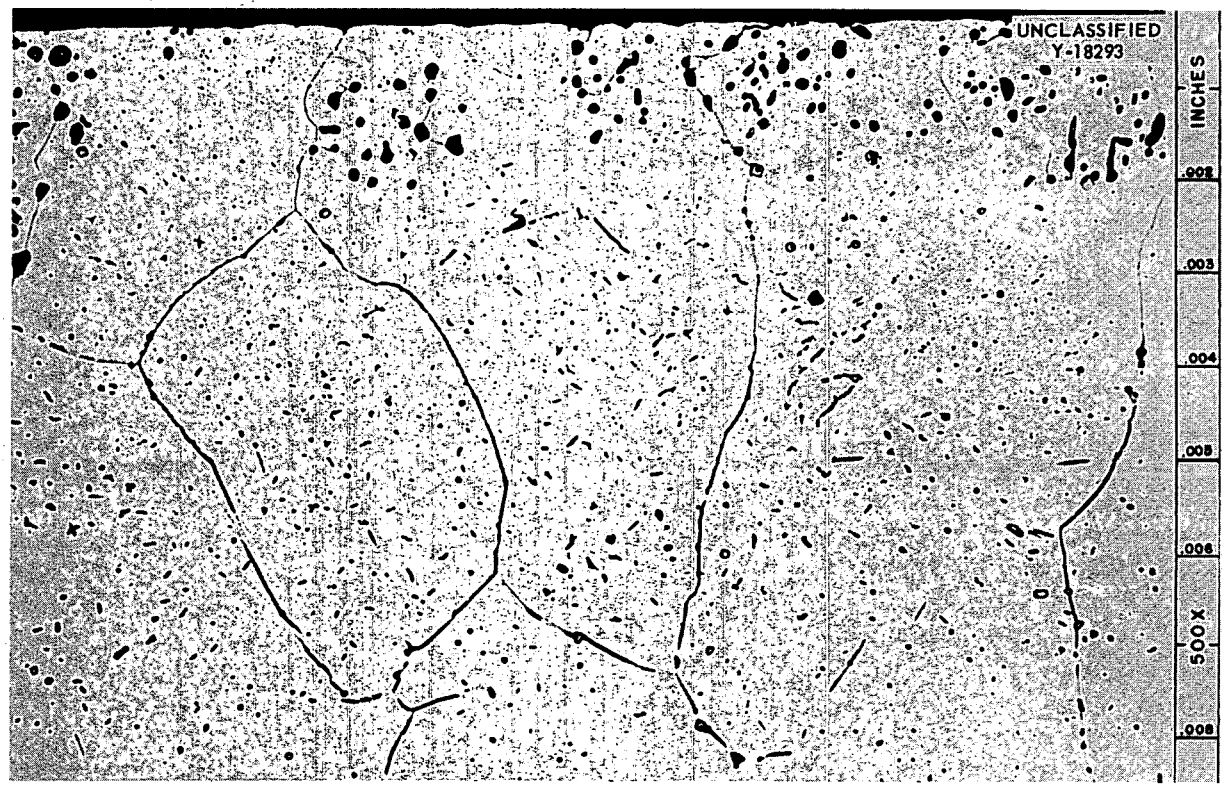

Fig. 39. Bath Zone of Inconel Capsule Following Exposure to $NaF-ZrF_4-UF_4$ (53.5-40-6.5 mole %) for 1000 hr at 1600°F. Etchant: 10% oxalic acid. 500X. Reduced 2%. (Secret with caption)

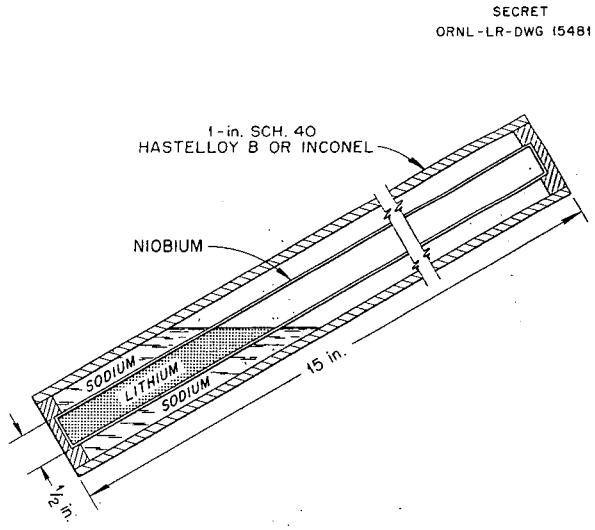

Fig. 40. Schematic Sketch of Niobium Seesaw Capsule.

CAST INCONEL–FUSED SALT STATIC TESTS

R. Carlander

Thermal-convection-loop tests of Inconel castings in an $NaF-ZrF_4-UF_4$ (50-46-4 mole %) wrought Inconel system performed by the Dynamic Corrosion Group[4] resulted in heavier attack than is normally noted on wrought Inconel. Metallographic examination of the as-received material revealed the presence of cracks, stringer porosity, and large grains with grain boundaries perpendicular to the surface. Therefore, several static tests of three Inconel castings, differing primarily in silicon content, were performed in an $NaF-ZrF_4-UF_4$ (50-46-4 mole %) bath in wrought Inconel capsules for 1000 hr at 1500°F. Examination of the tested specimens revealed that the casting with the highest silicon content (1.93%) was the

[4] J. H. DeVan, ORNL CF-56-2-56 (Feb. 13, 1956).

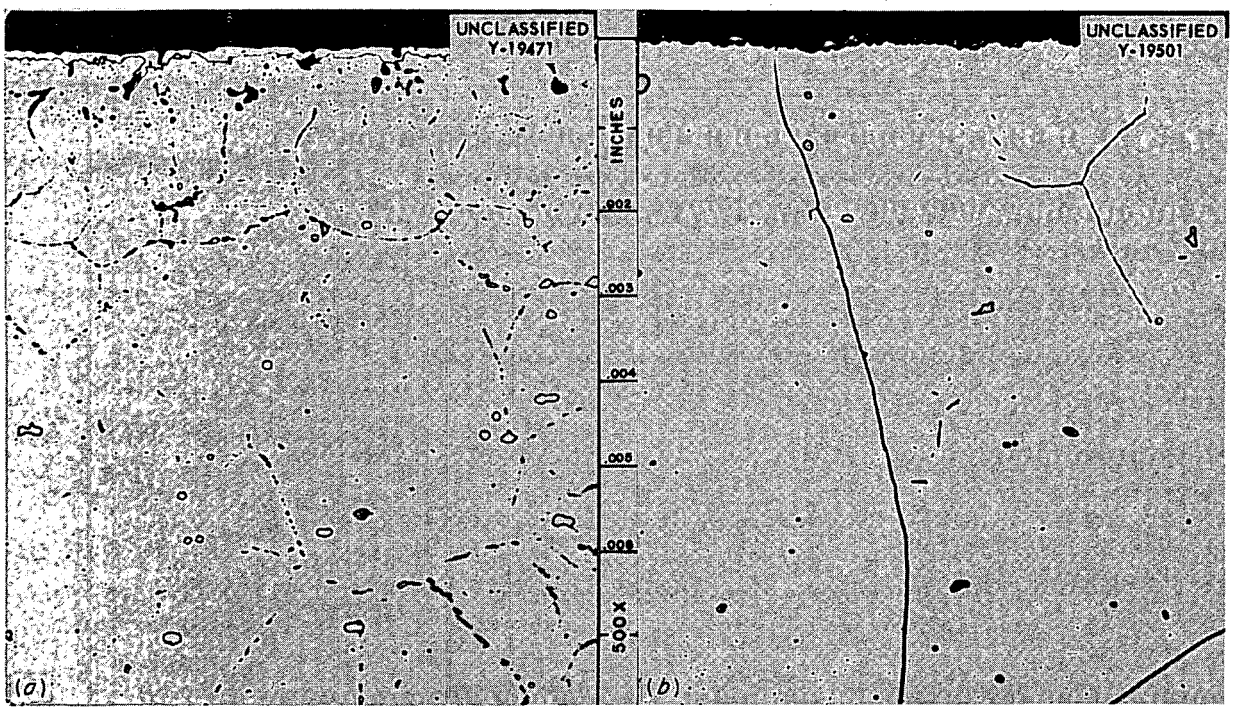

Fig. 41. (*a*) Hastelloy B and (*b*) Inconel Containers, Both of Which Contained Niobium, After Exposure to Sodium for 100 hr at 1535°F. Note dissimilar-metal mass-transfer layers on the surfaces of the Hastelloy B and the Inconel. Etchant: (*a*) 20 cc 10% chromic acid–30 cc HCl, (*b*) 10% oxalic acid. 500X. Reduced 10%. (Secret with caption)

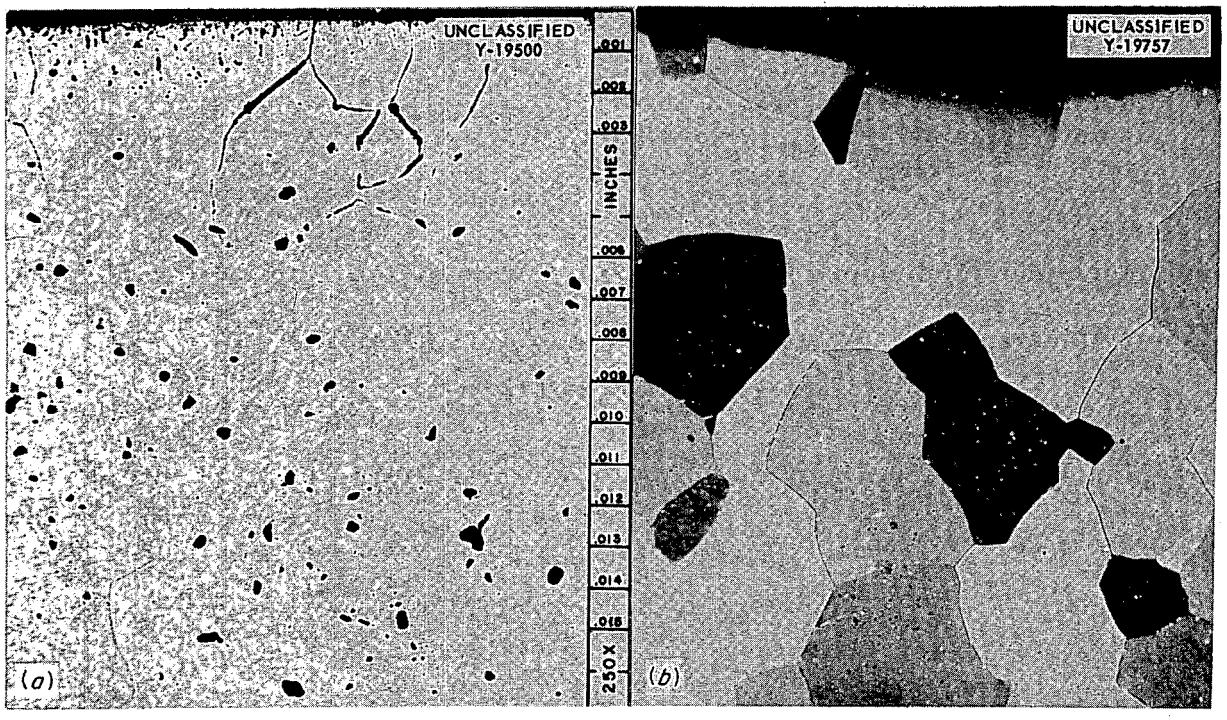

Fig. 42. (*a*) Inside Wall of Niobium Capsule Containing Lithium and (*b*) Inside Wall of Zirconium Capsule Containing Lithium After Testing for 100 hr at 1535°F. Etchant: (*a*) $HF\text{-}HNO_3\text{-}H_2O$ (25-25-50 vol %), (*b*) $C_2H_4O_2\text{-}HClO_4$ (10-1) electrolytic etch and polish. 250X. Reduced 11%. (Secret with caption)

TABLE 12. RESULTS OF TESTS OF ZIRCONIUM AND NIOBIUM IN LITHIUM AND IN SODIUM IN SEESAW APPARATUS

Test duration: 100 hr
Hot-zone temperature: 1535°F
Cold-zone temperature: 995°F

Test	Material	Bath	Attack (mils)	Metallographic Notes
A	Niobium capsule	Lithium on inner surface	2	Intergranular penetration found on both the inner and the outer surfaces
		Sodium on outer surface	2	
	Hastelloy B container	Sodium on inner surface	1.5	Attack in the form of voids; small amount of dissimilar-metal mass transfer detectable at 500X
B	Niobium capsule	Sodium on inner surface	None	Cracks found on outer surface; but not clearly evident that the cracks were due to sodium attack
		Sodium on outer surface	1.5	
	Inconel container	Sodium on inner surface	None	Surface roughened; small amount of dissimilar-metal mass transfer detectable at 500X
C	Zirconium capsule	Lithium on inner surface	None	
		Sodium on outer surface	None	
	Hastelloy B container	Sodium on inner surface	1.5	Attack in the form of voids
D	Zirconium capsule	Sodium on inner surface	None	

least attacked, while the casting with the lowest silicon content was the most severely attacked. In all cases, the attack was a combination of subsurface voids and intergranular penetration. The depth of subsurface voids on the Inconel castings was 3–4 mils – compared to 2–4 mils on the wrought Inconel capsules. The intergranular penetration, however, varied from 3 mils on the high-silicon casting to 12 mils on the low-silicon casting. This difference is attributed to the aforementioned porosity and to the grain boundaries running perpendicular to the surface of the castings. The results of metallographic examinations are given in Table 13. Photomicrographs of the wrought Inconel capsule and of the cast Inconel specimen No. 321 are shown in Fig. 43. It may be noted that in every test the wrought Inconel container was more corrosion resistant than the cast Inconel. The anomalistic results indicate that more work should be performed on the cast Inconel–fused salt system.

HIGH-TEMPERATURE CORROSION RESISTANCE OF MOLYBDENUM AND HASTELLOY B TO RUBIDIUM

R. Carlander

Because of its desirable properties, low cross section (0.56 barns), low melting point (102°F), and high boiling point (1260°F), rubidium was chosen as a possible coolant in a "High-Temperature Vapor-Cycle Power Plant Study" conducted by a Reactor School study group. Since high temperatures were to be obtained in such a power plant, corrosion studies with rubidium were

TABLE 13. RESULTS OF NaF-ZrF_4-UF_4 (50-46-4 MOLE %) CAST INCONEL STATIC TESTS

Cast Inconel No.	Silicon Content (%)	Depth of Attack (mils)		Metallographic Notes of Cast Inconel
		Wrought Inconel Capsule	Cast Inconel Specimens	
321	1.04	4	12	Subsurface voids to depth of 4 mils, intergranular penetration to depth of 12 mils; no apparent cracks
322	1.93	2	3	Subsurface voids and intergranular penetration to depth of 3 mils; no apparent cracks
323	1.34	2	8	Subsurface voids to depth of 3 mils, intergranular penetration to depth of 8 mils; no apparent cracks

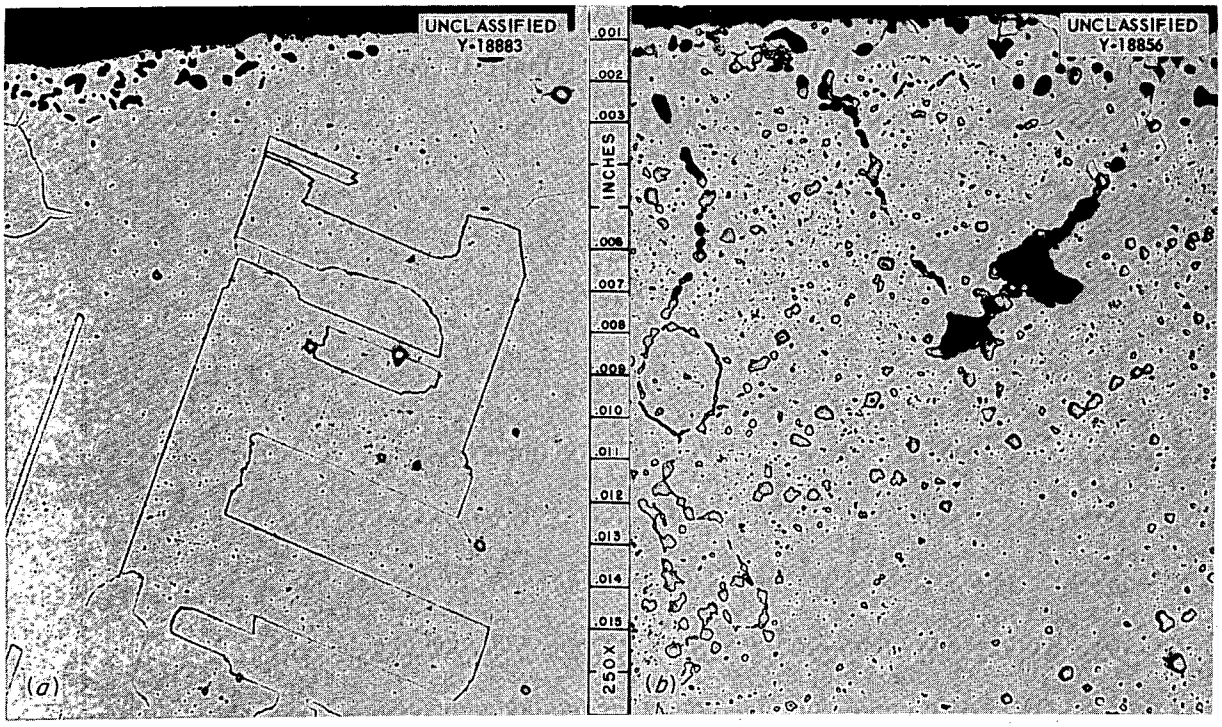

Fig. 43. (*a*) **Bath Zone of Wrought Inconel Capsule and** (*b*) **Cast Inconel Specimen No. 321 Tested Statically in NaF-ZrF_4-UF_4 (50-46-4 mole %) for 1000 hr at 1500° F.** Etchant: aqua regia. 250X. Reduced 11%. (Secret with caption)

undertaken on molybdenum and on alloys of the Ni-Mo type (Hastelloy B). Preliminary corrosion studies of Inconel in static and dynamic rubidium have been previously reported. Static tests of rubidium in Inconel at 1500 and 1650°F showed a maximum attack of 2 mils after 100 hr.[5] A boiling rubidium-Inconel thermal-convection loop which was operated at a hot-leg temperature of 1520°F produced no mass transfer but did produce an intergranular penetration in the hot leg to a depth of 1 mil after 312 hr.[6] Two standpipe tests of rubidium in Hastelloy B were performed for 500 hr at bath-zone temperature of 1400 and 1500°F (cold-zone temperatures for both tests, 1000°F). Tests of rubidium in Hastelloy B and rubidium in molybdenum were performed for 500 hr in a tilting type furnace (1 cpm). The hot zone of the Hastelloy B seesaw capsule was maintained at 1600°F (cold zone, 1000°F) and the hot zone of the molybdenum seesaw capsule was maintained at 1900°F (cold zone, 1350°F). The temperatures of the various portions of the test capsules and the results of metallographic examination are given in Table 14. No mass transfer occurred in any of the tests. The attack (½–2 mils) in the Hastelloy B standpipe tests (Fig. 44) was a combination of subsurface voids and intergranular penetration. The attack (1 mil) in the Hastelloy B seesaw capsule (Fig. 45) was in the form of subsurface voids. No attack occurred in the molybdenum seesaw capsule (Fig. 46), but an increase in grain size occurred on the outside surface of the hot zone. The results indicate that molybdenum and alloys of the Ni-Mo type would be suitable high-temperature containers for rubidium.

[5]E. E. Hoffman *et al.*, *ANP Quar. Prog. Rep. Sept. 10, 1954*, ORNL-1771, p 86.

[6]E. E. Hoffman, W. H. Cook, and C. F. Leitten, *ANP Quar. Prog. Rep. Dec. 10, 1954*, ORNL-1816, p 87.

TABLE 14. SUMMARY OF THE TEST CONDITIONS AND METALLOGRAPHIC EXAMINATION OF HASTELLOY B AND MOLYBDENUM CORROSION TESTS IN RUBIDIUM

Test	Temperature (°F)	Depth of Attack (mils)	Metallographic Notes
		Standpipe No. 1	
Hastelloy B			
Bath zone	1400	1	1 mil of voids and intergranular attack
Boiling zone	1535	1.5	1.5 mils of intergranular attack, 1 mil of voids
Vapor zone	815	0.5	0.5 mil of voids, no intergranular attack
		Standpipe No. 2	
Hastelloy B			
Bath zone	1500	2	2 mils of intergranular attack, 1 mil of voids
Boiling zone	1550	1.5	1.5 mils of intergranular attack, 1 mil of voids
Vapor zone	995	1	1 mil of voids, no intergranular attack
		Seesaw Test No. 1	
Hastelloy B			
Hot zone	1600	1	1 mil of voids, no intergranular attack
Cold zone	1000	1	1 mil of voids, no intergranular attack
		Seesaw Test No. 2	
Molybdenum			
Hot zone	1900	No attack	No attack, but recrystallization of grains on the outer surface of the hot zone
Cold zone	1350		

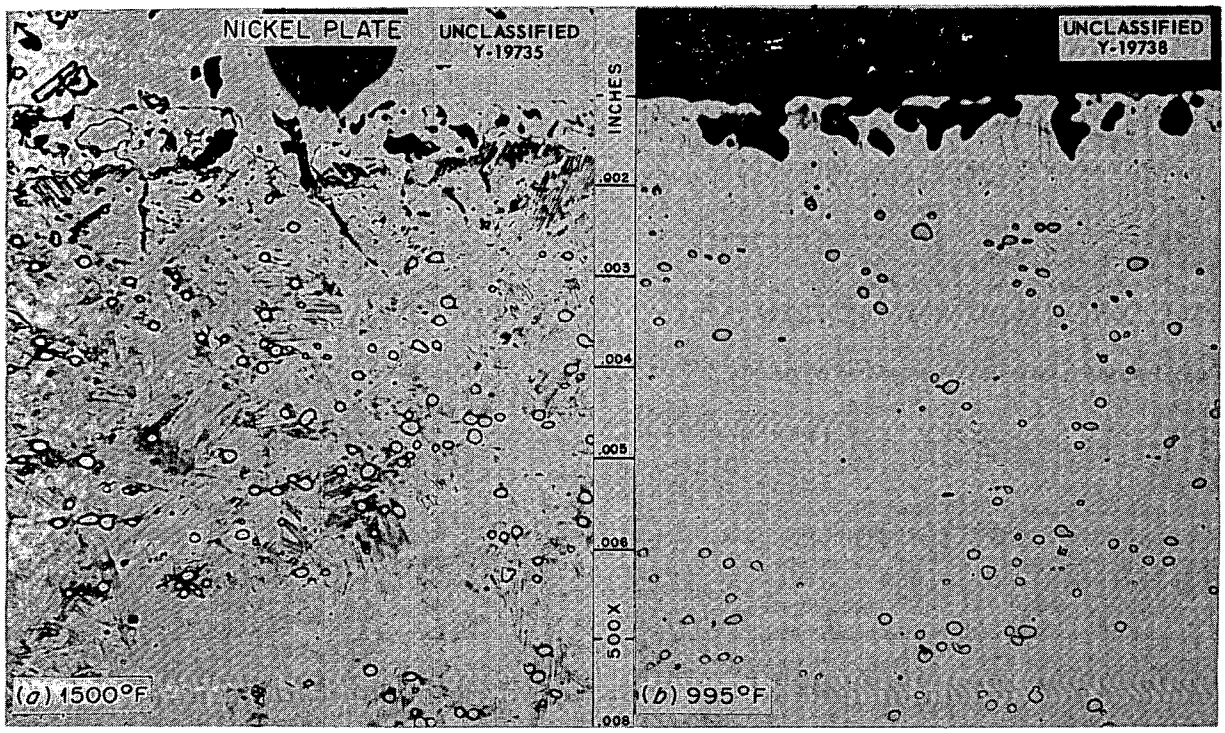

Fig. 44. (*a*) **Bath Zone and** (*b*) **Vapor Zone of Hastelloy B Standpipe Test No. 2 After Exposure to Rubidium for 500 hr.** Etchant: 80 cc H_2O_2–20 cc H_3PO_4. 500X. Reduced 4%. (Secret with caption)

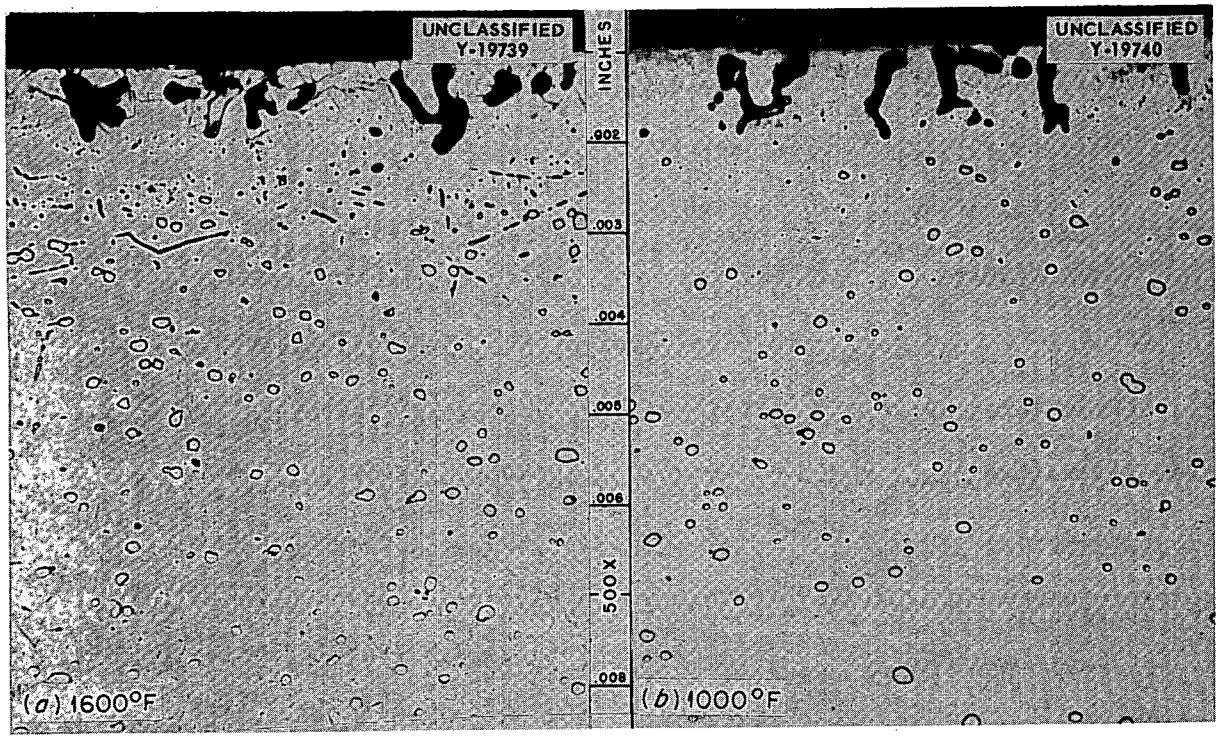

Fig. 45. (*a*) **Hot Zone and** (*b*) **Cold Zone of Hastelloy B Seesaw Capsule After Exposure to Rubidium for 500 hr at 1600°F.** Etchant: 80 cc H_2O_2–20 cc H_3PO_4. 500X. Reduced 4%. (Secret with caption)

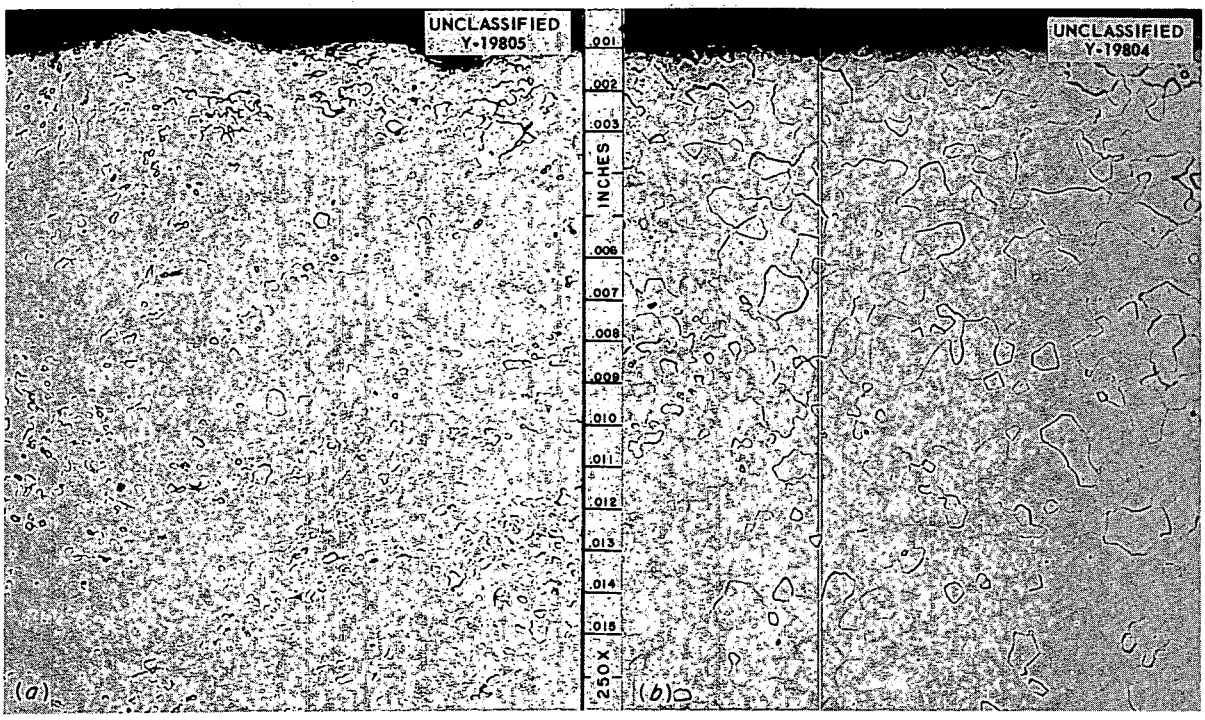

Fig. 46. (*a*) Inside Wall and (*b*) Outside Wall of the Hot Zone of the Molybdenum Seesaw Capsule After Exposure to Rubidium for 500 hr at 1900°F. Etchant: 40 cc H_2O_2; 50 cc NH_4OH. 250X. Reduced 11%. (Secret with caption)

THE CARBURIZATION OF VARIOUS ALLOYS BY MOLTEN SODIUM

E. E. Hoffman R. Carlander

The carburization and decarburization of various alloys by molten sodium contaminated with carbon has been observed. The carburization of stainless steel, for instance, results in precipitation at the grain boundaries of a complex iron-chromium carbide. The precipitation depletes the adjacent grain boundary areas in chromium, and thus forms areas of a different "stainless" composition. This phenomenon renders the grain boundaries more susceptible to intergranular corrosion. Hence, an effort was made to study the various factors that affect the carburization of various alloys by sodium.

Specimens (2 in. × 1 in. × $\frac{1}{8}$ in.) of Hastelloy B, and types 310, 316, and 430 stainless steel were measured, polished, and weighed prior to testing. The specimens were loaded into capsules of the same material, filled with sodium plus 1, 5, and 10 wt % additions of graphite, and sealed under vacuum. The capsules were then tested in static sodium at 1500°F for 100 hr. Upon completion of the tests, the specimens were removed from the capsules, cleaned and weighed, and a portion of each was analyzed chemically and metallographically. The results of the chemical analyses are presented in Table 15. The results of metallographic examination are given in Table 16.

Of the four materials tested, Hastelloy B and type 310 stainless steel (Figs. 47*a* and 48*a*) exhibited the least amount of carburization, while types 430 and 316 stainless steel (Figs. 47*b* and 48*b*) were heavily carburized.

Figure 49, a compilation of all the data, clearly illustrates that type 430 stainless steel was the alloy most susceptible to carburization. Also, the depth of carburization of the stainless steels increased with increasing graphite additions but leveled off for Hastelloy B. Furthermore, although the depth of carburization of type 316 stainless

TABLE 15. CARBON ANALYSIS, TOTAL CARBON PICKUP, AND TOTAL WEIGHT CHANGE OF VARIOUS ALLOYS AFTER EXPOSURE TO SODIUM AND GRAPHITE FOR 100 hr AT 1500°F

Capsule Material	Nominal Composition (wt %)	Graphite Added to Sodium (wt %)	Carbon Found in 3-mil Surface Cut (wt %)	Total Carbon Pickup (mg)	Total Weight Change of Specimen (mg)
Hastelloy B	28 Mo–5 Fe–0.12 C max–bal Ni	1	0.680	2.6	25.8
		5	0.577	16.4	46.8
		10	1.118	22.4	47.1
Type 310 stainless steel	25 Cr–20 Ni–0.25 C max–bal Fe	1	0.388	0.5	39.3
		5	0.994	8.8	47.2
		10	1.43	No analyses	55.5
Type 316 stainless steel	17 Cr–12 Ni–0.10 C max–bal Fe	1	0.606	10.1	48.1
		5	1.09	30.7	90.6
		10	2.35	50.2	119.3
Type 430 stainless steel	16 Cr–0.12 C max–bal Fe	1	0.267	10.7	36.3
		5	1.30	25.2	81.3
		10	1.47	55.4	153.4

TABLE 16. METALLOGRAPHIC EXAMINATION OF VARIOUS ALLOYS AFTER EXPOSURE TO SODIUM WITH GRAPHITE ADDITIONS FOR 100 hr AT 1500°F

Carbon Added to Sodium (wt %)	Depth of Carburization (mils)			
	Hastelloy B	Stainless Steels		
		Type 310	Type 316	Type 430
1	5	2	0–10 (varied over the surface)	4
5	8	4	10	10
10	8	6	13	24

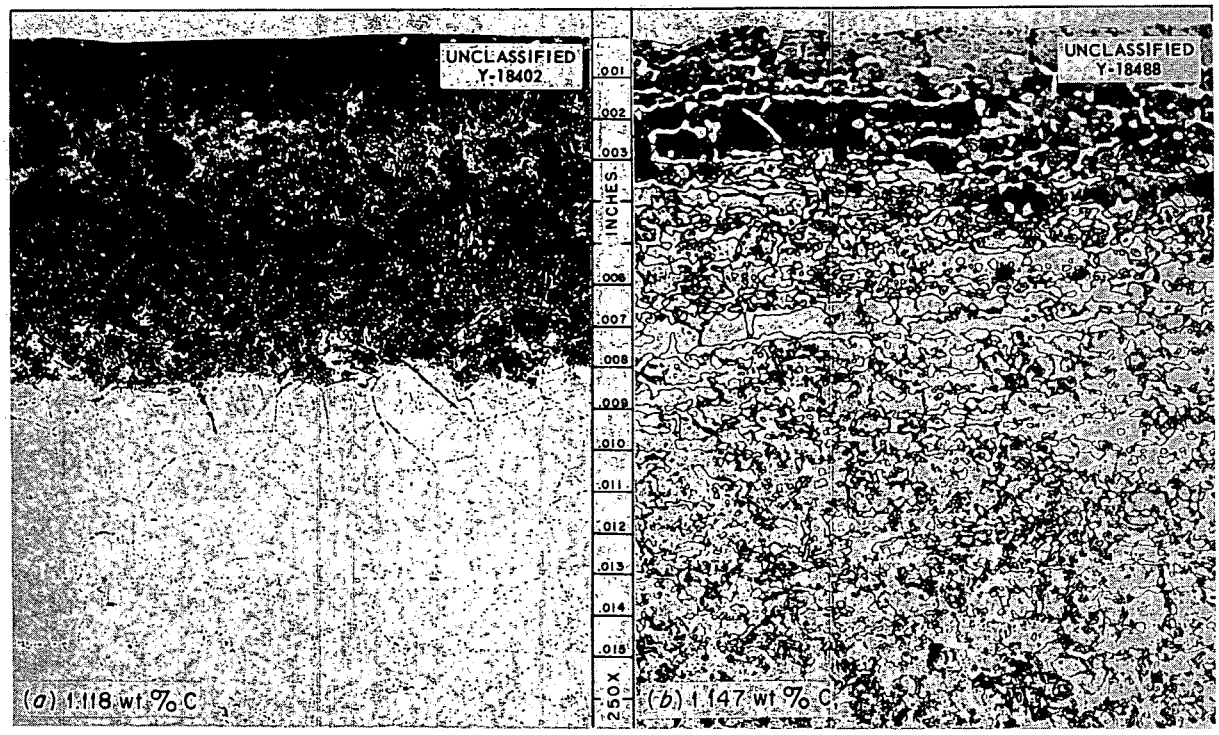

Fig. 47. (*a*) Hastelloy B and (*b*) Type 430 Stainless Steel After Exposure to Sodium + 10 wt % Graphite for 100 hr at 1500°F. Etchant: (*a*) phosphoric acid–H_2O_2 and (*b*) glyceria regia. 250X. Reduced 11%.

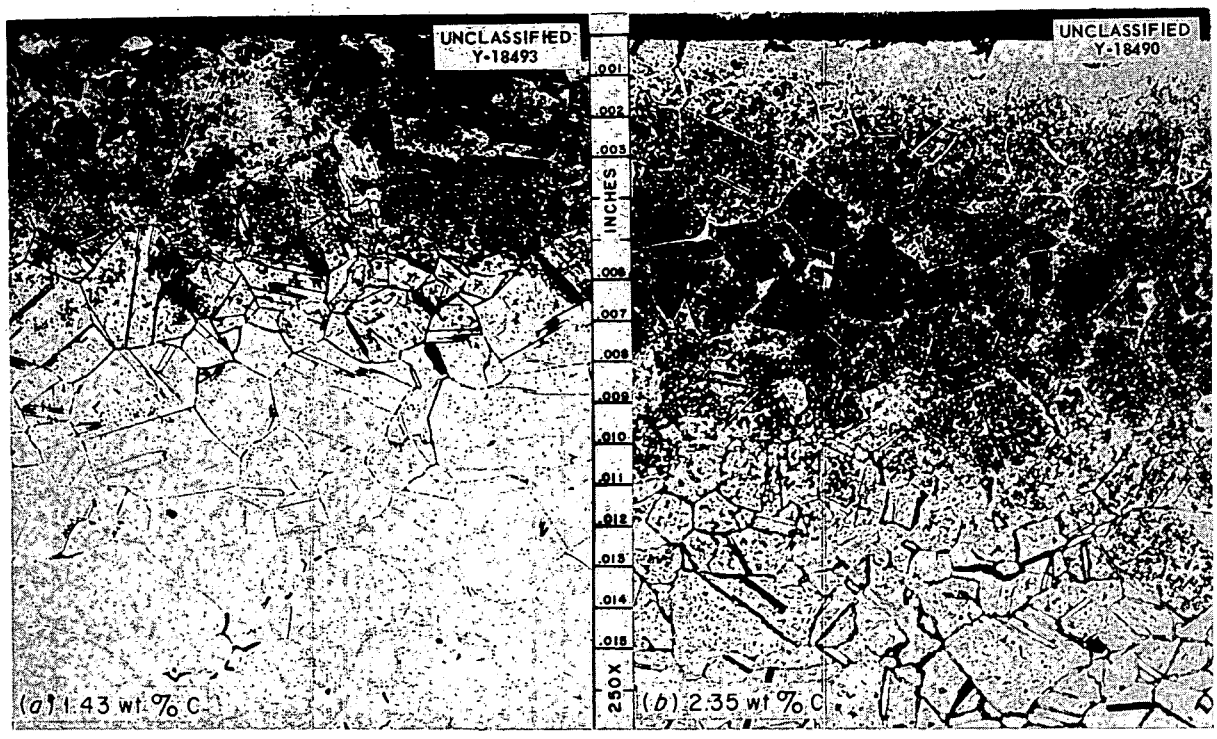

Fig. 48. (*a*) Type 310 and (*b*) Type 316 Stainless Steel After Exposure to Sodium + 10 wt % Graphite for 100 hr at 1500°F. Etchant: glyceria regia. 250X. Reduced 11%.

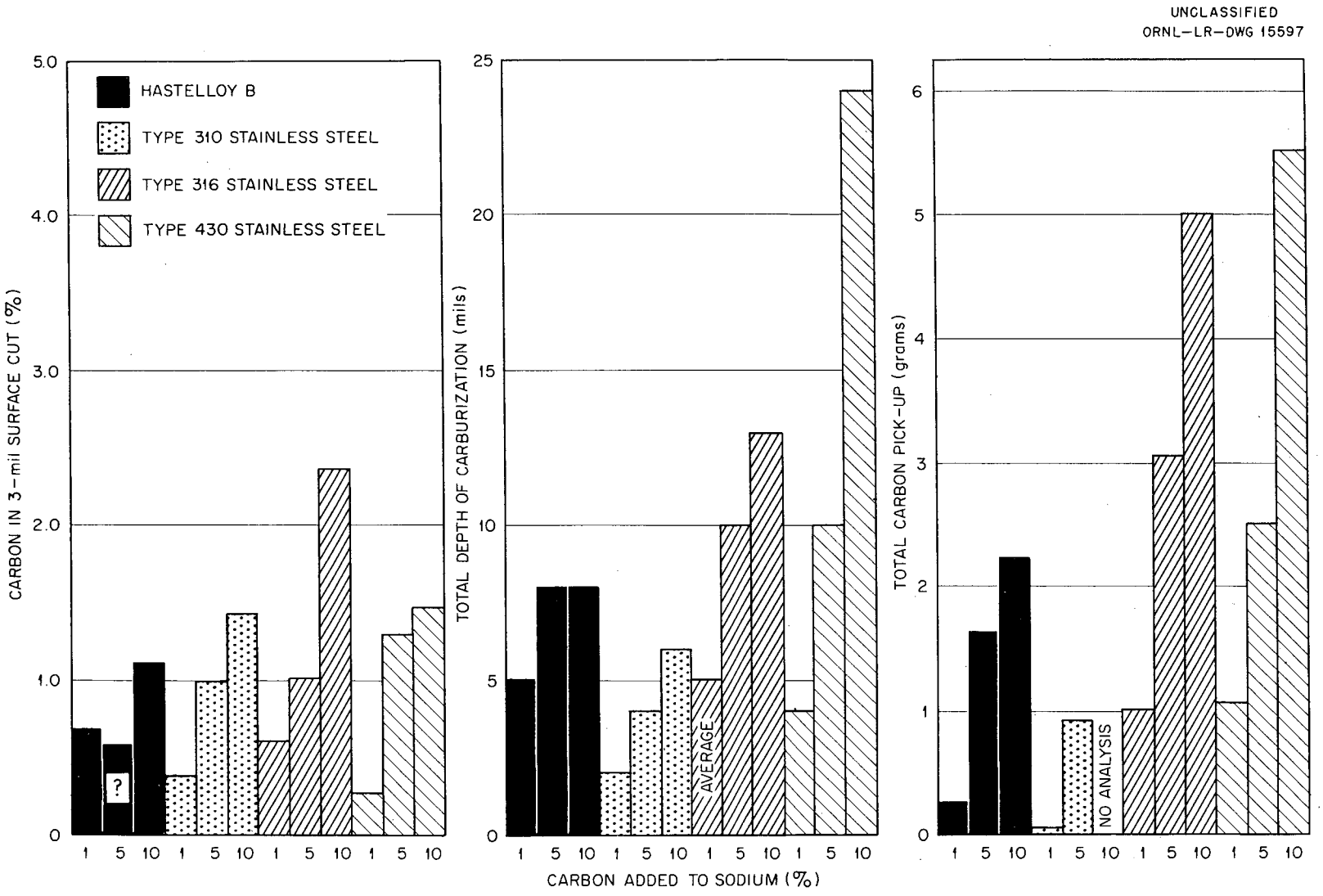

Fig. 49. Carburization of Various Alloys as a Function of the Per Cent Carbon Added to the Sodium.

steel was less than that of type 430 stainless steel, the total amount of carbon pickup was approximately on the same level.

CORROSION OF INTERMETALLICS BY STATIC SODIUM AND FUSED SALTS

W. H. Cook

Intermetallics of NiAl, NiAl + 5% Ni, NiAl + 4% Zr, and MoAl have been tested for 100 hr in static sodium and in static NaF-ZrF_4-UF_4 (53.5-40.0-6.5 mole %) at 1500°F. No attack was found on the specimen tested in the sodium. Those tested in the fused salt were severely attacked. Table 17 is a summary of the test results which were obtained by metallographic comparisons of untested and tested specimens. Chemical analyses of the test media are being made.

All the intermetallics had a common phase that may have been an oxide added by the fabricator for strengthening purposes.[7] This phase constituted less than 5% of the surface of any sectioned intermetallic. It was homogeneously distributed in all specimens with the exception of the NiAl + 5% Ni, in which some segregation was apparent. In addition to this common phase, all the intermetallics had one major phase except for the NiAl + 4% Zr, which contained two additional phases.

In the NiAl + 4% Zr, the major phase was present as well-bonded globular particles, and the three minor phases were located in the few open spaces between the particles of the major phase. The NiAl + 5% Ni specimens were the only ones in which any porosity was found, and it was negligible in these.

For the NiAl-base intermetallics the fused-salt attack was most likely due to the aluminum; the attack began intergranularly and advanced into the grains. The differences in the extent of the fused-salt attacks on the NiAl-base intermetallics were probably caused by differences in the accessibility of the NiAl to the fused salt. In the NiAl + 5% Ni specimen, it was noted that the attack was most severe where the "oxide" phase was concentrated. It was assumed that oxide was quickly corroded away which allowed the fused salt to attack the intermetallic.

The severe attack in the case of the NiAl + 4% Zr can probably be explained by the removal of both the common phase and zirconium. These corrosion tests indicate that the NiAl in the NiAl-base intermetallics was attacked whenever it was exposed to NaF-ZrF_4-UF_4 (53.5-40.0-6.5 mole %) at 1500°F.

[7] G. Stern, *Refractory Type Materials for High Temperature Application*, NP-4527, p 139–40 (Aug. 1953).

TABLE 17. SUMMARY OF THE RESULTS OF INTERMETALLICS TESTED FOR 100 hr IN STATIC NaF-ZrF_4-UF_4 (53.5-40.0-6.5 MOLE %) AT 1500°F

Intermetallic	Attack (mils)			Notes
	Max	Av	Min	
MoAl				Quantitative measurements could not be made on the MoAl because of its extreme brittleness, but visual examination indicated that it had been attacked by the fused salt
NiAl	20	15	8	Attacked; attack produced alternate zones (bands) of degrees of porosity parallel to the surfaces of the specimen
NiAl + 5% Ni	32	8	3	Attacked; one end of specimen did not appear to be bonded as well as the remainder; maximum attack was found here
NiAl + 4% Zr	74	61	49	Attacked; attack severe to the depths indicated but was most severe along the edges for an average depth of 6 mils

The poor corrosion resistance of these intermetallics in the fused salt obviates further tests in this medium. However, the results of the sodium tests are encouraging enough to warrant more severe corrosion tests in this media.

POROSITY OF RARE-EARTH-OXIDE CERAMICS TO WATER AND TO MOLTEN SODIUM

W. H. Cook

The testing of ceramics of 45.0 to 49.5% Sm_2O_3–22.5 to 27% Gd_2O_3–bal primarily other rare-earth oxides (this was taken from the nominal composition given by the Lindsay Chemical Co. for their Code 920) for their porosity to water and to molten sodium has been completed. This is part of the work being done in the evaluation of these rare-earth-oxide ceramics for reactor-control-rod use. The results of these porosity studies are summarized in Table 18.

The sodium from the 500-hr test has been submitted for chemical analysis. The most adverse service conditions expected were used in the 500-hr test. Corrosion tests on shapes made from these rare-earth oxides have indicated negligible attack by sodium.[8] By assuming that the ceramic was not attacked in the sodium permeability tests and by using the density of sodium at its melting point, the porosity of the ceramic to sodium was calculated.

The chemical analysis of the sodium from the 500-hr test plus investigations being made on similar 1000- and 2000-hr corrosion should provide the necessary data to explain the differences in the water and the sodium porosities obtained for the 100- and 500-hr sodium permeability tests.

[8]W. H. Cook, *ANP Quar. Prog. Rep. June 10, 1956*, ORNL-2106, p 155.

SOLID-PHASE-BONDING SCREENING TESTS

W. H. Cook

Solid-phase-bonding screening tests have been made with cermets K150A (80% TiC–10% $NbTaTiC_3$–10% Ni) and K152B (64% TiC–6% $NbTaTiC_3$–30% Ni) in contact with molybdenum at 20,000 psi (calculated) for 100 hr in NaF-ZrF_4-UF_4 (50-46-4 mole %) at 1500°F. Bonding between K152B and molybdenum was observed with a low-power microscope. A thin film appeared to have been "transferred" in the contact area between the molybdenum and K152B. This was probably a Ni-Mo diffusion layer, but this has not been verified. In similar examinations of the contact areas of K150A and molybdenum, there was a thin black film observed in some areas on K150A, but there were no signs of solid-phase bonding. There was some deformation of the molybdenum in the contact areas.

No solid-phase bonding was observed for Stellite 6 in contact at 50,000 psi (calculated) with Stellite 6 for 200 hr in sodium at 1200°F. The Stellite 6 formed a $\frac{3}{16}$-in.-thick hard facing on Inconel specimens. There was only slight deformation of the Stellite 6 facings in the areas of contact. In some places outside the seating areas, the Stellite 6 appeared to be roughened by an etching effect.

TABLE 18. THE PERMEABILITY OF CERAMICS OF 45.0 TO 49.5% Sm_2O_3–22.5 TO 27% Gd_2O_3 (BAL PRIMARILY OTHER RARE-EARTH OXIDES) TO WATER AND TO MOLTEN SODIUM

Nominal Dimensions (in.)			Test Conditions in Sodium		Density[a] (g/cc)	Apparent Porosity (%)	
OD	ID	Length	Temperature (°F)	Time (hr)		To Water[a]	To Sodium
$\frac{7}{8}$ ×	$\frac{1}{2}$ ×	1[b]	1300	100	3.53	53.5	52
$1\frac{1}{4}$ ×	$\frac{3}{4}$ ×	1	1350[c]	500[c]	4.09	46.4	51.0

[a]The ceramic laboratory of the Metallurgy Division fabricated all test pieces and determined their densities and apparent porosities to water.

[b]The data on this piece have been reported previously (W. H. Cook, *ANP Quar. Prog. Rep. June 10, 1956*, ORNL-2106, p 155).

[c]The temperature was constant at 1350°F for the first 250 hr; during the concluding 250 hr, the temperature was cycled between 1350 and 1100°F three times each day in 3-hr periods.

DYNAMIC CORROSION

J. H. DeVan E. A. Kovacevich

FORCED CIRCULATION CORROSION STUDIES

J. H. DeVan

Fluoride Pump Loops

Further studies have been directed toward the interplay of loop surface area and loop volume in the corrosion of Inconel-fluoride systems. The fluorides circulated in these tests were mixtures of NaF-ZrF_4-UF_4 (50-46-4 mole %) designated as fuel 30. A relatively large cold-leg surface was employed in loop 7425-8 to evaluate effects contributed by the cold zone to the mass transfer of chromium in such systems. A tube bundle, composed of a top and bottom header with five connecting coils of $\frac{1}{4}$-in.-dia tubing, was used in place of a standard-size cooling coil of $\frac{1}{2}$-in. tubing[1] and resulted in a doubling of cold-leg surface over that of a standard loop. The volume of the cold leg was held, insofar as possible, the same as that for a standard loop, so that total loop volume would be unchanged.

A standard pump loop, 7425-10, operated concurrently with this loop and was designed as a control loop both for 7425-8 and for several previously-run series such as wall-temperature, temperature-gradient, and surface-area-to-volume experiments. Both 7425-8 and 7425-10 were intended to operate at a 1600°F maximum wall temperature with other conditions shown in Table 19. However, the loops after operation were found to have identical discrepancies in the recorders used to measure maximum wall temperature, resulting in a revised value of 1580°F. While a good comparison can still be made between these two tests, the lower wall temperature somewhat handicaps the use of 7425-10 as a standard loop for other test series.

[1] J. H. DeVan and E. A. Kovacevich, *Met. Semiann. Prog. Rep. April 10, 1956*, ORNL-2080, p 53.

TABLE 19. OPERATING CONDITIONS OF INCONEL PUMP LOOPS WHICH CIRCULATED NaF-ZrF_4-UF_4 (50-46-4 MOLE %)

Operating Conditions	Loop Number			
	7425-41	7425-43	7425-8	7425-10
Operating time, hr	1000	1000	1000	1000
Maximum fluoride mixture temperature, °F	1650	1500	1500	1500
Fluid temperature gradient, °F	200	200	200	200
Maximum tube wall temperature, °F	1700	1700	1580	1580
Reynolds number	2750	6500	10,000	10,000
Velocity, fps	2.06	4.47	6.5	6.5
Heater surface area, $in.^2$	262	262	262	262
Cooler surface area, $in.^2$	247	247	542	247
Ratio of cooler surface area to total loop volume, $in.^2/in.^3$	2.0	2.0	4.2	2.0
Ratio of heater surface area to total loop volume, $in.^2/in.^3$	2.1	2.1	1.94	2.1
Maximum attack, mils	10	9	4	$4\frac{1}{2}$

A maximum attack of 4 mils occurred in the case of loop 7425-8, which compares quite closely to an attack of 4½ mils in standard loop 7425-10. Cold-leg deposits were absent in both loops, and fuel analyses after test showed equivalent chromium contents, approximately 400 ppm. Thus the increase in cold-leg surface over the range of these tests produced no apparent effect on corrosion.

Some increase in the amount of mass transfer with increased cold-leg surface was expected on the basis of thermodynamic studies in fluoride salts of pure chromium and chromium in Inconel. These studies predict that mass transfer of Inconel in zirconium base fluorides should be rate-controlled, in part, by the amount of deposited chromium which can diffuse into the cold leg.[2] Such a process is related directly to cold-zone surface.

Examination has been completed of pump loop 7425-43, which is part of a series to study effects of bulk fluoride temperature on the corrosion of Inconel. The loop circulated the mixture NaF-ZrF_4-UF_4 (50-46-4 mole %) and operated with a 1700°F maximum wall temperature, a 1500°F maximum fluid temperature, and a 200°F fluid temperature drop. Another loop in this series, 7425-41, which was reported previously,[3] was operated at a similar maximum wall temperature and temperature drop but with a maximum fluid temperature of 1650°F. Other conditions for these two loops are compared in Table 19.

The maximum attacks recorded in both loops occurred in the regions of maximum wall temperature. As shown in Figs. 50 and 51, the attacks were quite similar, reaching 9 mils in the case of the 1500°F fluid temperature and 10 mils at 1650°F. The levels of chromium in solution in both loops, which are shown in Table 20, were also comparable, the value at 1500°F actually being the greater. If variations in Reynolds number are neglected, as argued in previous reports,[4] the small effect resulting from changes in bulk fluoride temperature in these tests is apparently explained by the similarity in maximum wall temperatures. The importance of this latter variable to corrosion in fluoride systems has been discussed previously.[1]

[2]W. R. Grimes, *ANP Quar. Prog. Rep. June 10, 1956*, ORNL-2106, p 96, esp 98–99.

[3]J. H. DeVan and E. A. Kovacevich, *Met. Semiann. Prog. Rep. April 10, 1956*, ORNL-2080, p 56.

[4]*Ibid.*, p 61.

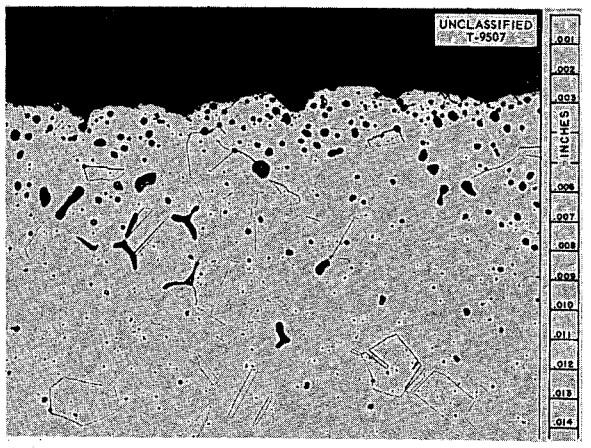

Fig. 50. Maximum Attack in Inconel Loop 7425-43, Operated 1000 hr with a 1700°F Maximum Wall Temperature, 1500°F Maximum Fluid Temperature. 250X. Reduced 36.5%.

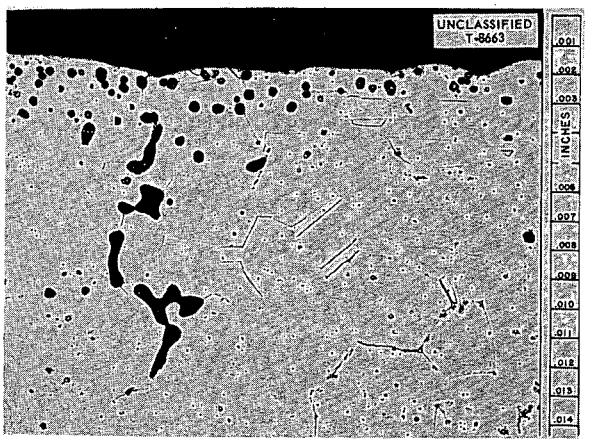

Fig. 51. Maximum Attack in Inconel Loop 7425-41, Operated 1000 hr with a 1700°F Maximum Wall Temperature, 1650°F Maximum Fluid Temperature. 250X. Reduced 36.5%.

TABLE 20. CHEMICAL ANALYSES OF FUEL CIRCULATED IN LOOPS 7425-41 AND 7425-43

Loop No.	Sample	U (%)	Ni (ppm)	Cr (ppm)	Fe (ppm)
7425-41	Fill	8.61	40	105	45
	Drain	10.3(?)	40	440	70
7425-43	Fill	9.20	50	55	70
	Drain	9.37	100	650	80

Two Inconel pump loops have been operated for 1000 hr with fuel No. 70, a fluoride mixture comprised of NaF-ZrF_4-UF_4 (56.0-39.0-5.0 mole %). The purpose of these tests was to compare the corrosion properties of this fuel mixture with those of the more familiar fuel No. 30. The lower ZrF_4 content in fuel 70 affords a considerable reduction in vapor pressure at reactor operating temperatures as compared to fuel 30.

The conditions of operation for these two loops, 7425-14 and 7425-15, are listed in Table 21. Operation of the loops, including the cleaning procedure, followed a pattern identical to that employed for Inconel–fuel 30 tests. Visual examination of loop 7425-14, which was operated with a 1500°F maximum fluid temperature, showed the presence of a few very small metallic crystals in the top section of the cooling coil and along the fluid–inert gas interface in the pump. These crystals, based on spectrographic examination, analyzed >5% Cr, >5% Zr, 2% Ni, and 0.2% Fe. Although fuel undoubtedly comprised a large portion of the crystals, the presence of chromium affords an indication of possible mass transfer. However, no crystals could be found in the examination of loop 7425-15, which operated with a temperature gradient similar to that of 7425-14 but at a higher fluid temperature (1650°F).

Maximum hot-leg attack, observed metallographically, was approximately the same for both loops, being reported as 7 mils. The attack occurred as light-to-moderate void formation, as shown in Fig. 52. A very thin metallic layer was noted in the cold legs of both loops and is pictured in Fig. 53. The layer is barely visible at the magnification of 500X used and is thus seen to be quite small. An analysis of this layer was not possible.

Analyses of fuel samples taken before and after operation are shown in Table 22.

Fig. 52. Hot-Leg Surface of Loop 7425-14 After Exposure to Fuel 70 at 1500°F. 250X. Reduced 34.5%. (Secret with caption)

TABLE 21. OPERATING CONDITIONS OF FLUORIDE PUMP LOOPS

Operating Conditions	Loop Number		
	7425-12	7425-14	7425-15
Loop material	Hastelloy B	Inconel	Inconel
Fluoride mixture	107	70	70
Operating time, hr	1000	1000	1000
Maximum fluoride mixture temperature, °F	1505	1525	1643
Temperature gradient, °F	200	200	200
Maximum tube wall temperature, °F	1555	1595	1712
Reynolds number	10,000	10,000	9500
Velocity, fps	3.2	4.8	2.6
Ratio of hot-leg surface to loop volume, $in.^2/in.^3$	2.08	2.08	2.08

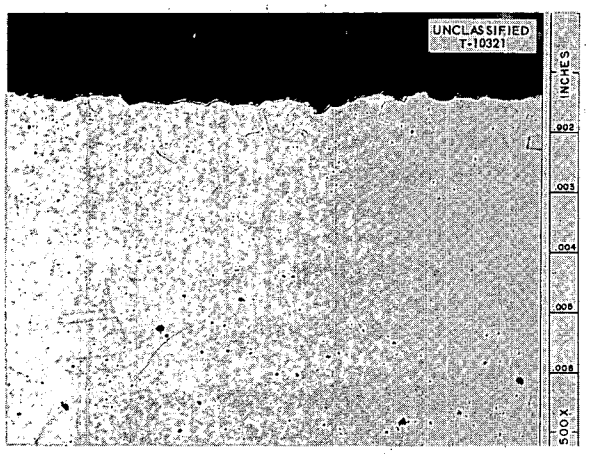

Fig. 53. Thin Layer Seen in Cold-Leg Specimen from Loop 7425-15.

TABLE 22. CHEMICAL ANALYSES OF FUEL CIRCULATED IN LOOPS 7425-14 AND 7425-15

Loop No.	Sample	Total U (%)	Ni (ppm)	Cr (ppm)	Fe (ppm)
7425-14	Fill	11.2	15	85	50
	Termination	11.4	30	290	90
7425-15	Fill	11.1	95	90	35
	Termination	11.6	4	255	110

Note that a buildup of chromium has occurred over the test period, although the termination samples showed somewhat less chromium than samples taken from loop 7425-10 reported above, which operated with fuel No. 30 under comparable conditions.

These results are in agreement with solubility measurements made by Materials Chemistry Division which indicate that decreases in zirconium content from the fuel 30 level will reduce slightly the equilibrium concentration of chromium.

The similarity in attacks in the two loops, which operated at different temperatures, is felt to have limited significance. Loops 7425-41 and 7425-10 (reported above), which operated under comparable conditions to these two loops but with fuel 30, revealed attacks of 4½ mils at the lower temperature and 9 mils at the higher temperature. The figure of 7 mils reported for both tests with fuel 70 does not represent an abnormally large deviation from either of these values obtained for fuel 30. Therefore the corrosion properties of fuel 70, in general, appear similar to those of fuel 30, although some tendency for layer formation in the cold leg appears to accompany the former fuel.

The operation of a Hastelloy B pump loop (7425-13) has verified the excellent corrosion resistance of this alloy to fluorides observed in thermal-convection-loop tests. The loop was constructed of ½-in.-OD × 0.035-in.-wall tubing and was identical in configuration and manner of heating to the standard loop design presently employed for Inconel corrosion tests. Operating conditions of the loop are given in Table 21. The fluoride mixture circulated was NaF-KF-LiF-UF_4 (11.2-41-45.3-2.5 mole %), designated as fuel 107.

Very little attack was seen on examination of this loop. Some pitting to a maximum depth of 1½ mils was observed along both the hot and cold legs, but the surfaces were quite similar to those of as-received tubing, as illustrated in Fig. 54. No deposits were found metallographically either in the hot or cold legs of the loop. A visual examination of the cold leg revealed small metallic-appearing deposits in one area, although on the basis of metallographic examination these appear to have been fluorides rather than metallic crystals.

Chemical analyses of the fuel before and after operation are tabulated in Table 23.

A small pickup in chromium, possibly reflecting small residuals of this element in the tubing or in the welds, and in iron may be noted together with a decrease in nickel. A molybdenum analysis was not obtained for the fuel before test, although this element would not seem to have been affected to a measurable degree during the test.

The operation of an Inconel pump loop, conducted as an endurance test with fuel 30, terminated because of a pump drive failure after 8300 hr. This failure resulted in a subsequent leak in the cold leg while the loop was being thawed to re-establish operation. The loop, 4935-6, was gas-fired and operated with a maximum fluoride temperature of 1450°F, a temperature drop of 200°F, a maximum wall temperature of 1550°F, and a Reynolds number of 10,000. Following the test the hot-leg surface was shown metallographically to be roughened with heavy intergranular void formation to a depth of 25 mils. The cold-leg

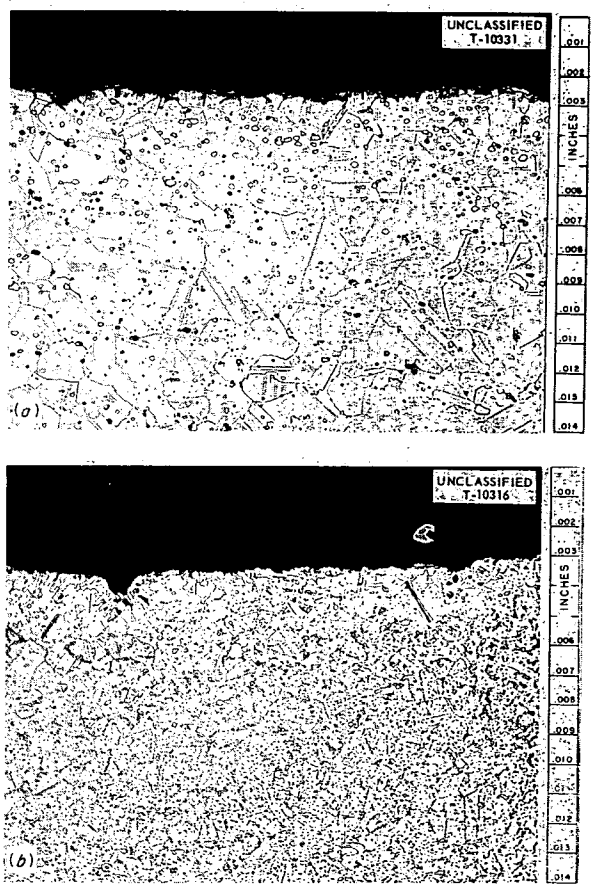

Fig. 54. Hastelloy B As-received Tubing (*a*) and Hot-Leg Sample (*b*) from Loop 7425-13 After Exposure to Fuel 107 for 1000 hr. Note increased amount of second phase resulting from aging at 1500°F. 250X. Reduced 35.5%. (Secret with caption)

surface was roughened with no evidence of mass-transferred deposits.

A second test involving an Inconel pump loop of relatively long duration was conducted by using electrical-resistance heating. This loop, 7425-9, also circulated fuel No. 30 and operated for 3000 hr. The maximum and minimum fluid temperatures employed were 1600 and 1300°F, respectively, with a Reynolds number of 5750. Wall temperature reached a maximum of 1700°F. Maximum attack in this loop was reported to be 14 mils, occurring in the area of highest wall temperature. Visual and metallographic examination revealed no deposits attributable to mass transfer in the cold zones.

TABLE 23. CHEMICAL ANALYSES OF FUEL CIRCULATED IN LOOP 7425-13

Sample	Total U (%)	Ni (ppm)	Cr (ppm)	Fe (ppm)	Mo (ppm)
Operating fill	12.5	215	35	60	
Terminating sample	13.2	80	195	105	7

The chromium buildup in the fuels during the course of operation in both the above loops was comparable to loops of 1000-hr durations. This fact agrees well with observations in a previous report[5] on the effect of time on fluoride corrosion. However, in this earlier report the rate of attack noted from 50 to 1000 hr was approximately 3-4 mils per 1000 hr and was constant with time. During the first 50 hr of operation, attack occurred at a much faster rate and gave rise to a threshold value of approximately 3 mils. A rate of 3-4 mils per 1000 hr, when added to an initial attack of 3 mils and extrapolated to times comparable to those of the above long-duration loops, gives a range of attacks considerably higher than those experimentally recorded for the loops. Thus it appears that the rate of attack does not remain linear with time beyond 1000 hr but tends to decrease; however, the operating conditions of the loops unfortunately are not similar enough to provide a comprehensive study of this decrease.

Sodium Pump Loops

An Inconel pump loop, 7426-6, has completed 1000 hr of operation with sodium which had been specially treated to remove oxide contamination prior to testing. Operating conditions for the loop were a 1500°F maximum fluid temperature and a 300°F temperature drop. Prior to the actual test, sodium was circulated through the loop under 1500°F isothermal temperature conditions to remove oxide films from both the hot and cold legs of the loop. This sodium was then dumped at 1500°F and replaced by a charge which had been cold-trapped and filtered in a service loop operated at 300°F. A circulatory cold trap maintained at 300°F was also used on this charge during the course of the

[5] J. H. DeVan and E. A. Kovacevich, *Met. Semiann. Prog. Rep. April 10, 1956*, ORNL-2080, p 53.

test. An evaluation of mass transfer in this loop showed the weight of deposit (15 g) to be equivalent to loops operating with normal sodium either with or without circulatory cold traps. Maximum thickness of this deposit was 18 mils; the hot leg showed heavy pitting and intergranular attack to a depth of 2 mils.

A relatively heavy deposit, also predominantly nickel, was found in Inconel loop 7426-12, operated at 1500°F with a temperature gradient of 400°F. The loop included a cold trap identical to that mentioned above. Deposits appeared predominantly in the economizer section of this loop, reaching thicknesses of 20 mils, as shown in Fig. 55. Intergranular attack in the hot zone was 2 mils. When scraped from the loop walls, the deposits were measured to be 21 g. This value is substantially higher than the value of 15 g reported above and would indicate temperature drop to be a more significant variable than found in earlier 500-hr tests.[6] In the case of both the above loops, deposits were analyzed to be approximately 10% Cr and 90% Ni.

An Inconel pump loop, 7426-11, which circulated sodium at a maximum temperature of 1350°F, revealed only scattered metal deposits in cold-zone sections after 1000 hr of operation. The loop employed a fluid temperature drop of 300°F and contained a bypass cold trap operated at 300°F. Deposits reached a maximum thickness of 3 mils, as shown in Fig. 56, and were also analyzed to be predominantly nickel. The hot leg of the loop showed slight intergranular attack to a depth of ½ mil. Comparing this loop with the above loop, it is seen that the amount of Inconel mass transfer is considerably more at 1500°F than at 1350°F.

A 316 stainless steel loop, 7426-14, has been operated 1000 hr with sodium at a maximum temperature of 1650°F. An examination of this loop, which employed a 300°F temperature drop, showed very little increase in mass transfer compared to a similar loop operated at 1500°F, described previously.[5] Deposits appeared as occasional clusters of metal crystals 3–5 mils thick and comprised a total weight of 1.7 g. An analysis of the deposits showed the following elements present: 5.5% Ni, 72.4% Cr, 22.0% Fe. The hot leg was attacked intergranularly to 2 mils, with small voids appearing to a depth of 5 mils. A loop of 310 stainless steel, 7426-13, run under similar conditions but at a maximum temperature of 1500°F, showed substantially more extensive deposits than the above

[6] G. M. Adamson *et al.*, *Met. Semiann. Prog. Rep. Dec. 10, 1955*, ORNL-1988, p 25.

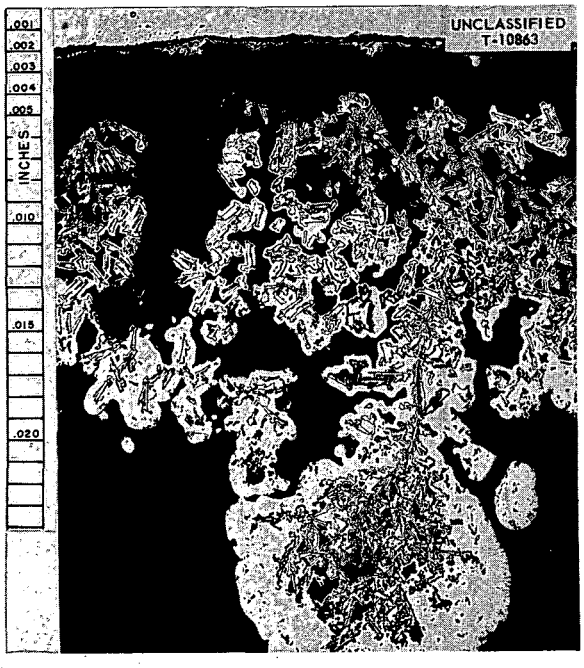

Fig. 55. Deposits Found in Inconel Pump Loop 7426-12 Operated with Sodium at 1500°F. 150X. Reduced 22%.

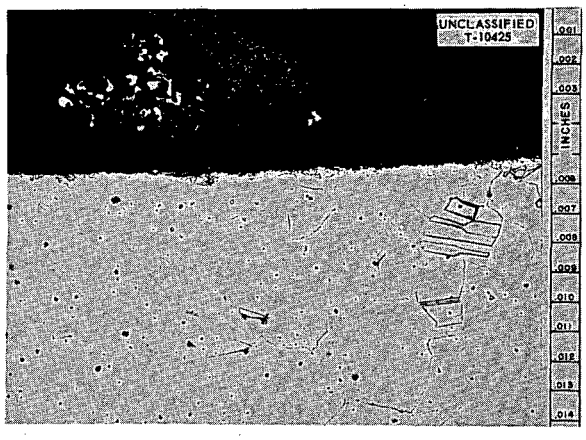

Fig. 56. Deposits Found in Inconel Pump Loop 7426-11, Which Circulated Sodium at 1350°F. 250X. Reduced 36%.

316 stainless steel loop. The total mass comprised by the deposit was only 2.25 g, although the deposit thickness reached 9 mils. Hot-leg attack in this loop was quite severe, with intergranular attack and void formation reaching 13 mils, as pictured in Fig. 57.

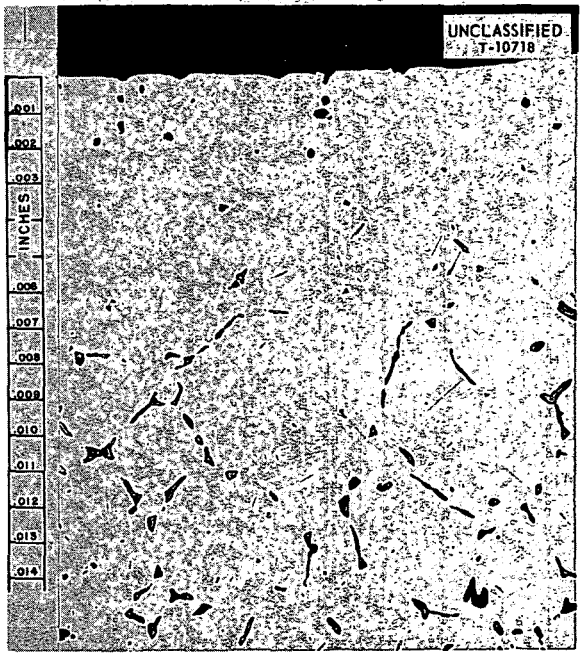

Fig. 57. Hot-Leg Attack in Type 310 Stainless Steel Loop After 1000 hr Operation with Sodium at 1500°F. 250X. Reduced 22%.

Sodium-Beryllium-Inconel Compatibility

Two Inconel pump loops have been operated at 1250 and 1300°F, respectively, with beryllium inserts contained in the hot legs. The insert was machined in the form of a hollow cylinder 2½ in. long and contained an Inconel island concentric within the insert. The insert was separated from the loop wall by a distance of 0.040 in. along one inch of its length and by 0.094 in. along another inch. The remainder of the insert was in direct contact with the Inconel. The Inconel island was spaced ¼ in. from the inside diameter of the insert. Following 1000-hr operation at the higher temperature, the beryllium insert revealed scattered void formation to 7 mils. Alloying between the beryllium and Inconel in contact with it produced a brittle layer approximately 3½ mils thick. In areas where a positive separation between the beryllium and Inconel was maintained, no attack or alloying was seen on the Inconel. In the lower temperature loop, also operated for 1000 hr, void formation in the beryllium progressed to 5 mils. Alloy formation between beryllium and Inconel was not reported even in areas assumed to be in direct contact. However, related compatibility studies would tend to indicate that alloyed products may have been lost in metallographic sampling. Both of the above loops operated with cold traps maintained at 300°F. No mass-transferred particles or layers were produced in either loop.

To determine whether increasing the beryllium surface area relative to Inconel will affect the compatibility of these materials in sodium, two pump loops were operated at 1250°F in which equivalent surface areas of beryllium and Inconel were in contact with flowing sodium. One of the tests incorporated an oxide cold trap while the other did not.

The beryllium, in the form of rectangular blocks, was contained in an Inconel can and was inserted in the hottest section of the loop, the remaining sections of which were constructed of Inconel. A temperature drop of 300°F existed between the hot and cold fluid temperatures in each test. After 1000-hr operation, no increase in the amount of mass transfer was seen in either of these tests compared to tests of smaller inserts in pump loops discussed above. The addition of a cold trap showed little effect on test results.

THERMAL-CONVECTION-LOOP STUDIES

E. A. Kovacevich

Inconel Castings

In order to evaluate the use of Inconel castings for large intricate sections required in the ART, three standard Inconel thermal convection loops with cast Inconel inserts in the hot leg were operated 500 hr with NaF-ZrF_4-UF_4 (50-46-4 mole %) and sodium at 1500°F. The castings, whose compositions are given in Table 24, contained approximately 1.2% manganese, 2% columbium, and a range of silicon contents from 1 to 2%. Inserts 321 and 322, which had the lowest and the highest silicon contents, respectively, were

tested with NaF-ZrF_4-UF_4 (50-46-4 mole %), while the remaining insert, 323, with an intermediate silicon content, was operated with sodium.

As shown in Table 25, very severe corrosion was evidenced in both cast specimens in contact with fluoride salts. Attack occurred not only in the form of subsurface voids typical of wrought Inconel, but, in addition, very deep intergranular penetrations appeared, reaching in the worst case to a depth of 70 mils, as shown in Fig. 58.

These intergranular penetrations, although a result of rapid attack of grain boundary constituents, were aided considerably by porosity and shrinkage cracks present in all the castings in the as-received condition, as shown in Fig. 59. The 1% level of silicon was found to be no better from the corrosion standpoint than the 2% alloy.

Metal deposits were seen metallographically and visually in the hot leg of both loops. Spectrographically, the deposits were predominantly nickel with aluminum, chromium, and iron reported as major elements. Silicon and manganese analyzed low in these deposits.

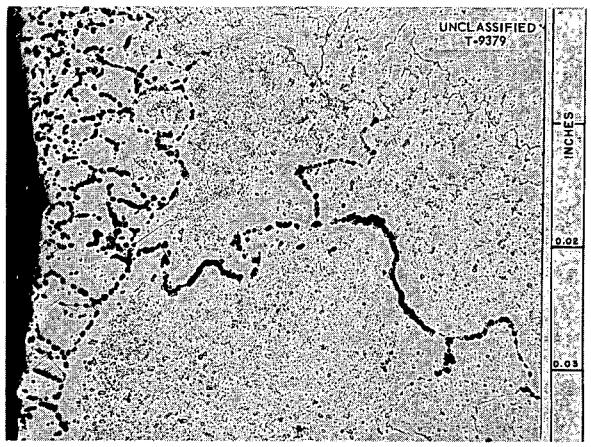

Fig. 58. Maximum Attack Near Cast-Weld Interface in Casting 321; Tested in Fuel 30, Loop 876. 100X. Reduced 34%. (Secret with caption)

TABLE 24. CHEMICAL ANALYSIS OF CAST INCONEL INSERTS OPERATING IN STANDARD INCONEL THERMAL-CONVECTION LOOPS

Cast Inconel Insert No.	Chemical Analysis (%)								
	Ni[a]	Cu	Fe	Si	Mn	C	Cr	Cb	S
321	70.49	0.01	8.20	1.04	1.22	0.23	16.67	2.08	0.005
322	69.79	0.03	8.20	1.93	1.17	0.22	16.51	2.09	0.006
323	70.44	0.02	8.10	1.34	1.16	0.22	16.67	2.00	0.004

[a]By difference.

TABLE 25. INCONEL THERMAL CONVECTION LOOPS OPERATING 500 hr WITH CAST INCONEL INSERTS IN THE HOT LEG WITH NaF-ZrF_4-UF_4 (50-46-4 MOLE %) AND SODIUM AT 1500°F

Loop No.	Insert No.	Coolant	Metallographic Results	
			Hot-Leg Attack (mils)	Cold-Leg Attack
876	321	Fuel 30	Cast section – 25 Weld interface – 70	Light surface roughening with a metal deposit present
877	322	Fuel 30	Cast section – 23 Weld interface – 25	Light surface roughening with evidence of metal crystals
878	Control	Fuel 30	10	No attack
879	323	Sodium	No attack	No attack, no deposits.

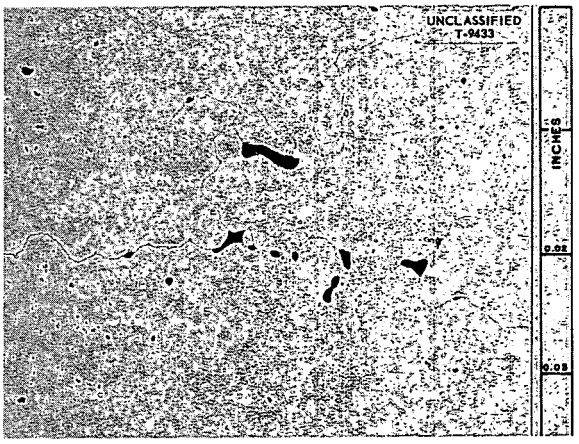

Fig. 59. Porosity in As-received Specimen of Casting 321. 100X. Reduced 36%.

Loop 879 (insert 323), which circulated sodium, revealed very little corrosion, <1 mil, in the insert section. Metallic deposits, which analyzed predominantly nickel, were seen macroscopically in the trap area, but were approximately in the same quantity as those observed in wrought Inconel loops.

Monel with Fuel 107

Six Monel thermal-convection loops, 806, 808, 809, 880, 881, and 882, completed 500, 545, 1027, 1000, 1339, and 1217 hr of operation, respectively, in NaF-LiF-KF-UF_4 (11.2-41.0-45.3-2.5 mole %) at 1500°F. The latter three loops were chromium-plated to afford oxidation protection after difficulties were encountered in earlier loops 808 and 809. These two loops were terminated before their scheduled operational time because of excessive oxidation of the outer tube wall. However, in the case of the chromium-plated loops 880 and 882, excessive oxidation occurred in areas where plating imperfections apparently existed. Metallographic results revealed 1 mil of hot-leg attack, as shown in Fig. 60, in all these loops. Formation of an intergranular precipitate was also observed in all hot-leg samples to a maximum depth of 3 mils.

Hastelloy Loops

Four Hastelloy X thermal-convection loops, which were constructed from ½-in.-dia tubing, operated 1000 hr with sodium and NaF-ZrF_4-UF_4 (50-46-4 mole %) at 1500°F. Loops 855 and 856, which operated with sodium, had no hot-leg attack and no evidences of metallic deposits in the cold leg. However, loops 857 and 983 which circulated NaF-ZrF_4-UF_4 (50-46-4 mole %) showed considerable hot-leg attacks to depths of 27 and 35 mils (Fig. 61). The cold legs of both loops showed surface roughening and evidences of metallic crystals. The fluoride in the trap area analyzed

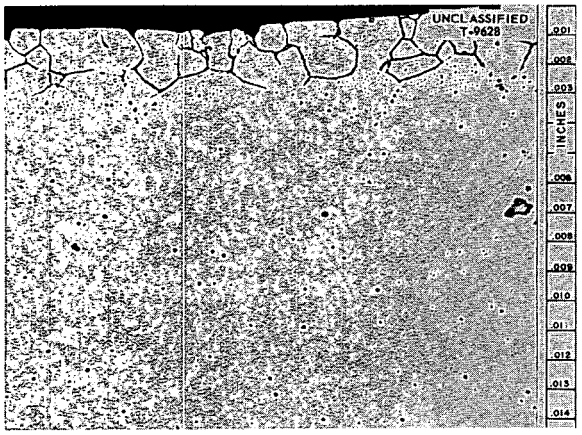

Fig. 60. Maximum Hot-Leg Attack in Monel Loop 809 Circulating Fuel 107 for 1027 hr at 1500°F. 250X. Reduced 36%. (Secret with caption)

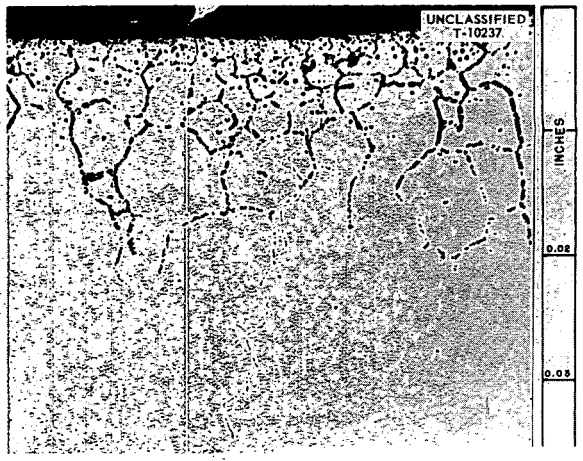

Fig. 61. Maximum Hot-Leg Attack in Hastelloy X Loop 983 Circulating Fuel 30 for 1000 hr at 1500°F. 100X. Reduced 32.5%. (Secret with caption)

26.6 wt % chromium in loop 857 and 16.6 wt % in loop 983.

Five loops, 872, 897, 873, 885, and 896, which were constructed of $\frac{3}{4}$-in. Hastelloy W tubing, also operated 1000 hr with sodium, $NaF-ZrF_4-UF_4$ (50-46-4 mole %), and $NaF-LiF-KF-UF_4$ (11.2-41.0-45.3-2.5 mole %). Loops 872 and 897, which circulated sodium, showed no hot-leg attack, as shown in Fig. 62 but had scattered metallic crystals in the cold leg which were found spectrographically to be predominantly nickel. Surfaces of the hot-leg samples were similar after test to the as-received samples of each loop. Loop 873, which circulated $NaF-ZrF_4-UF_4$ (50-46-4 mole %), showed no hot-leg attack or cold-leg deposits.

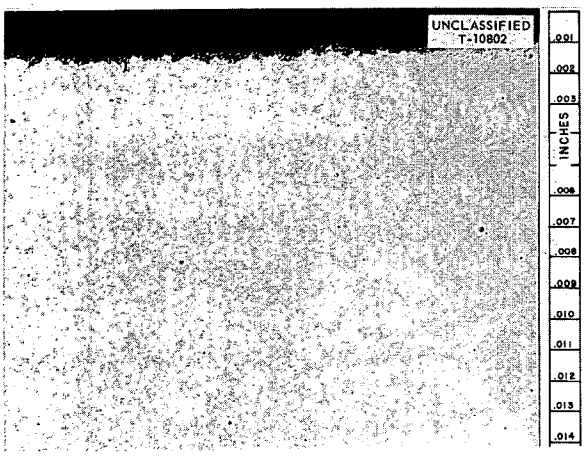

Fig. 62. Maximum Hot-Leg Attack in Hastelloy W Loop 897 Circulating Fuel 107 for 1000 hr at 1500°F. 250X. Reduced 32.5%. (Secret with caption)

The circulation of fuel 107, $NaF-LiF-KF-UF_4$ (11.2-41.0-45.3-2.5 mole %), in loops 885 and 896 resulted in maximum hot-leg attacks of 2 mils and $\frac{1}{2}$ mil, respectively. Cold-leg attacks appeared as light surface roughening with no evidences of metallic deposits or layers.

Loop 986, constructed of $\frac{1}{2}$-in. tubing of the composition 85% Ni–15% Mo, also was examined following operation for 1000 hr with fuel 107. This loop showed only 2 mils maximum hot-leg attack (Fig. 63). Cold-leg deposits were also absent.

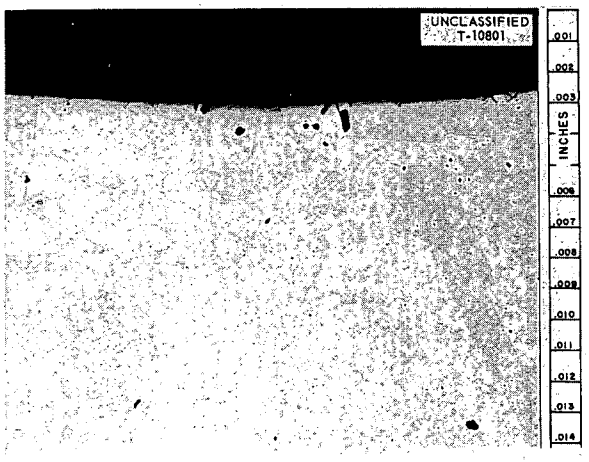

Fig. 63. Maximum Hot-Leg Attack in Loop 986, 85% Ni–15% Mo, Circulating Fuel 107 for 1000 hr at 1500°F. 250X. Reduced 32.5%. (Secret with caption)

Hastelloy B–Beryllium–Sodium Studies

Two Hastelloy B thermal-convection loops with beryllium inserts in the hot leg were operated 1000 hr with sodium at 1200 and 1300°F. The insert consisted of a hollow cylinder 6 in. long with a tube wall of 0.080 in. Spacing between the Hastelloy B and the beryllium was 0.020 ± 0.005 in. Holes were drilled at the top and the bottom of the insert to permit sodium flow on the outside of the beryllium. This aided in eliminating stagnant sodium areas in the system.

As seen in Table 26, maximum attack on the beryllium, which appeared as small voids, occurred on the outside diameter of the insert. In both loops, 899 and 900, no alloying occurred between the nickel and beryllium across the 0.020-in. separation, although where the beryllium came in direct contact with the Hastelloy B, alloying was observed. It appeared as a homogeneous layer 1 mil thick in loop 899 and as a two-phase layer 3 mils thick in loop 900. After operation, the insert from loop 900 had a grey scale on the outside diameter. However, this scale was absent in loop 899. The x-ray diffraction pattern identified this deposit as $Be_{21}Ni_5$. Cold-leg deposits were not reported in either loop.

TABLE 26. HASTELLOY B AND INCONEL THERMAL-CONVECTION LOOPS WITH BERYLLIUM INSERTS IN THE HOT LEG WHICH OPERATED 1000 hr WITH SODIUM AT VARIOUS TEMPERATURES

	Loop Number						
	899	900	912	913	914	915	916
Loop material	Hastelloy B	Hastelloy B	Inconel	Inconel	Inconel	Inconel	Inconel
Maximum fluid temperature, °F	1200	1300	1200	1250	1300	1400	1500
Corrosion, mils							
Loop material							
Hot leg	1	1	1	1	1	1	1
Cold leg	1	1	Surface rough	Surface rough	Surface rough	Surface rough	Surface rough
Sleeve							
Top section	2	1	Surface rough	Surface pits	Surface pits	1-mil attack and layer	½-mil attack and layer
Center section	1½	2	Surface pits	1	Surface pits	1	Pitting and layer
Bottom section	1½	1	Surface rough	Surface rough	1-mil attack and layer	1-mil attack and layer	1-mil attack and layer
Beryllium insert							
Inner top section	1	1	2	Surface pits	1	1	2
Inner center section	2	1	2	2	1	1	2
Inner bottom section	1	1	3	2	3	2	2
Outer top section	3	3	2	5	6	9	13
Outer center section	3	2	2½	7	5	8	10
Outer bottom section	1	1	3	3	6	8	8

Inconel-Beryllium-Sodium Studies

A series of five Inconel thermal-convection loops with beryllium inserts in the hot leg, similar to those used in the Hastelloy B–beryllium–sodium compatibility studies above, was operated for 1000 hr at 1200, 1250, 1300, 1400, and 1500°F. Metallographic examination of the Inconel adjacent to the beryllium insert, which was spaced 0.020 ± 0.005 in. from the Inconel, showed some alloy formation in tests conducted at temperatures of 1300°F and above. Typical nickel-beryllium alloying observed is shown in Fig. 64. Maximum attack on the beryllium, as shown in Table 26, increased with an increase in fluid temperature. This deeper attack occurred on the outside diameter of the insert. In all instances, a grey scale accompanied by a black deposit, as shown in Fig. 65, was observed on the outside and inside surfaces

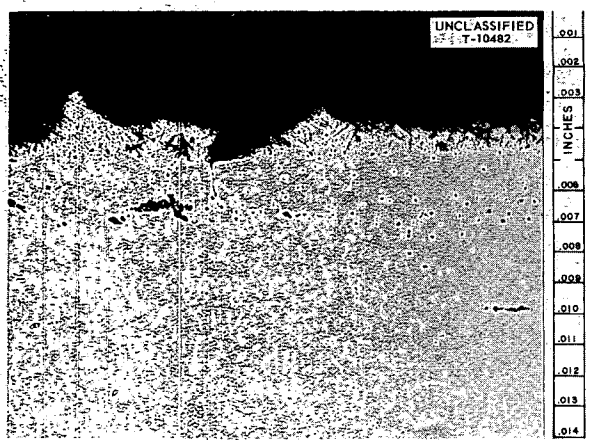

Fig. 64. Beryllium-Nickel Alloying in Loop 915 Operating with Beryllium Insert in the Hot Leg and with Sodium at 1400°F. 250X. Reduced 32.5%.

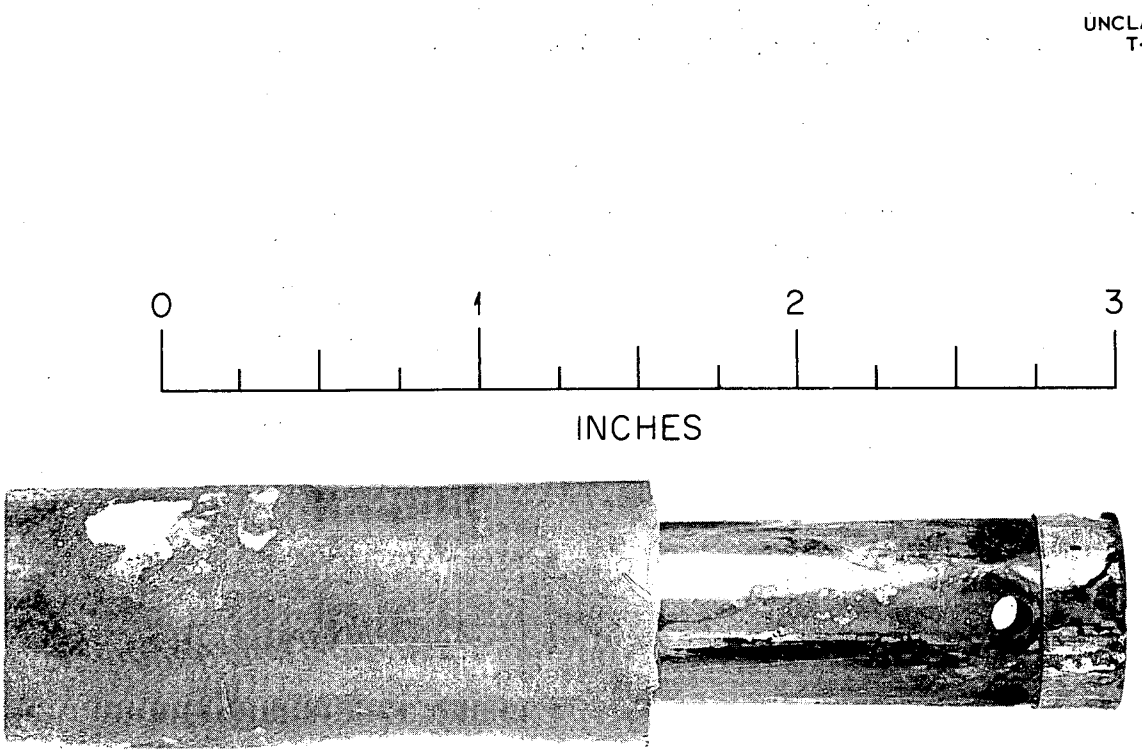

Fig. 65. Deposit on Beryllium Insert After Operation in Inconel Loop 913, Which Circulated Sodium 1000/hr at 1250°F.

of the insert after operation. This deposit was also identified by x-ray diffraction as $Be_{21}Ni_5$. The thickness of the nickel-beryllium layer reported by metallography ranged from 1 mil in loop 914 to a maximum depth of $3\frac{1}{2}$ mils in loop 915. The layer in loop 915 was reported as being two phases; however, in the other tests only one phase was observed. Metallic deposits were not seen in the cold leg of these loops.

Chemical analysis of the coolant in all tests after operation showed approximately 300 ppm of beryllium. A possible explanation for this relatively high beryllium concentration may be attributed to flaking of the $Be_{21}Ni_5$ scale into the sodium.

Specially Prepared Fluoride No. 30

Tests to determine the corrosion behavior of fuel 30 ($NaF-ZrF_4-UF_4$, 50-46-4 mole %) in which specially prepared ZrF_4 was used have been conducted in standard Inconel thermal-convection loops. The loops were operated at 1500°F for a period of 500 hr.

The fuel (batch EE 808) used in these experiments contained zirconium fluoride of special purity produced by the Materials Chemistry Division. The maximum hot-leg attack, as reported in Table 27, for these loops, 987 and 988, was 2 to 3 mils less than the attack observed in standard loops 860 and 861. These latter loops operated with standard fuel 30 (batch EE 526Pf2) containing commercial-grade zirconium fluoride normally used in the production of fuel 30. Note that in Table 28 a lower concentration of chromium after test appears in the fuels with specially-treated ZrF_4, which is in agreement with the lower attacks observed.

Another series of three standard Inconel thermal-convection loops, 858, 859, and 984, was operated for 500 hr at 1500°F with reclaimed fuel 30. The purpose of these tests was to determine the difference, if any, in corrosion results between standard fuel and fuel which had been used in other experimental tests and reclaimed. In all cases the fuel which comprised the initial batch of fuel before reclaiming had been used in Inconel systems.

TABLE 27. METALLOGRAPHIC RESULTS OF STANDARD INCONEL THERMAL-CONVECTION LOOPS OPERATED WITH STANDARD FUEL 30, RECLAIMED FUEL 30, AND FUEL 30 PRODUCED FROM SPECIALLY PREPARED ZIRCONIUM FLUORIDE

Operating Conditions: time, 500 hr; temperature, 1500°F

Loop No.	Coolant	Maximum Hot-Leg Attack (mils)
987	Fuel 30 (specially produced ZrF_4)	7
988	Fuel 30 (specially produced ZrF_4)	7
858	Reclaimed fuel 30 with plant helium*	8.5
859	Reclaimed fuel 30 with plant helium	5
984	Reclaimed fuel 30 with bottle helium**	6
860	Standard fuel 30 with plant helium	10.5
861	Standard fuel 30 with plant helium	9

*Plant helium (after scrubber column) −120 dew point reading.

**Bottle helium −60 to −70 dew point reading.

TABLE 28. CHEMICAL ANALYSIS OF FUEL 30 USED IN THERMAL-CONVECTION LOOPS 988, 987, 860, AND 861

Sample	Chemical Analysis						
	U (%)	Zr (%)	Na (%)	F (%)	Ni (ppm)	Cr (ppm)	Fe (ppm)
EE 808	8.78	38.1	11.2	42.0	40	45	60
EE 526Pf2	8.71				20	90	50
Loop 987							
Before	8.99				115	90	85
After	8.98				25	625	70
Loop 988							
Before	8.98				50	65	155
After	8.96				20	720	80
Loop 860							
Before	8.00				<2	80	95
After	8.50				15	1060	80
Loop 861							
Before	8.70				345 (?)*	150	105
After	8.79				35	820	100

*Filled at same time as loop 860.

The reclaiming procedure conducted by Materials Chemistry consisted of the addition of zirconium metal to the fuel, followed by hydrogen gas treatments to strip the fuel of predominant impurities. The resulting mixture was given a hydrogen fluoride treatment, followed by hydrogen bubbling.

The chemical analysis of the fuel before the treatment and after the treatment is shown in Table 29. It should be noted that a definite reduction in chromium was effected in the purification treatment through the addition of zirconium.

A summary of corrosion results, as shown in Table 27, indicates that the reduction of maximum hot-leg attack, 2 to 3 mils, which occurred in loops operated with reclaimed fuel was similar to that which occurred with the fuel containing the specially prepared zirconium fluoride. This reduction in attack may be attributed to the removal of impurities in the fuel through corrosion processes during previous operation. The decrease, as would at first be supposed, does not seem to be due to any effect on the initial equilibrium between chromium and UF_4, since, as seen in Table 29, chromium contents in this fuel were comparable to fuels as initially prepared.

However, it should be noted that any increase in U^{+++} content in these fuels resulting from changes in the processing used to prepare the fuels would cause a significant decrease in attack. This possibility unfortunately is difficult to evaluate through conventional chemical analyses.

TABLE 29. CHEMICAL ANALYSIS OF THE FUEL 30 USED IN RECLAIMED TESTS

Sample	Chemical Analysis			
	U (%)	Ni (ppm)	Cr (ppm)	Fe (ppm)
Before reclaiming	8.66	2	305	120
After reclaiming	8.21	220	110	135
Before operation (loop 858)	8.36	250	170	95
After operation (loop 858)	8.95	15	670	120
Before operation (loop 859)	7.57	2	120	115
After operation (loop 859)	8.84	30	620	100
Before operation (loop 984)	8.13	285	155	65
After operation (loop 984)	8.79	20	820	100

Special Fuels

A screening program is currently under way to evaluate the corrosion properties of numerous fluoride mixtures with Inconel systems. These fuels, which were prepared by Materials Chemistry, are being tested in standard Inconel thermal-convection loops for 500 hr at 1500°F. Standard thermal-convection-loop-filling procedures are followed; however, due to the limited availability of fuel, precleaning steps utilizing an extra fluoride fill are omitted.

The fluoride mixtures for which tests have been completed are tabulated in specific groups according to the variable being investigated (Table 30). Group 1 lists the zirconium-base fluorides in which alkali-metal-fluoride components (KF, LiF, RbF, and NaF) were interchanged, while the polyvalent-fluoride (ZrF_4 and UF_4) compositions, similar to that of fuel 30, remained constant. In these fluoride systems it is desired to establish the corrosion properties accompanying the various alkali fluorides in combination with ZrF_4. Fuels of the above type but with slightly higher alkali-fluoride contents also are included in this group.

In group 2, fluoride mixtures complexed with sodium and lithium were prepared with varying zirconium fluoride contents. The purpose of preparing these fuels was to determine the level of ZrF_4 below which such mixtures show corrosion behavior typical of fuel 12, of the Flinak systems, rather than behavior typical of the higher ZrF_4 fuels such as fuel 30.

To determine what effect an increase of uranium fluoride concentration in a zirconium base fluoride mixture has on corrosion of Inconel, the fuels listed in group 3 were investigated. This list of fuels is incomplete, with several fuels remaining to be evaluated.

The fuels in group 4 were programed to see whether mass transfer in beryllium fluoride systems is a function of the ratio of sodium fluoride to beryllium fluoride.

For tests in group 1 involving KF, LiF, RbF, and NaF systems in combination with ZrF_4, the lowering of the ZrF_4 from 46 to 40 mole % produced no significant effect on the attack in NaF systems and increased attack from 1 to 2 mils in the case of KF and RbF systems. The LiF system showed quite anomalous behavior in that attack decreased markedly with the decrease in ZrF_4.

TABLE 30. METALLOGRAPHIC DATA OF THE FLUORIDE MIXTURES WHICH COMPLETED 500-hr LOOP OPERATION AT 1500°F

Fuel No.	Mole Composition (%)	Loop No.	Metallography	
			Hot-Leg Attack (mils)	Cold Leg
		Group 1		
95	50 RbF–46 ZrF_4–4 UF_4	839	9	Metallic layer
		840	9	Metallic layer
WR-5	56 RbF–40 ZrF_4–4 UF_4	932	10	Layer + crystals
		933	11	Layer + crystals
94	50 KF–46 ZrF_4–4 UF_4	845	6.5	Metallic layer
		846	8	Metallic layer
WR-4	56 KF–40 ZrF_4–4 UF_4	930	7	Metallic layer
		931	9	Metallic layer
93	50 LiF–46 ZrF_4–4 UF_4	847	17.5	Layer + crystals
		848	19	Layer + crystals
WR-3	56 LiF–40 ZrF_4–4 UF_4	928	10	Layer + crystals
		929	10	Layer + crystals
WR-1	56 NaF–39 ZrF_4–5 UF_4	924	7	Layer + crystals
		925	9	Layer + crystals
WR-2	56 NaF–40 ZrF_4–4 UF_4	926	9	Layer + crystals
		927	7	Layer + crystals
30	50 NaF–46 ZrF_4–4 UF_4	860	10.5	None
		861	9	None
WR-13	75 LiF–21 ZrF_4–4 UF_4	948	14.5	Layer + crystals
		949	11	Layer + crystals
		Group 2		
WR-14	25 LiF–25 NaF–46 ZrF_4–4 UF_4	950	12	Layer + crystals
		951	11	Layer + crystals
WR-15	20 LiF–36 NaF–40 ZrF_4–4 UF_4	952	10	Layer + crystals
		953	11	Layer + crystals
WR-16	25 LiF–41 NaF–30 ZrF_4–4 UF_4	954	8.5	Metallic layer
		955	15	Crystals
82	55 LiF–20 NaF–21 ZrF_4–4 UF_4	841	14	Metallic layer
		842	12.5	Metallic layer
91	35 LiF–53 NaF–8 ZrF_4–4 UF_4	843	15	Metallic crystals
		844	10	Metallic layer
		Group 3		
WR-6	60 NaF–40 ZrF_4	934	5	Layer + fine crystals
		935	5	Layer + fine crystals

TABLE 30 (continued)

Fuel No.	Mole Composition (%)	Loop No.	Metallography	
			Hot-Leg Attack (mils)	Cold Leg
		Group 3		
WR-7	60 NaF–35 ZrF_4–5 UF_4	936	10.5	Layer + crystals
		937	10	Layer + crystals
WR-10	74 NaF–26 UF_4	942	15	Layer + crystals
		943	18	Layer + crystals
WR-11	74 LiF–26 UF_4	944	21	Layer + crystals
		945	20	Layer + crystals
WR-8	60 NaF–28 ZrF_4–12 UF_4	938	10	Metallic layer
		939	13	Metallic layer
WR-9	60 NaF–14 ZrF_4–26 UF_4	940	11.5	Layer
		941	9	Layer + crystals
		Group 4		
92	49.5 NaF–48 BeF_2–2.5 UF_4	853	12	Metallic layer
		854	12	Metallic layer
75	67 LiF–30.5 BeF_2–2.5 UF_4	851	17	Metallic layer
		852	17	Metallic layer
79	15 LiF–55 NaF–27.5 BeF_2–2.5 UF_4	849	11	Layer + crystals
		850	10	Layer + crystals
WR-17	50 NaF–47 BeF_2–3 UF_4	956	8	Layer + crystals
		957	9	Layer + crystals
WR-18	50 LiF–47 BeF_2–3 UF_4	958	20	Metallic layer
WR-19	25 LiF–25 NaF–47 BeF_2–3 UF_4	960	13	Metallic layer
		961	12	Metallic layer
WR-20	66 NaF–31 BeF_2–3 UF_4	962	9	Metallic layer and crystals
		963	9	Metallic layer and crystals
WR-21	33 NaF–33 LiF–31 BeF_2–3 UF_4	964	13	Metallic layer
		965	15	Metallic layer

The loops containing the higher alkali-metal-fluoride fuels, with the exception of the KF system, showed traces of metallic crystals in the cold leg. In analyzing the systems from the standpoint of interchanging the alkali-metal-fluoride component while maintaining the over-all composition constant (specifically MF-ZrF_4-UF_4, 50-46-4 and 56-40-4 mole %), it was observed that the KF system gave the least attack. At the beginning of the tests, it was expected that the LiF system would yield the least corrosion; however, as seen from the data, it produced the maximum attack.

To obtain further corrosion data for the KF-ZrF_4-UF_4 (50-46-4 mole %) which showed somewhat less attack than the other systems, two Inconel loops were operated under conditions similar to the above

loops, but for a longer period (1500 hr). An increase of operational time from 500 to 1500 hr with this fuel was accompanied by an increase in maximum attack of only 2 mils.

Tests to determine changes in the complexing of fluoride mixtures of sodium and lithium as the zirconium fluoride component is decreased (group 2) show little change in hot-leg attack to accompany the ZrF_4 decrease. However, in every instance other than the standard loops operated with fuel 30, evidence of metallic layers and/or evidences of metallic crystals were observed metallographically. The presence of LiF in such mixtures, even with 46% ZrF_4, does not affect the corrosion appreciably.

As seen in Table 30, an appreciable increase in attack was observed in the tests conducted with fuels having the 26 mole % UF_4. Also, metallography reported a metallic deposit, possibly uranium, in the hot legs of these loops operating with those fuels. However, an increase from 5 to 12 mole % uranium fluoride did not seem to affect the corrosion. No hot-leg deposits were noted in these loops which operated with the lower concentration of uranium fluoride.

In the bulk of the tests involving special fuels, especially those in group 4, metallic layers and/or metallic deposits were noted in the cold legs. However, because these tests were conducted for a relatively short duration, 500 hr, it is not possible to accurately assess the mass transfer properties. It should be noted that the effect of increasing the mole composition of LiF in the beryllium systems appears to also increase the maximum hot-leg attack. In the instances where the NaF is replaced with LiF in these systems, the attack has increased almost twofold.

MECHANICAL PROPERTIES

D. A. Douglas
C. W. Dollins
J. R. Weir, Jr.
J. W. Woods
C. R. Kennedy

Pratt & Whitney Aircraft

The work of the Mechanical Properties Group falls under two general categories: the development of data applicable to the design of the ART and the testing of materials which may be of interest for future reactor designs. In line with the primary objective, the results of tests on Inconel, lead, and beryllium are being reported. For future reactor design the properties of Hastelloy B, Hastelloy W, Hastelloy X, and a lithium-magnesium alloy have been investigated.

TESTING PROGRAM FOR ART MATERIALS

Stress Relaxation of Inconel

The evaluation of the creep and creep-rupture characteristics of Inconel under constant load and in various environments has been and continues to be of prime concern. Recently, however, equipment has been designed and constructed for the study of another facet of the high-temperature behavior of metals, that is, the decay or relaxation of stress under a constant strain. This phenomenon, commonly called relaxation, is time-temperature dependent and assumes particular importance in cases of thermally induced cyclic stresses. For example, if a structural member is held rigidly at both ends and the temperature is raised and then lowered rapidly, corresponding tensile and compressive loads will result. It is essential in the stress analysis of this situation to know how much the stress has decreased, that is, relaxed, and how much plastic strain has resulted in each condition before the reverse load is applied.

There have been many different machines and methods used by previous experimenters to determine the relaxation characteristics of metals; however, most of the work has been done in temperature ranges well below the annealing temperature of the material tested. Extrapolation of these results to higher temperatures does not give reliable values. Therefore, it was necessary that new experimental techniques be devised to achieve the accuracy desired for temperatures in the range of 1200 to 1800°F.

A test machine designed by the Mechanical Properties Group, shown in Fig. 66, eliminates most of the objectionable features of previous units and makes it possible to obtain the relaxation characteristics of materials near or above their annealing temperatures. The test is run by setting the extensometer to a desired strain and then applying stress to produce and maintain this strain by automatically controlling the load. This is accomplished by the extensometer control system shown in Fig. 66. The position of the electric contacts is established by micrometer screws on a 20-to-1 magnification extensometer similar to the Westinghouse design.[1] When the extensometer makes contact, the 4- or 5-v grid bias is cut out, and the grid glow relay opens the proper solenoid valve to control the hydraulic pressure and thus the stress on the specimen. Load rates from 0.001 to 0.05 in./in./min can be maintained by adjusting the needle valves in the pressure lines. The furnace is shunt-wound and is controlled by a Leeds & Northrup model H Speedomax recorder and DAT 60 controller which will control to 2°F with a temperature gradient over the 6-in. gage length of less than 5°F.

Results of relaxation tests of Inconel at 1300 and 1500°F are shown in Figs. 67 and 68. To produce a plot on which the complete relaxation characteristics can be shown, the first 0.1 hr is plotted linearly and thereafter on a semilog plot. The initial stresses obtained at both temperatures agree with stress-strain curves of Inconel at the respective temperature. Each curve shown in Figs. 67 and 68 is the average of 2 to 10 tests in which the material was tested at a load rate of 0.05 in./in./min, with varying prior plastic strain varying from 0 to 2%. It is significant that only one curve for each strain is shown, indicating that

[1] J. Boyd, *Am. Soc. Testing Materials, Proc.* 37(II), 218–232 (1937).

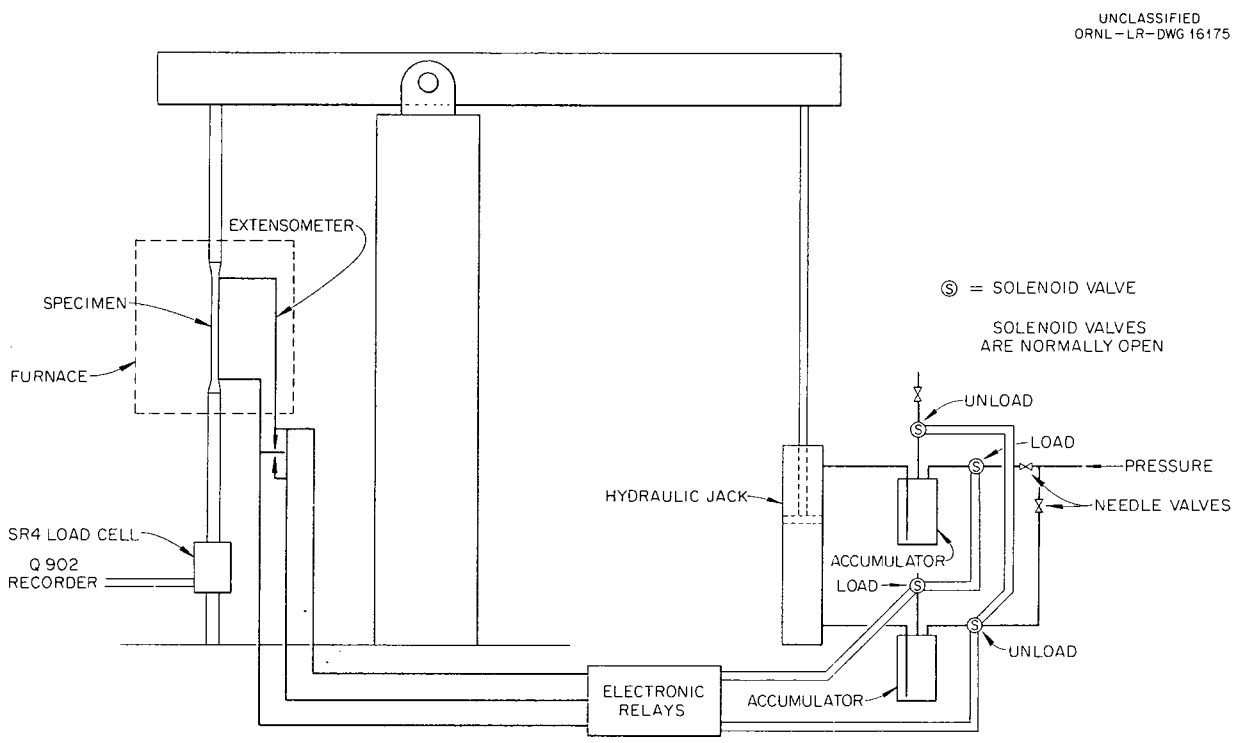

Fig. 66. Schematic Drawing of Relaxation Testing Machine.

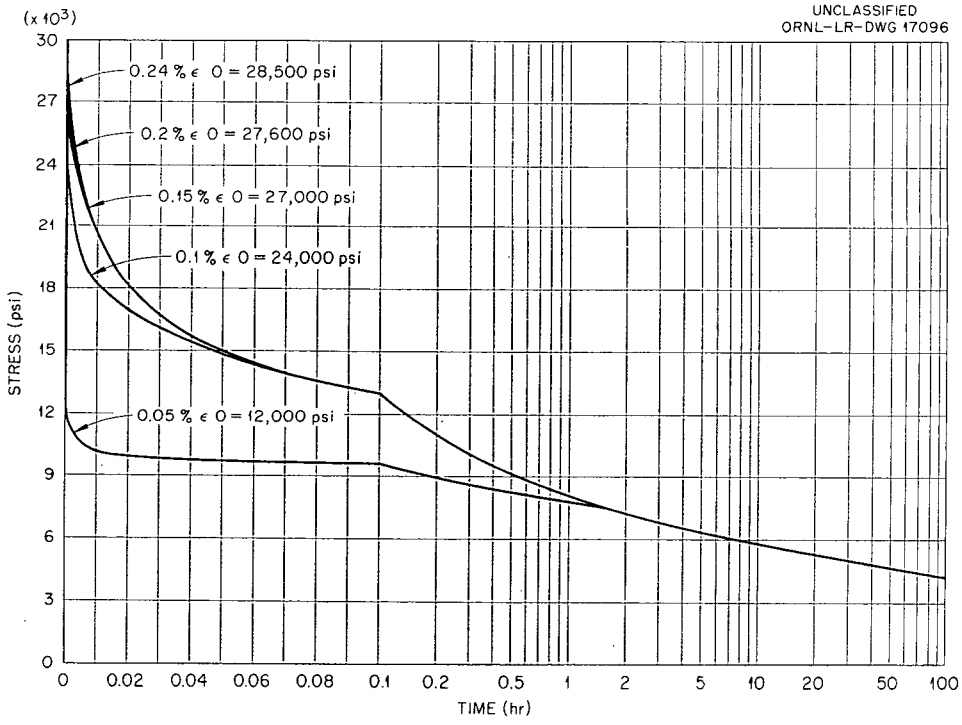

Fig. 67. Relaxation Characteristics of As-received Inconel at 1300°F.

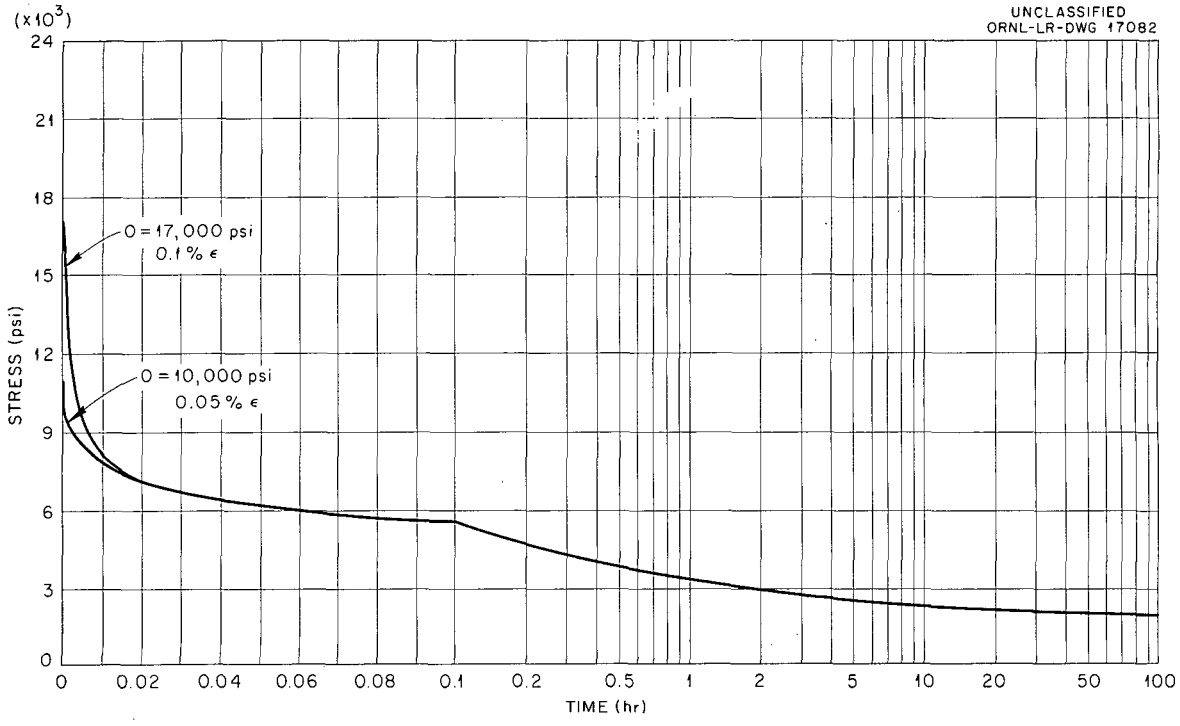

Fig. 68. Relaxation Characteristics of As-received Inconel at 1500°F.

prior plastic strain up to 2% at the test temperatures does not affect the relaxation characteristics of as-received Inconel. Tests at slower load rates produced slightly lower initial stresses, but after 0.01 hr the relaxation stresses are the same for all load rates. Thus an important trend is shown, namely, that the relaxation characteristics of the material vary with the strain until the proportional limit is reached, and that, for all strains above the proportional limit, the relaxation rate remains essentially the same. The strain corresponding to the proportional limit at 1300°F is about 0.1% and at 1500°F is 0.05%. This information can be used to determine the residual stresses in members which have undergone a thermal cycle and also to calculate the amount of plastic strain adsorbed by the material in each cycle.

Effect of Section Thickness on Creep-Rupture Properties of Inconel in Fused Salt No. 30

Data on the effect of section thickness on the rupture properties of Inconel tubes tested in fused salt No. 30 were presented previously.[2]

A testing program was subsequently initiated to determine the effect of section thickness on the creep-rupture properties and ductility of sheet Inconel in the liquid media. The creep-rupture data obtained from tests of 0.010-, 0.020-, 0.040-, 0.060-, and 0.125-in.-thick Inconel sheet at 1500°F in liquid No. 30 are presented in Fig. 69. Time to 2, 5, and 10% elongation and rupture is plotted vs specimen thickness. The rupture ductility for the various section thicknesses is also indicated.

The rupture behavior of the sheet Inconel is similar to that of the tubular material in that the 0.010- and 0.020-in.-thick sheets exhibit a much shorter rupture life than do the larger sections. However, the thin sheet material is more drastically affected by the corrosive media than the thin-wall tubes. This occurs because the corrosive reaction is occurring on both sides of the sheet specimen and only on one side of the tubular specimen.

One important conclusion that can be derived from these results is that the design data presented for the 0.060-in. sheet specimens tested in fused salt No. 30 are applicable to sections of greater thicknesses also, but this data cannot be used for components of less section thickness when the corrosive media are present.

[2] D. A. Douglas *et al.*, *Met. Semiann. Prog. Rep. April 10, 1955*, ORNL-2080, p 74 and J. W. Weir, *Met. Semiann. Prog. Rep. Oct. 10, 1955*, ORNL-1988, p 36.

Creep-Rupture Testing of a Lead Gamma-Shielding Alloy

An alloy of very pure lead containing 0.06% copper has been proposed as a gamma-ray shielding material. Present design calculations indicate that the maximum operating temperature of the lead shield will be approximately 230°F and that a tolerable deformation will be 0.5%/yr at 100-psi stress. Since the maximum temperature for which design data are available in the literature[3] is 150°F, a creep-rupture testing program was initiated to determine the strength of this alloy at the maximum expected operating temperature.

The results of the creep-rupture tests of cast bar stock at 230°F are summarized in Table 31. These data indicate that for this alloy the limiting design deformation of 0.5%/yr at 230°F and 100-psi stress will probably be exceeded. A better stress value lies between 50 and 100 psi. More tests will be run to determine a more accurate stress value for the design stress limitation.

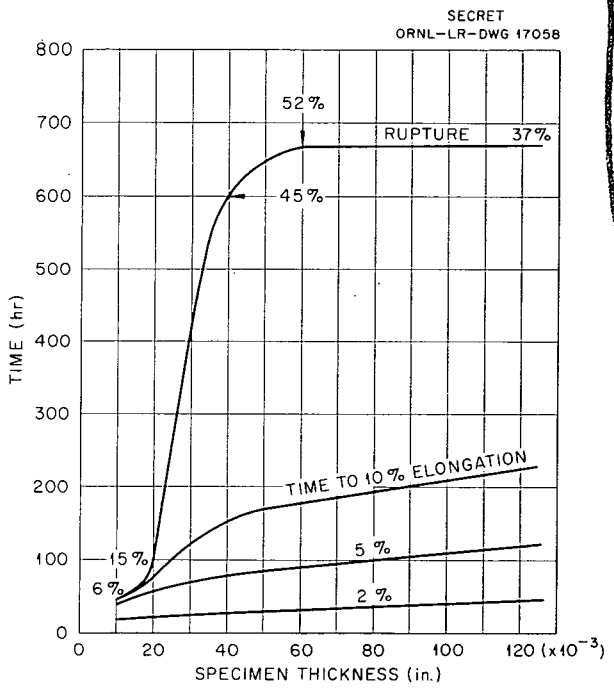

Fig. 69. Effect of Specimen Thickness on the Creep-Rupture Properties of Fine-Grain Inconel Tested in Liquid No. 30 at 1500°F and 3500 psi Stress.

Creep-Rupture Testing of Beryllium in Sodium

The selection of beryllium as the moderator material for the ART pointed up the critical need for mechanical property data on this metal at elevated temperatures. For the past two years The Brush Beryllium Co. in Cleveland, Ohio, under a research contract sponsored by ORNL, has been conducting creep and tensile tests in argon from 1000 to 1500°F. Their results show that the strength of beryllium decreases rapidly above 1200°F. It has also been demonstrated that the depth to which beryllium and Inconel will alloy increases rapidly above 1200°F. These facts make it necessary to impose a maximum temperature on the moderator for safe operation.

[3] C. W. Dollins, *Univ. Illinois Bull.* 45(65), (1948).

TABLE 31. SUMMARY OF CREEP RESULTS FOR A CAST LEAD SHIELDING ALLOY AT 230°F

Stress (psi)	Time (hr)	Total Elongation (%)	Creep Rate (%/hr)	Extrapolated Elongation in One Year (%)
20	1000	0.04	1×10^{-5}	0.1
	2000	0.05	1×10^{-5}	
50	1000	0.08	2×10^{-5}	0.2
	2000	0.1	2×10^{-5}	
100	1000	0.2	1×10^{-4}	1.0
	2000	0.3	1×10^{-4}	

In addition to the alloying problem there was some concern that the creep properties of beryllium might be adversely affected in a sodium environment. In order to explore this possibility, beryllium specimens were obtained from the stock being tested at the Brush laboratory; and creep tests were run at 1200°F in a sodium bath. A comparison of these results with those obtained in an argon environment by the Brush laboratory is shown in Table 32.

From these results it would appear that, in the absence of alloying, no deleterious effect on the creep properties of beryllium will occur in a pure sodium environment.

TESTING PROGRAM FOR POTENTIAL REACTOR MATERIALS

The design of the Pratt & Whitney Aircraft Reactor (PWAR) No. 1 and subsequent aircraft reactors makes it necessary that an alloy much stronger and more corrosive-resistant than Inconel be used for a structural material. It has been demonstrated that nickel-base molybdenum alloys have excellent resistance to corrosion in fused salts and good high-temperature strength. Thus, as part of a program aimed at obtaining better reactor materials, commercially available alloys of this type (such as Hastelloys B, W, and X) have been investigated. Nominal compositions for these alloys are given in Table 33.

Creep-Rupture Testing of Hastelloy B

Revised design curves data to replace those given previously[4] are shown in Figs. 70, 71, and 72 and were produced by creep testing solution-annealed Hastelloy B sheet stock in various environments at 1300, 1500, and 1650°F. A new design curve taken from creep testing solution-annealed Hastelloy B in argon and liquid No. 30 at 1800°F is shown in Fig. 73. It should be noted that the times to 0.5, 1, 2, 5, and 10% total strain at each temperature in the environments tested are essentially the same, and the only significant effect of environment is an increase in rupture life for stresses which produce a short rupture life. Of the environments tested, only those which alter the surface of the metal appear to affect the creep properties of the alloy. It can be seen from the above figures that only air (Fig. 71) and liquid No. 30 (Figs. 70–73) affect the creep properties of Hastelloy B. Air, of course, produces an adherent oxide film under isothermal conditions, and liquid No. 30 can be considered to have created a very thin surface film by a chemical alteration of the surface, as shown in Fig. 74.

Short-time high-temperature tensile properties of solution-annealed Hastelloy B are illustrated in Fig. 75, which gives the yield, ultimate strengths, and per cent elongation from 1000 to 1800°F. It is apparent that there is a distinct drop in the elongation and the ultimate strength around 1200°F. The drop in properties occurs at the same temperature range in which the type of fracture is transforming from predominately transgranular to intergranular. It is interesting to note the relatively

[4] D. A. Douglas *et al.*, *Met. Semiann. Prog. Rep. April 10, 1956*, ORNL-2080, p 74, Figs. 67–69.

TABLE 33. NOMINAL COMPOSITION OF HASTELLOYS B, W, AND X

Alloy	Composition (%)				
	Mo	Fe	Cr	C	Ni
Hastelloy B	28	5	1	0.1	Bal
Hastelloy W	24	5	5	0.1	Bal
Hastelloy X	9	24	22	0.1	Bal

TABLE 32. COMPARISON OF CREEP PROPERTIES OF BERYLLIUM IN ARGON AND SODIUM

Test Temperature (°F)	BeO Content (%)	Stress (psi)	Time to Rupture in Argon (hr)	Time to Rupture in Sodium (hr)
1200	1	4000	<10	144
1200	3	5000	<250	300

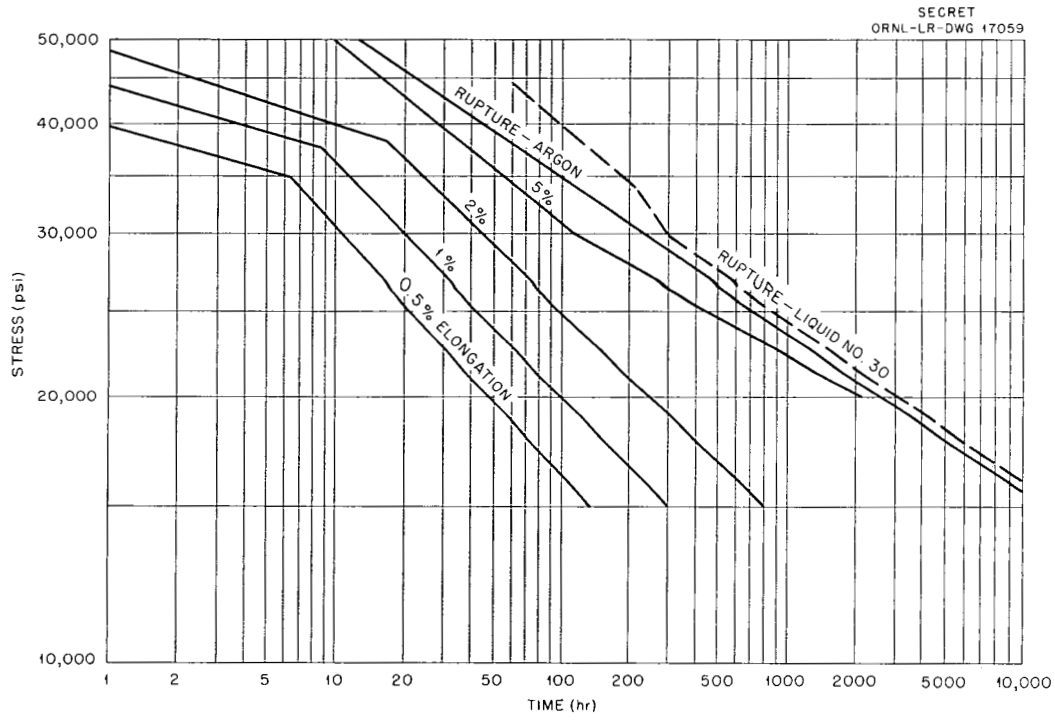

Fig. 70. Design Curve for Solution-annealed Hastelloy B Sheet Tested in Argon and Liquid No. 30 at 1300°F.

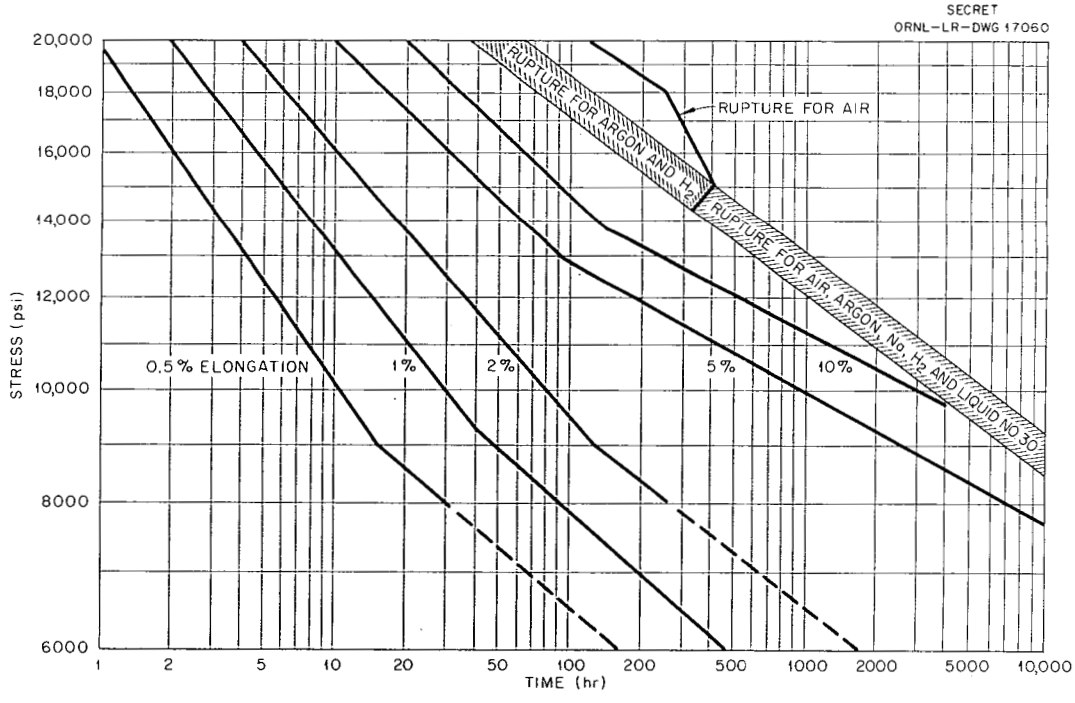

Fig. 71. Design Curve for Solution-annealed Hastelloy B Sheet Tested in Various Environments at 1500°F.

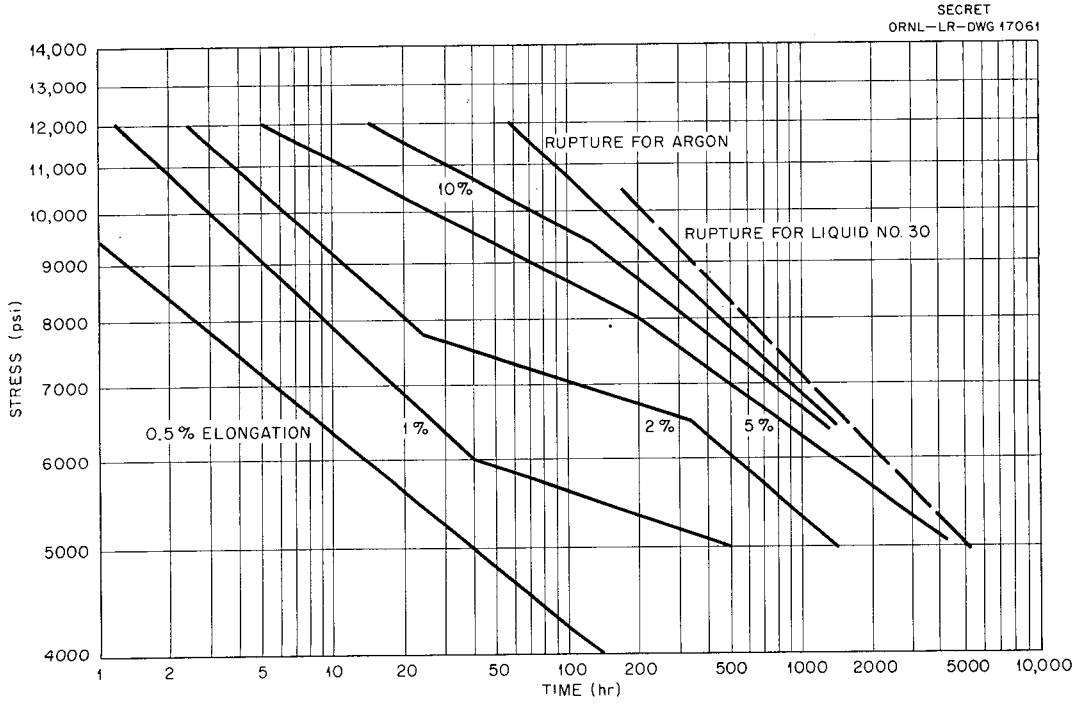

Fig. 72. Design Curve for Solution-annealed Hastelloy B Sheet Tested in Argon and Liquid No. 30 at 1650°F.

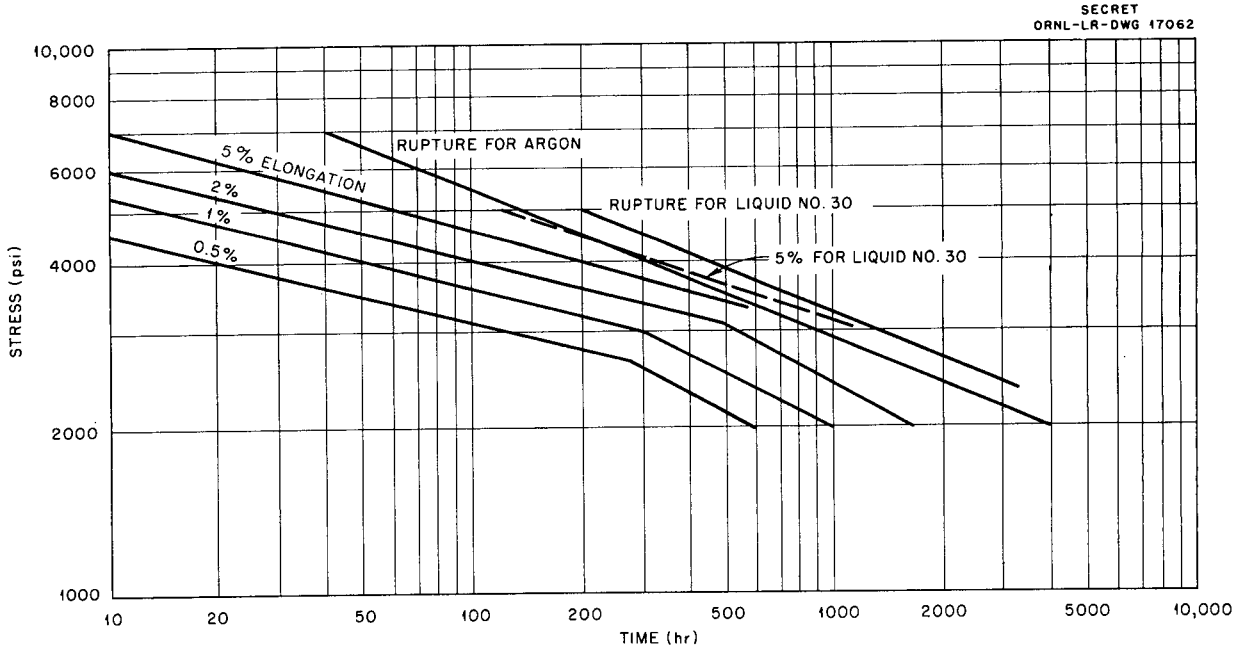

Fig. 73. Design Curve for Solution-annealed Hastelloy B Sheet Tested in Argon and Liquid No. 30 at 1800°F.

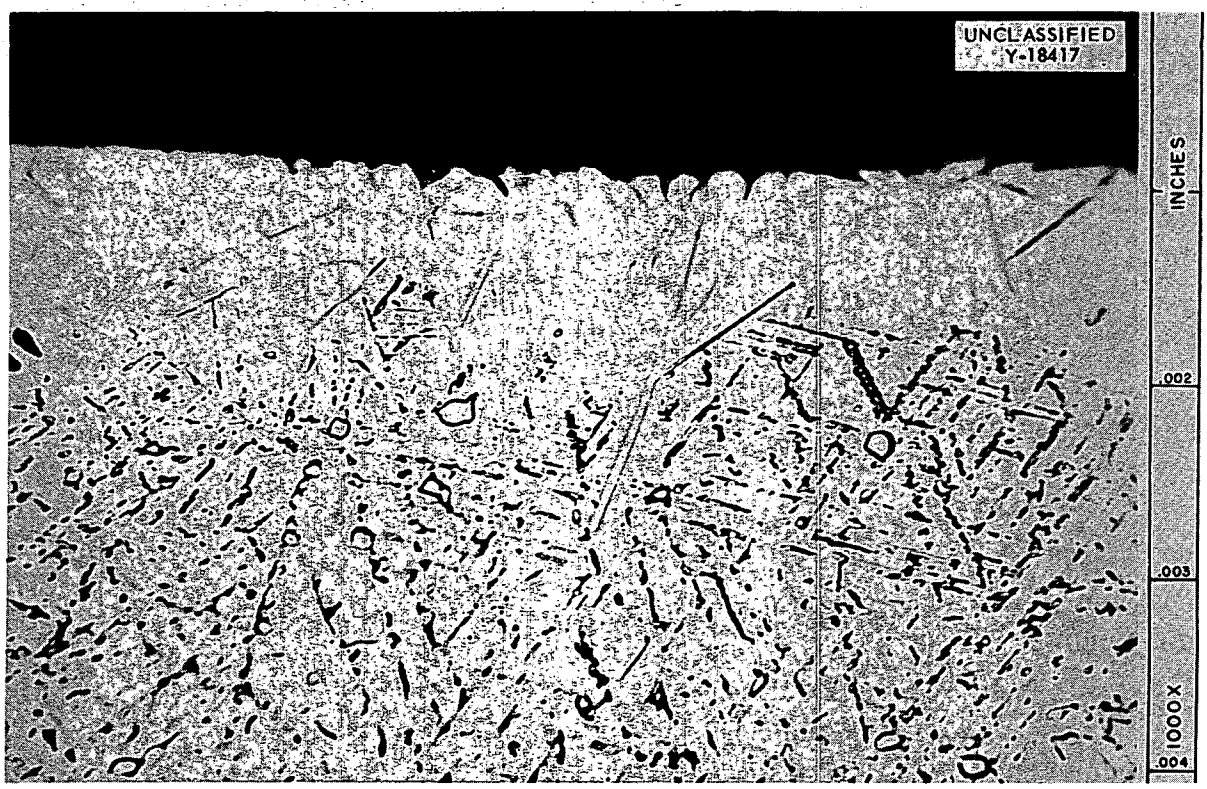

Fig. 74. Surface Effect on the Stressed Portion of a Hastelloy B Specimen After Exposure to Liquid No. 30 for 1700 hr and a Stress of 13,500 psi at 1500°F. (Secret with caption)

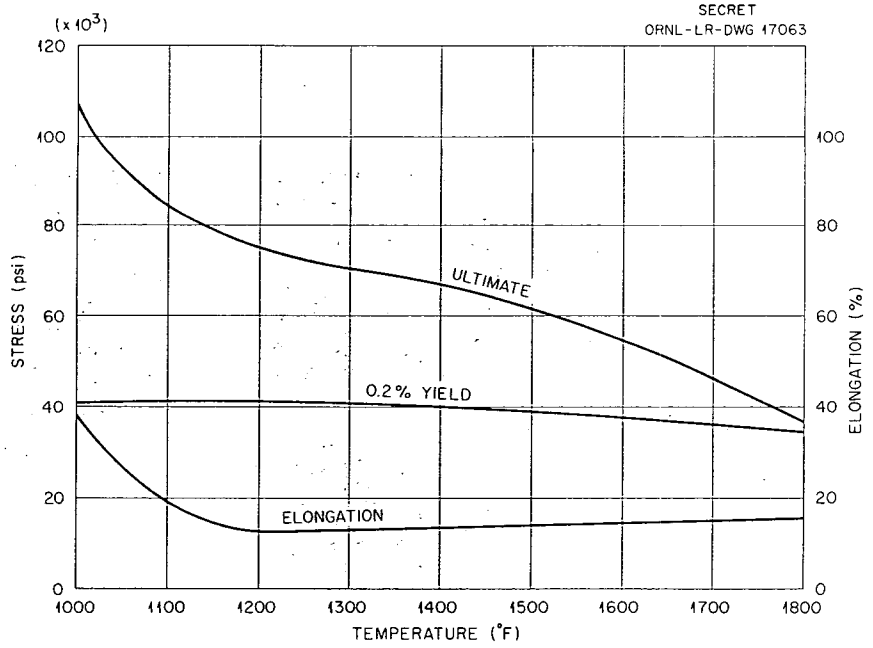

Fig. 75. Short-Time Tensile Data for Solution-annealed Hastelloy B Sheet at Temperatures 1000 to 1800°F.

small change in the yield strength with temperature.

Creep-Rupture Testing of Hastelloy W

Creep testing of Hastelloy W is now in progress, and design data are presented in Figs. 76 through 79 for solution-annealed sheet tested in argon at 1300, 1500, 1650, and 1800°F. Hastelloy W, having almost the same composition as Hastelloy B except for a small chromium addition and with a reduction of the molybdenum, has very similar creep properties. Although Hastelloy W exhibits less tendency to age than Hastelloy B, the alloy still experiences a decrease in creep ductility at 1300°F. This is shown in Fig. 76 by the absence of a 10% curve, indicating that the total strain at rupture was less than 10%.

Shown also in Figs. 76 through 79 are rupture points obtained from testing in liquids Nos. 30 and 107. The times to 0.5, 1, 2, 5, and 10% strain are essentially identical for the same stress and temperature. Tests run in liquid No. 107 indicate that this environment is inert and has no effect upon the creep properties of Hastelloy W. The effect of liquid No. 30 on the creep properties of Hastelloy W sheet appears to be very similar to that shown for Hastelloy B. Figure 80 shows the surface reaction of Hastelloy W tested in liquid No. 30.

Creep-Rupture Testing of Hastelloy X

As part of our efforts to aid Pratt & Whitney in their reactor program, a series of tests has been run to determine the effect of liquid No. 30 on the creep strength of Hastelloy X. This alloy has demonstrated reasonable creep strength and ductility at high temperatures in an air environment; however, it can be seen in Fig. 81 that the environment of liquid No. 30 has deleterious effects on its creep strength above 1500°F. Since liquid No. 30 has a proclivity to leach chromium, its effect was expected over the entire temperature range; however, at 1500°F the amount of corrosion is small, as seen in Fig. 82, and does not appear to detract from the creep strength of the alloy. In creep testing at temperatures of 1650 and 1800°F, as shown in Figs. 83 and 84, intergranular corrosion occurs, and a serious drop in the creep strength of the alloy results. From the above tests it would appear that Hastelloy X would not be a satisfactory structural material in contact with liquid No. 30 at temperatures above 1500°F.

Creep-Rupture Testing of an 80% Magnesium–20% Lithium Alloy

Creep-rupture testing of an 80% magnesium–20% lithium alloy, proposed as a neutron shielding material for a crew compartment, has recently been initiated. The results of the creep-rupture testing program for this alloy at 200°F in air are summarized in Fig. 85. Stress is plotted vs time to 0.2, 0.5, 1, 5, 10, and 20% elongation and rupture. The specimens being tested at stresses below 400 psi have not reached 0.2% elongation in 500 hr.

Because of the poor oxidation resistance exhibited by this alloy a chemical surface treatment, which greatly enhances the oxidation resistance, was developed by R. E. McDonald of the Fabrication Group, ANP Metallurgy. Briefly, this treatment consists of (1) a nitric acid dip, followed by a rinse in water, and (2) immersion in phosphoric acid until reaction ceases, followed by an acetone rinse.

The specimens from which the data in Fig. 85 were determined were given this treatment and no oxidation has been observed after 2000 hr. Tests will be run on a few untreated specimens for comparative purposes.

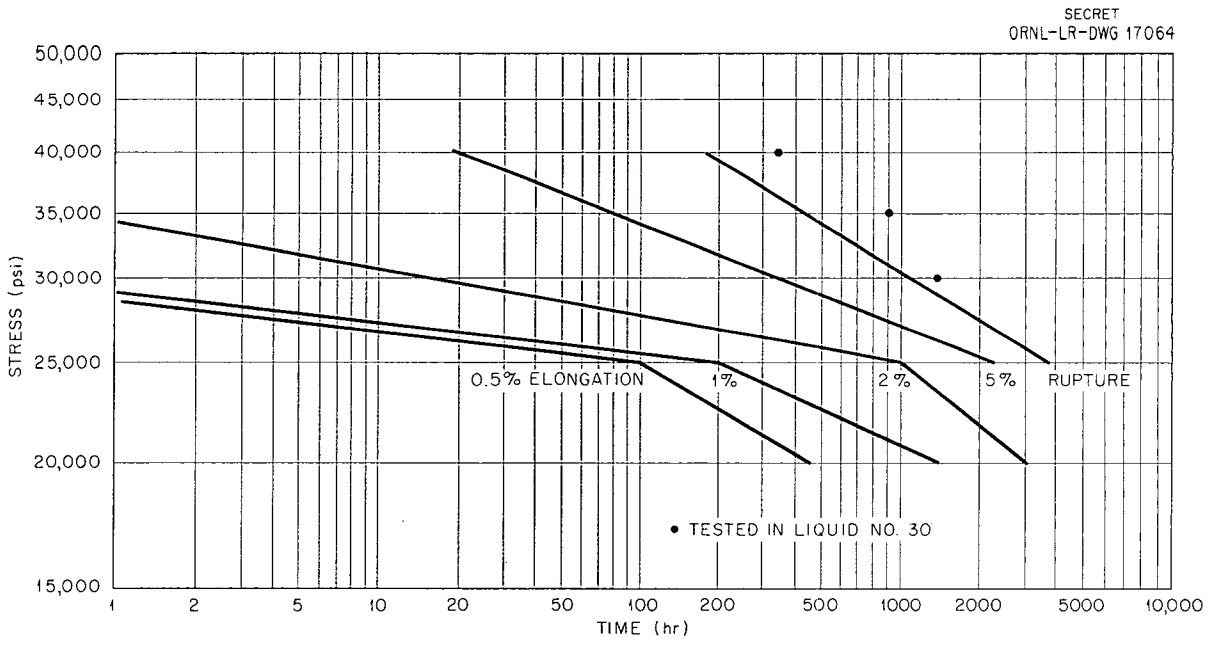

Fig. 76. Design Curve for Solution-annealed Hastelloy W Sheet Tested in Argon at 1300°F.

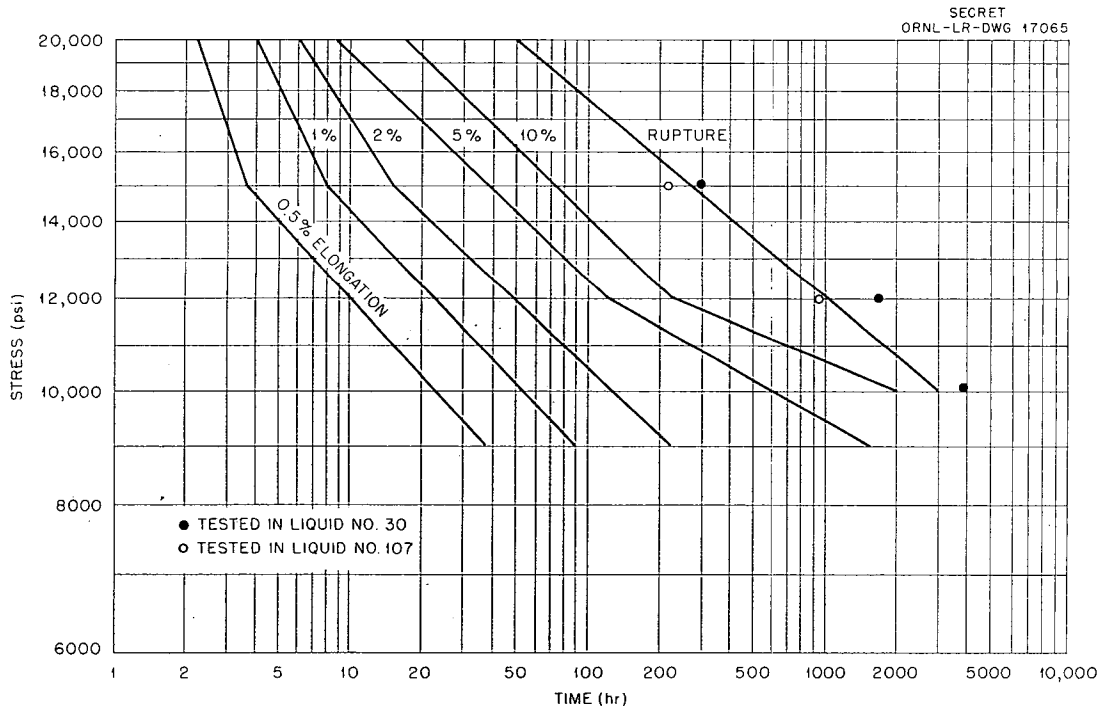

Fig. 77. Design Curve for Solution-annealed Hastelloy W Sheet Tested in Argon at 1500°F.

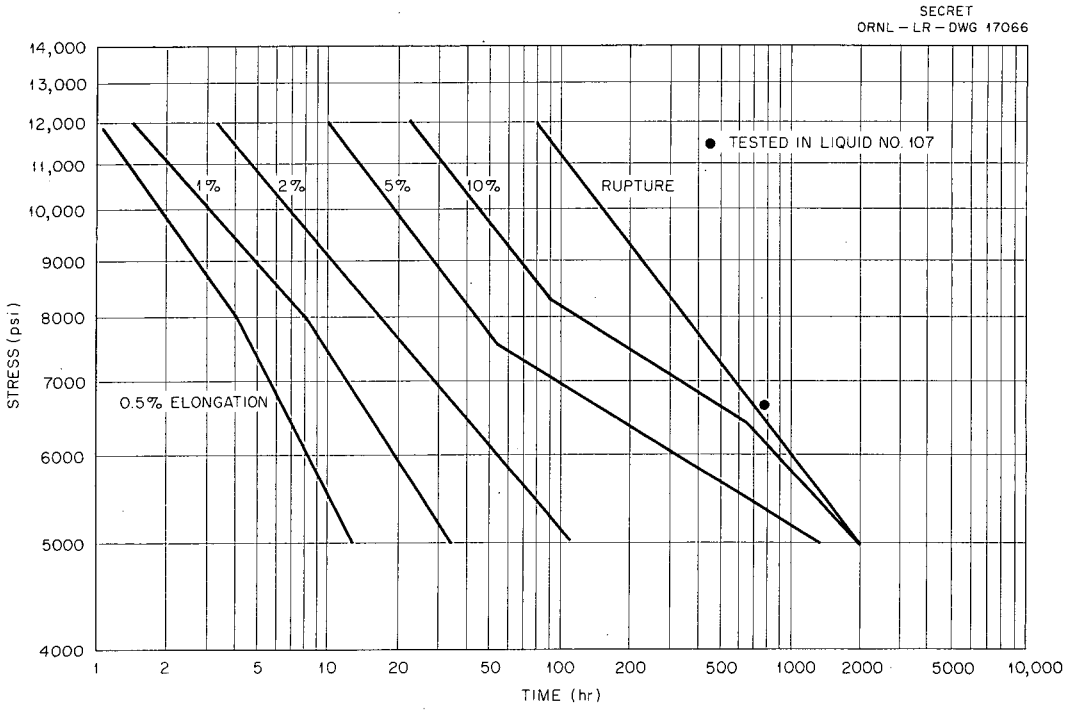

Fig. 78. Design Curve for Solution-annealed Hastelloy W Sheet Tested in Argon at 1650°F.

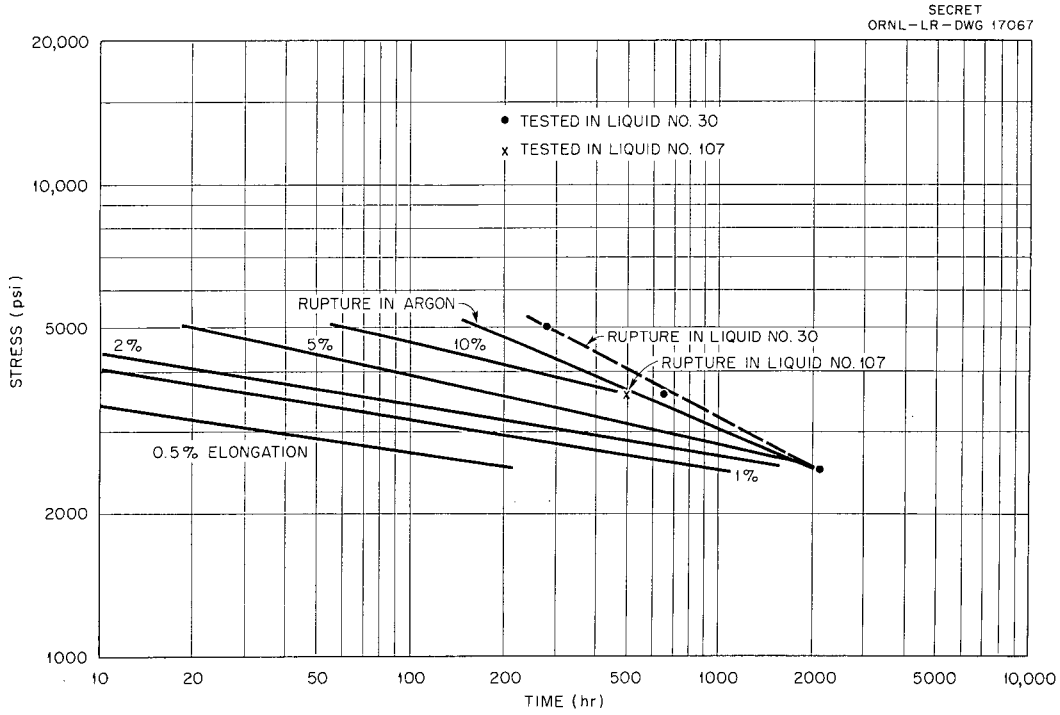

Fig. 79. Design Curve for Solution-annealed Hastelloy W Sheet Tested in Argon and Liquid No. 30 at 1800°F.

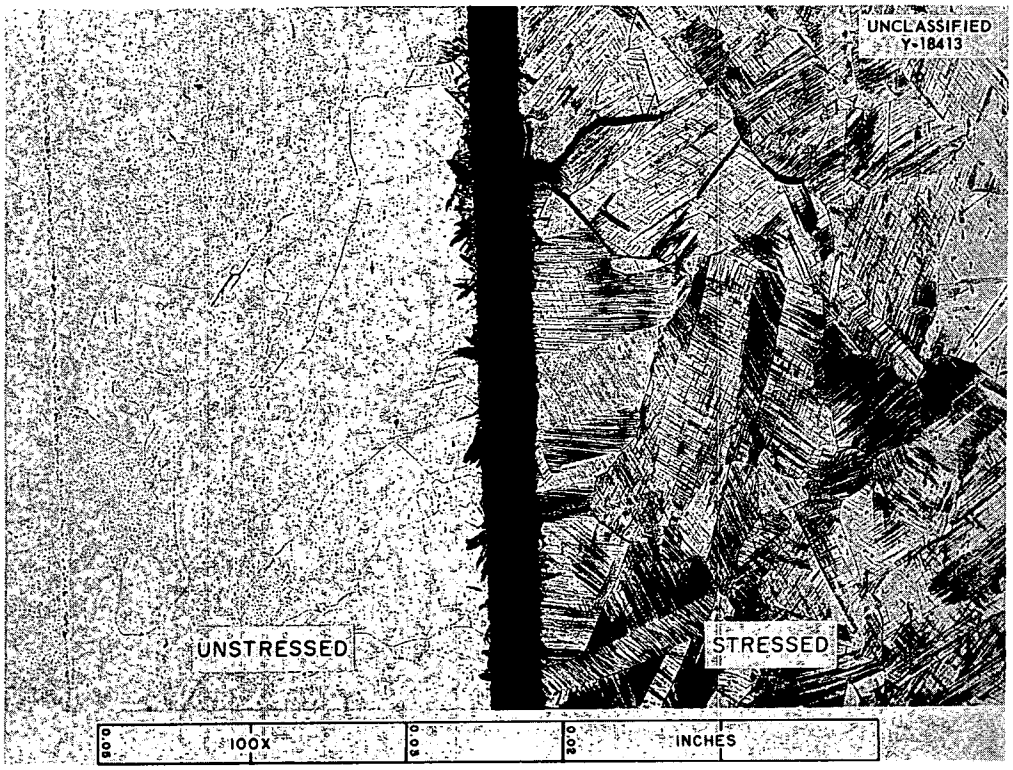

Fig. 80. Surface Effect of a Hastelloy W Specimen After Exposure to Liquid No. 30 for 1291 hr and a Stress of 35,000 psi at 1300°F. Reduced 16%. (Secret with caption)

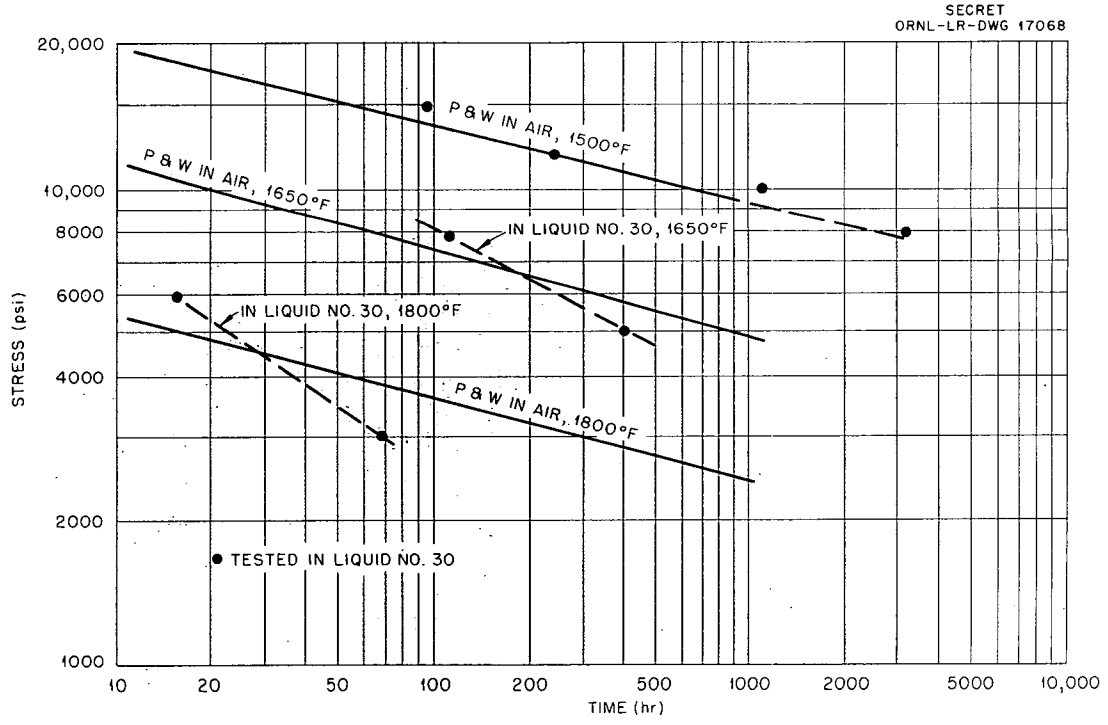

Fig. 81. Comparison of Stress-Rupture Properties of Hastelloy X in Air and in Liquid No. 30 at 1500, 1650, and 1800°F.

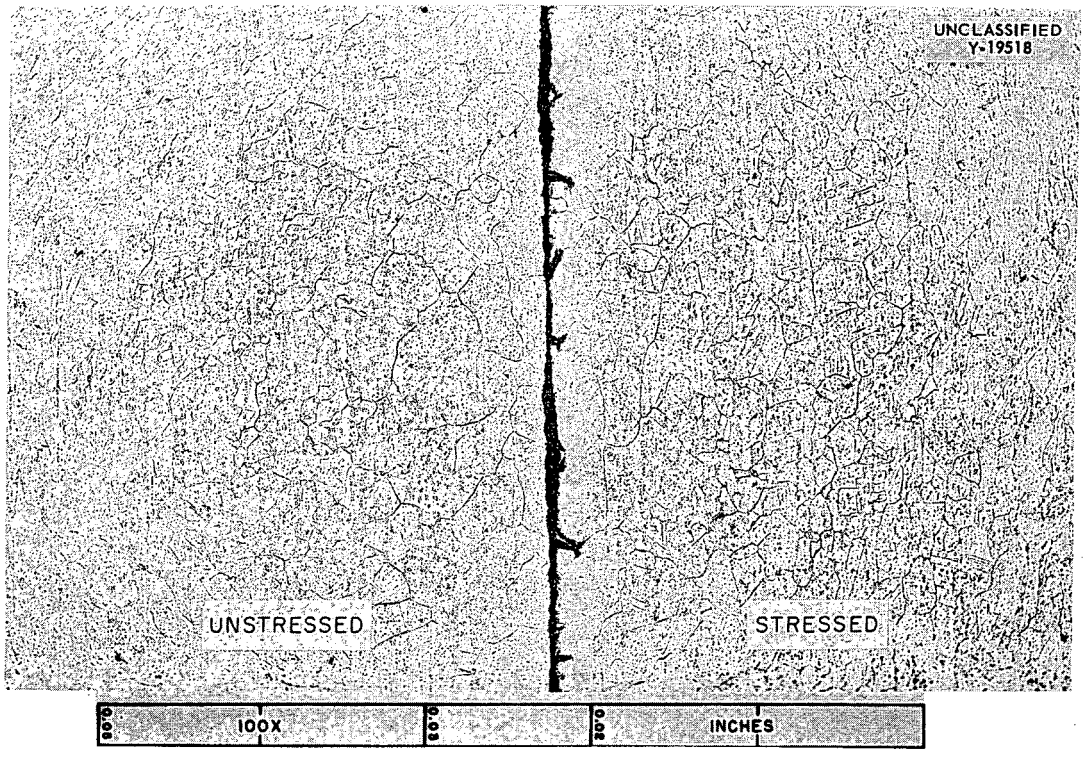

Fig. 82. Surface of the Stressed and Unstressed Portion of a Hastelloy X Specimen After Creep-Rupture Testing in Liquid No. 30 at 1500°F. Reduced 13%. (Secret with caption)

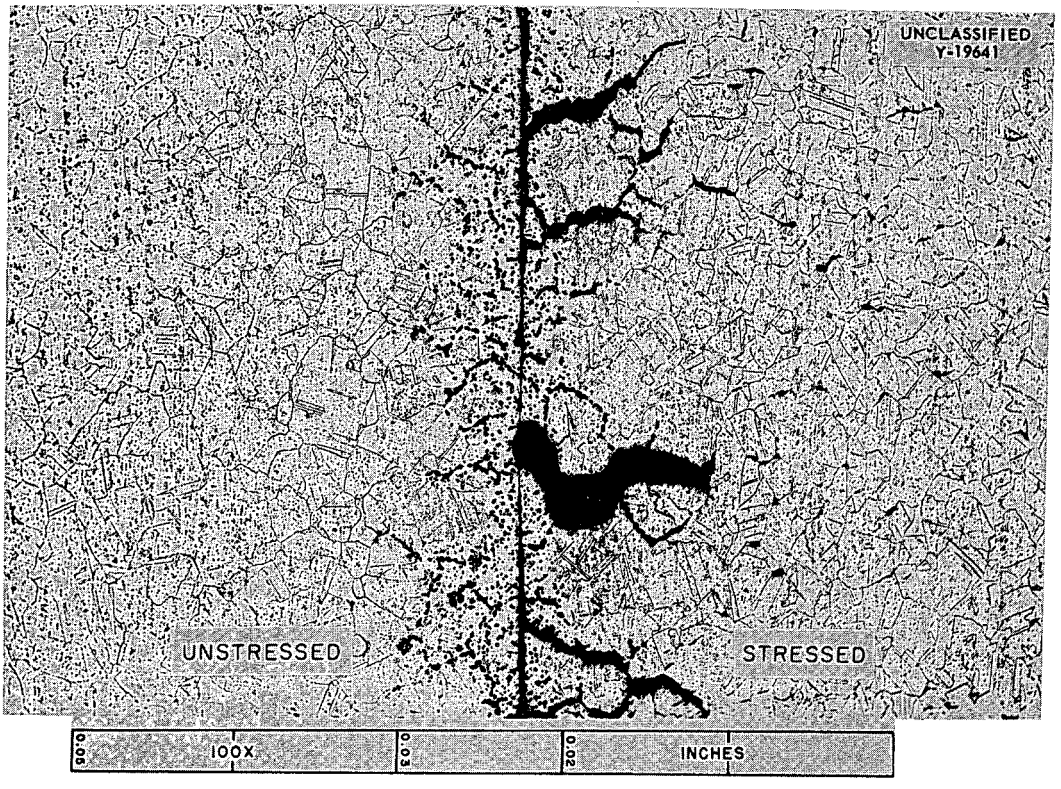

Fig. 83. Surface of the Stressed and Unstressed Portion of a Hastelloy X Specimen After Creep-Rupture Testing in Liquid No. 30 at 1650°F. Reduced 14%. (Secret with caption)

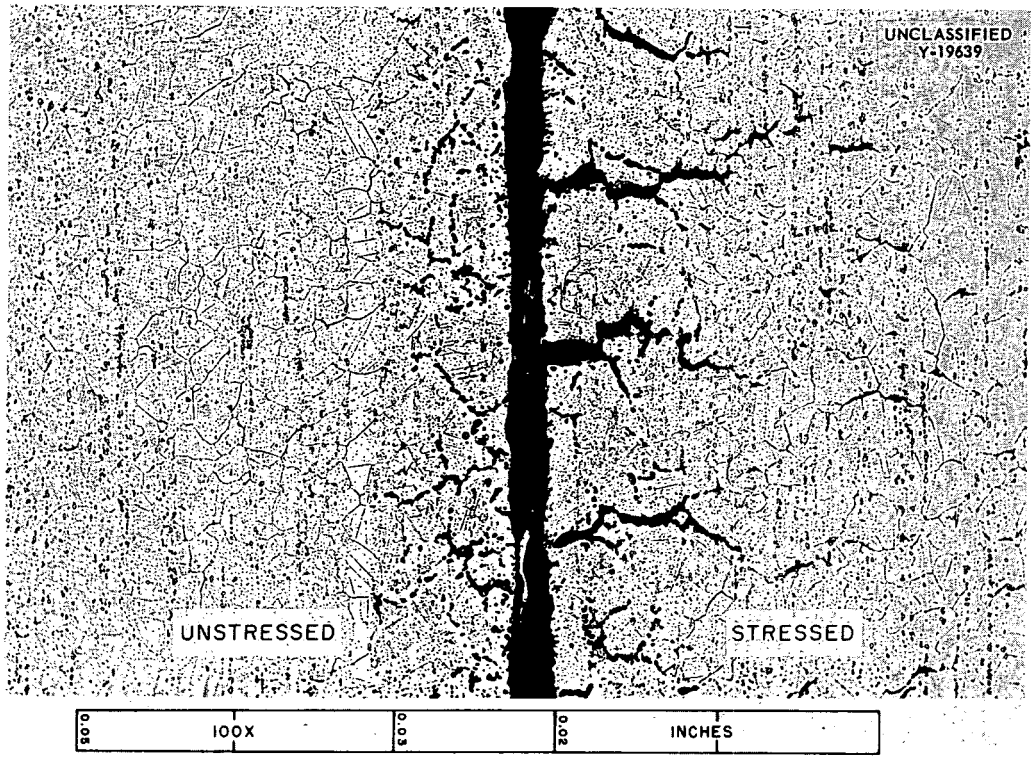

Fig. 84. Surface of the Stressed and Unstressed Portion of a Hastelloy X Specimen After Creep-Rupture Testing in Liquid No. 30 at 1800°F. Reduced 11%. (Secret with caption)

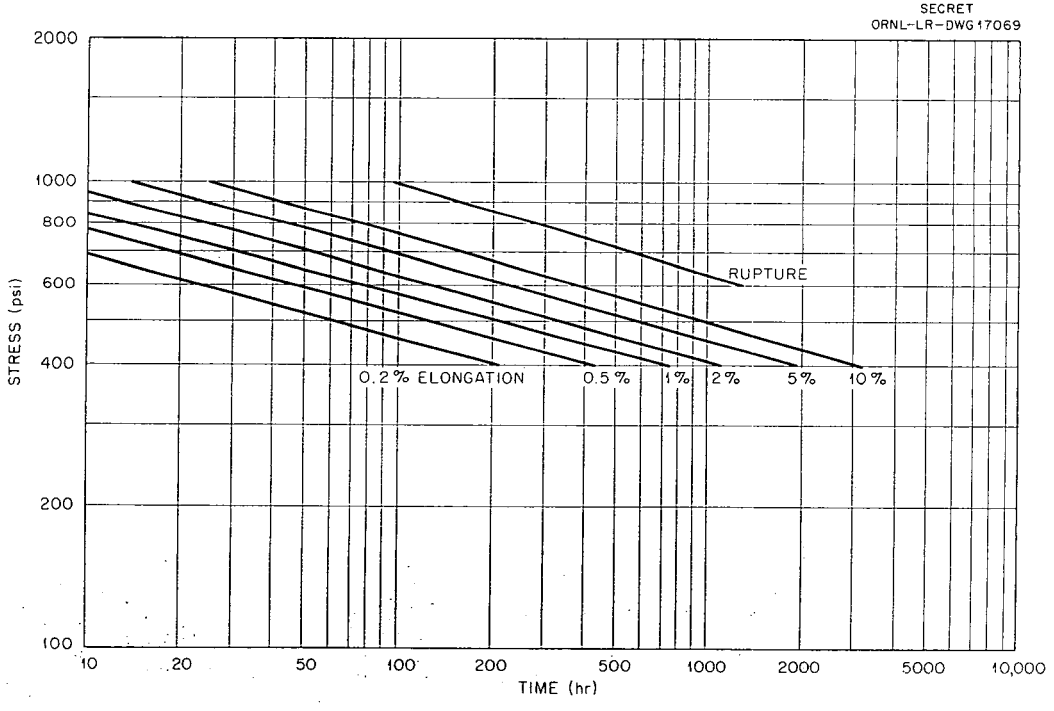

Fig. 85. Creep-Rupture Summary Graph for the Surface-treated Magnesium-Lithium Alloy Tested at 200°F in Air.

NONDESTRUCTIVE TESTING

R. B. Oliver J. W. Allen R. W. McClung

EDDY-CURRENT TESTING OF SMALL-DIAMETER TUBING

J. W. Allen

The results of the eddy-current inspection of 14,540 ft of CX-900 Inconel tubing are shown in Table 34. The undersize and oversize figures include rejections on both out-of-tolerance wall thicknesses and out-of-tolerance diameters, since the two appear inseparably in the cyclograph-type eddy-current readout.[1] The discontinuity indications were due to cracks, gouges, and the pickup of foreign metal on the inside of the tube.

[1] R. B. Oliver *et al.*, *Met. Semiann. Prog. Rep. April 10, 1956*, ORNL-2080, p 88.

In recent shipments the presence of foreign metal embedded in the inside wall of $^{3}/_{16}$-in.-OD × 0.025-in.-wall CX-900 Inconel tubing has been detected by the encircling-coil eddy-current test. Subsequent longitudinal macrosections of two such areas occurring in one 42-in. length are shown in Fig. 86, along with the eddy-current signal trace produced by this tube. These areas are indicated by the sharp downward spikes in the trace. They are similar to the spikes which result from short longitudinal cracks, except that the spikes are in the direction of increased wall thickness rather than in the direction of decreased wall thickness. Stains similar to the ones shown in Fig. 86 are yellow to red in color and are sometimes, but not

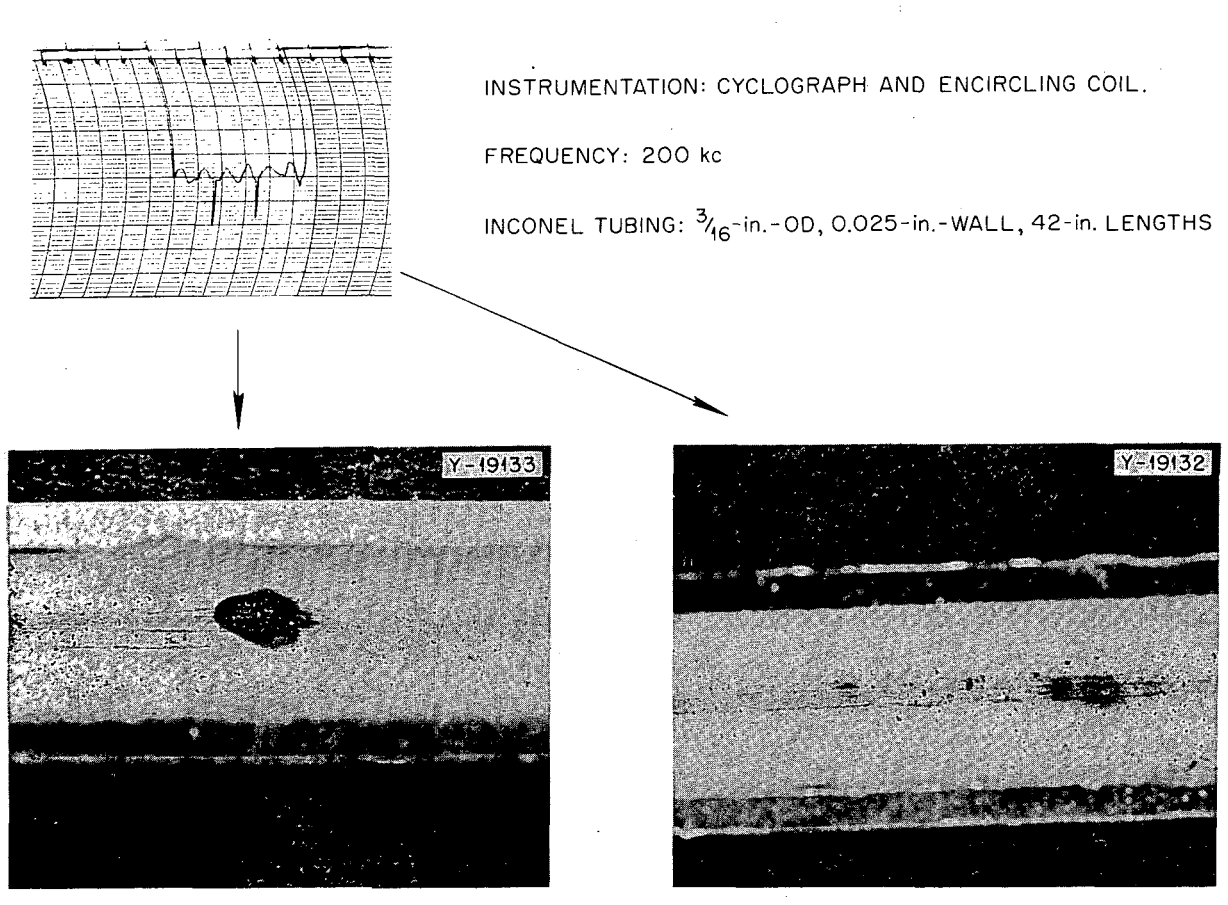

Fig. 86. Eddy-Current Signal Trace of Defective $^{3}/_{16}$-in.-OD × 0.025-in.-wall Inconel Tubing.

TABLE 34. EDDY-CURRENT INSPECTION RESULTS OF CX-900 INCONEL TUBING

Size	Total Pieces Inspected	Total Pieces Rejected	Rejections		
			Undersize	Oversize	Indications of Discontinuities
$\frac{3}{16}$-in. OD × 0.025-in. wall × 42-in. length	3003	167	71	57	39
0.229-in. OD × 0.025-in. wall × 78-in. length	229	3	3	0	0
0.242-in. ID × 0.035-in. wall × 132-in. length	236	6	6	0	0

always, present in the pickup areas. Transverse microsections through several of these areas have failed to reveal that these areas have a perceptible depth. This fact emphasizes that the pickup metal must have been highly permeable in order to have produced such large eddy-current indications, as shown in Fig. 86, which suggests that the foreign metal consists of bits of steel picked up from the mandrel over which the tubing was drawn. Further metallographic study and also microspark spectroscopy are planned on these areas.

INSPECTION OF TUBING BY ULTRASONIC METHOD

R. W. McClung

Large quantities of tubing are now being inspected by the immersed-ultrasonic technique. During the last report period 4224 pieces of $\frac{3}{16}$-in.-OD × 0.025-in.-wall × 42-in.-long CX-900 Inconel tubing were inspected, with 4143 lengths being accepted for critical use. Thus the rejection rate was slightly less than 2%, indicating a high-quality tubing. All the rejected lengths contained only very small, single defects. Metallographic examination of some of these defects was unsuccessful because of the difficulty of precisely marking the defect and because of the tendency of the metal to smear over small defects in polishing. Further metallographic studies are planned.

A total of 2360 ft of 0.242-in.-ID × 0.030-in.-wall thermocouple wall tubing in random lengths from 10 to 12 ft was inspected ultrasonically. Twenty-eight lengths were found to have one short defect each. One length had a series of short defects throughout the tube. Since the minimum usable length of this tubing was 10 ft, only about half of the rejected lengths were usable after removing the defective area. Thus the rejection rate was approximately 6%. Metallographic sectioning of a few of the defective areas disclosed a small gouge on the outside diameter of one tube approximately 0.005 in. deep × 0.012 in. wide × 32 in. long and a small outside-diameter crack approximately 0.003 in. deep on another tube. Again trouble was encountered because of the difficulty of precisely locating the defects and the problem of observing the indication in spite of the smearing during metallographic polishing.

Over 1000 ft of $\frac{3}{8}$-in.-OD × 0.035-in.-wall Hastelloy C tubing in random lengths was inspected ultrasonically with a resultant rejection rate of approximately 30%. Metallographic sectioning disclosed the presence of cracks or other discontinuities such as those illustrated in the following figures. Figure 87 is a macrograph of the inside surface along the weld. An apparent lack of fusion is present, accompanied by tiny tears along the weld-parent metal interface. Figure 88 is a micrograph showing an internal crack which did not extend to either the inside or the outside surface of the tube wall. It seems to be in the heat-affected zone adjacent to the weld. Figure 89 is an unetched sample of Hastelloy C tubing which exhibits two cracks, one of which seems to be approximately 0.015 in. deep and the shallower one about 0.005 in. in depth. Etching of this sample, as shown in Fig. 90, discloses greater depth on each of the cracks to about 0.020 in. on the deeper and 0.015 in. on the shallower. Figures 91*a* and *b* present another crack in the etched and unetched condition, respectively. It may again be noted that the crack, although it is about 0.015 in. deep, does not

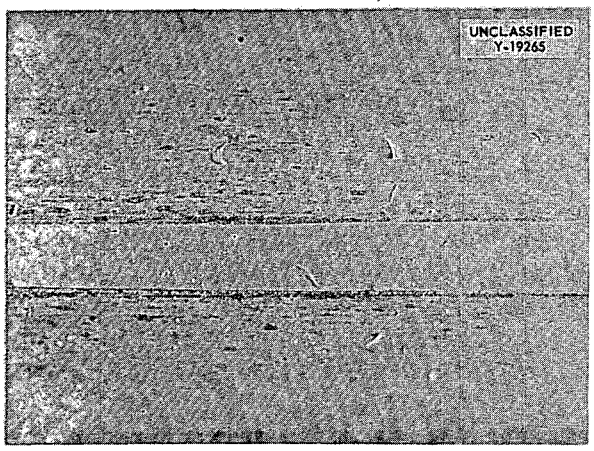

Fig. 87. Macrograph of the Inside Surface of Weld-drawn Tubing.

extend to either surface. Again difficulty was noticed in the preparation of metallographic sections due to the problem of smearing the soft matrix over the defects in the polishing operation. However, a greater degree of success was achieved in locating the defects in this material than in the Inconel tubing. This can probably be attributed to the larger size defect which seems to regularly occur in Hastelloy tubing.

Over 1000 ft of $\frac{3}{8}$-in.-OD × 0.035-in.-wall CX-900 Inconel tubing in random lengths was examined ultrasonically with a total rejection of approximately 25 ft. The few defects which were detected seemed to be very small. In general the quality of this tubing seemed to be quite high as is indicated by the rejection rate of less than 2.5%.

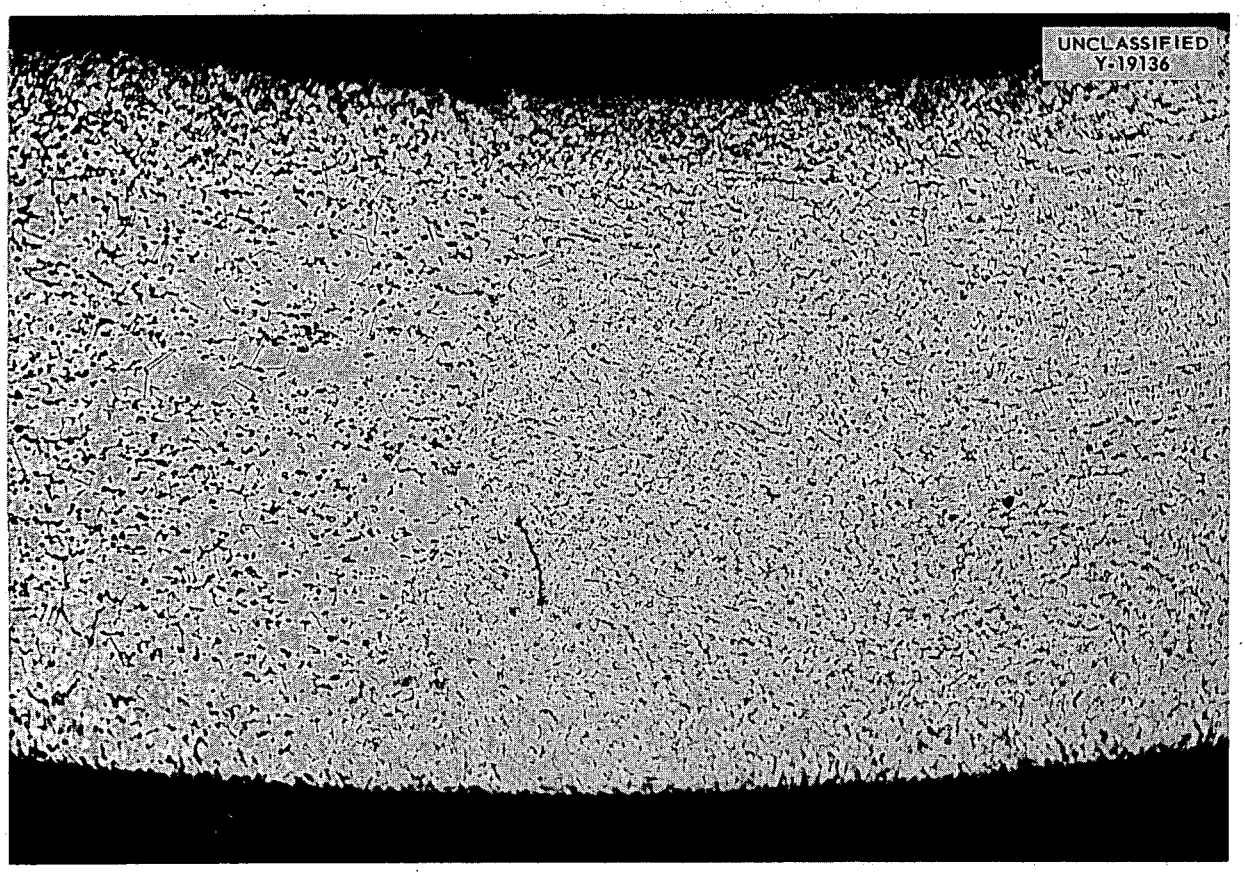

Fig. 88. Internal Crack in the Weld Bead of $\frac{3}{8}$-in.-OD × 0.035-in.-wall Hastelloy C Tube. Etched with chrome regia. 100X.

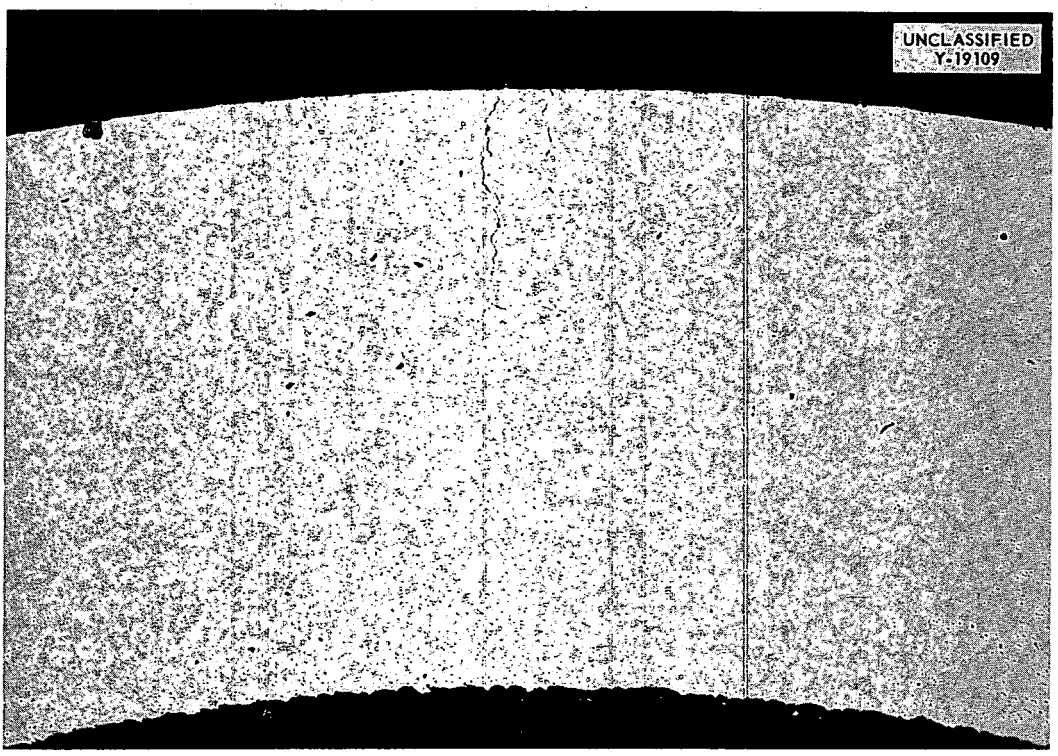

Fig. 89. Intergranular Cracking in Hastelloy C Tube. Not etched. 100X. Reduced 11%.

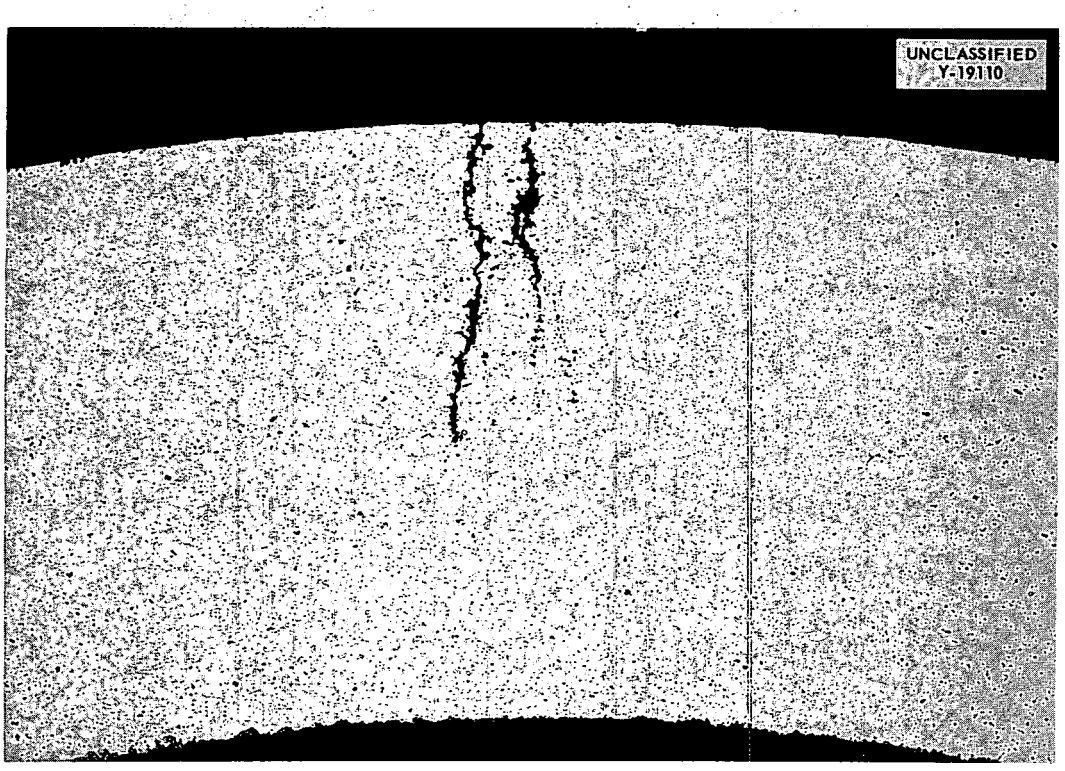

Fig. 90. Intergranular Cracking in Hastelloy C Tube. Etched with chrome regia. 100X. Reduced 11%.

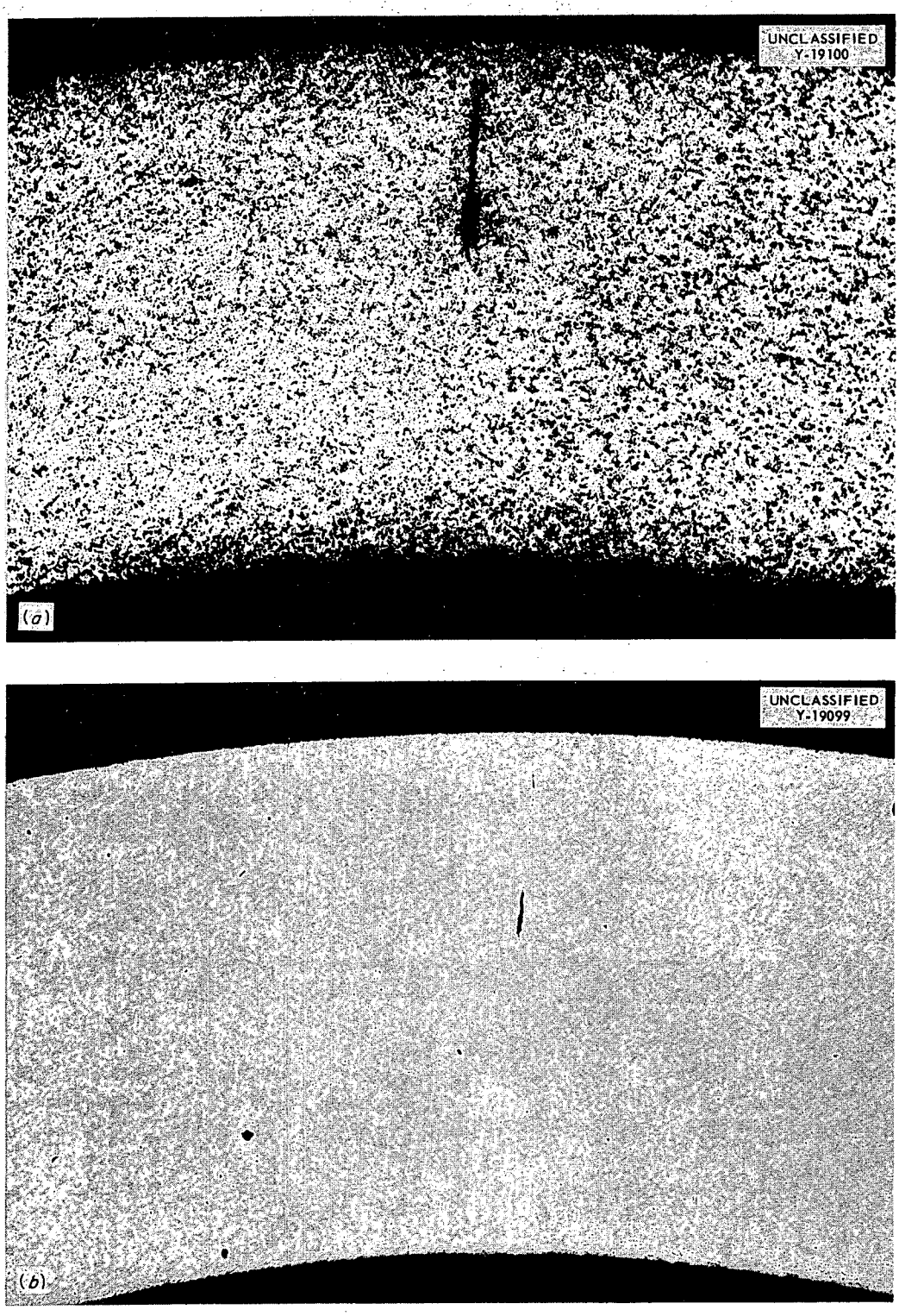

Fig. 91. Cracking in Hastelloy C Tubing. (*a*) Etched with chrome regia. (*b*) Unetched. 100X. Reduced 13.5%.

Metallography failed to disclose any defect of appreciable size.

Two hundred twenty-nine pieces of 0.229-in.-OD × 0.025-in.-wall × 78-in.-long CX-900 Inconel tubing were examined ultrasonically with 31 pieces being rejected.

An attempt is being made to correlate all defects found by ultrasound and other inspection methods. With the larger defects this is normally possible. However, for many of the very small indications, particularly on the inside diameter of the tube, ultrasound seems to be the only feasible detection method. It is hoped that, despite the inherent difficulties, metallographic work will continue to provide additional information concerning the nature of the defects.

ULTRASONIC PIPE INSPECTION

J. K. White R. B. Oliver

No development work on the ultrasonic method for the inspection of pipe had been planned, because the literature had reported several apparently adequate techniques. A short investigation showed that, for high precision work, it would be necessary to improve upon contact techniques by eliminating contact pressure, surface finish, and coupling thickness as variables; it was also decided that the suppression of Rayleigh or surface waves was a prerequisite to quantitative interpretation of results. Development of an immersed method solved these problems and achieved these further advantages:

1. Simple continuous adjustment of the incident angle of the sound beam is permitted.
2. The water column provides a delay line which allows the very strong initial signal to pass through the amplifier before the weaker inspection signals return to the instrument.
3. Collimation may be achieved; thus a limit can be placed on angle of incidence.

Figure 92 shows the pipe inspection facility devised for utilizing the immersed ultrasonic method. It consists of a tank 26 ft long, 14 in. wide, and 20 in. deep; variable-speed, motor-driven, lathe-headstock-adjustable, skewed-roller supports; a motor-driven translation guide; a hand-held, transducer-positioning jig; and instrumentation. In use, the pipe to be inspected is immersed in treated water in the tank, supported by the rollers, and rotated by the lathe headstock. The positioning jig shown in Fig. 93 is equipped

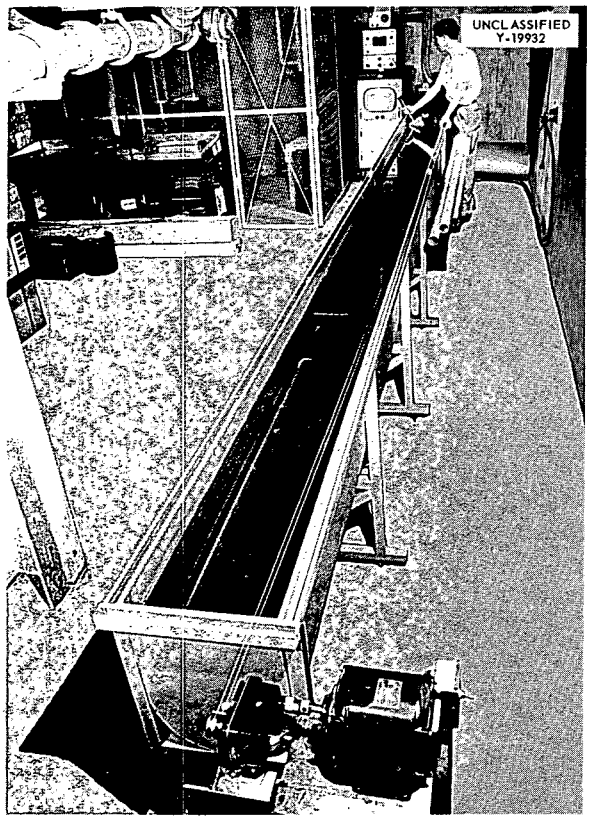

Fig. 92. Facilities for Inspection of Pipe by the Immersed Ultrasonic Method.

with a series of templates to fit any common pipe sizes. It holds the piezoelectric transducer in a steady position relative to the longitudinal axis of the pipe. As the pipe is rotated, the transducer and guide are manually translated along the pipe at a steady rate as directed by the motor-driven guide. Thus the transducer path describes a helix circumscribing the pipe, and, provided the guide is properly set, the beam of ultrasonic energy produced by the transducer covers the entire pipe.

Instrumentation shown in Fig. 94 consists of the model 424A Immerscope (Curtiss Wright Corp., Caldwell, New Jersey); the B-scan, the large console under the Immerscope; and a small audible alarm, the small upper box, designed at ORNL. The Immerscope excites a lithium sulfate crystal, causing it to emit high-frequency sonic vibrations. This ultrasonic beam is transmitted into the water bath and into the pipe wall. Any discontinuity of the pipe wall reflects the sound beam which

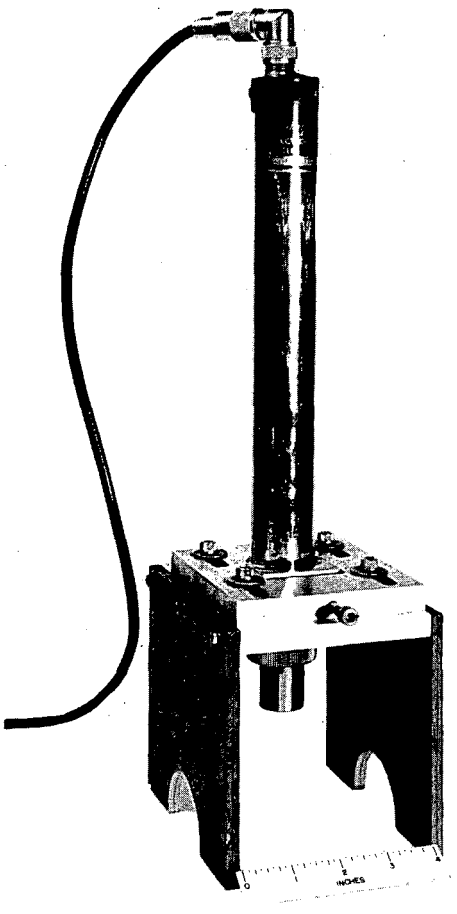

Fig. 93. Method of Mounting Ultrasound Search Unit to Inspect Pipe.

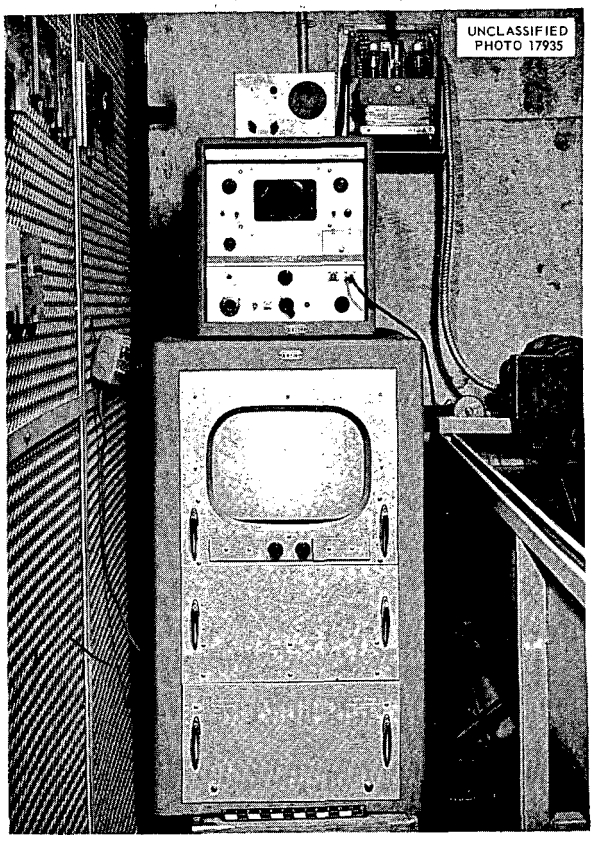

Fig. 94. Instrumentation for the Immersed Ultrasonic Inspection of Pipe.

is received by the crystal, amplified by a wide-band amplifier, and presented as a time-amplitude plot on the small oscilloscope. The "B-scan" takes the same data plus a signal for rotation of the pipe and plots pipe rotation against time of travel on a larger oscilloscope. This latter plot is easier to interpret because the oscilloscope utilizes a persistent phosphor, and information being plotted may be compared with information of the past several seconds. This is more easily understood than the instantaneous plot shown by the Immerscope or "A-scan." The audible alarm calls the attention of the operator to indications which might otherwise be missed.

As a reference standard to establish acceptance or rejection of pipe, longitudinal notches are cut in the inside and outside surfaces of a sample length of pipe with the same dimensions and composition as the pipe being inspected. These notches are 1 in. long, 5% of wall thickness deep, and only as wide as is necessary for fabrication; both notches are located on the same circumference of the pipe. It is considered imperative to use an inside-diameter reference notch to prove inspection of the inner surfaces. Reference notches on the inside diameter have been difficult to make and to measure. At the present time the ultrasonic inspection is our best measuring method. New machining techniques are being investigated so that an inside-diameter notch of known depth may be produced.

Since the installation of the pipe inspection facility in April 1956, and until August 1956, over 6000 ft of pipe, ranging from $\frac{3}{8}$-in. IPS sched-40 pipe to 7-in.-OD × 0.54-in.-wall tubing, has been inspected with good success.

INSPECTION OF THIN SHEET

J. W. Allen R. W. McClung
R. B. Oliver

Sheet material has extensive application in power reactors and in most cases this formed sheet will function both as a container for fluids and as a heat transfer medium between the two fluids. Since high heat fluxes and thermal stresses are involved, the presence of laminar defects is very undesirable. The only known method for detecting such defects in sheet poses, currently, a difficult mechanical problem. This situation has motivated an investigation to develop a simpler and better inspection method. Liquid-penetrant, radiographic, and eddy-current methods cannot work because of the unfavorable defect orientation. The ultrasonic resonance method was not an adequate approach, since it is not capable of resolving small defects and it inherently requires a slow contact scanning of the sheet. The conventional pulse-echo ultrasonic inspection, even with a pulse length as short as 1 μ, is not practical for sections thinner than 0.20 in. The transmission-attenuation technique is capable of detecting small laminations in thin sections, but, since it requires a critical alignment of two transducers on opposite sides of the sheet, it is a very difficult method to apply to the inspection of large or nonplanar areas.

A new ultrasonic method has been proposed by this group and preliminary experiments have given promising results. This method requires a pulse of ultrasound having a duration of 5 to 20 μ and tuned to such a frequency that the sheet thickness is an exact multiple of the half-wave length. With these conditions the ultrasound reverberates or rings between the two sheet surfaces for a period of time that is several times greater than the pulse duration. When a lamination exists in the sheet this ringing is decreased, both in duration and amplitude, as a function of the area of the lamination relative to the transducer area. To test this method, flat-bottom holes with several different areas were milled into one side of a sheet of Inconel to various depths. Preliminary experiments with this method by using existing equipment were successful in that most of these reference defects were located.

To properly instrument this test method, the reflectoscope has been drastically altered. The pulse repetition was increased from 60 to 500 pulses per second, appropriate filters were added to the circuits, a variable sweep delay circuit was added to permit immersed scanning, and external connections have been provided for synchronization signals. This last change will permit the addition of gated alarm circuits and various data-presentation and recording units in the near future.

INSPECTION

A. Taboada
R. Heestand
G.M. Tolson
A. Goldman

SPECIFICATIONS

A. Taboada A. Goldman

A number of specifications have been written in order that the metallurgical requirements of the ANP project may be met in the purchase of materials. These specifications are for:

MMS-1	Small Diameter Inconel Tubing
MMS-2	Hastelloy B Tubing
MMS-3	Hastelloy B Welded Pipe
MMS-4	Hastelloy B Plate and Sheet
MMS-5	Hastelloy B Rod and Bar
MMS-6	CX-900 Inconel Sheet or Strip or Tubing for Expansion Joint Bellows
MMS-7	Inconel Plate for Hot Forming Application
MMS-8	Inconel Fittings
MMS-9	Seamless Inconel Pipe
MMS-10	CX-900A Inconel Hot Formed Bar
MMS-11	Inconel Tubing (Sizes Other Than Those Covered by MMS-1)

WELD INSPECTION

A. Taboada

The following inert-gas shielded-arc Inconel weldments were inspected in the Y-12 shops:

Total Number Inspected	Number Rejected	Per Cent
4959	539	11

The rejectable conditions noted were porosity, cracks, misalignment, lack of fusion, and lack of penetration. It may be noted that approximately 60% of the rejected welds required only repair in order to obtain an acceptable weldment. An additional 813 noncritical welds were fabricated and inspected on NaK filters, fuel sampler units, and experimental thermocouple welds.

MATERIAL INSPECTION

A. Taboada G. M. Wilson

The following Inconel material (see Table 35) was inspected by radiographic, dye-penetrant,

TABLE 35. INCONEL MATERIAL INSPECTED

Type Material	Total Inspected	Amount Rejected	Per cent
Tubing: regular, ft	1,602	268	17
CX-900, ft	20,370.5	1951	10
Pipe, $\frac{1}{8}$-in. to 6-in. IPS sched 40, ft	7,492	855	11
Rod, 1-in. to 8-in. dia, ft	1,044	18	2
Plate and sheet: regular, ft^2	4,959	230	5
CX-900, ft^2	359	1	0.3
Fittings: $\frac{3}{4}$-in. to 8-in. IPS sched 40	84	1	1
Reducers, various sizes	78	0	0
Ells, $1\frac{1}{2}$-in. to 2-in. IPS sched 40	18	0	0

ultrasonic, and visual techniques. Most of this material was requested for use in the fabrication of component parts and the piping systems of the ETU and ART assemblies.

In addition, three hundred 78-in. lengths of 0.229-in.-OD × 0.025-in.-wall CX-900 tubing were received for inspection. Upon destructive examination of one tube, a medium blanket of oxide was noticed. Further examination by borescope revealed that 90% of the tubes examined were affected. Consequently, the entire lot was rejected.

Also rejected, in addition to the above, was 1861 ft of 0.250-in.-OD × 0.025-in.-wall regular Inconel. This tubing did not meet purchase specifications, in that numerous indications of defects greater than 5% of the wall thickness were found.

An extensive examination of defects found during the various inspection methods on thin-wall Inconel tubing has been performed in order that an evaluation of inspection methods may be made. The results to date indicate that, due to the various sizes and shapes of defects encountered on both the outside and inside surfaces, a continuation of all inspection methods presently performed will be required in order to detect detrimental flaws.

Figures 95 through 100 show the photomacrographs and photomicrographs of typical defects found by the various inspections performed in the Y-12 area. It may be noted that re-examination of the defective areas by the methods which had previously found them to be acceptable failed to detect these flaws in most cases.

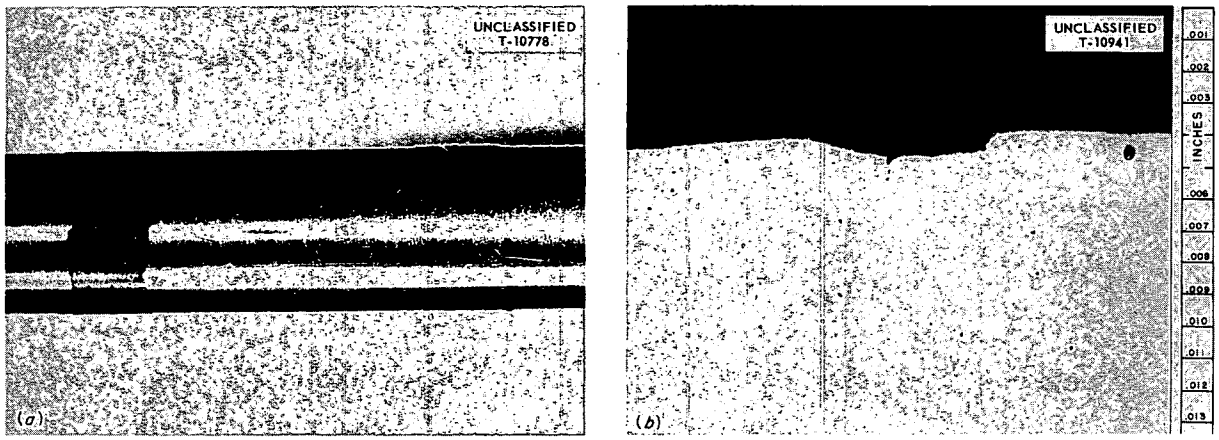

Fig. 95. Typical Defect Rejected on Visual Examination. (*a*) Macrograph. 3X. (*b*) Micrograph. 250X. Reduced 30.5%.

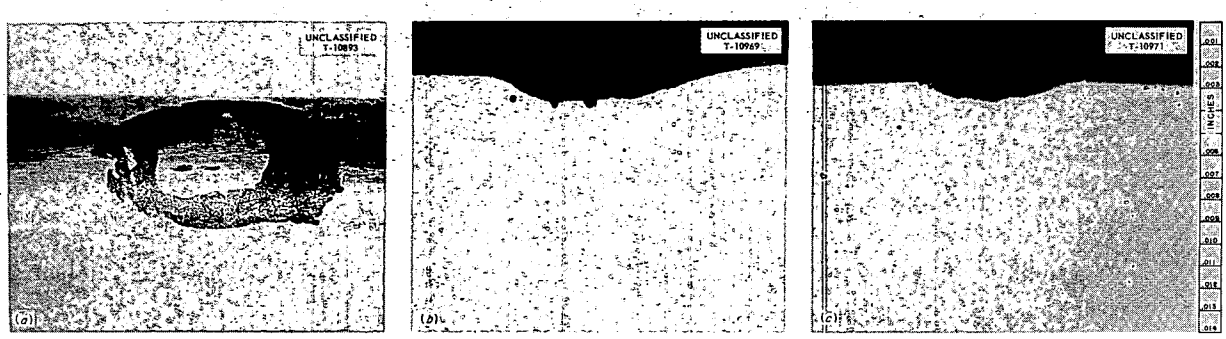

Fig. 96. Typical Defect Rejected on Pentrex Penetrant Examination. (*a*) Macrograph. 8X. (*b*) Micrograph. 250X. (*c*) Micrograph. 250X. Reduced 52%.

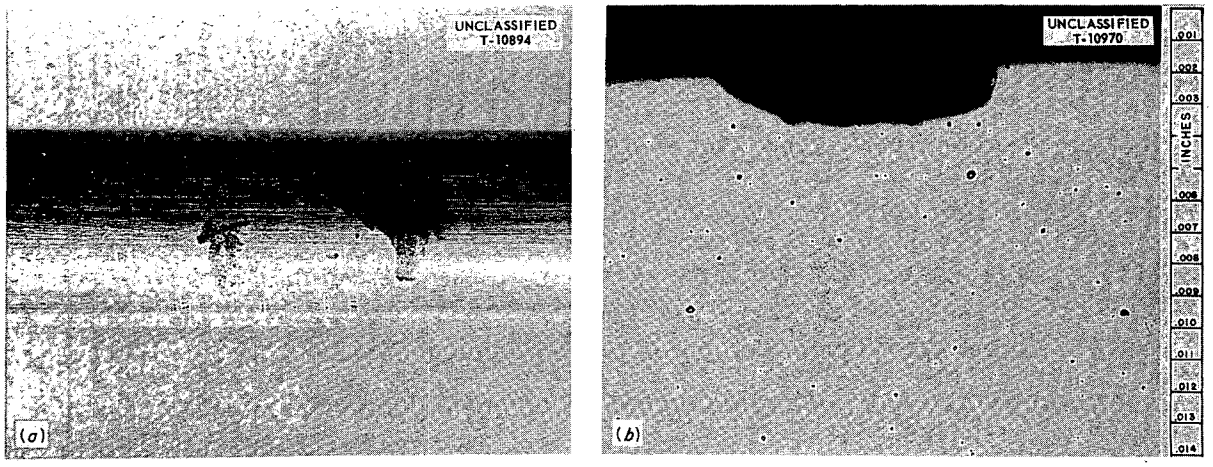

Fig. 97. Typical Defect Rejected on Pentrex Penetrant Examination. (*a*) Macrograph. 8X. (*b*) Micrograph. 250X. Reduced 31%.

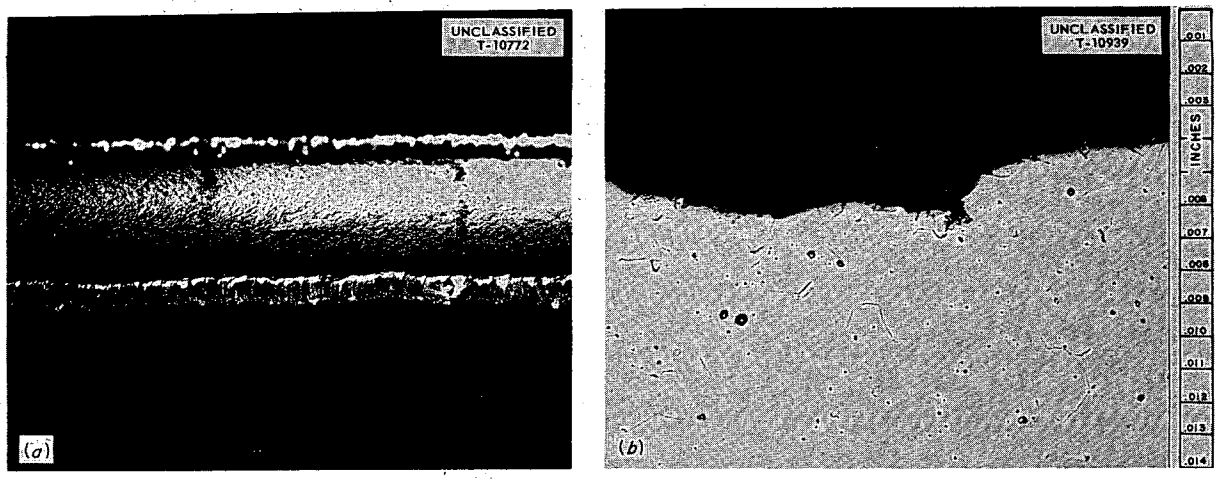

Fig. 98. Typical Defect Rejected on Radiographic Inspection. (*a*) Macrograph. 8X. (*b*) Micrograph. 250X. Reduced 28%.

OTHER MATERIAL

Sixty feet of Inconel "W" tubing was received and inspected for use in fabrication of thermal-convection loops. All of this material was found to be acceptable for this application.

The Hastelloy B material shown in Table 36 was examined by visual, dye-penetrant, radiographic, and reflectoscope techniques.

Because of numerous surface conditions, the pipe and tubing required reworking by centerless

TABLE 36. HASTELLOY B MATERIAL EXAMINED

Type	Total Inspected	Total Rejected	Per Cent
Pipe	160 ft	5 ft	3
Tubing	208 ft	136 ft	65
Plate and sheet	116 ft^2	0 ft^2	0
Rod and bar	244 ft	43 ft	18

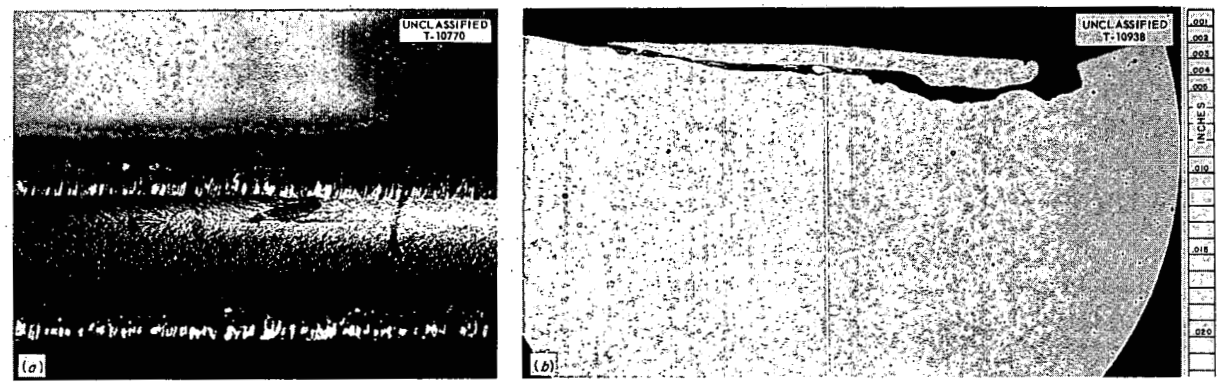

Fig. 99. Typical Defect Rejected on Radiographic Inspection. (*a*) Macrograph. 8X. (*b*) Micrograph. 150X. Reduced 42%.

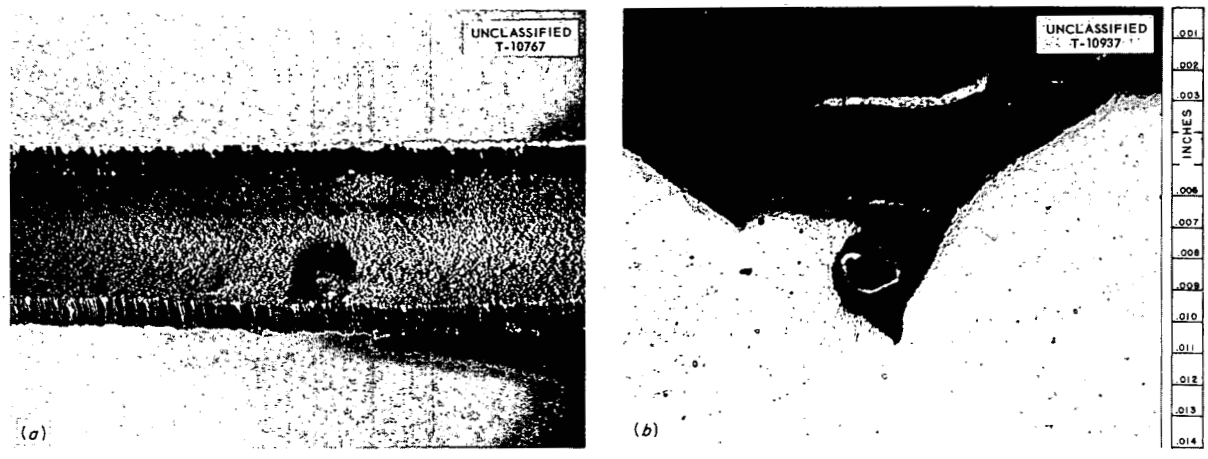

Fig. 100. Typical Defect Rejected on Radiographic Inspection. (*a*) Macrograph. 8X. (*b*) Micrograph. 250X. Reduced 31%.

grinding. Other defects noted were cracks and porosity.

A waiver was made on fine and medium size porosity, resulting in the rejection of only those areas with cracks and large porosity.

Because of failure of electrical Calrods in service, radiographic inspection of these units has been requested. Those units which are found to have improper orientation of the conduit are subject to rejection. A total of 150 units, 3½ ft each, have been examined and found to be acceptable.

COMPONENT PARTS FABRICATED BY OUTSIDE VENDORS

R. L. Heestand[1]

Sixty thermal-convection loops were received and the welds were inspected by the dye-penetrant method. Thirty-six of these loops were found to have welds which showed numerous indications of cracks, pinholes, and other defects. These loops were sent to the Y-12 shops to be repaired where

[1]On loan from Pratt & Whitney Aircraft.

necessary, and reinspected. The remainder were accepted for use.

Thirty-eight pieces of Inconel plate were inspected prior to shipment for fabrication into dished heads, then re-examined for manufacturing defects upon return. Several were found to have numerous pitted conditions, apparently caused by a foreign material being embedded during the pressing operation. Four heads were found to have cracks running from the edge inward which appeared to be as deep as ½ in. These areas were repaired by grinding and welding. Re-examination by radiographic techniques revealed that two of the heads were acceptable and the remaining two still contained crack conditions. Apparently these cracks were not completely ground out, with the result that further propagation occurred when heat was applied.

Four small heat exchanger units and the accompanying fabrication data and inspection reports were received for acceptance. Inspection results indicated that, while several minor conditions were apparent, these units were acceptable for test service.

Three high-conductivity-fin ½-Mw radiators and the accompanying fabrication data, inspection reports, and braze control samples were received for inspection. Inspection results indicated that two of these units were acceptable with minor conditions. The rejection of the third unit was recommended on the basis of the results found in the evaluation of the control sample and the x-ray films. This unit was subsequently accepted by the project engineer for test service.

FLUORESCENT-PENETRANT INSPECTION OF TUBING

G. M. Tolson

The installation of the fluorescent-penetrant equipment to be used in the inspection of small-diameter, thin-wall tubing has been completed. Tests are now being performed to compare the fluorescent-penetrant method with the dye-penetrant type of inspection used heretofore. Indications are that it will be possible to ensure higher quality tubing with the new method because of its higher sensitivity. The fluorescent penetrant revealed small pinholes and tight laplike defects which were not discernible by the dye-penetrant method. Exploration of some of these areas by polishing showed them to be as deep as 0.002 in. in some cases. However, the greater sensitivity of the new method will present some problems initially because experience will be required before the indications of superficial imperfections can be distinguished from indications of true defects.

RADIOGRAPHIC INSPECTION

A. Taboada G. M. Tolson

Since Eastman Kodak has discontinued the manufacture of type A industrial x-ray film, an effort is being made to evaluate the replacement film, type AA, and other films in order that the radiographic requirements of the ANP program may be successfully attained.

Specifications pertaining to the radiographic inspection of materials and fabricated component parts are being developed. These specifications will be designed to specify the various techniques required in the use of both x-ray equipment and gamma source radiation in order that a high degree of film quality may be attained from both in-plant inspection groups and outside vendors.

QUALIFIED WELDERS EMPLOYED IN ANP PROGRAM

A. Goldman

The number of qualified welders presently being utilized in the ANP program is shown in Table 37.

An estimate of the number of qualified welders to be required of ORNL is now being prepared. Qualification of these welders is expected to begin as soon as these requirements are known.

A qualification program is now under way at the Paducah installation. No welders have qualified to date.

TABLE 37. QUALIFIED WELDERS IN THE ANP PROGRAM

Location	Welding Procedure Specification		
	PS-1	PS-2	Both PS-1 and PS-2
Y-12 Plant, Oak Ridge			22
Outside vendors:			
York Corp., York, Pa.	8		
Griscom-Russell Corp., Massillon, Ohio	2		
Black, Sivalls & Bryson, Tulsa, Okla.	5		
Process Engineering, Inc., Mathuen, Mass.	2		
Struthers-Wells Corp., Warren, Pa.	1		
Total	19	1	22

WELDING AND BRAZING

P. Patriarca
R. E. Clausing
A. E. Goldman
G. M. Slaughter
E. J. Wilson

MEASUREMENT OF WELD SHRINKAGE IN INCONEL CORE SHELLS

A series of tests are being carried out to determine the weld shrinkage to be expected during the welding fabrication of the Inconel core shells for the ART facility. Since comparisons of the weld shrinkage formulas given in the literature with preliminary results obtained at ORNL revealed wide discrepancies, it was decided that actual experiments yielding empirical data would be necessary.

As a means of obtaining useful preliminary information, a program of welding Inconel plates under controlled conditions and close observations was initiated. Based upon the results of these tests, the welding of large Inconel hoops was begun. These tests were performed in a manner as nearly duplicating the fabrication problems and restrictions of the actual core shells as was possible. The experimental procedure used on the $\frac{1}{4}$-in. thickness is described and compared with that to be expected for other thicknesses.

Each test for the initial program consisted in the inert-arc welding of two $\frac{1}{4}$-in. Inconel plates, each 6 × 20 in., in accordance with techniques described in Procedure Specification PS-1. A 50-deg bevel with a $\frac{1}{16}$-in. land was machined on one long edge of each plate. A total of nine tests was performed.

Each pair of plates was assembled as shown in Fig. 101. The root gap was fixed at $\frac{1}{8}$-in. by using four $\frac{1}{8}$-in. tool-steel spacers. The plates were held against a flat horizontal plate by means of C-clamps. Two large clamps were used to draw the plates tightly against the tool-steel spacers. The edges of the plates were securely taped to prevent air leakage into the gap, since only the torch gas was used to supply backing gas and weld coverage.

A $\frac{1}{2}$-in.-long tack weld was placed at each end of the root gap, and two more $\frac{1}{2}$-in.-long tack welds were equally placed along the root gap. The clamps were removed after tack welding and the spacers driven out. Shrinkage measurements were taken and the plates again fastened to the flat base. The root pass was applied after the tack welds had been wire-brushed and the edges feathered. Measurements of the root-pass shrinkage were taken.

The plates were then assembled in the vertical welding jig as shown in Fig. 102. The remaining five weld passes per plate were deposited in accordance with the sequence shown. Figure 103 illustrates the completed weld test in the vertical jig. Dial-gage readings were taken at 1-min intervals during the deposition of the final passes, and micrometer measurements were taken after the final pass. Shrinkage measurements and welding data for the last four tests are shown in Table 38.

It can be seen that the results of these tests were in close agreement, although two different welding operators were used. Using these results, two tests were made with $\frac{1}{4}$-in. Inconel plates, 6 by 138 in., bent into hoops approximately 44 in. in diameter and welded by means of an identical inert-arc welding procedure. One edge of each hoop was beveled 50 deg, leaving a $\frac{1}{16}$-in. land. The hoops were placed on the welding positioner bed in a horizontal plane in the manner shown in

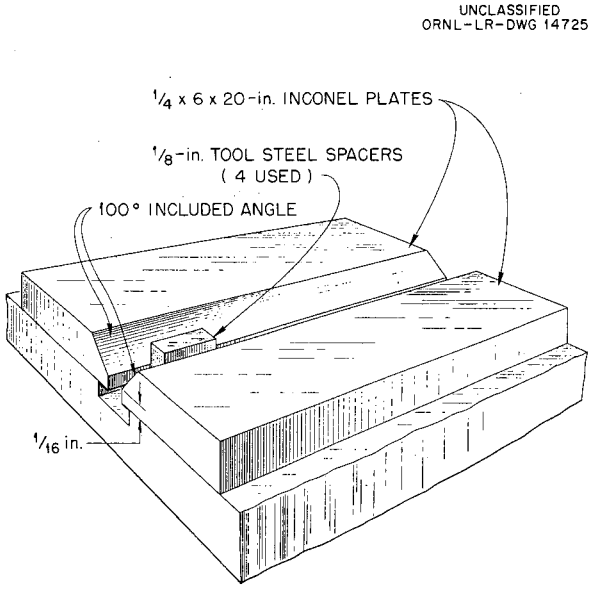

Fig. 101. Assembly of Inconel Weld-Shrinkage Test Plates Prior to Welding.

Fig. 104. As shown in Fig. 105, tool-steel spacers, 4 in. long and $\frac{1}{8}$ in. thick, were placed between the beveled edges at 6-in. intervals to maintain the root gap. Large C-clamps were used to draw the two hoops tightly against the spacers. Smaller C-clamps were halved and tacked to the bottom hoops to aid in the alignment of the upper hoop. Asbestos string was used to seal the gaps between the spacers prior to tacking. The area behind the root gap was sealed with a cover formed from 0.010-in. annealed brass sheet and masking tape, and purged for 30 min prior to tacking. Tack welds

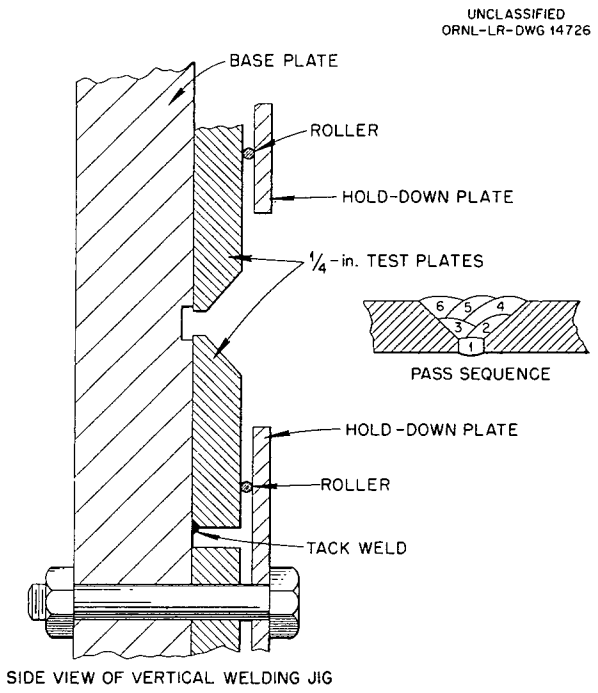

Fig. 102. Assembly of Test Plates in Vertical Welding Jig.

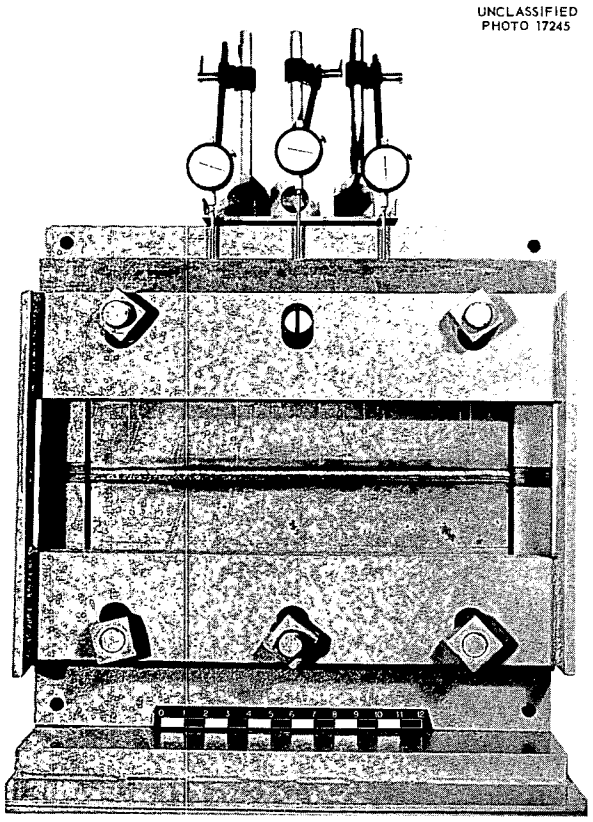

Fig. 103. Completed Weld-Shrinkage Plate Test in the Vertical Jig.

TABLE 38. SHRINKAGE MEASUREMENTS AND WELDING DATA FOR FLAT-PLATE TESTS

Test No.	Welder	Number of Passes	Time Required (min)	Rod Used (in.)	Amps Used	Shrinkage (in.)			Dial-Gage Shrinkage* (in.)		
						Max	Min	Av	Max	Min	Av
106	Gleen	6	61	198	80 (root) 105–110	0.157	0.121	0.141	0.092	0.082	0.087
107	Gleen	6	60	226	75–80 (root) 105–110	0.148	0.132	0.139	0.104	0.096	0.100
108	Hembree	6	79	231	80 (root) 105–110	0.157	0.106	0.138	0.103	0.093	0.098
109	Hembree	6	64	236	80 (root) 105–110	0.154	0.104	0.136	0.102	0.092	0.097

*Five final passes only; dial-gage readings on tests 100 and 101 are erroneous due to slip in the dial-gage actuating arm during tests.

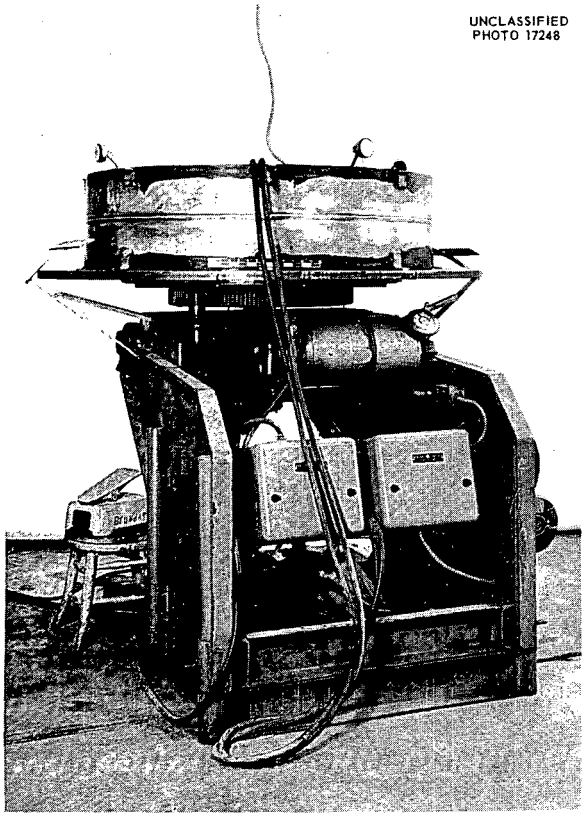

Fig. 104. Weld-Shrinkage Hoop Test on Welding Positioners, Illustrating Dial-Gage Locations.

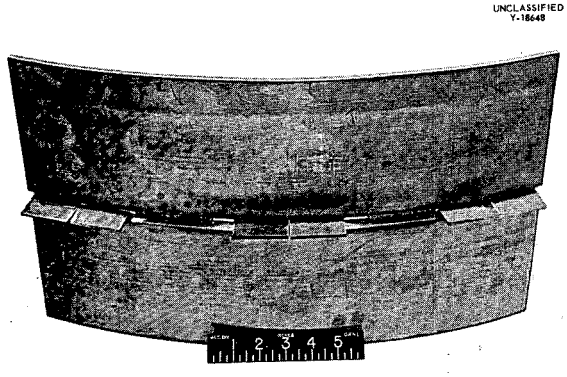

Fig. 105. Simulated Weld-Shrinkage Hoop Test, Illustrating Tool-Steel Spacer Locations.

were placed between the spacers, with alignment checked constantly. After removal of the tool-steel spacers, the root pass was deposited. No dressing of the land or feathering of the tack welds was permitted prior to the root-pass deposition.

After completion of the root pass, the weld was wire-brushed, and the five final weld passes were deposited by using the same sequence as described in Fig. 103. For these welds two welding operators were used, 180 deg apart around the hoop, and the positioner was slowly rotated. As shown in Fig. 106, four dial gages were used to record the final-pass shrinkages. The welders worked on a 15-min-work–5-min-rest cycle. Micrometer readings and dial-gage measurements are shown in Table 39. Figure 107 illustrates a plot of the dial-gage reading for hoop test No. 1. Within the limits of this investigation, the following conclusions can be drawn:

Plates. – The results of the last four tests on plates indicated that under controlled conditions

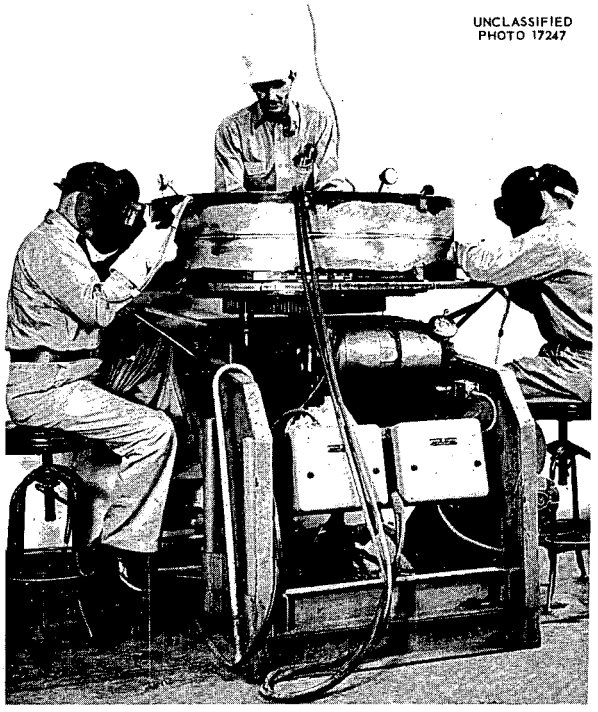

Fig. 106. Weld-Shrinkage Hoop Test.

TABLE 39. SHRINKAGE MEASUREMENTS AND WELDING DATA FOR HOOP TESTS

Test No.	Number of Passes	Arc Time Required (min)	Rod Used (in.)	Amps Used	Shrinkage (in.)			Dial-Gage Shrinkage* (in.)		
					Max	Min	Av	Max	Min	Av
1	6	314	1218	80 (root) 110–120	0.126	0.111	0.1194	0.095	0.080	0.088
2	6	310	1188	80 (root) 110–120	0.138	0.115	0.1261	0.102	0.088	0.095

*Five final passes only; does not include tack shrinkage or root shrinkage.

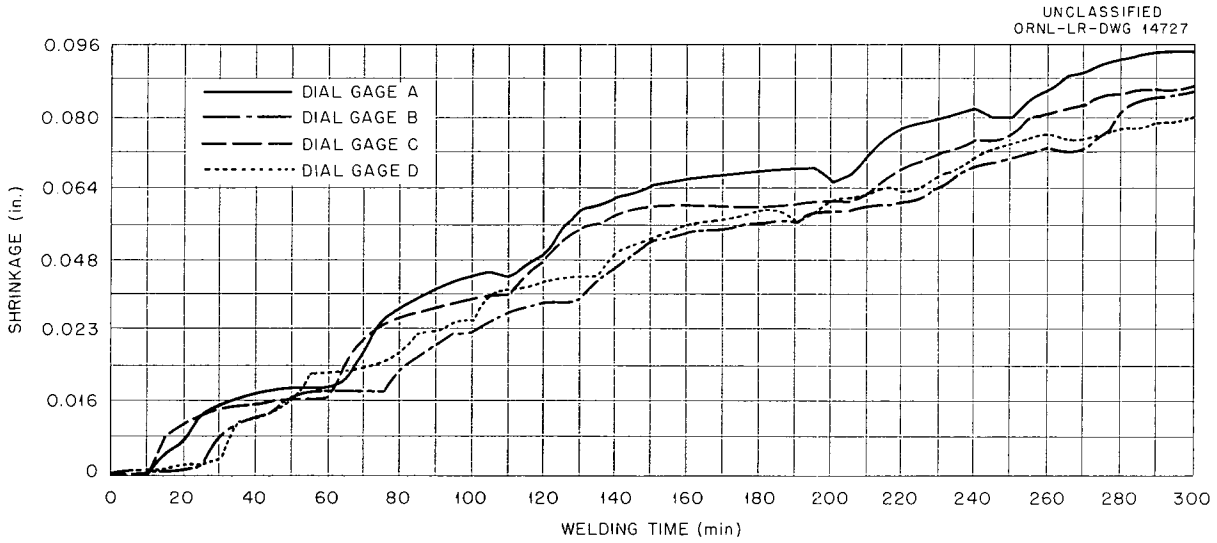

Fig. 107. Plot of Dial-Gage Readings for Hoop Test No. 1.

the effect of the welding variables can be minimized so that a welding operator can essentially duplicate his performance from test to test when manually welding. Also, for a given set of conditions, two welders can nearly duplicate each other's performance.

The use of various lengths of tool-steel spacers in the tack welding of the plates caused wide variations in the resulting tack-welding shrinkage. The amount of tack-welding shrinkage was found to be inversely proportional to the length of the spacers.

Hoops. – The results of the tests on the hoops indicated that the inevitable variations in conditions and techniques, during welding progression around the circumference, cause greater variations in shrinkage within a hoop than the variations observed from hoop to hoop.

The over-all results indicate that for $\frac{1}{4}$-in. Inconel plate, inert-arc welded by two welding operators, under the same conditions as utilized for these tests, the transverse shrinkage to be expected will be from 0.111 to 0.138 in., with an average value being 0.120 in. The longitudinal shrinkage to be expected will be 0.250 to 0.375 in. for a circumferential length of 138 in.

Similar tests were conducted on $\frac{1}{16}$-, $\frac{1}{8}$-, and $\frac{3}{8}$-in.-thick material, and the results of all experiments are summarized in Table 40. It should be noted that the data are pertinent only under the conditions utilized for these tests. Each change

TABLE 40. SUMMARY OF WELD SHRINKAGE DATA

Inconel Section Size (in.)	Width × Diameter Hoop Size, (in.)	Transverse Shrinkage (in.)				Recommended Design Allowance, Transverse Shrinkage (in.)	Longitudinal Shrinkage (in./in.)
		Av	Max	Min	Greatest Deviation, Station to station		
1/16	12 × 45	0.024	0.026	0.018	0.005	0.024 ±0.010	0.00045
1/8	12 × 10.5	0.051	0.056	0.044	0.009	0.051 ±0.010	Not measurable
1/8	12 × 22	0.041	0.045	0.036	0.010	0.041 ±0.010	Not measurable
1/4	12 × 44	0.120	0.138	0.111	0.011	0.120 ±0.015	0.002–0.003
3/8	12 × 52	0.168	0.184	0.155	0.014	0.168 ±0.020	0.002–0.003

in the variables present may cause extreme variations in the actual weld shrinkage encountered.

FABRICATION OF PRIMARY PUMP VOLUTES

Extensive experimentation has been conducted to determine the approximate weld shrinkage to be expected in the fabrication of primary pump volutes. The information obtained from these tests has been used to successfully fabricate three of these Inconel volutes, one by metallic-arc welding and two by inert-arc welding procedures.

Primary pump volute No. 1 incorporated the use of metallic-arc welding (coated-electrode), and the shrinkage obtained compared favorably with that obtained on simulated test components. However, radiographic inspection of the weld revealed porosity of unacceptable levels. Therefore, in order to ensure acceptable quality, the exclusive use of inert-arc welding was specified for joining of future volutes.

It was recognized that the magnitude of weld shrinkage would differ significantly for the two welding processes. Since the existing data could not be used to predict these dimensional changes, an additional shrinkage test was conducted.

Two test pieces were machined from 2-in. Inconel plate and welded in accordance with the procedure described in Fig. 108. Micrometer measurements were made at four radial sections, as described in Fig. 109, prior to and after each subsequent operation. The completed test is shown in Fig. 110. The results of the micrometer measurements are summarized in Table 41.

These data provided a first approximation of the shrinkage to be expected when welding of primary volute No. 2 was undertaken. A 0.125-in. shrinkage allowance was incorporated into the joint design, and, after machining, the volutes were scribed as shown in Fig. 111. Micrometer measurements were made before and after each operation at each intersection shown.

The volute is shown assembled for welding in Fig. 112. The welding procedure used was essentially the same as that used in the primary pump test, that is, eight passes in the downhand position, with the exception that as many as six additional passes were required to complete the weld at the volute exit, where the section was in the order of

UNCLASSIFIED
ORNL–LR–DWG 16166

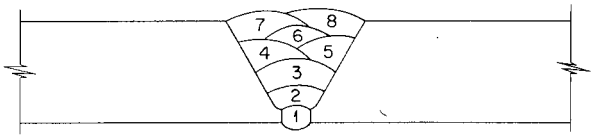

PASS NUMBER	ELECTRODE SIZE (in.)	ELECTRODE MATERIAL	CURRENT (amp)
1*	3/32 in.	INCO 62	90
2	3/32 in.	INCO 62	140
3	1/8 in.	INCO 62	170
4–8	1/8 in.	INCO 62	190

* ROOT PASS: 6 TACKS, EACH APPROXIMATELY 2 in. IN LENGTH, FOLLOWED BY TIE-INS BETWEEN TACKS.

Fig. 108. Inert-Arc-Welded Primary Pump Shrink Test No. 1.

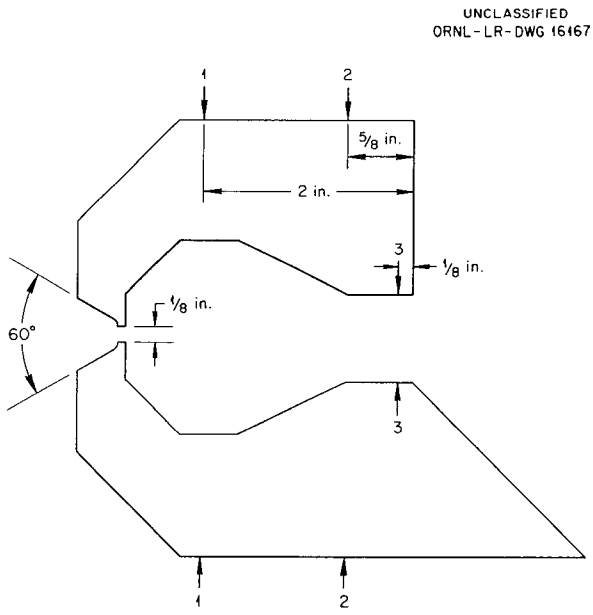

Fig. 109. Micrometer Measurement Details – Inert-Arc-Welded Primary Pump Shrink Test.

1 in. in thickness. The completed volute is shown in Fig. 113.

The results of micrometer measurements are summarized in Tables 42, 43, and 44. It may be noted that the shrinkage experienced was somewhat less than that desired.

Since the volute entrance dimension is considered to be the most critical in the primary pump, the data presented in Table 44 were analyzed, and a shrinkage allowance of 0.115 in. was selected for incorporation into the joint design of primary pump No. 3.

The volutes for pump No. 3 were machined, assembled, welded, and annealed, using comparable procedures and micrometer measurements made before and after each important operation. The data are summarized in Tables 45, 46, and 47. It may be noted from Table 47 that adjusting the shrinkage allowance to 0.115 in. satisfied within reasonable limits the dimensional requirements of the volute entrance. A further refinement is planned for primary pump No. 4. A shrinkage allowance of 0.110 in. will be incorporated into the joint design.

TABLE 41. DATA ON INERT-ARC-WELDED PRIMARY PUMP TEST NO. 1

Position	Dimensions				
	Before Welding (in.)	After Welding (in.)	Change (mils)	After Annealing** (in.)	Net Change (mils)
A 1*	0.366	0.244	0.122	0.240	0.126
B 1	0.382	0.254	0.128	0.248	0.134
C 1	0.388	0.264	0.124	0.259	0.129
D 1	0.378	0.249	0.129	0.244	0.133
A 2*	0.377	0.259	0.118	0.254	0.122
B 2	0.381	0.260	0.121	0.254	0.127
C 2	0.388	0.268	0.120	0.264	0.124
D 2	0.384	0.263	0.121	0.257	0.127
A 3	0.468	0.349	0.119	0.346	0.122
B 3	0.469	0.348	0.121	0.343	0.126
C 3	0.469	0.349	0.120	0.345	0.124
D 3	0.469	0.348	0.121	0.344	0.125

*Add 3.317-in. micrometer correction to readings shown at positions 1 and 2.

**1950°F for 2 hr; furnace cool, 500°F/hr.

UNCLASSIFIED
PHOTO 17788

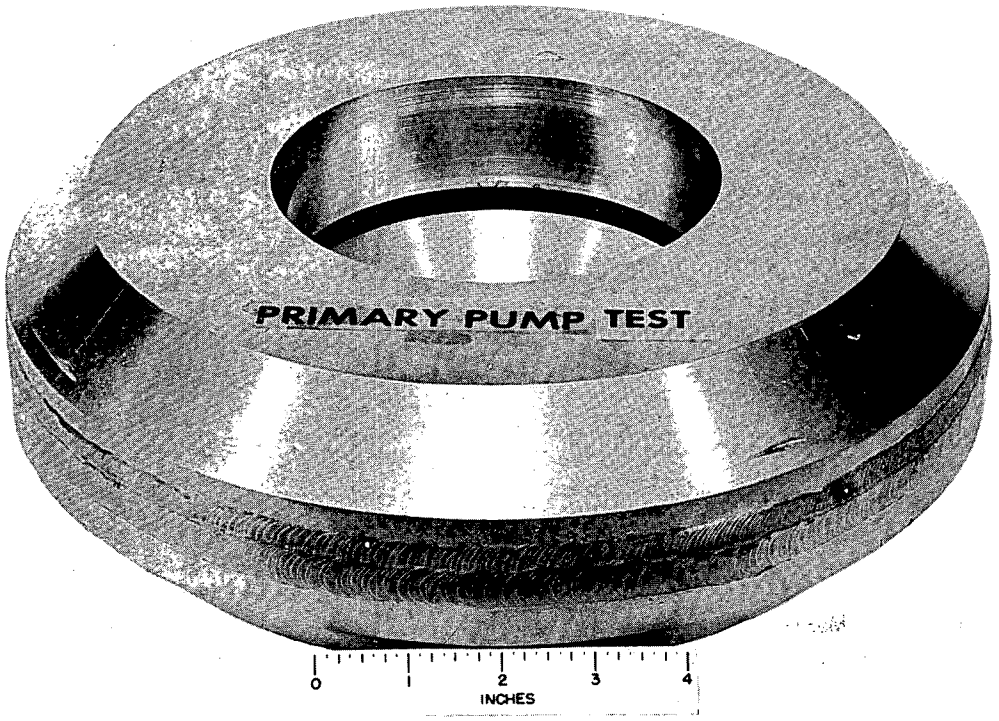

Fig. 110. Inert-Arc-Welded Primary Pump Weld-Shrinkage Test.

TABLE 42. DATA ON PRIMARY PUMP NO. 2

Angular Position (deg)	Dimensions* – Radial Position A				
	Before Welding (in.)	After Welding (in.)	After Annealing** (in.)	Total Change (mils)	Deviation from Ideal Change of 0.125 in. (mils)
0	0.754	0.646	0.648	–106	–19
200	0.765	0.649	0.647	–118	–7
220	0.771	0.655	0.652	–119	–6
240	0.758	0.641	0.639	–119	–6
260	0.763	0.642	0.641	–122	–3
280	0.763	0.639	0.639	–124	–1
300	0.777	0.654	0.654	–123	–2
320	0.778	0.653	0.654	–124	–1
340	0.773	0.644	0.647	–126	+1

*Add 3.317-in. micrometer correction to readings shown.
**1950°F for 2 hr; furnace cool, 500°F/hr.

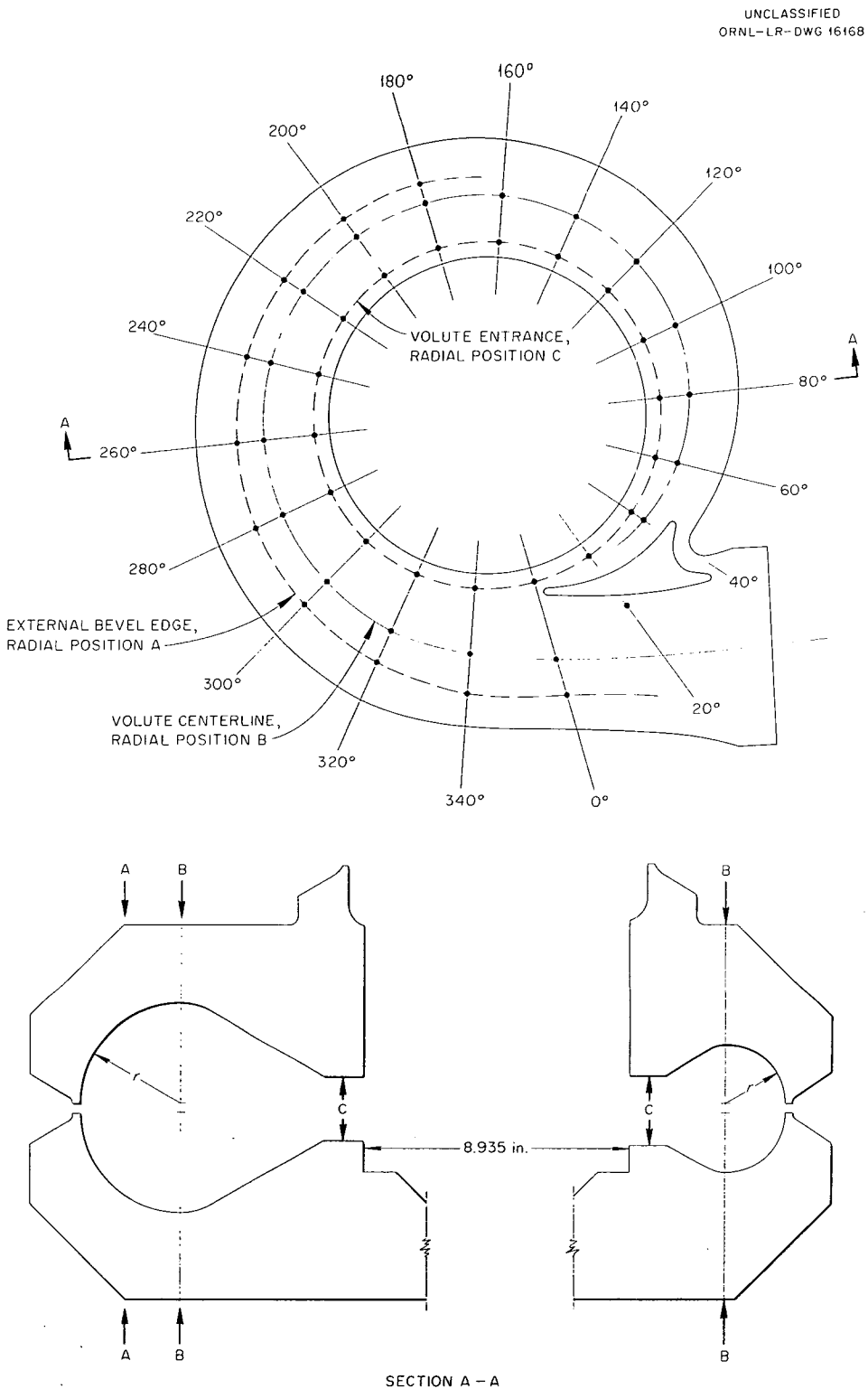

Fig. 111. Micrometer Measurement Details – Primary Pump Volute No. 2.

UNCLASSIFIED
PHOTO 17583

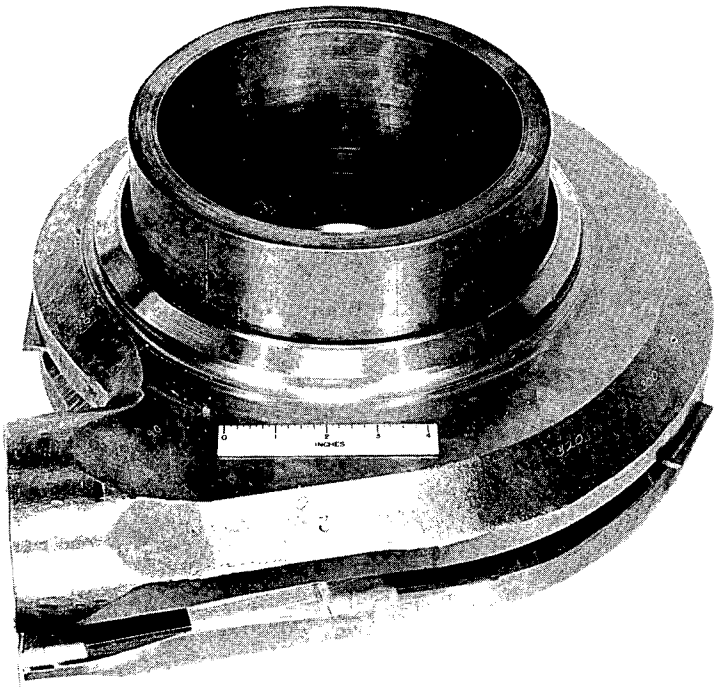

Fig. 112. Primary Pump Volute Assembled for Welding.

UNCLASSIFIED
PHOTO 17879

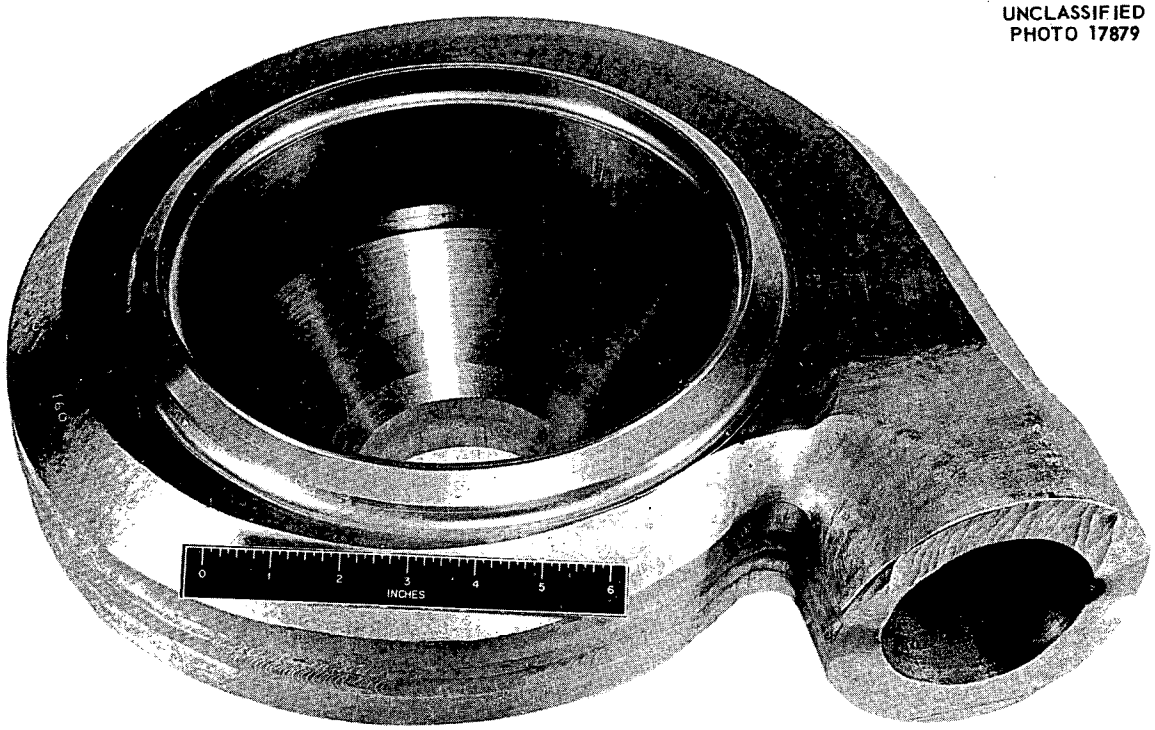

Fig. 113. Primary Pump Volute No. 2 After Inert-Arc Welding and Annealing.

TABLE 43. DATA ON PRIMARY PUMP NO. 2

Angular Position (deg)	Dimensions* – Radial Position B				
	Before Welding (in.)	After Welding (in.)	After Annealing** (in.)	Total Change (mils)	Deviation from Ideal Change of 0.125 in. (mils)
0	0.804	0.690	0.689	–115	–10
20	0.771	0.665	0.665	–106	–19
40	0.802	0.696	0.694	–108	–17
60	0.787	0.675	0.674	–113	–12
80	0.778	0.664	0.662	–116	–9
100	0.774	0.659	0.656	–118	–7
120	0.771	0.655	0.653	–118	–7
140	0.779	0.664	0.661	–118	–7
160	0.773	0.656	0.654	–119	–6
180	0.766	0.650	0.649	–117	–8
200	0.779	0.665	0.663	–116	–9
220	0.777	0.668	0.663	–111	–14
240	0.764	0.649	0.648	–116	–9
260	0.771	0.654	0.652	–119	–6
280	0.776	0.659	0.657	–119	–6
300	0.780	0.664	0.663	–117	–8
320	0.784	0.668	0.667	–117	–8
340	0.794	0.674	0.673	–121	–4

*Add 3.317-in. micrometer correction to readings shown.
**1950°F for 2 hr; furnace cool, 500°F/hr.

Any shrinkage in excess of 0.650 in. will be prevented by the use of Inconel spacers where needed.

EXAMINATION OF HIGH-CONDUCTIVITY FIN RADIATORS

R. J. Gray[1] P. Patriarca

PWA-2 Failure

A 500-kw high-conductivity fin radiator, known as PWA HCF radiator No. 2, failed on December 23, 1955, as the result of a leak. This radiator had been under test for a period of 1199 hr in a temperature range of 1000 to 1600°F. Five hundred forty-six hours of this service was under conditions of NaK temperature differences as imposed by cold air forced across the fin surfaces. The radiator, as received from the test site, is shown in Fig. 114.

Examination Procedure and Results. – The entire radiator was leak-checked by pressurizing under water and observing the origin of the air bubbles. This procedure revealed the point of failure, as indicated by the arrow in Fig. 114. The radiator was then sectioned for further examination, as shown in Fig. 115. The side portions of the support members were removed with a rubber-bonded masonry wheel in a portable electric handsaw adjusted for a shallow cut. Each bank of fins was separated by slicing the support members and

[1]Metallography Group.

TABLE 44. DATA ON PRIMARY PUMP NO. 2

Angular Position (deg)	Dimensions* – Radial Position C				
	Before Welding (in.)	After Welding (in.)	After Annealing** (in.)	Total Change (mils)	Deviation from Desired Dimension of 0.660 ± 0.010 in. (mils)
0	0.780	0.675	0.674	–106	14
20	0.781	0.678	0.677	–104	17
40	0.784	0.681	0.680	–104	20
60	0.785	0.679	0.674	–111	14
80	0.785	0.678	0.679	–106	19
100	0.784	0.675	0.675	–109	15
120	0.783	0.674	0.674	–109	14
140	0.781	0.673	0.673	–108	13
160	0.780	0.673	0.672	–108	12
180	0.781	0.673	0.673	–108	13
200	0.781	0.675	0.673	–108	13
220	0.782	0.676	0.674	–108	14
240	0.782	0.676	0.674	–108	14
260	0.782	0.675	0.674	–108	14
280	0.782	0.674	0.674	–108	14
300	0.782	0.674	0.673	–109	13
320	0.781	0.673	0.673	–108	13
340	0.781	0.673	0.674	–107	14

*Dimensions shown are absolute micrometer measurements.
**1950°F for 2 hr; furnace cool, 500°F/hr.

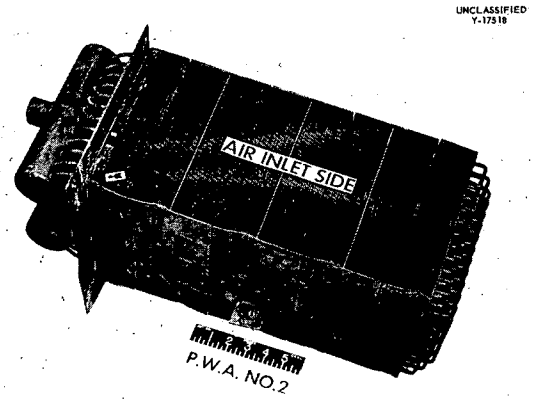

Fig. 114. PWA Radiator No. 2 Failure. Arrow indicates origin of failure.

bottom-flanged plate, as shown, with a fine-tooth, high-speed steel hacksaw blade in a portable electric drill equipped with a portable power-saw attachment. The failed area was then carefully removed for metallographic preparation on a standard wet cutoff machine equipped with an abrasive wheel.

The failed area is shown enlarged in Fig. 116. This section was again pressurized under water to locate the exact position of the leak before additional preparation for metallographic examination was undertaken. The failure was found to exist in the corner tube C-1 on that periphery which faced the side support member. The support member was subsequently removed for unobstructed observation of the emergence of the water bubbles. A photomicrograph of the failure is shown in Fig. 117.

TABLE 45. DATA ON PRIMARY PUMP NO. 3

Angular Position (deg)	Dimensions* – Radial Position A				
	Before Welding (in.)	After Welding (in.)	After Annealing** (in.)	Total Change (mils)	Deviation from Ideal Change of 0.115 in. (mils)
0	0.741	0.597	0.597	–144	+29
180	0.723	0.604	0.602	–121	+6
200	0.723	0.604	0.601	–122	+7
220	0.719	0.598	0.596	–123	+8
240	0.716	0.593	0.593	–123	+8
260	0.719	0.594	0.593	–126	+11
280	0.725	0.597	0.596	–129	+14
300	0.737	0.604	0.606	–131	+16
320	0.730	0.594	0.599	–131	+16
340	0.733	0.594	0.596	–137	+22

*Add 3.317-in. micrometer correction to readings shown.

**1950°F for 2 hr; furnace cool, 500°F/hr.

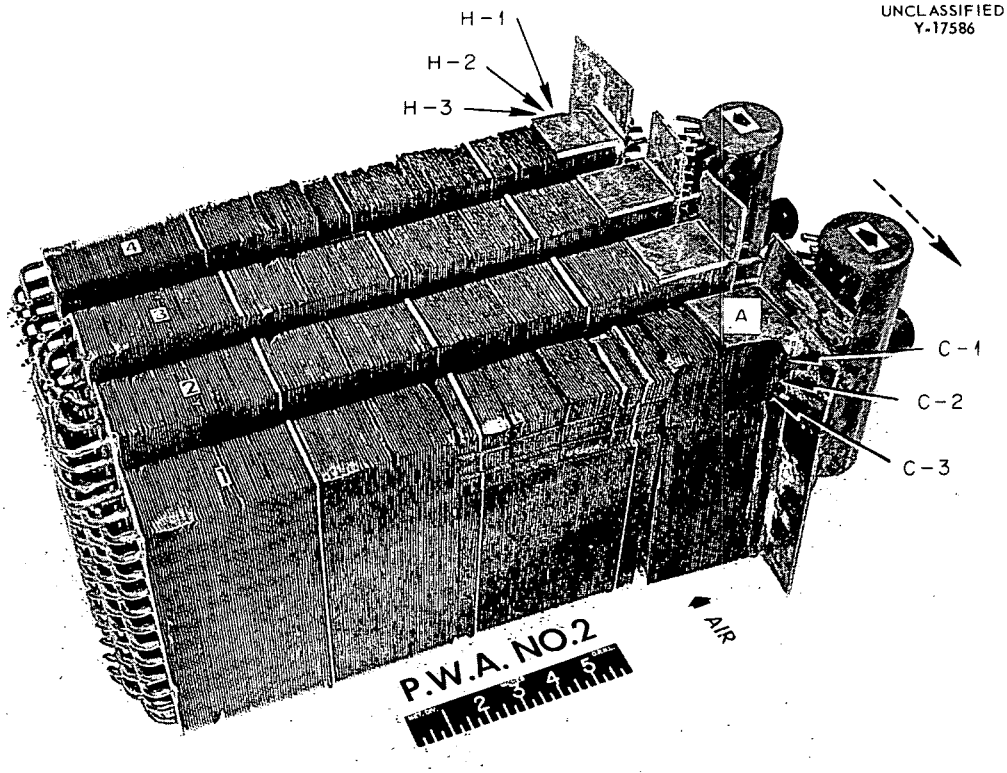

Fig. 115. PWA Radiator No. 2 After Sectioning. Section A was used for metallographic examination. C-1, C-2, and C-3 indicate tubes from the air inlet side, and H-1, H-2, and H-3 indicate tubes from the air exit side which were examined. Dotted arrow indicates viewing direction of photomicrograph.

TABLE 46. DATA ON PRIMARY PUMP NO. 3

Angular Position (deg)	Dimensions* – Radial Position B				
	Before Welding (in.)	After Welding (in.)	After Annealing** (in.)	Total Change (mils)	Deviation from Ideal Change of 0.115 in. (mils)
0	0.741	0.616	0.608	−133	+18
20	0.755	0.651	0.645	−110	−5
40	0.780	0.678	0.673	−107	−8
60	0.770	0.666	0.662	−108	−7
80	0.738	0.629	0.625	−113	−2
100	0.738	0.626	0.624	−114	−1
120	0.734	0.619	0.618	−116	+1
140	0.728	0.614	0.610	−118	+3
160	0.728	0.611	0.610	−118	+3
180	0.728	0.610	0.609	−119	+4
200	0.723	0.606	0.603	−123	+8
220	0.725	0.608	0.605	−125	+10
240	0.728	0.609	0.606	−128	+13
260	0.728	0.608	0.606	−128	+13
280	0.733	0.609	0.606	−127	+12
300	0.735	0.609	0.607	−128	+13
320	0.735	0.607	0.603	−132	+17
340	0.735	0.606	0.603	−132	+17

*Add 3.317-in. micrometer correction to readings shown.

**1950°F for 2 hr; furnace cool, 500°F/hr.

Tubes C-1, C-2, and C-3 were mounted intact and carefully ground down to the failure to permit examination of a longitudinal cross section of the tubes as seen against the direction of air flow. The failure in tube C-1 is shown in the composite of Figs. 118 and 119. The neckdown of the tube wall is evident, indicating a tensile fracture similar to that observed in York HCF radiator No. 1.

The composite of Figs. 120 and 121 shows a cross section of the tube C-2, and the composite of Figs. 122 and 123 shows a cross section of tube C-3. It may be noted that incipient fractures exist in both these tubes.

Three tubes, H-1, H-2, and H-3, taken from the air exit face and corresponding in position to tubes C-1, C-2, and C-3 in the air inlet face, were prepared for examination in a similar manner. Only tube H-1 exhibited evidence of incipient fracture. Figure 124 is a photomicrograph of this fracture as viewed in the direction of air flow.

Conclusions and Recommendations. – PWA HCF radiator No. 2 failed as a result of the initiation of a fracture in a braze alloy fillet by shear forces and the propagation of this fracture through the tube wall by tensile forces or combinations thereof during transient periods of operation.

TABLE 47. DATA ON PRIMARY PUMP NO. 3

Angular Position (deg)	Dimensions* – Radial Position C				
	Before Welding (in.)	After Welding (in.)	After Annealing** (in.)	Total Change (mils)	Deviation from Desired Dimension of 0.660 ± 0.010 in. (mils)
0	0.773	0.663	0.656	−117	-4
20	0.774	0.670	0.662	−112	+2
40	0.775	0.673	0.669	−106	+9
60	0.775	0.672	0.671	−104	+11
80	0.775	0.671	0.671	−104	+11
100	0.774	0.668	0.668	−106	+8
120	0.774	0.666	0.666	−108	+6
140	0.774	0.665	0.665	−109	+5
160	0.774	0.665	0.665	−109	+5
180	0.774	0.665	0.663	−111	+3
200	0.774	0.665	0.663	−111	+3
220	0.774	0.665	0.662	−112	+2
240	0.774	0.665	0.661	−113	+1
260	0.774	0.664	0.659	−115	−1
280	0.774	0.663	0.658	−116	−2
300	0.773	0.660	0.654	−119	−6
320	0.773	0.659	0.653	−120	−7
340	0.773	0.660	0.653	−120	−7

*Dimensions shown are absolute micrometer measurements.

**1950°F for 2 hr; furnace cool, 500°F/hr.

Since the incidence of incipient fractures is associated exclusively with the presence of support members or plates, it is recommended that these transverse restraints be removed entirely. This can be accomplished as suggested previously by use of a high-conductivity fin to provide transverse support at 2- or 4-in. intervals[2] and the brazing procedure modified accordingly.

[2]R. J. Gray and P. Patriarca, *Metallographic Examination of ORNL Radiator No. 1 and York Radiator No. 1 Failures*, ORNL CF-55-10-129, (Oct. 31, 1955).

The tensile loading contributing to the York failure was attributed at the time of examination to the restraining influence of the support member which extended up the side of the radiator. In view of this conclusion the support members of subsequent radiators, including PWA No. 2, were slit as shown in Fig. 114 prior to installation. It may be noted, however, that the radiator as "redesigned" retained the use of a bottom flanged plate, a top plate, and the four support members. During the brazing cycle the NaK tubes were brazed to these members resulting in a relatively

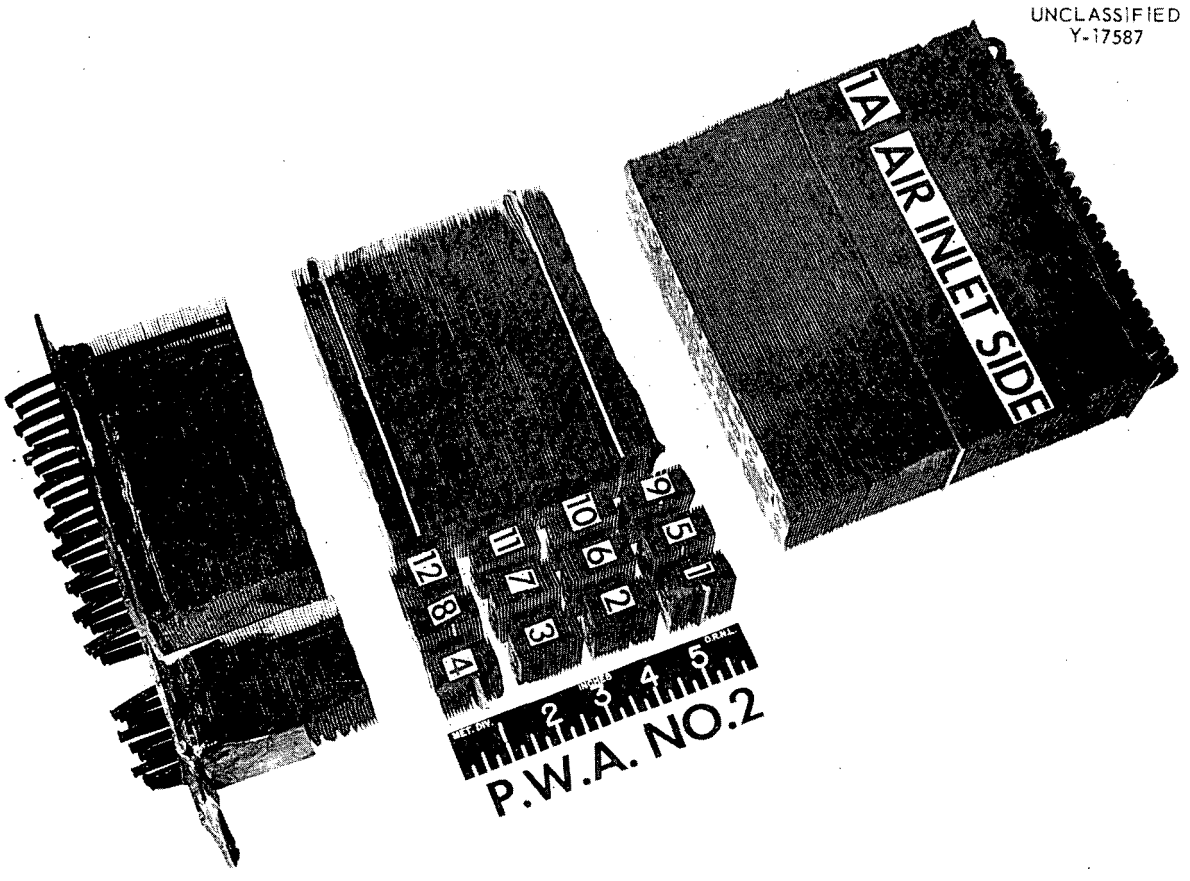

Fig. 116. PWA No. 2 Section A with Failed Tubes C-1 and Adjacent Tubes C-2 and C-3.

rigid condition at each of five transverse sections across the radiator matrix.

Local differences in rates of heating and cooling, particularly between the air inlet face and the remainder of the radiator during blower startup, could therefore be assigned the responsibility for the development of tensile loading.

This condition could be partially relieved by slicing the support members and plates in a manner similar to that utilized during dissection for metallographic examination as shown in Fig. 115.

The development of tensile forces alone, however, cannot be assigned the full responsibility for failure. The incidence of numerous incipient fractures in this radiator has been related to the presence of a support member or heavy plate. Over 13,000 tube-to-fin joints have been examined metallographically without the observation of a single incipient fracture. The relative mass and thermal conductivity of the support members and plates as compared with the high-conductivity fins could result in significant differences in cooling rates during transient periods. These could result in lateral forces responsible for initiation and propagation of fractures in tube-to-support-member braze joints in any portion of the radiator.

York-4 Postexamination

On March 3, 1956, a 500-kw high-conductivity fin radiator, known as the York HCF radiator No. 4, was removed from service after 1356 hr in test. This radiator was tested in a temperature range of

Fig. 117. Failed Tube (C-1) from PWA No. 2 as Viewed from the Support-Member Side of the Radiator After Removal of Support Plate.

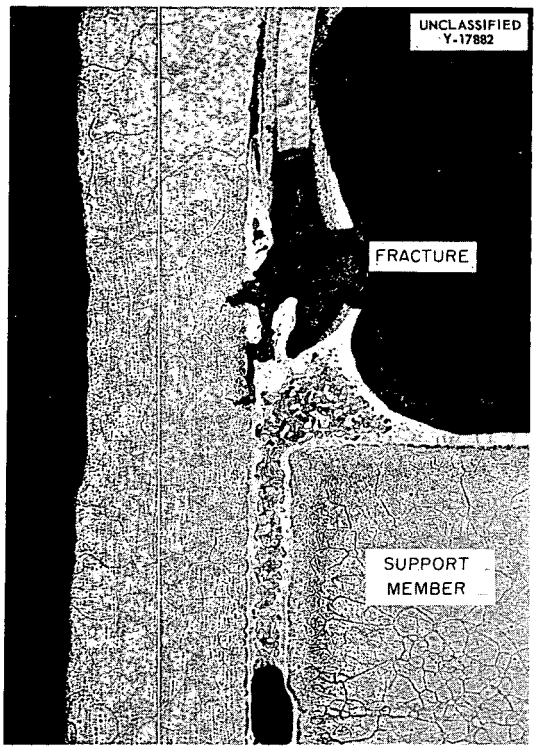

Fig. 119. Longitudinal View of Opposing Walls from the Failed Tube C-1 in PWA Radiator No. 2 Viewed Against the Air Flow. Note neckdown at fracture. 75X. Reduced 23.5%.

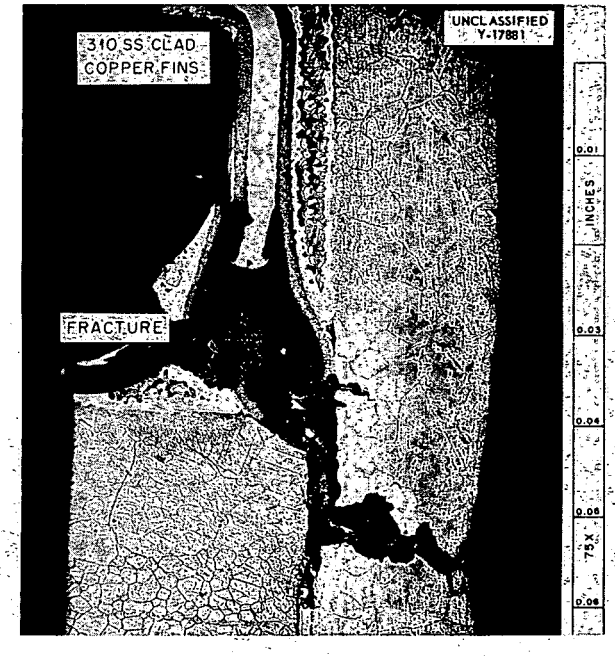

Fig. 118. Longitudinal View of Opposing Walls from the Failed Tube C-1 in PWA Radiator No. 2 Viewed Against the Air Flow. Note neckdown at fracture. 75X. Reduced 35%.

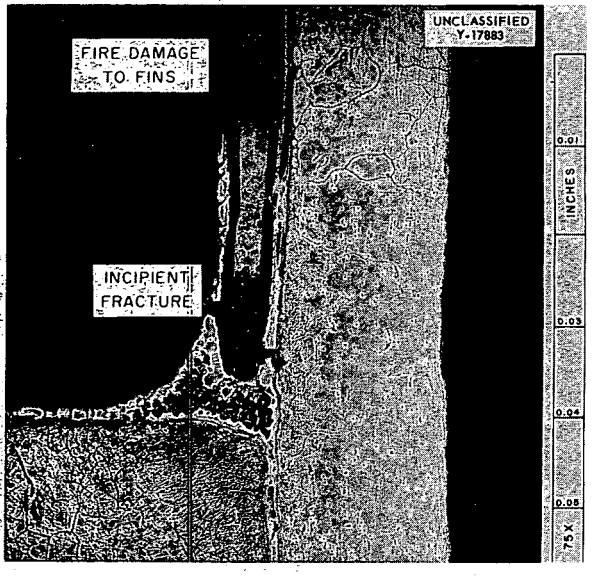

Fig. 120. Longitudinal View of Tube C-2 Adjacent to Failed Tube C-1 in PWA Radiator No. 2 as Viewed Against the Air Flow. Note incipient fracture, which has progressed into tube wall. 75X. Reduced 34.5%.

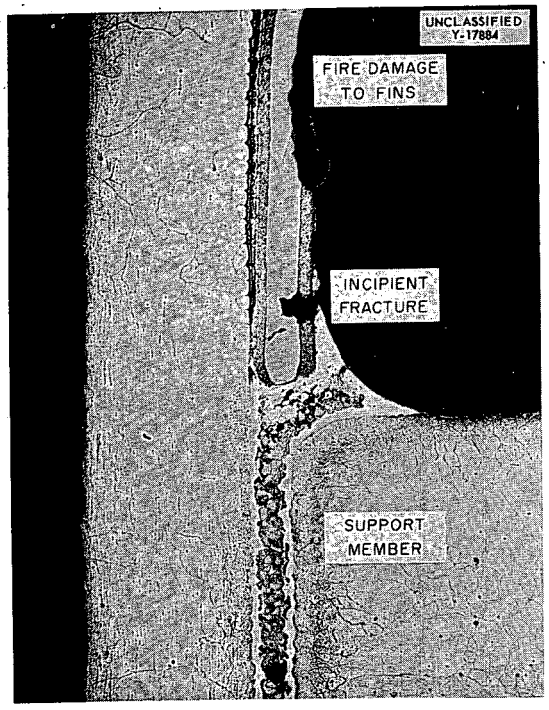

Fig. 121. Longitudinal View of Tube C-2 Adjacent to Failed Tube C-1 in PWA Radiator No. 2 as Viewed Against the Air Flow. Note incipient fracture, which has progressed into tube wall. 75X. Reduced 35%.

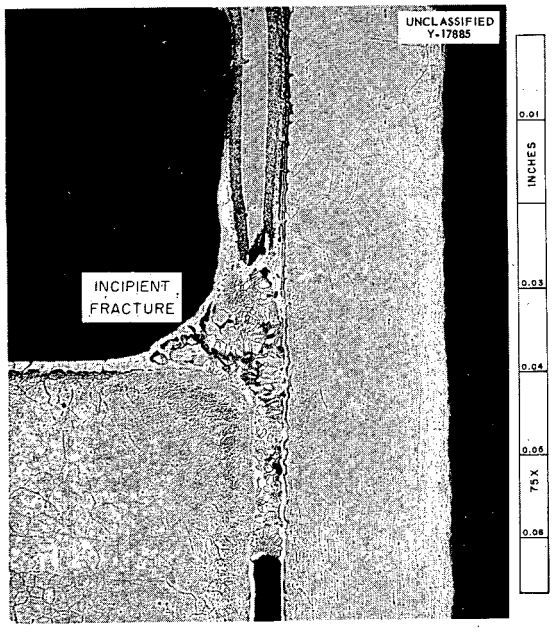

Fig. 122. Longitudinal View of Tube C-3 from PWA Radiator No. 2 as Viewed Against the Air Flow. Note fracture within the eutectic structure of braze metal. 75X. Reduced 41%.

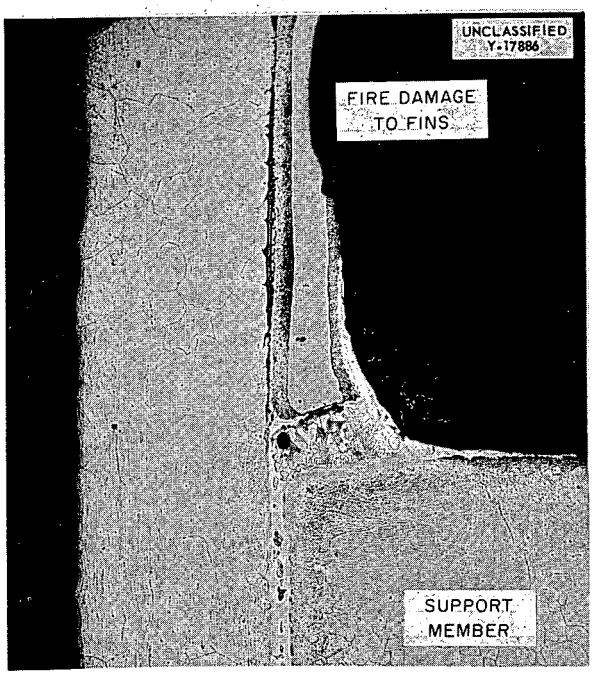

Fig. 123. Longitudinal View of Tube C-3 from PWA Radiator No. 2 as Viewed Against the Air Flow. Note fracture within the eutectic structure of braze metal. 75X. Reduced 28.5%.

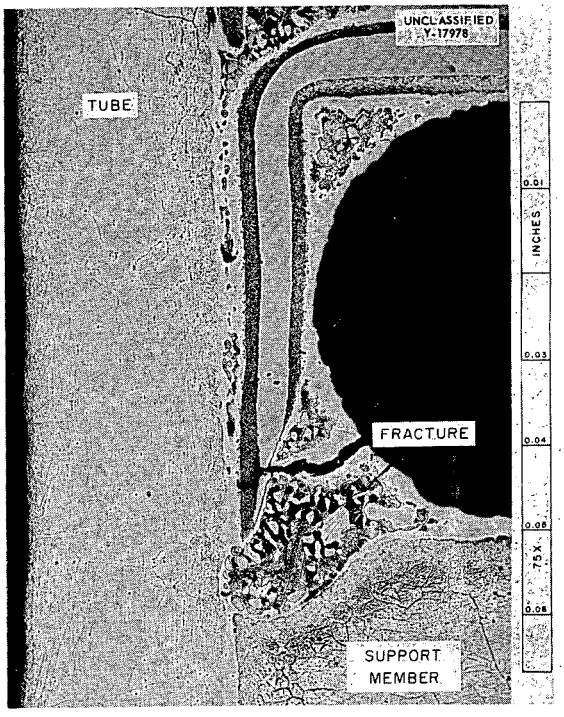

Fig. 124. Corner Tube H-1 from Air Exit Face of PWA Radiator No. 2 as Viewed in the Direction of the Air Flow. 75X. Reduced 39%.

1000 to 1600°F, with 748 hr of test under ΔT conditions.

The radiator was modified by removal of the side plates, cutting of the horizontal spacer plates, and slicing of the base plate through the middle parallel to the air flow.

Twenty-four specimens were cut from the radiator, as shown in Figs. 125 and 126. Each specimen contained a portion of three tubes, each joined to 15 or more fins. The specimens were cross-sectioned to reveal two opposed joint areas and were then mounted and examined at 80X.

A total of 2757 joint areas was examined. The percentages of fin-to-tube adherence and the degree of oxidation of the fin collars were noted. Table 48 illustrates the results of this examination in comparison with five previously examined radiators. As was noted in the examination of prior radiators, the presence of cracking was found to be associated with tube-to-support-plate joints and tube-to-sump-plate joints.

York-9 Postexamination

On May 28, 1956, a 500-kw high-conductivity fin radiator, known as the York HCF radiator No. 9, was removed from service after 1283 hr in test. This radiator was tested in a temperature range

Fig. 125. York HCF Radiator No. 4.

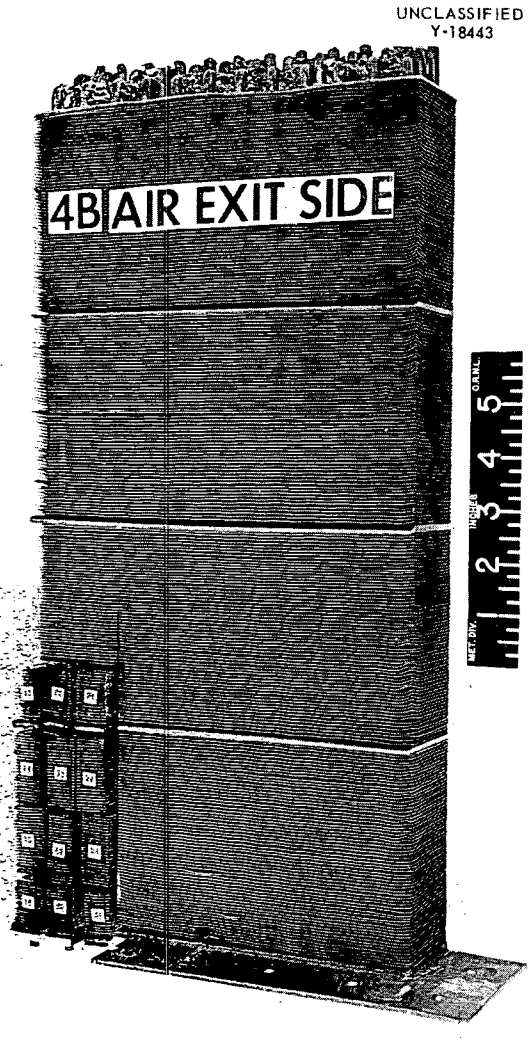

Fig. 126. York HCF Radiator No. 4.

TABLE 48. SUMMARY OF TUBE-TO-FIN STUDIES OF SEVERAL HCF RADIATORS

	York No. 4	York No. 3	York No. 1	PWA No. 2	ORNL No. 3	ORNL No. 1
Number of joint areas examined	2757	2684	3847	3210	2282	4150
Per cent of joint areas having 75–100% adherence	60.7	90.4	67.4	100	87.7	91.8
Per cent of joint areas having 50–74% adherence	18.8	5.9	13.0		3.5	4.2
Per cent of joint areas having 25–49% adherence	5.5	1.1	7.3		1.4	1.4
Per cent of joint areas having 0–24% adherence	15.0	2.6	12.3		7.4	2.6
Per cent of joint areas having nonoxidized copper fins	61.9	84.5	75.4	100	12.1	59.3
Per cent of joint areas having slightly oxidized copper fins	19.5	7.5	22.0		2.5	20.1
Per cent of joint areas having heavily oxidized copper fins	18.6	8.0	2.6		85.4	20.6
Number of hours of 1000–1600°F service	1356	361	152	1199	716	608

of 1000 to 1600°F, with 695 hr of test under ΔT conditions. The radiator was fabricated with a revised design which included the following modifications:

1. Side plates were omitted.
2. Rigid support plates, base plate, and top plate were omitted.
3. Sump plates were fashioned from fin material.
4. Air shields on the top and bottom were made from 0.010-in. nickel sheet, cut with over-size holes as shown in Fig. 127.
5. The radiator was brazed on its side, using a slurry of Coast Metals No. 52 brazing alloy.

Twenty-four metallographic samples were removed from the unit as described in the foregoing section, "York-4 Postexamination," and were examined microscopically. No cracks were found in the tube-to-sump-plate areas and no evidence of incipient cracking was noted, indicating that the design modifications employed were beneficial.

METALLOGRAPHIC EXAMINATION OF INTERMEDIATE HEAT EXCHANGER FAILURE

Tests on the fluid-30-to-NaK heat exchanger, designated as IHE-3, were terminated as a result of detection of a leak in tube bundle No. 1 after a total of 1794 hr of operation in the temperature range of 1100 to 1500°F. The unit was operated under conditions of ΔT for 1015 hr of this total time, and a total of 21 thermal cycles was applied over this period.

The NaK inlet and outlet headers of tube bundle No. 1 were separated from the heat exchanger to facilitate examination and inspection. Top and bottom views of the NaK inlet head are shown in Figs. 128 and 129, respectively. The general location of the failure is evident in the latter figure, in that a dark reaction product can be distinguished from the lighter solidified fluid 30. Forty tubes in the failed area were individually inspected with dye-penetrant and a borescope, and at least five tubes were found which contained obvious cracks. Figure 130 is a photograph of the NaK inlet head after dissection with an abrasive cutoff wheel to permit the examination of individual tubes. Each tube was numbered for the subsequent investigation, and the nomenclature is presented in Fig. 131.

The frequency and severity of cracking as detected in the initial inspection were more pronounced in the forward rows of tubes, that is, those with short

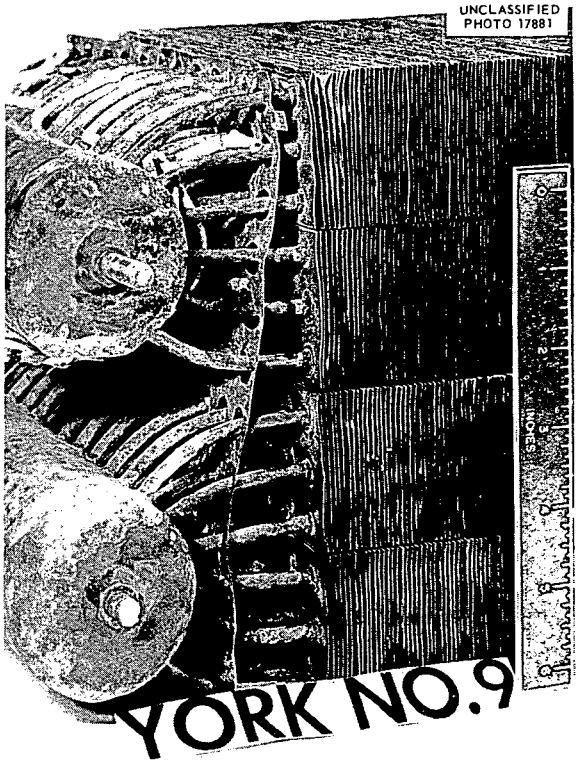

Fig. 127. Close-up of York HCF Radiator No. 9, Illustrating 0.010-in. Nickel Sheet Air Shield.

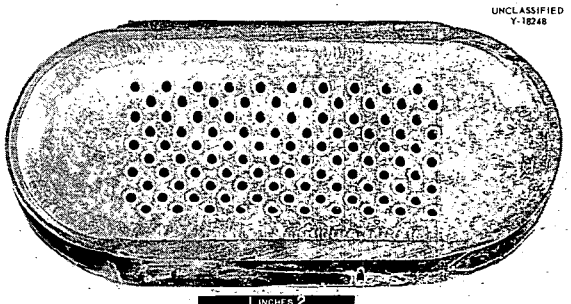

I H E NO.3
FAILURE

Fig. 128. Top Side of IHE No. 3, NaK Inlet Head, Showing Tube Welds.

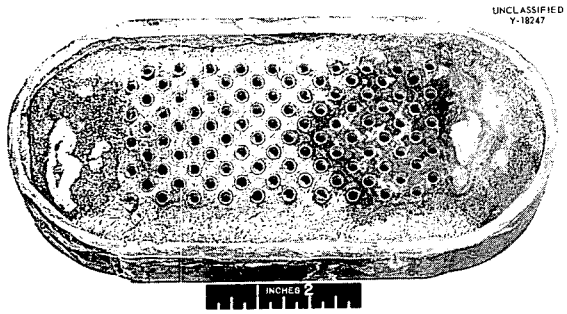

I H E NO.3
FAILURE

Fig. 129. Bottom Side of IHE No. 3, NaK Inlet Head, Showing Dark Reaction Product.

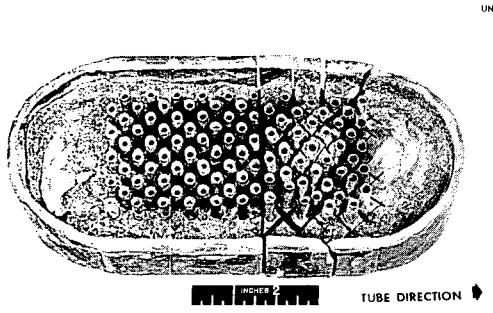

I H E NO.3
FAILURE

Fig. 130. NaK Inlet Head After Dissection for Further Examination.

bends. The distance from the tube bends to the headers was significantly shorter for the first row of tubes, for example, $3\frac{1}{4}$ in. as compared with 6 in. for the last row of tubes. For a given expansion of the 6-ft over-all straight length of tubes as a result of heating, a substantial degree of strain occurs in these locations. As would be expected, cracking was more pronounced on the tension side of the tube. A crack in the tensile side of tube No. 2 could be seen upon visual examination, and a photograph is shown in Fig. 132. Further evidence of the tube distortion at the headers can be

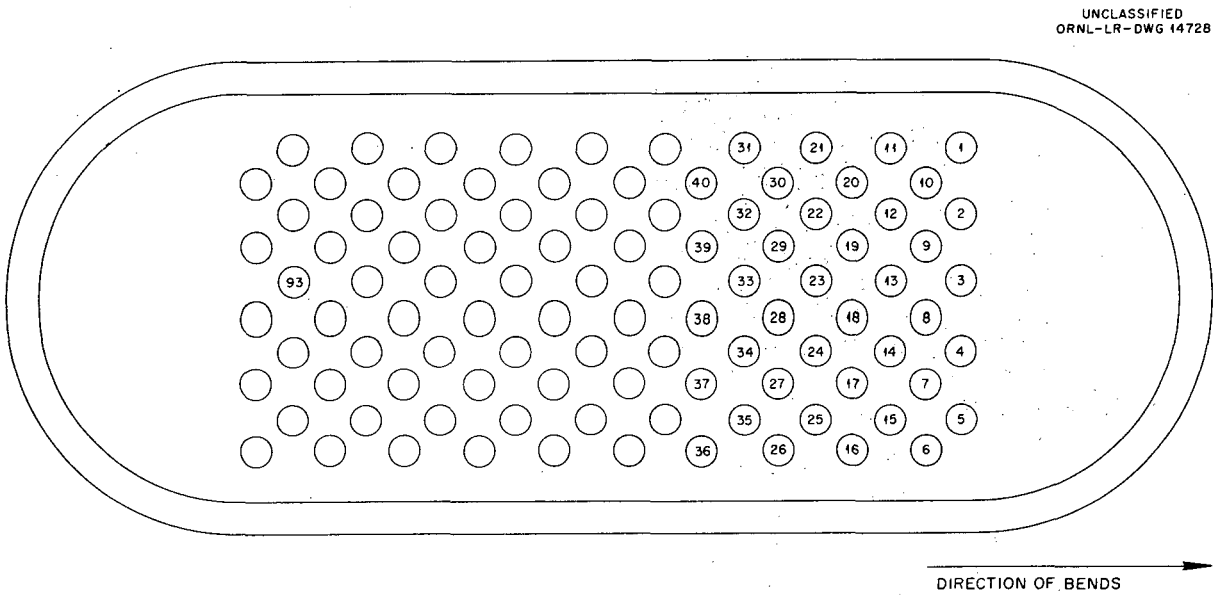

Fig. 131. Tube-Sheet Configuration and Dissection Nomenclature. IHE No. 3 failure.

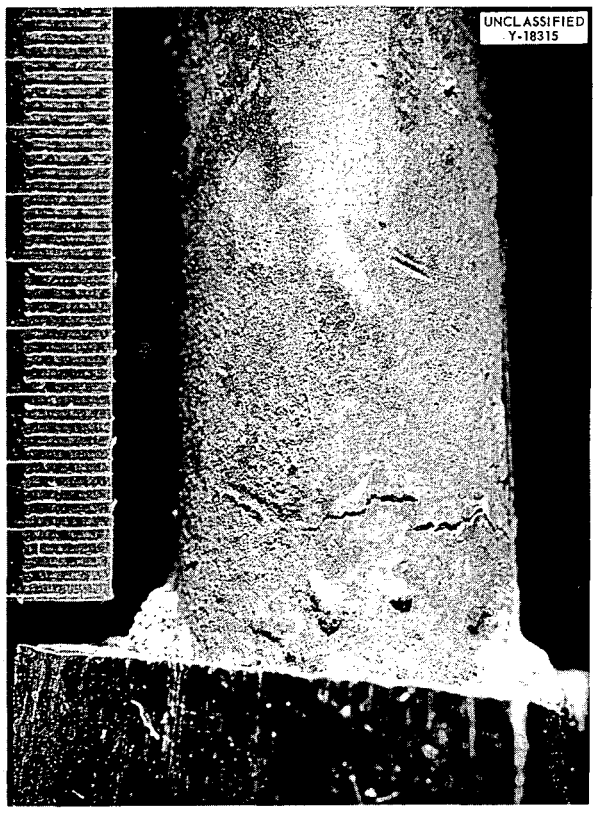

Fig. 132. Crack on Tension Side of Tube No. 2.

seen in Fig. 133, a photograph of the NaK outlet head.

Several of the tubes of interest were then mounted intact in Castolite and polished to the approximate center line for metallographic examination. Figure 134, a photomicrograph of the tensile side of tube No. 3, illustrates typical severe cracking and fluid 30 corrosion. A similar condition is evident in Fig. 135, a panorama of the tension side of tube No. 17. It may be noted that the opposite face of this tube, a panorama of which is shown in Fig. 136, does not exhibit as serious a condition. It appears that corrosion and stresses combine to form an abnormally unfavorable condition.

The extent of fluid 30 corrosion was investigated in tube No. 93 to ensure that the large degree of attack observed in the previous samples did not result from the reaction of the two fluids at the location of the failures. Figure 137 indicates that general severe corrosion was prevalent throughout the tubes in this header. A photograph illustrating a typical condition on the inner tube wall is shown in Fig. 138. Cracking and fluid 30 corrosion from the outer tube wall are also in evidence. A white deposit was found in the cracks in some areas, the appearance of which is shown in Figs. 139 and 140, low- and high-magnification photomicrographs of a crack and deposit. The nature of this deposit,

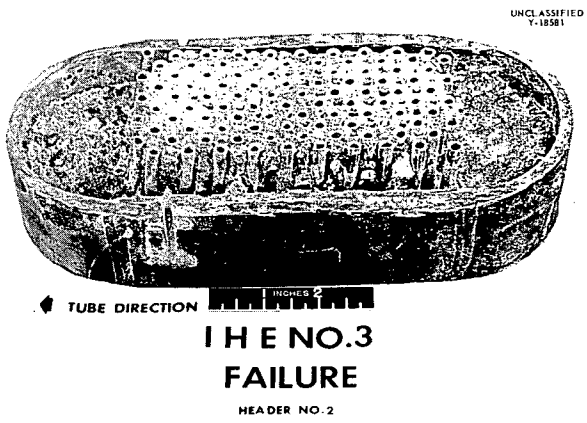

Fig. 133. Bottom Side of IHE No. 3, NaK Outlet Head, Showing Bending of Tubes.

as well as a detailed investigation of the mass transfer and corrosion behavior in the heat exchanger, will be studied by other groups.

CONTINUOUS FURNACE PRODUCTION OF SINTERED CM-52 RINGS

The use of a sintered Coast Metals No. 52 brazing ring for the side brazing of ART radiators is dependent upon the achievement of production rates adequate to reduce the cost per ring to a figure which can compete with the present means of preplacing the brazing alloy. An experimental pilot plant has been built which has attained a production rate of more than 8000 rings/hr. In the first production run, 33,000 rings were made in 5 hr, and it is felt that this will definitely establish a

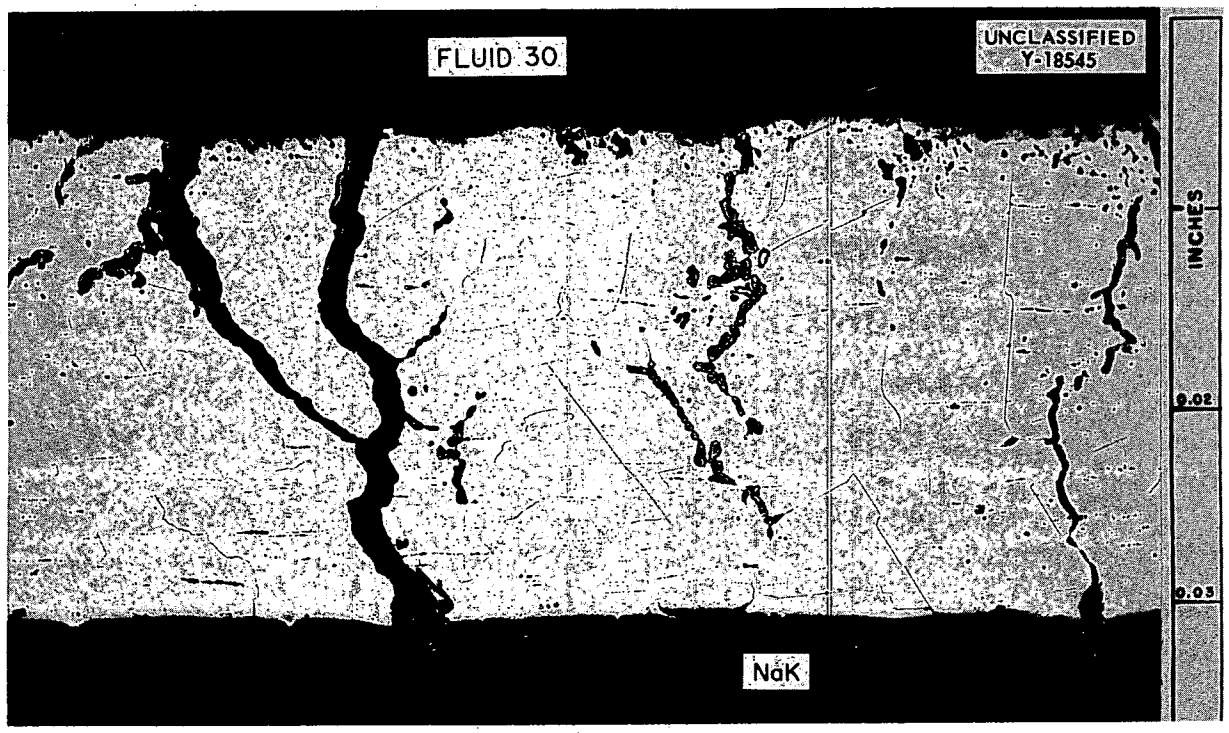

Fig. 134. Cracks in Tension Side of Tube 3. Etchant: electrolytic oxalic acid. 100X.

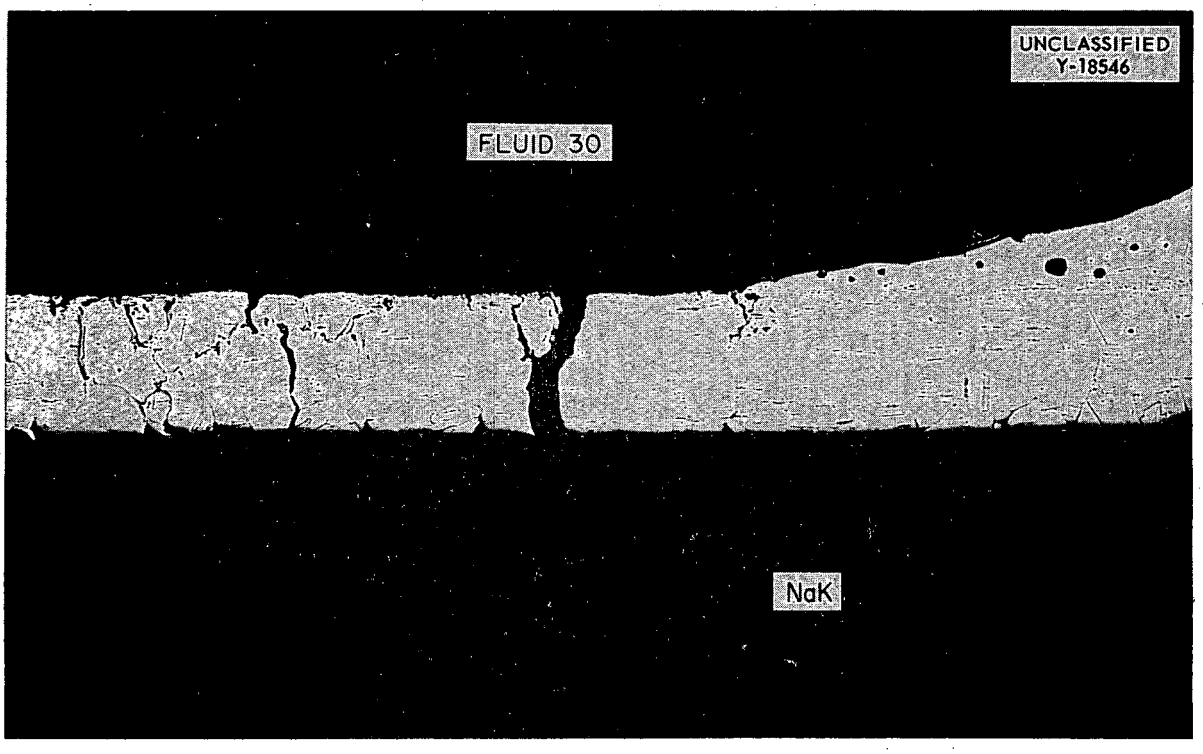

Fig. 135. Panorama of Tension Side of Tube No. 17 Showing Gross Cracking and Corrosion. Etchant: electrolytic oxalic acid. 33X.

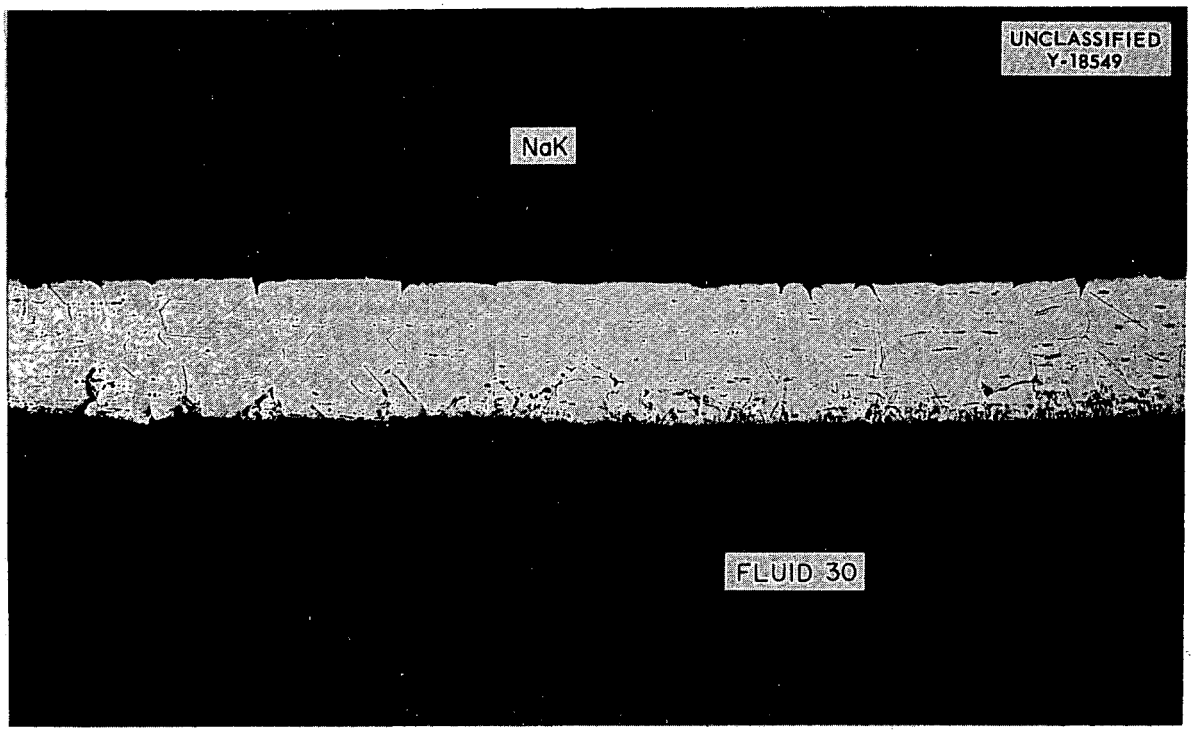

Fig. 136. Panorama of Compression Side of Tube No. 17 Showing Corrosion and Occasional Cracking. Etchant: electrolytic oxalic acid. 33X.

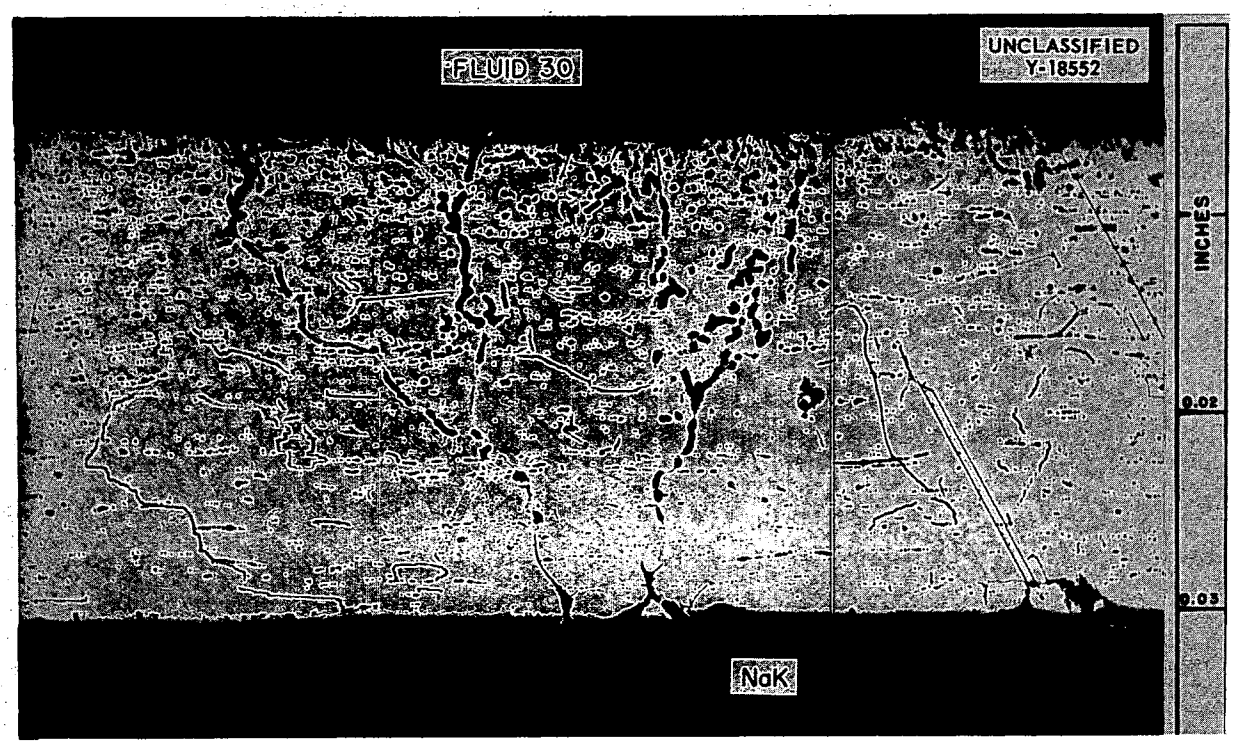

Fig. 137. Photomicrograph Showing Severe Corrosion on Tension Side of Tube 93. Etchant: electrolytic oxalic acid. 100X.

Fig. 138. Inner Surface of Tube 17. Cracking and corrosion from the outer surface are evident. Etchant: electrolytic oxalic acid.

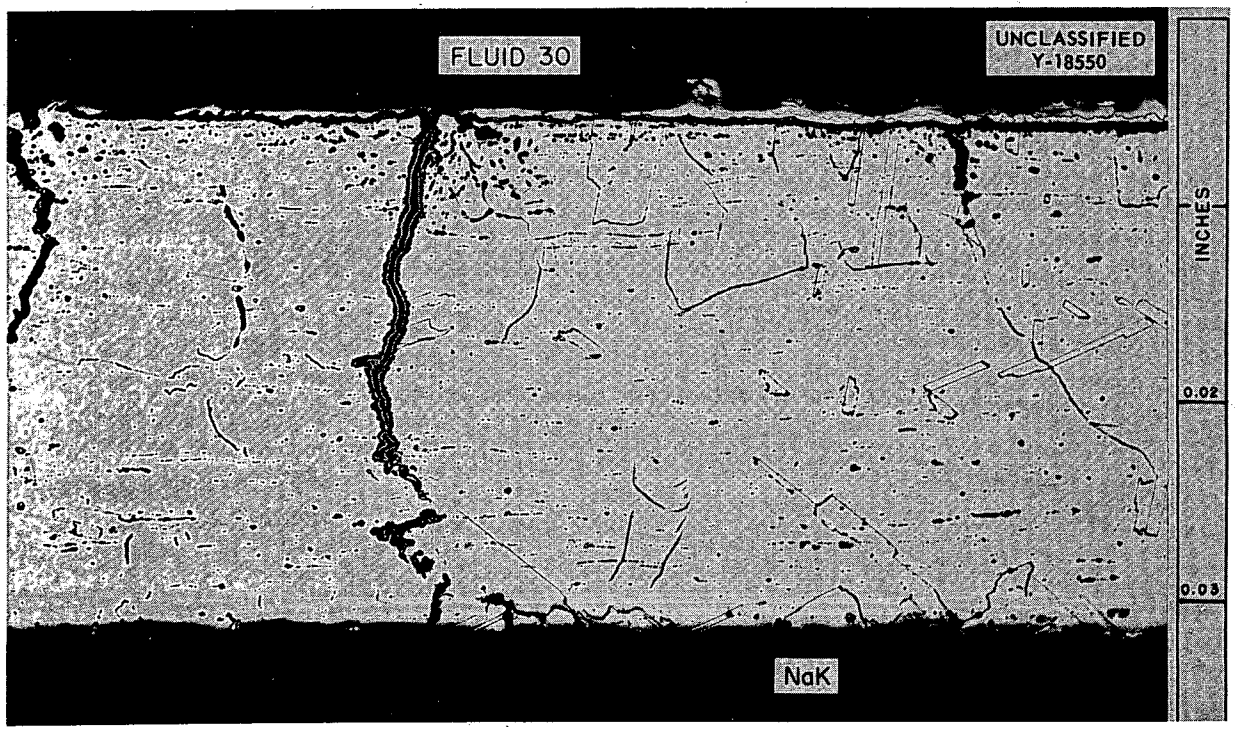

Fig. 139. Crack and Deposit in Tension Side of Tube 19. Etchant: electrolytic oxalic acid. 100X.

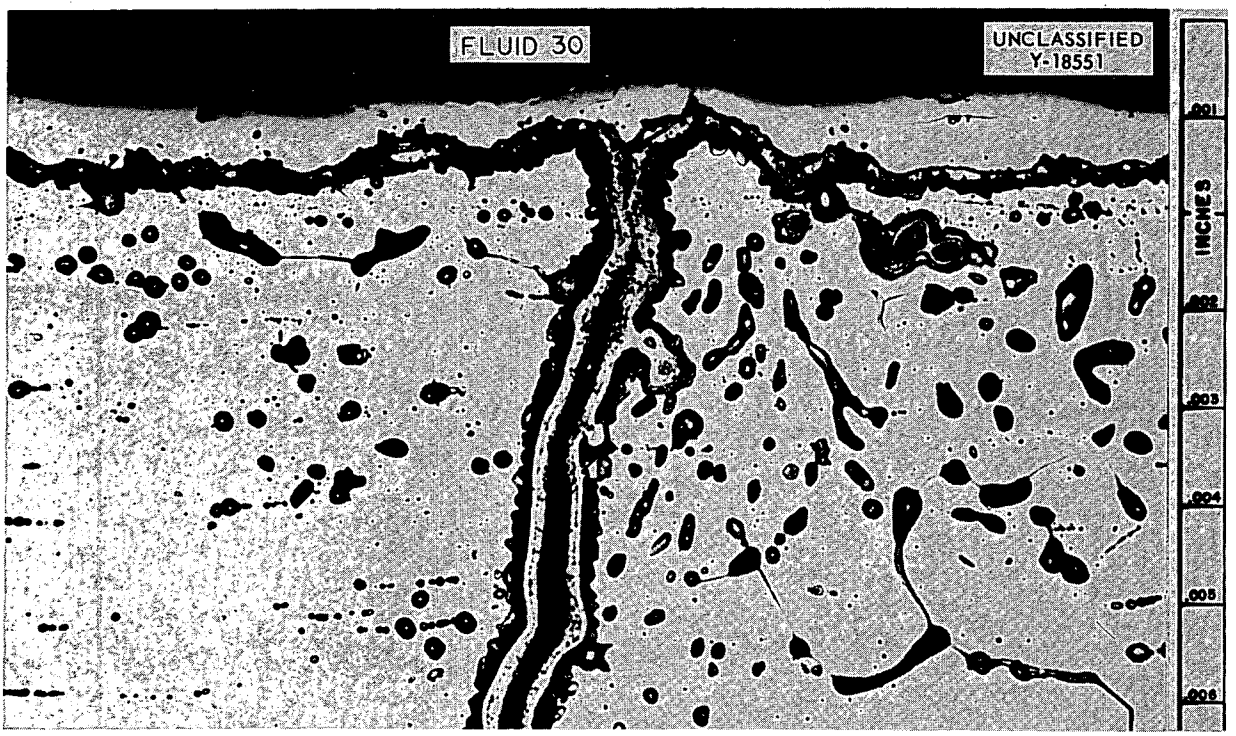

Fig. 140. High-Magnification View of Crack and Deposit. Etchant: electrolytic oxalic acid. 500X.

satisfactory cost for ring production. Of course, there are other factors which may influence the use of the ring, such as application techniques and the quality of the joints produced by the two methods.

As in previous experiments, graphite molds were prepared by using a tool similar to the one shown in Fig. 141 in a drill press. The depth of cut was adjusted to yield rings weighing 4.5 g per hundred. The size of this ring is based on the quantity of alloy required to produce an acceptable tube-to-fin joint by using 0.188-in.-OD tubing and a fin made with existing ORNL fin dies. The molds were loaded flush with CM-52 powder and stacked four high, with each mold serving as a lid for the one below it and with a graphite block serving as a lid for the top mold in a manner similar to that shown in Fig. 142.

The furnace used for this pilot plant is described in the schematic diagram shown in Fig. 143. This furnace is essentially a two-section unit, the first of which serves as a preheater and the second of which adjusts the temperature to the narrow range in which satisfactory rings are produced and maintains this temperature long enough to allow the entire mass of the molds to reach this temperature. A continuous stainless steel ribbon runs through the furnace and is driven by a variable-speed drive shown in Fig. 144. When this equipment is operated at a belt speed of 5 in./min, 9000 rings may be produced in 1 hr; however, the control of furnace temperature becomes quite critical. This equipment, therefore, is best operated at 4-in./min, producing 7200 rings/hr or approximately 50,000 per 8-hr day.

A thermal cycle which produced satisfactory rings is shown in Fig. 145. This graph was reproduced from a recording of the output of a thermocouple attached to a set of molds passing through the furnace at 4 in./min.

Proper control of temperature permits the easy removal of the sintered rings from the molds by the use of the vibrating tool shown in Fig. 146. The rings may be grit-blasted or tumbled in CM-52, if necessary, to remove any traces of carbon or small surface imperfections. If the temperature is

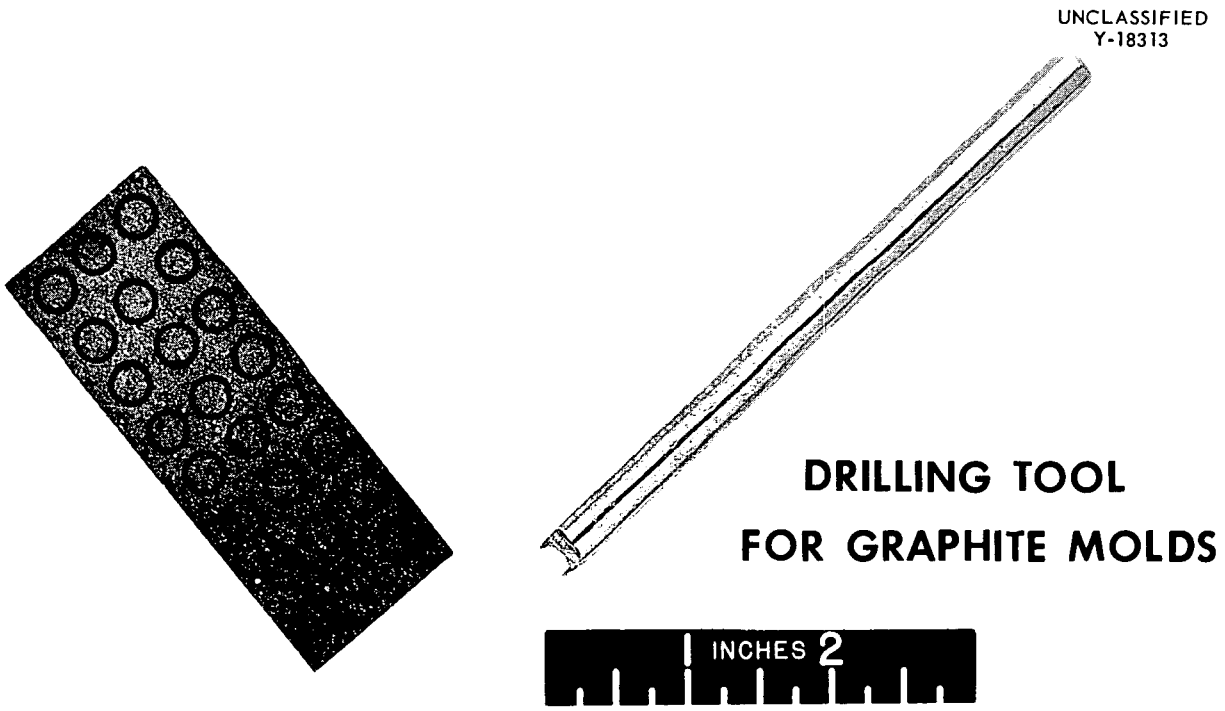

Fig. 141. Drilling Tool for Graphite Molds.

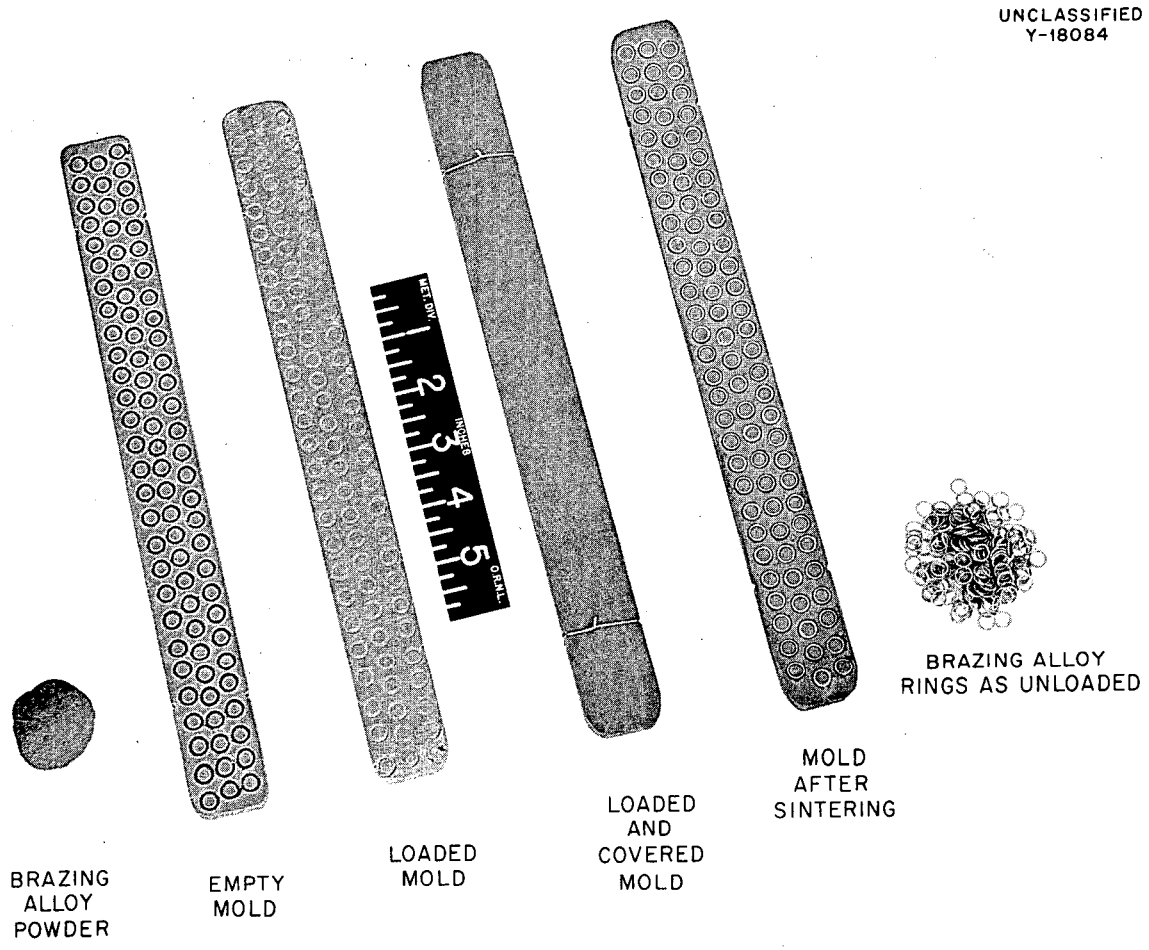

Fig. 142. Graphite Molds for Continuous Furnace Production of Sintered CM-52 Brazing Rings.

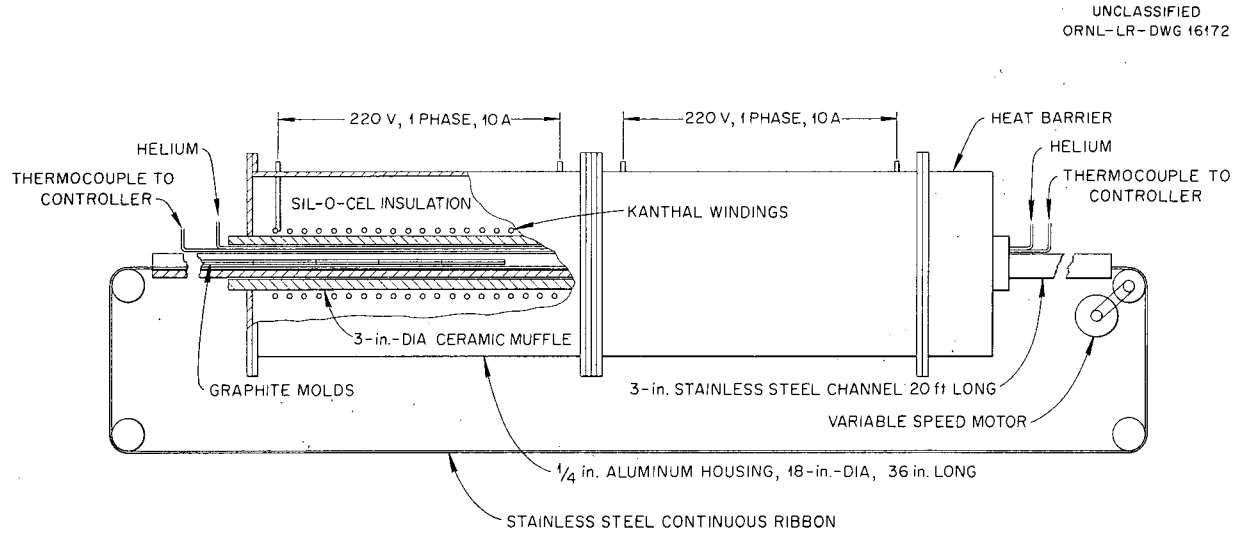

Fig. 143. Continuous Furnace for Production of Sintered CM-52 Brazing Rings.

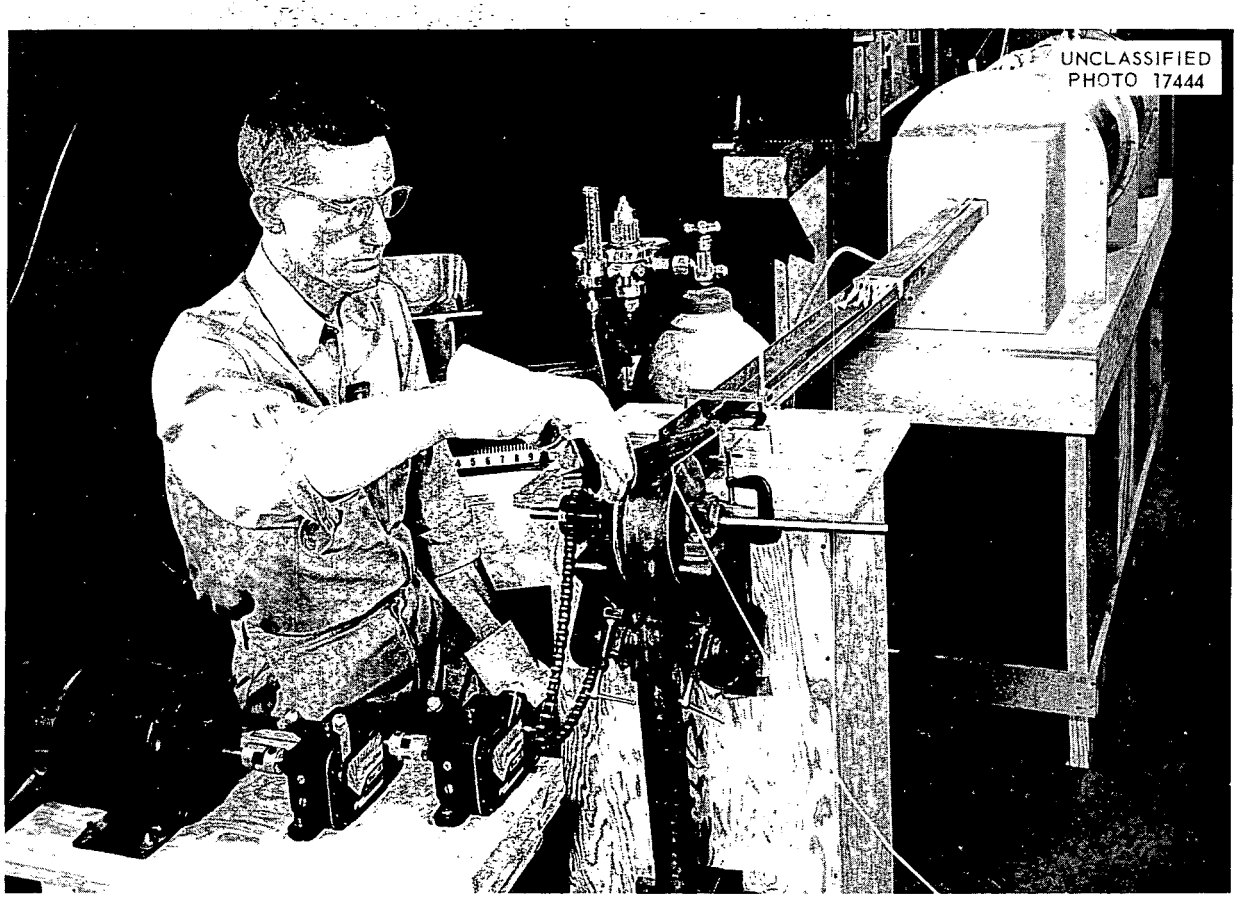

Fig. 144. Photograph of Continuous Ring Furnace.

carefully controlled (within a 5°C range), rings with no rejects and very good surface finish will be produced. Rings of satisfactory quality are produced within a range of about 10°C.

Temperature is adjusted and controlled by a Variac and a Brown Pyr-O-Vane with the Brown Flex-A-Pulse unit installed. The Variac serves as a fine temperature adjustment, moving the control point to above and below the set point on the Pyr-O-Vane by a few degrees.

Two men can easily operate this equipment at speeds up to 5-in./min, loading and emptying molds, inspecting rings, and making all necessary equipment adjustments. Power consumption is negligible, and capital costs are low. Brazing alloy costs are less than 0.1 cent per ring. These data should provide a reasonable means of evaluating vendor's production and costs.

Several improvements may be made on the existing equipment; however, they would only lessen the manual labor and not increase the production rate. Larger equipment could easily be built and should offer no major problems. With equipment of greater production capacity, labor-saving devices, such as the automatic mold filler now being built, could probably allow a furnace team to produce 10,000 rings per man.

Cost Estimate

The data shown in Table 49 are based upon a summary of information obtained from the operation of the above furnace. This furnace is capable of continuous production of good-quality rings at a rate of 7200 rings per hour of operation, exclusive of warmup periods. This warmup period will probably require 1 to 1½ hr at each startup to stabilize

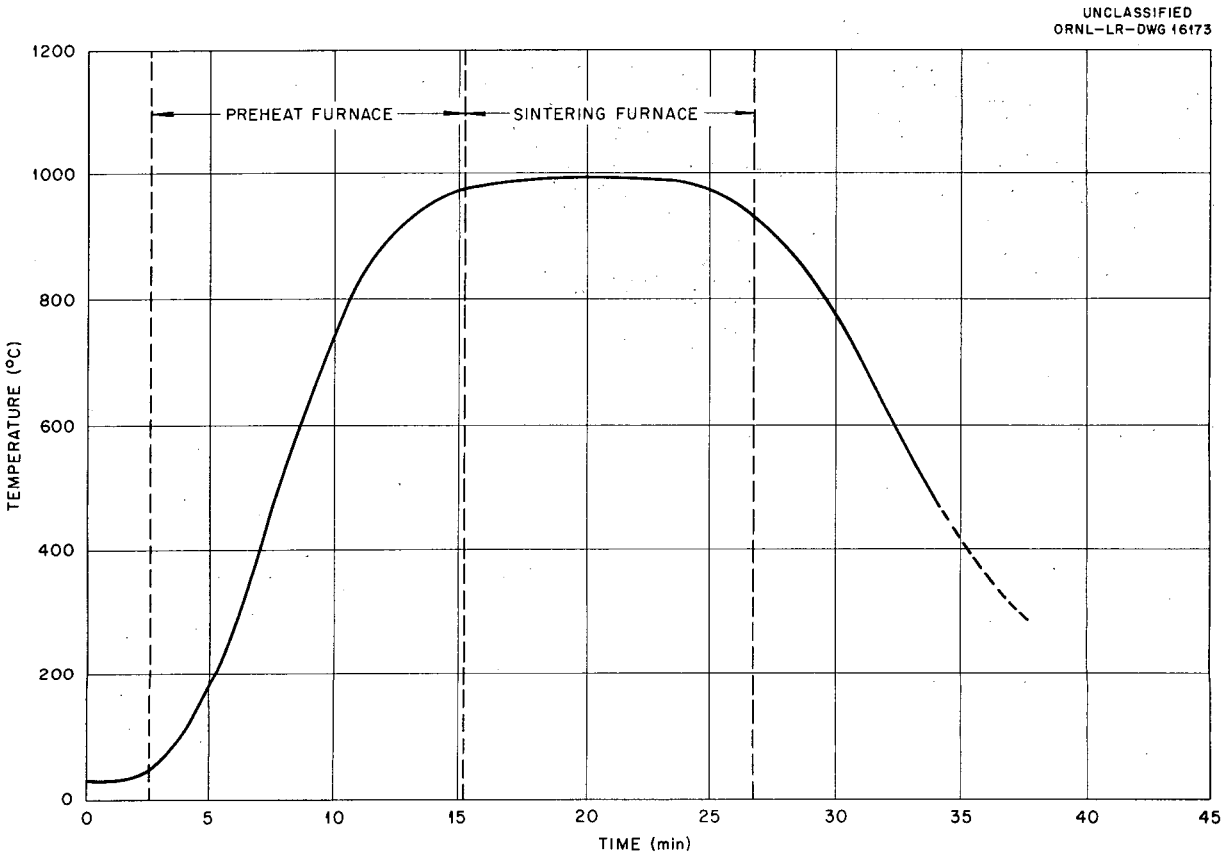

Fig. 145. Sintering Cycle at 4 in./min.

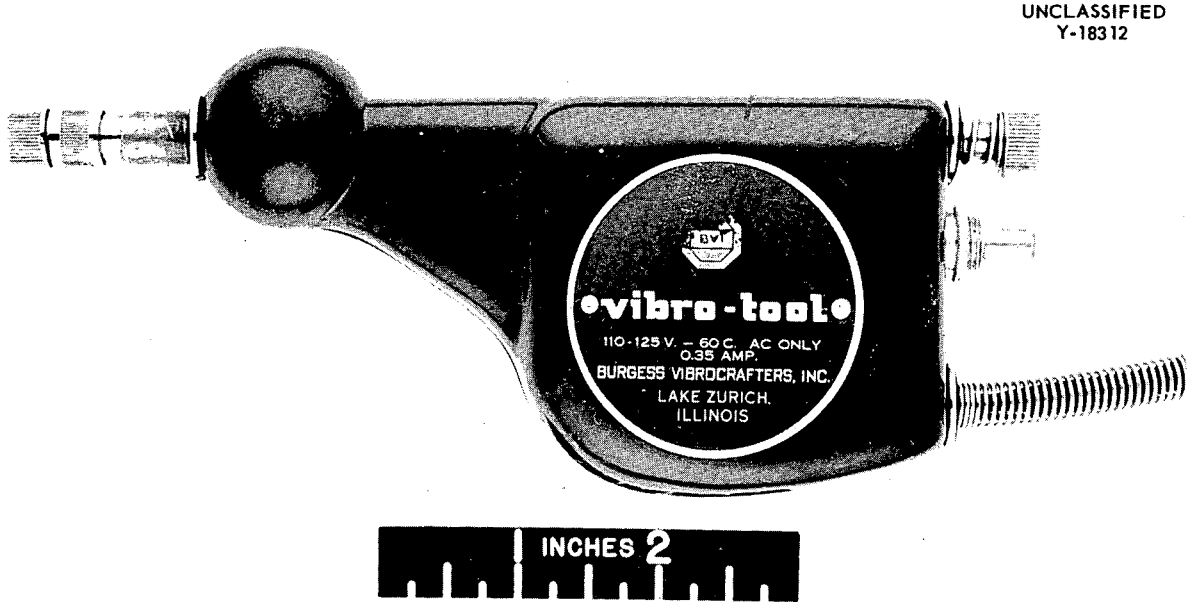

Fig. 146. Vibrating Tool for Removing Rings From Molds.

TABLE 49. COSTS FOR SINTERED CM-52 BRAZING RING PRODUCTION

	Operational Costs (based on 7200 rings/hr)	
	Per hr	Per Ring
Electricity, 4 kw at 5¢/kwhr	$ 0.20	$0.00003
Helium, 50 ft^3 at 3¢/ft^3	1.50	0.00021
Labor, assuming 2 men at $5.00	10.00	0.00139
CM-52, 1 lb at $7.00/lb	7.00	0.00097
Replacement of graphite molds, $0.94 per hr*	0.94	0.00013
	$19.64	$0.00273
	Capital Costs	
Furnace and equipment	$2000.00	
Instrumentation	$1000.00	

*Manufacturing and material cost for each mold is estimated at $1.30 and will probably produce 10,000 rings during its lifetime for a cost of $0.00013 per ring.

furnace temperatures under operating conditions and permit good control.

During the first production run of 5 hr duration, 33,000 rings were made at rates up to 9000/hr. It was felt, however, that at a production rate of 7200 rings/hr better quality and closer control were obtained. The table lists the estimated cost of operation to produce 7200 inspected and sorted rings per hour on a continuous basis, using existing equipment.

Based on cost per ring, only total capital costs and operational labor would vary appreciably if the equipment were scaled up. It is necessary to use two men to operate the pilot plant, although neither is fully utilized. As stated before, it is conceivable that a production of 10,000 rings per man-hour might be attained by using suitable labor-saving devices in conjunction with larger equipment.

FABRICATION OF CERMET VALVE COMPONENTS

A description of the high-temperature cermet-bonding procedure used in the fabrication of several valve components was presented in the previous semiannual report.[3] At the relatively high temperatures required for bonding (~1350°C), the cermets lose strength to such an extent that, occasionally, significant distortion or warpage of the cermet body is observed.

In view of this difficulty, a modification in fabrication procedure was developed which has permitted the successful fabrication of disks and seats for four different test-valve assemblies. The minimum temperature for consistent bonding was determined for each cermet composition and was found to vary with cermet type (i.e., K-151A, K-152B, or K-162B). These temperatures are shown in Table 50.

TABLE 50. MINIMUM TEMPERATURE FOR CONSISTENT BONDING OF CERMET VALVE COMPONENTS

Trade Designation	Binder	Bonding Temperature (°C)
K-151A	20% Ni	1350
K-152B	30% Ni	1335
K-162B	25% Ni–5% Mo	1340

[3] P. Patriarca, A. E. Goldman, and G. M. Slaughter, *Met. Semiann. Prog. Rep. April 10, 1956*, ORNL-2080, p 114.

Occasionally these optimum temperatures were found to vary slightly with different components of the same general composition. This observation can probably be related to variations in the compacting and sintering procedure in the original manufacture of the cermet bodies. Accordingly, each component was treated as an individual problem.

Observation ports were machined in the nickel transition layer to permit a visual determination of the initiation of bonding. This visual observation was found to be an essential addition to the precise control and measurement of temperatures for the consistent prevention of distortion of the cermets. These ports are clearly visible as black spots when the assembly in the furnace hot-zone is viewed with dark glasses. When the liquid reaction product forms, however, these ports are filled and disappear with the simultaneous formation of a fillet which can also be detected by careful observation through dark glasses. Cooling rates of approximately 1000°C/hr were used to minimize stresses during cooling.

The close control afforded by these modifications made it unnecessary to incorporate the use of the ceramic supports described in a previous memorandum.[2] Slight variations in settling which were observed occasionally were easily compensated for by a machining operation on the nickel face of the cermet-to-nickel subassembly.

Exploded views of the two steps employed in the fabrication of the valve disks are shown in Figs. 147 and 148. The cermet-to-nickel subassembly in the latter figure was copper-brazed to the Inconel shank by conventional dry-hydrogen techniques. Cooling rates of approximately 400°C/hr were used to prevent cracking. The stages used in the fabrication of the seat-ring components are shown in Figs. 149 and 150.

Four assemblies of each type have been successfully fabricated. After grinding in the ORNL Research Shops, the cermets will be evaluated in the ARE Division testing facilities.

QUALIFICATION OF WELDERS

The testing and evaluation of welder's qualification test specimens is an integral part of the fabrication of various components by vendors. Test welds are submitted to visual, radiographic, mechanical, and metallographic examination, and the welders are evaluated accordingly. A summary of the status of these tests to date is presented in Table 51.

WELDABILITY STUDIES OF NICKEL-MOLYBDENUM ALLOYS

The use of nickel-molybdenum alloys as structural materials for reactor applications requires that they possess adequate weldability characteristics.

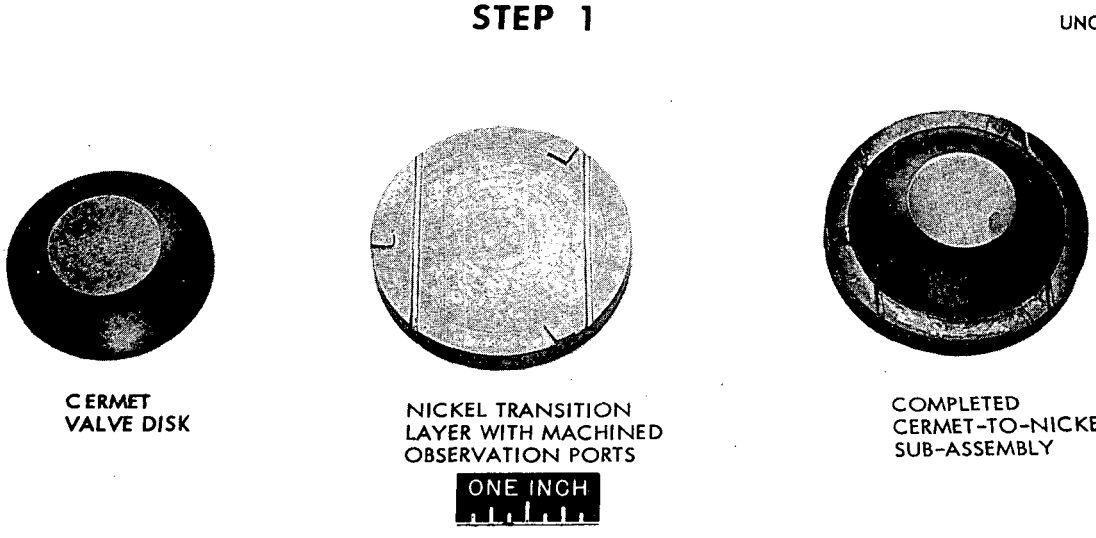

Fig. 147. Valve Disk Fabrication – Step 1.

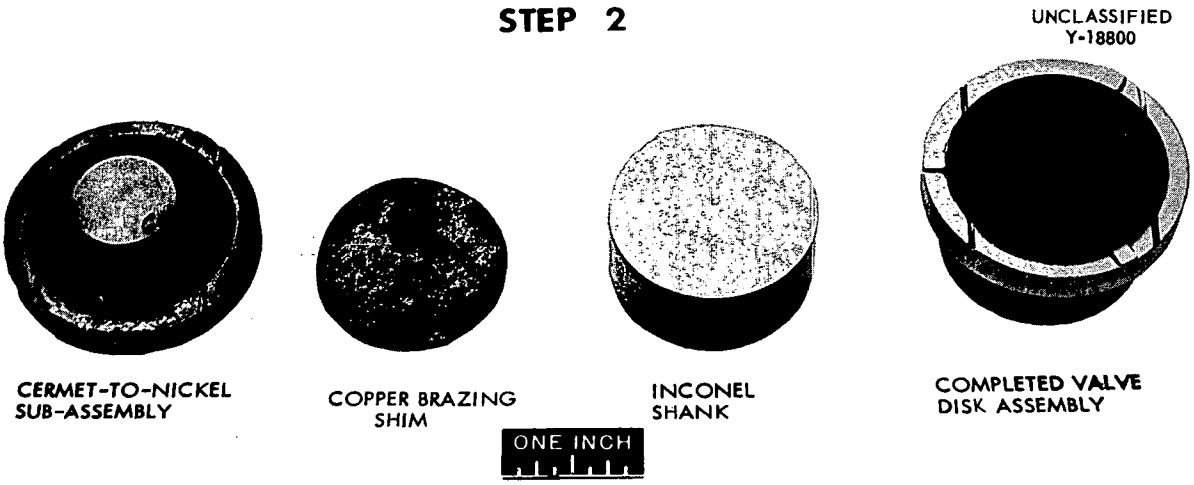

Fig. 148. Valve Disk Fabrication – Step 2.

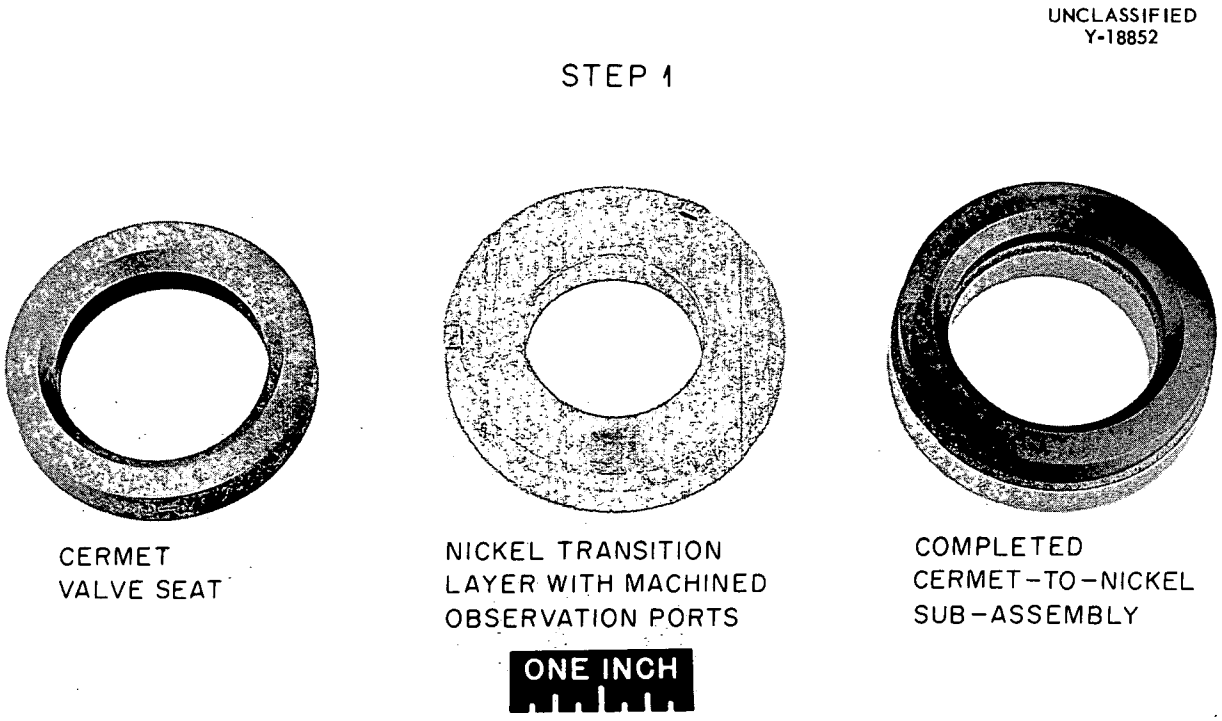

Fig. 149. Valve Seat Fabrication – Step 1.

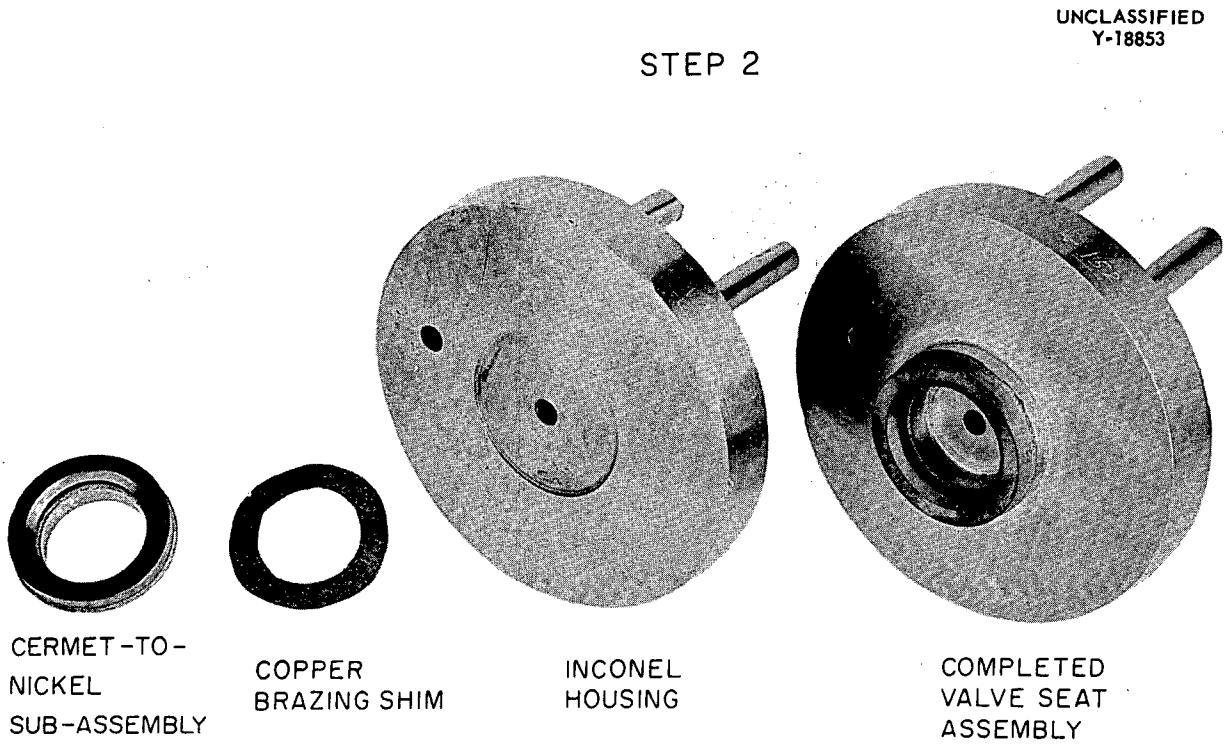

Fig. 150. Valve Seat Fabrication – Step 2.

TABLE 51. STATUS OF WELDERS' QUALIFICATION TESTS

Vendors	Number of Welders in Test	Number of Welders Who Passed Test		
		2G	5G	Fillet
York Corp.	13	13	13	8
Black, Sivalls, & Bryson	5	5	5	5
Griscom-Russell	3	3	3	2
Process Engineering	4	3	2	2
Alcoa Products	2	0	0	0
Struthers-Wells	5	1	1	1
Sharples	1	1	1	0

To obtain background information on the weldability of several alloys now under development, welding studies are being conducted on commercially available Ni-Mo type alloys and on the 85 Ni–15 Mo alloy.

Ten weld test plates have been made with base material of ½-in. thickness. The weldments are being subjected to dye-penetrant and radiographic inspection followed by all-weld-metal and transverse-tensile tests and bend tests at both room and elevated temperatures. The results will be reported in the next annual report. A summary of the types of weld test plates is presented in Table 52.

TABLE 52. SUMMARY OF NI-MO ALLOY TEST-PLATE DATA

Plate No.	Plate Composition	Filler Metal Composition	Type of Mechanical Test
1	Hastelloy B	85 Ni–15 Mo	Longitudinal
2	Hastelloy B	Hastelloy B	Longitudinal
3	Hastelloy B	Hastelloy B	Transverse
4	Hastelloy B	Hastelloy B	Longitudinal
5	Hastelloy W	Hastelloy W	Longitudinal
6	Hastelloy W	Hastelloy W	Transverse
7	Hastelloy W	Hastelloy W	Longitudinal
8	Hastelloy B	Hastelloy B	Longitudinal
9	Hastelloy B	Hastelloy W	Transverse
10	Hastelloy W	85 Ni–15 Mo	None (extensive porosity and weld-metal cracking)

FABRICATION

J. H. Coobs H. Inouye
J. P. Page T. K. Roche
Metallurgy Division

M. R. D'Amore R. E. McDonald
Pratt & Whitney Aircraft

V. M. Kolba
The Glenn L. Martin Co.

J. E. Spruiell
University of Tennessee Co-op Student

DEVELOPMENT OF NICKEL-MOLYBDENUM-BASE ALLOYS

H. Inouye T. K. Roche

The present available supply of Hastelloy B and W tubing is prepared by redrawing tubing formed from welded strip, and it is not of high quality. Since these alloys are characterized by high-temperature strength and resistance to fused-salt corrosion, a source of seamless tubing is desired; therefore, considerable effort has been devoted to the study of extrusion techniques for the production of seamless tubing of these Hastelloys and other related alloys.

Extrusion and Redrawing of Hastelloy W

Early attempts to extrude tube blanks of Hastelloy W failed. In these experiments forged billets canned in Inconel were extruded at 2050 and 2100°F at an extrusion ratio of 7:1. Severe fracturing of the tube blank occurred during the extrusion process, at least in part, as a result of melting. An excessive temperature rise as a result of the rapid deformation of the material was found to have caused this difficulty. During the period of this report, the alloy was successfully extruded by changing the extrusion temperature and rate, as noted below. Other conditions, which were identical in both cases, are as follows:

Billet	Forged Hastelloy W; canned in Inconel
Billet size	3-in. OD, 1⅛-in. ID, 3 in. long
Die size	1½-in., 30-deg cone
Mandrel size	1 in.
Extrusion ratio	7:1

The rate of extrusion was controlled by regulating the flow of high-pressure water to the ram of the extrusion press by means of a throttle valve. The rate settings, in terms of the number of turns that this valve was opened, were 3½ and 3¾ for the unsuccessful extrusions and 2½ for the successful extrusion. Actual extrusion rates, in feet per minute, were not determined during these experiments. The preheating temperature used for the successful extrusion was 2200°F, as compared to 2050 and 2100°F used for unsuccessful extrusions.

It was concluded from this work that Hastelloy W could be extruded on a laboratory scale by raising the extrusion temperature and reducing the extrusion rate so as to allow time for metal flow and to minimize the deleterious effects of generated heat. The successful and unsuccessful tube-blank extrusions are illustrated in Fig. 151.

Results of processing the successful tube blank of Hastelloy W, shown in Fig. 151, to 0.187-in.-OD, 0.025-in.-wall tubing by the Superior Tube Co. indicate the feasibility of producing small-diameter seamless tubing of Hastelloy-type alloys. This extrusion yielded 25 ft of tubing, which was examined by non-destructive testing techniques and was determined to be of the high quality required for heat-exchanger applications. Longitudinal and transverse sections of the tube wall are shown in Figs. 152 and 153, respectively.

Extrusion of Hastelloys B, W, and X on a Commercial Scale

An experiment at the Huntington Works of the International Nickel Company on March 27, 1956, was performed in order to determine the feasibility of producing tube-blank extrusions of Hastelloys B, W, and X on a commercial scale. The experiment was carried out as a cooperative effort between Oak Ridge National Laboratory, International Nickel Company, and Haynes Stellite Company.

Forged and machined billets of the Hastelloys were prepared by Haynes Stellite Company. Based

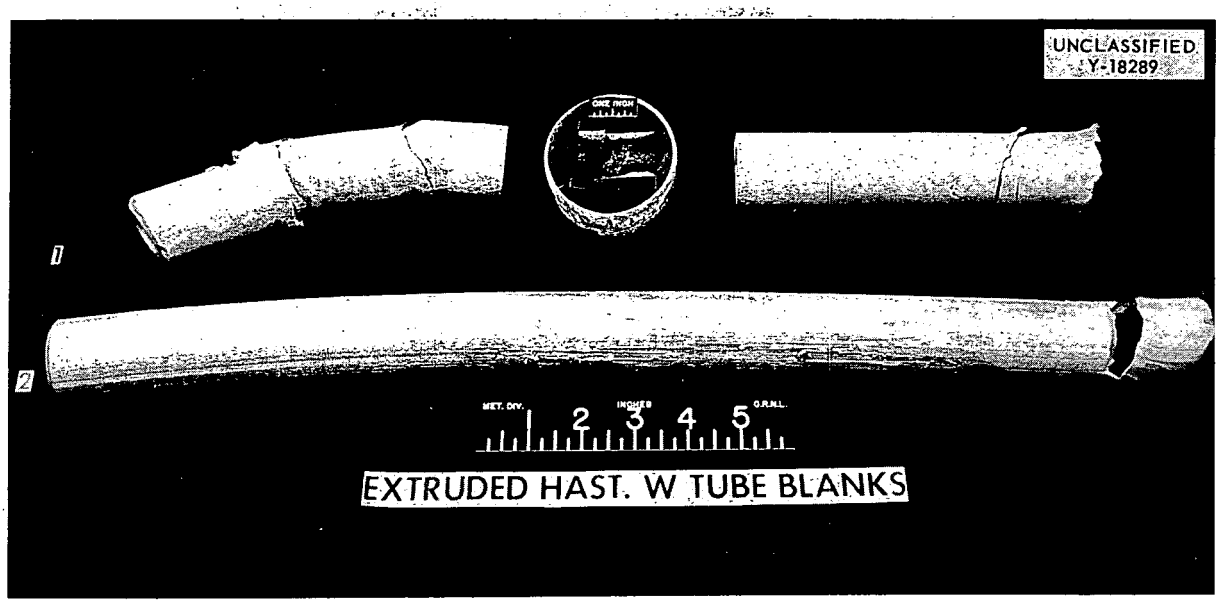

Fig. 151. Seamless Tube Blanks Extruded from Forged Hastelloy W Billets Canned in Inconel. Tube 1 was extruded at a fast rate at 2100°F. Tube 2 was extruded slowly at 2200°F.

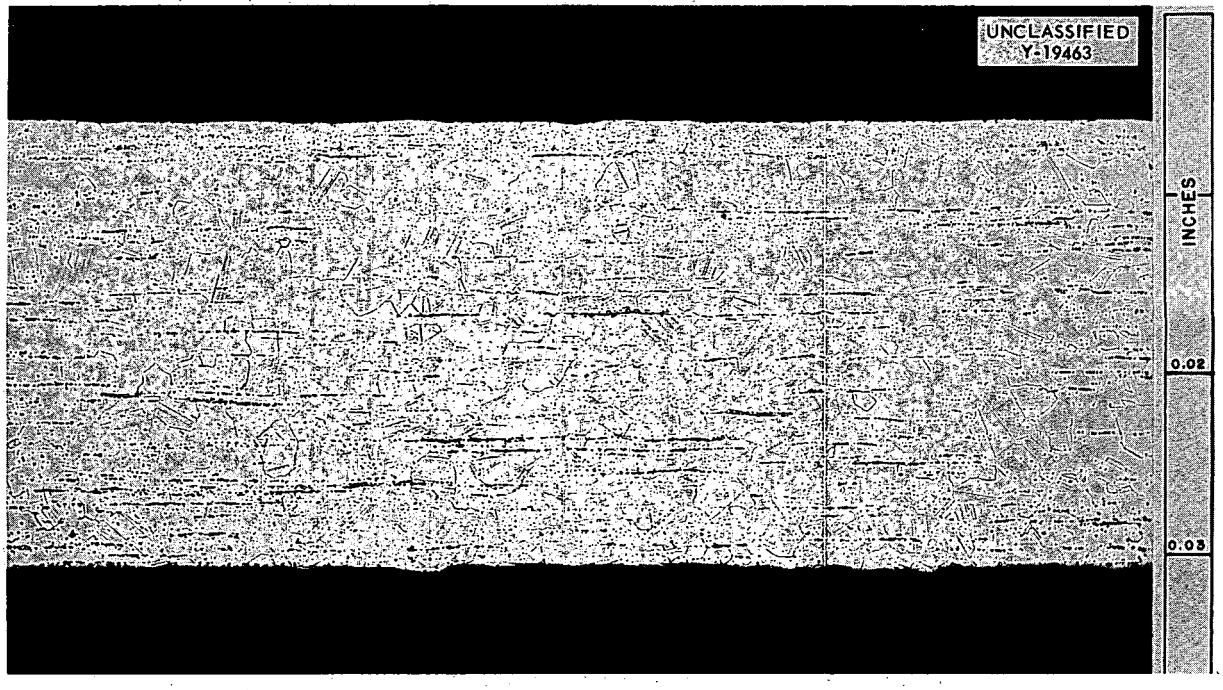

Fig. 152. Longitudinal Section of Seamless Hastelloy W Tubing, 0.187-in. OD × 0.025-in. Wall. Etchant: chrome regia. 100X. Reduced 3%.

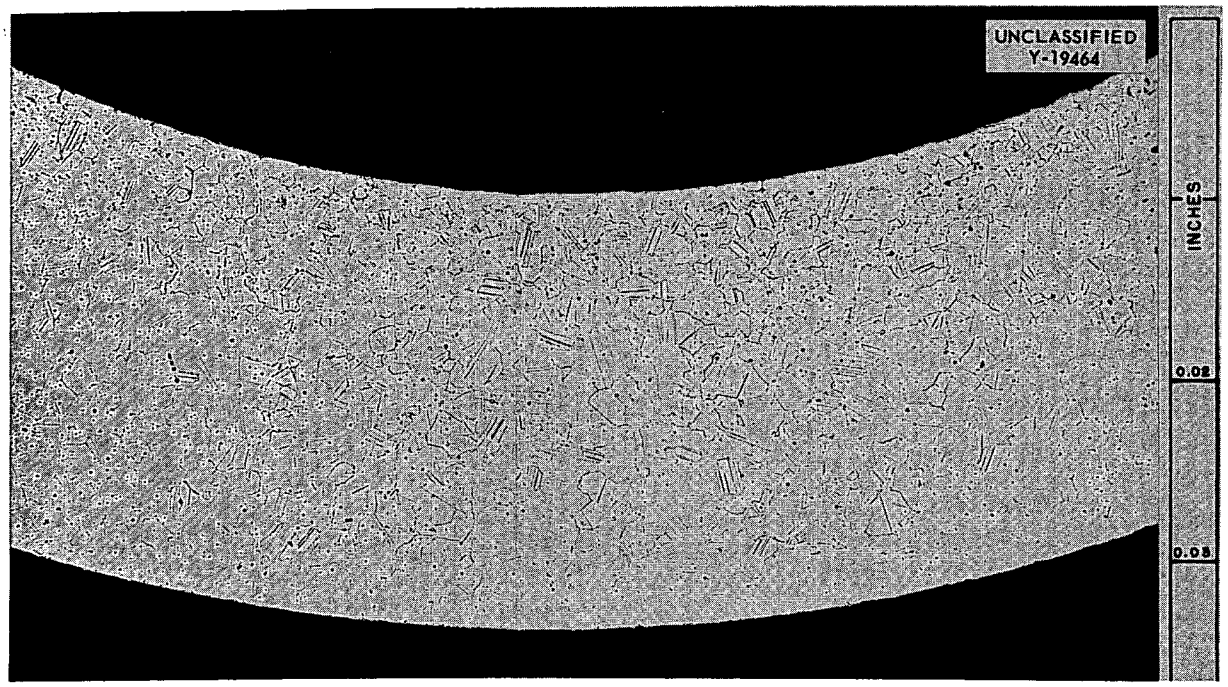

Fig. 153. Transverse Section of Seamless Hastelloy W Tubing. Etchant: chrome regia. 100X. Reduced 3%.

upon extrusion experience on a laboratory scale at ORNL, as described above, a schedule was prepared for the extrusion of the Hastelloy B billets. Since small tube blanks had been prepared successfully by use of a slow extrusion rate at 2200°F, it was proposed that the larger billets be extruded at as slow a rate as practical. The extrusion temperature could be lower, of course, because of the larger size of the billet. The results of the Hastelloy B extrusions, which are summarized in Table 53, were reported to ORNL by International Nickel Company upon completion of the experiment. The extruded tube blanks of Hastelloy B are shown in Figs. 154 and 155.

Although the Hastelloy W and X billets were not extruded under the direction of ORNL, the fabrication of these alloys is of interest to the over-all alloy-development program. The available results of these extrusions are presented in Table 54.

The following general conclusions have been drawn regarding the extrusion of 6.9-in.-OD, 10-in.-long billets of Hastelloys B, W, and X:

1. Forged billets of Hastelloys B, W, and X can be successfully extruded into tube blanks.
2. Canning of the billets with $\frac{1}{8}$-in.-thick type 316 stainless steel appears to be advantageous from the standpoint of reducing the extrusion pressure. Because of the number of variables involved, however, this conclusion needs to be confirmed.
3. The larger mass of the commercially produced billets made possible the use of lower soaking temperatures at smaller extrusion ratios (i.e., 5.5:1) than were found to be optimum for the extrusion of small laboratory billets.
4. For successful extrusion of these alloys, it is necessary that the billets be upset with sufficient pressure to start the material through the die and then be extruded at a relatively slow rate to prevent hot-short cracking.

These were the first successful attempts to extrude these materials on a large scale, and it now appears to be feasible that seamless tubing of these alloys can be produced. Three Hastelloy B tube blanks and one Hastelloy W tube blank are scheduled to be reduced to 1-in. pipe and small-diameter tubing for use at ORNL.

TABLE 53. EXTRUSION OF HASTELLOY B BILLETS BY INTERNATIONAL NICKEL COMPANY FOR OAK RIDGE NATIONAL LABORATORY

Billet dimensions: 6.900-in. OD, 2.500-in. ID, 10 in. long
Machined size of billets canned on outside diameter only: 6.650-in. OD, 2.50-in. ID, 10 in. long
Machined size of billets canned on outside diameter and inside diameter: 6.500-in. OD, 2.75-in. ID, 10 in. long
Machined size of uncanned billets: 6.900-in. OD, 2.50-in. ID, 10 in. long
Product dimensions: outside diameter, as indicated below; inside diameter, 2.250 in.

Billet No.[a]	Billet Preparation		Nose Radius (in.)	Extrusion Temperature[b] (°F)	Total Soaking Time (min)	Extrusion Ratio	Product Outside Diameter (in.)	Extrusion Pressures (tsi)			Extrusion Rate of Billet Length (ips)	Usable Length of Product (in.)
	On Outside Diameter	On Inside Diameter						Peak	Minimum	Running		
B-1	Uncanned	Uncanned	1	2050	220	5.5:1	3.685	77.1	77.1	77.1	1.2	41
B-2	Canned	Uncanned	0.5	2050	201	5.5:1	3.685	71.3	66.8	68.3	1.2	51
B	Canned	Canned	0.5	2050	187	5.5:1	3.685	68.3	61.0	62.3	1.2	47
B-7	Uncanned	Uncanned	1	2150[c]	100	5.5:1	3.685	74.3	62.3	68.3	1.3	47
B-8[d]	Uncanned	Uncanned	1	2150[c]	110	7:1	3.462	77.1	77.1	77.1	0	0
B-10	Uncanned	Uncanned	1	2150	65	7:1	3.462	75.8	71.3	68.3	1.4	58
BB[d]	Uncanned	Uncanned	1	2150	75	7:1	3.462	77.1	77.1	77.1	0	0
BBB	Canned	Uncanned	0.5	2150	65	7:1	3.462	74.3	68.3	69.7	1.2	62
B-3	Canned	Uncanned	0.5	2150	70	7:1	3.462	72.8	68.3	69.7	1.4	70
B-5	Canned	Uncanned	0.5	2200	100	10:1	3.135	77.1	74.3	77.1	0.5	81
B-4	Canned	Canned	0.5	2200	105	12.25:1	3.000	77.1	71.3	72.8	1.5	99

[a] Listed in extrusion order.
[b] Soaked in gas furnace, except as indicated.
[c] Soaked in salt bath after preheating to 700°F
[d] Billet stalled.

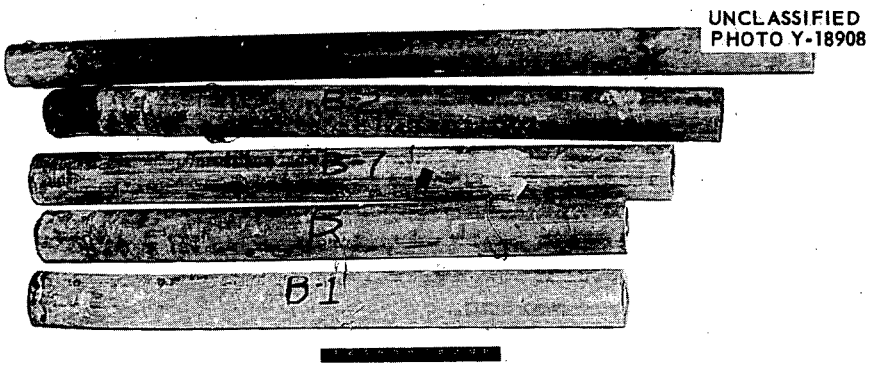

Billet	Extrusion Temperature (°F)	Extrusion Ratio
BBB	2150	7:1
B-2	2050	5½:1
B-7	2150	5½:1
B	2050	5½:1
B-1	2050	5½:1

Fig. 154. Hastelloy B Tube Blank Extrusions Fabricated by the International Nickel Company.

Billet	Extrusion Temperature (°F)	Extrusion Ratio
B-4	2200	12¼:1
B-5	2200	10:1
B-3	2150	7:1
B-10	2150	7:1

Fig. 155. Hastelloy B Tube Blank Extrusions Fabricated by the International Nickel Company.

TABLE 54. EXTRUSION OF UNCANNED HASTELLOY W AND X BILLETS BY INTERNATIONAL NICKEL COMPANY

Billet dimensions: 6.900-in. OD, 2.50-in. ID, 10 in. long; nose radius, 1 in.
Product dimensions: outside diameter, as indicated; inside diameter, 2.250 in.

Billet Material	Extrusion No.	Extrusion Temperature* (°F)	Extrusion Ratio	Outside Diameter of Product (in.)	Usable Length of Product (in.)
Hastelloy W	12**	2150	12.25:1	3.00	0
	13	2150	7.9:1	3.28	67
Hastelloy X	14	2150	7.9:1	3.28	67
	15	2150	7.9:1	3.28	67
	16	2150	10:1	3.135	85
	17**	2150	12.25:1	3.00	0
	18	2200	12.25:1	3.00	104
	19	2200	12.25:1	3.00	104

*Soaked in gas furnace.
**Billet stalled.

Extrusion and Redrawing of Special Alloys

The study of alloys which are based on the nickel-molybdenum-alloy system and which contain 15 to 20% molybdenum has progressed. It is hoped in this study to find a solution to the problem of embrittlement of the Hastelloy-type alloys as a result of aging. At present the only readily apparent solution is to change the composition of the alloys.

It was reported previously that the corrosion resistance to fused salts of the binary alloys of nickel and molybdenum which contain more than 15% molybdenum was exceptionally good but that the high-temperature strength of the alloys was not adequate. Thus, in order to obtain alloys with greater strength the special alloys described below are being studied. In addition, ternary alloys have been made that will be tested in order to determine the effect of a third element on the corrosion resistance of these alloys in fused salts.

A number of extrusion experiments have been conducted on the various alloys, and the material will be used for evaluation in thermal-convection loops. Drawing of the extruded tube blanks by the Superior Tube Co. has been generally satisfactory. The processing procedure for "as-extruded" 1.5-in.-OD, 0.25-in.-wall tube blanks is as follows:

1. initially condition the tube blanks by machining (results in an average weight loss of 50%);
2. reduce tube to 0.875-in. OD and 0.095-in. wall;
3. anneal at 2050°F in a dry-hydrogen atmosphere and water quench;
4. draw rod and sink to final size with intermediate anneals;
5. finish by sand blasting and rotary polishing.

An average yield of 70% is being obtained from the blanks after the initial conditioning operation. It has been found in the processing of these alloys that lighter cold reductions per pass must be taken than in the case of stainless steel or Inconel. A 20% reduction in area per pass is considered optimum.

Battelle Memorial Institute Compositions. – Extrusion experiments were conducted on promising compositions with the intention of producing seamless tubing for corrosion testing. This work was done in cooperation with Battelle Memorial Institute in the development of nickel-molybdenum-base alloys for high-temperature use. Initially, ten forged billets, representing portions of 220-lb air-melted heats, were fabricated. The results of the experiments are presented in Table 55.

Although fast extrusion at a ratio of 5.4:1 resulted in cracking on the inside, all these tube

TABLE 55. RESULTS OF EXTRUSION EXPERIMENTS ON SPECIAL ALLOYS PREPARED BY BATTELLE MEMORIAL INSTITUTE

Alloy No.	Nominal Compositions (wt %)						Extrusion Conditions			Results
	Ni	Mo	Nb	Ti	C	Mn	Temperature (°F)	Ratio	Rate*	
B-2897	77	20	1	1	0.12	0.80	2060	5.4:1	3	Back of tube cracked on inside
							2100	5.4:1	3	Back of tube cracked on inside
B-2898	76	20	1	2	0.12	0.80	2060	5.4:1	3	Back of tube cracked on inside
							2100	5.4:1	3	Back of tube cracked on inside
							2150	7:1	2¼	Good tube blank obtained
							2150	7:1	2¼	Good tube blank obtained
B-2899	78	20	1		0.20	0.80	2060	5.4:1	3	Back of tube cracked on inside
							2150	5.4:1	3	Back of tube cracked on inside
							2125	5.4:1	3	Back of tube cracked on inside
							2150	7:1	2¼	Good tube blank obtained

*Number of turns that the valve on the high-pressure water to the extrusion ram was opened; see discussion above.

blanks were salvaged at the Superior Tube Company by drilling the as-extruded tube blank, thereby increasing the inside diameter from ¾ to 1 in. before tubing reducing. Slow extrusion at a ratio of 7:1 proved beneficial from the standpoint of obtaining more sound tube blanks of these alloys. Tube No. 6, shown in Fig. 156, is representative of a good extrusion obtained from these alloys. As is typical of most extrusions of these high-strength nickel-molybdenum-base alloys, a certain amount of surface roughening was found on the inside, but it was not so severe as it appears to be in Fig. 156. Slight conditioning of the blanks before redrawing will eliminate these defects. The cause of this roughening is not completely understood at this time.

The results of processing the extrusions from alloys B-2897, B-2898, and B-2899 to 0.500-in.-OD, 0.035-in.-wall tubing are tabulated in Table 56. The response of these compositions to cold tube-forming techniques was only moderately successful. Examples of the difficulties encountered are illustrated in Fig. 157. Metallographic examination of the failure found in the tube blank of alloy B-2898 (20% Mo–1% Nb–2% Ti–0.80% Mn–0.12% C–bal Ni) revealed the stringering of second-phase particles (i.e., carbides) to be the probable source of difficulty, as shown in Fig. 158.

All attempts to produce seamless tubing of alloy B-2899 (20% Mo–1% Nb–0.80% Mn–0.20% C–bal Ni) failed. Of the two extrusions of this composition seen in Fig. 157, one developed a longitudinal crack along its length while on the draw bench; and the other failed during the initial tube-reducing operation. Examination of these cracks again revealed that stringering of the numerous precipitates was the source of failure.

In view of the results obtained, it is apparent that carbon levels of 0.20% or greater in the Ni-Mo alloys being investigated will render tube-forming success improbable; and a carbon level of 0.12% is marginal in this respect.

A second series of alloys received from Battelle Memorial Institute is listed in Table 56 under alloy numbers B-3275 through B-3278. These compositions were received in the form of forged extrusion billets, swaged impact tensile specimens, and rolled creep-rupture specimens. The impact tensile specimens were sent to Rensselaer Polytechnic Institute for weldability studies, and the creep-rupture specimens will be tested at ORNL in fluoride fuel No. 107. Extrusion experiments were conducted at ORNL on two forged billets of each composition to investigate the feasibility of producing seamless tubing of the alloys. The tube blanks were extruded at 2150°F at a ratio of 7:1. All compositions were fabricated successfully and sent to Superior Tube Co. for redrawing.

Results of tubing fabrication from the extruded tube blanks are also shown in Table 56. One tube

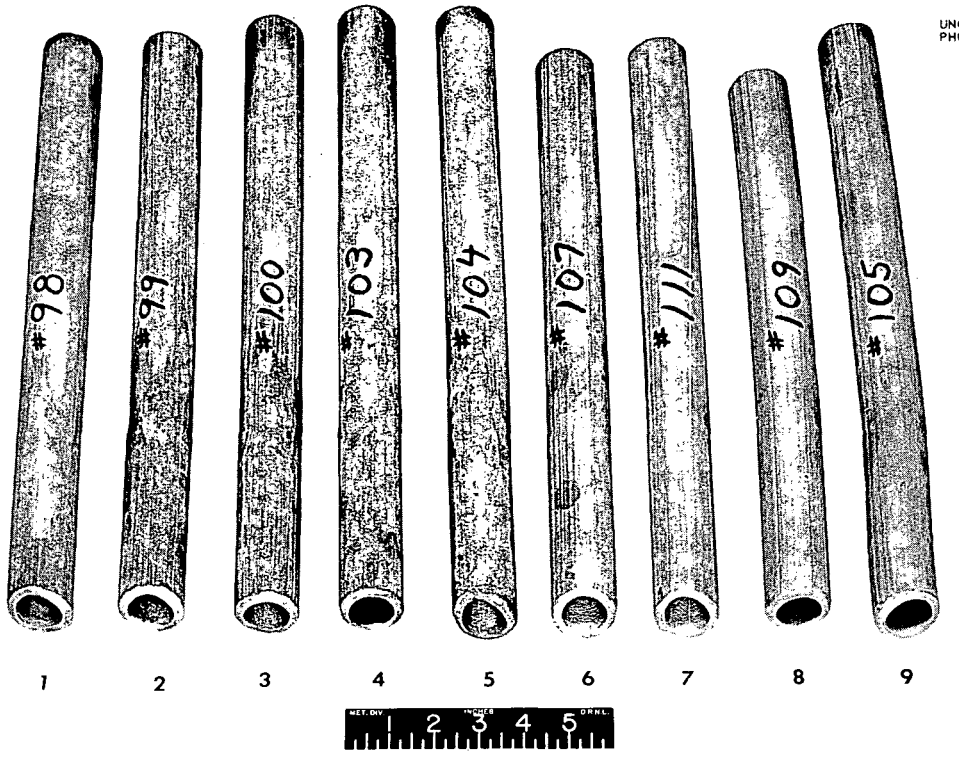

	Mo	Cr	Cb	W	Al	Ti	Mn	C	Ni
1	15	5	3	3	0.5				BAL
2	17				0.5				BAL
3	15		3	3	0.5				BAL
4	15				1	1.5			BAL
5	15		3	3	0.5			0.25	BAL

	Mo	Cr	Cb	W	Al	Ti	Mn	C	Ni
6	20		1			2	0.80	0.12	BAL
7	17	3						0.06	BAL
8	17	5						0.06	BAL
9			HASTELLOY B						

Fig. 156. Extruded Tube Blanks from a Variety of Nickel-Molybdenum Alloys.

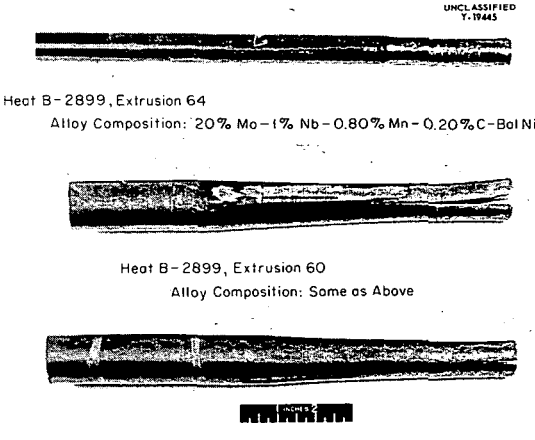

Fig. 157. Failures in Tube Blanks During Cold Reduction.

blank of alloy B-3276 (20% Mo–7% Cr–2% Nb–1% Fe–0.80% Mn–0.12% C–bal Ni) and both tube blanks of alloy B-3278 (20% Mo–7% Cr–2% Al–0.80% Mn–0.12% C–bal Ni) failed on the tube reducer. These failures were not analyzed metallographically but were assumed to have been caused by the carbide stringering problem, as shown in Fig. 158. The compositions which were successfully processed to seamless tubing will be evaluated for their corrosion resistance by thermal-convection loop testing in fluoride fuel No. 107.

International Nickel Company Compositions. – As reported in the last semiannual report, 40-lb heats of five special alloys were received from International Nickel Company for corrosion testing and strength evaluation. The nominal compositions of these alloys are given in Table 57.

Four extrusion billets, 3 in. in diameter and 3 in. in length, were machined from each ingot; three

TABLE 56. RESULTS OF REDRAWING BATTELLE AND INCO ALLOYS TO 0.500-in.-OD, 0.035-in.-WALL TUBING

Alloy No.	Nominal Composition (wt %)	Number of Extruded Tube Blanks	Total Length of Tubing Received		Yield* (%)	Number of Loops Requested	Remarks
			Feet	Inches			
	Battelle Alloys						
B-2897	Ni–20 Mo–1 Nb–1 Ti–0.80 Mn–0.12 C	2	9	2	40	1	
B-2898	Ni–20 Mo–1 Nb–2 Ti–0.80 Mn–0.12 C	4	19	6		2	One tube blank split on tube reducer
B-2899	Ni–20 Mo–1 Nb–0.80 Mn–0.20 C	4	0	0	0	0	Two tube blanks split on tube reducer; two split on draw bench
B-3275	Ni–20 Mo–7 Cr–0.80 Mn–0.12 C	2	26	3		2	
B-3276	Ni–20 Mo–7 Cr–2 Nb–1 Fe–0.80 Mn–0.12 C	2	11	4		1	One tube blank split on tube reducer
B-3277	Ni–20 Mo–7 Cr–2 Nb–1 Fe–1 Al–0.80 Mn–0.12 C	2	27	6		2	
B-3278	Ni–20 Mo–7 Cr–2 Al–0.80 Mn–0.12 C	2	0	0	0	0	Both tube blanks split on tube reducer
	INCO Alloys						
T-23011	Ni–15 Mo–5 Cr–3 Nb–3 W–0.5 Al–0.02 C	2	11	11	43	1	
T-23012	Ni–17 Mo–0.5 Al–0.02 C	1	12	0	69	1	
T-23013	Ni–15 Mo–3 Nb–3 W–0.5 Al–0.02 C	3	27	6	76	2	
T-23014	Ni–15 Mo–1.5 Ti–1 Al–0.02 C	1	7	4	80	1	
T-23015	Ni–15 Mo–3 Nb–3 W–0.5 Al–0.25 C	2	0	0	0	0	Both blanks failed on tube reducer

*Per cent yield after conditioning tube blanks.

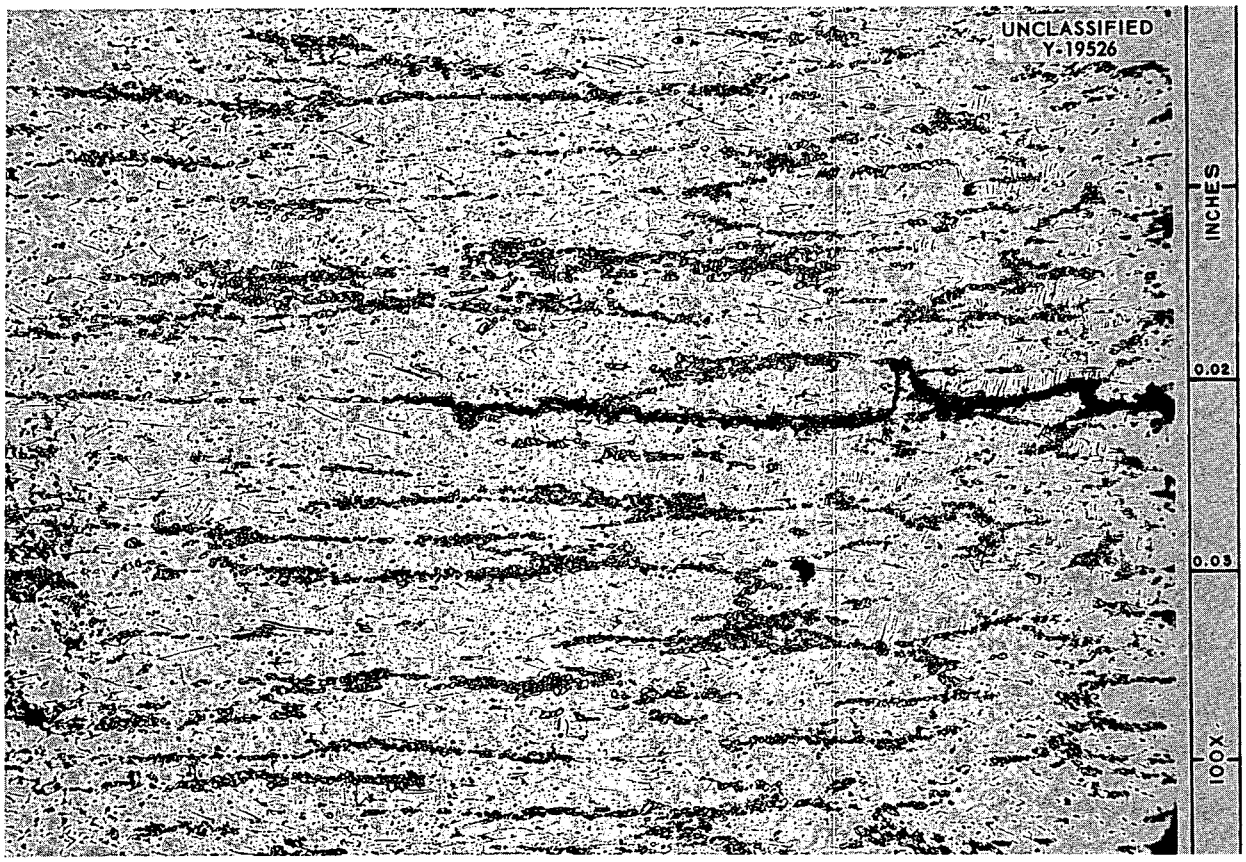

Fig. 158. Longitudinal Section of Tube Blank of Alloy 2898 Showing Crack Propagation Along Carbide Stringers. Etchant: chrome regia.

were for tube blanks and one was for rod fabrication. The rod extrusions were for rolling into 0.065-in. strip for the preparation of test specimens for strength evaluation. The initial tube-blank-extrusion experiments involving one billet of each composition met with little success. When a fast extrusion rate was used, the alloys demonstrated the hot-short tendencies of Hastelloy B, with the exception of alloy T-23013, 15% Mo–3% Nb–3% W–0.5% Al–78.5% Ni. The results of this initial experiment are presented in Table 57.

Before the remaining billets of these alloys were extruded, the results obtained in the fabrication of Hastelloy W at a slow extrusion rate were sufficiently favorable to prompt an alteration in the extrusion conditions for the special compositions. Two billets, T-23012 and T-23014, were extruded slowly at 2200°F with a $\frac{3}{4}$-in.-dia mandrel at an extrusion ratio of 5.4:1. Both alloys responded satisfactorily, but the mandrel broke within the tube blank in each case. With a decreased rate of extrusion, the billet remained in contact with the mandrel for an excessive length of time, and the resultant overheating of the tool caused a subsequent decrease in its ultimate strength. The utilization of a 1-in.-dia mandrel alleviated this problem. The final results of slow extrusion of these alloys at 2200°F are presented in Table 58. Extrusions 1 through 5, shown in Fig. 156, are representative of the good tube blanks obtained from these special compositions.

The results of processing the tube blanks of the INCO compositions to 0.500-in.-OD, 0.035-in.-wall tubing by the Superior Tube Co. are tabulated in Table 56. For the most part this limited amount of data indicates that these compositions are amendable to tube-producing practice, with one exception: alloy T-23015 with 0.25% C could not be successfully tube reduced.

Requests have been made for the construction of thermal-convection loops from the various lengths

TABLE 57. NOMINAL COMPOSITIONS AND RESULTS OF PRELIMINARY ATTEMPTS TO EXTRUDE SPECIAL ALLOYS PREPARED BY THE INTERNATIONAL NICKEL COMPANY

Extrusion ratio: 5.4:1
Mandrel size: $\frac{3}{4}$-in. diameter

Alloy No.	Composition (wt %)								Extrusion Temperature (°F)	Results
	Mo	Cr	W	Nb	Al	Ti	C	Ni		
T-23011	15	5	3	3	0.5			73.5	2060	Extruded tube blank shattered
T-23012	17				0.5			82.5	2175	Extruded tube blank shattered
T-23013	15		3	3	0.5			78.5	2100	Good tube blank obtained
T-23014	15				1	1.5		82.5	2010	Press stalled
T-23015	15		3	3	0.5		0.25	78.25	2080	Tube blank cracked on the inside

TABLE 58. RESULTS OF THE FINAL EXTRUSIONS OF SPECIAL ALLOYS PREPARED BY THE INTERNATIONAL NICKEL COMPANY

Mandrel size: 1-in. diameter

Alloy No.	Extrusion Ratio	Extruded Shape	Number of Successful Extrusions
T-23011	7:1	Tube blank	2
T-23012	7:1	Tube blank	1
T-23013	7:1	Tube blank	2
T-23014	7:1	Tube blank	1
T-23015	7:1	Tube blank	2
T-23011	6.25:1	Rod	1
T-23012	6.25:1	Rod	1
T-23013	6.25:1	Rod	1
T-23014	6.25:1	Rod	1
T-23015	6.25:1	Rod	1

of tubing prepared from the four other compositions in order that these compositions can be evaluated for corrosion.

Hot rolling of the extruded rods was only moderately successful. The rolling temperature was varied between 1925 and 2100°F, and the scheduled reduction was approximately 10% per pass. In general, the lower temperature proved to be more satisfactory for minimizing edge cracking. Each alloy was hot-rolled to 0.250-in. strip, pickled, annealed at 2050°F for 1 hr, and cold-finished to 0.065-in. strip, with an intermediate anneal at 2050°F for $\frac{1}{2}$ hr. Final annealing of each alloy was scheduled to yield a grain size of ASTM 6–7. Alloy T-23015 edge-cracked severely during hot rolling. The other alloys, for which edge cracking did not interfere with the machining of sound test specimens, will be evaluated for strength.

ORNL Compositions. – The basic nickel-molybdenum alloy containing 15 to 20% molybdenum possesses corrosion resistance on a par with that of Hastelloy B, better ductility and fabricability, but poorer strength properties. Consequently, alloy additions to the basic composition are required for improving the strength properties. The elements being investigated as strengtheners are Ti, Al, W, Nb, Cr, Fe, and V. In order to determine the effect of these elements individually on corrosion resistance and in order to establish the maximum quantity of each element that can be present without adverse effect on corrosion resistance, ternary alloys have been prepared that contain 17 wt % molybdenum, the elements listed below in the amounts shown, and the balance nickel.

Element Added	Quantity Added (wt %)
Cr	3, 5, 7, 10
W	2, 4
Ti	2, 4
Nb	2, 4
Al	2, 4
Fe	4

Vacuum-induction heats of each composition were prepared in 36-lb ingots. A small amount of carbon was added to each charge to bring the resultant carbon level to 0.06%. It was possible to machine three tube-blank extrusion billets from each ingot for the fabrication of sufficient tubing to make three standard thermal-convection loops for corrosion testing.

The extrusion of tube blanks at 2150°F of the ternary alloys which are listed in Table 59 presented no unusual difficulties when a slow extrusion rate of ~1 in. of billet length per second at a ratio of 7:1 was used. One exception was the Ni–17% Mo–4% Al composition, which offered relatively high resistance to plastic deformation.

The yield of tubing from the redrawn tube blanks has been satisfactory, although no sound product was received from the 4% Al or 4% Ti alloys. A summary of these results is also shown in Table 59. Another attempt will be made to fabricate

TABLE 59. RESULTS OF REDRAWING ORNL ALLOYS TO 0.500-in.-OD, 0.035-in.-WALL TUBING

Alloy No.	Nominal Composition (wt %)	Extruded Tube Blanks	Total Length of Tubing Received		Yield* (%)	Number of Loops Requested	Remarks
			Feet	Inches			
30-1	Ni–17 Mo–3 Cr–0.06 C	3	30	10	76	2	
37A-1	Ni–20 Mo–3 Cr–0.02 C	1	8	2	69	1	
30-2	Ni–17 Mo–5 Cr–0.06 C	3	36	3	81	3	
43A-3	Ni–20 Mo–7 Cr–0.02 C	1	8	4	73	1	
30-6	Ni–17 Mo–7 Cr–0.06 C	2	23	7		2	
30-4	Ni–17 Mo–10 Cr–0.06 C	2	21	6	81	2	
30-7	Ni–17 Mo–2 Al–0.06 C	3	34	2		3	
30-17	Ni–17 Mo–4 Al–0.06 C	2	0	0	0	0	Both tube blanks split
30-8	Ni–17 Mo–2 Ti–0.06 C	3	31	5		3	
30-18	Ni–17 Mo–4 Ti–0.06 C	3	28	2	0	0	Tubing cracked
30-9	Ni–17 Mo–2 W–0.06 C	3	31	7		3	
30-19	Ni–17 Mo–4 W–0.06 C	3	34	1		3	
30-10	Ni–17 Mo–2 V–0.06 C	3	33	4		3	
30-20	Ni–17 Mo–4 V–0.06 C	3	32	7		3	
30-11	Ni–17 Mo–4 Fe–0.06 C	3	29	9		3	
30-12	Ni–17 Mo–3 Nb–0.06 C	3	31	4		3	
30-21	Ni–17 Mo–5 Cb–0.06	3					Processing incomplete
30-13	Ni–16 Mo–1.5 Ti–1 Al–0.06 C (INOR-3)	3	35	10		3	
30-14	Ni–16 Mo–1.5 Ti–2 Al–0.06 C (INOR-4)	3	33	10		3	
30-15	Ni–15 Mo–2 Nb–2 W–0.06 C (INOR-5)	2					Processing incomplete
30-16	Ni–16 Mo–5 Cr–1.5 Ti–1 Al–0.06 C (INOR-6)	3	32	0		3	

*Per cent yield after conditioning of tube blanks.

tubing from an ingot of Ni–17% Mo–4% Al which has been received from the Superior Tube Co.

Tubes 7 and 8 of Fig. 156 are representative of the extruded tube blanks of the ternary alloys. These particular samples are alloys bearing chromium, which is a desirable addition for imparting oxidation resistance to the base composition. Previous tests of chromium-bearing nickel-molybdenum alloys in fuel mixture No. 30 indicated that chromium additions in excess of 5% decreased corrosion resistance; however, at least 7% chromium is required to make the alloy resistant to oxidation.

In addition to the ternary alloys, 36-lb vacuum-induction melts of the INOR-3, -4, -5, and -6 compositions were prepared and extruded into tube blanks. These alloys have the same compositions as the production-size heats prepared by the International Nickel Company.

In all extrusion experiments carried out to date, difficulty was encountered occasionally with billets that failed to extrude to completion. This trouble was attributed to excessive chilling of the billets by the cold ram at the slow extrusion rates being used. Therefore, a new billet was designed that has mild-steel nose and tail plates tack welded to it. It was expected that the plates would allow the billet to start through the die more easily, as well as to transfer the chilling action by the ram to a more easily extruded material. The mild steel is cropped from the tube blank after extrusion. Steel washed back on the outside surface of the tube is machined off before the tube blank is reduced to tubing.

Improved lubrication of the billet was obtained by coating the container of the press, as well as the mandrel, with Necrolene grease prior to each extrusion. Low-melting Fiberglas mats are also placed around the hot billets as they are introduced into the extrusion press. This lubrication practice has resulted in lowering the pressure required for the extrusion of these materials.

Production of Commercial-Size Heats of Special Alloys by International Nickel Company

In order to gain production experience with special nickel-molybdenum-base alloys, the International Nickel Company has prepared 4800-lb heats of six alloys which, according to experience at INCO, should possess elevated temperature strength superior to that of Inconel. The status of these alloys is indicated in Table 60. Material from each composition has been submitted to New England Materials Laboratory and Rensselaer Polytechnic Institute for stress-rupture testing and weldability studies, respectively. It has been requested that the material of each composition remaining for processing be fabricated into seamless tubing, plate, sheet, wire, and rod for carrying out a complete evaluation program on each alloy. One composition, heat Y-8198, was not forged successfully during initial ingot breakdown, and, as a result, the material that remains is only sufficient for fabricating a small amount of plate and sheet product.

Consumable-Arc-Melting Experiment

As indicated previously,[1] arrangements were made with Battelle Memorial Institute for the preparation of arc-melted ingots of nickel, Hastelloy B, Hastelloy W, a 76% Ni–17% Mo–7% Cr alloy, and an 83% Ni–17% Mo alloy. The melts were to be made by the consumable-electrode process so as to take advantage of the high arc temperatures for vaporizing "tramp" elements in an effort to improve the strength and fabricability of these alloys. Electrodes of the first three alloys were supplied to Battelle in the form of extruded rods. The special nickel-molybdenum alloys were prepared by vacuum melting, and the electrodes were fabricated by threading together extruded rods of the material.

The electrodes have been melted and returned to ORNL for evaluation. Suitable test specimens will be fabricated from the ingots in order to determine whether arc melting is instrumental in improving the properties of these alloys.

OXIDATION OF HASTELLOY B

H. Inouye J. E. Spruiell

It was reported previously[2] that oxidation of Hastelloy B in air at 1500°F was not excessive. When the alloy was thermally cycled from 1500°F to below about 660°F, however, the rate was increased by an order of magnitude as a result of spalling of the protective $NiMoO_4$ scale from the

[1] T. K. Roche and H. Inouye, *Met. Semiann. Prog. Rep. April 10, 1956*, ORNL-2080, p 124, esp 125.

[2] H. Inouye, and J. H. Coobs, *ANP Quar. Prog. Rep. Dec. 10, 1954*, ORNL-1816, p 103.

TABLE 60. STATUS OF 4800-lb HEATS OF INCO ALLOYS

Chemical Analyses

Heat No.	Amount (%)												
	Ni	Mo	Cr	Al	Ti	W	Cb + Ta	C	Mn	Fe	S	Si	Cu
Y-8195	78.44	20.29						0.01	0.47	0.28	0.002	0.47	0.02
Y-8197	76.72	16.17	5.28					0.04	0.54	0.69	0.002	0.52	0.02
Y-8196	79.86	16.11		1.08	1.62			0.01	0.53	0.18	0.001	0.57	0.02
Y-8198	77.83	16.97		1.96	1.68			0.01	0.49	0.49	0.001	0.53	0.02
Y-8200	78.59	13.15	5.30			2.69	2.15	0.10	0.94	1.66	0.002	0.68	0.02
Y-8199	74.01	16.01	5.30	1.15	1.69			0.02	0.57	0.59	0.003	0.62	0.02

Heat No.	Total Weight (lb)	Material Processed				Scrap Weight (lb)	Material Sent to:					
							New England Materials Laboratory			Rensselaer Polytechnic Institute		
		Cross Section (in.)	Length Feet	Length Inches	Weight (lb)		Diameter (in.)	Length (ft)	Weight (lb)	Diameter (in.)	Length (ft)	Weight (lb)
Y-8195 (INOR-1)	4720	4 × 6	15	2	1404	2495	½	26	21	½	13	10
		8¾ (dia)		20	390							
		8¾ (dia)		10	400[a]							
Y-8197 (INOR-2)	4614	3 × 3	3		106	2585	½	44	36	7/16	20	12
		3 × 3	28		890							
		8¾ (dia)		31	585[c]							
		8¾ (dia)		10	400[a]							
Y-8196 (INOR-3)	4621	4 × 5	16		1152	3095	½	49	40	½	26	21
		3 × 3	3		113							
		8¾ (dia)		10	200[b]							
Y-8198 (INOR-4)	4370	3 × 3	3		113[c]	4195[d]	½	51½	41	½	26	20
Y-8200 (INOR-5)	4469	3 × 3	3		102	2250	½	54½	41	7/16	26	16
		3 × 3	36		1175							
		8¾ (dia)		25	485							
		8¾ (dia)		10	400[a]							
Y-8199 (INOR-6)	4557	3 × 3	34		1095	2665	½	23½	18	½	11	9
		8¾ (dia)		30	570							
		8¾ (dia)		10	200[b]							

[a] Extrusion billets – two pieces.
[b] Extrusion billet – one piece.
[c] Billet split on one end.
[d] Billets split on forging.

metal surface. This spalling is caused by a phase transformation in the $NiMoO_4$ layer at about 660°F.

The oxidation of Hastelloy B in static air has now been investigated at 1200, 1400, 1600, and 1800°F. Data were obtained for mechanically polished specimens exposed to air at the various temperatures for 168 hr. The increases in the specimen weights were determined at frequent intervals in order to obtain oxidation-rate curves. The total increases in weight of the specimens during the tests at the various temperatures are shown in Table 61. The curves of weight gain vs time were parabolic at all test temperatures, and, thus, the oxide scale appears to be protective.

The oxidation rate of the alloy at 1200°F is very low, and the superficial scale which forms does not spall upon cooling. Preliminary x-ray data show that this scale is principally NiO.

Thus far in these studies of the oxidation characteristics of nickel-molybdenum alloys, evidence has been found that the formation of $NiMoO_4$ depends upon the molybdenum content. However, its formation may also be a function of temperature, as indicated in the tests described above.

SHIELD PLUG FOR ART PUMP

J. P. Page J. H. Coobs

It was previously proposed that the shield plugs surrounding the pump-impeller shafts on the ART incorporate three separate shielding materials, including a thin disk of neutron-shielding material, a disk of zirconia for thermal shielding, and a high-density, low-conductivity cylinder for gamma shielding. Since no standard materials would fulfill the desired properties, several ZrO_2 bodies were prepared and their thermal conductivity was determined, and a suitable gamma-shielding material was developed which consisted of a mixture of tungsten carbide and Hastelloy C powders hot pressed to a density of 12.0 g/cm^3.

A preliminary report entitled "Shield Plug for ART Impeller Pumps" has been published as ORNL CF-56-8-40, which gives a fairly complete account of the development work involved.

NEUTRON SHIELD MATERIALS FOR HIGH-TEMPERATURE USE

M. R. D'Amore J. H. Coobs

Neutron Shield for the ART

The neutron shield for the ART incorporates a double layer of boron-containing materials which have a total boron density of at least 1.2 g/cm^3. A Cu-B_4C layer 0.100 in. thick is used nearest the neutron source to minimize radiation damage to the second layer, which consists of B_4C tiles 0.265 in. thick.

Clad Cu-B_4C. – The Allegheny Ludlum Steel Corp. is being considered as a potential supplier of the Cu-B_4C (6.6% B_4C) shield material. This material is roll-clad with type 430 stainless steel and has a total thickness of 0.100 in.

A plate approximately $7\frac{3}{4} \times 23 \times 0.100$ in., fabricated by Allegheny Ludlum, was evaluated. The evaluation included surface finish, radiography, bend tests, tensile tests, thickness uniformity, core density measurements, microstructures, and clad-core bonding. No pinholes were evident in the 10-mil-thick cladding stripped from the core material, although the surface finish on the cladding was rough. No segregation of the B_4C or cracking of the core was observed, and the clad was well bonded to the core material. The density of the Cu-B_4C cermet, measured by the water displacement method, was 97.9% of theoretical. Small specimens that had been cut parallel and transverse to the rolling direction were bent to

TABLE 61. RESULTS OF OXIDATION TESTS OF HASTELLOY B EXPOSED TO STATIC AIR FOR 168 hr

Number of Tests	Test Temperature (°F)	Average Total Weight Gain* (g/cm^2)	Remarks
4	1200	0.00031	Oxide did not spall on cooling
3	1400	0.00095	Oxide spalled on cooling
3	1600	0.0025	Oxide spalled on cooling
2	1800	0.0095	Oxide spalled on cooling

*Weight gain of Inconel in 168 hr at 1500°F = 0.00004 g/cm^2.

a radius of curvature of $^{9}/_{16}$ and $^{27}/_{32}$ in., respectively, before fracture occurred. The plate tapered along the length from a maximum thickness of 0.099 in. to a minimum thickness of 0.092 in. The dispersion of B_4C particles in the copper matrix was excellent. The room-temperature tensile strength for the material is tabulated in Table 62.

The tensile specimens were punched out with a blanking die and were 5 in. long, with a 2-in. gage length. The as-punched tensile specimen showed no elongation and failed at the yield point of the material. Specimen 4 was prepared by stripping the clad from the Cu-B_4C core prior to punching the specimen.

B_4C Tiles. – Sample tiles of B_4C-base material submitted by the Norton Company and The Carborundum Company were evaluated for possible use in the outer layer of the neutron shield. These tiles will be held in place in the shield by use of metal cans, to eliminate possible shifting of fragments resulting from radiation damage.

Two sets of four sample tiles each were received from The Carborundum Company. The tiles were bonded with silicon and fabricated by a casting and sintering process. Radiographs of the first set of four tiles revealed large voids. The macroporosity was eliminated in the second set of tiles by a revision in the manufacturing process. The boron density of the eight tiles as determined by chemical analysis varied between 0.889 and 1.15 g/cm^3. The minimum boron density of 1.26 g of boron per cubic centimeter specified for the ART tiles appears difficult to achieve in a cast and sintered B_4C-SiC tile.

The Norton Company submitted tiles of both technical-grade and high-purity B_4C, hot-pressed to densities of 1.9 to 2.34 g/cm^3. A high-purity B_4C tile with a density of 2.0 g/cm^3 was found by analysis to contain 1.48 g of boron per cubic centimeter. No voids or foreign particles were detected in any of the hot-pressed tiles.

Representative specimens cut from sample tiles submitted by each company were irradiated in the LITR for a six-week period. A cursory examination of the irradiated specimens indicates that the two materials have equivalent resistance to radiation damage at exposures of less than 3% burnup of B^{10} atoms. No volume change or cracking of the specimens was observed, nor was any gas evolution detected during irradiation of either material.

Since the hot-pressed tiles are preferable because of their higher boron density, and no other significant difference in properties is evident, the contract for production of the tile bodies was awarded to the Norton Company.

Boride Dispersions in a Metallic Matrix

Dispersions of BN and CaB_6 particles in iron and nickel were investigated as possible substitutes for Cu-B_4C. Compacts containing 21 vol % CaB_6 dispersed in iron and those containing 30 vol % BN dispersed in nickel were successfully fabricated by roll cladding of pressed and sintered powder cores. The plates were sectioned and the CaB_6-Fe and BN-Ni cores were examined for evidence of reaction by x-ray diffraction techniques. A reaction had occurred in the CaB_6-Fe

TABLE 62. ROOM-TEMPERATURE STRENGTH OF TYPE 430 STAINLESS-STEEL-CLAD Cu-B_4C

Specimen Number	Orientation	Condition	Yield Strength (psi), 0.2% Offset	Tensile Strength (psi)	Elongation (% in 2 in.)
1	Transverse to rolling direction	As punched	24,500	24,500	0.0
2	Transverse to rolling direction	Annealed 20 min at 1650°F	20,000	31,200	5.6
3	Parallel to rolling direction	Annealed 20 min at 1650°F	19,900	34,000	7.5
4	Core material unclad; transverse to rolling direction	Annealed 20 min at 1650°F	15,100	21,400	3.5

material during the fabrication process, resulting in formation of Fe_2B. No reaction was detected between BN and nickel, confirming the compatibility test results for this material reported in ORNL-2012.[3] Clad specimens of both materials have been prepared for irradiation testing in the LITR.

Combinations of CaB_6-Ni and BN-Fe were also investigated; CaB_6-Ni compacts formed a liquid phase at 1800°F during sintering. No reaction was observed between BN and iron. However, difficulties in fabrication were experienced, and work on BN-Fe was discontinued in favor of the BN-Ni compositions. The BN-Ni cermet appears attractive as a high-temperature shield material, since it is easily fabricated and the components are compatible at 2000°F for long periods.

Boron Steels

The study of boron steels for use in a compression ring between the beryllium reflector and support strut ring was continued.

The tensile strength at 1300°F of an as-cast alloy containing 0.75% B was 14,775 psi with no elongation. Billets of the alloy were extruded into rod at 1900°F, using an extrusion ratio of 6.5:1 with no difficulty. Tensile specimens will be machined from the wrought material to determine the effect of hot working on the mechanical properties of the alloy.

The compatibility of 1 and 3% B-Fe alloys and Inconel was determined at 1300°F. Diffusion couples were prepared by hot rolling composites of the two materials at 1900°F. Metallographic observation of the Inconel and B-Fe alloy interface revealed that no diffusion of boron into the Inconel had occurred during the hot-rolling operation. Examination of diffusion couples after 500 hr at 1300°F showed that layers 1 to 1.5 mils thick in the 1% B–Fe alloy and 0.5 mil thick in the 3% B–Fe alloy were depleted in boron, indicating that diffusion of boron from the boron steels is not serious at this temperature.

Radiation-damage specimens were fabricated from a boron–stainless steel alloy for testing in the LITR and MTR. The composition of the alloy is basically type 304 stainless steel, with the nickel content increased to about 14% and a boron addition of 1.07%. The boron addition to the melt contained 84.6% B^{10} and 15.4% B^{11}. The specimens will be irradiated both unstressed and stressed at 500 psi, at temperatures from 1300 to 1700°F in the LITR, and at 1600°F in the MTR.

Recent work[4] by other investigators has revealed low ductility in boron-containing stainless steels after irradiation. In view of these results the feasibility of using a duplex ring composed of Inconel and clad Cu-B_4C was investigated. However, the compressive creep strength of the Cu-B_4C was insufficient for the required load. Present plans are to build up the ring with a number of canned B_4C tiles.

Miscellaneous Investigations

The electrophoretic deposition of uniform copper coatings on B_4C tiles was investigated by The Vitro Mfg. Co. This method of coating was proposed as an alternate means of preventing diffusion of boron from the tiles and for confining fragments of tiles produced by radiation damage.

It was found that, by proper control of several variables, uniform, adherent copper coatings about 5 mils thick could be produced on full-sized tiles by deposition of cuprous oxide, followed by sintering in a mixture of argon and hydrogen. A final report on this investigation, entitled "Boron Containing Coatings," No.-V-2059-2-0, was recently published by Vitro.

CREW-COMPARTMENT SHIELDING

R. E. McDonald
Pratt & Whitney Aircraft

Work was continued on protective coatings and claddings for the 20% Li–80% Mg alloy proposed for crew-compartment shielding. A technique was developed which produces a bright surface, using a two-step treatment with concentrated phosphoric acid and acetone. The surface produced tarnished slightly when exposed to air but is stable at 300°C and for long periods at lower temperatures. Using specimens with surfaces prepared by this method, roll cladding with 2S aluminum and AZ31 magnesium alloy was investigated. The 2S clad material produced a brittle bond, while the AZ31 alloy failed to bond, even to itself.

[3] H. Inouye and M. R. D'Amore, *ANP Quar. Prog. Rep. Dec. 10, 1955*, ORNL-2012, p 162.

[4] J. J. Lombardo, *Tensile and Impact Test Results on Irradiated Boron-Stainless Steel*, WAPD-SFR-FF-192 (June 28, 1955).

In order to further evaluate the mechanical properties of the 20% Li–80% Mg alloy, more sheet specimens were prepared. A 0.250-in.-thick sheet was mechanically cleaned of mill scale and corrosion products, was given the phosphoric acid–acetone treatment, and was hot-rolled at 250°C to a thickness of 0.070 in. New specimens were machined from this sheet and kept under mineral oil until tested. Tensile and stress-rupture data on new and old batches are presented in Table 63 for comparison. It is evident that the cleaned and coated material from the new batch has considerable more ductility and longer rupture life than the original material.

Fixtures are being designed to test the alloy at constant temperature, in a protective medium, without the film produced by the phosphoric acid–acetone treatment.

Powder metallurgy techniques were investigated as a different approach to the shielding-material problem, using dispersions of lithium compounds in aluminum. Lithium oxide was chosen as the lithium source, being the most stable of the lithium compounds and possessing the highest melting point. A mixture of 50-50 vol % Li_2O-Al powder was cold-pressed and hot-rolled in a 2S aluminum picture frame. Composite sheet produced by this method shows a continuous aluminum matrix, even distribution of the lithium oxide, and good bonding. This volume per cent results in 20 wt % Li in the core and a lithium density of 0.452 g/cm^3, as compared with a lithium density of 0.288 g/cm^3 in the 20% Li–80% Mg alloy. Ratios of clad to core of 1:2, 1:4, 1:6, and 1:8 were fabricated successfully.

On the basis of the success of the Li_2O-Al composite sheet, Li_2O-Mg was investigated. This combination would produce lighter sheet and a higher per cent lithium for a given volume per cent. The picture frame was made from AZ31, because M-1 alloy was not available. No solid-phase bonding with AZ31 could be obtained. The Li_2O-Mg compact and AZ31 interface was brittle, and the finished sheet was cracked throughout.

Possible techniques for roll cladding the 20% Li–80% Mg alloy were investigated further. As reported earlier, aluminum forms a brittle intermetallic compound with the alloy, and thus aluminum-clad sheets have no ductility. In an effort to overcome this difficulty, nickel foil was used as a diffusion barrier, and some bonding resulted. Further work with nickel and other barrier materials is contemplated.

TABLE 63. TENSILE AND STRESS-RUPTURE DATA FOR 20% Li–80% Mg ALLOY

Specimen	Temperature	Elongation (%)	Average Tensile Strength* (psi)	Average Yield Strength (psi)
Old batch	Room	35	12,500	11,230
New batch	Room	48	12,775	10,650
Old batch	200°F	45	3,000	2,970
New batch	200°F	94	3,200	2,940

Specimen	Coating	Rupture Data*	
		Elongation (%)	Rupture Life (hr)
Old batch	None	48	125
	Grease	90	315
	HNO_3 dip and grease	100	220
New batch	Phosphoric acid–acetone and grease	32	1050
	Grease	35	566

*All tests at room temperature and 3000 psi.

TUBULAR CONTROL RODS

M. R. D'Amore

The feasibility study on extrusion of undersized control rods was continued. A simulated control-rod billet consisting of a type 316 stainless steel can with a core composed of 34 vol % Al_2O_3 (to simulate Lindsay oxide) in nickel powder was extruded at 2150°F to a 1½-in.-OD × ¾-in.-ID tube. The billet was designed to determine the feasibility of (1) extruding thin (~0.050-in.-thick) inner and outer cladding on control-rod cores and (2) preparing cores by tamping the loose powder mixture into the billet cans.

Evaluation of the extruded tube showed that the cladding thickness was satisfactory. However, tamping of the loose powder does not appear promising as a core preparation method. Transverse sections of the extruded tube revealed the core cross section to be fairly uniform except in one area. This nonuniform area can be attributed to the sintering and concomitant shrinkage of the core during the preheat operation, which can result in the following effects:

1. A longitudinal crack can develop in the core due to shrinkage around the inner clad layer.
2. A void area can form between the core and the outer clad which causes buckling of this layer during extrusion.

Either effect will result in a nonuniform core in the extruded tube.

A Hastelloy X billet containing a hot-pressed core of 30 wt % Lindsay oxide (balance nickel) has been prepared for extrusion.

Tensile specimens are being machined from plates of 30 wt % Lindsay oxide (balance nickel) cermet clad with Inconel, which were fabricated by hot rolling with the picture-frame technique. The specimens will be used to investigate the effect of the Lindsay oxide particle size on the elevated-temperature tensile strength of the cermet. The oxide particle sizes being investigated are in the following ranges: 1 to 3, 1 to 200, and 52 to 200 μ.

The thermal conductivity of a 30 wt % Lindsay oxide (balance nickel) specimen was measured between 165 and 554°C, and the results are shown in graph form in Fig. 159. The slopes and intercepts of the two lines were calculated from test results, using the least-squares method.

SEAMLESS TUBULAR FUEL ELEMENTS

M. R. D'Amore

Two three-ply tube blanks containing cores of 30 vol % Al_2O_3 (to simulate UO_2) dispersed in type 302-B stainless steel were redrawn from 1.0-in. OD × 0.125-in. wall to 0.187-in. OD × 0.015-in. wall at the Superior Tube Co. The inner and outer layers of the three-ply composites were type 316 stainless steel. The finished tubing was

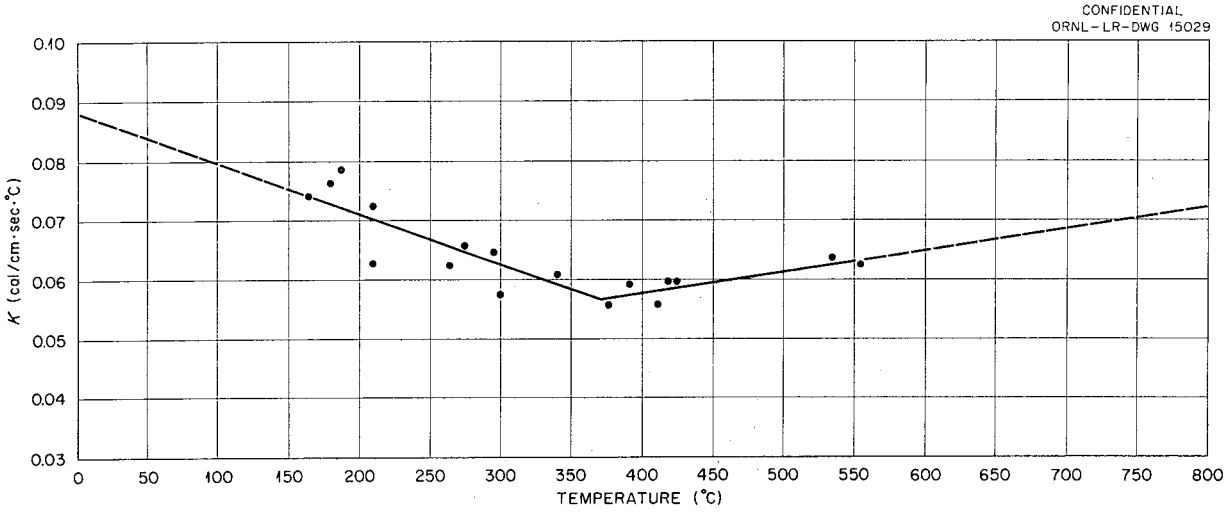

Fig. 159. Thermal Conductivity of 70% Nickel–30% Lindsay Oxide Specimen.

received and has been evaluated, along with samples taken at various stages in the reduction schedule.

The first extruded tube, for which the core was prepared by hot pressing a mixture of −325 mesh Al_2O_3 and stainless steel powder, exhibited tensile fractures in the core after 30% total reduction. The finished tubing had severe fractures in the core.

The second extruded tube blank was prepared by tamping the powder mixture into the billet can, using −105 +325 mesh Al_2O_3 in type 302-B stainless steel. Examination of the redrawn tubing did not reveal any tensile fractures in the core. However, the relatively large particles of Al_2O_3 were fractured and tended to form stringers, finally resulting in longitudinal cracking of the core as the total reductions increased. Radiographs of the finished tubing revealed the core fractures in tube No. 1 but did not show the longitudinal cracks in the core of tube No. 2.

An evaluation report on the redraw properties and structure of this tubing is being forwarded by Superior Tube Co. The results will be correlated with our examination.

It is evident from the evaluation of the redrawn tubing that the core containing the larger Al_2O_3 particles was stronger than the core with the fine Al_2O_3 particle dispersion. Tamping of a loose powder mixture into a billet can appears to be a satisfactory method for preparing cores of 30 vol % Al_2O_3 dispersed in 70 vol % of type 302-B stainless steel.

The study of flow patterns in three-ply extruded tubes containing cermet cores was continued, with the extrusion of two three-ply billets to 1¼-in.-OD × ¾-in.-ID tubes at 2150°F. The billet can material was type 316 stainless steel, and the cores were fabricated by hot pressing a powder mixture of type 304 stainless steel and 30 vol % Al_2O_3. A 29-deg taper was machined into the ends of the core of one billet in an effort to eliminate core end defects in the extruded tube and thus improve material recovery. This taper resulted in a slight reduction in the length of the defect.

The second billet contained a core made in three sections to determine whether nonuniform areas will appear at the interface between core sections. The extruded tube is being sectioned for examination.

The Allegheny Ludlum Steel Corp. has extruded two 5⅜-in.-dia × 12-in.-long three-ply billets containing cores of Al_2O_3 in stainless steel. The cores and billet can were fractured severely during extrusion. A third billet was prepared with cermet cores sintered at a higher temperature and was carefully welded to avoid cracking or leaks. Extrusion of this billet was quite successful. Sections are being redrawn, and a full evaluation will be reported later.

NIOBIUM

H. Inouye V. M. Kolba
J. P. Page

Evaluation of Arc-melted Niobium

Evaluation of arc-melted niobium has been initiated. The object of this investigation will be to compare physical and mechanical properties of this material with niobium prepared by conventional powder-metallurgy techniques.

Macroetching of a section of an arc-cast and cold-worked ingot has revealed the large-grained, severely distorted structure typical of such a fabrication history. An attempt to cold roll a section of the as-received ½-in. plate was terminated after two 3% passes, when some end cracking was noticed.

The cracked ends were cut off, and the remaining material was annealed 1 hr at 1100°C at a vacuum of 2×10^{-5} mm Hg. This 0.458-in.-thick section was then successfully cold rolled to a 10-mil strip, a reduction in thickness of about 98%. The hardness jumped from 160 VHN (2.5-kg load) to 190 VHN in the first few passes, then climbed very slowly to 206 at 98% reduction in thickness. Samples were taken at several stages in the reduction, split into thirds, and annealed for ½ hr at 850, 1050, and 1150°C in high vacuum. These will be examined metallographically to determine the amount of reduction necessary to produce fine-grained material after annealing.

Nb-UO_2

Two batches of niobium powder made from wrought sheet were analyzed and were found to be somewhat contaminated. These powders were prepared by the hydriding of cold-rolled sheet, followed by crushing, leaching, and finally vacuum

annealing to remove hydrogen. The analytical results are presented in Table 64.

The Nb-3-C batch was chosen to make five Nb–30 wt % UO_2 compacts for sintering and reaction studies. The UO_2 used had previously been hi-fired in a hydrogen atmosphere. The compacts were 82% dense as compacted and had good green strength. These compacts are being sent to GE-ANPD for sintering at 2000°C.

Attempts to secure high-purity powder from commercial sources have been unsuccessful.

TABLE 64. ANALYSIS OF NIOBIUM POWDER

Sample	Amount (%)				VHN
	C	O_2	N_2	H_2	
Nb-2-C	0.042	0.29	0.018	8.2×10^{-4}	292
Nb-3-C	0.103	0.18	0.019	5.8×10^{-4}	179

Nb-U Alloy

A finger melt of an alloy of 80% Nb–20% U was made. Segregation in the initial casting was noted but was reduced by subsequent remelting. The hardness of the as-cast sample was R_B 86. Attempts to cold roll the as-cast material proved unsuccessful. A sample of the alloy was encapsulated and hot rolled successfully at 1050°C to a reduction of 85%. Metallographic examination of the hot-rolled structure revealed that the as-cast structure had not been broken up during the rolling process. The as-rolled hardness was R_B 95.

At present, vacuum-annealing tests are being conducted on the hot-rolled alloy at 1100, 1200, and 1300°C to determine the recrystallization temperature of the alloy, after which further rolling studies will be made.

FABRICATION OF HYDRIDES

R. E. McDonald

A survey of available literature on the fabrication of hydrides has been completed, and the hydriding furnace and purification system being built by the Ceramics Group are nearly ready. Yttrium and zirconium and their alloys will be hydrided and fabricated, and the compatibility of various barrier materials will be studied.

HIGH-TEMPERATURE REACTIONS OF METALS AND CERAMICS

G. P. Smith

HIGH-TEMPERATURE SPECTROPHOTOMETRY

C. R. Boston

Absorption spectra of liquids at ordinary temperatures have been used for several decades to measure the kinetics of reactions in solution. In recent years significant advances have been made in the interpretation of ultraviolet and visible absorption spectra of ions in solution in terms of electron energy states,[1] so that it appears hopeful that such spectral data will prove useful in answering basic questions about chemical bonding in complex ions in solution.

In order to extend measurements of absorption spectra to fused salt solutions, a high-resolution, recording spectrophotometer has been constructed in which the samples can be heated to 800°C under carefully controlled conditions. With this instrument high accuracy is obtained up to optical densities of 3.5 over the spectral range of 200 to 800 mμ at temperatures below 600°C. At higher temperatures the accuracy is somewhat less because of the background of thermal radiation. This defect can be eliminated in the short-wavelength region if it becomes necessary.

Preliminary measurements of absorption spectra have been made for molten silver bromide in the wavelength range 600–800 mμ and for silver bromide–rubidium bromide mixtures in the wavelength range 450–800 mμ. Three runs were made on pure silver bromide by sealing off under vacuum a quartz optical cell containing the previously dehydrated salt. Light paths through solution were varied by means of solid quartz spacers. The spectra were very reproducible over periods of 2 to 3 hr at 500–600°C and after various temperature cycles.

The very important absorption bands in the ultraviolet region (200 to 400 mμ) were not measured because their optical density exceeded 3.5 with the shortest path lengths used (0.1 mm). Interpretation of the spectra will have to be postponed until, by using still shorter path lengths, the ultraviolet absorption bands have been measured.

[1] See, for example, S. A. Shchukarev and O. A. Lobaneva, *Doklady Akad. Nauk S.S.S.R.* 105, 741 (1955); R. Lacroix, *Arch. sci. (Geneva)* 8, 317–321 (1955).

HIGH-TEMPERATURE NUCLEAR MAGNETIC RESONANCE MEASUREMENTS

J. J. McBride

A preliminary investigation into the use of nuclear magnetic resonance techniques as a means of elucidating some aspects of structure in fused salts has been started. The work has had the continuing invaluable assistance of R. Livingston of the Chemistry Division, whose magnet and associated electronic circuitry will be used in the tests.

The work to date has consisted principally in developing a furnace, RF coil, and sample holder assembly which is electrostatically and electromagnetically shielded and thermally insulated, but still small enough to fit in a 1½-in. magnet gap. Construction of a workable assembly, beset with many problems, is now close to completion. When the assembly is completed, nuclear magnetic resonance measurements will be made on fused sodium hydroxide near its melting point. It is hoped that both a sodium and a proton resonance can be observed.

FILM FORMATION ON METALS

J. V. Cathcart

The investigation of the oxidation characteristics of the alkali metals has been continued with a series of oxidation-rate determinations for potassium at −50 and −20°C. As in previous experiments, the potassium specimens were in the form of thin evaporated films, and the rate measurements were made manometrically. The details of the experimental procedure have already been reported.[2]

Figure 160 shows an oxidation curve for potassium at −50°C. This result must be checked further, but it appears that potassium forms a highly protective oxide at this temperature. (The term "protective oxide" refers to an oxide formed under conditions where the oxidation rate is a continually decreasing function of time.) At

[2] J. V. Cathcart, L. L. Hall, and G. P. Smith, *The Oxidation Characteristics of the Alkali Metals I. The Oxidation Rate of Sodium Between −79 and 48°C*, ORNL-2054 (May 22, 1956).

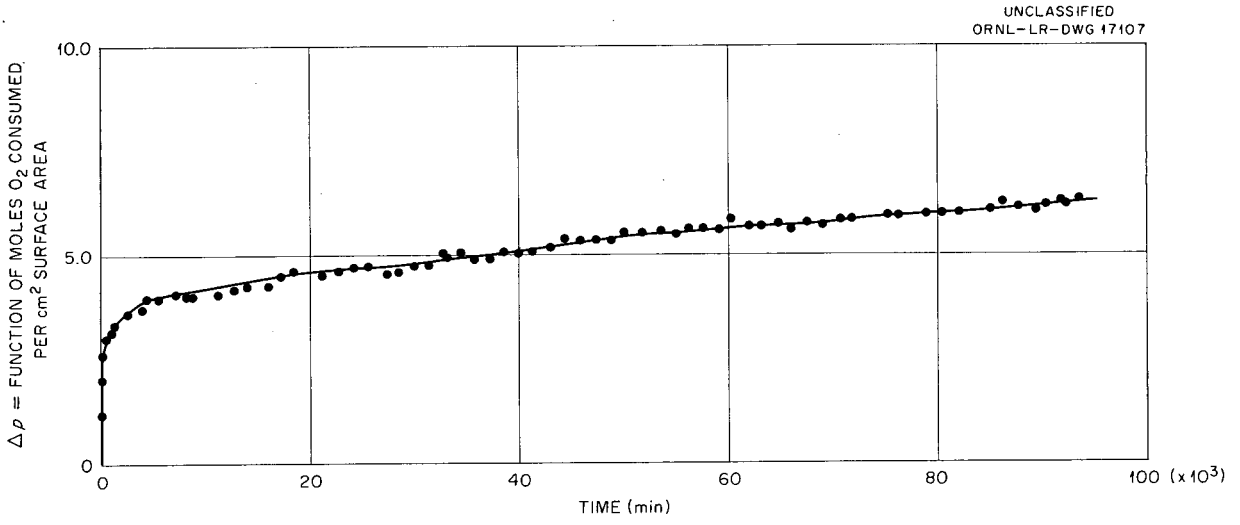

Fig. 160. Oxidation of Potassium at –50°C, Showing Protective Film Formation.

–20°C (see Fig. 161) a large increase was observed in the average oxidation rate as compared with that measured at –50°C. As may be seen in Fig. 161, the oxidation rate, initially very large, decreased sharply after a few minutes of oxidation, but after about 200 min began increasing again. Thus at –20°C the oxide formed on potassium gradually transformed from a protective to a nonprotective film.

The pattern of oxidation behavior exhibited by potassium conforms with that already established for sodium and rubidium.[3] Contrary to generally accepted theoretical predictions, none of these metals obey a linear oxidation rate equation. All three metals appear to undergo protective oxidation at sufficiently low temperatures, but at some higher temperature they form oxides which, although initially protective, become nonprotective as the oxidation proceeds. This transition occurs at a temperature between –50 and –20°C for potassium, while for sodium, which is less reactive toward oxygen than potassium, the transition was observed in the neighborhood of 48°C. Rubidium is considerably more reactive than either potassium or sodium and does not form a completely protective oxide even at –79°C (the lowest temperature investigated); however, a comparison of the results obtained at –79 and –50°C suggests that at a temperature slightly below –79°C protective oxidation also occurs for rubidium.

[3]J. V. Cathcart, *Met. Semiann. Prog. Rep. April 10, 1956*, ORNL-2080, p 137.

No satisfactory explanation has yet been obtained for the observed oxidation characteristics of the alkali metals, and to this end investigations of the composition and microscopic texture of the oxide films formed on these metals are being undertaken.

REACTIONS BETWEEN ALLOYS AND SODIUM HYDROXIDE MELTS[4]

G. P. Smith M. E. Steidlitz

Studies have been made of reactions between alloys and fused sodium hydroxide in which rate processes in the solid alloy played a prominent role in the reaction mechanism. The alloys studied were composed of nickel, which is relatively inert toward sodium hydroxide melts, and one or two of the reactive metals iron, molybdenum, and chromium. The reactions all consisted of the selective leaching of the reactive constituents, but the details of mechanism differed for different kinds of alloys. These studies are described in a series of reports[5] which are abstracted below.

[4]In cooperation with E. E. Hoffman of the Corrosion Group.

[5]G. P. Smith, M. E. Steidlitz, and E. E. Hoffman, *Two-Phase Corrosion Products Formed in the Reaction Between Fused Sodium Hydroxide and Inconel*, ORNL-2129 (to be published); G. P. Smith and E. E. Hoffman, *The Action of Sodium Hydroxide Melts on Alloys of Nickel, Molybdenum and Iron at 815°C*, ORNL-2131 (Oct. 23, 1956); and G. P. Smith and E. E. Hoffman, *Microstructures of Corrosion Products Formed in the Reaction Between Fused Sodium Hydroxide and Iron-Rich Alloys of Iron, Chromium and Nickel*, ORNL-2156 (to be published).

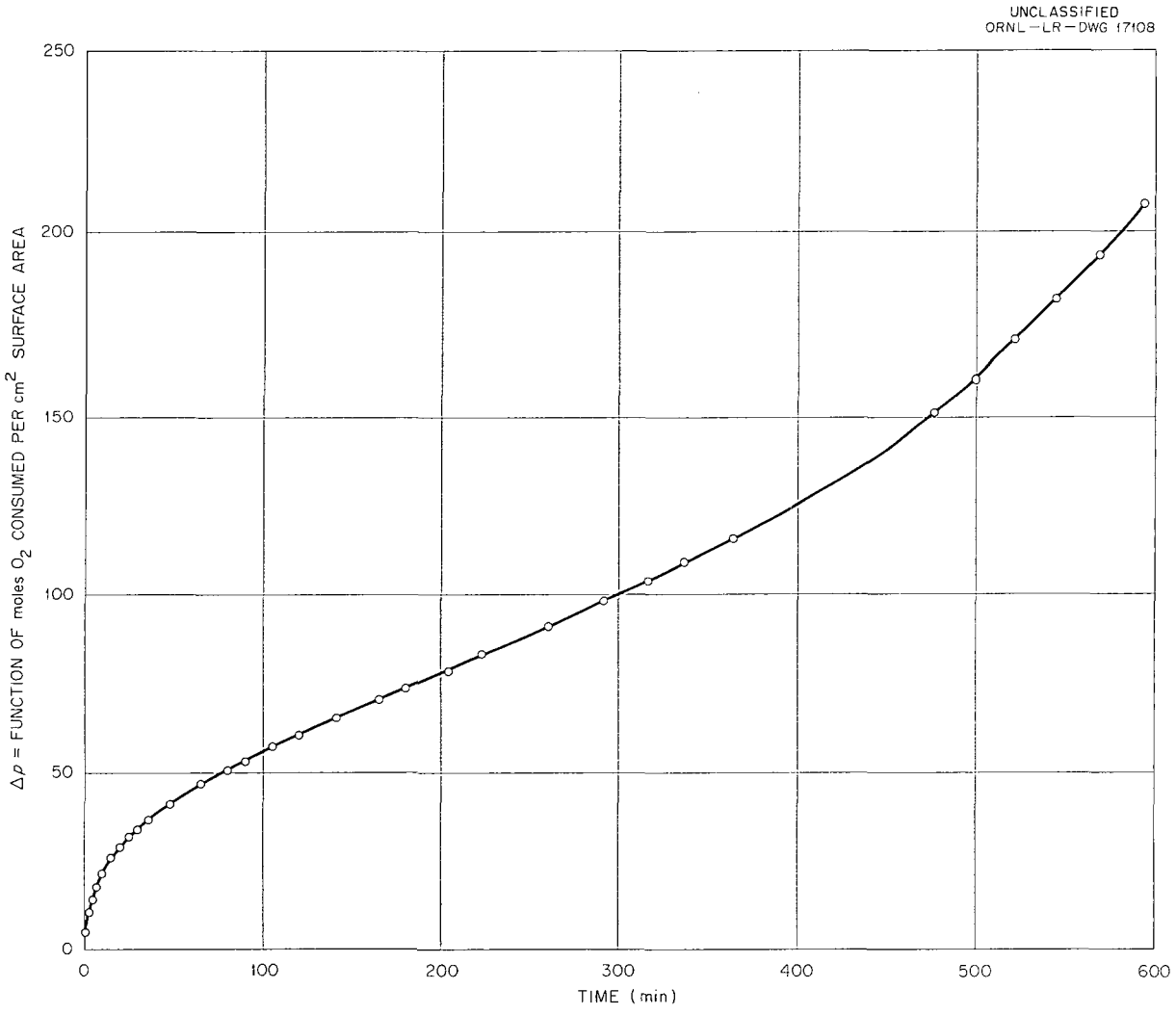

Fig. 161. Oxidation of Potassium at –20°C, Showing the Transition from Protective to Nonprotective Films.

A study was made of the reaction between Inconel[6] and sodium hydroxide melts over the temperature range 450 to 815°C for times up to 400 hr under blanketing atmospheres of hydrogen and helium. Both commercial Inconel and specially prepared high-purity alloys were studied.

It was shown that the reaction consisted of the selective leaching of iron and chromium from their terminal solid solution with nickel. The reaction products, shown to be a mixture of oxides and sodium oxysalts, grew in a network of narrow channels which, starting from the hydroxide-metal interface, penetrated along preferred paths into the underlying Inconel. These paths consisted of intergranular boundaries and certain crystallographic directions in the transgranular regions.

A photomicrograph of such a network is shown in Fig. 162 at a magnification of 1000X. This picture shows the early stages of network growth when the corrosion product is largely confined to intergranular regions. However, a number of very straight, narrow channels are to be seen penetrating transgranular regions.

It was found that the rate of advance of the corrosion-product network changed only by a small

[6]Nominal composition: 78% Ni, 15% Cr, and 7% Fe.

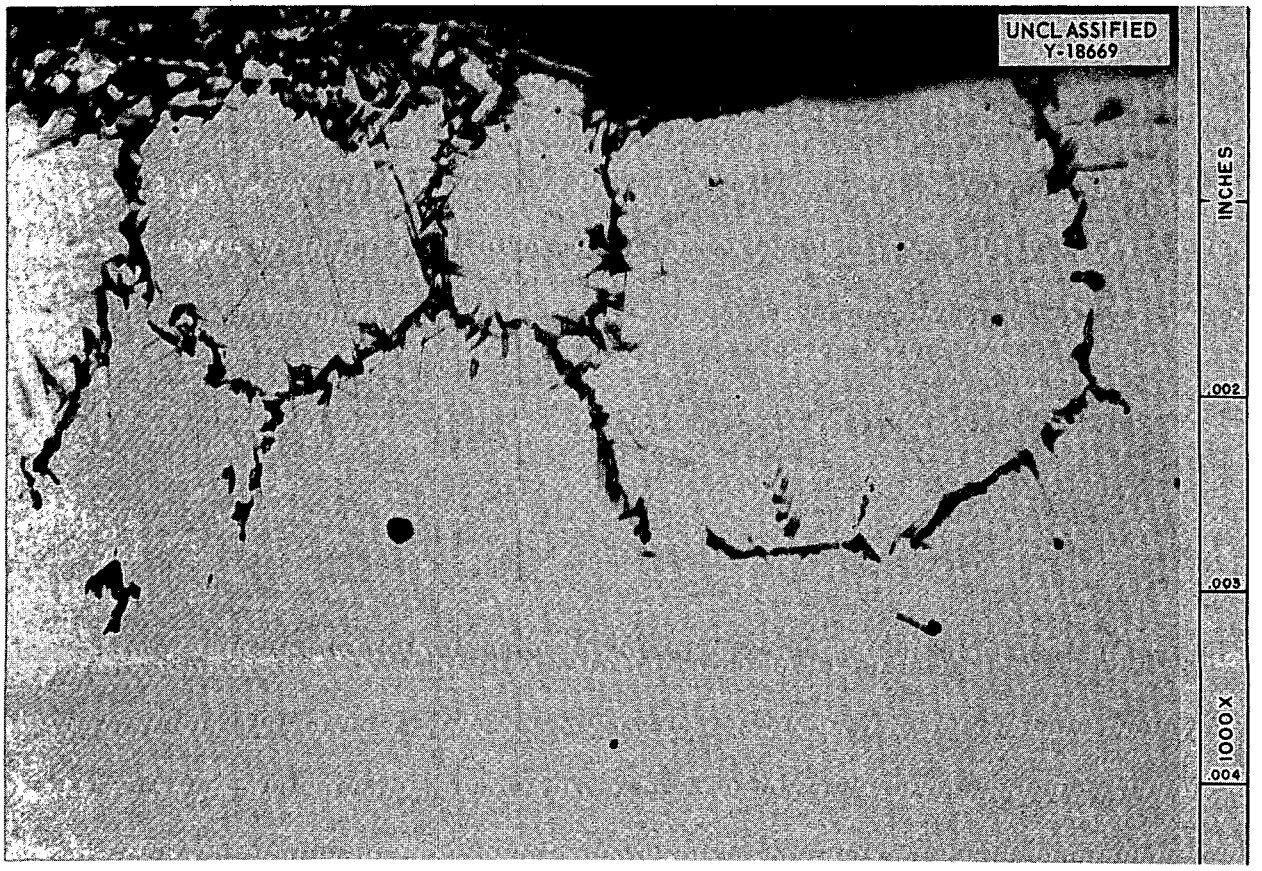

Fig. 162. Corrosion-Product Network Formed in Inconel After Exposure to a Sodium Hydroxide Melt for 100 hr at 600°C.

amount with increasing depth of penetration. It was deduced from this result that the rate-controlling process in the corrosive reaction was localized at the advancing ends of the network and that transport processes along the network exerted only a secondary influence.

The volume of reaction product was much greater than the decrease in volume of alloy, caused by the leaching of metal atoms from alloy lattice sites, so that a considerable stress was localized at the advancing tips of the reaction-product network. Inasmuch as residual stress from prior cold work was found to increase the susceptibility of Inconel to attack, it was proposed that the self-generated stress at advancing ends of the reaction-product network played an important role in localizing the rate-controlling processes at those sites.

In two-phase corrosion-product regions where the reaction had substantially subsided, a grain coarsening occurred, probably under the influence of a decrease in interfacial free energy.

Studies were made of the reaction between iron-rich alloys of iron, nickel, and chromium and sodium hydroxide at 815°C for 100 hr. The alloys used were both commercial stainless steels and high-purity alloys.

The reaction-product layer formed by the action of sodium hydroxide melts on these alloys was structurally similar to that formed on Inconel, described above, in that it consisted of a network of channels, filled with reaction product and located along preferred paths in a metallic matrix.

Many of these reactions produced a substantial quantity of sodium which, during test, existed as a gas at roughly 0.5 atm pressure over the hydroxide melt.

Studies were made of the reaction between fused sodium hydroxide and high-purity, terminal solid solution, nickel-rich alloys of nickel, molybdenum, and iron at 815°C for 100 hr. The reaction mechanism was found to involve the selective leaching of iron and molybdenum from their terminal solid solution with nickel. The resulting decrease in volume of the alloy occurred by the formation of very elongated pits rather than by a uniform decrease in specimen thickness. A cross section through such pits is shown in Fig. 163.

SELF-DECOMPOSITION OF FUSED HYDROXIDES

G. F. Petersen

Studies of the self-decomposition of fused hydroxides previously reported[7] are being continued. At present an apparatus is under construction which should allow a much greater accuracy of measurement.

[7] M. E. Steidlitz and G. P. Smith, *ANP Quar. Prog. Rep. Dec. 10, 1955*, ORNL-2012, p 133.

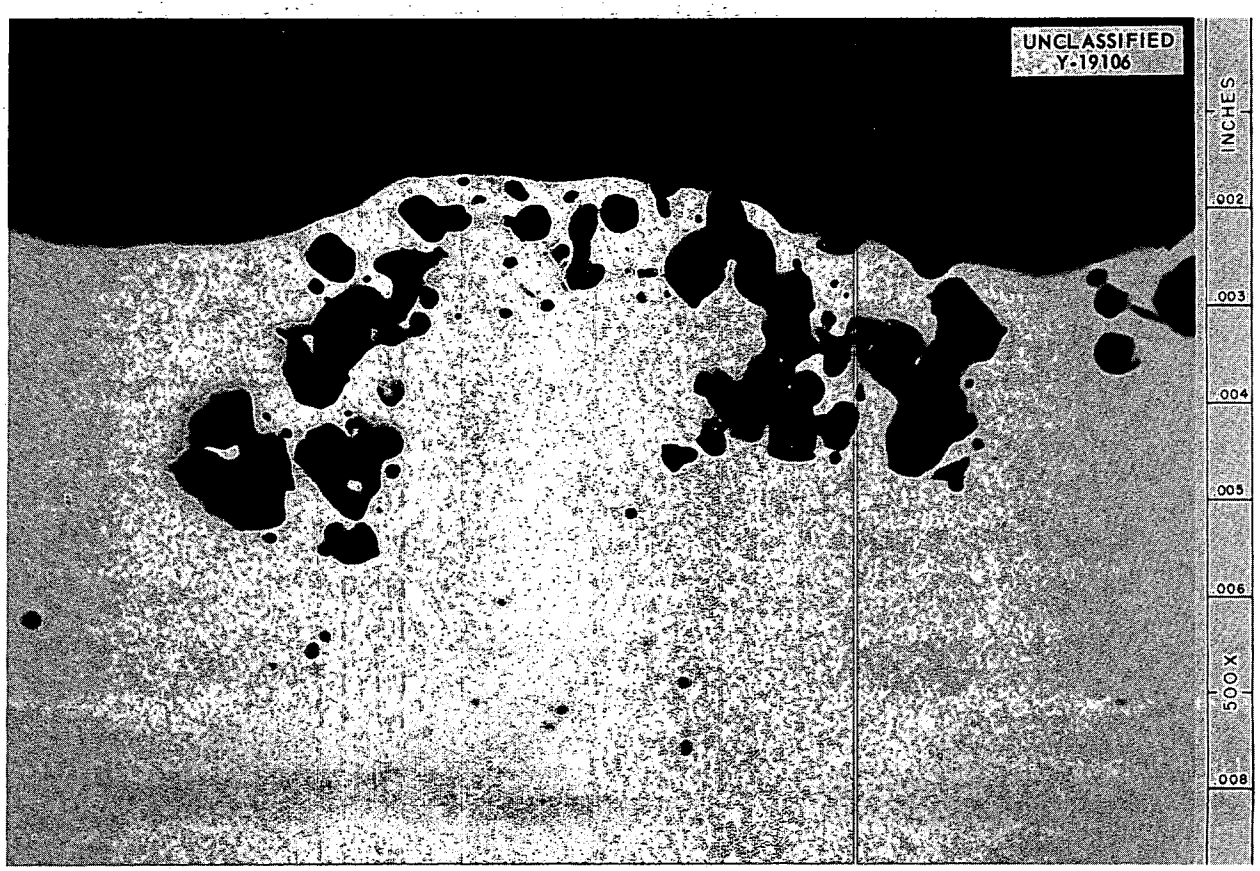

Fig. 163. Deep Pits Formed by the Reaction Between Fused Sodium Hydroxide and an Alloy Containing 70% Ni, 15% Fe, and 15% Mo.

HRP METALLURGY

G. M. Adamson, Jr.

HRP METALLURGY

G. M. Adamson

W. J. Fretague
J. P. Hammond
W. J. Leonard
M. L. Picklesimer
G. B. Wadsworth
C. H. Wodtke
O. Zmeskal

Zirconium alloys have been found which will form oxides that are comprised almost completely of a densely packed phase. The zirconium-niobium alloys with and without other additions have been examined fairly well up to 35% total alloy content. In the higher part of this range (25–35%) the bulk alloy oxides produced by air oxidation at 1000°C contain over 95% of the orthorhombic compound $6ZrO_2 \cdot Nb_4O_5$.

The thin tightly adhering film produced by low-temperature oxidation has been, to date, monoclinic in phase structure, regardless of the alloy studied. The improved corrosion resistance under irradiation conditions of a 15% niobium alloy is probably not related to phase stabilization of the oxide film.

Subsize impact tests on Zircaloy-2 have failed to reveal any significant changes in impact values as a result of aging up to 1500 hr at 250°C or to 1000 hr at temperatures as high as 450°C.

Procedures have been developed by which a flattened ring may be used as a preplaced root insert in inert-arc welding of A-55 titanium pipe. The quality is comparable to that obtained by conventional filler metal techniques.

If 6 Al–4 V titanium alloys are to be used in critical welded assemblies, it has been shown that they will have to be given a post-welding heat treatment in order to have satisfactory mechanical properties.

PHYSICAL METALLURGY

M. L. Picklesimer G. B. Wadsworth
O. Zmeskal

Morphology of Zircaloy-2

As a part of the effort to determine the best material for a homogeneous reactor core tank, a metallographic study on the heat-treated structures of zirconium alloys has been carried out. The alloys which have been studied are Zircaloy-2, -2W, -3A, -3B, and -3C and crystal-bar material. Conclusions on the temperature range of the alpha-plus-beta fields, the rates of grain growth and structures at various temperatures, the preferred orientation, and the nature of the inclusions were presented in the last report.[1] During this period, additional data have been obtained on Zircaloy-2 which will permit the following conclusions:

1. Specimens of Zircaloy-2 which had been held at 840 and 860°C for seven days and then water-quenched showed the same amount and the same distribution of the beta phase as the short-time (30 min to 2 hr) specimens that had been prepared previously. Thus the phase boundary temperatures reported previously[1] for the short-time specimens are valid for the "equilibrium" conditions.

2. Preferred orientation determinations (by x-ray diffraction) on Zircaloy-2 core tank material in the as-received condition and in the "randomized" heat treated condition (beta-quenched, cold-rolled 20% reduction, and annealed at 800°C for 30 min) showed that the as-received material had a very high degree of preferred orientation,[2] with little or no ductility predicted for the direction normal to the plate surface. The randomizing heat treatment resulted in a very-fine-grained material, ASTM No. 8 or smaller, with a considerable randomization of the structure. The intensity peaks of the inverse pole figure[2] were moved approximately 20 deg away from the (0001) pole, and the value of the peak intensity was cut by a factor of 2, indicating the probability of an increase in ductility in the direction normal to the plate surface, with still almost isotropic mechanical properties in the plane of the plate. Metallographic examination of specimens given the same heat treatment but with reductions of 10 and 15% instead of 20% has shown that these reductions result in a large grain size after annealing, ASTM No. 2 or larger, and that a cold reduction of 20% after beta-quenching is necessary to give fine-grained material.

---

[1] M. L. Picklesimer and G. B. Wadsworth, *Met. Semiann. Prog. Rep. April 10, 1956*, ORNL-2080, p 145.

[2] C. J. McHargue, *Met. Semiann. Prog. Rep. April 10, 1956*, ORNL-2080, p 211.

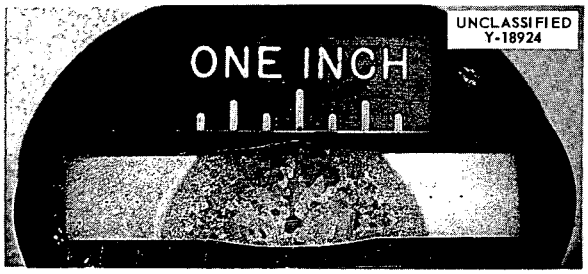

Fig. 164. Macrograph of Multipass Weld in Zircaloy-2 Plate.

A multipass weld in Zircaloy-2 plate has been examined metallographically, and a hardness traverse of the weld has been made. A macrograph of the weld is given in Fig. 164, the hardness traverse of the weld is shown in Fig. 165, and representative micrographs of areas of the weld and base metal are given in Figs. 166, 167, and 168. The base material had many long thin stringers in the plane of rolling. In the heat-affected zone of the weld these stringers opened up into voids, Fig. 166, and there is no clearly defined fusion line, except as shown by the dis-

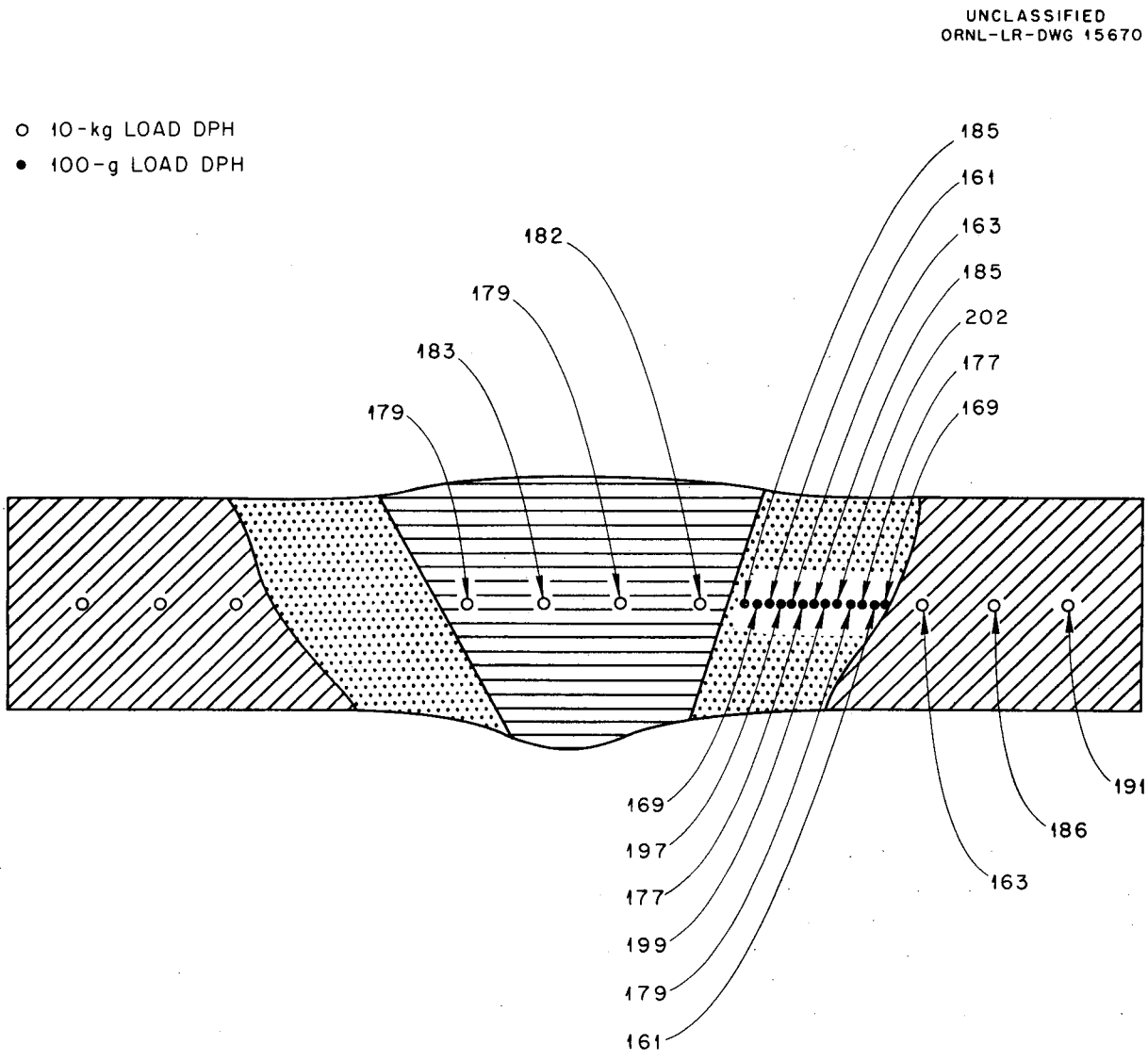

Fig. 165. Hardness Traverse of Zircaloy-2 Weldment.

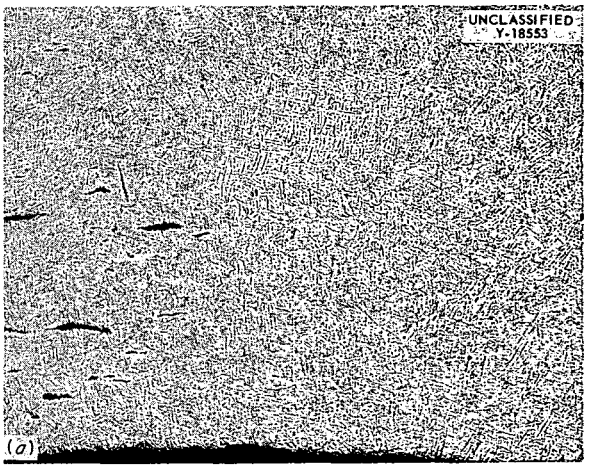

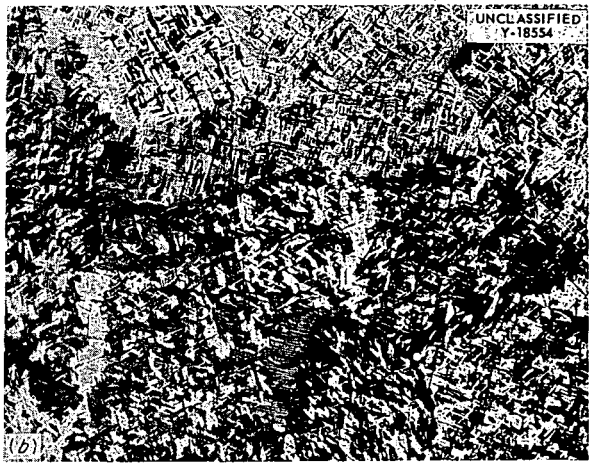

Fig. 166. Structure and Stringers in Fusion Zone of Zircaloy-2 Weldment. (*a*) Bright field. (*b*) Polarized light. 50X. Reduced 29%.

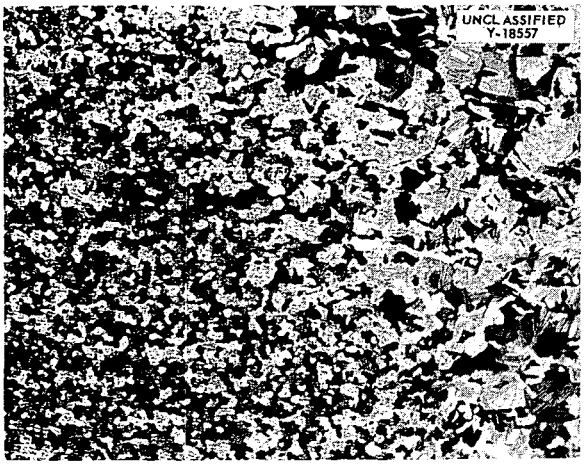

Fig. 167. Structure of Heat-affected Zone in Zircaloy-2 Weldment. Polarized light. 100X. Reduced 30%.

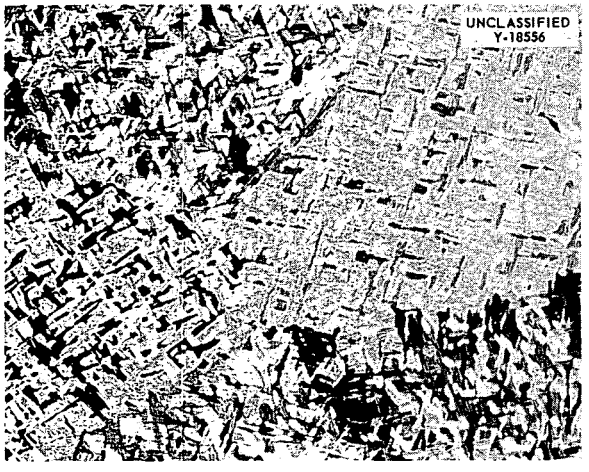

Fig. 168. Structure of Deposited Weld Metal in Zircaloy-2 Weldment. Note large beta grains and basket-weave structure. Polarized light. 100X. Reduced 30%.

appearance of the stringers. Figure 167 shows the heat-affected zone from the essentially unaffected, partially cold-worked base metal into an alpha recrystallization zone, into the alpha-plus-beta zone, and into the all-beta zone. The structure of the deposited weld metal is shown in Fig. 168. The structures shown in Figs. 166 and 167 and the hardness traverse shown in Fig. 165 demonstrate the very rapid change of structure and properties as the weld zone is approached.

Zirconium Alloy Development

An alloy development program has been started for the purpose of developing zirconium alloys with a corrosion resistance in uranyl sulfate greater than that found with Zircaloy-2. This program is coordinated with the study of zirconium oxide films. Corrosion tests by the HRP Corrosion Section on the prepared alloys have shown that thus far only the zirconium-niobium system has shown promise of improvement in corrosion resistance. The efforts are now centered on trying to increase the corrosion resistance of this system and to understand why it is more resistant.

Crystal-bar and sponge-base zirconium alloys containing Nb, Mo, Fe, Ta, Pd, and Pt as binary and ternary alloy additions have been arc-cast as

100-g castings. The castings have been homogeneized, water-quenched, hot- or cold-rolled to strip, and cut into heat-treatment metallographic specimens. They have been given a variety of heat treatments ranging from a study of the effects of quenching temperatures from 700 to 1100°C to aging the cold-worked and the quenched structures at temperatures from 300 to 800°C for times from 15 min to two weeks. Most of the work has been concerned with the 15% Nb alloys with Mo, Pd, and Pt as ternary additions. Difficulties in etching procedure for satisfactory microstructures prevented, for a considerable time, examination of the specimens held at 700°C and below. A recent development in etchants has finally permitted examination of these specimens. The examinations are not complete, but a number of conclusions can be drawn from the work completed:

1. All alloys containing up to 20% Nb with and without ternary additions up to 5% do not show fully retained beta on water quenching from 800°C and above. A Widmannstätten pattern of markings of a second phase is always present. These markings have been tentatively identified as alpha zirconium.

2. The addition of either 5% Pd or Pt to zirconium will permit the retention of a completely beta structure when quenched from 800°C or above. The addition of 10% of either element causes the appearance of a second phase, not alpha zirconium, when the material is held at temperatures from 800 to 1100°C, with the amount of the second phase decreasing with increasing temperature. Tempering treatments below 800°C led to the conclusion that the eutectoid composition and the eutectoid temperature are near 5% and 700°C for both the Zr-Pd and Zr-Pt systems. Decomposition of the retained beta occurred very rapidly at 600 and 700°C, with complete decomposition occurring in less than 1 hr at temperature.

The examination of the specimens held below 600°C has not been completed to an extent sufficient for conclusions to be drawn.

Zirconium-Hydrogen Studies

In a homogeneous reactor, under irradiation the solutions may decompose and liberate hydrogen and oxygen. It is known that the addition of hydrogen to zirconium may result in a brittle alloy. This study was undertaken to determine, first, whether hydrogen would be picked up by the zirconium under reactor operating conditions and, second, what the effects would be if the hydrogen were picked up. Procedures for adding controlled amounts of hydrogen to zirconium and of identifying the phases have been developed and reported previously.[1] It has also been shown that under equilibrium conditions the hydrides are found within the grains of crystal-bar zirconium and in the grain boundaries of the Zircaloy alloys.

A number of crystal-bar zirconium and Zircaloy-2 specimens have been hydrided in the modified Sievert's apparatus and step-cooled (100°C every 30 min) or oil- or mercury-quenched from 900°C. Hydrogen contents from less than 5 to 1000 ppm H_2 have been used. Oil and mercury quenching has been accomplished in the apparatus by putting the quenching medium in the bottom of the specimen tube, freezing and keeping frozen with a liquid-nitrogen bath until the hydrogen addition and desired heat treatment at temperature had been completed, removing the liquid-nitrogen bath and permitting the quenching medium to melt, and dropping the specimen into the quenching bath. With the use of mercury, extremely rapid rates of quenching may be obtained. Hydrogen contents of more than 130 but less than 250 ppm H_2 can be retained in supersaturated solution in crystal-bar zirconium (alpha) by quenching into mercury from 600°C. Micrographs of crystal-bar zirconium containing approximately 500 ppm H_2, step-cooled from 900°C, and mercury-quenched from 900°C are shown in Fig. 169. The second phase present in all cases in these two micrographs is hydrides. Zircaloy-2 specimens with contents of 100 and 870 ppm H_2 and step-cooled from 900°C are shown in Fig. 170. The white-appearing phases are hydrides, while the remainder of the grain boundary material is composed of the Fe, Ni, and Cr intermetallics. The metallographic preparation procedure for the identification of the hydrides was reported previously.[1]

Study of Oxide Films on Zirconium Alloys

The observation by members of this Division that ordinary zirconia is subject to radiation damage – namely, that the monoclinic phase is transformed to the more densely packed phase by neutron bombardment – led J. R. Johnson,[3]

[3] J. R. Johnson, *Development of a Cubic Oxide Protective Film on Zirconium*, ORNL-2029 (Jan. 30, 1956).

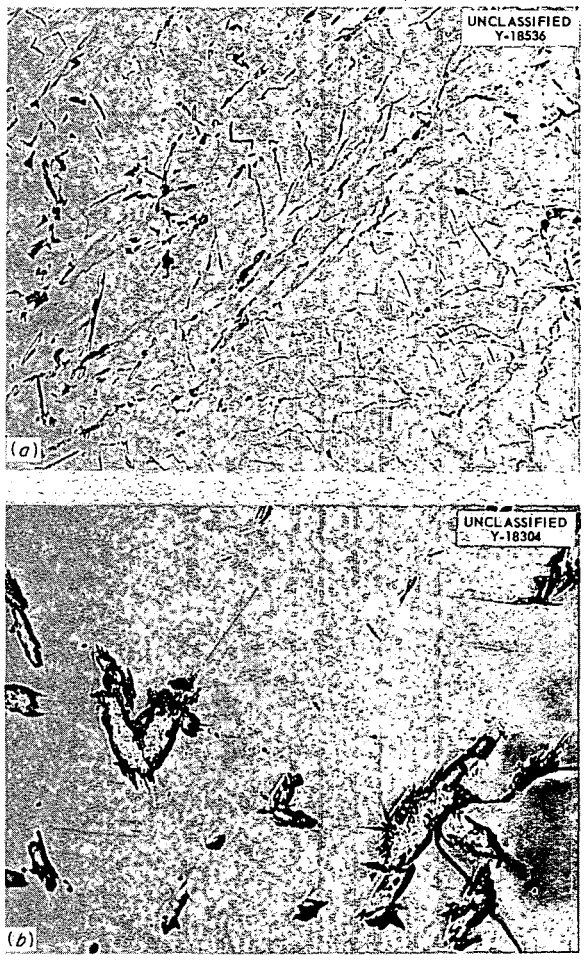

Fig. 169. Change in Size and Distribution of Hydrides with Cooling Rate in Crystal-Bar Zirconium. (*a*) Mercury-quenched. (*b*) Step-cooled. Bright field. 500X. Reduced 30%.

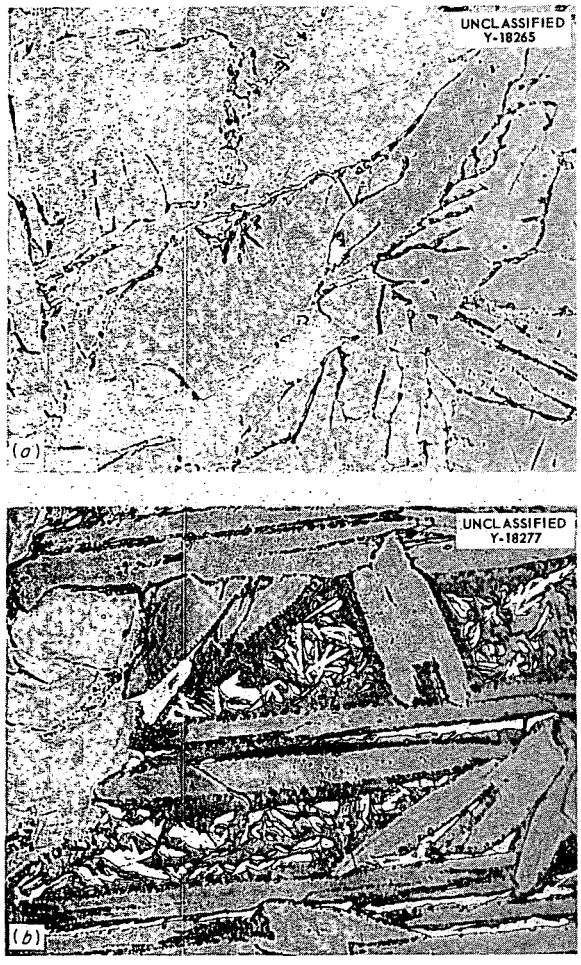

Fig. 170. Structure of Cooled Zircaloy-2–Hydrogen Alloys. (*a*) 100 ppm H_2. (*b*) 870 ppm H_2. 500X. Reduced 30%.

formerly of the Ceramics Group, to propose the key idea that led to this current oxidation study.

Johnson proposed that the reason for the accelerated corrosion of zirconium and of Zircaloy-2 by HRP uranyl sulfate solutions under irradiation was a result of this irradiation-induced transformation of the monoclinic film to a more densely packed state. The volume changes resulting from this transformation presumably could produce cracks in the film which would then act as reaction paths and accelerate the corrosion. Therefore a program was undertaken with the goal of producing an oxide film on a zirconium alloy which would be stabilized in the sense that it would consist principally of the densely packed phase and thus would not transform under irradiation.

In previous work[3] it was shown that the addition of oxides of Ca, Mg, Y, Ce, and Nb to zirconia would result in a stabilization of the high-temperature phase. More effective stabilization was found when tin and vanadium oxides were added with the niobium oxide. The only metal on this list that increased the corrosion resistance when added to zirconium was niobium.

As a continuation of this work approximately 50 different alloys have been evaluated to determine the degree to which the more densely packed phase is formed in the oxide. The available data are presented in Table 65. The procedure has

TABLE 65. VARIATION IN PERCENTAGE OF DENSELY PACKED PHASE IN OXIDES OF ZIRCONIUM ALLOYS WITH OXIDIZING TEMPERATURE

Alloy* Composition (wt %)		Oxidation Conditions		
		600°C for ¼ hr	800°C for ¼ hr	1100°C for ½ hr
Niobium				
5		15	20	35
10		35	35	70
15		30	65	80
20		25	40	65
33		45		100
Niobium and Sponge Zirconium				
15		30	40	80
20		15	65	95
Molybdenum				
5		5		0
10		10	5	0
Palladium				
5		0	0	0
10		5	<5	<5
Platinum				
5		15		0
10		15		0
Yttrium				
5		5		0
Manganese				
2		0		0
Silicon				
2		10		0
Indium				
5		0		0
Uranium				
10		10		5
Titanium				
5		15		5
Niobium-Molybdenum				
10	5	40	60	65
15	5	40	75	90
20	5	55		>95
20	7	50		>95
Niobium-Tantalum				
10	5	35	50	60
20	3	30		>95
20	5	35		>95

TABLE 65 (continued)

Alloy* Composition (wt %)			Oxidation Conditions		
			600°C for ¼ hr	800°C for ¼ hr	1100°C for ½ hr
Niobium-Iron					
10	1		10	20	55
10	2		20	30	50
15	1		30		70
Niobium-Tin					
7.5	2		35	40	65
15	3		45	65	85
Niobium-Palladium					
10	2		30		65
15	2		40		80
Niobium-Vanadium					
20	3		75		>95
20	5		85		>95
Niobium-Platinum					
15	2				80
15	5		30		80
Niobium-Chromium					
20	4		20		80
Niobium-Manganese					
20	3		45		85
Niobium-Nickel					
20	1				90
Niobium-Molybdenum-Tantalum					
10	5	5	35	65	90
Niobium-Yttrium-Tin					
8	2	2	35	35	40

*Unless noted otherwise, remainder of all alloys was crystal-bar zirconium.

been set up in four separate stages:

1. air oxidation of alloy powders (filings or saw cuttings), bulk oxide;
2. air oxidation of alloy plates (strip or slices from castings), thick films;
3. "soup" oxidation of alloy plates, thin films;
4. film formation in pure oxygen, thick and thin films.

The oxidation of powders was used as the first step of the diffraction study, since by comparing the intensities of their strongest reflections the realtive amounts of the various phases in the oxide may be determined. Because of distortions arising from coherency between the metal and oxide, the x-ray diffraction patterns are distorted and it is not possible to use this technique on thin films.

In the work with the powders it has been shown that those elements which promoted the formation of the densely packed phase in the oxide films on the alloys were also beta-phase stabilizers in the alloy. (Incidentally, the converse is not true; that is, all beta stabilizers are not stabilizers of the densely packed phase in zirconia. For example, palladium is a powerful beta stabilizer of zirconium, but it has no tendency to produce a densely packed phase in the oxide film on the alloy.)

In niobium alloys the densely packed phase is the orthorhombic compound, shown by Roth to be $6ZrO_2 \cdot Nb_2O_5$. Increasing the niobium content of the alloys resulted in more compound in the surface oxide, until at the composition equivalent to the stoichiometric composition of the compound, that is, 33 wt % niobium, the oxide can be made completely $6ZrO_2 \cdot Nb_2O_5$. In ternary alloys with niobium at 20% the oxide formed at 1100°C was almost all compound.

There is a strong temperature dependence of the amount of densely packed phase formed in the oxide. In many of the alloys studied, increasing the oxidation temperature increased the amount of densely packed phase formed in the oxide. The binary molybdenum alloys showed the reverse behavior; whereas about 10% of a densely packed phase (probably tetragonal) was formed in the oxide at 600°C, none was formed at 1100°C. This was probably due to the complete volatilization of molybdenum oxide from the scale. However, when molybdenum is present as a ternary addition to niobium-zirconium alloys, it apparently is not lost by high-temperature oxidation but, rather, has a definite enhancing effect in increasing the amount of compound formed. Binary alloys with yttrium, uranium, titanium, and platinum also formed more of the densely packed phase at the lower temperature of oxidation than they did at the higher. The rapid decrease in the amount of the densely packed phase in the oxide film as the oxidation temperature is lowered would indicate that the oxide film formed on zirconium alloys at 300°C in "soup" is probably the monoclinic phase.

In addition to the principal phases, that is, monoclinic and some form of a more densely packed structure, other phases have been noted in the scales of several alloys. The only phases of this latter group that have been identified are those that have not reacted with or dissolved in the principal phases. The yttrium alloy at 600°C formed Y_2O_3 in addition to the monoclinic and cubic zirconia phases, but none was found at 1100°C and only the monoclinic phase resulted. In addition to the monoclinic and densely packed phases, the uranium alloy formed U_3O_8 at both temperatures. Platinum alloys at 1100°C had elemental platinum in the scale, in addition to the monoclinic phase; this was the case both in binary and ternary alloys.

Schwartz and co-workers at Battelle examined films *in situ* on alloy specimens oxidized in high-temperature water and reported the presence of tetragonal ZrO_2 in some of them, although the monoclinic phase is reported as the principal phase in all of them. Schwartz found only the monoclinic phase in the film in place on a plate specimen of 15% niobium, treated at ORNL in UO_2SO_4 for 200 hr. Klein has examined the films on Zircaloy-2 in-pile loop specimens and has concluded that monoclinic zirconia is the only oxide phase present.

Tightly adherent films can be produced by high-temperature oxidation, but only when the time of exposure is short (2 to 5 min at 1100°C). A film so produced on a 33% niobium alloy had only a small amount of orthorhombic compound, but the same alloy in powder form, oxidized at the same temperature for 20 min, yielded an oxide that was completely composed of the compound $6ZrO_2 \cdot Nb_2O_5$.

A more comprehensive study of the thin films produced in "soup" is required, but the evidence at hand indicates that low-temperature oxidation does not produce significant quantities of the densely packed oxide phase in comparison to the amount of monoclinic phase. This appears to be true regardless of the alloy within the group studied. It seems unlikely that the improved corrosion resistance of the 15% niobium alloys under irradiation conditions is due to the phase structure of the oxide film.

MECHANICAL METALLURGY

W. J. Fretague

Impact Strength of Zirconium Alloys

In a previous report[4] data were presented which indicated that changes in the mechanical properties, mainly impact strength, of Zircaloy-2 may be occurring under homogeneous reactor operating conditions. These tests are being confirmed, but, in addition, out-of-pile studies have been started so as to confirm that the effects are radiation-induced. In these tests the impact specimen geometry and heat treatment will be studied, as well as possible aging effects.

Zircaloy-2 multibreak, subsize impact specimens[4] have been broken after being held at elevated temperatures for various times. During aging, the specimens were capsulated in evacuated Vycor tubing.

[4] W. J. Fretague, *Met. Semiann. Prog. Rep. Oct. 10, 1955*, ORNL-1988, p 93.

The results of the impact tests are tabulated in Table 66 and plotted in Figs. 171 and 172. Aging up to 1585 hr at 250°C does not seem to cause any change in the Zircaloy samples. The impact values for specimens aged at temperatures above 250°C are higher than those for the controls and

TABLE 66. IMPACT VALUES OF ZIRCALOY-2 SPECIMENS AGED AT ELEVATED TEMPERATURES

Condition	Impact Values (in.-lb) at Break Temperatures of					
	100°C	23°C	90°C	150°C	200°C	254°C
Control	8	15	16	27	32	60*
At 250°C for 500 hr	10	13	22	24	38	60*
At 250°C for 1085 hr	9	12	20	29	34	52*
At 250°C for 1585 hr	8	14	20	28	36	50*
At 300°C for 1008 hr	13	24	30	36	44	58*
At 350°C for 1008 hr	12	20	25	34	53*	50*
At 400°C for 1008 hr	12	18	25	36	42	57*
At 450°C for 1008 hr	13	20	26	37	52*	57*

*Specimen broke on rebound of hammer or did not break completely, thus giving a value which may be low.

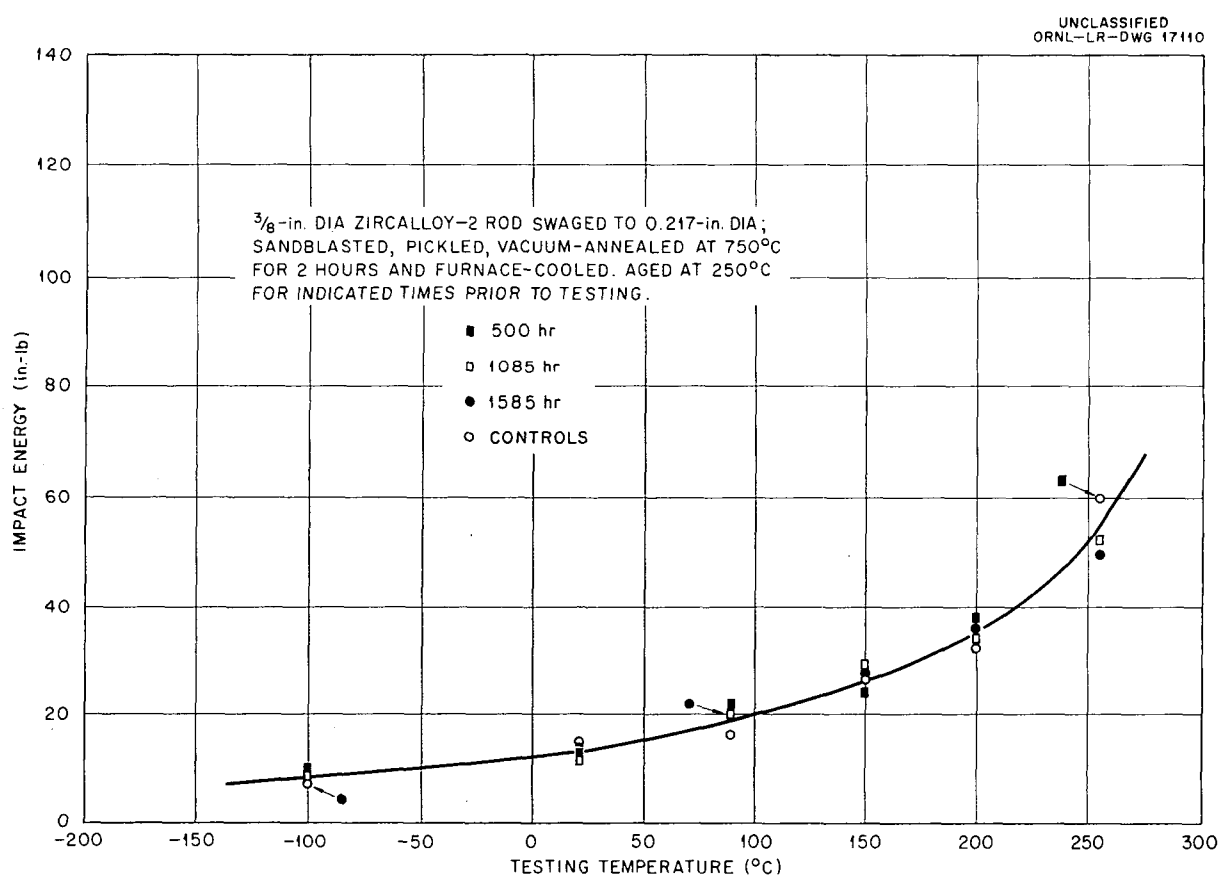

Fig. 171. Impact Energy vs Testing Temperature for Zircaloy-2 Aged at 250°C for Various Times.

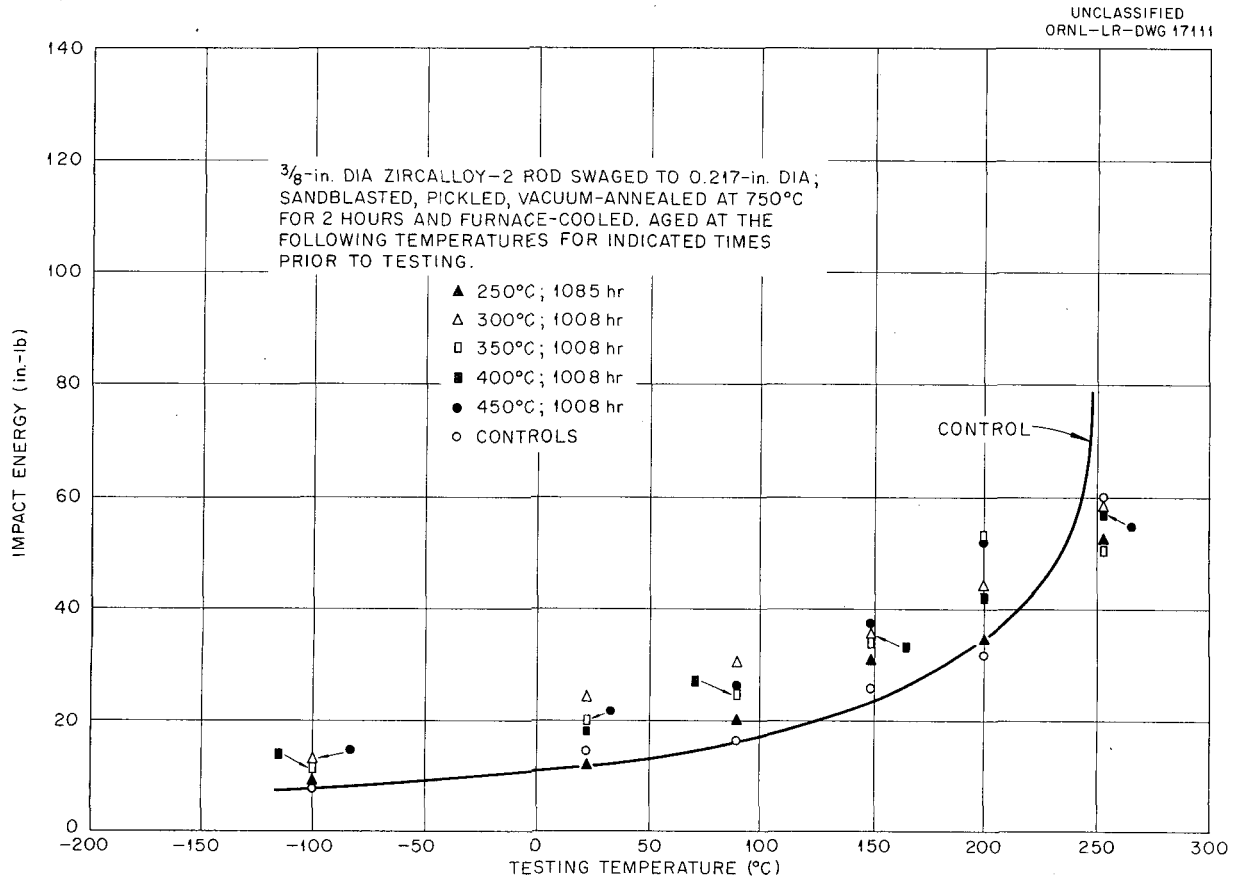

Fig. 172. Impact Energy vs Testing Temperature for Zircaloy-2 Aged 1000 hr at Various Temperatures.

those aged at 250°C, but not appreciably so. While from these data it cannot be said that no changes are occurring, it can at least be said that no significant embrittlement has occurred.

WELDING DEVELOPMENT

W. J. Leonard C. H. Wodtke

Titanium Welding Procedures

In order to provide a formal qualification of the recently developed Titanium Welding Procedure, four titanium pipe welds were made in 2½-in. sched-40, RC-55A pipe, using RC-40K welding wire. Both 2G and 5G welding positions were qualified. Bend tests and tensile tests as required by ASME-Boiler and Pressure Vessel Code 1952 were adhered to, with additional specimens taken for microscopic examination and microhardness tests. All specimens satisfactorily passed the required tests. The physical and mechanical properties data are given in Table 67.

The guided bend tests were made with specimens approximately 1 in. in width and bent on a radius of 2½ times the wall thickness. Figure 173 is a photograph of two weld specimens (root and face) showing the appearance after bending. All samples were sound, showing no cracks or fissures.

Since the use of a preplaced insert is generally preferred to hand feeding filler wire when consistent high quality root passes are desired, the use of inserts was tried in titanium welding. The Electric Boat (EB) type of inserts, made by machining ⅛-in.-dia wire, was tried extensively in both plate and pipe. Difficulty was experienced in obtaining a root pass of proper geometry and penetration. The use of high heat inputs, which were necessary to melt the insert and have it pull up in the welding groove properly, resulted in increased contamination of the weld metal and

TABLE 67. MECHANICAL PROPERTIES OF TITANIUM WELDS

Specimens	Welding Positions	Tensile Strength (psi)	Microhardness (VHN, 100-g Load)
Q-1	2G	81,824	204
Q-1	5G	81,619	194
Q-1	5G	84,824	194
Q-2	5G		207
Q-2	2G	81,411	196
Q-3	5G	83,106	255
Q-3	2G	81,757	228
Q-4	5G	83,642	217
Q-4	2G	80,139	221

greater hardnesses than those obtained in root passes made by conventional methods. The use of low heat resulted in improper flow of the molten insert into the welding groove, with resultant porosity and lack of proper penetration in the weld metal. A welding technique was eventually arrived at in which the heat input used was sufficiently high to prevent porosity and yet give proper penetration. The resultant root reinforcement was very small, being about flat with the inner base metal wall of a pipe, and the hardness of the weld metal averaged about 30 VHN higher than that obtained by conventional welding. The fit-up prior to welding was critical and greatly influenced the resultant properties of a weld.

A flat-type insert made by flattening a $\frac{3}{32}$-in.-dia wire to an approximate ellipsoid shape, as shown in Fig. 174, was then developed. Initial work in welding this type of joint indicated that the variations in penetration and root reinforcement with the heat input were not so critical as with the EB-type insert. The porosity again was inversely proportional to the heat input used in welding. Hardnesses of the weld metal were still higher than desired. By changing the included angle to 100 to 110 deg as shown in Fig. 174 and lowering the heat input, sound root passes of proper penetration and geometry were obtained with practically the same hardnesses as those made by conventional methods. The fit-up of the insert in relation to the root face was not critical. Varying

UNCLASSIFIED
T-10558

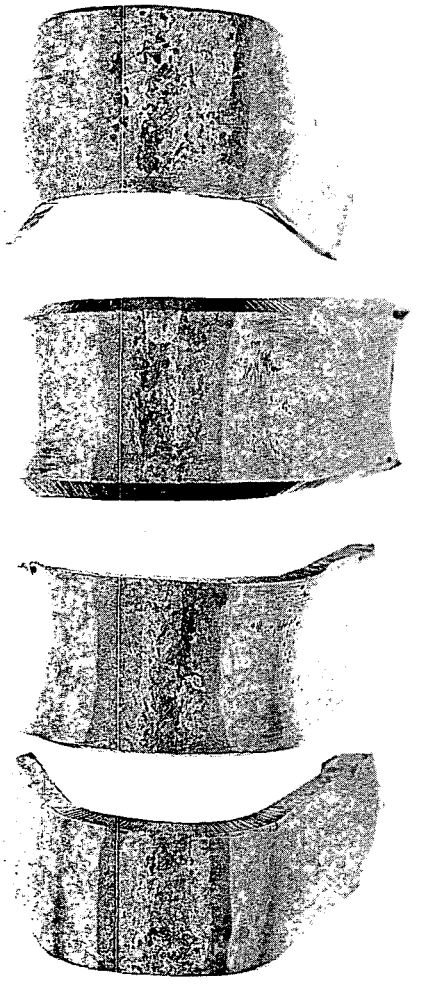

Fig. 173. Appearance of Root and Face-Bend Samples from Titanium Weld Specimens.

the position of the insert from a position where the bottom of the insert and base metal were almost flush to where the bottom of the insert protruded 0.100 in. below the base metal had no pronounced effect on the resultant root pass.

The weldability of an alpha-plus-beta type of titanium alloy (6 Al–4 V) was investigated. A $\frac{1}{16}$-in. sheet of the alloy in the as-received condition (annealed and pickled) was welded with filler wire of the same composition, using a single pass. The same welding technique, developed for

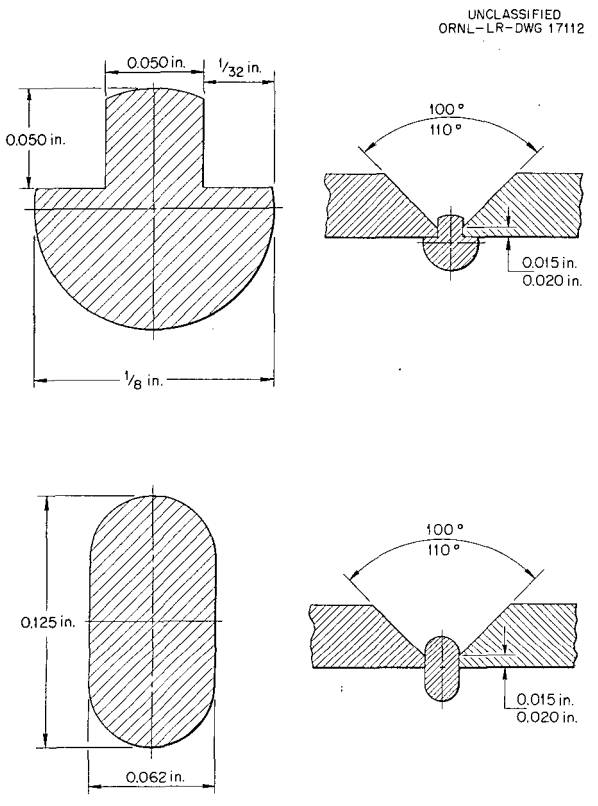

Fig. 174. Design and Position of Preplaced Titanium Weld Root Inserts.

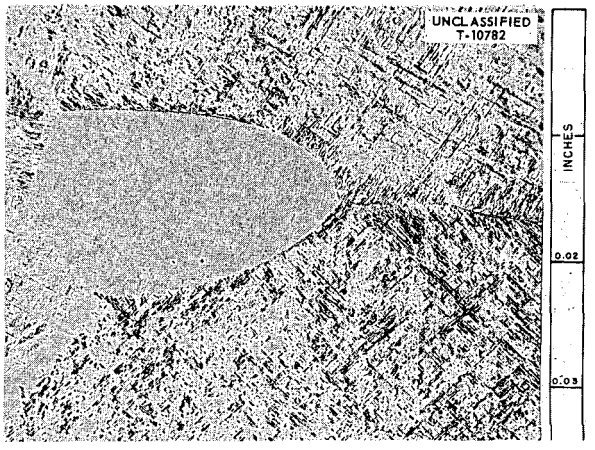

Fig. 175. Weld Structure in 6 Al–4 V Titanium Alloy. 100X.

welding unalloyed titanium in air, was used. Nondestructive tests, such as liquid penetrant testing and radiography, indicated a sound weld. The appearance of the weld was very satisfactory, indicating a minimum amount of contamination. Four sections along the 14-in. length of weld were examined microscopically. Figure 175 is a photomicrograph of typical weld-metal structure. The heat-affected zone exhibited a coarse recrystallized structure of the Widmanstätten type, similar in appearance to the weld metal. The microhardness averages of the weld metal, heat-affected zone and unaffected base metal were 339, 362, and 355 VHN, respectively.

Seven bend specimens were taken transverse to the weld and were bent in a special guided bend test jig. Three root face bends and three face bend tests were made on a radius of bend 4 times the specimen thickness. One root bend specimen was bent on a radius of twice the thickness.

The six specimens, bent on a radius of $4t$, broke when bent through an angle ranging from approximately 10 deg for the lowest specimen to 45 deg for the highest specimen. The seventh specimen, bent at $2t$, broke at less than 10-deg bend. All specimens broke in the heat-affected zone of the base metal. For comparison, good quality unalloyed titanium (Ti-55A or equivalent) of the same gage will bend 180 deg on a $2t$ radius. These results indicate an embrittling of alpha-plus-beta titanium alloy base metal during the welding cycle and that a postheat treatment after welding will possibly be required in order to secure weldment satisfactory for critical applications.

APPLIED METALLURGY

J. E. Cunningham

PROCESS METALLURGY

R. J. Beaver

ARMY PACKAGE POWER REACTOR (APPR)

Manufacturing of the Initial Loading of APPR-1 Fuel Elements

R. J. Beaver E. C. Edgar[1]

In order to comply with the request by the AEC to demonstrate a package power reactor at Fort Belvoir, Va. in December 1956, it was necessary to interrupt the final phases of fuel element development and initiate fabrication of the APPR-1 reactor components five months in advance of the anticipated date. By July 30, 1956, a full loading of 38 stationary fuel elements, 7 control-rod fuel elements, and 7 absorber sections for the control rods were manufactured and shipped to Alco Products, Inc., Schenectady, N.Y. Slightly more than 1200 fuel plates were fabricated, with a rejection rate of 17%. The finished APPR-1 stationary and control-rod fuel elements are illustrated in Figs. 176 and 177, respectively.

During the production of the fuel elements, it was discovered that the 304L material was being carburized and sensitized after the prolonged heat treatments required in the manufacturing specification. An appreciable number of fuel elements contained plates which had probably been intergranularly attacked after cleaning in a 15% HNO_3–5% HF aqueous solution. These fuel elements were not recommended for the APPR-1 but were approved for testing in the critical facility at Alco Products, Inc.

Sensitization of APPR-1 Fuel Plates

R. C. Waugh C. F. Leitten
W. R. Burt[2]

During manufacturing of APPR-1 fuel plates it was observed that after the anneal-flattening procedure, which consisted of slowly heating a pack of plates to 1125°C, annealing at that temperature for 3 hr, and furnace cooling, the plates were often slightly oxidized and contaminated with the Al_2O_3-separating material. At the same time, difficulty was experienced with excessive braze flow onto the cladding of the fuel core during brazing. It was felt that this condition could be eliminated if the plates were chemically cleaned prior to brazing. Manufacturing procedures were modified to include a cleaning treatment in a 15% HNO_3–5% HF aqueous solution prior to assembling plates for brazing. This modification was made with the assumption that the cladding material was type 304L stainless steel, which is not subject to severe intergranular attack by the acid. However, it was shortly discovered that the fuel plates were intergranularly attacked after the acid treatment. The extent of attack on a plate which had been subjected to three anneal-flattening cycles is illustrated in Fig. 178. It is apparent that in this instance the attack is quite severe.

It seemed apparent that the cladding material after the extended heat treatment was no longer a 304L type stainless steel, but was one containing sufficient carbon to make it sensitive and subject to intergranular attack in the aforementioned acid. It appeared possible that carbon was diffusing from the 0.07 wt % C matrix stainless steel in the core into the 0.03 wt % C stainless steel cladding. A thorough investigation was conducted to determine the cause and extent of sensitization of the 304L stainless steel clad, its effect in the application of this material in APPR, and the possible substitution of type 347 stainless steel.

The results and correlations are summarized herein; additional detailed information will be contained in a topical report to be published shortly. The investigation was divided into two phases: (1) to determine the effect of each processing heat treatment on carbon diffusion into and sensitization of the 304L cladding and (2) to determine whether or not the sensitized cladding of the material can be restricted by the substitution of type 347 stainless steel for either or both of the present type 304B fuel core matrix material and type 304L cladding material. The criteria for evaluating the extent of carbon diffusion and sensitization of cladding material were metallographic examination and Strauss testing.

[1] On loan from ALCO.

[2] Summer employee from Cornell.

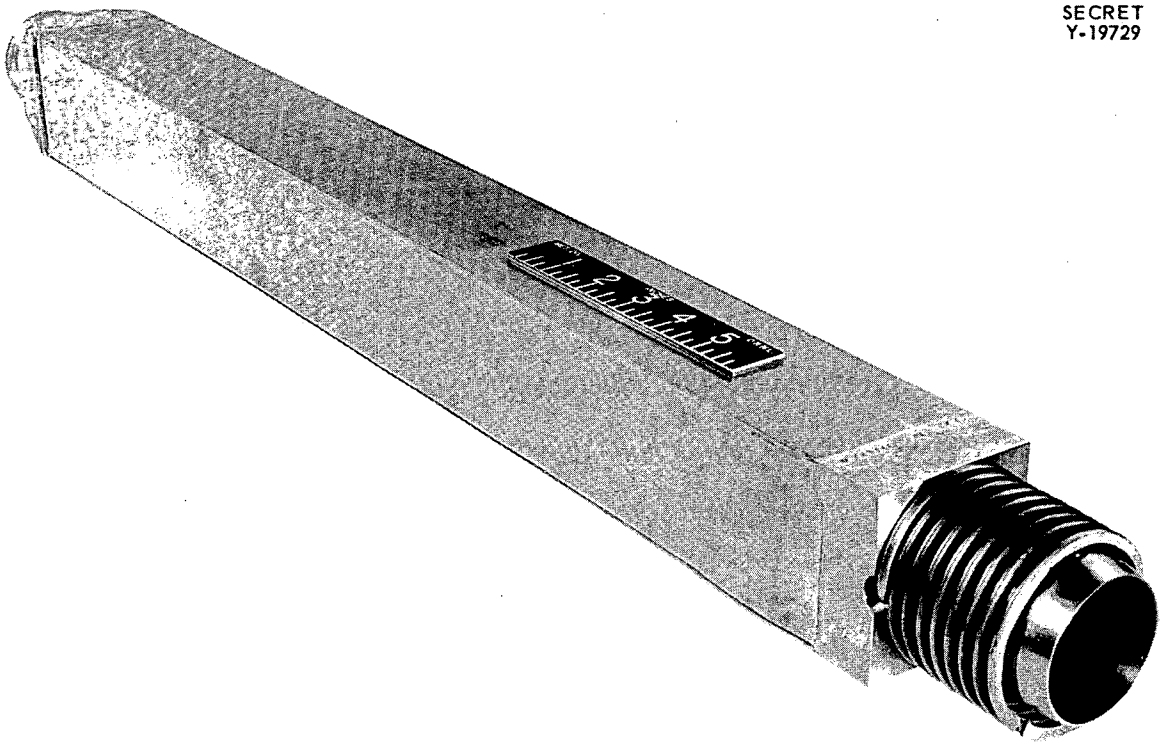

Fig. 176. Stationary Fuel Element.

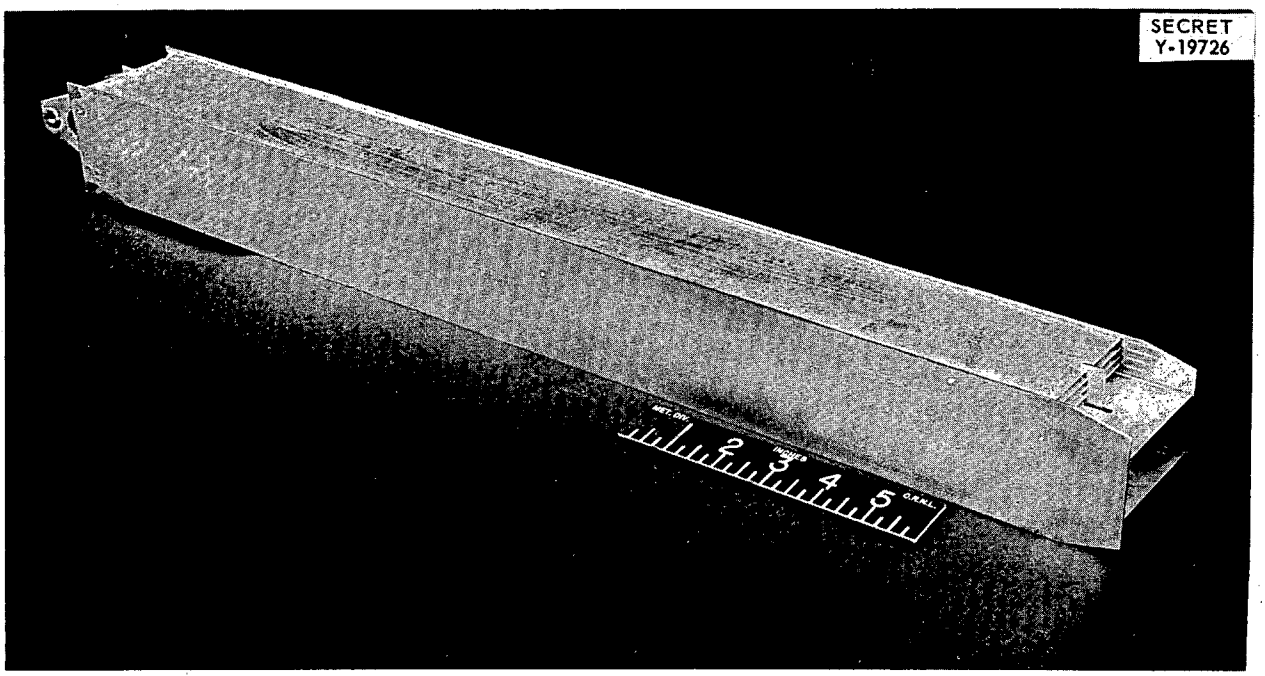

Fig. 177. Control-Rod Fuel Element.

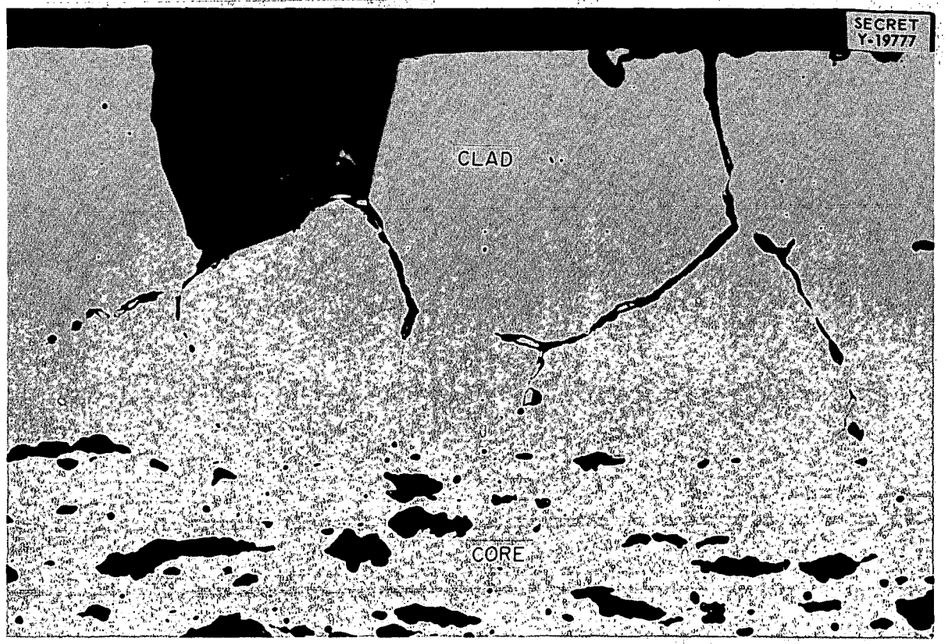

Fig. 178. Cross Section of APPR-1 Fuel Plate in Which the Stainless Steel Cladding Had Become Carbonized and Sensitized, Showing Severe Intergranular Attack After Treatment in 15% HNO_3–5% HF Aqueous Solution.

The results of phases 1 and 2 are summarized in Tables 68 and 69, respectively, and, for the present materials combination of 304B (0.07 wt % C) fuel core matrix and 304L (0.03 wt % C) cladding, the following conclusions can be drawn:

1. Carbon diffusion into the clad occurs during hot rolling, but the chromium carbide network does not extend to the surface of the plate.

2. The subsequent heat treatments specified in the manufacturing procedures cause complete diffusion of carbon and the formation of a chromium carbide network completely to the surface of the clad. The additional carbon in the clad results in a material which lies within the carbon specifications for type 304 stainless steel. The material therefore failed the Strauss test and would also be expected to be intergranularly attacked by an aqueous solution containing 15% HNO_3 and 5% HF.

3. The carbon in the 304B stainless steel is the important contributor to the carbon increase in the clad and masks any contribution of carbon to B_4C, ZrB_2, and UO_2.

For the substitution of types 347 and 347B in various combinations with types 304L and 304B the following conclusions can be drawn:

1. Type 347B fuel core matrix–type 304L clad: After an anneal-flattening heat treatment, the cladding material is susceptible to partial failure in a Strauss test. The chromium carbide network which forms throughout the cladding material is not sufficiently continuous to cause complete failure in a Strauss test.

2. Type 304B or 347B fuel core matrix–type 347 clad: Although the cladding contains isolated patches of chromium carbide at the intersection of 3 grain boundaries after the heat treatments specified in APPR-1 fuel element manufacturing, the material passes the Strauss test and is not susceptible to intergranular attack.

TABLE 68. EFFECT OF MANUFACTURING HEAT TREATMENTS ON CARBURIZATION AND SENSITIZATION OF 304L STAINLESS STEEL CLAD APPR-1 FUEL PLATES

LEGEND

NIA No intergranular attack
PIA Partial intergranular attack
CIA Complete intergranular attack
F Frame
SC Inward from clad surface
R Strauss control specimen

S Strauss-tested specimen
GBS Grain boundary separation
CN Continuous Cr_4C network
DN Discontinuous Cr_4C network
EN Erratic Cr_4C network
C Clad

	Hot Rolled Plate, Not Pickled	Hot Rolled and Pickled	Cold Rolled, Previous Pickling	First Flatten Anneal, H_2O-Al_2O_3	First Flatten Anneal, NBC-Al_2O_3	Second Flatten Anneal, H_2O-Al_2O_3	Second Flatten Anneal, NBC-Al_2O_3	First Flatten Anneal, H_2O-Al_2O_3, Brazed	First Flatten Anneal, NBC-Al_2O_3, Brazed	Second Flatten Anneal, H_2O-Al_2O_3, Brazed	Second Flatten Anneal, NBC-Al_2O_3, Brazed
304L frame and clad, 304B core, no boron compound	1*, NIA None – C 0.017 in. – F – DN R S – no GBS	9, NIA None – C 0.020 in. – F – EN R S – no GBS	2, NIA None – C 0.012 in. – F – EN R S – no GBS	3, CIA Through – C – CN Through – F – DN R – no GBS S – GBS	7, CIA Through – C – CN Through – F – DN R S – GBS	6, CIA Through – C – CN Through – F – DN R – no GBS S – GBS	10, CIA Through – C – CN Through – F – DN R – no GBS S – GBS	4, PIA (0.001 in.) Through – C – DN Through – F – DN R – no GBS S – slight GBS	8, PIA (0.002 in.) Through – C – DN Through – F – DN R – no GBS S – slight GBS	5, CIA Through – C – DN Through – F – DN R – no GBS S – GBS	11, CIA Through – C – CN Through – F – DN R – no GBS S – GBS
304L frame and clad, 304B core, B_4C poison	12, NIA 0.003 in. – C – DN 0.032 in. – F – DN R S – no GBS	13, NIA 0.004 in. – C – CN 0.021 in. – F – DN R S – no GBS	14, NIA 0.002 in. – C – DN 0.025 in. – F – EN R S – no GBS	19, CIA, E Through – C – CN Through – F – DN R – no GBS S – GBS	15, CIA, E Through – C – CN Through – F – DN R – no GBS S – GBS	21, CIA Through – C – CN Through – F – DN R – no GBS S – GBS	18, CIA Through – C – CN Through – F – DN R – no GBS S – GBS	20, PIA (0.002 in.) Through – C – CN Through – F – DN R – no GBS S – slight GBS	16, PIA (0.002 in.) Through – C – CN Through – F – DN R – no GBS S – slight GBS	22, CIA Through – C – EN Through – F – EN R – no GBS S – GBS	17, PIA (0.002 in.) Through – C – CN Through – F – DN R – no GBS S – slight GBS
304L frame and clad, 304B core, ZrB_2 poison	23, NIA 0.003 in. – C – EN 0.080 in. – F – EN R S – no GBS	24, NIA 0.003 in. – C – DN 0.073 in. – F – DN R S – no GBS	25, NIA 0.002 in. – C – EN 0.042 in. – F – EN R S – no GBS	26, CIA Through – C – CN Through – F – DN R – no GBS S – GBS	30, CIA Through – C – CN Through – F – DN R – no GBS S – GBS	29, CIA Through – C – CN Through – F – DN R – no GBS S – GBS	33, CIA Through – C – CN Through – F – DN R – no GBS S – GBS	27, PIA (0.002 in.) Through – C – CN Through – F – DN R – no GBS S – GBS	31, PIA (0.002 in.) Through – C – EN Through – F – EN R – no GBS S – slight GBS	28, CIA Through – C – CN Through – F – DN R – no GBS S – GBS	32, CIA Through – C – EN Through – F – EN R – no GBS S – GBS

*Specimen No.

TABLE 69. EFFECT OF MANUFACTURING HEAT TREATMENTS ON CARBURIZATION AND SENSITIZATION OF SUBSTITUTE STAINLESS STEEL COMBINATIONS FOR APPR-1 FUEL PLATES

LEGEND

NIA No intergranular attack	F Frame
PIA Partial intergranular attack	C Clad
CIA Complete intergranular attack	R Strauss control specimen
CN Continuous Cr_4C network	S Strauss-tested specimen
DN Discontinuous Cr_4C network	GBS Grain boundary separation
EN Erratic Cr_4C network	

Fabrication Operation	Combination of Materials					
	304L Frame and Clad, 347 Core		347 Frame and Clad, 304B Core		347 Frame and Clad, 347 Core	
	B_4C	ZrB_2	B_4C	ZrB_2	B_4C	ZrB_2
Cold-rolled	46*, NIA	49, PIA	37, NIA	43, NIA	52, NIA	55, NIA
	0.0045 in. – C – DN	0.0045 in. – C – DN	None – C	None – C	None – C	None – C
	0.041 in. – F – DN	0.026 in. – F – DN	None – F	None – F	None – F	None – F
	R – no GBS	R – rupture	R	R	R – rupture	R – rupture
	S – no GBS	S – rupture	S – no GBS	S – no GBS	S – rupture	S – rupture
Single anneal $H_2O + Al_2O_3$	47, PIA	50, PIA (0.002 in.)	38, NIA	44, NIA	53, NIA	56, NIA
	Through – C – DN	Through – C – DN	Through – C – EN	Through – C – EN	Through – C – EN	Through – C – EN
	Through – F – DN	Through – F – DN	Through – F – EN	Through – F – EN	Through – F – EN	Through – F – EN
	R – no GBS	R – no GBS	R – no GBS	R – no GBS	R – no GBS	R – no GBS
	S – no GBS	S – slight GBS	S – no GBS	S – no GBS	S – no GBS	S – no GBS
Single anneal and simulated braze	48, NIA	51, NIA	39, NIA	45, NIA	54, NIA	57, NIA
	Through – C – DN	Through – C – DN	Through – C – EN	Through – C – EN	Through – C – EN	Through – C – EN
	Through – F – EN	Through – F – DN	Through – F – EN	Through – F – EN	Through – F – EN	Through – F – EN
	R – no GBS	R – no GBS	R – no GBS	R – no GBS	R – no GBS	R – no GBS
	S – no GBS	S – no GBS	S – no GBS	S – no GBS	S – no GBS	S – no GBS

*Specimen No.

It is evident from the experimental results that the substitution of type 347 for 304L as the cladding material permits specified APPR-1 manufacturing procedures to be followed without encountering sensitization of the cladding material. The type 347 material also has a smaller grain size than 304L stainless steel after the required heat treatments, which is conducive to improved corrosion resistance. The experimental results do not reveal any advantage in substituting 347B material for 304B material as the fuel core matrix material, although a fuel plate in which all the stainless steel is stabilized may be desirable.

APPR CORROSION TESTING

R. C. Waugh

Static Testing. – Miniature fuel plate specimens and brazed T-joints of interest to the APPR program have been autoclave-tested by J. L. English of the REED Division, and results are summarized in Table 70. Metallographic examinations of the tested specimens have not been completed.

Dynamic Testing. – Prior to the manufacture of the APPR-type fuel element for testing in the Submarine Thermal Reactor (STR), a 3-plate element was prepared and shipped to Westinghouse Atomic Power Division (WAPD) for corrosion testing in their dynamic loop. The material combination consisted of a fuel core containing UO_2 dispersed in a 304B (0.07 wt % C) matrix and clad with 304L (0.03 wt % C). Manufacturing procedures were similar to the present procedures specified for APPR fuel elements, which include heat treatments that have recently been shown to cause carburization and sensitization of the 304L cladding. Evaluation of the cladding material in this fuel unit by chemical analysis, metallographic examination, and Strauss testing revealed that the original 304L cladding had been carburized and could be typed as a 304 stainless steel.

The corrosion testing of this element at WAPD consisted of 6245 hr in 500°F water, which contained 24 cc of H_2 per kiloliter and 10 cc of N_2 per kiloliter (O_2 undetectable) at a velocity of 38.2 fps. Although no corrosion rate data were obtained by WAPD, metallographic examination at ORNL revealed negligible surface corrosion products. It was concluded that the fuel element was very satisfactory even though the cladding material, as tested, was a sensitized type 304 stainless steel.

APPR-1 Absorber Section

C. F. Leitten

A composite plate, containing a dispersion of 3.2 wt % boron in electrolytic iron powder (enriched to the 92% level in B^{10}) and clad with wrought type 304L stainless steel, has been successfully fabricated by utilizing powder-metallurgy techniques for preparation of the core and roll-bonding procedures for cladding into composite plate. Powder-metallurgy processing of the core consisted of dry-blending the enriched boron and iron powder for 2 hr, cold-pressing at 33 psi, sintering at 1120°C for 1 hr in a dry purified hydrogen atmosphere and coining to final dimensions at 33 psi.

Billets were assembled by using the conventional picture-frame technique, in which boron-containing core is fitted into a rectangular hole machined into the stainless steel frame, to which a tube is attached for evacuating the billet subsequent to welding cover plates to the frame. After evacuation the tube is sealed and the billet is rolled to plate at 1100°C with a 10% reduction per pass and a total reduction of 91%. The billet is partially protected from excessive oxidation by preheating and reheating in a hydrogen muffle during the rolling sequences. After being stress relieved at 900°C, the plates are radiographed, machined to size, and welded into the absorber section shown in Fig. 179.

Irradiation-Testing of Stainless Steel Clad Plates Containing Boron Dispersed in Electrolytic Iron

C. F. Leitten

The boron-bearing material recently being considered as the poison in the APPR-1 control rod consists of a 3.2 wt % elemental boron dispersion in iron which is prepared by powder metallurgy and clad with 0.030-in. wrought type 304L stainless steel. The boron is enriched boron containing 92% B^{10}. A series of miniature plates has been prepared and an irradiation testing program in the MTR, as listed in Table 71, has been initiated. In the event that there is no irradiation damage to the specimen irradiated at 60% burnup of B^{10}

TABLE 70. SUMMARY OF APPR STATIC AUTOCLAVE TESTS

Temperature, 295°C; pressure, 1200 psi
Distilled and demineralized water: pH, not less than 6; total dissolved solids, 2 to 3 ppm
Resistivity, not less than 0.3 megohm-cm.

Environment No.	Additions	
	Hydrogen (cc/liter)	Oxygen (cc/liter)
1	0.0	1.0
2	50.0	1.0
3*	25.0	1.0

Category	Specimen Description	Environment No.	Exposure Time (hr)	Weight Change** (mg/cm^2)
Clad plate with holes drilled in clad	34 wt % UO_2–0.5 wt % B_4C in iron matrix	2	100	+0.13
	Same	2	500	+0.11
	34 wt % UO_2–0.5 wt % B_4C in pre-alloyed stainless steel	2	100	+0.19
	Same	2	500	–0.03
Unclad specimens of as-rolled core	34 wt % UO_2–0.5 wt % B_4C in pre-alloyed stainless steel matrix	2	10	–0.10
	Same	2	25	–0.17
	Same	2	50	+0.09
	Same	2	100	–0.03
Clad specimens with edges exposed	Iron plate clad with stainless steel	2	100	–1.0
	Same	2	500	–0.88
	34 wt % UO_2–0.5 wt % B_4C in iron matrix clad with stainless steel	2	100	+0.15
	Same	2	500	+0.47
	Elemental stainless steel plate clad with stainless steel	2	100	–0.07
	Same	2	500	–0.09
	34 wt % UO_2–0.5 wt % B_4C in elemental stainless steel matrix	2	100	Negligible
	Same	2	500	+0.02
	34 wt % UO_2–0.5 wt % B_4C in pre-alloyed stainless steel matrix	2	100	+0.30
	Same	2	500	+1.17
	Prealloyed stainless steel plate clad with stainless steel	2	100	–0.11
	Same	2	500	–0.05

TABLE 70 (continued)

Category	Specimen Description	Environment No.	Exposure Time (hr)	Weight Change** (mg/cm^2)
Brazed joints of 304L stainless steel	Coast Metals NP braze alloy	1	720	Negligible
	GE 81 braze alloy	1	720	Zero
	Low melting Nicrobraze alloy	1	720	Negligible
	GE 75 braze alloy	1	720	+0.26
	Pd-Ni-Si braze alloy	1	720	Negligible
	80% Cu–20% Ni braze alloy	1	720	+0.11
	85% Cu–15% Ni	1	720	Negligible
	90% Cu–10% Ni	1	720	+0.09

*Environment No. 3 results not yet available.

**The weight change noted for the specimens in categories 1–3 are based upon delivered weights, and those in category 4 are based upon as-scrubbed weights.

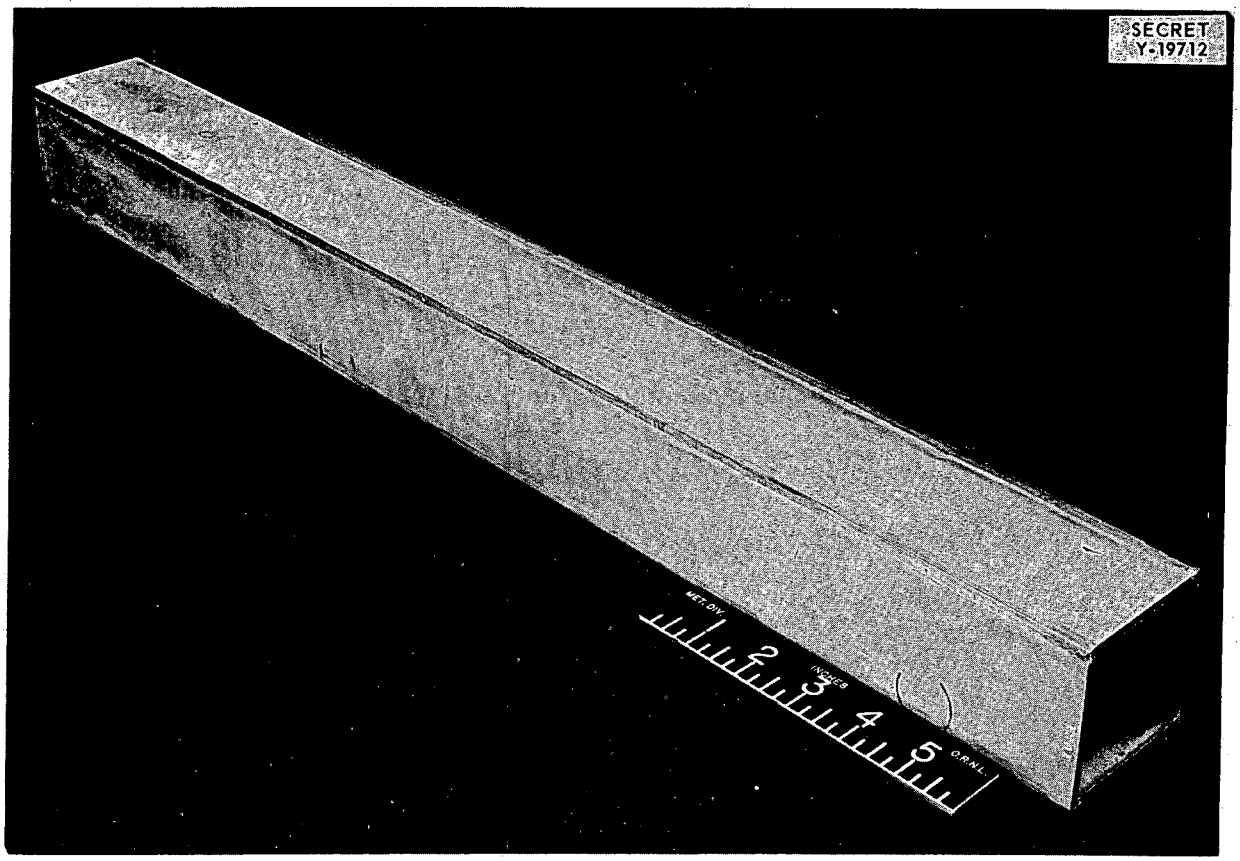

Fig. 179. APPR-1 Welded Absorber Section.

TABLE 71. IRRADIATION-TESTING OF MINIATURE COMPOSITE PLATES CONSISTING OF A DISPERSION OF ENRICHED ELEMENTAL BORON IN AN IRON MATRIX, CLAD WITH WROUGHT TYPE 304L STAINLESS STEEL

Sample No.	Per Cent B^{10} of APPR* Design Loading	Burnup of B^{10} Atoms (at. %)
1**	100	20
2**	100	40
3**	100	60
4**	100	80
5**	100	90
6	60	60
7	60	90
8	120	60
9	120	90

*The designed B^{10} loading for APPR-1 is 14.1 g per plate or 2.86 wt % B^{10} in the core mixture.

**Sampler in test at MTR.

atoms, a full size absorber section of this combination of materials will be substituted for the cadmium section in the MTR shim rod and tested in the active lattice of the MTR.

FOREIGN REACTOR FUEL ELEMENT PROGRAM

R. J. Beaver J. A. Milko
J. H. Erwin W. C. Thurber

The specification that uranium for foreign application be limited to 20% enrichment in the U^{235} isotope has created need for development of a reliable fuel alloy or a dispersion for the conventionally designed curved-plate MTR-type research reactor. Fabrication difficulties were experienced at ORNL with the UO_2-aluminum dispersion-type fuel element which was manufactured for the Geneva Conference Reactor. A program has been initiated at ORNL with the purpose of selecting a material which will be reliable and suitable for manufacturing aluminum fuel elements for foreign reactors. The program includes investigation of the following alloys or dispersions which are to contain 45 to 55 wt % uranium: uranium-aluminum alloy, UC and UC_2 dispersions in aluminum, UO_2 dispersions in aluminum, U_3O_8 dispersions in aluminum, and UAl_2 dispersions in aluminum.

Considerable emphasis has been placed on and progress has been made with the uranium-aluminum alloy containing 48 wt % uranium. Preliminary work has been initiated to determine the compatibility of the uranium carbides with aluminum. Although it is possible to manufacture fuel elements which contain a dispersion of UO_2 in aluminum, the fundamental cause of the dimensional instability which occurs during elevated-temperature heat treatments is not known, and efforts are being directed toward resolving this problem. The compounds U_3O_8 and UAl_2 have the disadvantage of lower concentration of uranium; however, their compatibility with aluminum is to be determined.

Melting and Casting of a Nominal 48 wt % Uranium–Aluminum Alloy

J. H. Milko

Investigations have been initiated to determine the effect of solidification rate, as influenced by the graphite mold size, on segregation in this alloy. Dimensions of the cylindrical graphite molds are listed in Table 72. All melts were prepared and cast in air. Pertinent results are listed in Table 73, and microstructures are illustrated in Fig. 180. The locations of the various samples are shown in Figs. 181 and 182. These results indicate the following:

1. The greatest variation in the uranium content may be expected in the central longitudinal section of the cast cylinders.
2. The transverse variation in the uranium content within any position of the height of the cylinders is rather small.
3. The most rapid solidification occurs with a mold wall thickness of 2 in. Beyond this value, the increase in solidification rate may not be increased appreciably.
4. Small grain size may be obtained with a mold wall thickness of 2 in.
5. Although there appears to be a trend of more segregation with a more rapid solidification, as evaluated by the average spread, this trend may not be correct because of the influence of suspected gas porosity.

TABLE 72. PERTINENT DATA OF FOUR CASTINGS PRODUCED IN GRAPHITE MOLDS

Casting Designation	Mold Dimensions (in.)				Wall Thickness (in.)	Volumes (in.^{3})		Areas (in.^{2})		Time to Reach 625°C (min)
	ID	Internal Height	OD	Outer Length		Metal	Graphite	Mold Cavity	Outer Surface	
S-1	3	8	4	8½	½	56.52	50.24	82.46	123.76	7.49
S-2	3	8	5	9	1		120.10		173.56	3.44
S-3	3	8	7	10	2		328.13		289.78	0.87
S-4	3	8	9	11	3		642.92		331.12	0.84

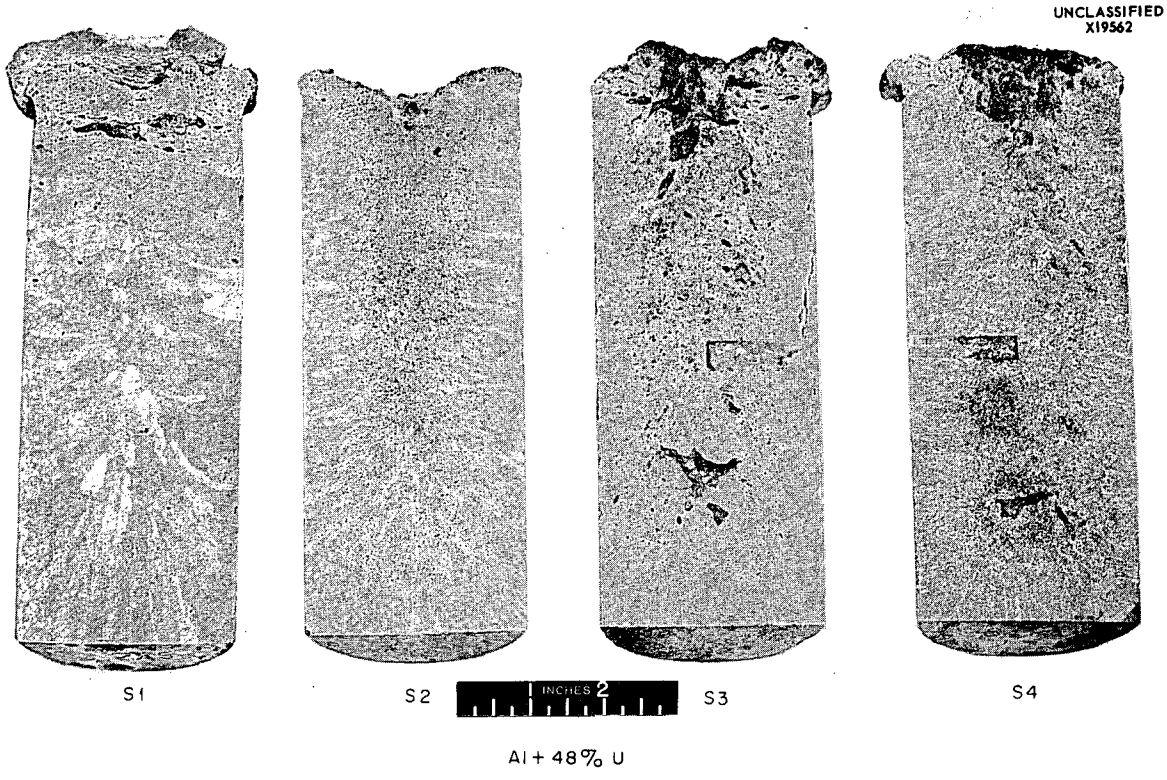

Fig. 180. Microstructures of Sectional Cylinders Produced in Molds of Dimensions as Given in Table 72.

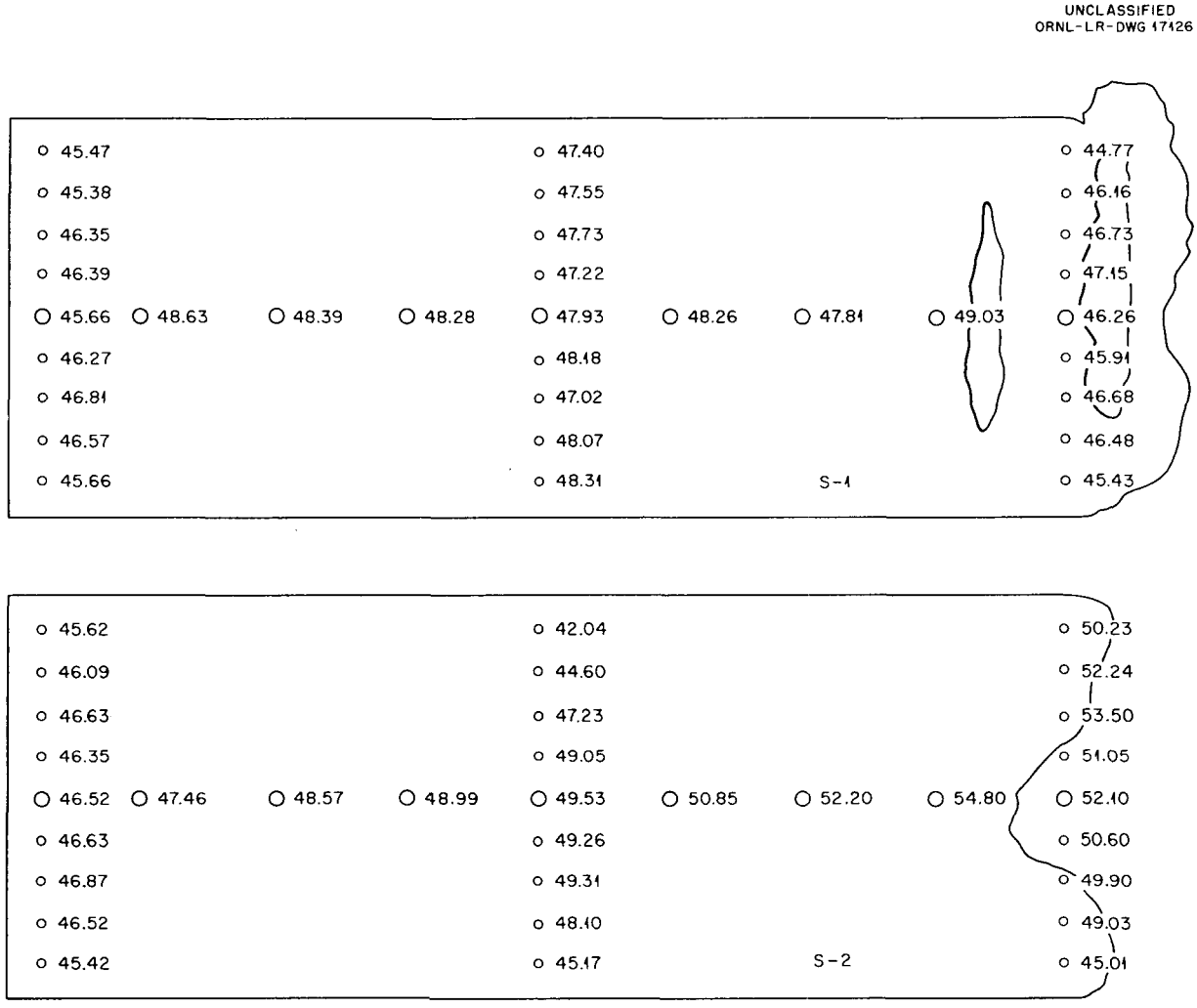

Fig. 181. Drilling Pattern and Uranium Contents of Sectional Cylinders S-1 and S-2, Produced in Molds Having Dimensions as Given in Table 72.

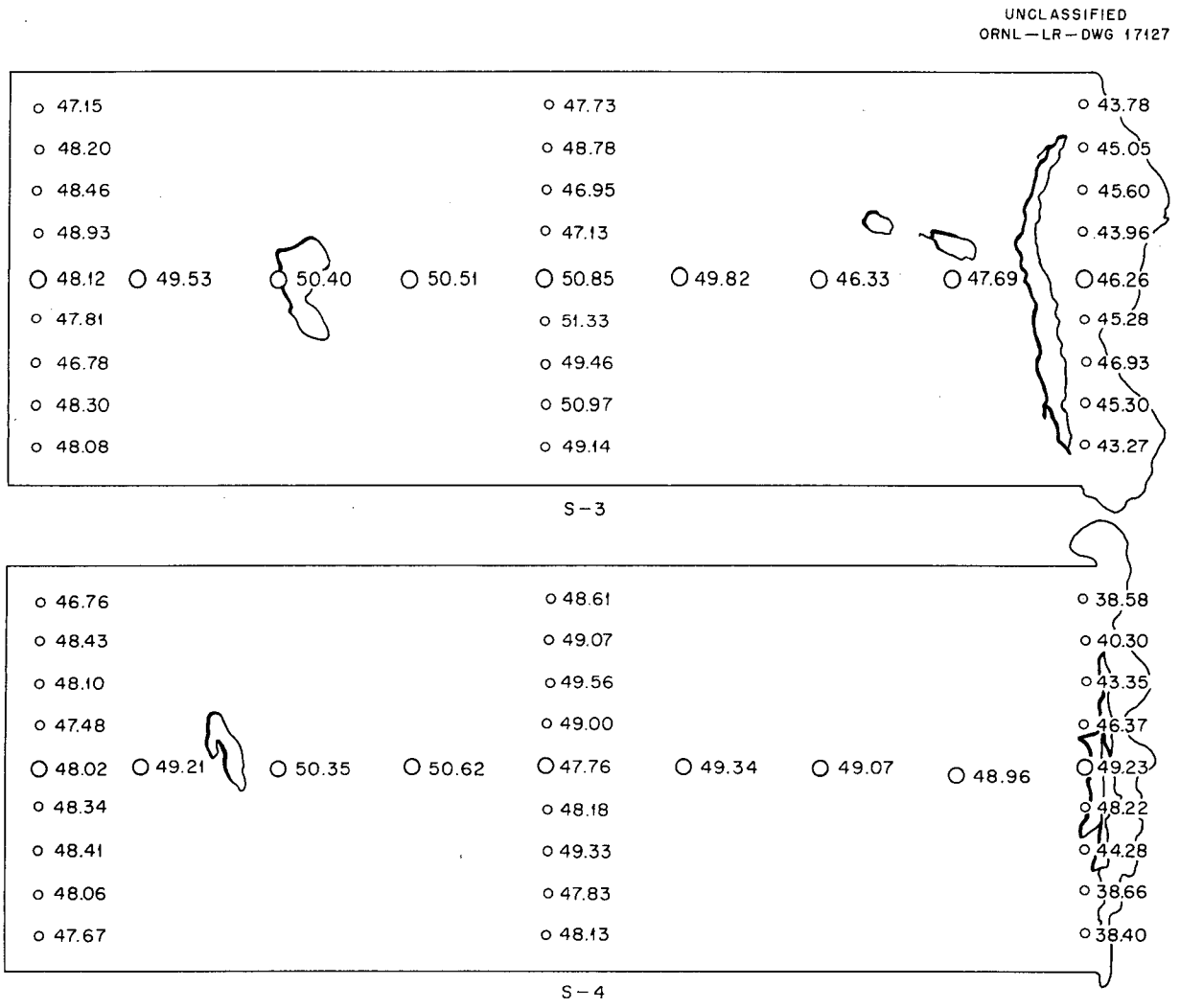

Fig. 182. Drilling Pattern and Uranium Contents of Sectioned Cylinders S-3 and S-4, Produced in Molds Having Dimensions as Given in Table 72.

TABLE 73. VARIATION OF URANIUM CONTENT IN FOUR CASTINGS WHOSE MOLD WALL THICKNESS VARIED FROM ½ TO 3 in.

	Casting Designation			
	S-1	S-2	S-3	S-4
Mold temperature, °C	65			
Pour temperature, °C	1175			
Mold wall thickness, in.	½	1	2	3
Time to 625°C, min	7.49	3.44	0.87	0.84
Uranium content, wt %				
Entire casting				
Maximum	49.03	54.80	51.33	50.62
Minimum	44.77	45.01	43.27	38.40
Spread	4.26	9.79	8.06	12.22
Average	46.95	48.41	47.69	47.08
Longitudinal center				
Maximum	49.03	54.80	50.85	50.62
Minimum	45.66	46.52	46.26	48.02
Spread	3.37	8.28	4.59	2.60
Average	47.80	50.11	48.83	49.07
¼ in. from bottom				
Maximum	46.91	46.86	48.93	48.43
Minimum	45.38	45.42	47.15	46.76
Spread	1.43	1.44	1.78	1.67
Average	46.06	46.29	47.98	47.92
4¼ in. from bottom				
Maximum	48.31	49.53	51.33	49.56
Minimum	47.02	42.04	47.13	47.76
Spread	1.29	7.49	4.20	1.80
Average	47.65	47.14	49.15	48.61
8¼ in from bottom				
Maximum	47.15	53.50	46.93	49.23
Minimum	44.77	45.01	43.27	38.40
Spread	2.38	8.49	3.66	10.83
Average	46.28	50.41	45.05	43.04
Average spread*	2.55	7.10	4.46	5.82

*Average of 5 spreads in the various locations of the casting.

Manufacturing of Fuel Element Containing 48 wt % Uranium–Aluminum Alloy

J. H. Erwin

Efforts have been directed to fabricate composite fuel plates and braze assemblies in a manner similar to that presently used in manufacturing the conventional MTR-type fuel element. Two principal problems have been encountered, namely, (1) serious thinning of the type 1100 aluminum cladding and (2) erratic bonding when high-strength alloys are substituted for the type 1100 aluminum cladding material. Because of the difference in plasticity between the 48 wt % uranium–aluminum alloy and the type 1100 aluminum cladding at the hot-rolling temperature of 580°C, the nominally 0.016-in.-thick cladding reduces to as low as 0.002 in. in localized areas above the ends of the rolled core. This condition is markedly improved by the substitution of higher-strength type 6061 or 6951 aluminum as the cladding material and a decrease in the total reduction in thickness ratio from 6/1 to 5/1. However, with the substitution of the materials at these total reduction values, erratic bonding results in pronounced blisters, which frequently occur during brazing of the fuel elements. Efforts are being directed to roll-clad the alloy cover plate and frame material with type 1100 aluminum, so that during roll-bonding of the composite fuel plate, the bonding process will be confined to type 1100 aluminum surfaces.

Extrusion of 48 wt % Uranium–Aluminum Alloy

J. H. Erwin

Excessive edge-cracking has been experienced in hot-rolling slabs of nominal 48 wt % uranium–aluminum alloy to plate material from which fuel cores may be punched. Although this difficulty has been markedly minimized by framing the alloy in type 1100 aluminum, a more attractive method for obtaining fuel core material appears to be extrusion of cylindrical billets into flat plates. Preliminary work has revealed that ¾-in.-dia rods of this material can be readily extruded from 3-in.-dia × 6-in.-long billets at a temperature of

510°C and a pressure of approximately 65 tsi through a bellmouthed die with an entrance at 90 deg included angle. Lubricants consisted of Necrolene in the container and powdered lead on the die face. Microstructure of the extruded alloy is illustrated in Fig. 183 and may be compared with the rolled alloy shown in Fig. 184.

SPERT B DEVELOPMENT

R. J. Beaver J. H. Erwin

Efforts have been made to manufacture an aluminum fuel element for the SPERT B program at Phillips Petroleum Co. (PPCO) which is stronger than previous aluminum fuel elements and which permits insertion and removal of several of the fuel plates. The fuel element is to contain four flat fixed plates, brazed into position, with sufficient additional grooves in the side plates to permit insertion or removal of 20 additional plates. The age-hardenable type 6061 aluminum alloy has been substituted for type 1100 aluminum as the side plate material in the fuel element and for the cladding material of the fuel plate. Considerable difficulty has been experienced with erratic bonding between types 1100 and 6061 aluminum while roll-cladding fuel plates by using a 6/1 reduction in thickness. Roll-cladding the type 6061 aluminum cover plates with type 1100 aluminum confines bonding of the composite fuel plate to type 1100 aluminum surfaces and has resulted in satisfactorily bonded plates. Experimental fuel elements have been brazed and quenched in air with no appreciable distortion, and the aluminum alloy has been age-hardened to tensile strengths approaching 32,000 psi. Water-quenching resulted in severe distortion of the fuel element.

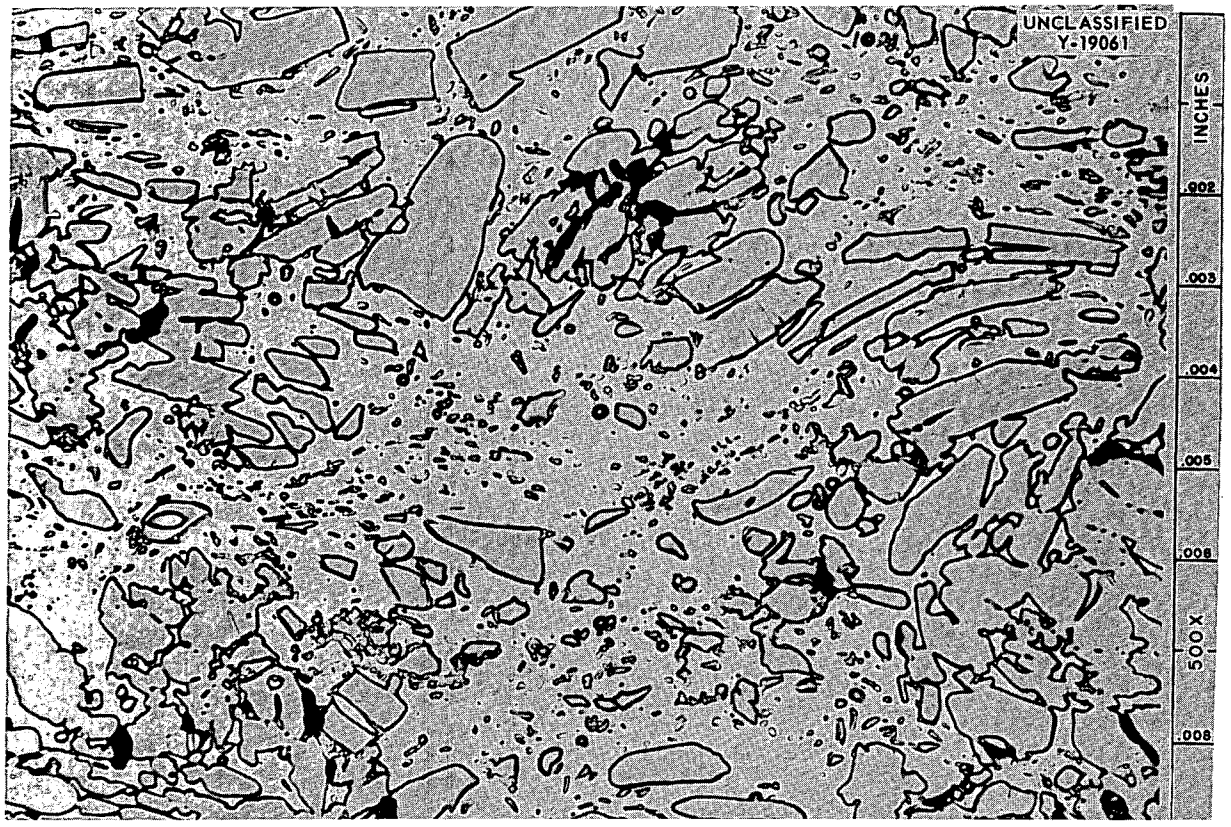

Fig. 183. Aluminum–42 wt % Uranium Alloy Extruded at 950°F, 16/1 Reduction Ratio. 500X. Reduced 2%.

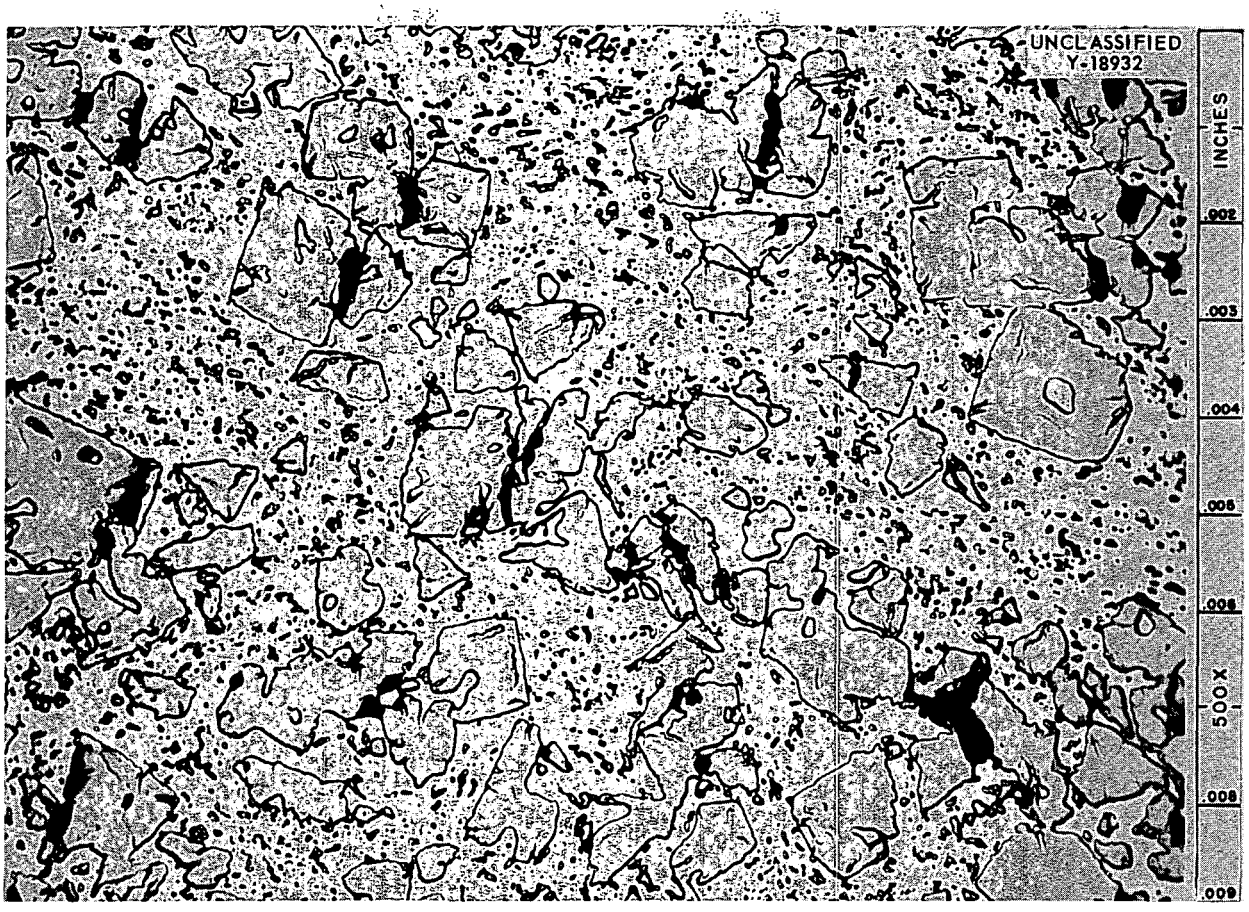

Fig. 184. Aluminum–42 wt % Uranium Alloy Hot Rolled at 1100°F, 16/1 Reduction Ratio.

HIGH-STRENGTH ALUMINUM FUEL ELEMENTS

J. H. Erwin

One of the sources of difficulties with the aluminum MTR-type fuel element is the softness of the type 1100 aluminum as a result of the extended elevated-temperature heat treatments and brazing cycle. Consequently the material is prone to damage during handling in the reactor and to possible distortion under differential pressure conditions. Results have been obtained from pressure-testing of fuel elements in which types 5050 and 6951 aluminum alloys were substituted for the conventional type 1100. The design data and test results are listed in Tables 74 and 75, respectively. It is apparent that the IDX-11 fuel element compares quite favorably with IDX-8, the predecessor of the present MTR Mark XI element, and appears to offer higher strength, 15% reduction in aluminum, and 23% reduction in the metal-to-water ratio when compared with the present MTR fuel element. After five months in the BSF water, IDX-10 element showed no greater attack than the type 1100 aluminum BSR fuel elements. The fuel element is illustrated in Fig. 185.

MANUFACTURE OF FUEL ELEMENTS CONTAINING 10 wt % PLUTONIUM–ALUMINUM ALLOY

R. J. Beaver J. H. Erwin

A cooperative program has been undertaken by Los Alamos Scientific Laboratory and ORNL to manufacture six fuel elements containing plutonium in the form of a 10% plutonium–aluminum alloy for irradiation in the MTR. The fuel elements are similar to the MTR fuel elements, with nearly identical manufacturing procedures. Los Alamos has prepared evacuated aluminum billets, containing the Pu-Al alloy core, which ORNL has successfully fabricated into composite plate. Some difficulty was experienced in meeting plate

TABLE 74. DESIGN DATA OF MTR-TYPE FUEL ELEMENTS

Unit No.	Aluminum Type		Thickness (in.)	Groove Depth (in.)	Fuel Plates		
	Side Plate	Fuel Plate			Number	Thickness (in.)	
						Top and Bottom	Intermediate
IDX-7*	1100	1100	0.125	0.071	18	0.060	0.060
IDX-8*	1100	1100	0.187	0.057	19	0.075	0.050
IDX-10	6951	5050	0.125	0.071	18	0.060	0.060
Mark XI	1100	1100	0.187	0.087	19	0.065	0.050
IDX-11	6951	5050	0.102	0.048	19	0.050	0.050
IDX-12	6951	5050	0.102	0.048	20	0.045	0.045

*J. P. Sanders, *Deformation of MTR Fuel Element in Static Pressure Tests*, ORNL CF-55-4-24 (May 9, 1955).

UNCLASSIFIED
Y-19746

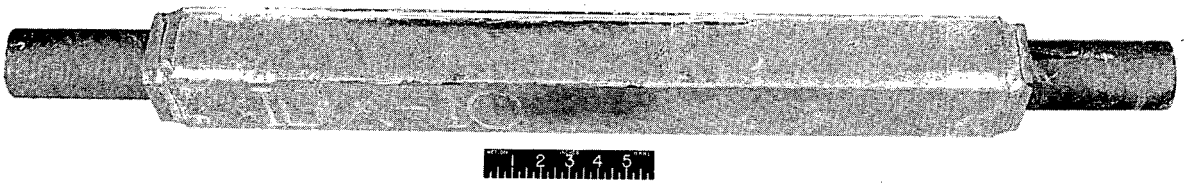

Fig. 185. IDX-10 Fuel Unit After Five Months in the BSF Pool.

TABLE 75. DEFLECTION OF MTR-TYPE FUEL ELEMENTS UNDER STATIC PRESSURES

Unit No.	Deflection (mils) at Indicated Pressure (psi)							
	5	10	15	17.5	20	25	30	0*
IDX-7**	4	14	75					17
IDX-8**	5	7	13	22	36			10
IDX-10	5	9	16	17	21	28	37	6
IDX-11	5	11	16	18	23			1
IDX-12	10	17	32	36	45			9

*Permanent set in unit after removal of the pressure.

**J. P. Sanders, *Deformation of MTR Fuel Element in Static Pressure Tests*, ORNL CF-55-4-24 (May 9, 1955).

dimensional tolerances because of the apparent softness of the 10% Pu–Al alloy compared with the 10% U–Al alloy.

DEVELOPMENT OF ALUMINUM-BORON BINARY ALLOYS AND ALUMINUM-URANIUM-BORON TERNARY ALLOYS FOR APPLICATION IN ALUMINUM FUEL ELEMENTS

R. J. Beaver J. A. Milko
W. C. Thurber

Alloy Development

Casting techniques for preparing homogeneous boron-aluminum cladding alloys and uranium-boron-aluminum core alloys for MTR-type fuel elements have been advanced during the current period.

Previous work[3] had indicated that finely divided AlB_{12}, both loose and compacted with aluminum powder, was unsatisfactory as a boron addition in uranium-boron-aluminum alloy fuel element cores. However, nickel-boron master alloys containing about 12 wt % boron have shown considerable promise as an alloying addition – both in the core and cladding material. Aluminum-boron alloys containing 2 to 5 wt % boron were successfully used in preparing cladding alloys.

The nickel-boron master alloy was prepared by arc-melting, under argon, pressed and sintered compacts of the elemental powders. The aluminum-boron master alloy was obtained from a commercial vendor.

Five core-alloy castings having the nominal composition 17% U–0.22% B–1.61% Ni–bal aluminum and three cladding-alloy castings having the nominal composition 0.10% B–0.73% Ni–bal aluminum were made by using the nickel-boron master alloy as a melt addition. One casting of each composition was poured into a horizontal slab mold fed from one end, while the remaining six slabs were poured into vertical molds fed from the top. With the exception of the U-B-Ni-Al alloy poured in the horizontal plane, good boron recovery and a high index of homogeneity[4] were manifest in every case as indicated in Table 76.

[3]W. C. Thurber and J. A. Milko, *Met. Semiann. Prog. Rep. April 10, 1956*, ORNL-2080, p 162.

[4]The index of homogeneity is an empirical value based on deviation of individual analyses from the mean boron content of the billet. Perfect homogeneity = 100.

TABLE 76. EVALUATION OF ALLOYS PREPARED WITH Ni-B ADDITIONS

Alloy	Boron Recovery (%)	Index of Homogeneity
U-B-Ni-Al	91	88
U-B-Ni-Al	83	78
U-B-Ni-Al	91	92
U-B-Ni-Al	90	92
U-B-Ni-Al[a]	61	50
B-Ni-Al	94	93
B-Ni-Al	92	74
B-Ni-Al[a]	85	96

[a]Horizontally cast slabs.

Sixteen castings of cladding alloy having the nominal composition 0.10% boron–balance aluminum were prepared by using aluminum-boron master alloys. Evaluation of these alloys is indicated in Table 77. It should be noted that both recovery and index of homogeneity are high and occasionally free from any erraticity. Although the recovery figure is reported as 100% in a majority of cases, the calculated recovery of boron was found to be actually greater than 100%. This discrepancy was probably due to segregation of boron in the master alloy.

TABLE 77. EVALUATION OF ALLOYS PREPARED WITH Al-B ADDITIONS

Alloy	Recovery (%)	Index of Homogeneity
Al + B	74	90
	82	99
	98	86
	100	87
	99	93
	100	94
	100	96
	100	92
	100	94
	100	98
	100	99
	100	96
	100	94
	100	94
	100	95
	100	84

Corrosion Testing

To evaluate the corrosion performance of cladding alloys containing boron, static corrosion tests in distilled water are being performed on boron-aluminum and boron-nickel-aluminum alloys. Two groups of samples are being tested. Group I samples received 75% cold-reduction, while group group II samples received a heat treatment analogous to that which MTR fuel plates receive.

Preliminary results of these tests are summarized in Table 78. After 1500 hr in distilled water all group I samples exhibited pitting and blistering. Blistering was also observed on group II samples after 200 hr under the same conditions. Group II samples tested for 200 hr in 60°C distilled water showed no blistering.

TABLE 78. STATIC CORROSION OF ALUMINUM ALLOYS IN DISTILLED WATER

Material	Composition	Temperature (°C)	Time (hr)	Weight Gain (mg/cm^2)	Comments
			Group I*		
Al + NiB	0.066% B, 0.75% Ni	100	1500	0.3, 0.3	Pitting and blistering
Al + NiB	0.152% B, 0.75% Ni	100	1500	0.4, 0.3	Pitting and blistering
Al + AlB	0.062% B	100	1500	0.3, 0.3	Pitting and blistering
Al + AlB	0.063% B	100	1500	0.3, 0.3	Pitting and blistering
1100 Al		100	1500	0.3, 0.3	Negligible attack, no blistering
			Group II**		
Al + NiB	0.091% B, 0.80% Ni	60	200	0.04, 0.05	Negligible attack
Al + NiB	0.091% B, 0.80% Ni	100	200	0.11, 0.12	Some blistering
Al + AlB	0.078% B	60	200	0.04, 0.06	Negligible attack
Al + AlB	0.078% B	100	200	0.04, 0.07	Some blistering
1100 Al		60	200	0.04, 0.04	Negligible attack

*Specimens cold-rolled about 75%.

**Specimens received simulated MTR heat treatment.

Irradiation Testing

An MTR prototype aluminum fuel element, in which boron was incorporated in the cladding of the fuel plates, was manufactured and delivered to the MTR for irradiation testing. Fabrication procedures were analogous to the conventional procedures for manufacturing MTR fuel elements. It was apparent during processing of this element that the aluminum-boron alloy cladding material was more prone to blistering than type 1100 aluminum. Eight per cent of the fuel plates fabricated was rejected for this reason. The concentration of the boron in the alloy clad varied from 0.82 to 0.14 wt %. The element contained a total of 1.92 g of boron.

METALLURGICAL MATERIALS AND PROCESSING

E. S. Bomar

R. E. Adams E. M. Benson
J. I. Federer

THORIUM – THE METALLEX PROCESS

E. S. Bomar

Consolidation Experiments

Thorium, amounting to about 35 lb of metal, was obtained from amalgam prepared by the Metallex process. Fifteen pounds of the metal was melted in a nonconsumable-electrode furnace at Armour Research Foundation to obtain information on the behavior of the metal in this type of equipment. The material is reported to have responded well to this treatment and to have formed a billet with a density of 11.45 g/cc. Only traces of mercury were observed to have collected in the furnace. The resulting 3-in.-dia billet was extruded into a $\frac{7}{8}$-in.-dia rod. The remaining 20 lb of thorium was hot-pressed in a manner similar to that described previously.[1] A 3-in.-dia extrusion billet was machined from the hot-pressed compact and then extruded into $\frac{7}{8}$-in. rod. This rod is scheduled for use as a consumable electrode in a melting experiment at Armour Research Foundation.

Retorting Experiments

The conclusion that the evolution of the uncombined mercury is accomplished without damage to compacts at heating rates as high as 12°C/min may be in error. The conclusion was based on the absence of a volume change when the samples were heated to 500°C in vacuum. Recent retorting runs of a $3\frac{1}{4}$-hr holding period at temperatures ranging from 90 to 240°C show that samples held at 140°C have fewer external flaws.

Transfer of iron, nickel, and chromium from the stainless steel container to the thorium charge was found not to occur during the retorting cycle.

Since a eutectic exists at 860°C in the iron-thorium system, it is necessary to isolate the thorium-bearing charge from the steel retort. Based on their too-high cost, their too-low melting points, or the presence of low-melting eutectics in the binary system with iron or thorium as a gage of usability for a container material, all elemental materials but silicon, vanadium, chromium, cobalt, niobium, molybdenum, tantalum, and tungsten were eliminated as potential liner materials. The relative suitability of these metals for use as liners was tested by retorting samples of thorium amalgam in contact with specimens of the above elements, then removing the bottom portion of each of the resulting thorium samples for chemical analysis. The silicon-thorium couple was an exception because these metals melted together. The analytical results are presented in Table 79. The last column in the table takes into account the variation in thermal-neutron absorption cross sections of the several metals.

Of the metals examined, tungsten and tantalum are the most inert in contact with thorium.

Future Work

The effort on the Metallex program has been further reduced, and the behavior of 5-in.-dia compacts will not be examined. A Metallex thorium rod will be used for a consumable-electrode arc-melting experiment. Continued support will be given to the Chemical Technology Division's laboratory work.

METALLURGICAL PROCESSING OF SPENT FUEL ELEMENTS

R. E. Adams

Carburization

Certain limitations in application of carburization as an aid to recovery of unburned uranium from spent stainless steel fuel elements have been observed. Two different methods were previously examined for treating the type 304 stainless steel elements used in earlier carburization experiments.[2] APPR elements being made at present contain a core made with type 302B stainless steel and are clad with type 304 stainless steel. Table 80 shows that, following similar carburizing and sensitizing treatments, the method based on

[1] E. S. Bomar, *Met. Semiann. Prog. Rep. April 10, 1956*, ORNL-2080, p 179.

[2] R. E. Adams, *Met. Semiann. Prog. Rep. April 10, 1956*, ORNL-2080, p 181.

TABLE 79. EVALUATION OF POTENTIAL LINER MATERIALS FOR USE IN RETORTING THORIUM AMALGAMS

Contact time: 1 hr
Contact temperature: 1200°C
Atmosphere: Vacuum of 0.04 μ

Metal	Method of Analysis	Amount of Metal in Thorium Sample (ppm)	$\frac{\sigma_a \times \text{ppm}}{\text{Atomic weight}}$
V	Colorimetric	28	2.6
Cr	Colorimetric	190	10.6
Co	Colorimetric	20	10.8
Nb	Spectrographic	36	0.4
Mo	Colorimetric	36	0.9
Ta	Activation	<0.10	<0.01
W	Activation	<0.01	<0.001

TABLE 80. DISTRIBUTION OF URANIUM AND STAINLESS STEEL AFTER TESTS ON AN APPR FUEL ELEMENT MATERIAL

Sample preparation: Carburized for 20 min at 1000°C
Homogeneized for 2 hr at 1150°C
Sensitized for 2 hr at 650°C
Carbon content, 0.3–0.5%

	Per Cent of Fuel Element Material Recovered					
	Type 304 Core*		Type 302B Core**			
			Test No. 1		Test No. 2	
	Uranium	Stainless Steel	Uranium	Stainless Steel	Uranium	Stainless Steel
$CuSO_4 + H_2SO_4$ corroding solution	0.1	6.7	0.2	4.1	0.6	6.5
HNO_3 leaching solution	99.0	11.2	78.1	0.6	87.2	2.2
Solids	0.9	82.1	21.7	95.3	12.2	91.3

*Nominal composition: 18–20% Cr, 8–11% Ni, 2% max Mn, bal Fe.
**Nominal composition: 17–19% Cr, 8–10% Ni, 2% max Mn, 2–3% Si, bal Fe.

intergranular corrosion gives much lower uranium recoveries from the type 302B cores than from the type 304 cores.

DISSOLUTION IN TIN

J. I. Federer

Selective dissolution in tin and other molten metals is being examined as a possible means of recovering appreciable quantities of the non-fissionable metal contained in fuel elements as solids and the uranium in a nitric acid soluble form suitable for solvent extraction. This would result in a reduction in volume of the feed stream to the solvent-extraction column and recovery of a large portion of the waste in a form more suitable for permanent disposal than is possible with a

liquid. The aluminum-uranium fuel element was selected for the initial work.

The solubility of uranium in pure tin is reported[3] to be less than 0.01 wt % at 650°C. Since the solubility of aluminum in tin is about 75 wt % at 650°C, the possibility exists that the aluminum portion of a fuel element could be dissolved, leaving the uranium in suspension for removal by filtration. In practice, however, the solubility of uranium in tin-aluminum alloy increases with the aluminum concentration. Experiments have been performed on aluminum alloys containing 4 wt % of uranium. Figure 186 shows the dependence of uranium recovery on the aluminum content of the bath. Whether the scatter in the data was due to inadequate control of a sensitive metallurgical variable or to difficulties encountered in the chemical analyses was not determined. The trend to higher losses of uranium with increasing percentage aluminum in the bath and increased filtration temperature is apparent. X-ray diffraction patterns of the residue on the filter showed that the uranium is present in the bath as USn_3.

The aluminum content of the tin bath was reduced to 0.8 wt % by a second filtration at 275°C. The tin could then be recycled for additional aluminum-uranium alloy dissolution.

Dissolution experiments with zirconium in tin and zirconium in bismuth were also performed. The tentative phase diagram for zirconium-tin

[3] R. W. Buzzard and H. E. Cleaves, *J. Met.* and Ceramics 1, 25(1948); *Binary Alloys of Uranium*, TID-65, p 44 (July 1948).

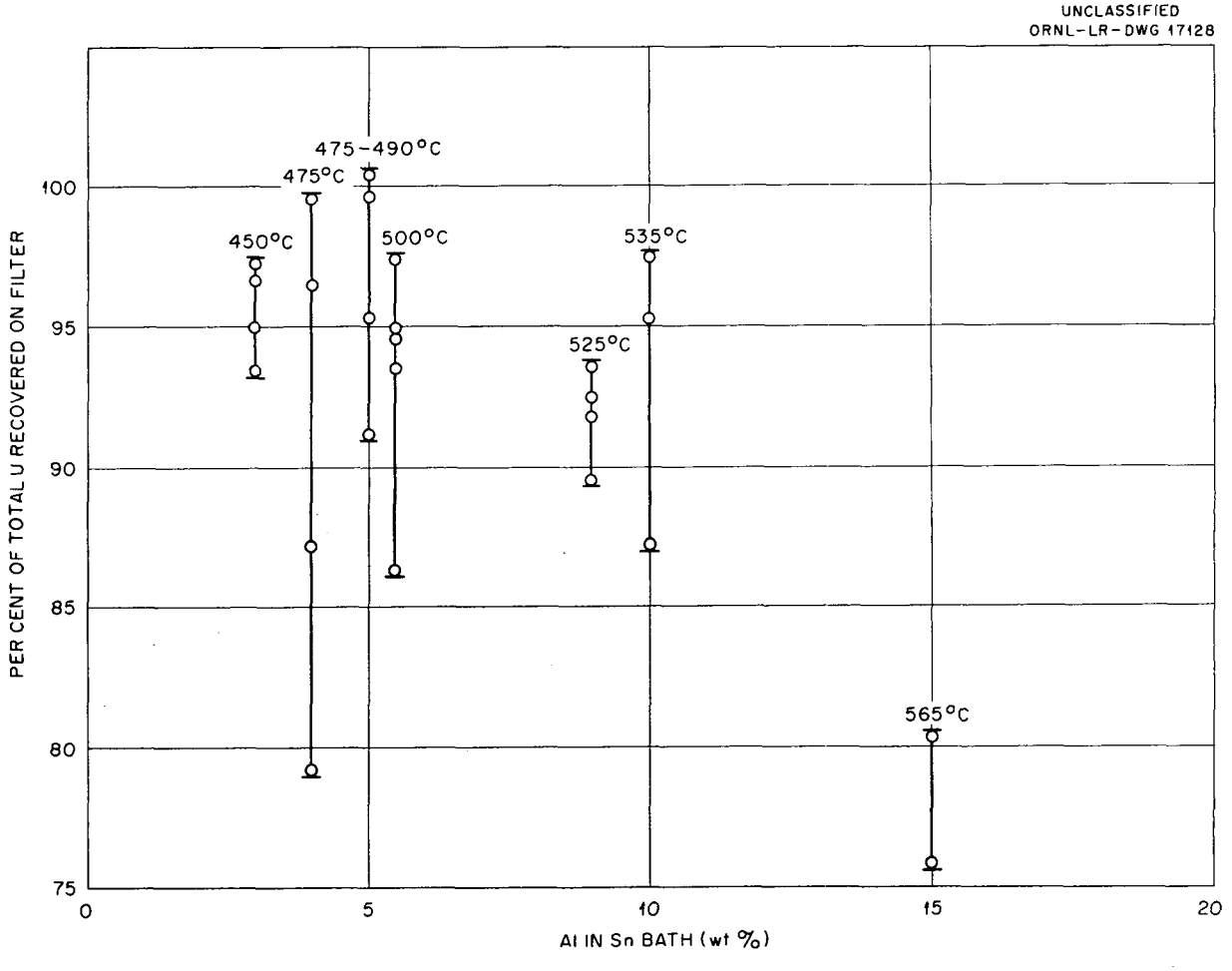

Fig. 186. Recovery of Uranium from Al-Sn-U Baths by Filtration.

shows a single liquid phase for 5 wt % zirconium in tin at temperatures greater than 500°C.[4] However, zirconium sufficient to form a 5 wt % alloy did not dissolve in tin even upon holding for 95 hr at 1000°C.

A solution of 5 wt % zirconium in bismuth was formed after 24 hr at 1000°C. Increasing the surface-to-volume ratio of subsequent zirconium samples by a factor of 8 led to almost complete dissolution in a bismuth bath after 24 hr at 600°C.

[4] *Phase Diagrams of Zirconium-Base Binary Alloys; A Study of the Systems of Zirconium with Tin, Molybdenum, Copper, Wolfram, Chromium, Silicon, Aluminum, and Magnesium; Final Report January 1, 1951–March 31, 1952,* Armour Research Foundation of Illinois Inst. Technol. COO-89, (April 14, 1952).

METALLOGRAPHY

R. J. Gray

R. S. Crouse
E. L. Long
T. M. Kegley
D. F. Stoneburner
J. R. Riddle
J. E. Van Cleve

METALLOGRAPHIC EXAMINATION OF HIGH-VELOCITY HEAT EXCHANGER (SHE NO. 1)

R. J. Gray

A small heat exchanger was built and operated by a group in the Aircraft Reactor Engineering Division to study conditions that might be encountered in the intermediate heat exchanger of the Aircraft Reactor Test (ART).[1] The small heat exchanger (SHE No. 1) was used to determine heat transfer characteristics, pressure drop characteristics, and corrosion and mass transfer effects as found in a multiple tube, fluoride salt–NaK, high-velocity heat exchanger.

The heat exchanger operated for a period of 1648 hr with a fluoride salt (fuel) and NaK. For the study of mass transfer effects, a wide temperature differential was maintained during the last 456 hr of its operation.

Following its operation, the heat exchanger, shown in Fig. 187, was sectioned for metallographic examination. The principal parts in the examination were the NaK-carrying Inconel tubes, identified by name in Fig. 188; principal areas of examination are identified as A, B, C, D, and E. The tubes were carefully cut into samples of suitable size and mounted in a non-pressure-setting plastic for metallographic grinding and polishing. Area A (Fig. 187) is shown in Fig. 189, with the fuel and NaK flow directions indicated. A sectioned view of area A is shown in Fig. 190. It was immediately noticeable that the inside surface of the tube in this area had been brightened by a reaction with the NaK flowing through the tubes. The NaK outlet temperature in this area was approximately 1495°F during the last 456 hr of test.

A photomicrograph made directly on the inner surface in contact with the NaK is shown in Fig. 191. The rate of attack is much deeper at the grain boundaries, with some uniform dissolution of the inner wall surface. Figure 192 is a longitudinal view of the tube and shows the NaK exposed surface, on which the intergranular attack is very pronounced.

Tube-to-header welds were also examined in the A area. A representative photomicrograph of a weld and tube exposed to NaK at the NaK exit end (hot) of this heat exchanger is shown in

[1] J. C. Amos, *Small Fluoride – NaK Heat Exchanger Test No. 1 (High Velocity Heat Exchanger Test)*, ORNL CF-56-1-187 (Jan. 2, 1956).

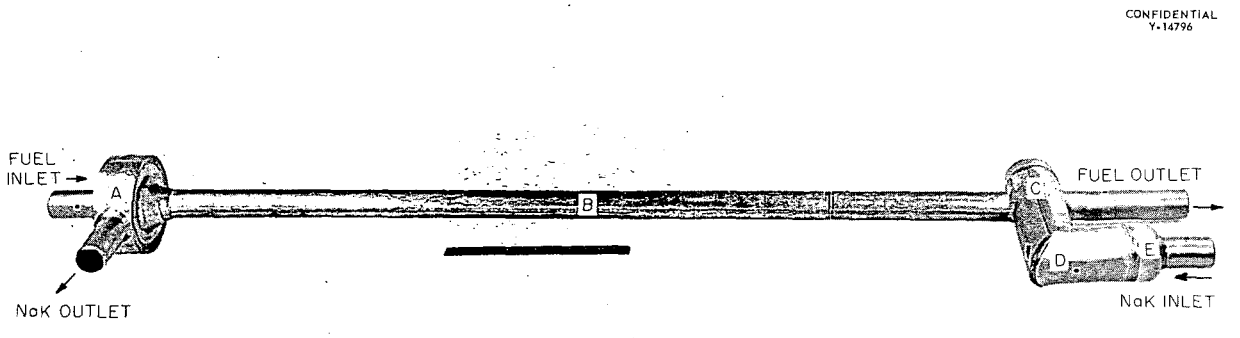

Fig. 187. High-Velocity Heat Exchanger (SHE No. 1). Arrows indicate flow direction of NaK and fuel. Letters indicate areas of metallographic examination.

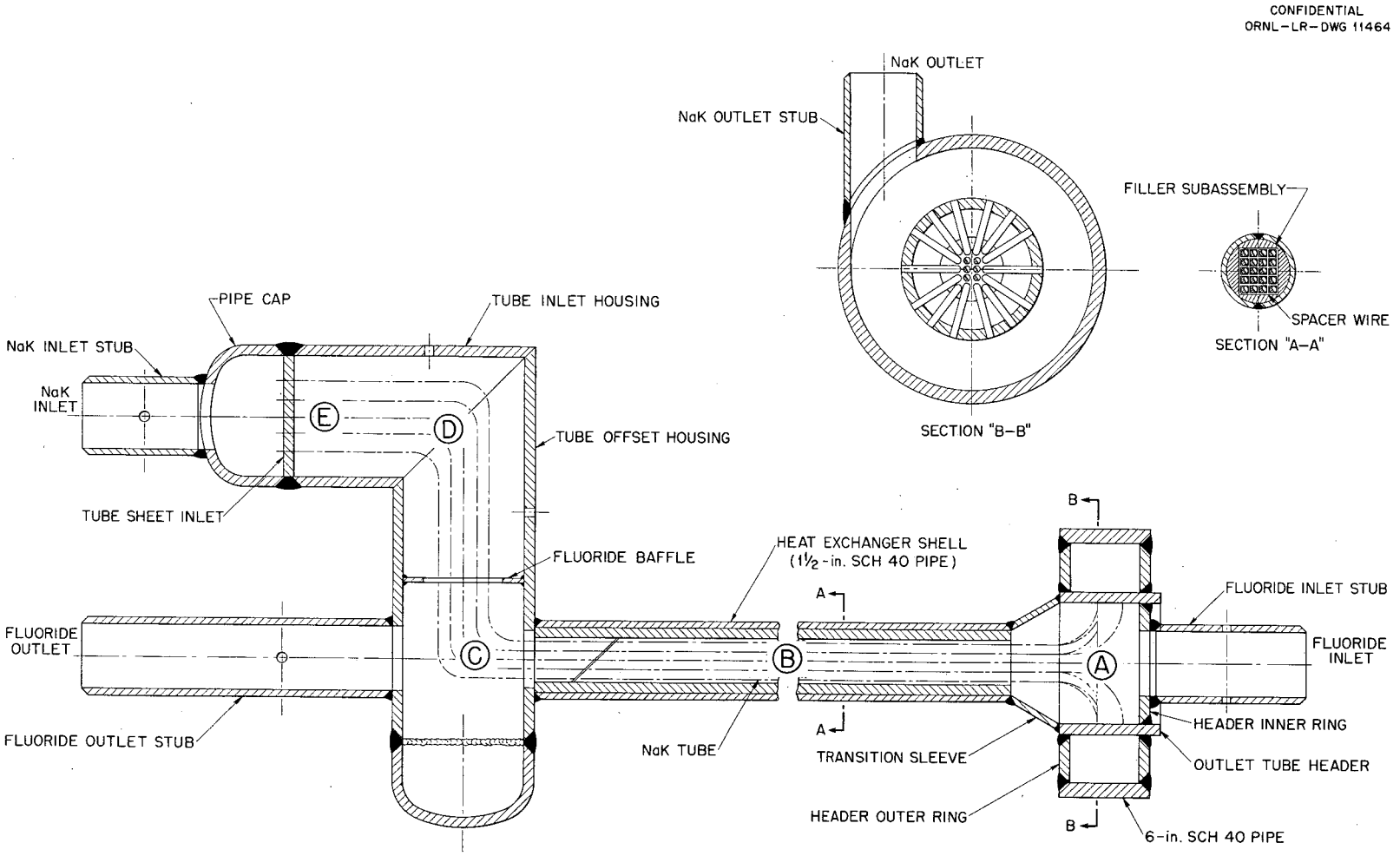

Fig. 188. High-Velocity Heat Exchanger. A, B, C, and E indicate areas of metallographic examination.

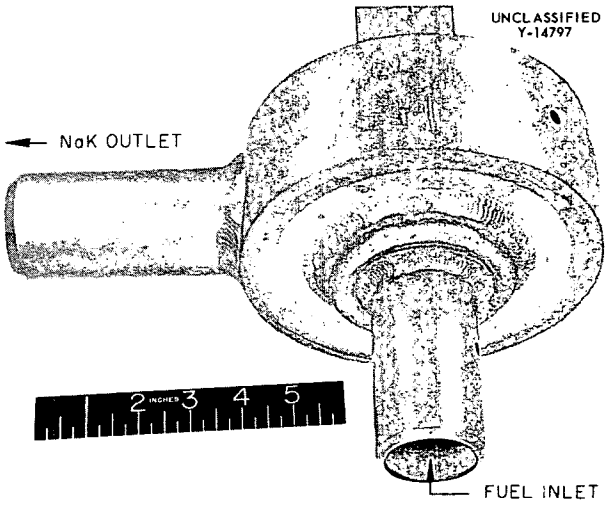

Fig. 189. High-Temperature End (Area A) of SHE No. 1 Before Sectioning.

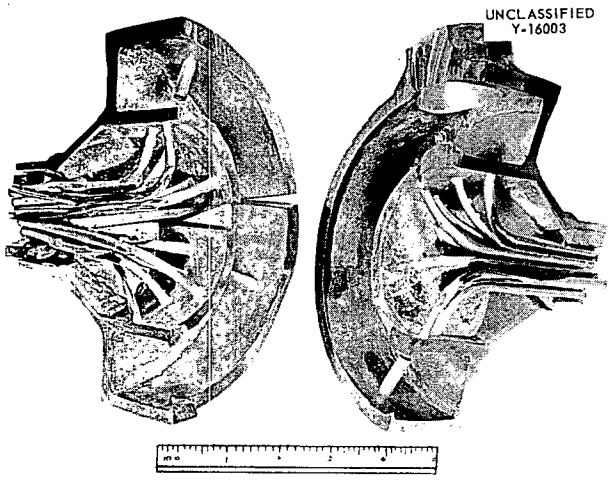

Fig. 190. High-Temperature End (Area A) of SHE No. 1 After Sectioning.

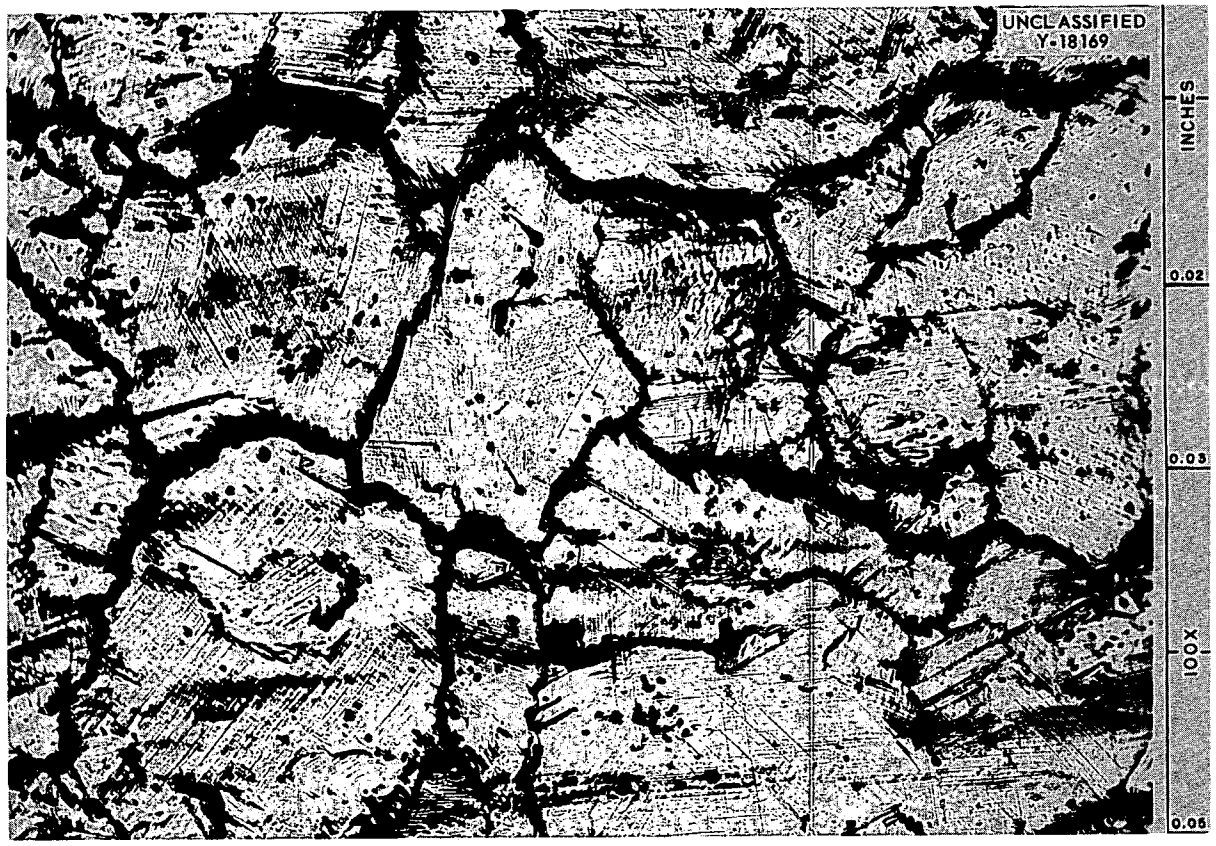

Fig. 191. Inner Surface (NaK Side) of Inconel Tube. Photo is made normal to the surface. Note selective attack at the grain boundaries. (Confidential with caption)

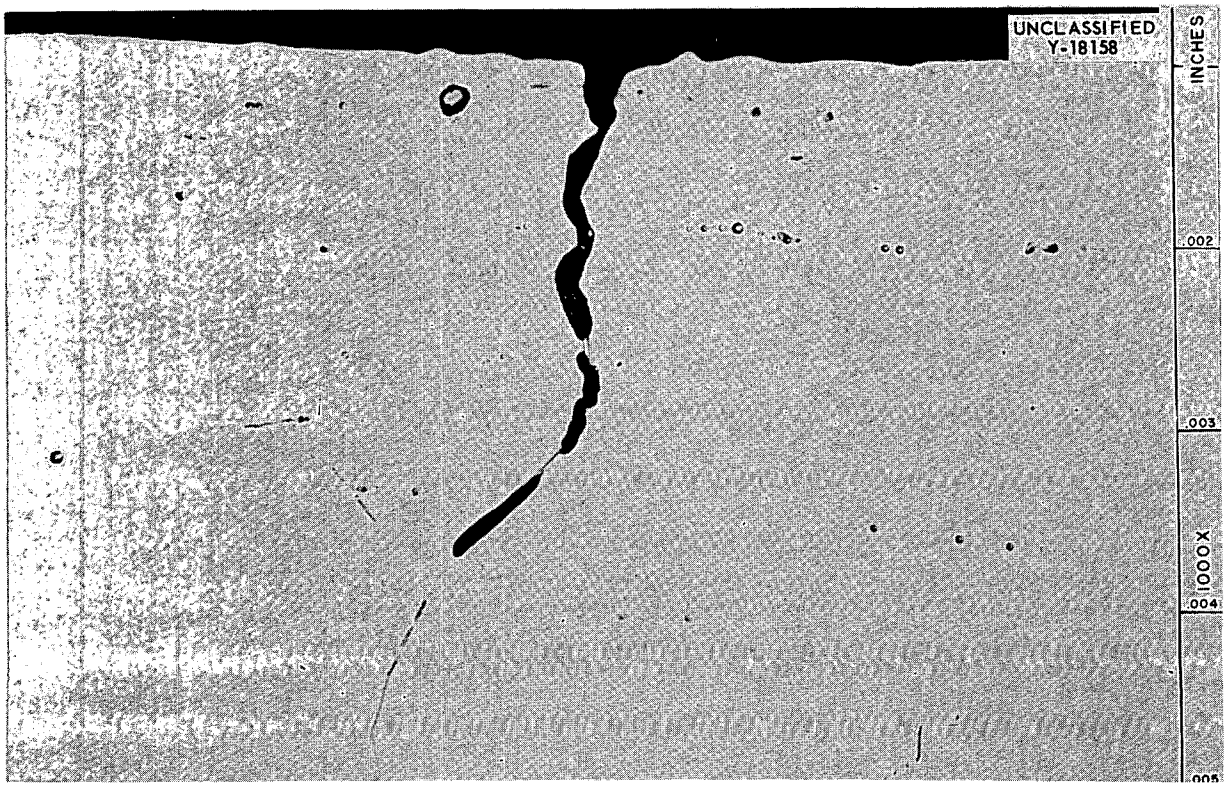

Fig. 192. Longitudinal View of Inconel Tube Exposed to NaK. Note the depth of selective attack at the grain boundaries. 1000X. Reduced 3%. (Confidential with caption)

Fig. 193. A photomicrograph at a higher magnification is shown in Fig. 194. It is evident that the depth of intergranular attack is not so deep as in the tubes and that there is no indication of selective attack in the cored structure typical of a weld.

A photomicrograph of an entire tube wall in area A is shown in Fig. 195. The outer surface of the tube exposed to the hot fuel also shows considerable attack by the depth of voids. The fuel inlet temperature in area A was approximately 1505°F for the last 456 hr of test. The grain size is noticeably large in the tubes, averaging about two grains across the entire wall. Along with this grain size the microstructure is free of much of the precipitate usually found in commercial-grade Inconel. The large grain size and the small amount of precipitate can be accounted for by the 1505°F (fuel) to 1495°F (NaK) operating temperature in area A and the probable elemental diffusion, at these temperatures, of Cr, Ti, Al, and C into the NaK and fuel. These elements are found as compounds of Ti-Al, Cr_3C_2, and $Cr_{23}C_6$ in Inconel. The cyclic triaxial stressed condition on the tubes at these temperatures would also accelerate grain growth.

A longitudinal view of the tube wall at about the center of the heat exchanger (area B) is shown in Fig. 196. It might be assumed that the operating temperatures in this location would be near the mean temperatures of the fuel (1455°F) and the NaK (1250°F). There is less elemental diffusion in this area, as indicated by the presence of precipitate on the fuel half of the tube wall. The amount and depth of subsurface voids on the fuel side are less, and the average depth of intergranular attack on the NaK side is slightly less, although there is still elemental diffusion into the NaK, as evidenced by the absence of precipitate.

The fuel outlet and NaK inlet header is shown in Fig. 197, with the examination areas C, D, and E indicated. A longitudinal examination at the first bend near the fluoride outlet is shown in Fig. 198 (area C). A comparison with the micro-

Fig. 193. Tube-to-Header Weld from Area A. Dark areas in the lower corners are due to field limitations of microscope.

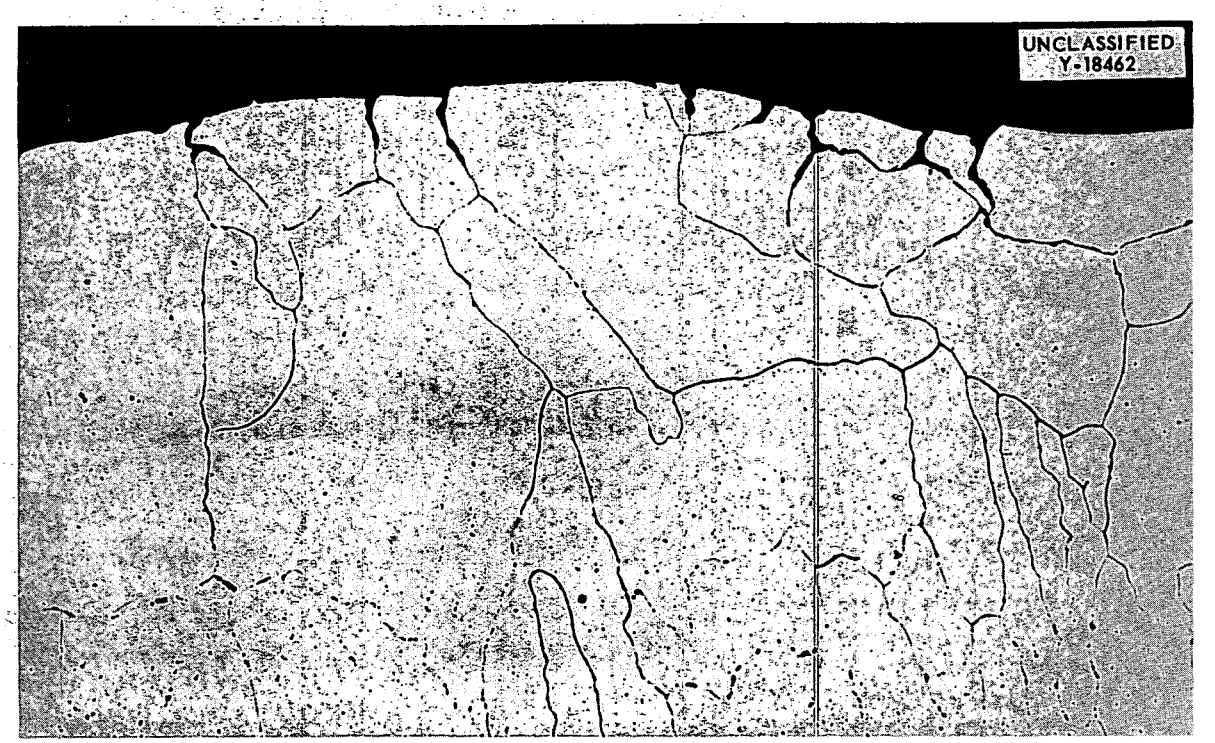

Fig. 194. Tube-to-Header Weld from Area A. Photomicrograph of area indicated in Fig. 193 at higher magnification. 250X.

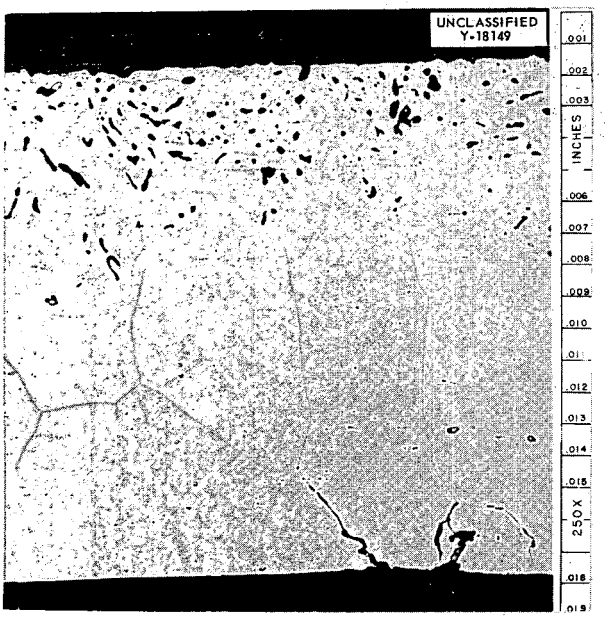

Fig. 195. Inconel Tube Wall from Area A. Fuel side is at top; NaK side is at bottom. 250X. Reduced 31.5%. (Confidential with caption)

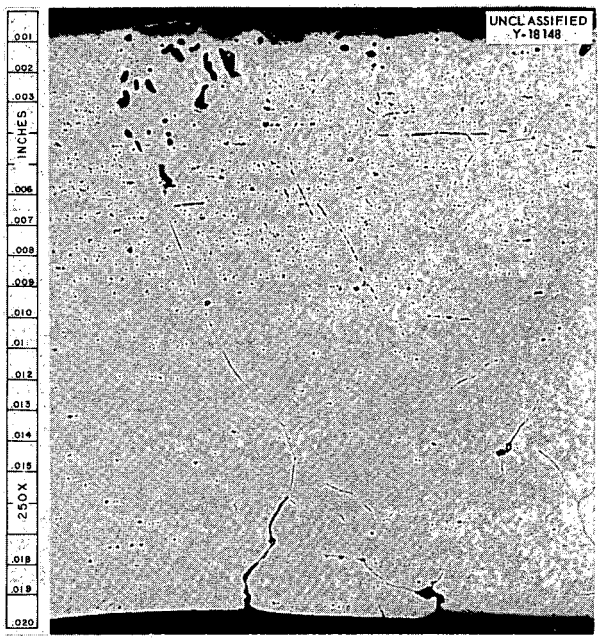

Fig. 196. Inconel Tube Wall from Area B. Fuel side is at top; NaK side is at bottom. 250X. Reduced 34%. (Confidential with caption)

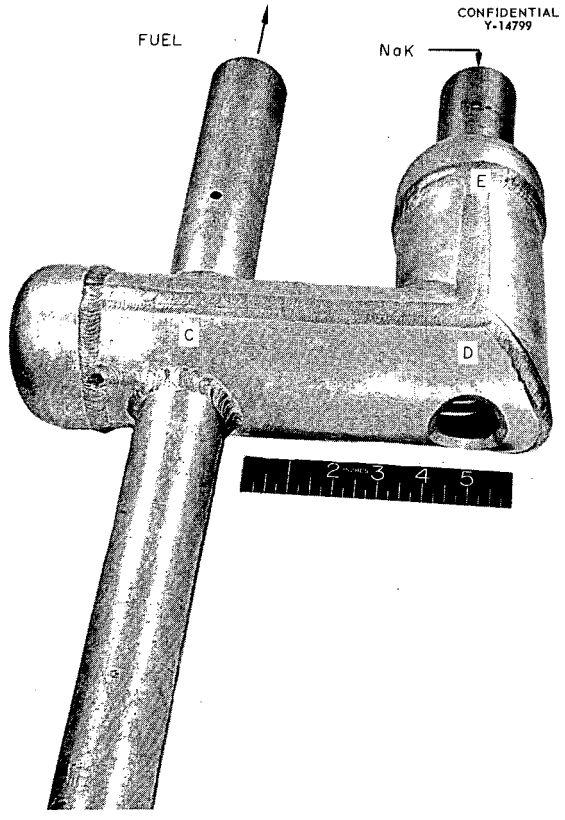

Fig. 197. Coldest End of High-Velocity Heat Exchanger Fuel Outlet and NaK Header.

Fig. 198. Inconel Tube Wall in Area C. Note small amount of subsurface voids on fuel side (top of photomicrograph) and absence of intergranular attack on NaK side (bottom). Note uniform distribution of precipitate. 250X. Reduced 26.5%. (Confidential with caption)

structures from areas B and A shows a heavier precipitate in the microstructure across the entire tube wall in area C, with no attack on the inner wall exposed to the NaK and a small amount of subsurface voids on the fuel side.

A longitudinal examination of the bend area D showed a mass transfer layer about 0.003 in. deep at the outer surface of the bend. There is a radical difference in the amount of mass transfer which exists on the inner surface of the tubes at the outside and inside bend, as shown in Figs. 199 and 200. Apparently, the flow of NaK impinging

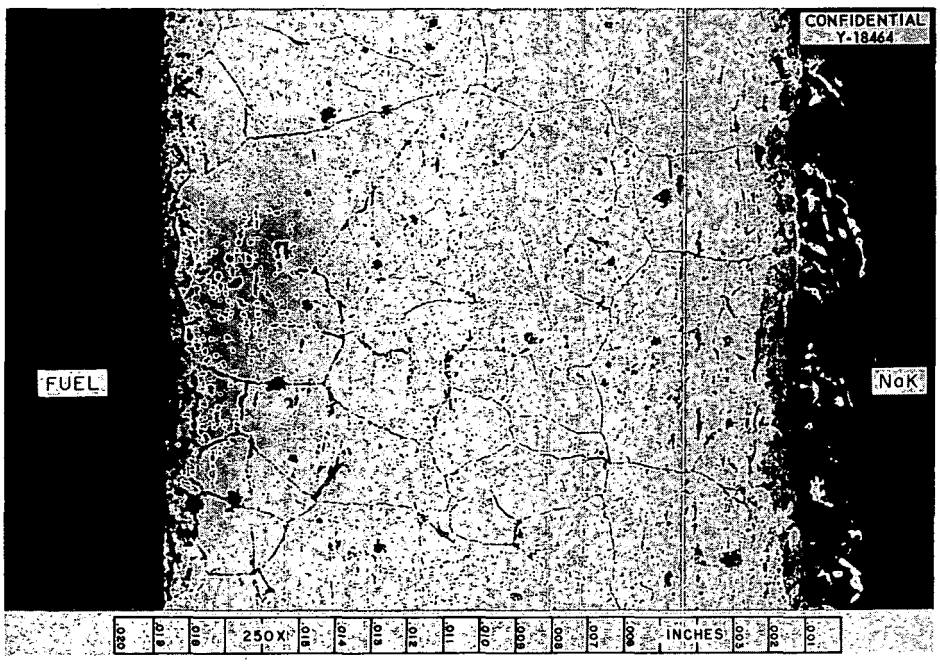

Fig. 199. Mass Transfer on NaK Side of Bend (Outer Bend) in Area D. Note difference in amount of deposit on diametrically opposite walls at the bend. 250X. Reduced 22%.

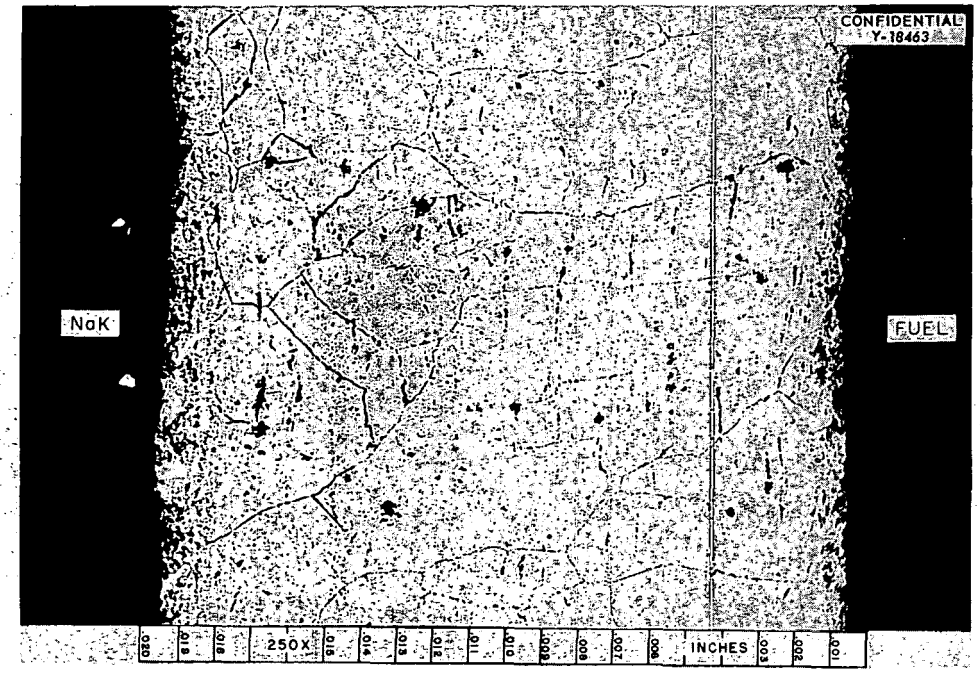

Fig. 200. Mass Transfer on NaK Side of Bend (Inner Bend) in Area D. 250X. Reduced 22%.

against the outer part of the bend accounts for the deposition being greater at the outer part than on the inner curvature. A more highly magnified photomicrograph of the deposit on the outside bend is shown in Fig. 201. The growth pattern of the deposit is curved with the flow direction. A spectrographic ratio analysis of the deposit as compared with Inconel is shown below:

	Deposit	Inconel
Ni-Fe ratio	7.9 to 1.0	9.5 to 1.0
Ni-Cr ratio	12.2 to 1.0	5.0 to 1.0
Cr-Fe ratio	1.0 to 1.5	1.9 to 1.0

The fuel side (outside) of the tube was also examined in area D, and a tightly adhering gold-colored layer about 0.0001-in. thick was found, as shown in Fig. 202. This layer was analyzed spectrographically as a titanium-rich layer and was identified by x ray as titanium oxide (TiO).

The tube-to-header welds at area E were examined primarily for comparison with the welds from the hot end (area A) of the heat exchanger. A longitudinal view of a weld from area E is shown in Figs. 203 and 204. The difference in operating temperature is very evident at area E, which operated at 1005°F (NaK) inside and 1405°F (fuel) outside. The heavy precipitate in the microstructure of the header plate tube wall and the weld is typical of welded Inconel subjected to this temperature. A difference in the amount of deposit is evident on the orifice of the tubes and just inside the weld. As mentioned previously, the flow velocity through the header plate has affected

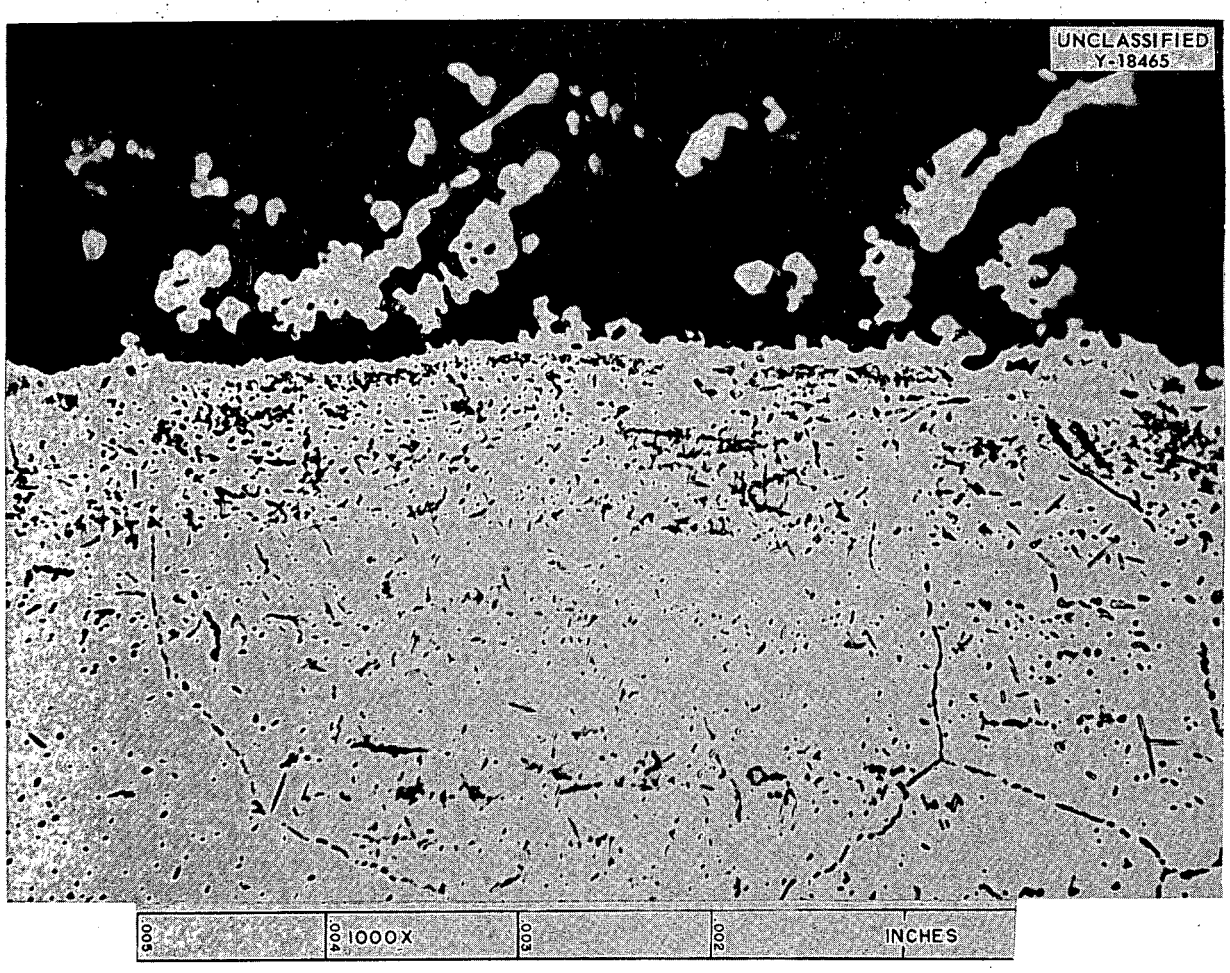

Fig. 201. Outer Bend, Area D, Similar to NaK Side Shown in Fig. 199. (Confidential with caption)

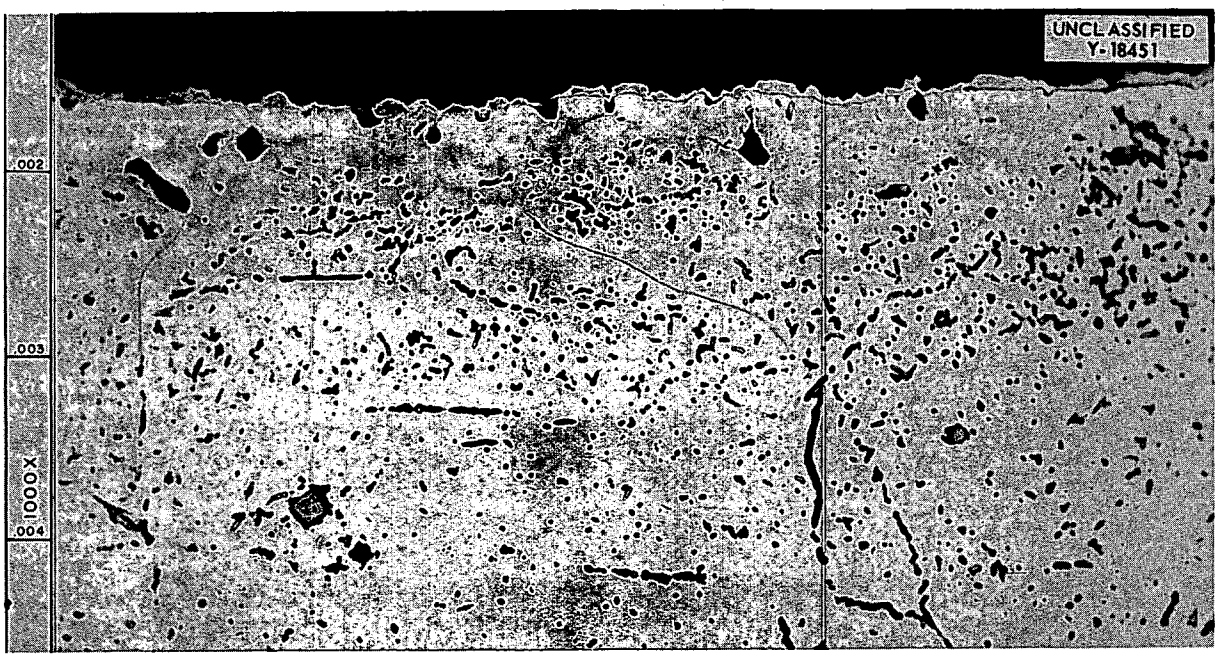

Fig. 202. Outer Surface (Fuel Side) in Area D. Note "gold"-appearing deposit on surface. 1000X. Reduced 3%. (Confidential with caption)

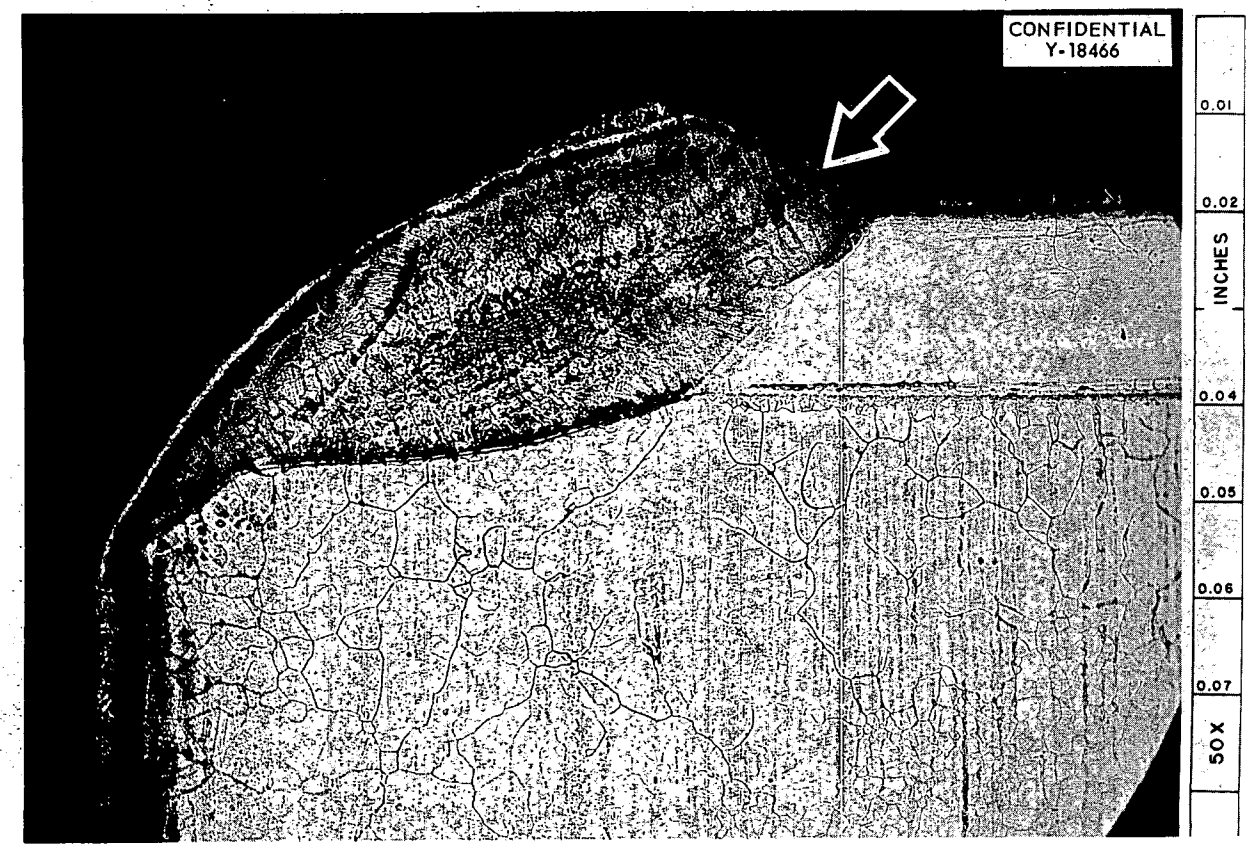

Fig. 203. Tube-to-Header Joint in Area E. Arrow indicates static area with very little mass transfer.

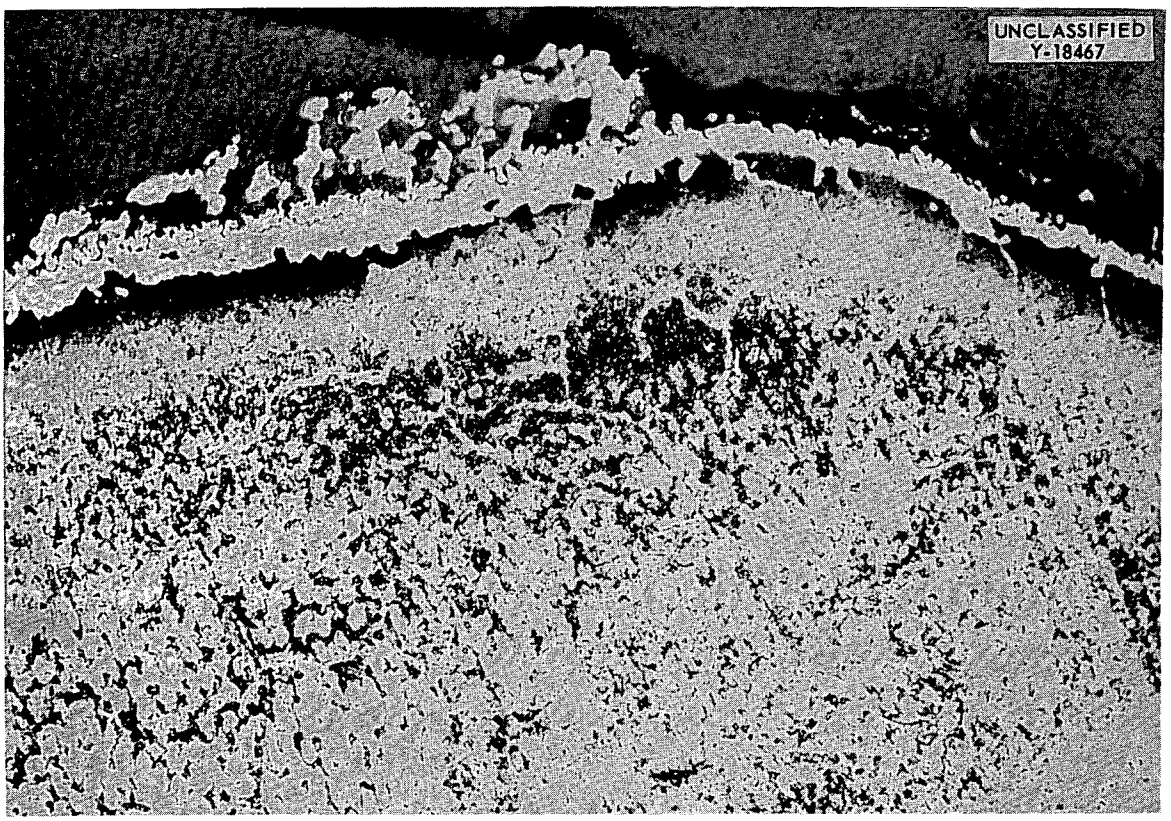

Fig. 204. Same as Fig. 203 but at Higher Magnification. Note deposit on NaK surface. 250X. (Confidential with caption)

the amount of deposit. Locations of comparative static conditions which would exist just inside the weld have little deposit.

METALLOGRAPHIC STUDY OF ISOTHERMALLY TREATED HASTELLOY B

J. R. Riddle R. J. Gray

Hastelloy B was given a series of isothermal treatments to determine structures present and to establish a guide to the metallography of the alloy. All other factors affecting microstructure were rigidly controlled. Specimens were $\frac{1}{16}$-in. sheet selected from the same heat and sealed in quartz under a partial pressure of argon. When possible, all samples were etched identically. All samples in each series other than those of the 1800°F series were etched for 5 sec, while the 1800°F series required 15 sec, and the solution-annealed sample required 20 sec. All etching was by immersion in a solution of equal parts of hydrochloric acid, 10% chromic acid, and water.

The alloy composition determined by wet chemical analysis is given below:

Element	wt %
Ni	65.1
Mo	27.5
Fe	4.86
C	0.05
Cr	0.03
Mn	0.87
Si	0.65
P	0.003
Ti	0.30
S	0.001
Al	0.20
Mg	0.67
Va	0.32

Shown in Figs. 205 through 210 are the more significant structures of the test. A report giving more detail will be published upon completion of x-ray studies. These studies should reveal the precipitate present in the 1300 to 1500°F treatments, which lie in the beta or gamma region of the Ni-Mo phase diagram. They should also confirm the presence of a stable delta phase in the 1650 and 1800°F heat treatments. The small spheroidal particles present in each series have been identified as complex carbides which originally formed as a eutectic, were broken up through rolling, and spheroidized during anneal.[2] Variations in Widmanstätten precipitates of 1300, 1400, and 1500°F treatments are attributed to changes in nucleation and growth rates with temperature. Stable nucleus size decreases with increasing degree of undercooling below the solvus and accounts for the finer dispersion of precipitate at lower temperatures.[3] This effect is aided by slower diffusion rates at lower temperatures.

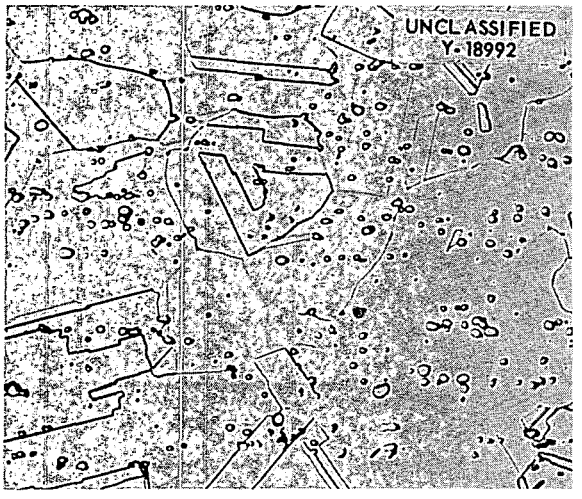

Fig. 205. Structure of Hastelloy B Prior to Isothermal Treatments. Heat-treated for 2 hr at 2100°F. 250X.

Hardness curves (Fig. 211) represent the average of four diamond pyramid impressions per specimen with a normal scatter of 8 to 12 points. Note the agreement between structure and hardness in the 1300 and 1400°F series which correspond to the embrittling effect produced by aging at these temperatures.

[2]Based on x-ray data obtained by T. K. Roche of ORNL.

[3]A. H. Geisler, "Precipitation from Solid Solutions of Metals," in *Conference on Phase Transformations in Solids*, p 398, Wiley, New York, 1951.

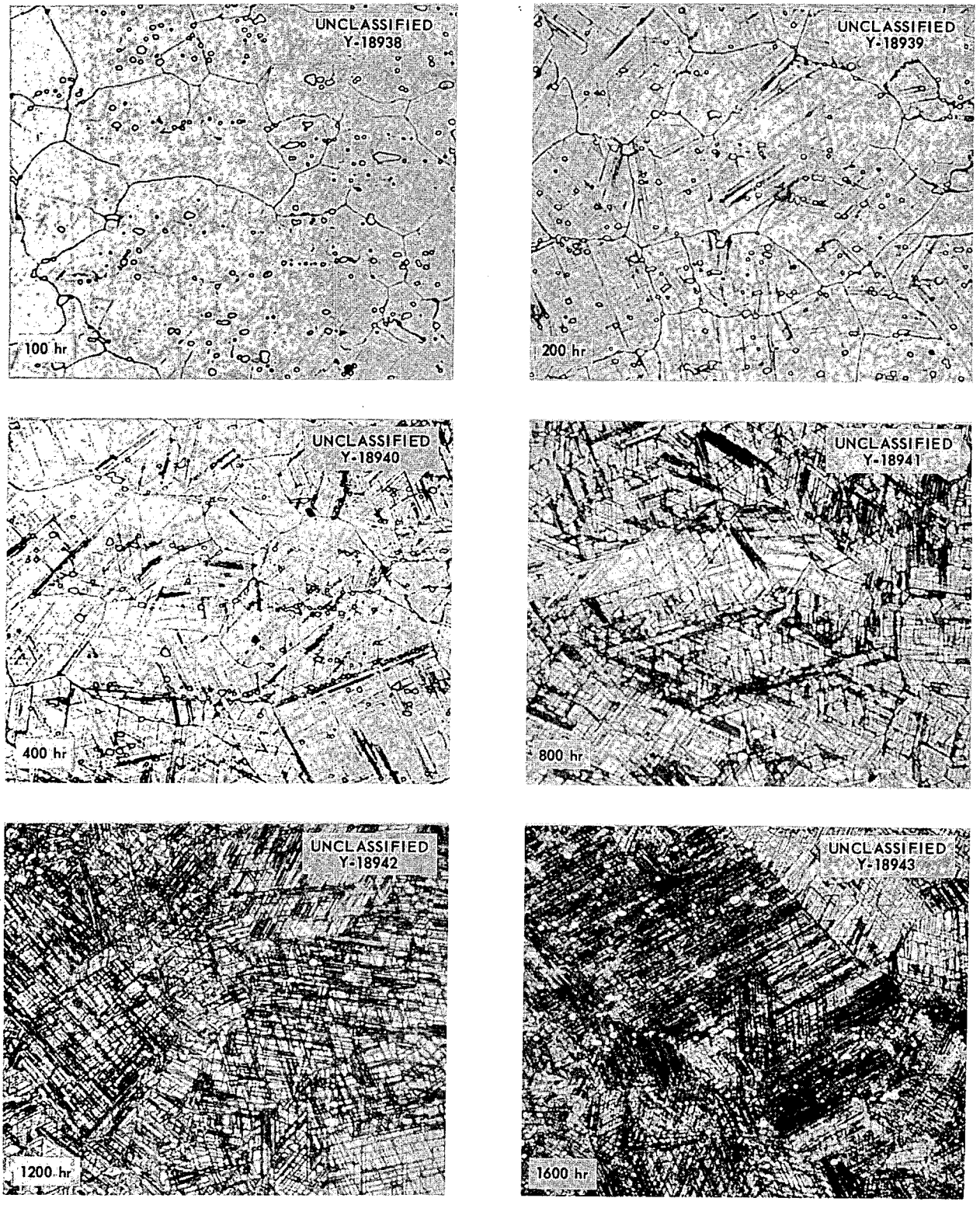

Fig. 206. Hastelloy B Heat-treated at 1300°F. 250X.

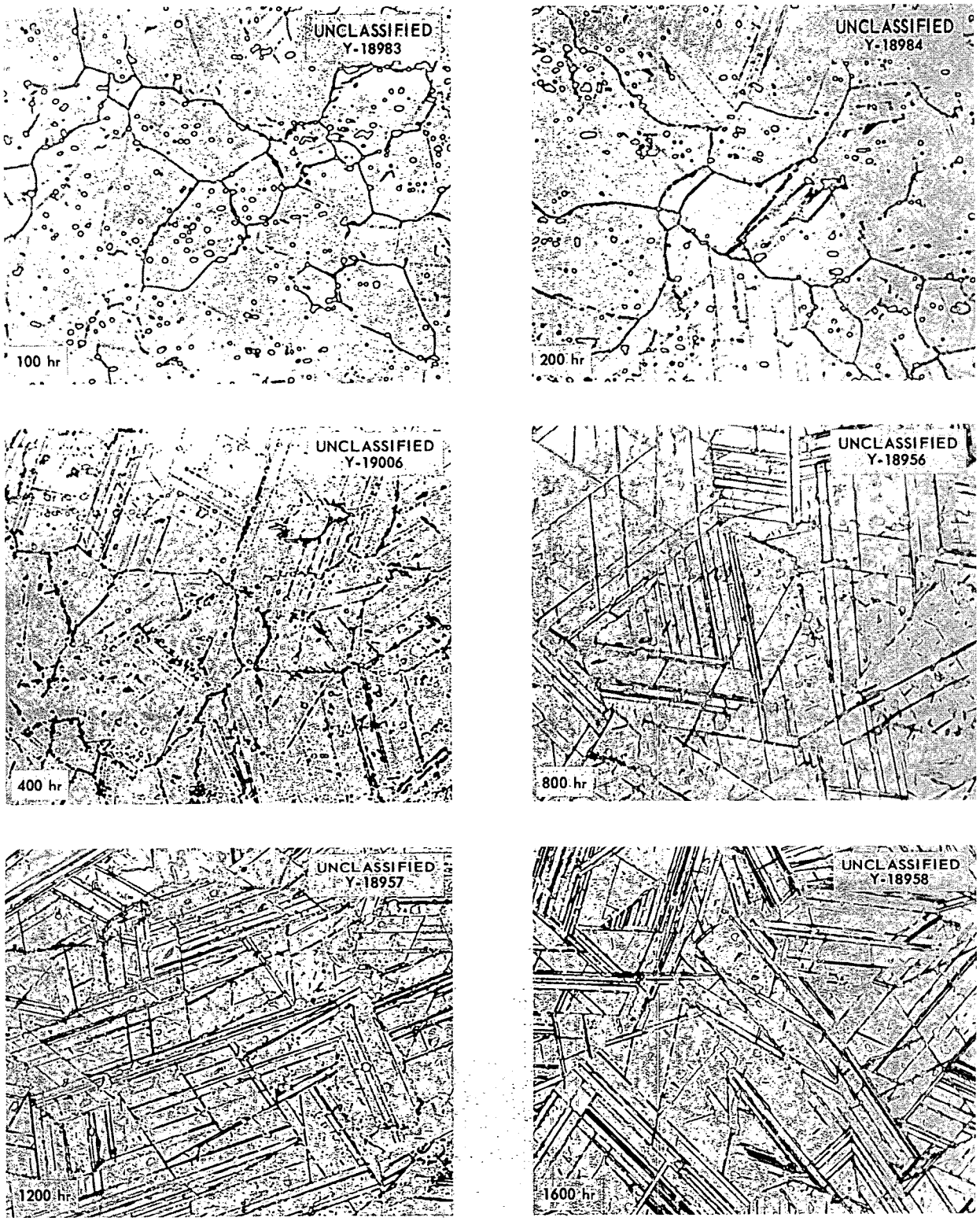

Fig. 207. Hastelloy B Heat-treated at 1400°F. 250X.

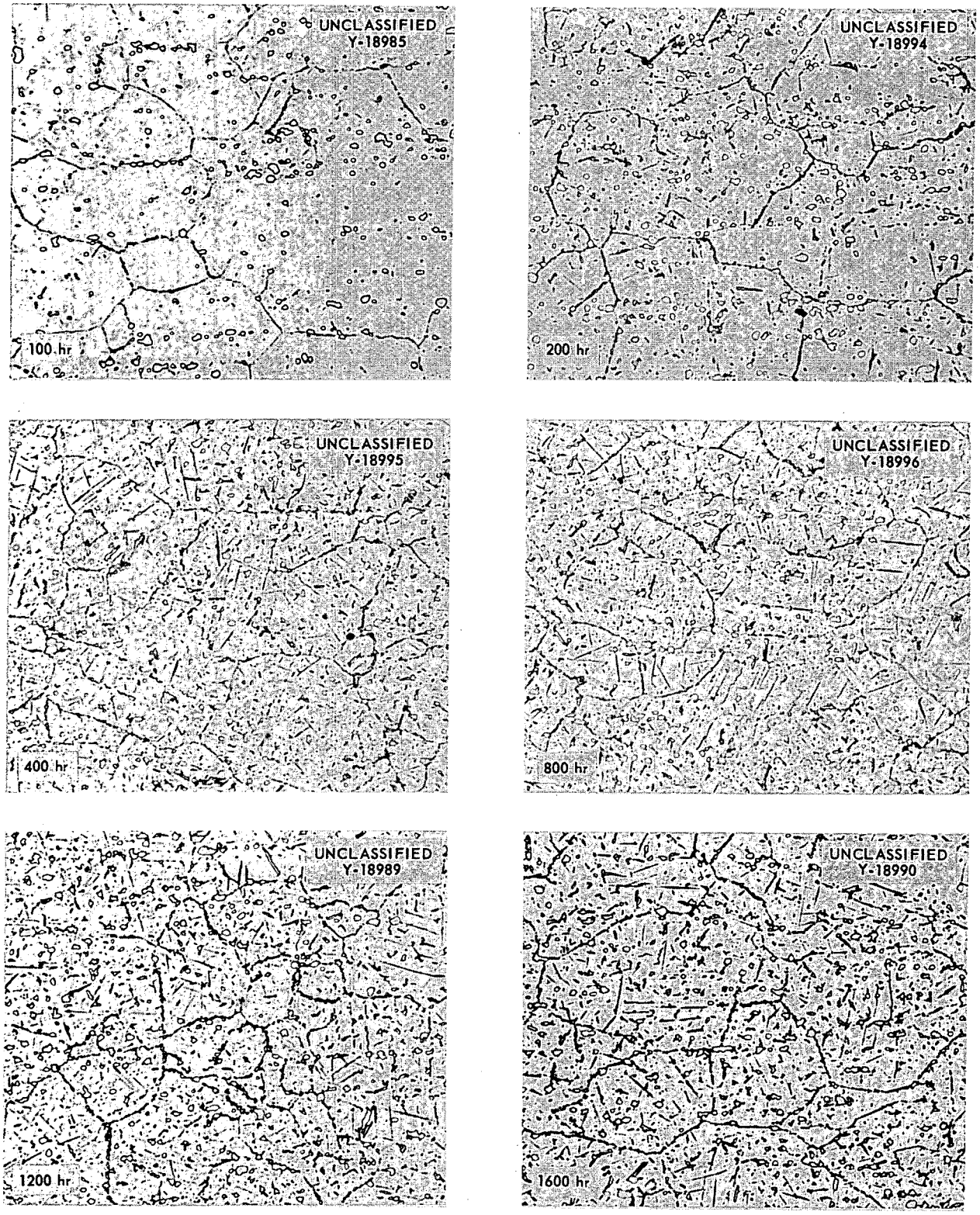

Fig. 208. Hastelloy B Heat-treated at 1500°F. 250X.

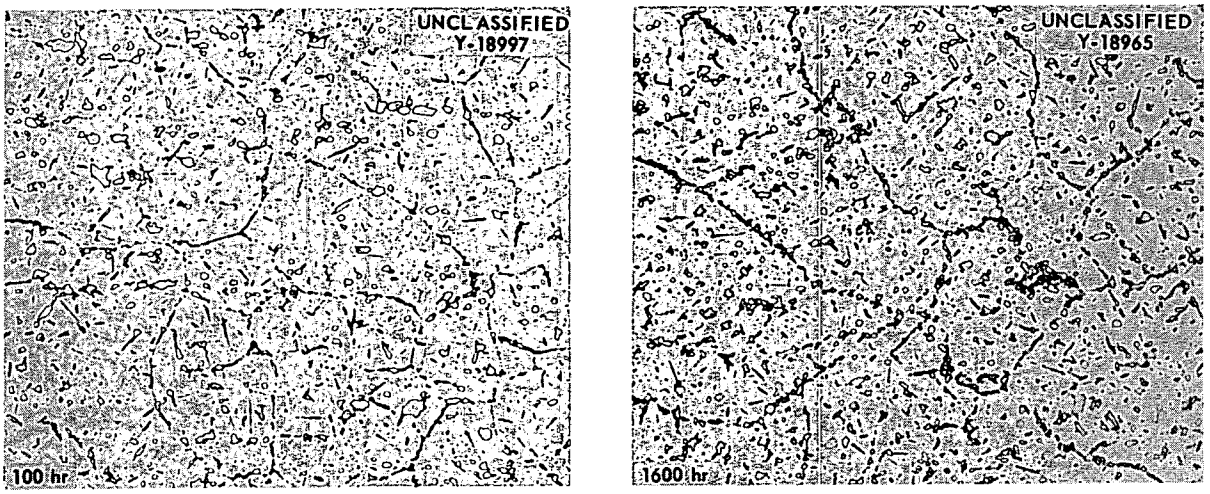

Fig. 209. Hastelloy B Heat-treated at 1650°F. 250X.

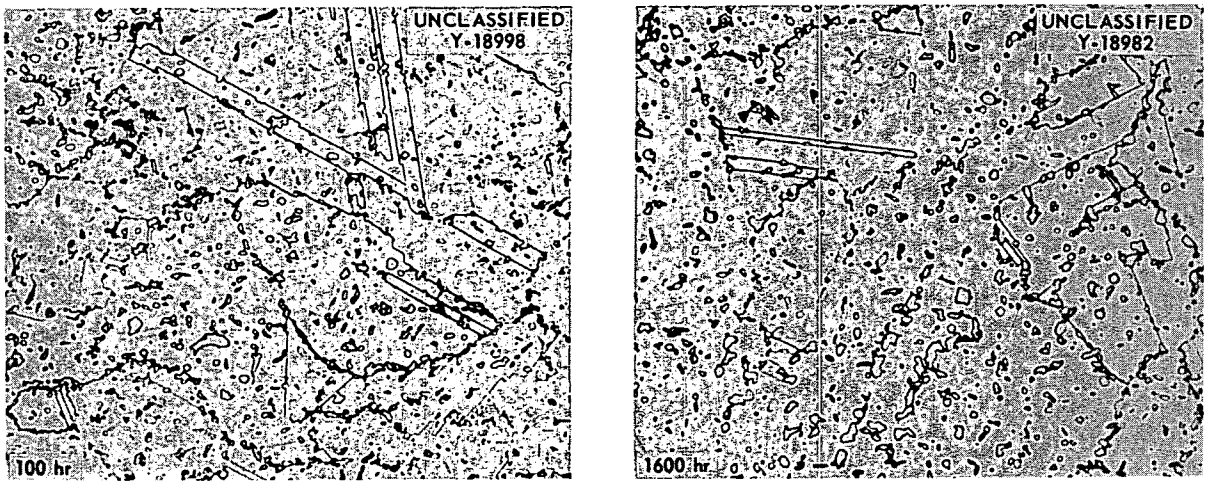

Fig. 210. Hastelloy B Heat-treated at 1800°F. 250X.

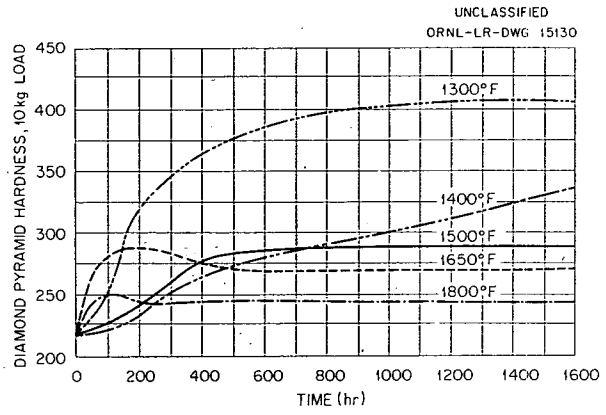

Fig. 211. Hastelloy B Hardness Curves.

CERAMICS RESEARCH

L. M. Doney

C. E. Curtis
S. D. Fulkerson
J. A. Griffin
R. L. Hamner
M. P. Haydon
F. P. Jeffers
J. M. Kerr
R. A. Potter
A. J. Taylor
A. G. Tharp
G. D. White
T. N. McVay[1]
T. S. Shevlin[1]

UO_3 CRYSTAL INVESTIGATION

A. J. Taylor

The UO_3 experiments designed to grow UO_3 crystals in large quantities, at high uranium yields, and in particular size ranges have indicated that rigid control of all process steps may be necessary, including processing of the uranium peroxide cake (UO_4 hydrate), which is the starting material in the crystal-growing process.

At the beginning of the experiments it was assumed that the knowledge gained from working with depleted cake would be directly applicable to normal, or enriched, cake. This assumption proved to be erroneous. When no significant progress toward the objectives had been gained after a series of 18 experiments with depleted cake, the cake was changed to normal. This was done to fill a small order for normal UO_2 made by this process. With the change, the process went completely awry. Autoclave pressure went abnormally high, and crystal size and yields became completely unpredictable and to some extent uncontrollable. A series of seven experiments established that in order to grow a batch of normal UO_3 crystals comparable in size and yield to some of the batches of depleted crystals it was necessary to revise the composition ratios R_1 and R_2 radically. It also became necessary to double the time in the autoclave. The best results with normal cake and UNH as a source of uranyl ion were not particularly good. A second source of uranyl ion (nitric acid additions) proved to be much less sensitive and gave some very encouraging results.

With UNH as the uranyl ion source the initial crystal grows as a needle similar in size and habit to Mallinckrodt gamma-phase UO_3 but different in composition as seen in the DTA patterns, Fig. 212. The orthorhombic bipyramid is a secondary crystal growth, not yet understood, in which the needles or primary growth often appear as inclusions.

With nitric acid additions providing the source of uranyl ion, the primary crystal growth seems to be the orthorhombic bipyramid. This offers the possible advantage of making time the one controlling variable in growing the largest percentage of crystals in a given size range.

A study is being made of the different peroxide cakes (depleted, normal, and enriched) to see how and why they differ and why they have such a marked effect on the crystal-growing process. Figure 213 shows the difference in crystal size and habit

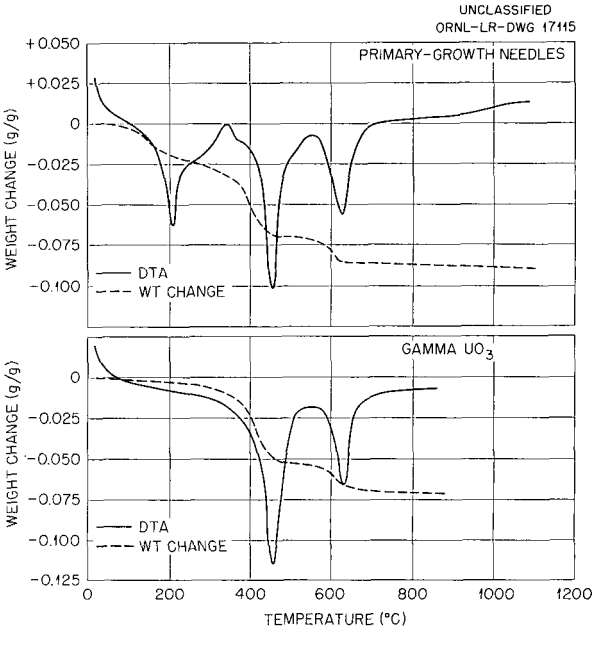

Fig. 212. DTA Patterns Showing Differences in Compositions Between Primary-Growth Needles and Gamma-Phase UO_3.

[1]Consultant.

UNCLASSIFIED
PHOTO 27026

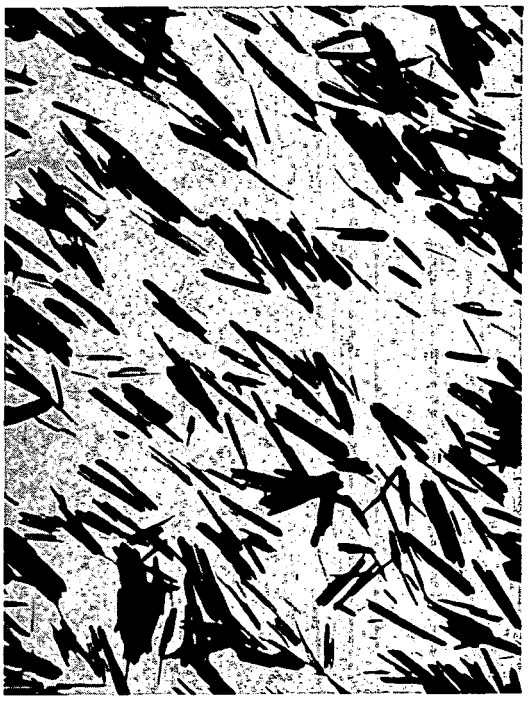

⟵ 1μ ⟶
NORMAL PEROXIDE CAKE

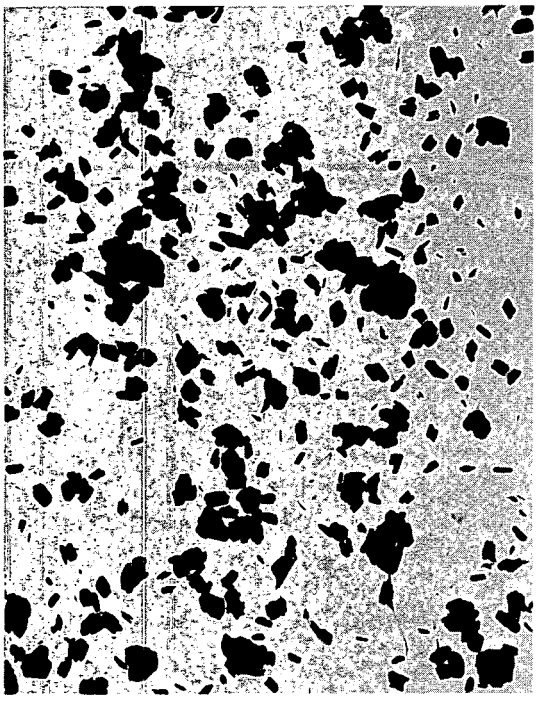

⟵ 1μ ⟶
DEPLETED PEROXIDE CAKE

Fig. 213. Electron Micrographs Showing Differences in Crystal Size and Habit Between Normal and Depleted Peroxide Cake.

between the depleted and normal UO_4. X-ray patterns have indicated that crystal size of the enriched UO_4 will be even smaller than that of the depleted UO_4. The DTA patterns of Fig. 214 indicate the differences in the reactivities of the three cakes and also indicate possible composition differences such as hydroxyl radicals substituting for water. The strong exothermic peak occurring at 286°C in the normal cake pattern is as yet unexplained.

The attempt to devise some means of separating platelets from whole crystals, as previously described, was not too successful. The tilted and vibrated surface made a much better separation than did the flowing column of water, but, since it could not be made continuous and was very slow, the investigation was dropped.

Si-SiC DEVELOPMENT

A. J. Taylor

A technique has been developed for fabricating thinner Si-SiC fuel plates in the interest of making the plates more resistant to thermal shock. Plate thickness has been reduced to 0.09 in., and plates have been successfully made without warping at 0.06 in. To make the plates thinner without warping, it was also necessary to cut the size to $1\frac{3}{4} \times \frac{3}{4}$ in. from the previous plate dimensions of $3 \times 1\frac{1}{8}$ in. The thinner skin resulted in a net increase in fuel content of 3 wt %, an increase from 7% to 10% UO_2.

The thinner plates should give advantages regarding neutron economy in a reactor, and in reduced thermal stresses or a slightly higher element surface temperature because of the reduction in

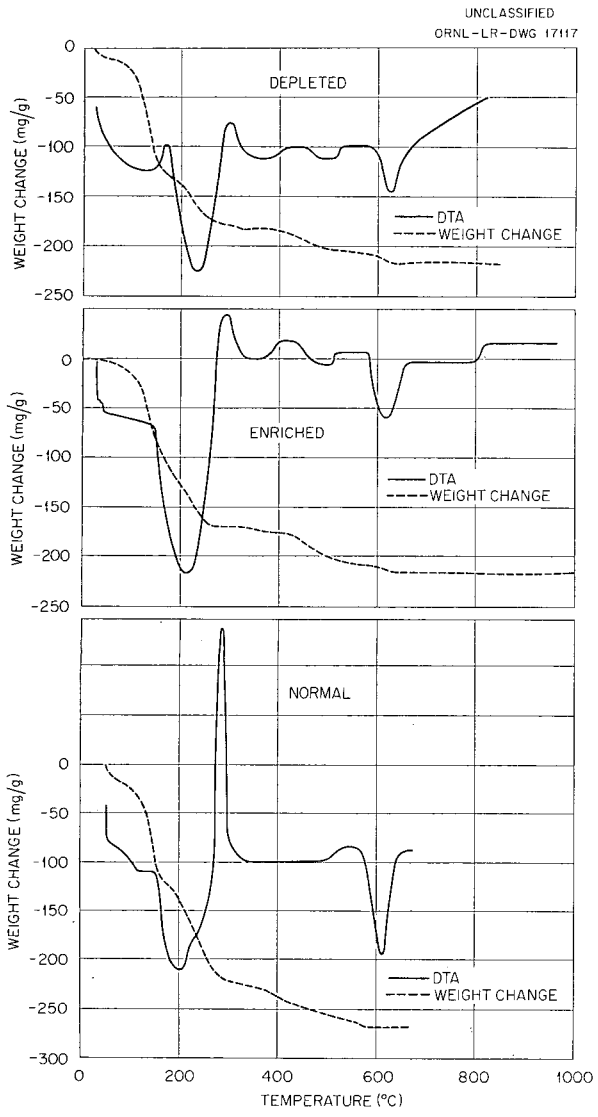

Fig. 214. DTA Patterns of Depleted, Normal, and Enriched Uranium Peroxide Cake.

temperature differential between core and skin. Some possible disadvantages to the thinner plates might be less resistance to stresses induced by differential expansion between the core and the skin and a decreased ability to retain gaseous fission products at elevated temperatures.

Fuel additions greater than 10 wt % in the thinner plates have not yet been successful with the use of a monolayer of coarse-grained UO_2. Work on the monolayer additions continues, but parallel to it has been included a revision of the core technique, in which the core is considerably thicker than the monolayer and consists of a mixture of UO_2 and graphite. The UO_2 is being added as coarse-grained particles rather than the fine-grained oxide.

Some experimental work is being done on a variation of the Si-SiC element, in which the fuel element will consist of a dense graphite core clad in Si-SiC.

METAL HYDRIDING SYSTEM

R. A. Potter

Erection of a system for the hydriding of zirconium and yttrium metals is nearing completion. The assembly is composed of a gas train for the purification of hydrogen, a vacuum pump for degassing, and two hydriding furnaces of such capacity as required to handle 4 × 12 in. billets.

The gas train consists of a Deoxo unit, two activated alumina driers, two Kanthall-element vertical muffle furnaces containing metal turnings of calcium in one and zirconium in the other. Both furnaces have been obtained, and Inconel muffles are being fabricated.

The zirconium hydriding furnace is a modified version of the furnaces used in the gas train and utilizes an Inconel muffle (being fabricated) equipped with a gas inlet and a vacuum outlet. Hydriding temperatures will be in the range 1600 to 1700°F. Zirconium billets will be heated in a vacuum to the desired temperature and soaked in a hydrogen atmosphere. Upon reaching the saturation point, the hydrogen flow will be discontinued and the heat shut off.

With the exception of an Inconel muffle and a power supply, the yttrium hydriding furnace has been completed. Glo-bar elements positioned vertically around the muffle permit operating temperatures in the range 2200 to 2300°F. Yttrium billets, when available, will be heated in a vacuum to 2300°F, the temperature will be dropped to 2200°F, hydrogen will be allowed to flow until the saturation point is reached, and then the hydrogen and heat will be discontinued.

One vacuum pump and one gas train will service both hydriding units for the present.

BeO PROTECTION TUBE

R. A. Potter

An attempt was made to extrude a thermocouple protection tube composed of BeO. The tube was to have an outside diameter of 0.25 in. and was to contain five 0.025-in. holes uniformly spaced. The attempt was a failure because of the die design, which has since been changed. A new die is in the process of being fabricated.

ZIRCONIUM CARBIDE STUDY

R. A. Potter

A 200-g sample of ZrO_2 was carburized in a graphite crucible and yielded a zirconium carbide containing approximately 9% combined carbon (theoretical, 11.64%). Graphite was added to the carbon-poor carbide and the mixture heated in accordance with the McKenna Menstruum process[2] in molten aluminum metal. Zirconium carbide is being extracted from the reaction product for free and combined carbon analysis.

CERAMIC COMPACTS FOR ANP

L. M. Doney J. A. Griffin

Approximately 77 porous rare-earth oxide compacts, more from code 920 Lindsay mix, were fabricated and delivered to the Control Rod Fabrication Group of ANP. The compacts are shown in Fig. 215.

[2]P. McKenna, *Metal Progr.* 36, 152–155 (1939).

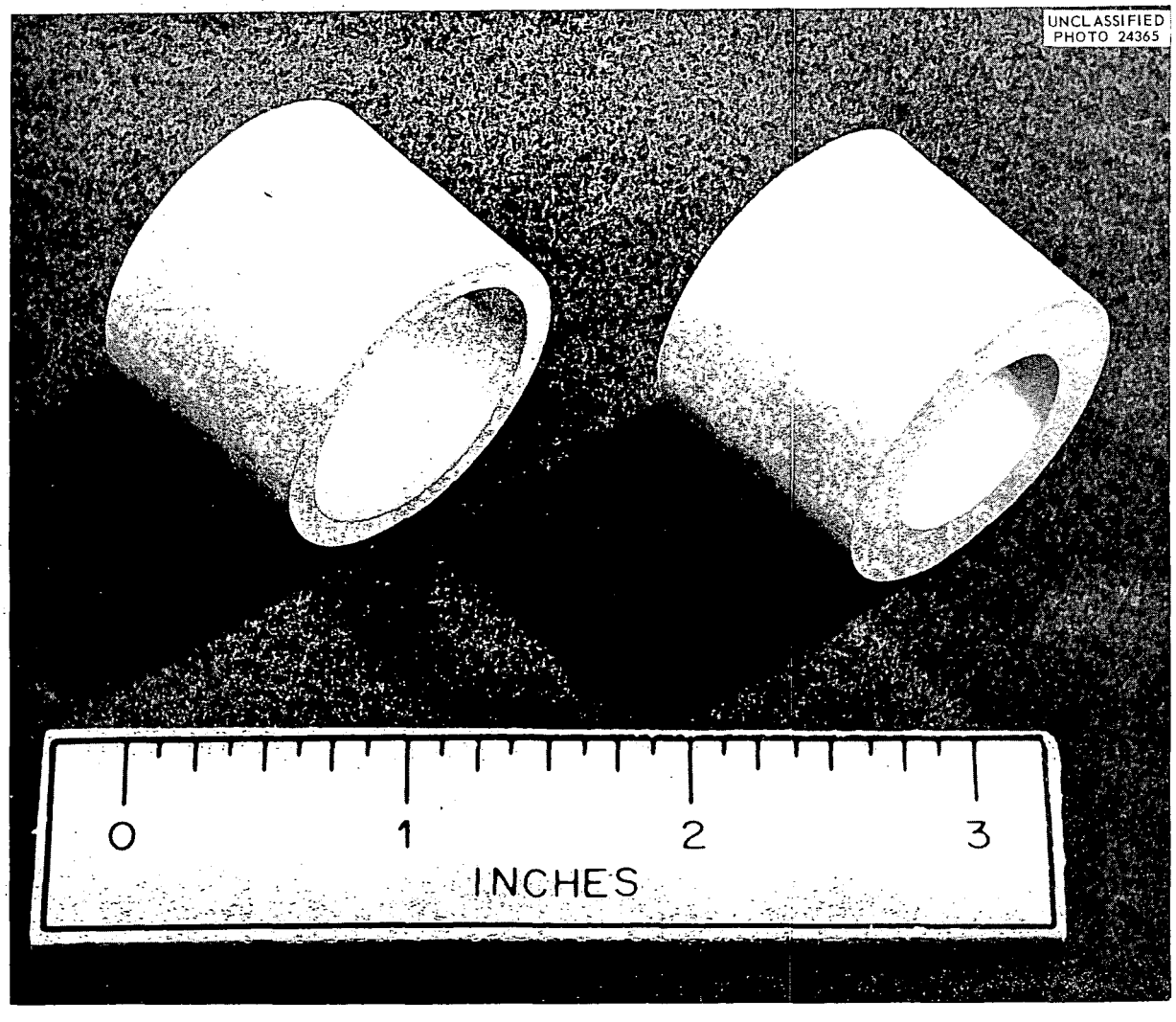

Fig. 215. Rare-Earth Oxide Ceramic Compacts for the ART Control Rod.

Two hundred and twenty-two disks of CaF_2 were fabricated for the Critical Experiment Group for use in the Pratt & Whitney critical experiment. The disks were about 0.790 in. in diameter and 0.070 in. in thickness and had a raised rim around each edge. The disks are to be used as foil holders for the uranium metal foil and the CaF_2 will simulate the presence of the fuel during the experiment.

Work is under way for the production of a refractory ceramic disk which will contain an appreciable quantity of cadmium; it is contemplated that these disks will be cadmium silicate. These disks are also for an assembly in the critical experiment work for Pratt & Whitney.

Fabrication of a rare-earth-oxide and nickel cermet for a critical experiment assembly is also under way. The cermet will be a right circular cylinder approximately 2.800 in. in outside diameter with about a $\frac{1}{4}$-in. wall.

ENTHALPY DATA FROM 0 TO 1200°C FOR PHYSICAL PROPERTY STUDIES OF CERAMIC MATERIALS

M. P. Haydon

One hundred and twenty-four "drops" were made in the ice calorimeter for heat content measurements. Of these, 27 were measurements of yttria and 97 were additional determinations of the enthalpy of the platinum sample container or basket. The platinum data were continued in an effort to verify the previously reported discontinuities in SiO_2 and UO_2.

The yttrium oxide enthalpy data showed evidence of at least one discontinuity at some point between 460 and 500°C. The smoothed curve of the preliminary values, not corrected for "drift," is shown in Fig. 216, together with the curves reported before on UO_2, SiO_2, and Si-SiC. The three suspected anomalies shown for uranium oxide, silica glass, and yttrium oxide will be investigated more fully after the irregularities in the platinum basket data have been satisfactorily analyzed.

The 97 additional points on the platinum basket enthalpy curve gave for the most part a much closer fit to the published data[3] than the first scattered runs had indicated. However, between 400 and 500°C, a definite dip of about 5 cal/g occurs from

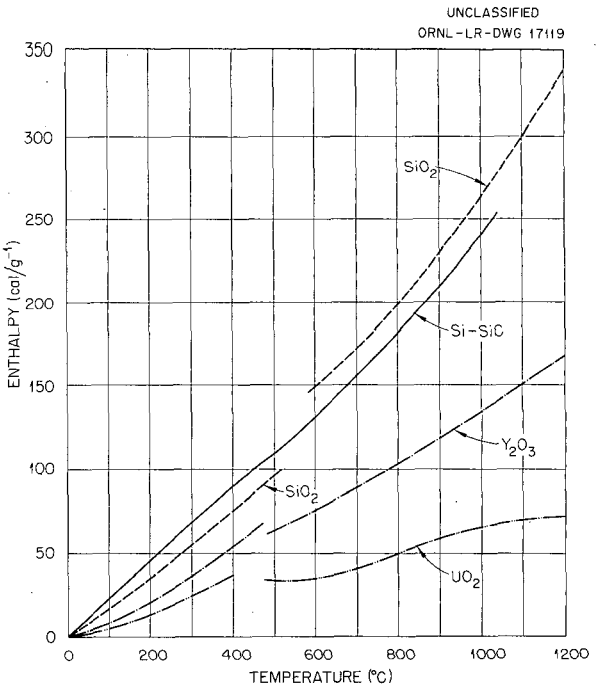

Fig. 216. Derived Enthalpy vs Temperature.

an expected value of 15 cal. A 20% spread in data is found in the 700 to 800°C region, and between 1000 and 1200°C there is a 16% drop from the published values. These discrepancies are sufficiently greater than the average error to be considered as an effect of the sample rather than having occurred as a result of the misfunction of the calorimeter system. A search of literature has disclosed that other investigators have noticed an erratic behavior of platinum in heat content and other physical properties determinations. Improper annealing, variation with temperature of the number of electrons, stresses from repeated quenching, possible contamination by silicon resulting in "hot-" and "cold-shortness," displacement of the chemical equilibrium, order-disorder transformations, recrystallization at high temperatures, polymorphous transition points, impurities, and strains are mentioned as possible explanations for anomalous behavior.

An electrical resistivity experiment is being devised as a means of determining the purity of the basket in present use. Regular "drop" experiments with new samples of platinum wire are planned to help in determining the true enthalpy values for the specimen holder so that the values for the eight

[3] K. K. Kelley, *Contributions to the Data on Theoretical Metallurgy. X. High-Temperature Heat Content, Heat-Capacity, and Entropy Data for Inorganic Compounds*, U.S. Bur. Mines, Bull. 476, 1949.

ceramic materials already measured may be corrected and verified.

DENSITY MEASUREMENTS – PYCNOMETER TECHNIQUES

M. P. Haydon

Specific gravity bottles fitted with thermometers and overflow capillaries were used to determine the densities of three ceramic materials. The values obtained are given below:

	Density (g/ml)
TAM zirconium oxide, 1860°C	
−100 mesh	5.735 ±0.014
As-received	5.707 ±0.042
Spodumene, 1100°C	
−100 mesh	2.377 ±0.007
Uranium dioxide, 1750°C	
−325 mesh	10.4640 ±0.275

The erratic results of the uranium oxide determinations were probably due to the hygroscopic nature of the material. Additional runs with precautions directed at moisture uptake during weighing are planned.

HIGH-TEMPERATURE X-RAY EXAMINATION OF HASTELLOY B

G. D. White

Physical property vs temperature measurements on Hastelloy B indicated a possible inversion at approximately 600°C. X-ray diffraction traces of this material were taken at temperatures up to 700°C. The only change in the tracings with increasing temperature was a shift in d values due to the thermal expansion of the specimen.

OPTICAL PROPERTIES OF YF_3

G. D. White

Crystals of YF_3 approximately 30 μ across the longest dimension were grown in order to measure their optical properties, which are given below:

Biaxial	$2V \sim 90$ deg
$\alpha = 1.536$	$\gamma = 1.568$
Colorless	

FLUORIDE FUEL COMPOUNDS

T. N. McVay

The usual petrographic examinations of fluoride compounds have been continued as in the past.

A bulletin containing optical and x-ray data on a large number of fluoride compounds is being assembled by H. Insley, T. N. McVay, R. E. Thoma, and G. D. White. This material is now being typed and should be ready for publication by the middle of September.

EFFECT OF LEAD ION ON THE UO_2 LATTICE PARAMETER

A. G. Tharp

B. Wasserstein[4,5] has suggested that it is possible to determine the age of uranium oxide ores by determining the lattice parameter change induced in cubic UO_2 by the formation of tetravalent lead ion by the radioactive decay of uranium. To prepare specimens for x-ray diffractometric study, Wasserstein heated samples of composition UO_{2+x} in hydrogen at 950°C, and for samples of composition UO_{2-x} he heat-treated them in an oxidizing atmosphere. In both instances a stoichiometry of UO_2 after heating is claimed. These observations are not consistent with previous observations in the uranium-oxygen system.[6]

To evaluate the observations of Wasserstein, synthetic samples of UO_2 containing lead ion were prepared for x-ray analysis, the most direct and and accurate method for determining whether or not lead ions would go into solid solution with UO_2 and, if so, the effect that this would have on the lattice parameter of UO_2. The UO_2 used in the preparations was obtained from decomposing ammonium diuranate. Baker and Adamson chemically pure lead monoxide was used as a source of lead ion. Free-energy calculations show that higher oxides of lead are unsatisfactory since they will decompose and oxidize UO_2 to a higher uranium oxide.

The first series of UO_2-PbO samples was prepared by heating to 1000°C for 2 hr in an inert

---

[4] B. Wasserstein, *Nature*, 174, 1004 (1954).

[5] B. Wasserstein, *Nature*, 176, 159, esp 160 (1955).

[6] J. J. Katz, E. Rabinowitch, *The Chemistry of Uranium*, NNES vol VIII-5, McGraw-Hill, New York, 1951.

atmosphere. Subsequent chemical analysis showed that the preparations contained practically no lead. Since PbO is not appreciably volatile at 1100°C, the lead ions must have been reduced, with subsequent volatilization of lead metal.

The next series of samples was prepared by heating at 700°C for 2 hr. From an initial lead content of 5, 10, and 15 mole % PbO, chemical analysis after heating showed 3.6, 7.8, and 11.7 mole % PbO. Petrographic analysis did not establish whether or not the lead was present as PbO.

X-ray analysis showed the presence of two phases; both phases gave face-centered cubic diffraction patterns. This suggests the presence of two CaF_2-type uranium oxide phases. Lattice parameters were determined for the pure UO_2 and the preparations. The following values, accurate to ±0.001 Å, were obtained:

	Å
UO_2, 0% PbO	5.465
UO_2, 3.6% PbO	5.465
UO_2, 7.8% PbO	5.464
UO_2, 11.7% PbO	5.465

The second phase gave a diffraction pattern unsuitable for lattice parameter determinations.

The third series of preparations was made by heating 5, 10, 15, 25, and 50 mole % PbO with UO_2. Examination by x ray showed that the preparations contained large amounts of metallic lead – the amount increasing with increasing PbO content. The 50 mole % pattern was so poor that lattice parameters could not be obtained for the UO_2 phase. The preparations with an initial PbO content of 15 and 25 mole % gave $a_0 = 5.468$ Å. The lattice parameters for the other preparations were not determined.

These experiments suggest that PbO is not soluble in UO_2 unless it is in very small quantities. It was positively shown that UO_2 will reduce lead monoxide to lead metal and form a higher oxide of uranium at temperatures near 800°C.

There remains the possibility that Wasserstein's method of age determination of uranium oxide ores is still valid. Lead dioxide formed by the radioactive decay of uranium could remain in the lattice without reacting with the uranium dioxide. To synthetically evaluate age determinations by x-ray methods UO_2-PbO_2 samples should be prepared and should be heated for several days at temperatures near 200°C.

WASTE DISPOSAL

R. L. Hamner

Heat Experiment No. 7

Heat treatment No. 7 was a laboratory-scale "hot pot" experiment designed to simulate conditions in Pilot Pit No. 1, that is, to pour the clay-flux slurry ungelled. The heating and sintering characteristics were compared with those of heat experiment No. 6, reported previously,[7] in which a gel was formed.

Mix No. 15 was poured as a thin slurry into the same shell used for heat experiment No. 6. A spiral Calrod heater was used, placed so that it would be in the center of a 6-in. cake. Approximately the same end result was achieved as with No. 6 with respect to power input and equilibrium vs time (200 w to attain 800°C in a 5-gal pot in a total time of about 14 days). However, the sintered cakes from these experiments differed in color and structure; there was considerably more variation in color in experiment No. 7, which indicates more inhomogeneity, and the porous structure of No. 7 was in the form of hollow pipes whereas that of No. 6 was more randomly oriented.

Pilot Pit No. 2 – Analysis of Final Cake

Visual examination of the final cake showed it to be apparently inhomogeneous with regard to composition. It was also apparent that heat distribution throughout the cake was poor, portions near the heaters being hard-sintered whereas some sections had not reached drying temperature; this is attributed to heater design and thermal conductivity of the mass.

Samples were taken from various locations within the cake and analyzed. X-ray analyses showed very distinct lines for $NaNO_3$ in some of the samples, indicating very low temperatures in these regions. No reaction products were identified. Petrographic analyses confirmed these results.

[7] S. D. Fulkerson and R. L. Hamner, *Met. Semiann. Prog. Rep. April 10, 1956*, ORNL-2080, p 198.

The inhomogeneity of the cake is pointed out by the chemical analyses shown in Table 81.

Heat Experiment No. 8

For the purpose of better design for auxiliary heaters that might be used in waste disposal pits such as Pilot Pit No. 1, it was considered necessary to determine the thermal conductivity of the clay-flux mix.

This experiment was designed for a cake 1 ft thick and 18 in. in diameter. A finger-type Calrod heater served as the heat source, being placed so that it would be located in the center of the sintered cake. Temperatures were measured by four thermocouples, one at the heater and the others placed radially in a line 2, 6, and 8 in. from the heat source. Since the mass could not be brought to the dry, as-sintered state with the finger heater, it was necessary to first bring it to 550°C (lowest temperature for fixation) on a hot plate and then to transfer it to an insulated shell for thermal conductivity measurements. The results are summarized below:

Maximum temperature attained	
On finger heater (T_1)	1839°F (1004°C)
2 in. from heater (T_2)	1119°F (604°C)
5 in. from heater (T_3)	780°F (416°C)
K between T_1 and T_2	4.676 Btu/ft^2·°F·hr per inch of thickness
K between T_2 and T_3	5.667 Btu/ft^2·°F·hr per inch of thickness

These data indicate that uniform efficient heating to fixation temperature by auxiliary heaters alone would be impractical because of the close spacing required.

Fixation of Radioisotopes in Clay-Flux Mixes and in Hope Solution Residue

Counts were made on leach solutions after 11 months' contact with clay-flux mix No. 15, which had been tagged with Sr^{90}, Ce^{144}, Ru^{106}-Rh^{106}, Cs^{137}-Ba^{137}, and mixed fission products and fired at temperatures from 850 to 1750°F.

With the exception of the Sr^{90}-tagged mix fired to 850°F and the mixes containing Cs^{137}-Ba^{137}, there was no appreciable radioactivity in the leach solutions. This is consistent with previous results obtained after short-time leaching.

To determine the effectiveness of the Al_2O_3 residue from the dried and fired Hope solution in fixing radioisotopes, samples tagged with mixed fission products were fired at temperatures from 500 to 1000°C and placed in leach water. The ratio of activity in the leach water to possible activity was on the order of 10^{-2} after three weeks. This ratio for clay-flux mixes such as Nos. 5 and 15 is on the order of 10^{-3}.

Monitoring of Radioactive Gases

A satisfactory technique for the monitoring of radioisotopes evolved during firing of clay-flux mixes has not yet been established. However, a

TABLE 81. CHEMICAL ANALYSES OF SAMPLES FROM PILOT PIT NO. 1

Sample Number	Constituents (%)											
	Si	Fe	Al	Ca	Mg	CO_3	Cl	PO_4	K	Na	SO_4	NO_3
1	8.30	2.91	15.1	10.6	0.72	6.2	<0.05	0.27	0.36	11.9	0.16	1.75
2	10.9	3.48	13.5	3.58	0.46	1.41	<0.05	0.20	1.08	9.0	0.085	18.7
3	26.0	4.37	8.95	3.28	0.69	0.18	<0.05	0.41	2.2	7.4	0.20	0.62
4	9.37	2.90	11.1	5.16	0.48	0.91	<0.05	0.19	0.88	11.5	0.031	28.1
5	15.7	2.87	15.0	10.4	0.65	1.65	<0.05	0.25	0.82	10.1	0.41	0.73
6	5.86	2.22	11.0	7.4	0.53	2.4	<0.05	0.22	1.28	13.8	0.19	32.0
7	10.4	3.56	16.3	8.4	0.70	3.51	<0.05	0.37	0.89	13.1	0.69	0.94
8	11.1	3.26	17.6	6.6	0.55	4.39	<0.05	0.36	1.30	10.7	0.63	0.048
Standard error	2	2	2	2	5	5		5	5	5	5	5

preliminary run was made with the count rate recorder for the evolution of Ru^{106}-Rh^{106} from Hope solution and its residue up to 1000°C. No appreciable activity was noted until 425°C had been reached. At this temperature there was a burst of activity, which subsided at approximately 450°C. During this period yellowish fumes, indicating nitrate evolution, were also noted, and so it is possible that at least part of the Ru^{106}-Rh^{106} evolution was due to entrainment rather than to gaseous evolution.

New Compositions for Fixation

The new compositions listed in Table 82 were mixed and fired to 800, 1000, and 1200°F for leaching experiments.

Petrographic Examination of Clay-Flux Mixes

To determine the feasibility of identifying phases in clay-flux mixes which fix radioisotopes, compositions 5 and 15, untagged, were fired at temperatures of 500 to 1100°C and examined petrographically. Quartz, which presumably plays no part in fixation, was the only crystalline phase which could be recognized in the samples. However, it was noted that samples fired below 900°C remained as a very-fine-grained material, which would have an enormous surface area for fixation.

Beryllium Oxide Specimens

R. L. Hamner

Beryllium oxide specimens $1\frac{1}{8} \times 1\frac{1}{4}$ in. and $1 \times \frac{1}{2}$ in., hot-pressed to a density of 97% theoretical, were submitted for corrosion testing.

The following properties were determined for a 4 × 4 × 2 in. hot-pressed block of BeO received from Saclay, France:

Bulk density (av)	2.956 (97.8% theoretical)
Porosity	0.00
Modulus of rupture, psi	42,527
Modulus of elasticity, psi	52,354,000
Linear coefficient of thermal expansion perpendicular to direction of pressing	
at 100–400°C	0.77×10^{-5} in./in./°C
at 400–700°C	0.85×10^{-5} in./in./°C
at 700–1000°C	1.16×10^{-5} in./in./°C
at 1000–1200°C	1.21×10^{-5} in./in./°C
av, 100–1200°C	0.98×10^{-5} in./in./°C
Linear coefficient of thermal expansion parallel to direction of pressing	
at 100–400°C	0.78×10^{-5} in./in./°C
at 400–700°C	0.92×10^{-5} in./in./°C
at 700–1000°C	1.07×10^{-5} in./in./°C
at 1000–1200°C	1.21×10^{-5} in./in./°C
av, 100–1200°C	0.97×10^{-5} in./in./°C

Boron

R. L. Hamner

Attempts were made to fabricate boron by adding small amounts of B_2O_3 and then hot-pressing. Specimens containing 5% B_2O_3 were hot-pressed at 900°C and 1500 psi. They had only 50% theoretical density.

TABLE 82. CLAY-FLUX COMPOSITIONS FOR RETENTION OF RADIOISOTOPES CONTAINED IN HOPE SOLUTION

Composition Number	Na_2CO_3 (g)	Limestone (g)	Phosphate Slimes, −100 mesh (g)	Tennessee Ball Clay, −100 mesh (g)	Hope Solution Plus Cs^{137}-Ba^{137} (ml)
28	30	30	200		250
29	30	30	100		250
30	30	30	50		250
37	30	30		200	250
38	30	30		100	250
39	30	30		50	250

FUNDAMENTAL METALLURGY

FUNDAMENTAL PHYSICO-METALLURGICAL RESEARCH

L. K. Jetter
J. O. Betterton, Jr.
D. S. Easton
C. J. McHargue
G. D. Kneip, Jr.
J. O. Scarbrough
J. C. Ogle
Metallurgy Division
W. K. Noyce
Summer Employee
R. J. Bohnhoff
Co-op Student

FUNDAMENTAL STUDIES OF ZIRCONIUM ALLOYS

J. O. Betterton, Jr. G. D. Kneip, Jr.
D. S. Easton J. Scarbrough
W. K. Noyce R. Bohnhoff

The objective of this group is to determine the factors which affect the alloys of group IVA elements. As reported in the past, a general phase-diagram program has been under way in order to determine the effects of adding solutes of different valency, Ag, Cd, In, Sn, Pb, and Sb, to zirconium. Recently, the work has been extended to include the effects of the same solutes on the axial ratio and upon the low-temperature specific heat of hexagonal zirconium. In the present discussion, the recent results on the Ag-Zr, Cd-Zr, In-Zr, Pb-Zr, and Sb-Zr phase diagrams will be given.

The Silver-Zirconium System

D. S. Easton J. O. Betterton, Jr.

The principal features of the constitution diagram of silver-zirconium were shown earlier[1,2] to be the presence of two intermediate phases, gamma and delta, at compositions Zr_2Ag and ZrAg, respectively, and a eutectoid decomposition of the beta phase in the zirconium-rich end. It was contended in the last report[3] that the phase boundaries of the beta phase were essentially independent of the variations in minor impurities in iodide zirconium, which have substantial effects upon the phase boundaries of the alpha phase. More detailed investigation with alloys prepared from batch No. 6 iodide zirconium (typical impurities present in this zirconium are 132 ppm Hf, 79 ppm C, 24 ppm Fe, 11 ppm Ni, 13–222 ppm O, 1–50 ppm N, all others <10 ppm) of the $\beta/(\alpha+\beta)$ boundary, however, has now shown a small displacement of this boundary (0.3–0.4 at. %) to lower silver contents, as compared with earlier results (see Fig. 217). Vickers hardness differences in

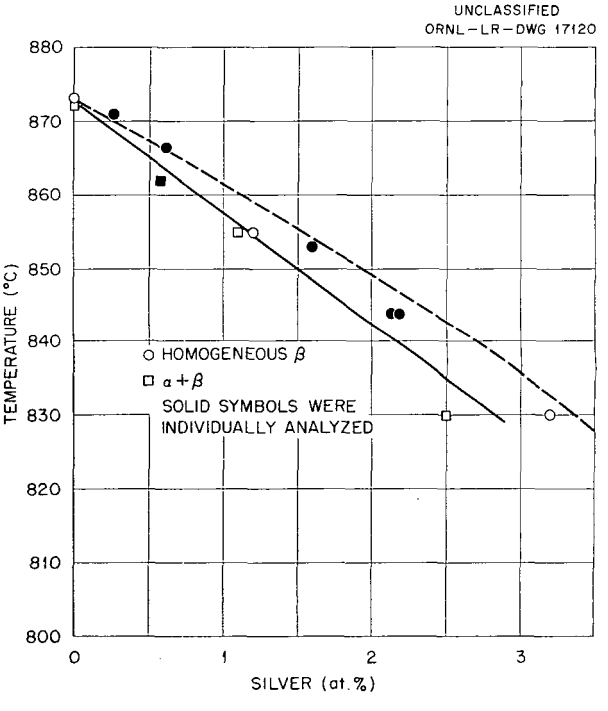

Fig. 217. Comparison of the $\beta/(\alpha+\beta)$ Phase Boundary in the Silver-Zirconium System, Determined Recently with Improved Alloys (Solid Line), with the Earlier Phase Boundary (Dashed Line).

[1] D. S. Easton, G. W. Cunningham, and J. O. Betterton, Jr., *Met. Semiann. Prog. Rep. April 10, 1954*, ORNL-1727, p 120.

[2] D. S. Easton and J. O. Betterton, Jr., *Met. Semiann. Prog. Rep. April 10, 1955*, ORNL-1911, p 16.

[3] D. S. Easton and J. O. Betterton, Jr., *Met. Semiann. Prog. Rep. April 10, 1956*, ORNL-2080, p 21.

the two sets of data suggest that the effect is due to the smaller contents of alpha-stabilizing hardening impurities in the new alloys.

The Cadmium-Zirconium System

D. S. Easton J. O. Betterton, Jr.

Attempts to make arc castings of cadmium-zirconium alloys have not been successful because of the high vapor pressure of cadmium. Alloys, however, have been prepared by annealing cadmium inside a zirconium container. Assemblies of this type were wrapped in zirconium and molybdenum foil and annealed at 581°C for five days and at 901°C for 12 days.

In the specimen annealed at 581°C most of the cadmium (nominally 19.7 at. %) diffused into the zirconium or formed intermediate phases, leaving little liquid cadmium in the interior of the container. A microstructure of the diffusion region is shown in Fig. 218, where two layers of intermediate phases appear on the interior surface of the alpha zirconium container. The results of x-ray and neutron activation analyses of specimens removed from the diffusion zone are given in Table 83 and show that the cadmium-rich layer has a composition in the vicinity of $ZrCd_2$ and a simple face-centered cubic structure, with $a = 4.37 \pm 0.01$ Å. The layer which is immediately adjacent to the zirconium was found to have a simple face-centered cubic structure, with $a = 4.43 \pm 0.01$ Å. The best indication of the composition of this phase was obtained from the specimen annealed at 901°C, in which, after the complete diffusion of the cadmium (nominally 8 at. %) into the zirconium, only the zirconium-rich intermediate phase was observed on the interior of the beta zirconium. Fragments of this phase were removed, and, as shown in Table 83, the composition was in the vicinity of Zr_2Cd.

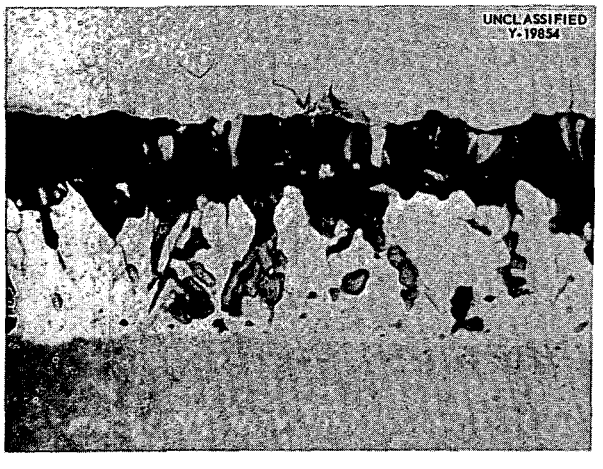

Fig. 218. Diffusion Couple Between Liquid Cadmium and Zirconium Quenched After 5 Days at 581 ± 15°C. The sequence of phases, with the Cd content decreasing from top to bottom is as follows: $ZrCd_2$ phase (microhardness 85 VHN), Zr_2Cd phase (microhardness 166 VHN, brittle and probably decomposed on quenching), alpha zirconium (microhardness 72 VHN). Unetched. 750X. Reduced 30%.

The phase diagram from the limited preliminary results above appears to consist of at least two intermediate phases of the approximate compositions Zr_2Cd and $ZrCd_2$. The former phase is in equilibrium with alpha zirconium of limited solubility at 581°C and with beta zirconium of limited solubility at 901°C. The microstructure of the Zr_2Cd phase shows that this phase is partially transformed during quenching. If this were by a eutectoid reaction below 581°C, the results would be consistent with those obtained by Pietrokowsky,[4] in which a face-centered cubic phase ($a = 4.3768$ Å) of the composition $Zr_{1-x}Cd_x$ ($x > 0.6$) is in equilibrium with alpha zirconium at 371°C. The face-centered tetragonal phase which Pietrokowsky observed in alloys containing 67, 75, and 80 at. % Cd after four days at 371°C was not observed in the present experiments at 581 or 901°C. Some information on the cadmium-rich end of the system was obtained from an interrupted casting experiment. The microstructure of the liquid phase indicated that cadmium forms a eutectic with an unidentified intermediate upon cooling.

On the basis of the preliminary experiments, the rate of diffusion of cadmium in zirconium appears to be quite appreciable. Additional experiments are required to determine if alloys of uniform composition can be prepared by longer anneals or by arc casting the diffused material.

The Indium-Zirconium System

W. K. Noyce J. O. Betterton, Jr.

In the earlier indium-zirconium phase-diagram study, the peritectoid region of the diagram was

[4] P. Pietrokowsky, *Trans. Am. Inst. Mining Met. Engrs.* 200, 219 (1954).

TABLE 83. RESULTS OF X-RAY AND ACTIVATION ANALYSES OF SAMPLES REMOVED FROM THE Zr-Cd DIFFUSION COUPLES

Location of Sample	Temperature (°C)	Analyzed Composition of Sample (at. % Cd)	Phases Present in the X-Ray Patterns*
Interior Zr container	581	0.54	Close-packed hexagonal, $a = 3.22$ Å, $c = 5.14$ Å
Zr container near interface	581	0.47	Close-packed hexagonal, $a = 3.23$ Å, $c = 5.15$ Å
Grindings near zirconium-rich intermediate phase	581	45.5	50% face-centered cubic, $a = 4.37$ Å 50% face-centered cubic, $a = 4.42$ Å
Coarse fraction of crushed residue from the interior of the assembly	581	63.2	75% face-centered cubic, $a = 4.37$ Å 25% face-centered cubic, $a = 4.44$ Å
Cadmium-rich intermediate phase	581	66.7	Face-centered cubic, $a = 4.37$ Å
Fine fraction of crushed residue from the interior of the assembly	581	72.2	Face-centered cubic, $a = 4.37$ Å
Zirconium-rich intermediate phase	901	37	Face-centered cubic, $a = 4.46$ Å
Interior Zr container	901	0.51	

*X-ray spacings are not determined more accurately than ±0.01 Å, since the precaution was not taken of protecting the samples from air oxidation during preparation. Extra lines at d spacings of 8.4, 7.1, 5.5, 4.9, 4.3, 3.3, and 2.9 Å were observed in diffraction patterns of the higher-cadmium samples. These lines are considered to be related to a reaction with the atmosphere.

made uncertain by the occurrence of a three-phase ($\alpha + \beta + \gamma$) structure in an alloy containing 11.4 at. % In at 1040°C. This specimen was suspected of contamination because it was the end piece of cold-rolled ingot and had slight cracks in its surface. A new set of alloys was prepared from batch No. 6 zirconium in the range 7.8–11 at. % In. The results of the anneals on these alloys which have been completed are shown in Fig. 219, which includes the results of the earlier study. The composition of these alloys has not yet been analyzed but is plotted on the basis of an empirical correction curve derived from the earlier indium-zirconium analyses. The results agree with the previous diagram and show by the presence of ($\alpha + \beta + \gamma$) structures at 1007°C that minor impurities remain in these alloys sufficiently great to prevent the determination of a single-temperature horizontal for the peritectoid reaction. Establishment of the fact that the beta phase is in equilibrium with the gamma phase at 1023 and 1039°C removes the earlier discrepancy from the phase diagram.

The Antimony-Zirconium System

J. O. Betterton, Jr.

Additional results on the zirconium-rich end of the zirconium-antimony system have been obtained and are shown with the earlier results in Fig. 220. A number of the microscopical specimens were individually analyzed (indicated by the filled symbols) and are in good agreement with the compositions indicated by weight changes.

Several of the final alloys used in the Sb-Zr and In-Zr investigations have been analyzed for minor impurities by the neutron activation and the vacuum-fusion (Pt bath) methods. The results are given in Table 84.

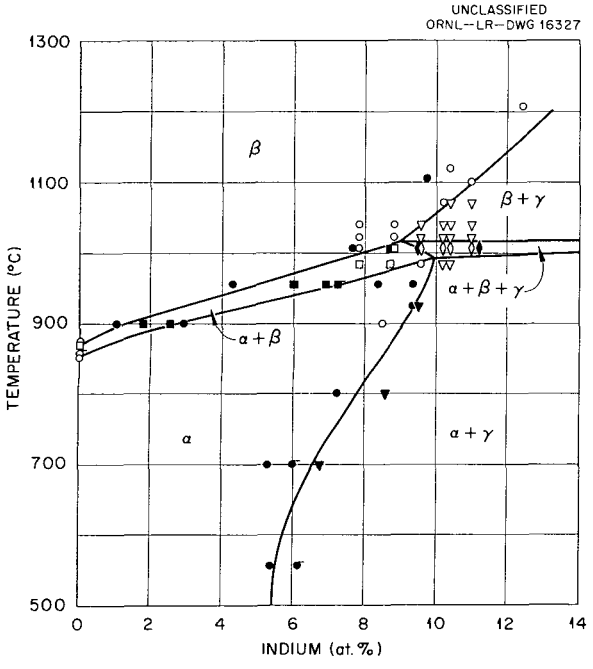

Fig. 219. Results of the Final Investigation of the Indium-Zirconium Phase Diagram in the Region 0–13 at. % Indium.

Zirconium-Lead System

G. D. Kneip, Jr. J. Scarbrough

An exceptionally pure bar of batch No. 6 iodide zirconium was chosen for the alloying studies of this system by neutron activation analyses and

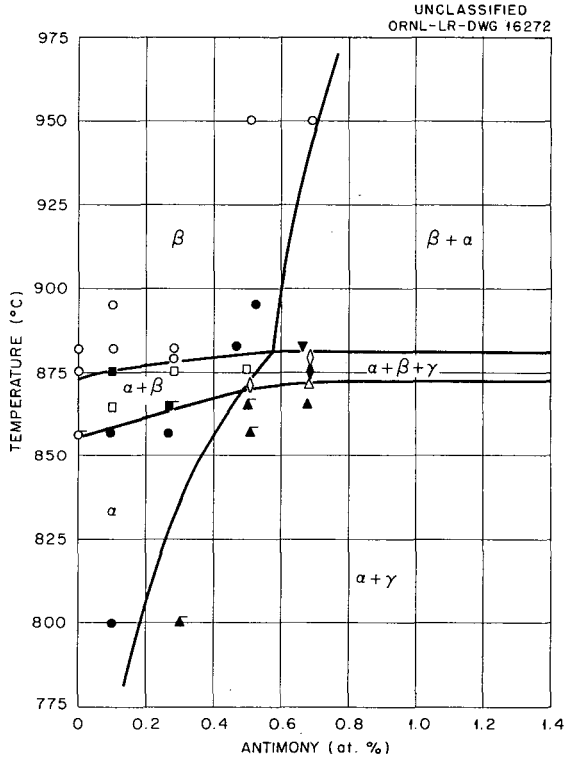

Fig. 220. Results of the Final Investigation of the Peritectoid Region of the Antimony-Zirconium System.

TABLE 84. MINOR IMPURITIES IN PHASE-DIAGRAM ALLOYS

	Amount by Neutron Activation (ppm)						Amount by Vacuum Fusion (Pt Bath) (ppm)		
	Cu	Fe	Mo	Ni	Si	W	H	O	N
Antimony-zirconium system	5.6	28		8.2	12	9	9	23	1
	7.3	29		1.0	15	12.5	10	26	2
Indium-zirconium system	18.0		6.1	49	34		3.8		
	16.0	50		21	8	4	3.6		
	10.0	83	6.7	45	67				
	<1.0			57	42	10			

for studies of the temperature width of the α/β transformation. The analysis of some of the metallic impurities, as given by the neutron activation method, is given below:

Metallic Impurity	Amount (ppm)
Fe	14.2
Ni	7.0
Cr	6.0
Si	13.0
Cu	0.6
Mo	1.4
W	0.05
Ta	17.00

For this material the α/β transformation takes place over the temperature range of approximately 10°C, or from 863 to 873°C.

Several zirconium-rich alloys have been made by arc melting on a water-cooled copper hearth in an argon atmosphere. The melting conditions were such that the casting apparatus could be evacuated to approximately 10^{-7} mm Hg and closed off from the pumps for leak testing prior to the introduction of the argon melting atmosphere. Leak rates of 2×10^{-6} mm_{Hg}·liter/min were obtained prior to arc melting to minimize oxygen and nitrogen contamination.

Alloys in the form of 20-g buttons were found to be segregated after melting six times, even though the button was turned over between each remelting. In order to remove this segregation it was found necessary to roll the ingots to approximately a $\frac{1}{16}$-in. sheet and then remelt them an additional six times.

The as-cast microstructures of the homogeneous alloys containing up to 6 at. % lead were all found to be a relatively fine-grained transformed beta structure. Lead increases the hardness of zirconium almost linearly up to 6 at. % lead, as shown in Fig. 221.

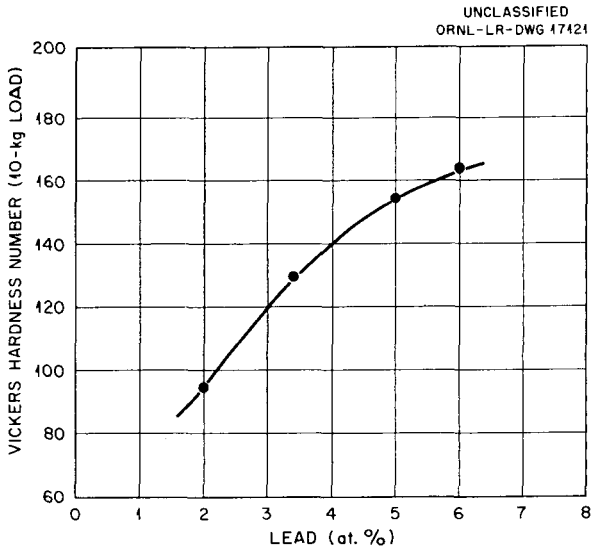

Fig. 221. Hardness of Arc-melted Zirconium-Lead Alloys.

Zirconium α/β Transformation

G. D. Kneip, Jr. R. Bohnhoff

Determination of a more accurate zirconium α/β transformation temperature than that previously obtained by thermal analysis[5,6] is desirable for the study of the effects of solutes on this transformation. Exceptionally pure zirconium which has been produced by the zone-refining process[7] is now available for the determination of the transformation temperature. The method of isothermal annealing was chosen as the most sensitive means of studying the transformation region. The preliminary results of this experiment are shown in Fig. 222. In general, the effects shown in the figure are consistent with the impurity movements expected in the zone-refining process. In the purest part of the rod the transformation is found to take place at 870 ± 3°C. The temperatures were measured with calibrated platinum–10% rhodium thermocouples, and the same precautions to prevent contamination during the annealing were taken as were described earlier.

PREFERRED ORIENTATION IN THORIUM SHEET

C. J. McHargue L. K. Jetter

In order to study the progressive development of preferred orientation and its effect on mechanical properties, textures have been determined for cold-rolled and annealed thorium sheet.

[5] R. Vogel and W. Tonn, *Z. Anorg. Chem.* 202, 292 (1931).

[6] G. W. Cunningham and J. O. Betterton, Jr., *Met. Semiann. Prog. Rep. April 10, 1954*, ORNL-1727, p 108.

[7] J. O. Betterton, Jr., G. D. Kneip, Jr., and R. J. Bohnhoff, *Met. Semiann. Prog. Rep. April 10, 1956*, ORNL-2080, p 230.

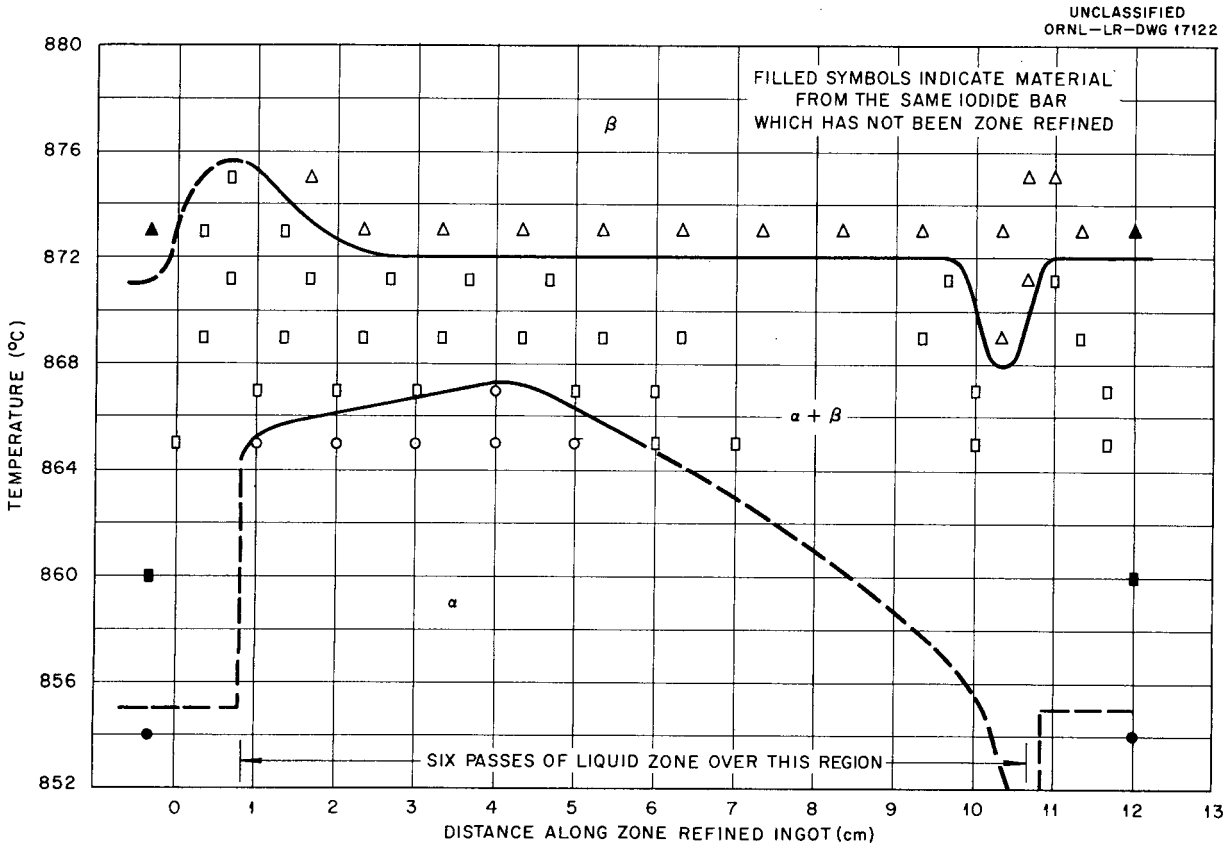

Fig. 222. Transition Temperature of Zone-refined Zirconium as a Function of Distance Along the Rod.

A 3.125-in.-dia billet of Ames thorium was extruded to a 1 × 2 in. bar at a rate of approximately 500 fpm and with a billet temperature of 850°C. Portions of this bar were cold-rolled to 0.250 and 0.050 in., which amounted to reductions in thickness of 75 and 95%, respectively. Reductions of the order of 25% per pass were used, and the direction of rolling was changed 180 deg after each pass. Vacuum-annealing treatments of 10 min at 900°C were given to specimens from each sheet.

X-ray diffraction specimens were 0.200-in.-dia spheres taken from the centers of the extruded bar and the 0.250-in. sheet. Pieces of the 0.050-in. sheet were bonded with an adhesive to give laminates from which 0.200-in. specimens were machined.

Pole-distribution data and axis-distribution charts were obtained by the usual ORNL method, using diffraction from the following planes: {111}, {002}, {022}, {113}, {222}, {004}, {133}, {024}, {224}, and {135}. Axis-distribution charts were obtained for the rolling and normal directions and, in some instances, the transverse direction.

Because of the nature of plastic flow in producing the 1 × 2 in. bar, a sheet-type texture would be expected to develop. The axis-distribution charts for the extrusion direction and for the direction normal to the 2-in.-wide face are illustrated in Fig. 223. It may be seen that the most prominent extrusion direction is <001> and that there is also a <114> component. The most preferred normal direction is also <001>, but there is a second component 3 deg from <034>. These preferred directions can be combined to give the components $\{001\}\langle\bar{1}00\rangle$ and the near $\{034\}\langle\bar{4}\bar{1}1\rangle$, as shown in Fig. 224. The distribution of transverse directions (normal to the 1-in.-wide face) was consistent with this selection of texture components. A

UNCLASSIFIED
ORNL-LR-DWG 14908

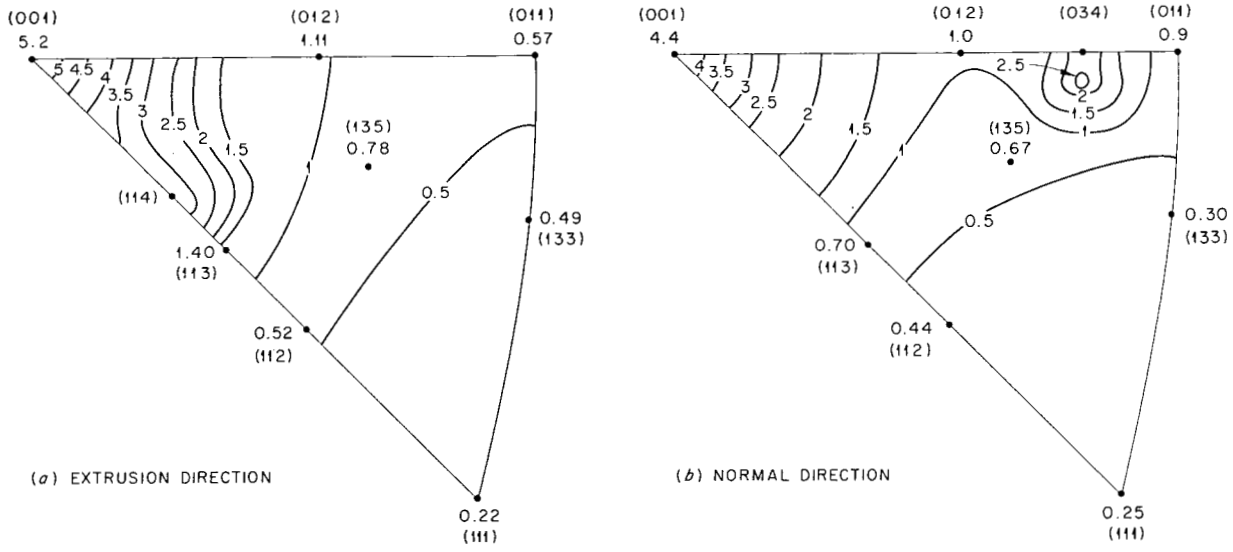

Fig. 223. Axis Distribution Charts for (*a*) Extrusion Direction and (*b*) Normal Direction of 1 × 2 in. Thorium Bar Extruded at 850°C and a Rate of 500 fpm.

UNCLASSIFIED
ORNL-LR-DWG 16755

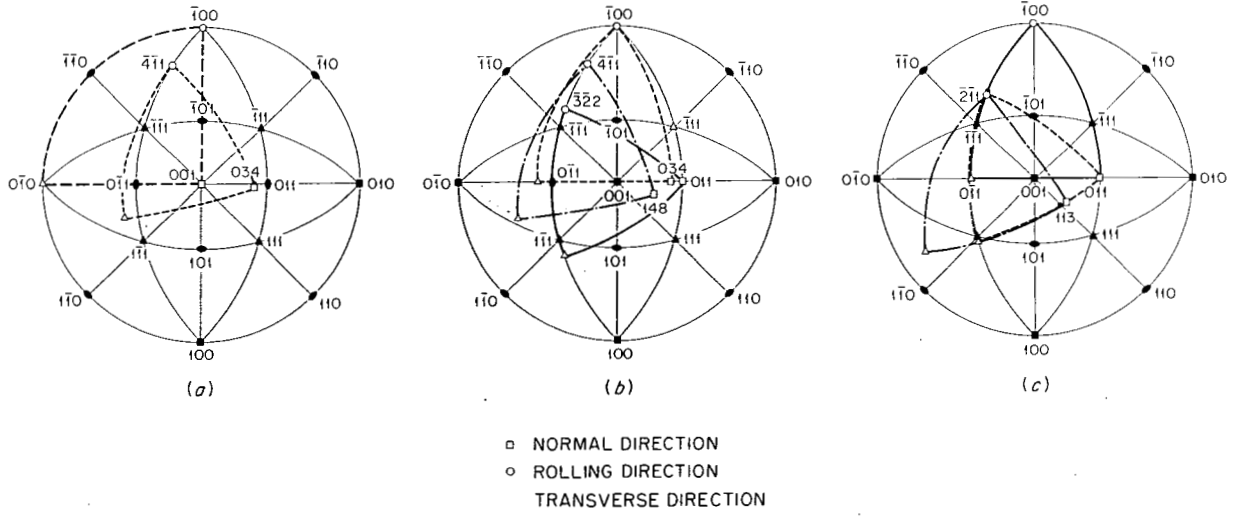

Fig. 224. Standard Stereographic Projection Illustrating the Components of the Sheet Textures of Thorium. (*a*) As-extruded 1 × 2 in. bar, near {034} <$\bar{4}\bar{1}1$>, {001} <$\bar{1}\bar{0}0$>. (*b*) Cold-rolled 75%, {011} <$\bar{3}\bar{2}2$>, {034} <$\bar{1}\bar{0}0$>, {148} <$\bar{4}\bar{1}1$>. (*c*) Cold-rolled 95%, {011} <$\bar{1}\bar{0}0$>, near {113} <$\bar{2}\bar{1}1$>, near {011} <$\bar{2}\bar{1}1$>.

metallographic examination showed that the bar was completely recrystallized in the as-extruded condition. These texture components, therefore, appear to have been developed when recrystallization occurred during the deformation process.

The axis-distribution charts for the rolling and normal directions of the sheet reduced 75% in thickness by cold rolling are given in Fig. 225. The more preferred rolling directions are <001>, with spread to and including <114>, and <223>. The crystallographic directions preferentially aligned with the normal direction are <148> and a position near <034>. Figure 224 shows that the texture components, therefore, are {148} <$4\bar{1}1$>, {011} <$3\bar{2}2$>, and {034} <$\bar{1}00$>.

The sheet cold reduced 95% in thickness developed the orientations shown in Fig. 226. The more preferred crystallographic directions of the rolling direction are <001> and a direction 2 deg from <112>. There is a spread of orientations between these along the <$1\bar{1}0$> zone. The normal directions are distributed primarily about <011> and a direction 3 deg from <113>. The components of the texture, shown in Fig. 224, are near {113} <$2\bar{1}1$>, {011} <$\bar{1}00$>, and near {011} <$2\bar{1}1$>.

The texture developed in the sheet cold rolled 75% and annealed 10 min at 900°C is shown in the axis-distribution charts of Fig. 227. The crystallographic direction preferentially aligned with the rolling direction was <001>, with some spread toward <013>. The normal direction was aligned with <017>. As shown in Fig. 228, the principal texture component is {017} <$\bar{1}00$>, an orientation slightly off the "cube" texture position.

Figure 229 shows the axis-distribution charts for the sheet cold rolled 95% and annealed 10 min at 900°C. The principal texture is the "cube" orientation, {001} <$\bar{1}00$>; however, a minor component with the approximate indices {013} <$0\bar{3}1$> is indicated by the spread in the distribution of both the rolling and normal directions.

The {148} <$4\bar{1}1$> component noted from the axis-distribution charts of the sample cold rolled 75% is not far from the near {123} <$2\bar{1}1$> component used by Smallman to describe his pole figures for cold-rolled thorium,[8] and from the components used by others to describe the textures of aluminum[9,10] and copper.[9] However, in the present

[8] R. E. Smallman, *J. Inst. Met.* 83(9), 408 (1955).

[9] H. Hu, P. R. Sperry, and P. A. Beck, *Trans. Am. Inst. Mining Met. Engrs.* 194, 76 (1952); *J. Metals* 5(1), 76 (1952).

[10] L. K. Jetter, C. J. McHargue, and R. O. Williams, *J. Appl. Phys.* 27, 368 (1956).

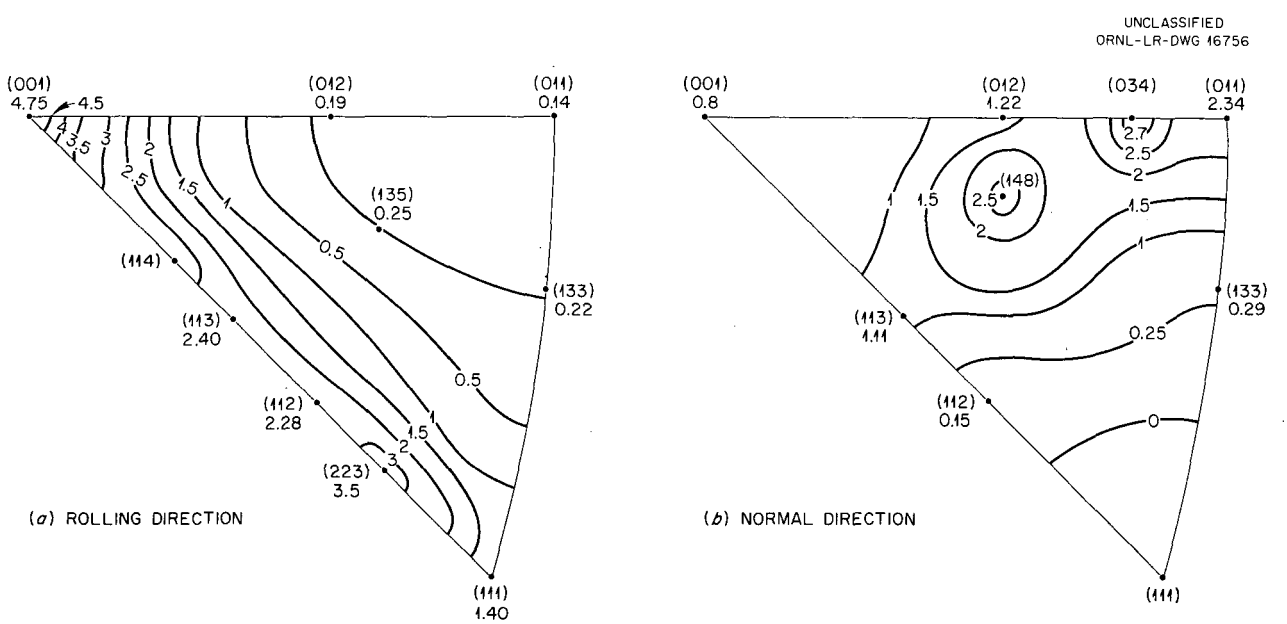

Fig. 225. Axis Distribution Charts for (*a*) Rolling Direction and (*b*) Normal Direction of Thorium Sheet Cold Rolled 75%. The starting texture was that in Fig. 220.

UNCLASSIFIED
ORNL-LR-DWG 14910

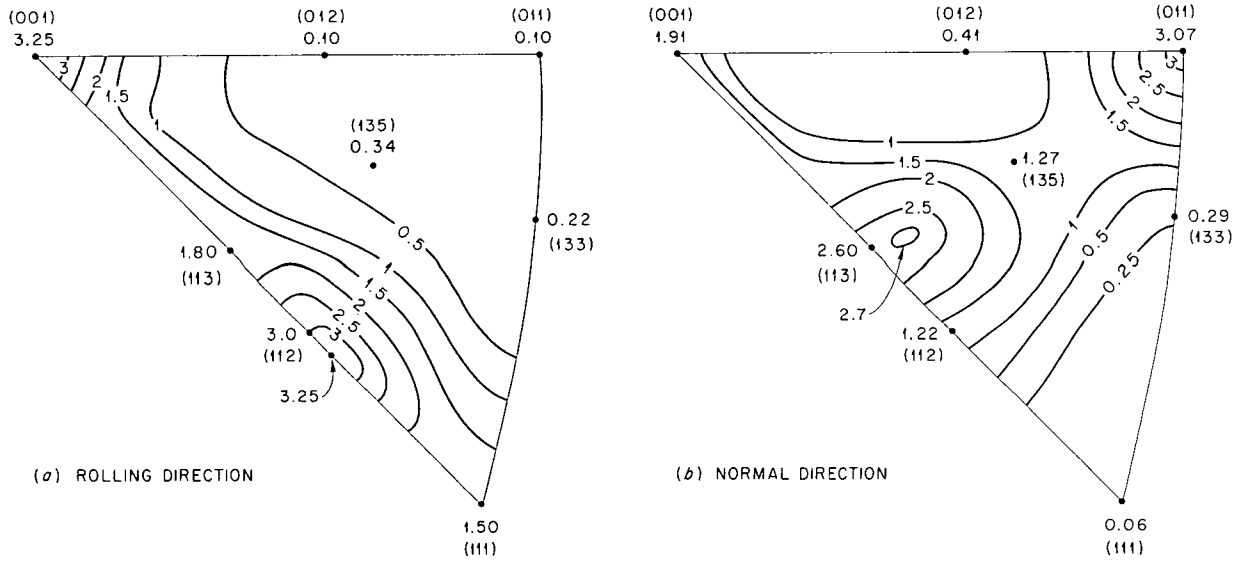

Fig. 226. Axis Distribution Charts for (*a*) Rolling Direction and (*b*) Normal Direction of Thorium Sheet Cold Rolled 95%. The starting texture was that in Fig. 220.

UNCLASSIFIED
ORNL-LR-DWG 15082

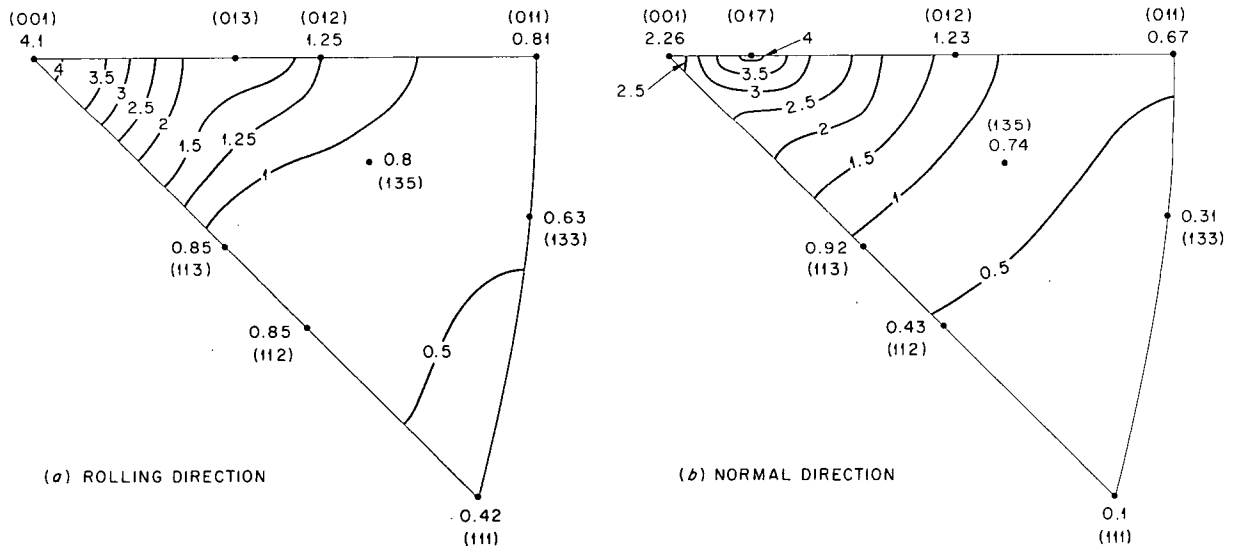

Fig. 227. Axis Distribution Charts for (*a*) Rolling Direction and (*b*) Normal Direction of Thorium Sheet Cold Rolled 75% and Annealed 10 min at 900°C.

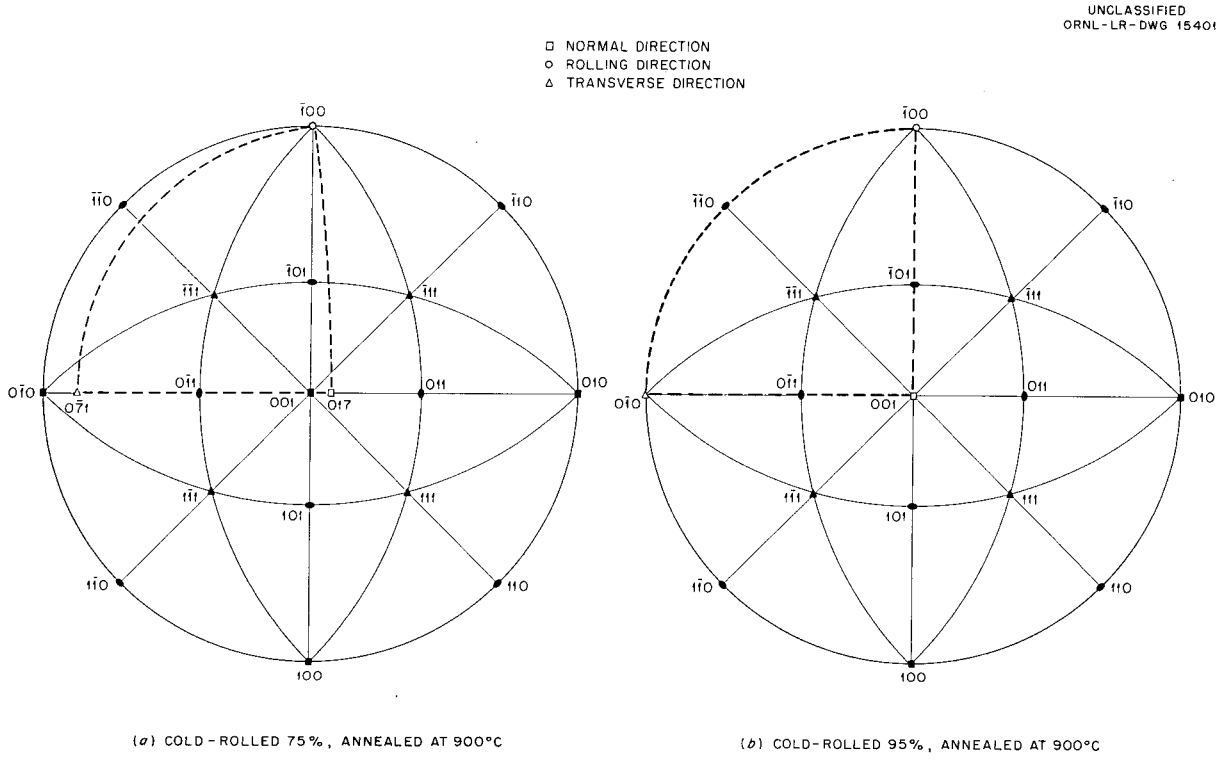

Fig. 228. Standard Stereographic Projection Illustrating the Components of Sheet Textures of Annealed Thorium. (*a*) Prior reduction of 75%. (*b*) Prior reduction of 95%.

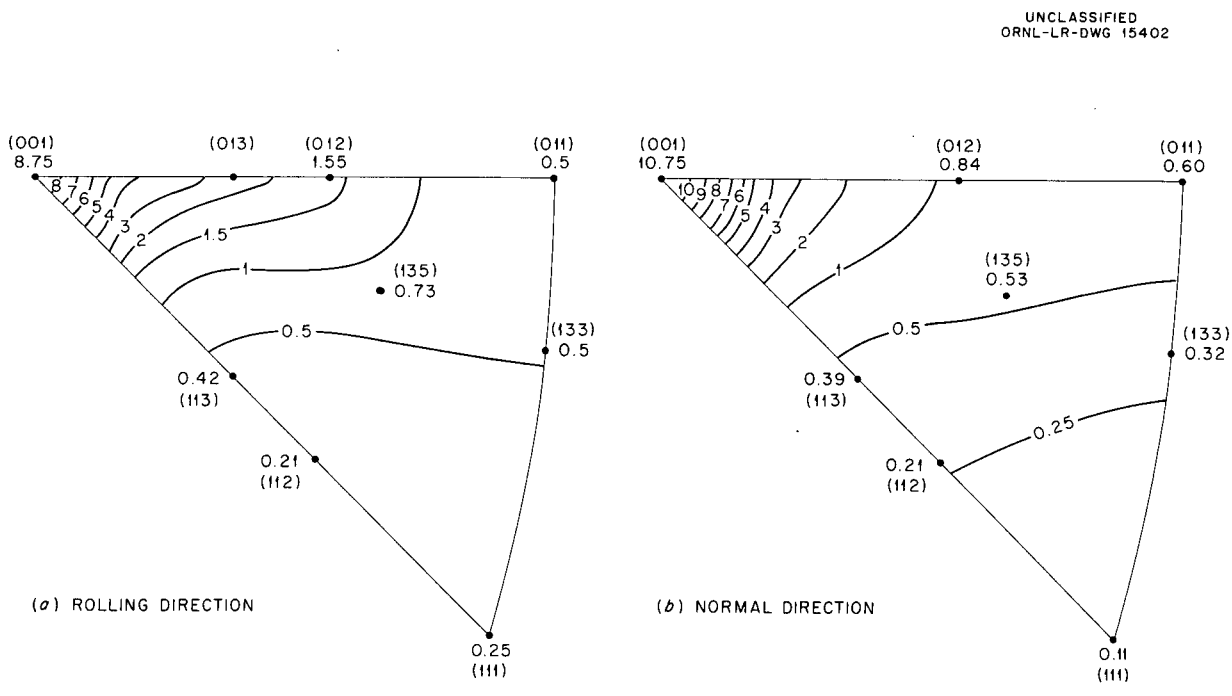

Fig. 229. Axis Distribution Charts for (*a*) Rolling Direction and (*b*) Normal Direction of Thorium Sheet Cold Rolled 95% and Annealed 10 min at 900°C.

study, two additional components were present, $\{011\}\langle\bar{3}\bar{2}2\rangle$ and $\{034\}\langle\bar{1}00\rangle$.

It was found that the $\{111\}$ and $\{002\}$ pole figures given by Smallman for resintered thorium cold rolled 95% can be described by two of the three texture components shown in Fig. 224c. These components were determined from the axis-distribution charts of Fig. 226. The near $\{113\}\langle\bar{2}\bar{1}1\rangle$ and near $\{011\}\langle\bar{2}11\rangle$ textures account for the regions of high density and for the major spreads of the conventional pole figures. Figure 230 shows the $\{111\}$ pole figure published by Smallman with the "ideal" positions of these orientations and the $\{123\}\langle\bar{2}\bar{1}1\rangle$ type. It is apparent that the selection of orientations to describe the texture cannot be readily made from the conventional pole figure.

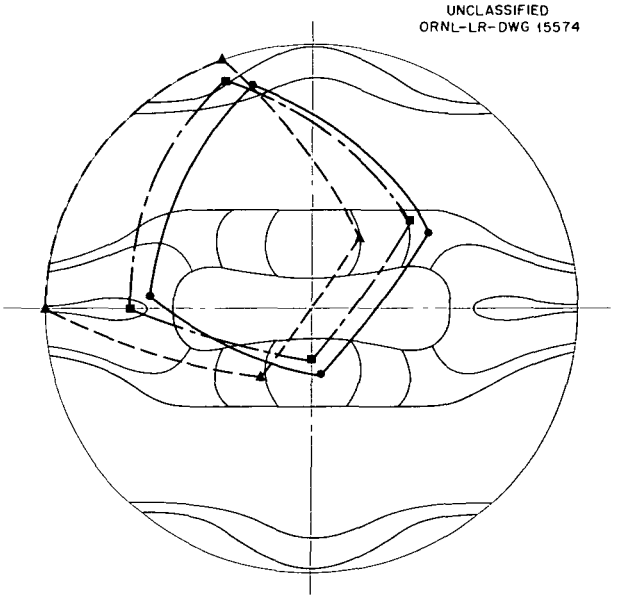

Fig. 230. The $\{111\}$ Pole Figure According to Smallman (Ref 8), Showing the "Ideal" Positions for ● Near $\{113\}\langle\bar{2}\bar{1}1\rangle$, Δ Near $\{011\}\langle\bar{2}\bar{1}1\rangle$, ■ $\{123\}\langle\bar{2}\bar{1}1\rangle$.

The preferred orientation obtained on rolling and subsequent annealing was $\{017\}\langle\bar{1}00\rangle$ for a 75% prior reduction and $\{001\}\langle\bar{1}00\rangle$ for a 95% prior reduction. Smallman apparently observed the "cube" texture for prior reductions of 60%, 80%, 90%, and 95%; however, since the orientation $\{017\}\langle\bar{1}00\rangle$ is only 8 deg from $\{001\}\langle\bar{1}00\rangle$, it is probable that by the conventional technique this difference would have been noted only as a spread about the latter orientation.

It was found that one texture component in the sheets given prior reductions of 75% and 95% could be related to the annealing textures by rotations about $\langle111\rangle$ axes. The reorientations that are necessary in order to cause the observed changes in texture are shown in Fig. 231. The four $\langle111\rangle$ axes of the $\{017\}\langle\bar{1}00\rangle$ orientation coincide with a $\langle111\rangle$ axis of each of the four equivalent orientations of the rolling texture components $\{148\}\langle\bar{4}\bar{1}1\rangle$. Thus, the annealing texture is related to each of the $\{148\}\langle\bar{4}\bar{1}1\rangle$ type orientations by a $\langle111\rangle$ rotation of 24 deg.

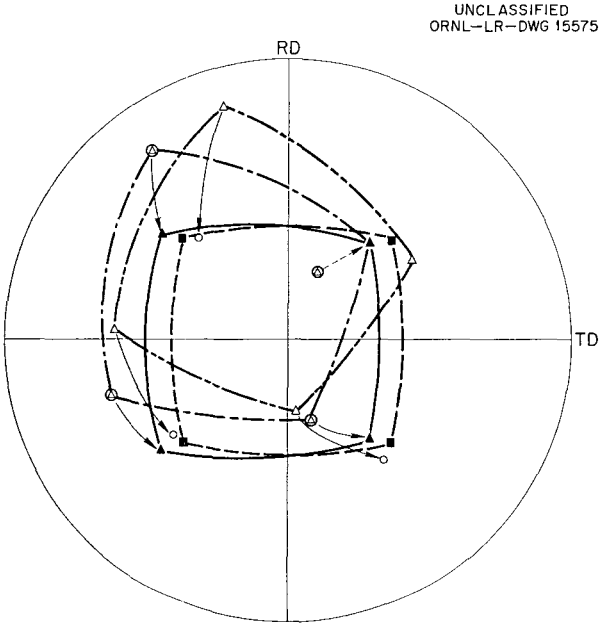

Fig. 231. Orientation Relationships Between Rolled and Annealed Components of Sheet Textures of Thorium. Ⓐ $\{148\}\langle\bar{4}\bar{1}1\rangle$, Δ $\{017\}\langle\bar{1}\bar{0}0\rangle$, ■ $\{001\}\langle\bar{1}\bar{0}0\rangle$, ▲ near $\{113\}\langle\bar{2}\bar{1}1\rangle$.

In the case of the 95% rolled sheet, the four $\langle111\rangle$ axes of a cube orientation are near a $\langle111\rangle$ axis of each of the four orientations of the rolling texture component $\{113\}\langle\bar{2}\bar{1}1\rangle$. A rotation of approximately 37 deg brings each of the four $\{113\}\langle\bar{2}\bar{1}1\rangle$ type orientations to a position near the $\{001\}\langle\bar{1}00\rangle$ orientation. This type of rotational relationship has previously been noted on several occasions, particularly in aluminum and copper.

Influence of Texture on Mechanical Properties

Because of the crystallographic nature of deformation mechanisms, the mechanical properties of metals should be expected to be influenced by textures. As a first approximation, the proportional limit of a specimen might be expected to vary as the reciprocal of the resolved shear stress. In other words, the more of the applied stress that is resolved in shear on a slip system, the more likely it is for slip to occur for a given applied stress level.

Table 85 shows the mechanical properties of an extruded rod containing 0.12% carbon, the textures of which have been previously reported.[11] Relative resolved shear stresses were determined for the peak position of each component by use of the relationship $\cos \phi \cos \lambda$, where ϕ is the angle between the stress axis and normal to the slip plane, and λ is the angle between the stress axis and slip direction. The ratio of the reciprocal resolved shear stresses (<111> to <114>) is 1.67, and the ratio of proportional limits 1.7. It was also noted that a marked anisotropy is shown for the modulus of elasticity, which was 13.35×10^6 for the rods with the <111> texture and was 7.65×10^6 for the rod with the <114> texture.

Table 86 shows the mechanical properties of the cold-rolled thorium sheet and the annealed thorium sheet for specimens taken at various positions with respect to the rolling direction. It can be seen again that the proportional limit varied inversely as the relative resolved shear stress for the most favored slip system. It was also observed that the tensile strength and the elongation were markedly influenced by the mechanical fibering of carbides and oxides. The fracture of the specimens taken parallel to the rolling direction and 22.5 deg to the rolling direction was perpendicular to the fibers but tended to parallel the fibers for all other positions. The relationship between rolling direction and fracture is shown in Fig. 232. Thus, the difference in properties of rods fabricated by different procedures is in part due to the different preferred orientations developed, as is the directionality of properties in the plane of rolled sheet. In the latter case, some of the properties are also influenced by mechanical fibering of undissolved constituents.

[11] L. K. Jetter and C. J. McHargue, *Met. Semiann. Prog. Rep. April 10, 1955*, ORNL-1911, p 11.

TABLE 85. MECHANICAL PROPERTIES OF EXTRUDED* THORIUM ROD (0.12% C)

	Extrusion Speed	
	Slow	Fast
Texture	96% <111> + 4% <001>	<114>
Yield strength, psi	45,650	26,250
Tensile strength, psi	50,600	30,500
Proportional limit, psi	38,050	22,000
Elongation, %	21	42
Reduction in area, %	37	70
Modulus of elasticity, psi	13.35×10^6	7.65×10^6
$\cos \phi \cos \lambda$	0.27	0.45

*Billet temperature, 850°C.

TABLE 86. MECHANICAL PROPERTIES OF THORIUM SHEET

	Direction of Stress Axis				
	Rolling Direction, 0 deg	22.5 deg	45 deg	67.5 deg	Tranverse Direction, 90 deg
95% Cold Rolled					
Yield strength, psi	50,100	47,800	47,850	50,950	51,500
Tensile strength, psi	54,500	54,500	53,550	55,000	55,750
Proportional limit, psi	23,250	18,850	20,750	18,500	19,600
Elongation, %	13	10	7.5	8	10
Modulus of elasticity, psi	10.8×10^6	13.8×10^6	11.1×10^6	11.25×10^6	11.4×10^6
Maximum relative resolved shear stress	0.408	0.499	0.469	0.492	0.491
$\frac{\text{(Relative shear stress)}}{\text{(Relative shear stress)}_{0\ \text{deg}}}$	1.0	1.2	1.15	1.2	1.2
$\frac{\text{(Proportional limit)}_{0\ \text{deg}}}{\text{(Proportional limit)}}$	1.0	1.2	1.1	1.25	1.2
Annealed 900°C					
Yield strength, psi	18,250	17,550	18,150	18,650	18,150
Tensile strength, psi	26,800	27,050	27,600	28,000	27,900
Proportional limit, psi	11,350	9,400	10,950	9,400	10,600
Elongation, %	60	62.5	57.5	48	48
Modulus of elasticity, psi	8.9×10^6	10.8×10^6	9.4×10^6	11.1×10^6	10.1×10^6
Maximum relative resolved shear stress	0.408	0.495	0.408	0.495	0.408
$\frac{\text{(Relative shear stress)}}{\text{(Relative shear stress)}_{0\ \text{deg}}}$	1.0	1.2	1.0	1.2	1.0
$\frac{\text{(Proportional limit)}_{0\ \text{deg}}}{\text{(Proportional limit)}}$	1.0	1.2	1.04	1.2	1.07

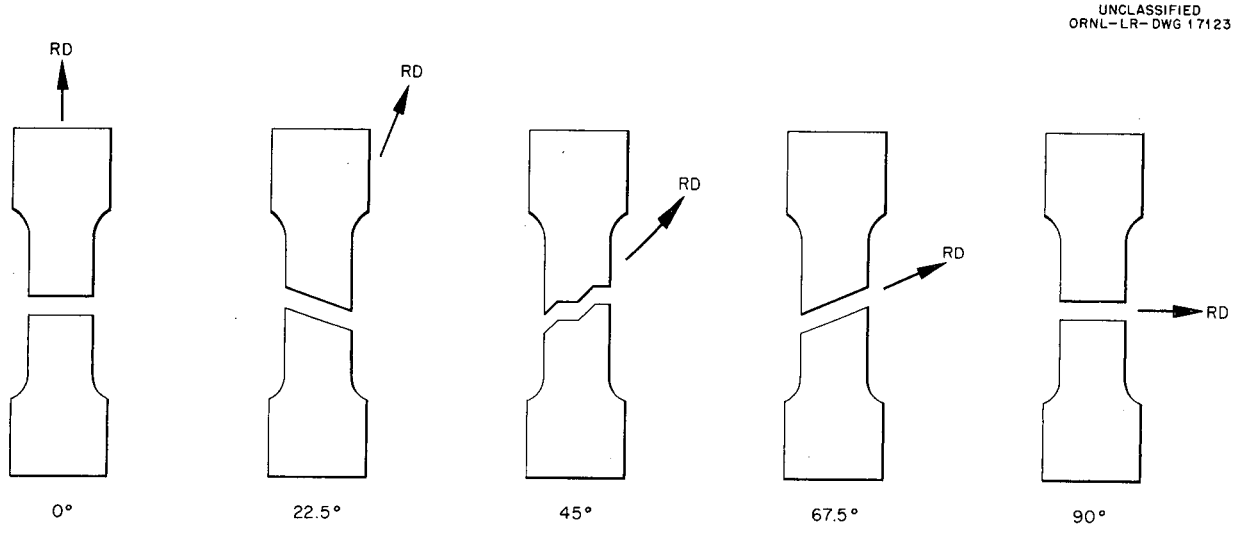

Fig. 232. Relationship Between Rolling Direction and Fracture in Tensile Specimens of Annealed Thorium Sheet. The arrow denotes the rolling direction, and the angle between rolling direction and tension axis is noted beneath each specimen.

METALLURGY DIVISION
AT
THE OAK RIDGE NATIONAL LABORATORY

NOVEMBER 15, 1956

DIRECTOR — J. H. FRYE, JR.; B. BYRUM, SEC.

ASSOCIATE DIRECTOR — W. D. MANLY*; J. MORRISON,* SEC.

ASSISTANT DIRECTOR — J. E. CUNNINGHAM*; M. WHITE,* SEC.

ADMINISTRATIVE ASSISTANT
L. E. BANKER*
M. BOLINGER, SEC.

FUNDAMENTAL METALLURGY

PHYSICO-METALLURGICAL RESEARCH
L. K. JETTER
B. BALLARD,* SEC.

PREFERRED ORIENTATION
C. J. MCHARGUE
J. C. ODLE

THEORETICAL ALLOYING
J. O. BETTERTON, JR.
G. D. KNEIP, JR.
D. S. EASTON
J. O. SCARBROUGH
D. O. WELCH (CO-OP)

X-RAY DIFFRACTION
H. L. YAKEL, JR.
B. BALLARD,* SEC.
R. W. STEELE
J. C. RICHTER

HRP METALLURGY
G. M. ADAMSON, JR.
F. LOVING,[1] SEC.
J. P. HAMMOND
W. J. LEONARD
M. L. PICKLESIMER
J. J. PRISLINGER
R. L. STEPHENSON
C. H. WODTKE
P. J. JONES
C. W. SMITH, JR.
M. A. WHEELER
J. J. WOODHOUSE, JR.

ADMINISTRATION
L. E. BANKER*

PROCUREMENT
R. J. STEERE
B. BOTHWELL
K. P. BAYNE

BUDGET ANALYST
R. G. CARDWELL, JR.

TIMEKEEPING
D. POE*

ANP METALLURGY
W. D. MANLY*
J. MORRISON,* SEC.
T. HIKIDO, USAF

GENERAL CORROSION
E. E. HOFFMAN
D. POE,* SEC.
R. CARLANDER (PWA)
W. H. COOK
D. H. JANSEN
J. L. GRIFFITH
J. W. HENDRICKS
J. E. POPE
L. R. TROTTER

DYNAMIC CORROSION
J. H. DEVAN
SEC. UNASSIGNED
E. A. KOVACEVICH
G. D. BRADY
E. J. LAWRENCE
M. A. REDDEN

HIGH TEMPERATURE REACTIONS
G. P. SMITH, JR.
M. BOND,* SEC.
C. R. BOSTON
J. V. CATHCART
J. J. MCBRIDE
G. F. PETERSEN
J. J. CAMPBELL
J. E. EPPERSON

NONDESTRUCTIVE TEST DEVELOPMENT
R. B. OLIVER
M. BOND,* SEC.
J. W. ALLEN
R. W. MCCLUNG
R. A. NANCE
J. K. WHITE[3]
R. O. CARDEN[3]
O. E. CONNER
R. A. CUNNINGHAM, JR.
W. J. MASON
A. C. SMITH[3]

INSPECTION
A. TABOADA
SEC. UNASSIGNED
A. E. GOLDMAN
R. L. HEESTAND (PWA)
G. M. TOLSON
R. M. EVANS
J. B. PHILLIPS

METALLURGY REPORTS OFFICE
W. R. HILL
W. DIXON
L. PYATT
F. FINN

FABRICATION
J. H. COOBS
B. BALLARD,* SEC.
M. R. D'AMORE (PWA)
H. INOUYE
V. M. KOLBA (GLM)
R. E. MCDONALD (PWA)
J. P. PAGE
T. K. ROCHE
W. R. JOHNSON
J. F. NEWSOME
J. E. SPRUIELL (CO-OP)

WELDING AND BRAZING
P. PATRIARCA
W. BOND,* SEC.
R. E. CLAUSING
E. A. FRANCO-FERREIRA
G. M. SLAUGHTER
E. J. WILSON, JR.
B. MCDOWELL
E. A. NICHOLS[3]
R. G. SHOOSTER
C. E. SHUBERT
F. S. TROTTER, JR.[3]
L. C. WILLIAMS

MECHANICAL PROPERTIES
D. A. DOUGLAS, JR.
D. POE,* SEC.
C. W. DOLLINS
C. R. KENNEDY (PWA)
J. R. WEIR, JR.
J. W. WOODS
F. L. BEELER
K. W. BOLING
E. BOLLING
J. T. EAST
J. D. HUDSON
V. G. LANE
B. MCNABB, JR.
E. B. PATTON, JR.
C. K. THOMAS
C. W. WALKER

MASS TRANSFER STUDIES
J. L. SCOTT
B. BALLARD,* SEC.
H. W. LEAVENWORTH, (PWA)

APPLIED METALLURGY
J. E. CUNNINGHAM*
M. WHITE,* SEC.

PROCESS METALLURGY
R. J. BEAVER
M. WHITE,* SEC.
L. L. HALL

METAL FABRICATION
J. H. ERWIN*
G. D. GOLDSTON
T. W. COFFEY

FUEL ELEMENT FABRICATION
J. H. ERWIN*
G. H. CALLAWAY
N. H. FLICKINGER
J. N. HIX
C. W. HOLLAND
W. W. PROAPS
L. QUEENER
H. J. WALLACE

ALLOY PREPARATION
W. C. THURBER
G. E. ANGEL
J. B. FLYNN

FUEL ELEMENT DEVELOPMENT
R. C. WAUGH
C. F. LEITTEN
J. W. GEER
C. HAMBY, JR.
E. R. TURNBILL

METALLURGICAL MATERIALS AND PROCESSING
E. S. BOMAR, JR.
M. WHITE,* SEC.
R. E. ADAMS
E. M. BENSON
J. I. FEDERER
R. A. PADGETT, JR.
J. H. TERRY

CERAMICS RESEARCH
L. M. DONEY
A. HOBBS, SEC.

GENERAL CERAMICS
C. E. CURTIS
S. D. FULKERSON
F. P. JEFFERS

FUNDAMENTAL CERAMICS RESEARCH
A. G. THARP

FUEL ELEMENT DEVELOPMENT
A. J. TAYLOR
R. L. HANNER

ANP MATERIALS
L. A. HARRIS
R. A. POTTER
G. D. WHITE
J. A. GRIFFIN

WASTE DISPOSAL
M. P. HAYDON
J. M. KERR

METALLOGRAPHY
R. J. GRAY
W. SHOCKLEY
R. S. CROUSE
E. L. LONG, JR.

X-10 LABORATORY
W. H. BRIDGES
J. R. RIDDLE
J. E. VANCLEVE, JR.
M. D. ALLEN
L. A. AMBURN, JR.
N. W. ATCHLEY
R. A. BOWMAN
C. K. H. DUBOSE
W. H. FARMER
R. L. FITZGERALD
J. C. GOWER
E. P. GRIGGS
T. J. HENSON
E. H. LEE
B. C. LESLIE
C. D. MATHES
C. E. ZACHARY

Y-12 LABORATORY
T. M. KEGLEY, JR.
D. F. STONEBURNER
E. R. BOYD
B. F. DAY
B. J. REECE
L. G. SHRADER

*MULTIPLE LISTING
[1]ON LOAN FROM REED
[2]ON LOAN FROM HRP METALLURGY
[3]ON LOAN FROM INSPECTION ENGINEERING